Pharmacological Regulation and Function of Store-Operated Calcium Channels

Bo Zeng

Doctor of Philosophy

The University of Hull and The University of York

Hull York Medical School

September 2012

Abstract

Store-operated Ca^{2+} entry (SOCE) is an important Ca^{2+} influx pathway existing in almost all types of mammalian cell. STIM1, ORAI and TRPC have been regarded as the molecular basis of SOCE. Once the endoplasmic reticulum (ER) Ca^{2+} store is depleted, STIM1 proteins move to the plasma membrane and activate ORAI and TRPC channels to allow Ca^{2+} influx. In this thesis, the pharmacological aspects and regulatory mechanisms of SOCE were investigated using HEK293 cells overexpressing STIM1, ORAI or TRPC genes. The expression and function of TRPC channels and their spliced variants in native cells were also examined.

Using live-cell imaging, the cytosolic clustering of STIM1-EYFP was observed after challenging with the compounds including 2-APB, flufenamic acid, 4-chloro-3-ethylphenol, U73122 and FCCP. The aggregation of STIM1 in the cytosol coud be a novel mechanism for the inhibition of SOCE, and the process did not rely on the depletion of ER Ca^{2+} store. The ryanodine receptor agonist 4-chloro-3-ethylphenol not only caused Ca^{2+} release and cytosolic STIM1 clustering, but also nonselectively inhibited ORAI1/2/3 and TRPC3/4/5/6 channels.

The sensitivity of TRP channels to metal ions was also investigated using patch clamp. Micromolar Cu^{2+} significantly increased the currents of TRPC3/4/5/6 channels. The glutamic acid (E542/E543) and cysteine (C554) residues in the extracellular pore region of TRPC4 were involved in the channel opening by Cu^{2+}. Moreover, Cu^{2+} showed inhibitory effect on TRPM2 channel.

TRPC1/3/4/6 and multiple alternatively spliced variants were detected in the human ovarian adenocarcinoma-derived SKOV3 cells. Blockade of TRPC channel activity by 2-APB, SKF-96365, TRPC pore-blocking antibodies or transfection with TRPC siRNA significantly inhibited SKOV3 cell proliferation. Overexpression of TRPC genes promoted colony growth of SKOV3 cells.

It is concluded that cytosolic STIM1 movement could be a new pharmacological target for SOCE. 4-Chloro-3-ethylphenol and Cu^{2+} are new modulators of ORAI and TRP channels. TRPC channels and their spliced variants are important for cancer cell growth. These findings provide novel insights into the pharmacology and pathophysiology of store-operated channels.

Contents

List of Figures

List of Tables

Acknowledgements

First and foremost I would like to express my sincere gratitude to my supervisor Dr. Shang-Zhong Xu for the continuous support during my PhD study. I appreciate all his contributions of time and knowledge that make my research exciting and productive. His guidance has given me extraordinary experiences through out the three years in Hull.

Besides my supervisor, I would like to thank the rest of my thesis advisory panel, Prof. Jonathan Bennett and Prof. Stephen Atkin, for their encouragement, insightful comments and valuable suggestions for my research.

My sincere thanks also go to the lab fellows Dr. Hongni Jiang and Nikoletta Daskoulidou, who have shared many delightful moments and boring time together with me. It is a pleasure to say thanks to Xudong Zhu, Rui Zhao and many other friends I met in Hull. All of you have brought me beautiful memories in these years.

I would like to express my most appreciation to my wife Guilan Chen for her love, dedication and confidence in me. And also many thanks to my parents, who have been supporting me with all their love throughout my life.

Lastly, I gratefully acknowledge the China Scholarship Council for sponsoring my PhD study in the University of Hull.

Declaration

I confirm that this work is original and that if any passages or diagrams have been copied from academic papers, books, the internet or any other sources these are clearly identified by the use of quotation marks and the references are fully cited.

I certify that, other than where indicated, this is my own work and does not breach the regulations of HYMS, the University of Hull or the University of York regarding plagiarism or academic conduct in examinations.

I have read the HYMS Code of Practice on Academic Misconduct, and state that this piece of work is my own and does not contain any unacknowledged work from any other sources.

Abbreviations

2-APB	2-aminoethyldiphenyl borate
4-CEP	4-chloro-3-ethylphenol
4-ClP	4-chlorophenol
4-CmC	4-chloro-m-cresol
ADPR	adenosine diphosphate ribose
AMP	adenosine monophosphate
ATP	adenosine triphosphate
BAPTA	1,2-bis(2-aminophenoxy)ethane-N,N,N',N'-tetraacetic acid
C-terminus	carboxyl-terminus
CAD	CRAC activation domain
CAD/SOAR	CRAC activation domain and STIM1-Orai activating region
CalyA	calyculin A
CC	coiled-coil regions
CCD	central core disease
CHE	chelerythrine
CytD	cytochalasin D
DAG	diacylglycerol
DES	diethylstilbestrol
DMSO	dimethyl sulfoxide
dNTPs	deoxyribonucleotide triphosphates
E3	the extracellular third loop
EC	excitation–contraction
EF	EF hand domain
EGTA	ethylene glycol-bis(2-aminoethylether)-N,N,N',N'-tetraacetic acid
eNOS	endothelial NO synthase
ER	endoplasmic reticulum
EYFP	enhanced yellow fluorescent protein
FACS	fluorescence-activated cell sorting
F-actin	filamentous actin
FBS	fetal bovine serum
FCCP	carbonyl cyanide 4-(trifluoromethoxy)phenylhydrazone

FFA	flufenamic acid
GPCR	G protein-coupled receptor
HAECs	human aortic endothelial cells
HEPES	4-(2-hydroxyethyl)-1-piperazineethanesulfonic acid
I_{CRAC}	Ca^{2+} release-activated Ca^{2+} current
IP_3	inositol 1,4,5-trisphosphate
IP_3R	inositol 1,4,5-trisphosphate receptor
I-V	current-voltage
LA	Luria agar
LB	Luria broth
mCFP	monomeric cyan fluorescent protein
mCherry	monomeric red fluorescent protein
MH	malignant hyperthermia
N-terminus	amino-terminus
NFA	niflumic acid
NFAT	nuclear factor of activated T-cells
NO	nitric oxide
OAG	1-oleoyl-2-acetyl-sn-glycerol
PAR2	proteinase-activated receptor 2
PBS	phosphate buffered saline
PI_3K	phosphatidylinositol 3-kinase
PIP_2	phosphatidylinositol 4,5-bisphosphate
PKA	protein kinase A
PKC	protein kinase C
PLC	phospholipase C
PM	plasma membrane
RNAi	RNA interference
RNase	ribonuclease
ROCK	Rho-associated protein kinase
ROCs	receptor-operated channels
ROS	reactive oxygen species
RTK	receptor tyrosine kinase
RyR	ryanodine receptor
SAM	sterile α motif

SCID	severe combined immunodeficiency
SERCA	sarco/endoplasmic reticulum Ca^{2+} ATPase
siRNA	small interfere RNA
SOAR	STIM1-Orai activating region
SOCE	store-operated Ca^{2+} entry
SOCs	store-operated channels
SR	sarcoplasmic reticulum
STIM1	stromal interaction molecule 1
TG	thapsigargin
TM	transmembrane segment
TPEN	*N,N,N'N'*-tetrakis(2-pyridylmethyl)-ethylenediamine
TRP	transient receptor potential
TRPA	transient receptor potential ankyrin
TRPC	transient receptor potential canonical
TRPM	transient receptor potential melastatin
TRPML	transient receptor potential mucolipin
TRPP	transient receptor potential polycystin
TRPV	transient receptor potential vanilloid

Chapter 1

Introduction

1.1. Introduction

Calcium is a crucial element for all living organisms. Apart from the content of calcium stored in certain tissues and bound to proteins, free calcium ions (Ca^{2+}) play a pivotal role in the regulation of physiological functions of the cells. Within a typical mammalian cell, the concentration of Ca^{2+} varies in different subcellular compartments. The Ca^{2+} concentration in the cytoplasm at resting state is generally within the range of 100-200 nM (Putney, 2010). In some organelles, such as endoplasmic/sarcoplasmic reticulum (ER/SR), mitochondria and lysosomes, the Ca^{2+} concentrations are much higher, which may achieve 1-2 mM (Bygrave and Benedetti, 1996). Due to such a big difference between the Ca^{2+} contents in cytoplasm and organelles, these organelles are termed as "Ca^{2+} stores", which serve as an important source of cytoplasmic Ca^{2+}. Another major Ca^{2+} source for a cell is the extracellular fluid, which contains a large amount of Ca^{2+} with relatively stable concentrations at 1-2 mM (Larsson and Ohman, 1978). The entering of extracellular Ca^{2+} into the cell, i.e., Ca^{2+} influx, is tightly controlled by various types of Ca^{2+}-permeable channels or transporters residing in the plasma membrane and regulated by intracellular Ca^{2+} stores.

1.2. Store-operated Ca^{2+} entry

In non-excitable cells, such as fibroblasts, platelets and endothelial cells, the most important pathway for cytoplasmic Ca^{2+} supplement is the so called "store-operated Ca^{2+} entry" (SOCE), which means that the Ca^{2+} influx from extracellular fluid is triggered by the Ca^{2+} release from the stores. The physiological signals that induce Ca^{2+} release in non-excitable cells are mostly generated by the stimulation of G protein-coupled receptors (GPCRs) by agonists at the cellular surface. The activation of GPCRs triggers the signal transduction from G proteins to phospholipase C (PLC), which cleaves the membrane constituent phosphatidylinositol 4,5-bisphosphate (PIP_2) into diacylglycerol (DAG) and inositol 1,4,5-trisphosphate (IP_3). The receptors of IP_3 (IP_3Rs) are Ca^{2+} channels located in the luminal membrane of the ER, and thus the elevated level of IP_3 in the cytoplasm will result in the activation of IP_3Rs and Ca^{2+} release from the ER. A decrease in the luminal Ca^{2+} level of the ER will eventually open the store-operated Ca^{2+} channels in the plasma membrane that mediate Ca^{2+} influx from extracellular liquid. As

SOCE is a fundamental process in many cell types, it plays important roles in various cellular functions, such as proliferation of endothelial cells (Abdullaev *et al.*, 2008), exocytosis (Bakowski *et al.*, 2003), migration and metastasis of cancer cells (Yang *et al.*, 2009a), and insulin secretion (Henquin *et al.*, 2012).

1.3. Discovery of store-operated Ca^{2+} entry

The association between Ca^{2+} release from stores and Ca^{2+} entry from extracellular medium was originally described in a series of studies by James W. Putney in the 1970s (Putney, 1976a; Putney, 1976b; Putney, 1977). As the fluorescent Ca^{2+} indicators were not available at that time, Putney used rat parotid acinar cells that express Ca^{2+}-dependent K^+ channels, in which the cytosolic Ca^{2+} levels can be indirectly monitored by observing the efflux rates of K^+ or Rb^+ (Putney, 1976a). He found that carbachol and phenylephrine, which are agonists for muscarinic and adrenergic receptors respectively, elicited a biphasic $^{86}Rb^+$ release from the cells preloaded with this radioisotope. The first phase of release was independent of extracellular Ca^{2+}, but the second phase could be blocked by external Ca^{2+} chelator and La^{3+}. These results suggested a fluctuation of intracellular Ca^{2+} levels after receptor stimulation, which was confirmed by direct Ca^{2+} assay using $^{45}Ca^{2+}$ in the same type of cells (Putney, 1976b). Further experiments demonstrated that carbachol, phenylephrine and substance P (an agonist of neurokinin 1 receptor) all induced the first phase of $^{86}Rb^+$ efflux by releasing Ca^{2+} from the same store, which was followed by Ca^{2+} influx from external solution that resulted in the second phase of $^{86}Rb^+$ efflux (Putney, 1977). A later independent study on rabbit smooth muscle cells showed that the amplitude of $^{45}Ca^{2+}$ influx in the cells with Ca^{2+} store depleted by repetitive stimulation with noradrenaline in Ca^{2+}-free solution was larger than that in cells kept in Ca^{2+}-free solution only (Casteels and Droogmans, 1981). This study suggested a direct pathway of communication between the Ca^{2+} store and extracellular medium. After a review on previous findings, Putney (1986) proposed a "capacitative Ca^{2+} influx" model for the receptor-regulated Ca^{2+} entry. In this model, the signalling molecule IP_3 controls the Ca^{2+} release from the store, which in turn regulates the Ca^{2+} influx from extracellular space. The depletion of Ca^{2+} store will automatically trigger Ca^{2+} entry into the cell, and when the store is refilled to a certain level the Ca^{2+} influx will be terminated.

The introduction of fluorescent Ca^{2+} indicators (Grynkiewicz et al., 1985), especially fura-2, has significantly accelerated the Ca^{2+} signalling research. By using these membrane-permeable probes, it became feasible to monitor intracellular Ca^{2+} level in a live cell in real time. Another landmark in SOCE research is the discovery of thapsigargin as a specific blocker of sarco/endoplasmic reticulum Ca^{2+} ATPase (SERCA) (Thastrup et al., 1989; Thastrup et al., 1990) . Depletion of SR/ER Ca^{2+} stores by thapsigargin does not rely on IP_3 signalling, thus providing a means to investigate the role of Ca^{2+} store depletion without concerning unknown effects of the second messengers generated by GPCR activation. It was soon demonstrated that depletion of Ca^{2+} store alone by thapsigargin was sufficient to induce Ca^{2+} influx across the plasma membrane in rat parotid acinar cells (Takemura et al., 1989; Takemura and Putney, 1989). Taking the advantage of thapsigargin, the existence of SOCE in various types of cells was then reported by a number of independent research groups across the world. The findings on the cells including immune cells, epithelial and endothelial cells, cancer cells and smooth muscle cells implied that SOCE may be an ubiquitous cellular process in both excitable and non-excitable cells (Parekh and Penner, 1997).

The application of patch-clamp techniques provided biophysical evidences for SOCE. Penner et al. (1988) reported a small inward current after Ca^{2+} store depletion by IP_3 in rat mast cells. A small Ca^{2+}-selective current was also observed in human leukemic T cells by Lewis and Cahalan (1989), who used a mitogenic lectin, phytohemagglutinin, to stimulate internal Ca^{2+} release and found the elicited current was voltage-independent. Although both studies had described the correlation between Ca^{2+} release and the inward Ca^{2+} current, the authors did not consider Ca^{2+} release as a direct signal that triggered the Ca^{2+}-influx current. The causal relation between Ca^{2+} store depletion and the accompanying inward Ca^{2+} current was firstly demonstrated by Hoth and Penner (1992) and the current was termed "Ca^{2+} release-activated Ca^{2+} current" (I_{CRAC}). The I_{CRAC} was characterised by an inward rectification, very high selectivity for Ca^{2+} and voltage-independence. Later, store-operated currents with different biophysical properties were identified in many types of non-excitable cells, such as human umbilical vein endothelial cells (Oike et al., 1994), pancreatic beta cells (Bordin et al., 1995; Bertram et al., 1995) and rat basophilic leukaemia cells (Hoth, 1995), and some excitable cells, such as

smooth muscle cells (Zakharov *et al.*, 2004) and sensory neurons (Gemes *et al.*, 2011).

1.4. STIM and Orai as molecular basis of store-operated Ca^{2+} entry

Although the presence of SOCE in various cell types was well demonstrated by intracellular Ca^{2+} measurement and electrophysiological recordings over the past three decades, the molecular identities of store-operated channels (SOCs) had remained elusive until the discovery of STIM1 (stromal interaction molecule 1) and Orai1 in 2005 and 2006, respectively (Roos *et al.*, 2005; Liou *et al.*, 2005; Vig *et al.*, 2006b; Feske *et al.*, 2006). The crucial role of STIM1 in SOCE was revealed by RNA interference (RNAi)-based gene-screening studies in *Drosophila* S2 cells, human Jurkat T and Hela cells, in which the knockdown of STIM1 expression significantly reduced thapsigargin-induced or receptor-triggered Ca^{2+} influx (Roos *et al.*, 2005; Liou *et al.*, 2005). STIM1 was found to be the Ca^{2+} sensor in the ER and translocate to the plasma membrane upon Ca^{2+} store depletion (Liou *et al.*, 2005; Zhang *et al.*, 2005). Genome-wide RNAi screen in *Drosophila* S2 cells and genetic linkage analysis of patients with defective SOCE in T cells identified Orai1, the essential component of SOCs located at the plasma membrane (Vig *et al.*, 2006b; Feske *et al.*, 2006; Zhang *et al.*, 2006). Coexpression of STIM1 and Orai1 reconstituted the function of SOCs and greatly potentiated I_{CRAC} (Peinelt *et al.*, 2006; Soboloff *et al.*, 2006; Mercer *et al.*, 2006). Further mutational studies on Orai1 validated its role as the pore-forming subunit of SOCs (Prakriya *et al.*, 2006; Vig *et al.*, 2006a; Yeromin *et al.*, 2006). The RNAi study by Liou *et al.* (2005) also found STIM2, the conserved analogue of STIM1 in vertebrates (Cai, 2007a). Sequence similarity search against *Drosophila* Orai characterised Orai1, Orai2 and Orai3 in human genome (Feske *et al.*, 2006), of which Orai1 and Orai2 are conserved in vertebrates, and Orai3 is specific for mammals (Cai, 2007b). Functional similarities were shared between STIM1 and STIM2 (Liou *et al.*, 2005), and among the three Orai isoforms (Mercer *et al.*, 2006). These fundamental studies established a principal machinery of SOCs, which has substantially facilitated our understanding on the physiological and pathophysiological regulation of SOCE.

1.5. Mechanism of STIM1/Orai1-mediated Ca^{2+} entry

STIM1 is an ER-localised protein with a single transmembrane segment (Fig. 1.1). The N-terminus of STIM1, which resides in the ER lumen, contains EF hand and sterile α motif (SAM) domains (Stathopulos *et al.*, 2008; Zheng *et al.*, 2008). The EF hand is a Ca^{2+}-binding motif and thus functions as a sensor to detect luminal Ca^{2+} level in the ER. The SAM domain is responsible for the oligomerisation of STIM1 proteins. The cytosolic part of STIM1contains two predicted coiled-coil regions, a serine/proline-rich and a lysine-rich domain (Deng *et al.*, 2009). A STIM1 segment within the coiled-coil regions was found to activate Orai1 channel directly, thus being named CRAC activation domain (CAD) (Park *et al.*, 2009) or STIM1-Orai activating region (SOAR) (Yuan *et al.*, 2009b). In addition, an acidic motif has been recognised from the first coiled-coil region of STIM1, and a basic motif was found in the CAD/SOAR (Korzeniowski *et al.*, 2010). Each Orai1 protein has four transmembrane segments, with both the N- and C-termini facing the cytosol (Fig. 1.1). An acidic motif within the coiled-coil region of the C-terminus of Orai1 is believed to interact with the CAD/SOAR of STIM1 (Muik *et al.*, 2008; Calloway *et al.*, 2009). As the two acidic motifs in STIM1 and Orai1 have substantial similarity and the basic motif in the CAD/SOAR can bind to either of them, a molecular switching model has been proposed for the CAD/SOAR-controlled Orai1 activation (Fig. 1.1) (Korzeniowski *et al.*, 2010). At resting state, the CAD/SOAR is inactivated by binding to the acidic motif of STIM1. This intramolecular bond is disrupted after Ca^{2+} ions disassociate from the EF hand of STIM1, and the CAD/SOAR is exposed the cytosol and binds the acidic motif of Orai1 when the distance between STIM1 and Orai1 is close enough.

In a cell, the depletion of ER Ca^{2+} store induces aggregation and translocation of STIM1 proteins toward the plasma membrane (Liou *et al.*, 2005). The interaction of STIM1 and Orai1 occurs in the junctional area between the plasma membrane and the ER (PM-ER junction), which may be pre-existing or newly formed after Ca^{2+} store depletion (Wu *et al.*, 2006). The subplasmalemmal STIM1 clusters are able to induce local aggregation of Orai1 channels, forming a large number of puncta at the plasma membrane (Xu *et al.*, 2006a; Luik *et al.*, 2006), and causing the opening of Orai1 channels, which allows massive Ca^{2+} influx into the cell to refill the Ca^{2+} store and regulate cellular functions.
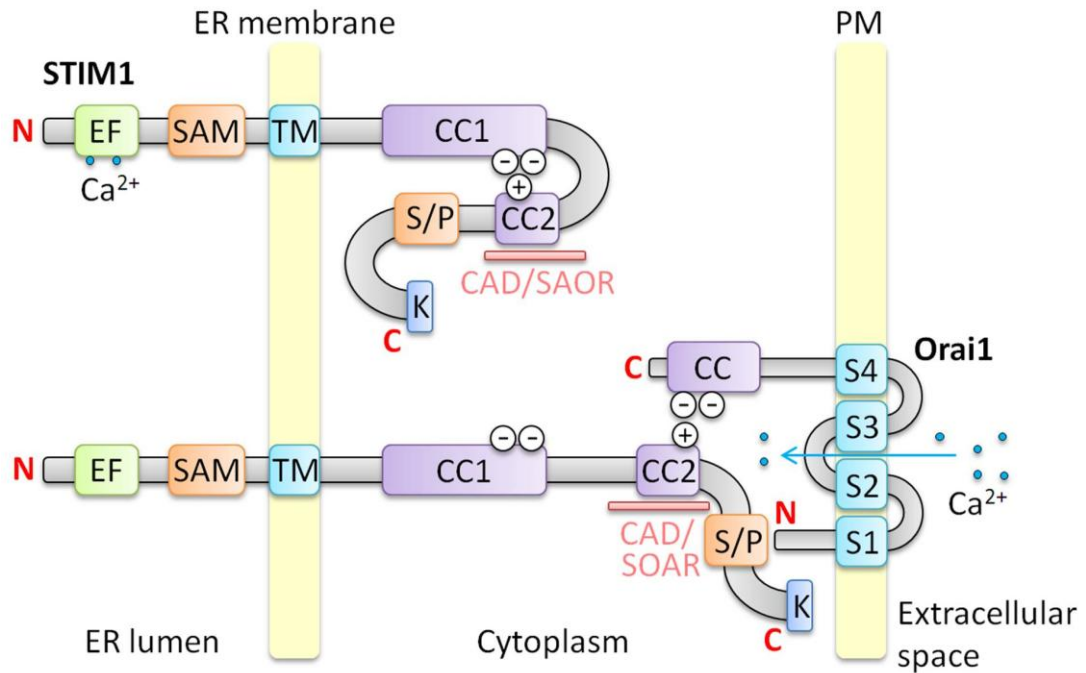
Fig. 1.1 Molecular mechanism of STIM1/Orai1-mediated Ca²⁺ influx. The upper part shows the structure of STIM1 at resting state, and the lower part illustrates the architecture of STIM1/Orai1 complex after Ca^{2+} ions disassociate from STIM1. The symbols of positive and negative charges indicate the basic and acidic motifs, respectively. Abbreviations: N, amino-terminus; C, carboxyl-terminus; EF, EF hand domain; SAM, sterile α motif; TM, transmembrane segment; CC, CC1 and CC2, coiled-coil regions; CAD/SOAR, CRAC activation domain and STIM1-Orai activating region; S/P, serine/proline-rich domain; K, lysine-rich domain; S1-S4, transmembrane segment 1-4.

1.6. TRPC channels in store-operated Ca²⁺ entry

Before the discovery of STIM1 and Orai1, the most possible candidates of SOCs have been considered to be transient receptor potential canonical (TRPC) channels. TRPC channels belong to the large family of TRP channels, which includes a total of 28 members in mammalian genome. These members are divided into six subfamilies according to the sequence similarities: TRPA1 (ankyrin), TRPV1-6 (vanilloid), TRPM1-8 (melastatin), TRPP1-3 (polycystin), TRPML1-3 (mucolipin) and TRPC1-7. Most TRP channels are non-selective cation channels with a selectivity of Ca^{2+} over Na^+ variable among different members. A number of TRP channels, in particular TRPCs, are activated following GPCR stimulation, and thus referred to as "receptor-operated channels" (ROCs). There is evidence that TRPC channels are potentiated by activated G proteins (TRPC4/5) (Jeon *et al.*, 2012), the PLC-cleavage product DAG (TRPC3/6/7) (Hofmann *et al.*, 1999; Okada *et al.*,

1999) and the depletion of Ca^{2+} store (Salido *et al.*, 2009). Among all TRPC members, TRPC1 has been most consistently considered a SOC channel in many cell types, such as salivary gland (Liu *et al.*, 2000), smooth muscle (Xu and Beech, 2001), DT40 (Mori *et al.*, 2002) and epithelial cells (Rao *et al.*, 2006). In these studies, inhibition of TRPC1 activity or knockdown of TRPC1 expression attenuated SOCE evoked by thapsigargin or GPCR agonists *in vitro*. In TRPC1-knockout mice, the endogenous SOCE was significantly reduced in salivary gland cells (Liu *et al.*, 2007), but not affected in platelets and cerebral artery smooth muscle cells (Varga-Szabo *et al.*, 2008a; Dietrich *et al.*, 2007), suggesting the essential role of TRPC1 in SOCE may be limited to some specific cell types. It has been showed that TRPC1 interacted with both STIM1 and Orai1, and formed a ternary complex (Ong *et al.*, 2007; Zhang *et al.*, 2010). Further studies in salivary gland cells demonstrated that the insertion of TRPC1 into the plasma membrane and its activation after Ca^{2+} store depletion were triggered by the Ca^{2+} influx through Orai1 channel (Cheng *et al.*, 2008; Cheng *et al.*, 2011). These studies provided an important mechanism for the functional interaction of STIM1, Orai1 and TRPC1 in salivary gland cells. TRPC1 was also reported to be gated by STIM1 directly through electrostatic interaction between the positively and negatively charged motifs in the C-termini of the two proteins (Zeng *et al.*, 2008), which may be a universal mechanism in HEK293 and other cell types. Apart from TRPC1, TRPC4 and TRPC5 were also found to interact with STIM1 (Yuan *et al.*, 2007). Considering that all TRPC isoforms, except TRPC2 (a pseudogene in human) and TRPC7, are able to form heterotetrameric channels, STIM1 was found to regulate TRPC3 and TRPC6 indirectly when they multimerise with TRPC1, TRPC4 or TRPC5 (Yuan *et al.*, 2007). Gene knockdown experiments suggested that TRPC3, TRPC4 and TRPC7 contributed to SOCE in DT40 (Vazquez *et al.*, 2001), HEK293 (Zagranichnaya *et al.*, 2005) or mesangial cells (Wang *et al.*, 2004b). Blockage of TRPC channels by antibodies revealed that TRPC1 and TRPC5 were required for SOCs in portal vein, coronary and mesenteric arteries, whereas TRPC6 and TRPC7 had such a role only in coronary artery and portal vein, respectively (Saleh *et al.*, 2008). An early and a recent study using endothelial cells from TRPC4-deficient mice validated the role of TRPC4 as a SOC channel (Freichel *et al.*, 2001; Sundivakkam *et al.*, 2012). There are also conflicting observations on the Ca^{2+} store-dependent activation of TRPC channels, which excluded the store-operated functionality of TRPCs. For example, RNA silencing of either TRPC1 or

TRPC4 did not affect the SOCE and I_{CRAC} in endothelial cells (Abdullaev *et al.*, 2008), and no functional association between TRPCs and STIM1/Orai1 was observed when they were coexpressed in HEK293 cells (Abdullaev *et al.*, 2008; DeHaven *et al.*, 2009). Collectively, these contradictory results may arise from the differences in the expression profile of STIM, Orai, TRPC and other unknown regulators of SOCE in various cell types. Nonetheless, TRPC channels are able to function as components of SOCs in at least some specific cell types. Future studies that recognise novel members and regulatory mechanisms of SOCs will be helpful to clarify the roles of TRPC channels in SOCE.

1.7. Physiological and pathophysiological functions of store-operated Ca^{2+} channels

1.7.1 Functions of STIM proteins and Orai channels

Although STIM1 and Orai1 proteins are widely expressed in a large variety of tissue and cell types, the genetic defects of STIM1 or Orai1 genes are mostly related to immune diseases in human and mice (Feske, 2009). A nonsense mutation in exon 3 of STIM1 gene, which results in a truncated STIM1 protein, caused immunodeficiency, autoimmune hemolytic anemia and other immune-related symptoms in the patients (Picard *et al.*, 2009). Studies using cells isolated from fetal STIM1-knockout mice demonstrated that STIM1 was essential for the activation of mast cells, T cells and macrophages (Baba *et al.*, 2008; Oh-Hora *et al.*, 2008; Braun *et al.*, 2009a). Patients bearing a nonsense mutation in Orai1 have a hereditary syndrome of severe combined immunodeficiency (SCID), which manifested decreased immune response and impaired Ca^{2+}-dependent gene expression in T cells (Feske *et al.*, 2006). In mast cells from Orai1-deficient mice the degranulation and cytokine secretion were defective, and the allergic reactions of the mice were inhibited *in vivo* (Vig *et al.*, 2008). Orai1-knockout mice also exhibited reduced B cell proliferation in response to receptor stimulation and attenuated cytokine production by T cells (Gwack *et al.*, 2008). These results consistently suggest that STIM1/Orai1-mediated SOCE is important for the immune functions. STIM2 has been found to share some functions of STIM1 in T cells, such as the regulation of cytokine production and nuclear translocation of the transcription factor NFAT (nuclear factor of activated T-cells) (Oh-Hora *et al.*, 2008). The functions of Orai2 and Orai3 in immune system are still lack of investigation thus far.

In addition to immune regulation, STIM and Orai also participate in the regulation of cardiovascular functions, and are involved in the development of cancer. STIM1 was found to promote pathological cardiac hypertrophy in rat models (Hulot *et al.*, 2011; Luo *et al.*, 2012). The activity of STIM1 and Orai1 is required for the proliferation and migration of vascular smooth muscle and endothelial cells (Potier *et al.*, 2009; Abdullaev *et al.*, 2008; Kuang *et al.*, 2010). The mice lacking STIM1 or Orai1 exhibited lowered activity of platelets and thus were less sensitive to ischemic brain infarction and arterial thrombosis (Grosse *et al.*, 2007; Varga-Szabo *et al.*, 2008b; Braun *et al.*, 2009b). The roles of STIM and Orai proteins in breast cancer cells have been investigated by different research groups. Yang *et al.* (2009a) demonstrated that STIM1/Orai1-mediated SOCE is critical for the migration and metastasis of breast tumour cells in mice. Motiani *et al.* (2010) found a correlative expression of oestrogen receptors and Orai3 in various breast cell lines and suggested that STIM1/2 operate Orai3 as major SOCs in breast cells with oestrogen receptors, whereas Orai1 plays the role as SOCs in breast cells lacking oestrogen receptors. Feng *et al.* (2010) unveiled a store-independent pathway for the activation of Orai1 that promoted the tumourigenesis of breast cancer cells, implying that Orai1 is a potential therapeutic target in the treatment of mammary tumours.

1.7.2 Functions of TRPC channels

TRPC1, which is the first identified mammalian TRP channel, has been proposed to function as component of store-operated (Xu and Beech, 2001), receptor-operated (Strubing *et al.*, 2001) and stretch-activated channels (Maroto *et al.*, 2005), and play diverse physiological roles in a range of cells such as cardiac, skeletal and smooth muscle cells, endothelial cells, neurons and salivary gland cells (Abramowitz and Birnbaumer, 2009). TRPC1-deficient mice showed significantly reduced SOCE upon agonist- or thapsigargin-stimulation in salivary gland cells (Liu *et al.*, 2007). Knock-out of TRPC1 protected the mice subjected to hemodynamic stress from cardiac hypertrophy by interrupting mechanosensitive signaling pathways (Seth *et al.*, 2009). Muscles from TRPC1 deficient mice displayed lower Ca^{2+} transients than that observed in muscles from wildtype mice. As a result, the TRPC1 deficient mice presented less force in muscle contraction and significantly decreased endurance for physical activity (Zanou *et al.*, 2010). Another study demonstrated that TRPC1 contributed to blood pressure regulation by negatively regulating endothelial Ca^{2+}-

activated K^+ channel-dependent vasodilatations in TRPC1-deficient mice (Schmidt *et al.*, 2010). TRPC1 was found to reside on the endoplasmic reticulum (ER) when expressed alone, but could interact with other TRPC channels, particularly TRPC4 and TRPC5, to form heterotetramers at the plasma membrane when they were coexpressed (Hofmann *et al.*, 2002; Alfonso *et al.*, 2008). Thus, it is proposed that TRPC1 may form heterotetrameric Ca^{2+}-influx channels at the plasma membrane and homotetrameric Ca^{2+}-release channels at the ER (Alfonso *et al.*, 2008).

Expression of TRPC3 have been detected in many tissues and cell types, but particularly high in brain, smooth and cardiac muscle cells (Clapham, 2003). The most studied cardiovascular diseases related to TRPC3 are hypertension and cardiac hypertrophy. Upregulation of TRPC3 was found in vasculature from hypertensive rats (Liu *et al.*, 2009), hypertrophic hearts from mice and rats (Bush *et al.*, 2006), and vascular endothelium of patients with malignant hypertension (Thilo *et al.*, 2009). The transgenic mice expressing a dominant negative TRPC3 in the heart exhibited attenuated cardiac hypertrophic response following either neuroendocrine agonist infusion or pressure-overload stimulation (Wu *et al.*, 2010a). In contrast, cardiac-specific overexpression of TRPC3 in mice induced spontaneous hypertrophy (Nakayama *et al.*, 2006). The hypertrophic growth of cardiomyocytes is considered to be mediated by NFAT, a Ca^{2+}-responsive transcriptional factor (Rohini *et al.*, 2010). The Ca^{2+} influx through TRPC3 may activate NFAT, and the activation of NFAT triggers the transcription of hypertrophic genes including TRPC3 itself (Nakayama *et al.*, 2006). This feedback loop augments the hypertrophic response, leading to the overgrowth of cardiomyocytes. The association between Ca^{2+} influx and NFAT activation also exists in vascular endothelial cells (Rinne *et al.*, 2009), which may relate to the pathology of more cardiovascular diseases. TRPC3 knockout mice exhibited an impaired walking behaviour (Hartmann *et al.*, 2008), but the cardiovascular function of these mice has not been investigated.

TRPC4 is expressed in endothelium, smooth muscle cells, intestinal pacemaker cells, neurons, adrenal glands and kidneys (Gees *et al.*, 2010). The best-characterised role for TRPC4 is in the regulation of endothelial permeability and vascular tone. In aortic endothelial cells isolated from wildtype and TRPC4-deficient mice, TRPC4 was found to be an indispensable component of SOCs acting as pore-forming subunits or other constituents of channel complexes (Freichel *et al.*, 2001). Both store-operated and agonist-induced receptor-operated Ca^{2+} entry were

absent in TRPC4-deficient endothelial cells. Moreover, endothelial-dependent vasorelaxation of aortic rings in response to stimulation is markedly impaired in TRPC4-deficient mice. In another study, lung endothelial cells from TRPC4-deficient mice failed to respond to thrombin-stimulated GPCR activation and corresponding Ca^{2+} influx was dramatically reduced compared to wildtype mice (Tiruppathi *et al.*, 2002). The abnormal Ca^{2+} influx in TRPC4-deficient endothelial cells was associated with a lack of thrombin-mediated actin-stress fiber formation and a reduced endothelial cell retraction response, suggesting TRPC4 is crucial for the regulation of microvascular permeability in the lungs of mice. TRPC4 is also involved in hypoxia-induced vascular remodelling (Fantozzi *et al.*, 2003). The expression of TRPC4 was upregulated by hypoxia and correlated directly with SOCE in human pulmonary artery endothelial cells. This TRPC4-related Ca^{2+} entry resulted in the activation of nuclear transcription factors and expression of vascular growth factors, leading to remodelling of blood vessels.

TRPC5 and TRPC4 share the highest homology among all members of TRPC subfamily. These two proteins have conserved structural elements in the N-termini and membrane-spanning regions, and only differ in the C-termini. TRPC5 is also expressed in multiple tissues, including cardiovascular system and central nervous system (Plant and Schaefer, 2003). TRPC5 has been reported to participate in endothelium-dependent nitric oxide (NO)-mediated vasorelaxation of blood vessels (Yoshida *et al.*, 2006). NO plays an important role in the cardiovascular system by controlling vasoconstriction and vasorelaxation. NO-induced Ca^{2+} influx in bovine aortic endothelial cells was prevented by transfection of siRNA or dominant negative isoform of TRPC5 (Yetik-Anacak and Catravas, 2006). This study also demonstrated that NO caused cysteine S-nitrosylation of TRPC5 on two cysteine residues in the S5-S6 loop region. Mutation of these cysteine residues to serine abrogated TRPC5 responses to NO. These two cysteine residues are also present at corresponding positions in TRPC1 and TRPC4, and both of them can be activated by NO (Freichel *et al.*, 2001). A mechanism is suggested that Ca^{2+} influx induced by NO-induced nitrosylation of TRPC channels may lead to increased endothelial NO synthase (eNOS) activity, which increases NO production and results in enhanced smooth muscle relaxation (Yoshida *et al.*, 2006). However, NO was also reported to inhibit Ca^{2+} entry in bovine vascular endothelial cells (Dedkova and Blatter, 2002). Other TRPC channel like TRPC3 may also participate in this process to generate

promiscuous Ca^{2+} signals observed in different studies (Kwan *et al.*, 2004). Knockout of TRPC5 diminished the innate fear levels of mice (Riccio *et al.*, 2009), which demonstrated its important role in the central nervous system.

Expression of TRPC6 was detected in various tissues and cells, such as lung, brain and smooth muscle cells (Freichel *et al.*, 2005). TRPC6-knockout mice showed an elevated blood pressure and increased vascular smooth muscle contractility, and this could only be partly recovered by the constitutively-active TRPC3 channels overexpressed in the smooth muscle cells of TRPC6-knockout mice (Dietrich *et al.*, 2005). Deletion of TRPC4 and TRPC6 in mice impaired smooth muscle contraction and intestinal motility, which was related to voltage-activated Ca^{2+} influx and depolarization of intestinal smooth muscle cells (Tsvilovskyy *et al.*, 2009). A TRPC5/TRPC6 activation cascade was found to participate in the regulation of endothelial cell migration (Chaudhuri *et al.*, 2008), and the mechanism has been well explained by a study in podocytes (Tian *et al.*, 2010). The authors suggest TRPC5 and TRPC6 regulate the cell migration by binding to different members of Rho GTPases. TRPC5 was present in a complex with Rac1 and TRPC6 was associated with RhoA, in which the former one promotes the cell migration and the latter one inhibits it.

Studies on TRPC7 are much less than that of other TRPC members and its exact role is still unclear. It is suggested that TRPC7 conducts Ca^{2+} in AT1-induced myocardial apoptosis via a calcineurin-dependent pathway and can thereby contribute to the process of heart failure (Satoh *et al.*, 2007). Ablation of both TRPC6 and TRPC7 genes in mice eliminated the light response in iris and retina, suggesting their essential roles in the mammalian melanopsin signalling pathway (Xue *et al.*, 2011).

1.8. Pharmacological modulators of store-operated Ca^{2+} channels

1.8.1. Chemical activators of store-operated Ca^{2+} channels

The principal way to activate SOCs is depleting Ca^{2+} from the ER/SR, which can be achieved by either stimulating Ca^{2+}-release channels in the ER/SR membrane, increasing the ER/SR membrane permeability to Ca^{2+}, or blocking Ca^{2+} transportation into the ER/SR (Fig. 1.2A).

GPCR agonists and IP$_3$: The GPCR agonist-induced IP$_3$ production is sufficient to trigger rapid Ca^{2+} release via IP$_3$Rs. The most widely used chemical agonists are carbachol and ATP, which activate muscarinic and purinergic receptors, respectively. The use of agonists to deplete the Ca^{2+} store from cell surface requires the expression of corresponding receptors in the cells, either endogenous or exogenous. Intracellular application of synthetic IP$_3$ is also able to activate IP$_3$Rs and thus induce SOCE (Taylor and Tovey, 2010; Smyth *et al.*, 2010).

RyR agonists: Another family of Ca^{2+}-release channels in the ER/SR is ryanodine receptors (RyRs). Potentiation of RyRs by caffeine and ryanodine has been shown to induce SR Ca^{2+} release and SOCE in smooth muscle cells (Ng *et al.*, 2007).

Ca^{2+} ionophore: An alternative way to stimulate Ca^{2+} release is to increase the Ca^{2+} permeability of the ER/SR membrane using ionomycin. Ionomycin is a Ca^{2+} ionophore that carries Ca^{2+} through the membrane. It is suggested that ionomycin at low concentrations (<1 μM) only affects the permeability of intracellular membranes and has little effect on the plasma membrane, which renders it the ability to activate SOCs without damaging the cells (Putney, 2010).

SERCA inhibitors: The importation of Ca^{2+} from cytoplasm into the ER/SR is in the charge of SERCA, a class of Ca^{2+} pumps. The activity of SERCA can be blocked by thapsigargin and cyclopiazonic acid. As a passive process relying on the endogenous Ca^{2+}-leaking activity, the depletion of Ca^{2+} store by thapsigargin and cyclopiazonic acid is very slow, compared to the effects of GPCR and RyR agonists. However, because the inhibition of SERCA by thapsigargin is essentially irreversible (Lytton *et al.*, 1991), the subsequent SOCE and membrane current are more persistent (Oike *et al.*, 1994; Liu and Gylfe, 1997).

Ca^{2+} chelators: Chelating cytosolic Ca^{2+} by BAPTA, EGTA or TPEN can also prevent Ca^{2+} from being transported into the store. The onset of Ca^{2+} store depletion depends on the Ca^{2+} affinity and concentration of the chelators (Zweifach and Lewis, 1996; Chvanov *et al.*, 2008). Chelation of cytosolic Ca^{2+} is required in the eletrophysiological recordings of I_{CRAC}, with BAPTA or EGTA as an essential component of the internal solution.
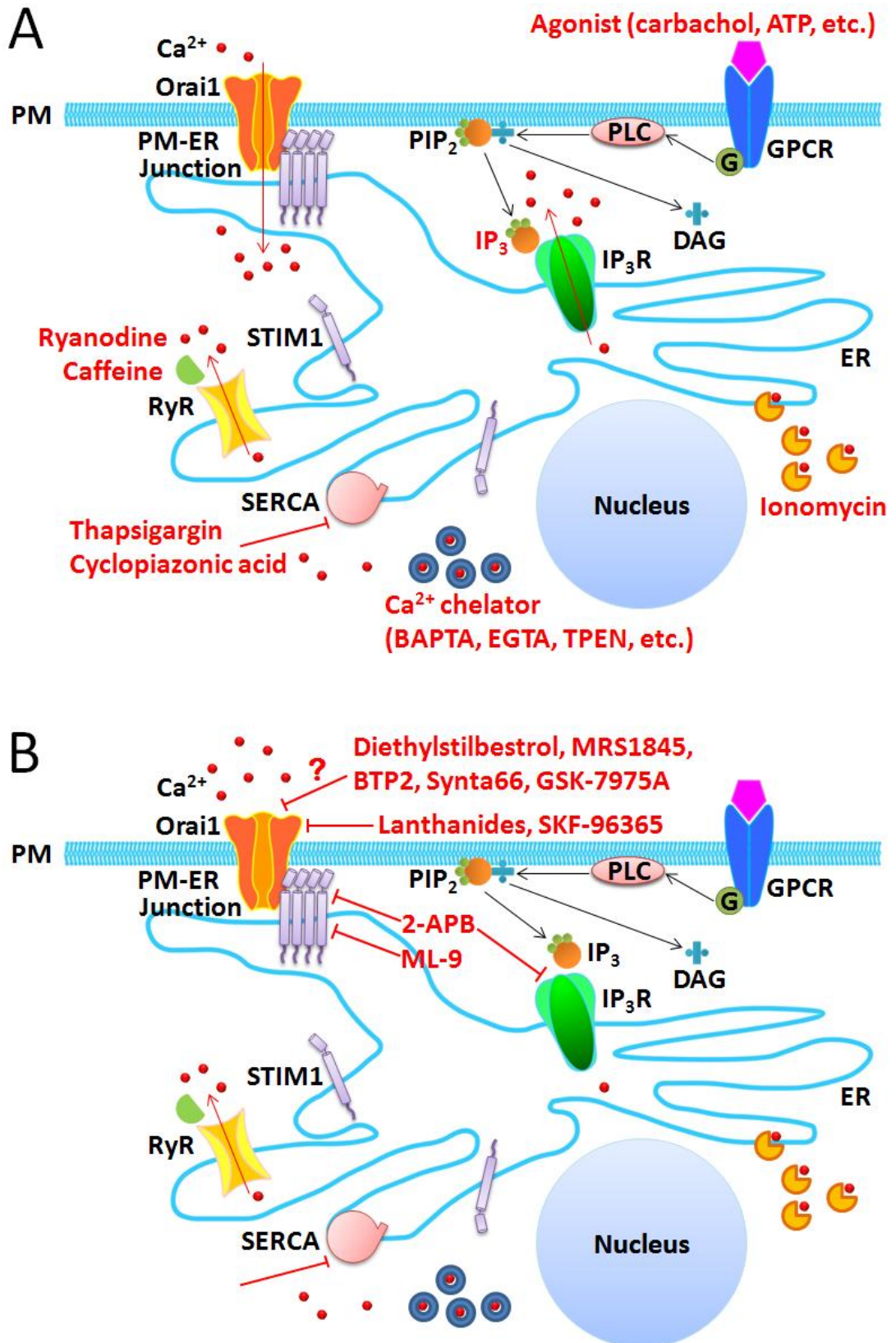
Fig. 1.2 Pharmacological mechanisms of chemical modulators of store-operated Ca^{2+} channels. (A) activators. (B) inhibitors. The question mark suggests that the mechanism is unclear.

1.8.2. Chemical inhibitors of store-operated Ca^{2+} channels

A number of small-molecule inhibitors of SOCs have been identified. Some of these chemicals, such as 2-aminoethyldiphenyl borate (2-APB) and ML-9, have inhibitory effect on the formation of STIM1 puncta at the plasma membrane, whilst others are most likely to block the pore-forming channels directly (Fig. 1.2B).

2-APB: 2-APB is generally considered an inhibitor of SOCs; however, it seems to directly facilitate Orai channels overexpressed in HEK293 cells. In cells coexpressing STIM1/Orai1 or STIM1/Orai2, an inward-rectifying current was developed immediately after the exposure to 10-100 µM 2-APB, and then the current was rapidly diminished (Peinelt *et al.*, 2008; DeHaven *et al.*, 2008). The transient potentiation of Orai1 and Orai2 by 2-APB relied on the pre-existence of STIM1/Orai complex induced by Ca^{2+} store depletion, suggesting that the conformation of Orai1 and Orai2 proteins determines their response to 2-APB (Peinelt *et al.*, 2008). 2-APB within the range 20-100 µM substantially activated Orai3 overexpressed alone or together with STIM1, without dependence on Ca^{2+} store depletion (Peinelt *et al.*, 2008; DeHaven *et al.*, 2008; Zhang *et al.*, 2008; Yamashita *et al.*, 2011). The 2-APB-induced Orai3 current showed both inward and outward rectification, which was attributed to the non-selective channel permeability to divalent and monovalent cations (DeHaven *et al.*, 2008; Zhang *et al.*, 2008). The inhibitory effect of 2-APB on global SOCE may be caused by, at least in part, its influence on STIM1. In cells overexpressing fluorescent protein-tagged STIM1, application of 50 and 100 µM 2-APB not only prevented the formation of STIM1 puncta after Ca^{2+} store depletion, but also disassembled STIM1 puncta already existed (Peinelt *et al.*, 2008; DeHaven *et al.*, 2008; Tamarina *et al.*, 2008). In addition to the complex actions on STIM1 and Orai channels, 2-APB at concentrations higher than 50 µM also inhibited IP_3Rs and TRPC channels (Maruyama *et al.*, 1997; Xu *et al.*, 2005a; Zagranichnaya *et al.*, 2005; Harteneck and Gollasch, 2011).

Lanthanides: La^{3+} was found to inhibit agonist-induced Ca^{2+} influx since the 1970s (Putney, 1976a; Putney, 1976b). Another lanthanide, Gd^{3+}, has been shown to potently suppress native and Orai-mediated CRAC currents with a lowest concentration of 50 nM (Zhang *et al.*, 2006; Yeromin *et al.*, 2006). La^{3+} and Gd^{3+} are also blockers of TRPC channels at micromolar or higher concentrations, with the

exception that TRPC4 and TRPC5 are potentiated within the range 10-100 μM (Jung *et al.*, 2003). Lanthanides are generally used in solutions without serum and multivalent anions, as these components may form metal-protein complex or insoluble salts (Putney, 2009).

Diethylstilbestrol: The synthetic oestrogen diethylstilbestrol has been reported to inhibit SOCs in human platelets, rat basophilic leukemia and vascular smooth muscle cells (Zakharov *et al.*, 2004). The inhibition on I_{CRAC} and SOCE was dose-dependent (IC_{50} within 0.1-1 μM) and reversible. Diethylstilbestrol was also found to reversibly block TRPC5 channel overexpressed in HEK293 cells with an IC_{50} around 10 μM (Naylor *et al.*, 2011). Apart from this, the effect of diethylstilbestrol has not been tested on exogenously expressed Orai and other TRPC channels.

ML-9: ML-9 is a myosin light chain kinase inhibitor. It was found to inhibit agonist-induced Ca^{2+} influx and SOCE in endothelial cells (Watanabe *et al.*, 1996) and monocytes/macrophages (Tran *et al.*, 2001), respectively. The effect of ML-9 on SOCs is considered to be independent of myosin light chain kinase, but related to STIM1. The action of ML-9 on STIM1 is similar to that of 2-APB. It blocked the formation of STIM1 puncta following Ca^{2+} store depletion, and also reversed the pre-existed puncta of a constitutively active STIM1 mutant (Smyth *et al.*, 2008). There is no report about the modulation of Orai or TRPC channels to date.

BTP2: BTP2 is another potent blocker of SOCs. It was originally identified as a most effective inhibitor of NFAT activation and T cell cytokine production among a number of pyrazole derivatives (Trevillyan *et al.*, 2001; Chen *et al.*, 2002). It was then found to inhibit SOCE with IC_{50} ranging from 10 to 300 nM in different cell types (Ishikawa *et al.*, 2003; Zitt *et al.*, 2004; He *et al.*, 2005). The activity of TRPC3 and TRPC5 channels overexpressed in HEK293 cells was also substantially blocked by BTP2, with the IC_{50} of 300 nM for the Ca^{2+} influx and 3 μM for the whole-cell currents (He *et al.*, 2005).

SKF-96365: SKF-96365 was firstly reported to inhibit receptor-mediated Ca^{2+} entry (Merritt *et al.*, 1990), and later found to be a general blocker of CRAC and TRPC channels (Boulay *et al.*, 1997; Hsu *et al.*, 2001; Kozak *et al.*, 2002; Ohana *et al.*, 2009). The IC_{50} of SKF-96365 on SOCE in different cell types is in the range of 1-3 μM (Liu *et al.*, 2011; McGahon *et al.*, 2012).

MRS1845: MRS1845 was screened out from a series of 1,4-dihydropyridines as the most potent and relatively selective compound to inhibit SOCE in leukemic HL-60 cells, with an IC_{50} of 1.7 μM (Harper *et al.*, 2003). The inhibitory effect of MRS1845 on SOCE was then confirmed by studies using human neutrophils, salamander photoreceptors and rat pituitary cells (Lee *et al.*, 2005a; Szikra *et al.*, 2008; Yamashita *et al.*, 2009).

Synta66 and GSK-7975A: A recent study has compared the potency of five SOC inhibitors in platelets, including 2-APB, SKF-96365 and MRS1845, and two new compounds, Synta66 and GSK-7975A (van Kruchten *et al.*, 2012). The potency of the five compounds on the inhibition of SOCE in platelets was ranked as Synta66>2-APB>GSK-7975A>SKF-96365>MRS1845, and the IC_{50} of Synta66 was ~0.6 μM (van Kruchten *et al.*, 2012). These results suggest that Synta66 may be a promising inhibitor of SOCs, with further studies required to illustrate its selectivity on Orai, TRPC and other channels.

1.9. Aims of this study

In this PhD project, I aimed to investigate the mechanisms underlying the activation and inhibition of SOCs by pharmacological and physiological modulators in HEK293 cells overexpressing STIM1, ORAI and TRP channels, and the pathological roles of TRPC channels in human ovarian cancer cells.

New discoveries on the following topics will be demonstrated:

(1) The pharmacological profile of STIM1, incluing the effects of ER and motichondrial Ca^{2+} store regulators, SOC inhibitors, signalling pathway blockers, and cytoskeleton depolymerising and stabilising agents.

(2) Identification of novel small-molecule inhibitors of STIM1/ORAI and TRPC channels, including 4-chloro-3-ethylphenol, 4-chloro-*m*-cresol and 4-chlorophenol.

(3) Activationof TRPC channels and inhibition of TRPM2 channel by Cu^{2+}.

(4) Function of TRPC channels in human ovarian cancer cells, including the roles of TRPCs in cell proliferation, colony growth and cell cycle progression.

Chapter 2

Materials and Methods

2.1. Materials

2.1.1. Chemicals

Sodium chloride (NaCl), potassium chloride (KCl), magnesium chloride ($MgCl_2$), calcium chloride ($CaCl_2$), sodium hydroxide (NaOH), hydrochloric acid (HCl), potassium phosphate monobasic (KH_2PO_4), sodium phosphate dibasic (Na_2HPO_4), ethylene glycol-bis(2-aminoethylether)-*N,N,N′,N′*-tetraacetic acid (EGTA), D-glucose, cesium chloride (CsCl), 4-(2-hydroxyethyl)-1-piperazineethanesulfonic acid (HEPES), 1,2-bis(2-aminophenoxy)ethane-*N,N,N′,N′*-tetraacetic acid (BAPTA), cesium-methanesulfonate (Cs-methanesulfonate), dimethyl sulfoxide (DMSO), thapsigargin (TG), 2-aminoethyldiphenyl borate (2-APB), SKF-96365, diethylstilbestrol (DES), colchicine, cytochalasin D (CytD), caffeine, 4-chloro-3-ethylphenol (4-CEP), 4-chloro-*m*-cresol (4-C*m*C), 4-chlorophenol (4-ClP), genistein, wortmannin, Y-27632 dihydrochloride, GF109203X, chelerythrine (CHE), 1-oleoyl-2-acetyl-sn-glycerol (OAG), U73122 hydrate, calyculin A (CalyA), flufenamic acid (FFA), niflumic acid (NFA), sodium azide, hydrogen peroxide (H_2O_2), carbonyl cyanide 4-(trifluoromethoxy)phenylhydrazone (FCCP), forskolin, adenosine 5′-diphosphoribose sodium salt (ADP-Ribose), copper sulphate ($CuSO_4$), gadolinium chloride ($GdCl_3$), mercury chloride ($HgCl_2$), Fura-PE3/AM, carbenoxolone, Triton X-100, propidium iodide and deoxyribonucleotide triphosphates (dNTPs) were purchased from Sigma-Aldrich (Poole, UK).

2.1.2. Cell culture materials

D-MEM/F-12 cell culture medium, trypsin-EDTA solution, penicillin and streptomycin were purchased from Invitrogen (Paisley, UK). Endothelial cell growth medium and supplements were purchased from PromoCell (Heidelberg, Germany). Fetal bovine serum (FBS), G418 disulfate salt, tetracycline, ampicillin, kanamycin, Luria broth (LB) and Luria agar (LA) media were purchased from Sigma-Aldrich (Poole, UK). Super optimal broth with glucose was purchased from Invitrogen (Paisley, UK). Cell culture dishes, flasks, pipettes, pipette tips and cryotubes were purchased from SARSTEDT (Leicester, UK). Glass coverslips were purchased from VWR International (Lutterworth, UK).

2.1.3. Enzymes, DNA ladders, nucleic acid extraction and purification kits

Phusion High-Fidelity DNA Polymerase was purchased from New England BioLabs (Hitchin, UK). M-MLV reverse transcriptase, ribonuclease (RNase) inhibitor, GoTaq Green PCR Master Mix, restriction endonucleases (HindIII, BamHI, XbaI, ApaI, EcoRI and BglII), T4 DNA ligase and 100 bp DNA ladder were purchased from Promega (Southampton, UK). RNase, TRIzol reagent and 1 kb Plus DNA ladder were purchased from Invitrogen (Paisley, UK). QIAprep Spin Miniprep Kit, QIAquick PCR Purification Kit and QIAquick Gel Extraction Kit were purchased from QIAGEN (Crawley, UK).

2.1.4. Plasmids, human cell lines and *E.coli* competent cells

The pEYFP-N1/STIM1 vector encoding STIM1 fused to the N-terminus of EYFP (STIM1-EYFP) was kindly provided by Prof. Alexei V. Tepikin at the University of Liverpool. The pIRES-TRPC1-GFP, pcDNA3-TRPC3 and pcDNA3-TRPC6 vectors were gifts from Prof. Craig Montell at the Johns Hopkins University. The pcDNA3-TRPC4 vector was from Prof. Mike X. Zhu at the University of Texas, Houston. The RFP-C1 and mCFP-C3 vectors were from Dr. Zhige Wu at the University of Dundee. The pIRES-EYFP vector was purchased from Clontech (Mountain View, California, USA). The pGEM-T vector was purchased from Promega (Southampton, UK). The pcDNA4/TO vector and T-REx HEK293 cell line were purchased from Invitrogen (Paisley, UK). TRPC5 and TRPM2 cell lines, in which the expression of exogenous genes is regulated by tetracycline, were generated by Dr. Shang-Zhong Xu and stored in the laboratory. Primary human aortic endothelial cells (HAECs) were purchased from PromoCell (Heidelberg, Germany). Human ovarian adenocarcinoma cells (SKOV3) were purchased from LGC Promochem (Middlesex, UK). The JM109 and DH5α *E. coli* competent cells were purchased from Promega (Southampton, UK) and Invitrogen (Paisley, UK), respectively.

Table 2.1 Primers used in gene cloning and plasmid construction

Primer name	Sequence (5'-3')
HindIII-GFP-F	TTTT<u>AAGCTT</u>CGCCACCATGGTGAGCAAGG
BamHI-GFP-R	TA<u>GGATCC</u>CTTGTACAGCTCGTCCATGC
TRPC1mut-F	GTTGCTCACAACAAGATTTCAATGGGACAGATGTTA
TRPC1mut-R	TCTGTCCCATTGAAATCTTGTTGTGAGCAACCACTTTG
TRPC1S-F	GATGTGCTTGGGAGAAATGC
TRPC1E1-F	GGGAGGTGAAGGAGGAGAAT
TRPC1E13-R	TGCACTAGGCAGCACATCA
TRPC1E4E5-R	CAAGACGAAACCTGGAATGC
TRPC1E8E11-F	TGGTATGAAGGGTTGGAAGAC
TRPC1E8E11-R	AATGACAGCTCCCACAAAGG
XbaI-TRPC1-F	ATA<u>TCTAGA</u>GATGATGGCGGCCCTGTACC
ApaI-TRPC1-R	GT<u>GGGCCC</u>TTAATTTCTTGGATAAAACATAGC
TRPC4E6E11-F	CGAAAGGGTTAACCTGCAAA
TRPC4E7E9-F	CAATGTCATCTCTCTGGTTGTTC
TRPC4E12-R	CCTGTAACCCCAGTGTGTCC
TRPC4E-R	ATGCTGTGTTCTTACCCCT
TRPC4-E542Q-E543Q-F	ATTGTACTTCTATTATCAACAAACGAAAGGGTTAACCTGC
TRPC4-E542Q-E543Q-R	CCCTTTCGTTTGTTGATAATAGAAGTACAATTGATTTAGG
TRPC4-C555W-F	CCTGCAAAGGCATAAGATGGGAAAAGCAGAATAATGCATTTTCAACG
TRPC4-C555-R	CATCTTATGCCTTTGCAGGTTAACCCTTTCGTTTCTTC
TRPC4-T549-R	TTAACCCTTTCGTTTCTTCATAATAGAAGTACAATTGATTTAGGC
TRPC4-E556Q-F	CCTGCAAAGGCATAAGATGTCAAAAGCAGAATAATGCATTTTCAACG
TRPC4-K557E-F	CCTGCAAAGGCATAAGATGTGAAGAGCAGAATAATGCATTTTCAACG

Table 2.1 Primers used in gene cloning and plasmid construction (continue)

BamHI-TRPC3-F	TA<u>GGATCC</u>ATGGAGGGAAGCCCATCCCTGAG
EcoRI-TRPC3-R	GC<u>GAATTC</u>CAGGTTGCTGCATCATTCACATCTC
BamHI-TRPC6-F	AA<u>GGATCC</u>ATGAGCCAGAGCCCGGCGTTC
EcoRI-TRPC6-R	CG<u>GAATTC</u>GCATTATCTATTGGTTTCCTCTTG
TRPC3E3E5-F	TGGAGATCTGGAATCAGCAG
TRPC3E3E5-R	GAGGCATTGAACACAAGCAG
TRPC6E8E12-F	TACGATGGTCATTGTTTTGC
TRPC6E8E12-R	TCTGGGCCTGCAGTACATATC
BglII-ORAI1-F	AAT<u>AGATCT</u>GCGGCGTGCTCCATGCATCC
EcoRI-ORAI1-R	ATG<u>AATTC</u>GGGCCTAGGCATAGTGGCTG
BglII-ORAI2-F	AGT<u>AGATCT</u>CCCACCATGAGTGCTGAGCTT
EcoRI-ORAI2-R	TA<u>GAATTC</u>CCTCACAAGACCTGCAGGCT
BamHI-ORAI3-F	TA<u>GGATCC</u>AGGATGAAGGGCGGCGAG
EcoRI-ORAI3-R	TAT<u>GAATTC</u>TCACACAGCCTGCAGCTCC
ORAI1-F	AGGTGATGAGCCTCAACGAG
ORAI1-R	CTGATCATGAGCGCAAACAG
ORAI2-F	CATAAGGGCATGGATTACCG
ORAI2-R	CGGGTACTGGTACTGCGTCT
ORAI3-F	GGCTACCTGGACCTCATGG
ORAI3-R	GGTGGGTACTCGTGGTCACT
Lifeact-GFP-F	<u>ATTCGAAAGCATCTCAAAGGAAGAA</u>GTGAGCAAGGGCGAGGAGCTGTTC
Lifeact-Kozak-R	<u>TTCTTGATCAAATCTGCGACACC</u>CATGGTGGCGAAGCTTAAGTTTAAACG
Lifeact-G	<u>GGTGTCGCAGATTTGATCAAGAAATTCGAAAGCATCTCAAAGGAAGAA</u>G

The underlined sequences indicate recognition sites of restriction endonucleases or the Lifeact-coding sequence.

Table 2.2 Primers used in the detection of TRPC variants in SKOV3 cells

Primer pair	Forward primer (5'-3')	Reverse primer (5'-3')
TRPC1-P1	GATGTGCTTGGGAGAAATGC	CAAGACGAAACCTGGAATGC
TRPC1-P2	TGCACCTGTCATTTTAGCTG	CAAGACGAAACCTGGAATGC
TRPC1-P3	TGGTATGAAGGGTTGGAAGAC	GGTATCATTGCTTTGCTGTTC
TRPC1-P4	TGGTATGAAGGGTTGGAAGAC	AATGACAGCTCCCACAAAGG
TRPC1-P5	TGCTTACCAAACTGCTGGTG	AACTGTTTTGCCGTTTGACC
TRPC3-P0	AACAAGCAAGGGTGACCTTC	GAGGCATTGAACACAAGCAG
TRPC3-P1	AAGGGTGCCAGGATCGAG	GAGGCATTGAACACAAGCAG
TRPC3-P2	TGGAGATCTGGAATCAGCAG	GAGGCATTGAACACAAGCAG
TRPC3-P3	CTGGGTCTGCTTGTGTTCAA	ATGGACAGCATCCCAAAGTC
TRPC3-P4	TGACTTCCGTTGTGCTCAAATATG	CCTTCTGAAGTCTTCTCCTTCTGC
TRPC4-P1	CTCCAGCTTCGATCGTTTTC	TCTGAACTGGACACGCATTC
TRPC4-P2	CTCGGATCCCATCACTTCAG	TCCCATGATTCTCGTGGATT
TRPC4-P3	CGAAAGGGTTAACCTGCAAA	CAGGACTTCAAAGCGGAAAC
TRPC4-P4	GGATCAGACGAGAAGTTCCAG	TAGTCCTGAAGTCCGCCATC
TRPC4-P5	TCTGCAGATATCTCTGGGAAGGATGC	AAGCTTTGTTCGAGCAAATTTCCATTC
TRPC4-P6	CAATGTCATCTCTCTGGTTGTTC	TGGTATTGGTGATGTCTTCTCAAG
TRPC4-P7	CAATGTCATCTCTCTGGTTGTTC	CCTGTAACCCCAGTGTGTCC
TRPC4-ε	CAATGTCATCTCTCTGGTTGTTC	ATGCTGTGTTCTTACCCCT
TRPC5	TGAGAACGAGAACCTGGAG	TACTCGGCCTTGAACTCATTC
TRPC6-P1	GCCTTGCTACGGCTACTACC	TCCCAGAAAAATGGTGAAGG
TRPC6-P2	AGTTTTAAGACACTGTTCTGG	TTCTGATATTGTCTTGGAGG
TRPC6-P3	TACGATGGTCATTGTTTTGC	TCTGGGCCTGCAGTACATATC
TRPC7	ATCTTCGTGGCCTCCTTCAC	AACGCTGGGTTGTATTTGGC

Table 2.3 Small interfere RNA (siRNA) used in this study

siRNA name	Sequence (5'-3')
si-TRPC1	GCCCGGAAUUCUCGUGAAU[dT][dT]
si-TRPC1_as	AUUCACGAGAAUUCCGGGC[dT][dT]
si-TRPC4	UGCUCCCUAUAGAGACCGC[dT][dT]
si-TRPC4_as	GCGGUCUCUAUAGGGAGCA[dT][dT]
si-TRPC5	GCAACCUUGGGCUGUUCAU[dT][dT]
si-TRPC5_as	AUGAACAGCCCAAGGUUGC[dT][dT]
si-TRPC6	GCAUGACUCGUUUAGCCAC[dT][dT]
si-TRPC6_as	GUGGCUAAACGAGUCAUGC[dT][dT]

The TRPC3, Bcl-2 and scramble siRNA used in this study were commercial products and the sequences are not available.

2.1.5. Oligonucleotides and antibodies

PCR primers (Table 2.1 and 2.2) and custom small interfere RNA (siRNA) (Table 2.3) were ordered from Sigma-Aldrich (Poole, UK). The TRPC3 siRNA was purchased from Santa Cruz Biotechnology (Santa Cruz, USA). The Bcl-2 and scramble siRNA were purchased from Upstate Biotechnology (New York, USA). Oligo d(T) and random primers were purchased from Promega (Southampton, UK). Rabbit polyclonal anti-TRPC antibodies against the extracellular third loop (E3) region near the channel pores or targeting to C-termini were generated and the specificities were verified in previous studies (Xu *et al.*, 2005b; Xu *et al.*, 2006b).

2.2 Methods

2.2.1. Gene cloning and plasmid construction

2.2.1.1. Identification of novel TRPC1 and TRPC4 spliced variants in human aortic endothelial cells

Human aortic endothelial cells (HAECs) were cultured in endothelial growth medium with supplements and 10% FBS, and maintained at 37 °C in a humidified atmosphere with 95% air and 5% CO_2. Total RNA was extracted from HAECs using TRIzol reagent according to the manufacture's instruction. The mRNA was reverse-

transcribed to cDNA using M-MLV reserve transcriptase and oligo d(T) primers. TRPC1 and TRPC4 fragments were amplified from the cDNA with different primer pairs using GoTaq Green Master Mix. The PCR mixture contained 1 µl cDNA (~200 ng), 0.5 µM forward primers, 0.5 µM reverse primers, and 1× GoTaq Green Master Mix. The PCR conditions were an initial denaturation at 95 ^{o}C for 30 s, 35 cycles of 94 ^{o}C for 30 s, 57 ^{o}C for 30 s and 72 ^{o}C for 1 min, and a final extension at 72 ^{o}C for 5 min. PCR products were analysed by electrophoreses on 1.5% agarose gel containing 0.5 µg/ml ethidium bromide. Positive bands were cut from the gel under UV light and purified with a QIAquick Gel Extraction Kit. The purified TRPC1 fragments were directly sent to Eurofins MWG Operon (London, UK) for sequencing. The purified TRPC4 fragments were ligated into pGEM-T vectors using T4 DNA ligase at room temperature for 4 h. The ligation mixtures were gently mixed JM109 *E. coli* competent cells, placed on ice for 30 min, heat-shocked at 42 ^{o}C for 1 min, transferred into super optimal broth with glucose and cultured at 37 ^{o}C for 1 h in a shaking incubator (300 rpm). The cells were then spread on LB agar plates containing 100 µg/ml ampicillin and incubated at 37 ^{o}C overnight. On the next day the bacterial colonies were picked into LB medium and cultured at 37 ^{o}C for 2 h. Positive colonies were characterised by PCR using cell suspensions as templates. The PCR mixture contained 1 µl cell suspension, 0.5 µM forward primers, 0.5 µM reverse primers, and 1× GoTaq Green Master Mix. The PCR conditions were an initial denaturation at 95 ^{o}C for 30 s, 30 cycles of 94 ^{o}C for 30 s, 57 ^{o}C for 30 s and 72 ^{o}C for 1 min, and a final extension at 72 ^{o}C for 3 min. The colonies showing a positive band in the PCR products were inoculated into 5 ml LB medium containing 100 µg/ml ampicillin and cultured at 37 ^{o}C overnight in a shaking incubator (200 rpm). The plasmids were extracted using a QIAprep Spin Miniprep Kit and sent for sequencing. The sequences were aligned with MEGA 4 software (Tamura *et al.*, 2007) to find out insertions and deletions.

2.2.1.2. Cloning of fluorescent protein genes into pcDNA4/TO vectors

The coding sequences of enhanced yellow fluorescent protein (EYFP), monomeric red fluorescent protein (mCherry) and monomeric cyan fluorescent protein (mCFP) were amplified with the primers HindIII-GFP-F and BamHI-GFP-R from the vectors pIRES-EYFP, RFP-C1 and mCFP-C3, respectively. The PCR mixture contained 1× Phusion HF Buffer, 200 µM dNTPs (50 µM each), 0.5 µM forward primers, 0.5 µM

reverse primers, 40 pg/µl template DNA, and 0.02 units/µl Phusion High-Fidelity DNA Polymerase. The PCR conditions were an initial denaturation at 98 ^{o}C for 30 s, 35 cycles of 98 ^{o}C for 10 s and 72 ^{o}C for 1 min, and a final extension at 72 ^{o}C for 5 min. PCR products were analysed by electrophoreses on 1.5% agarose gel containing 0.5 µg/ml ethidium bromide and successful amplifications were characterised by a band of 733 bp under UV light. The PCR products were purified with a QIAquick PCR Purification Kit. The purified PCR products and pcDNA4/TO plasmids were digested with HindIII and BamHI restriction endonucleases at 37 ^{o}C overnight. The digested PCR products and plasmids were electrophoresed on 1% agarose gel and then the gel slices containing the DNA bands were cut out under UV light. The DNA fragments in the gel slices were purified with a QIAquick Gel Extraction Kit. The EYFP, mCherry and mCFP-encoding DNA fragments were ligated into digested pcDNA4/TO plasmids and transformed into JM109 *E. coli* competent cells. Positive colonies were characterised by PCR using cell suspensions as templates. The PCR mixture contained 1 µl cell suspension, 0.5 µM HindIII-GFP-F and BamHI-GFP-R primers, and 1× GoTaq Green Master Mix. The PCR conditions were an initial denaturation at 95 ^{o}C for 30 s, 30 cycles of 94 ^{o}C for 30 s, 65 ^{o}C for 30 s and 72 ^{o}C for 45 s, and a final extension at 72 ^{o}C for 5 min. The colonies showing a 733-bp band in the PCR products were inoculated into 5 ml LB medium containing 100 µg/ml ampicillin and cultured at 37 ^{o}C overnight in a shaking incubator (200 rpm). The plasmids were extracted using a QIAprep Spin Miniprep Kit. Small amount of cell suspensions were mixed into LB medium containing 20% glycerol and stored in a -80 ^{o}C freezer. The three constructs generated in this section were named pcDNA4/TO-EYFP, pcDNA4/TO-mCherry and pcDNA4/TO-mCFP.

2.2.1.3. Cloning of TRPC1and TRPC1δ into pcDNA4/TO-mCFP vectors

TRPC1δ is a newly identified isoform with exon 9 deletion compared to the longer isoform of TRPC1 (NM_003304) (see result in Chapter 2). The complete coding sequence of TRPC1δ was produced by PCR mutagenesis from pIRES-TRPC1-GFP vector. Primers TRPC1mut-F and TRPC1mut-R were designed to anneal with the 5' end of exon 10 and 3' end of exon 8, respectively. Each primer has an overhang sequence at the 5' end complementary to each other so that they can bind to each other and skip the exon 9 during PCR. As direct amplification of TRPC1 plasmid

with TRPC1mut-F and TRPC1mut-R failed, a multistep mutagenesis method was used to delete exon 9 from the full-length TRPC1 gene as following steps:

(1) Amplification of exon1-8 with primers TRPC1E1-F and TRPC1mut-R (1239 bp);

(2) Amplification of exon10-13 with primers TRPC1mut-F and TRPC1E13-R (654 bp);

(3) Overlapping amplification of exon1-13 (1861 bp, without exon 9) with primers TRPC1E1-F and TRPC1E13-R, using products from Step 1 and 2 as template;

(4) Amplification of the backbone of the TRPC1 plasmid with primers TRPC1mut-F and TRPC1E4E5-R (~6 kb);

(5) Hybridisation of DNA fragments from Step 3 and 4, the single-stranded gaps were repaired by DNA polymerase in a routine PCR;

(6) Transformation of product from Step 5 into JM109 *E. coli* competent cells, characterisation of positive colonies (with exon 9 deleted) by PCR with primers TRPC1E8E11-F and TRPC1E8E11-R (405 bp for TRPC1δ);

(7) Extraction of pIRES-TRPC1δ-GFP plasmids from positive clones and sequencing.

Phusion High-Fidelity DNA Polymerase was used in Step 1-5, and GoTaq Green Master Mix was used in Step 6.

The coding sequences of TRPC1 and TRPC1δ were amplified with the primers XbaI-TRPC1-F and ApaI-TRPC1-R from the vectors pIRES-TRPC1-GFP and pIRES-TRPC1δ-GFP, respectively. The PCR mixtures contained 1× Phusion HF Buffer, 400 μM dNTPs (100 μM each), 0.5 μM each primer, 40 pg/μl template DNA, and 0.02 units/μl Phusion High-Fidelity DNA Polymerase. The PCR conditions were an initial denaturation at 98 °C for 30 s, 35 cycles of 98 °C for 10 s, 60 °C for 30 s and 72 °C for 2 min, and a final extension at 72 °C for 7 min. The expected product sizes for TRPC1 and TRPC1δ were 2298 bp and 2154 bp, respectively. The PCR products were purified, digested with XbaI and ApaI, ligated into pcDNA4/TO-mCFP vector, and transformed into JM109 *E. coli* competent cells. Positive colonies were screened by PCR with primers TRPC1E8E11-F and TRPC1E8E11-R (549 bp for TRPC1, 405 bp for TRPC1δ) using GoTaq Green

Master Mix. The PCR conditions were an initial denaturation at 95 ^{o}C for 30 s, 30 cycles of 94 ^{o}C for 30 s, 57 ^{o}C for 30 s and 72 ^{o}C for 30 s, and a final extension at 72 ^{o}C for 3 min. Plasmids pcDNA4/TO-mCFP-TRPC1 and pcDNA4/TO-mCFP-TRPC1δ were extracted from positive clones and the vector structures were confirmed by sequencing.

2.2.1.4. Constructs for fluorescent protein-tagged TRPC4 and TRPC4 mutants in pcDNA4/TO vectors

The constructs pcDNA4/TO-mCFP-TRPC4α, pcDNA4/TO-EYFP-TRPC4α, pcDNA4/TO-EYFP-TRPC4β1, pcDNA4/TO-EYFP-TRPC4ε1, pcDNA4/TO-EYFP-TRPC4α-E542Q/E543Q, pcDNA4/TO-EYFP-TRPC4α-C555W, pcDNA4/TO-EYFP-TRPC4α-E556Q and pcDNA4/TO-EYFP-TRPC4α-K557E were generated in this section. Full-length TRPC4α coding sequence (NM_016179) was cut from pcDNA3-TRPC4 vector by BglII and ApaI, and ligated into pcDNA4/TO-mCFP and pcDNA4/TO-EYFP plasmids digested with BamHI and ApaI. The ligation products were transformed into JM109 *E. coli* competent cells. Positive colonies were screened by PCR with primers TRPC4E7E9-F and TRPC4E12-R (956 bp) using GoTaq Green Master Mix. The PCR conditions were an initial denaturation at 95 ^{o}C for 30 s, 30 cycles of 94 ^{o}C for 30 s, 57 ^{o}C for 30 s and 72 ^{o}C for 1 min, and a final extension at 72 ^{o}C for 5 min. Successful cloning was confirmed by sequencing.

TRPC4β1 and TRPC4ε1 are two new TRPC4 isoforms identified from HAECs in this study (see result in Chapter 2). TRPC4β1 has a deletion of 255 bp in exon 11 compared to TRPC4α, whilst TRPC4ε1 has a 15-bp longer exon 8 and also the 255-bp deletion in exon 11. To make the full-length coding sequences of TRPC4β1 and TRPC4ε1, the DNA fragment including exon 8-12 was cut off from pcDNA4/TO-EYFP-TRPC4α plasmid and replaced by corresponding parts in TRPC4β1 and TRPC4ε1. Firstly, partial sequences of all TRPC4 isoforms were amplified from cDNA of human aortic endothelial cells with primers TRPC4E6E11-F and TRPC4E12-R. The expected product sizes for TRPC4α/β1/ε1 were 1137/882/897 bp, respectively. The PCR mixture contained 1× Phusion HF Buffer, 200 μM dNTPs (50 μM each), 0.5 μM each primer, 10 ng/μl cDNA, and 0.02 units/μl Phusion High-Fidelity DNA Polymerase. The PCR conditions were an initial denaturation at 98 ^{o}C for 30 s, 35 cycles of 98 ^{o}C for 10 s, 64 ^{o}C for 30 s and 72 ^{o}C for 30 s, and a final extension at 72 ^{o}C for 3 min. The PCR products were purified and digested with

KpnI (recognition site in exon 8) and XhoI (in exon 12). After digestion, the DNA fragments were separated by electrophoresis in 1.5% agarose gel. The exon 8-12 fragments for TRPC4β1 (405 bp) and TRPC4ε1 (420 bp) were harvested from the gel, whilst the TRPC4α exon 8-12 fragment (660 bp) and other two flanking fragments (374 and 103 bp) were discarded. The pcDNA4/TO-EYFP-TRPC4α plasmids were also digested by KpnI and XhoI, and the linear plasmids without exon 8-12 (~8 kb) were purified from the gel. The TRPC4β1 and TRPC4ε1 fragments were then ligated into the linear plasmids without exon 8-12 and transformed into JM109 *E. coli* competent cells. Positive colonies were screened by PCR using GoTaq Green Master Mix. As the products of TRPC4β1 and TRPC4ε1 generated by primers TRPC4E7E9-F and TRPC4E12-R were difficult to be separated in the gel (701 bp for TRPC4β1, 716 bp for TRPC4ε1), another primer TRPC4E-R was used in pair with TRPC4E7E9-F, which produce a 283-bp fragment from TRPC4ε1, but have no amplification from TRPC4β1. The PCR conditions were an initial denaturation at 95 ^{o}C for 30 s, 30 cycles of 94 ^{o}C for 30 s, 56 ^{o}C for 30 s and 72 ^{o}C for 45 s, and a final extension at 72 ^{o}C for 3 min. Successful cloning was confirmed by sequencing.

Point mutations in the pore-forming region of TRPC4 were introduced by PCR mutagenesis using pcDNA4/TO-EYFP-TRPC4α plasmid as template. The E542Q/E543Q mutant was generated by PCR amplification with overlapping primers TRPC4-E542Q-E543Q-F and TRPC4-E542Q-E543Q-R. The C555W mutant was generated by overlapping primers TRPC4-C555W-F, TRPC4-C555-R and TRPC4-T549-R. The E556Q mutant was generated by overlapping primers TRPC4-E556Q-F, TRPC4-C555-R and TRPC4-T549-R. The K557E mutant was generated by overlapping primers TRPC4-K557E-F, TRPC4-C555-R and TRPC4-T549-R. The expected product size for all mutant plasmids was ~8.8 kb. The PCR mixtures contained 1× Phusion GC Buffer, 800 μM dNTPs (200 μM each), 0.5 μM each primer, 40 pg/μl template DNA, and 0.02 units/μl Phusion High-Fidelity DNA Polymerase. The PCR conditions were an initial denaturation at 98 ^{o}C for 30 s, 35 cycles of 98 ^{o}C for 10 s and 72 ^{o}C for 4 min, and a final extension at 72 ^{o}C for 10 min. The PCR products were directly transformed into DH5α *E. coli* competent cells. Colonies were cultured and the extracted plasmids were sequenced to confirm the successful introduction of point mutations in the gene.

2.2.1.5. Constructs for fluorescent protein-tagged TRPC3 and TRPC6 in pcDNA4/TO vectors

Full-length TRPC3 coding sequence (U47050) was amplified with the primers BamHI-TRPC3-F and EcoRI-TRPC3-R from the vector pcDNA3-TRPC3. TRPC6 (BC093660) was amplified with the primers BamHI-TRPC6-F and EcoRI-TRPC6-R from the vector pcDNA3-TRPC6. The PCR mixtures contained 1× Phusion HF Buffer, 400 µM dNTPs (100 µM each), 0.5 µM each primer, 40 pg/µl template DNA, and 0.02 units/µl Phusion High-Fidelity DNA Polymerase. The PCR conditions were an initial denaturation at 98 ^{o}C for 30 s, 35 cycles of 98 ^{o}C for 10 s, 70 ^{o}C for 30 s and 72 ^{o}C for 1.5 min, and a final extension at 72 ^{o}C for 7 min. The expected product sizes were 2575 bp and 2815 bp for TRPC3 and TRPC6, respectively. The PCR products were purified, digested with BamHI and EcoRI, ligated into pcDNA4/TO-mCherry and pcDNA4/TO-mCFP vectors, and transformed into DH5α *E. coli* competent cells. Positive colonies were screened by PCR with primers TRPC3E3E5-F and TRPC3E3E5-R (351 bp), and TRPC6E8E12-F and TRPC6E8E12-R (476 bp), using GoTaq Green Master Mix. The PCR conditions were an initial denaturation at 95 ^{o}C for 30 s, 30 cycles of 94 ^{o}C for 30 s, 56 ^{o}C for 30 s and 72 ^{o}C for 30 s, and a final extension at 72 ^{o}C for 3 min. Plasmids from positive clones were further confirmed by sequencing. The constructs generated in this section were named pcDNA4/TO-mCherry-TRPC3 and pcDNA4/TO-mCFP-TRPC6.

2.2.1.6. Constructs for fluorescent protein-tagged ORAIs in pcDNA4/TO vectors

The constructs pcDNA4/TO-mCherry-ORAI1, pcDNA4/TO-mCFP-ORAI1, pcDNA4/TO-mCherry-ORAI2, pcDNA4/TO-mCFP-ORAI2 and pcDNA4/TO-mCFP-ORAI3 were generated in this section. Full-length ORAI1, ORAI2 and ORAI3 coding regions were amplified from cDNA of HAECs. The paired primers BglII-ORAI1-F and EcoRI-ORAI1-R, BglII-ORAI2-F and EcoRI-ORAI2-R, and BamHI-ORAI3-F and EcoRI-ORAI3-R were used. The expected product sizes for ORAI1, ORAI2 and ORAI3 were 939 bp, 790 bp and 902 bp, respectively. The PCR mixture contained 1× Phusion HF Buffer, 200 µM dNTPs (50 µM each), 0.5 µM each primer, 10 ng/µl cDNA, and 0.02 units/µl Phusion High-Fidelity DNA Polymerase. The PCR conditions were an initial denaturation at 98 ^{o}C for 30 s, 35 cycles of 98 ^{o}C for 10 s, 68 ^{o}C for 30 s and 72 ^{o}C for 1 min, and a final extension at

72 ^{o}C for 5 min. PCR products were purified from the gel after electrophoresis using a QIAquick Gel Extraction Kit. ORAI1 and ORAI2 were digested with BglII and EcoRI, and cloned into pcDNA4/TO-mCherry and pcDNA4/TO-mCFP vectors cut by BamHI and EcoRI. ORAI3 was digested with BamHI and EcoRI, and ligated into pcDNA4/TO-mCFP vector in a same way. The ligation products were transformed into DH5α *E. coli* competent cells and positive colonies were screened by PCR with paired primers ORAI1-F/R (238 bp), ORAI2-F/R (210 bp) and ORAI3-F/R (176 bp) using GoTaq Green Master Mix. The PCR conditions were an initial denaturation at 95 ^{o}C for 30 s, 30 cycles of 94 ^{o}C for 30 s, 56 ^{o}C for 30 s and 72 ^{o}C for 20 s, and a final extension at 72 ^{o}C for 3 min. Plasmids extracted from positive clones were sent for sequencing to confirm the successful cloning of the three ORAI genes.

2.2.1.7. pcDNA4/TO-Lifeact-mCFP

The Lifeact peptide is the first 17 amino acids at the N-terminus of the yeast protein Abp140, which binds to filamentous actin (F-actin) in eukaryotic cells (Riedl *et al.*, 2008). The Lifeact-encoding sequence was introduced into pcDNA4/TO-mCFP vector by PCR mutagenesis to create a Lifeact-mCFP fused gene. Three overlapping primers Lifeact-GFP-F, Lifeact-Kozak-R and Lifeact-G were used and the expected product size for the whole plasmid was ~5.8 kb. The PCR mixture contained 1× Phusion HF Buffer, 600 μM dNTPs (150 μM each), 0.5 μM each primer, 40 pg/μl template DNA, and 0.02 units/μl Phusion High-Fidelity DNA Polymerase. The PCR conditions were an initial denaturation at 98 ^{o}C for 30 s, 35 cycles of 98 ^{o}C for 10 s, and 72 ^{o}C for 3 min, and a final extension at 72 ^{o}C for 7 min. The PCR product was directly transformed into DH5α *E. coli* competent cells. Positive colonies were characterised by PCR with primers Lifeact-G and BamHI-GFP-R (761 bp) using GoTaq Green Master Mix. The PCR conditions were an initial denaturation at 95 ^{o}C for 30 s, 30 cycles of 94 ^{o}C for 30 s, 65 ^{o}C for 30 s and 72 ^{o}C for 45 s, and a final extension at 72 ^{o}C for 3 min. Plasmids were extracted from positive clones.

2.2.2. Generation of stably transfected cell lines

2.2.2.1. STIM1 cell line

T-REx HEK293 cells were cultured in D-MEM/F-12 medium supplemented with 10% FBS, 100 units/ml penicillin and 100 mg/ml streptomycin, and maintained at

37 °C in a humidified atmosphere with 95% air and 5% CO_2. The cells were seeded in a 35-mm culture dish and grown for 24 h to reach 90% confluency. STIM1-EYFP plasmids (3 µg) and 5 µl Lipofectamine 2000 transfection reagent (Invitrogen, paisley, UK) were separately mixed with 250 µl Opti-MEM I Reduced Serum Medium (Invitrogen, Paisley, UK), and kept at room temperature for 5 min. The two mixtures were merged into one tube, shaken vigorously and then incubated at room temperature for 20 min. During incubation, the DMEM/F-12 medium was removed from the cell culture dish and replaced by 1 ml Opti-MEM medium. Then the plasmid-Lipofectamine mixture was gently dropped into the dish. The dish was rocked for several times and moved into the incubator. The Opti-MEM medium was changed back to DMEM/F-12 medium 6 h later. On the next day (~24 h after transfection), G418 was added into the cell culture dish to a final concentration of 400 µg/ml. The cells were maintained for 1 week under G418 selection and the medium was changed on the 2nd, 3rd, 4th and 6th days to remove dead cells. The survived cells were trypsinized and seeded into 60-mm culture dishes at a density of 500 cells/dish. Cells were cultured in medium without G418 and grew into clumps after 5-7 days. After inspecting STIM1-EYFP expression under a Nikon Eclipse Ti-E inverted fluorescence microscope, cell clumps showing EYFP fluorescence (excitation/emission wavelengths of 500/535 nm) were manually picked out from the dishes by 200-µl tips on a pipetman. These cells (in ~20 µl medium) were carefully transferred into 50 µl 0.05% trypsin/EDTA solution and kept at room temperature for 3 min. Then the cells were mixed into DMEM/F-12 medium and cultured as usual. The cells were stored in medium containing 10% DMSO in liquid nitrogen when it is necessary.

2.2.2.2. TRPC1, TRPC4, TRPC3, TRPC6, ORAI1, ORAI2 and ORAI3 cell lines

The tetracycline-regulated gene expression cell lines including TO-mCFP-TRPC1, TO-mCFP-TRPC1δ, TO-EYFP-TRPC4α, TO-EYFP-TRPC4β1, TO-EYFP-TRPC4ε1, TO-EYFP-TRPC4α-E542Q/E543Q, TO-EYFP-TRPC4α-C555W, TO-EYFP-TRPC4α-E556Q, TO-EYFP-TRPC4α-K557E, TO-mCherry-TRPC3, TO-mCFP-TRPC6, TO-mCherry-ORAI1, TO-mCherry-ORAI2 and TO-mCFP-ORAI3 were generated by transfecting corresponding plasmids into T-REx HEK293 cells. For each transfection, 3 µg plasmids and 5 µl Lipofectamine were mixed in Opti-MEM medium and incubated with the cells for 6 h. The cells were trypsinized and seeded into 60-mm culture dishes at a density of 500 cells/dish 24 h after

transfection. After 5-7 days of culture with 1 μg/ml tetracycline in the DMEM/F-12 medium, the cell clumps showing mCFP, EYFP or mCherry fluorescence under microscope were picked out and cultured as usual. The excitation/emission wavelengths for mCFP and mCherry were 440/480 and 540/590 nm, respectively.

2.2.2.3. STIM1/TRPC1, STIM1/ORAI1, STIM1/ORAI2 and STIM1/ORAI3 cell lines

The STIM1-EYFP plasmids were transfected into TO-mCFP-TRPC1, TO-mCherry-ORAI1, TO-mCherry-ORAI2 and TO-mCFP-ORAI3 cells to generate STIM1-EYFP/TO-mCFP-TRPC1, STIM1-EYFP/TO-mCherry-ORAI1, STIM1-EYFP/TO-mCherry-ORAI2 and STIM1-EYFP/TO-mCFP-ORAI3 cell lines, in which the expression of STIM1 is stable and the expression of ORAI genes is regulated by tetracycline. The transfection and selection procedures were similar to that used in the generation of STIM1 cell line (Section 2.2.2.1).

2.2.2.4. STIM1/TRPC4 and STIM1/TRPC6 cell lines

The pcDNA4/TO-mCFP-TRPC4α and pcDNA4/TO-mCFP-TRPC6 plasmids were transfected into STIM1 cells to generate STIM1-EYFP/TO-mCFP-TRPC4α and STIM1-EYFP/TO-mCFP-TRPC6 cell lines. The transfection and selection procedures were similar to that described in Section 2.2.2.2.

2.2.3. Live-cell imaging and Ca^{2+} measurement

The cells were seeded on 13-mm glass coverslips and cultured for 24-48 h. Live-cell images for mCFP, EYFP and mCherry fluorescence were captured using the microscope equipped with a Nikon Plan Fluor 100×/1.30 oil objective (Nikon, Tokyo, Japan) and a CCD camera (ORCA-R2, Hamamatsu, Japan). The images were analysed with NIS-Elements 3.2 software (Nikon, Tokyo, Japan). For intracellular Ca^{2+} measurement, STIM1/ORAI1 cells were loaded with 2 μM Fura-PE3/AM in standard bath solution for 30 min at 37°C, followed by 5 min wash in Ca^{2+}-free solution at room temperature. Cells were excited alternately by 340 and 380 nm light and emission was collected via a 510-nm filter. Images were sampled every 5 s in pairs for the two excitation wavelengths. The ratio of 340/380 nm fluorescence was used to represent the intracellular Ca^{2+} level. The standard bath solution contained (mM): NaCl 130, KCl 5, $MgCl_2$ 1.2, HEPES 10, D-glucose 8,

and $CaCl_2$ 1.5 (pH 7.4). Ca^{2+}-free solution contained (mM): NaCl 130, KCl 5, $MgCl_2$ 1.2, HEPES 10, D-glucose 8, and EGTA 0.4 (pH 7.4). All experiments were performed at room temperature. The n values given are the numbers of cells from at least three independent Ca^{2+} imaging experiments.

2.2.4. Patch-clamp recordings

Patch-clamp recordings were performed at room temperature (23-26°C). The currents were amplified with an Axopatch 200B or Axoclamp 2B patch clamp amplifier controlled by pClamp software 10 (Molecular Devices, Wokingham, UK). For whole-cell and outside-out recordings, a 1-s ramp voltage protocol ranging from −100 mV to +100 mV was applied at a frequency of 0.2 Hz. Signals were sampled at 3 kHz and filtered at 1 kHz (low pass). Step pulses from -100 mV to 100 mV were used to record single-channel activities under outside-out configuration. The voltage increment for each step was 10 mV and the duration for each pulse was 3 s. The microelectrodes with resistance of 3-5 MΩ were made from borosilicate glass caplillaries (1.2 mm O. D. x 0.69 mm I. D., Harvard Apparatus, Kent, UK) using a glass micropipette puller (Narishige, London, UK). The standard bath solution was used in all recordings. The recording chamber had a volume of 200 µl and was perfused at a rate of about 5 ml/min.

The pipette solution for ORAI1/2/3 recordings contained (mM): 145 Cs-methanesulfonate, 10 BAPTA, 10 HEPES and 8 $MgCl_2$ (pH titrated to 7.2 using CsOH). In some experiments 1 µM TG was added into the pipette solution to deplete the Ca^{2+} stores. The pipette solution for TRPC4/5/3/6 recordings contained (mM): 115 CsCl, 10 EGTA, 2 $MgCl_2$, 10 HEPES, and 5.7 $CaCl_2$ (pH 7.2 adjusted with CsOH, osmolarity ~290 mOsm adjusted with mannitol, and the calculated free Ca^{2+} was 200 nM). For TRPM2 recordings the same 200 nM free Ca^{2+} pipette solution with additional 0.5 mM ADP-ribose was used.

2.2.5. Detection of TRPC spliced variants in SKOV3 cells

SKOV3 cells were cultured in D-MEM/F-12 medium supplemented with 10% FBS, 100 units/ml penicillin and 100 µg/ml streptomycin, and maintained at 37°C under 95% air and 5% CO_2. Total RNA was extracted from cultured cells using TRIzol reagent. The mRNA was reverse-transcribed to cDNA using M-MLV reserve

transcriptase and random primers. The primer sets were designed across introns and the sequences were given in Table 2.2. The PCR mixture contained 1 μl cDNA (~200 ng), 0.5 μM forward primers, 0.5 μM reverse primers, and 1× GoTaq Green Master Mix. The PCR conditions were an initial denaturation at 95 ^{o}C for 30 s, 35 cycles of 94 ^{o}C for 30 s, 57 ^{o}C for 30 s and 72 ^{o}C for 1 min, and a final extension at 72 ^{o}C for 5 min. PCR products were examined on 2% agarose gel, purified with a QIAquick Gel Extraction Kit and confirmed by direct sequencing.

2.2.6. Cell proliferation and colony growth assays

Cell proliferation was determined by WST-1 assay (Roche, Burgess Hill, UK), which reflects the metabolic activity of cultured cells. SKOV3 cells were seeded in 96-well microplates, and then incubated with drugs or antibodies, or transfected with siRNA. After desired time of the treatment, the cells were incubated with WST-1 in phenol red-free D-MEM/F-12 medium for 2-4 h. During this incubation period, viable cells convert WST-1 to a water-soluble formazan dye. The absorbance of formazan dye in each well was measured on a microplate reader with a test wavelength at 450 nm and a reference wavelength at 630 nm. The 630 nm background absorbance was subtracted from the 450 nm measurement, which produced a value correlating with the number of viable cells in each well.

For colony growth assay, SKOV3 cells were transfected with TRPC cDNA plasmids using Lipofectamine 2000, and plated in 60-mm culture dishes at a density of 500 cells per dish to allow the formation of cell colonies after 3-8 days culture. The colonies were fixed with 25% methanol, stained with 0.5% crystal violet dye in phosphate buffered saline (PBS), and automatically counted by CellC software (Selinummi *et al.*, 2005). For soft agar colony assay, the bottom layer of agar (0.7 %) was prepared in a 35-mm culture dish with 1.5 ml of D-MEM/F-12 medium containing agar, 10% FBS, 50 μg/ml penicillin and 50 μg/ml streptomycin. After solidification of the bottom layer, SKOV3 cells were suspended in 1 ml medium containing 0.35% agar at a density of 5000 cells/ml and poured into the dish to form a second layer. The dish was kept at 4 ^{o}C for 5 min and then the solidified second layer was covered with 1 ml medium to prevent the agar layer from drying out. The cells were incubated at 37°C in a humidified incubator and the top layer of medium was gently changed every 3 days. After 21 days of culture, the cells were stained

with 0.005% crystal violet and the cell colonies with diameters >100 μm were counted under a light microscope with a 4× objective.

2.2.7. Transfection of TRPC siRNA into SKOV3 cells

For cell proliferation assay, TRPC siRNAs were transfected into SKOV3 cells using Lipofectamine 2000. The wells or dishes without siRNA (no siRNA) or with scramble siRNA or non-specific pool siRNA were set as negative control in parallel. The Bcl-2 siRNA was used as positive control. For cell cycle experiment, SKOV3 cells were transfected with TRPC siRNAs using the Neon electroporation system (Invitrogen, paisley, UK). The cells were resuspended to a density of 5×10^{6}/ml and mixed with 200 nM siRNA, and then pulsed twice at 1,170 V for 30 ms in a 100 μl tip. After electroporation the cells were maintained in antibiotic-free medium for 72 h and harvested for flow cytometry assay.

2.2.8. Cell cycle and apoptosis analyses

Simultaneous measurement of cell cycle and apoptosis was conducted using flow cytometric assay with propidium iodide staining as described by Riccardi and Nicoletti (2006). SKOV3 cells at 70-80% confluency in a 100-mm culture dish were trypsinized, washed with PBS, fixed with 70% cold ethanol, incubated with DNA extraction buffer (0.2 M Na_2HPO_4, 0.004% Triton X-100, pH 7.8) , treated with RNase (200 μg/ml) and stained with propidium iodide (20 μg/ml). The cells were then analysed with BD FACSCalibur Flow Cytometry System with the CellQuest software (Becton Dickinson, Oxford, UK). Events were counted at the limit of 20,000 or 10,000 for the drug-treated or siRNA-transfected groups. Cell debris was gated out according to the scatter plot and the percentages of cells at different phases of cell cycle were calculated based on the histogram plot of fluorescent intensities.

2.2.9. Statistics

All values are expressed as mean ± SEM. The paired *t* test was used to assess the statistical difference between two groups and a *P* value less than 0.05 was considered as significant.

Chapter 3

**Localisation and Electrophysiological Properties of STIM1, ORAI
and TRPC Proteins in the Stably Transfected HEK293 Cells**

3.1. Introduction

Store-operated Ca^{2+} entry (SOCE) is implemented by the Ca^{2+}-sensing protein STIM1 at the ER and Orai (and possibly TRPC) channels at the plasma membrane. The subcellular localisation of these proteins is important for their roles as store-operated channels (SOCs). STIM1 senses the ER Ca^{2+} level with its N-terminus and regulates Orai and TRPC channels with the C-terminus (Yuan *et al.*, 2007; Zeng *et al.*, 2008; Korzeniowski *et al.*, 2010). The translocation of STIM1 from the ER to the subplasmalemmal regions is the key and unique signalling process in SOCE. STIM1 has been reported to gate Orai1/2/3 and TRPC1/4/5 channels directly, and TRPC3/6 channels indirectly (Yuan *et al.*, 2007; Zeng *et al.*, 2008; Liao *et al.*, 2008; Vaca, 2010). The diversity of these pore-forming subunits has rendered SOCs a broad range of cellular functions (Yuan *et al.*, 2009a; Vaca, 2010). Apart from the differences among the members of Orai and TRPC families, alternative splicing of a single Orai or TRPC gene may also produce channel isoforms with distinct functions. Comparing with other Orai and TRPC genes, TRPC1 and TRPC4 have exhibited much higher splicing activities. There are more than ten spliced variants of human TRPC1 and TRPC4 reported in GenBank, but the functional studies on these isoforms are very limited (Dedman *et al.*, 2011; Mery *et al.*, 2001; Schaefer *et al.*, 2002). As the alternatively spliced variants of other members of TRP channels, e.g. TRPV1, TRPM3 and TRPM8, have been shown to possess distinct functions compared to their full-length counterparts (Wang *et al.*, 2004a; Oberwinkler *et al.*, 2005; Gracheva *et al.*, 2011; Bidaux *et al.*, 2012), it is very important to examine the functional properties of the spliced variants TRPC1 and TRPC4.

In a mammalian cell, there are hundreds of different types of ion channels expressed (Gabashvili *et al.*, 2007). The endogenous activities of these miscellaneous channels make it difficult to study the function of a certain type of ion channels, particularly in non-excitable cells. SOCE is believed to be the most important Ca^{2+} influx pathway in non-excitable cells, and the currents mediated by SOCs are generally very small (whole-cell currents at lower picoampere level) in native cells (Parekh and Penner, 1997; Parekh and Putney, 2005). After the discovery of STIM1 and Orai1 as the most important components of SOCs, a relatively huge store-operated current (100-800 nA for a whole cell) was obtained by overexpressing STIM1 and Orai1 in HEK293 and Jurkat T cells (Peinelt *et al.*, 2006; Soboloff *et al.*, 2006;

Mercer *et al.*, 2006). The use of STIM1/Orai1-overexpressing cells has greatly promoted the functional research of SOCs. Moreover, the overexpression systems of TRPC channels have also been proved to be very useful in physiological and pharmacological studies. Many new interaction proteins and modulators of these channels have revealed by using TRPC-overexpressing cells (Yuan *et al.*, 2003; Xu *et al.*, 2005b; Xu *et al.*, 2008a; Harteneck and Gollasch, 2011).

In this chapter, I identified and cloned the alternatively spliced isoforms of TRPC1 and TRPC4 from human aortic endothelial cells (HAECs). Considering the advantages of ion channel-overexpressing cells as research tools, I generated stable overexpression cell lines for fluorescent protein-tagged STIM1, ORAI and TRPC channels. The inducible protein expression system composed of T-REx HEK293 cells and pcDNA4/TO vectors was used, in which the expression of transfected genes is repressed in the absence of tetracycline and induced in the presence of tetracycline. To verify the functional properties of these cell lines, channel activators including thapsigargin (TG, for STIM1 and ORAI1/2/3), 2-aminoethyldiphenyl borate (2-APB, for ORAI3), Gd^{3+} (for TRPC4/5) and trypsin (for TRPC3/4/5/6)were used in fluorescent microscopy and patch-clamp recordings.

3.2. Results

3.2.1. Novel TRPC1 and TRPC4 variants expressed in HAECs

Alternatively spliced isoforms of TRPC1 and TRPC4 were detected by PCR with different sets of primers across introns and the cDNA of HAECs was used as template. The PCR products generated by primer pairs TRPC1S-F/TRPC1E4E5-R, TRPC1E8E11-F/TRPC1E8E11-R and TRPC4E6E11-F/TRPC4E12-R showed multiple bands in agarose gel after electrophoresis, indicating the existence of spliced variants of TRPC1 and TRPC4 in HAECs (Fig. 3.1). Three alternatively spliced isoforms of TRPC1 were identified by direct sequencing, including TRPC1α (full-length), TRPC1β (exon 3 deletion) and a new isoform with exon 9 deletion (named as TRPC1δ in this thesis) (Fig. 3.2A and C). In addition, three spliced variants of TRPC4 were identified by sequencing the subcloned PCR products in pGEM-T vectors. The longer isoform was TRPC4α, and two new shorter isoforms were characterised and named as TRPC4β1 and TRPC4ε1 (Fig. 3.2B and C).

TRPC4β1 has three more nucleotides deleted in exon 11 compared to the TRPC4β isoform reported in GenBank (NM_001135955). TRPC4ε1 has the same deletion as TRPC4β1, but bears an additional 15 bp fragment after exon 8, which is the feature
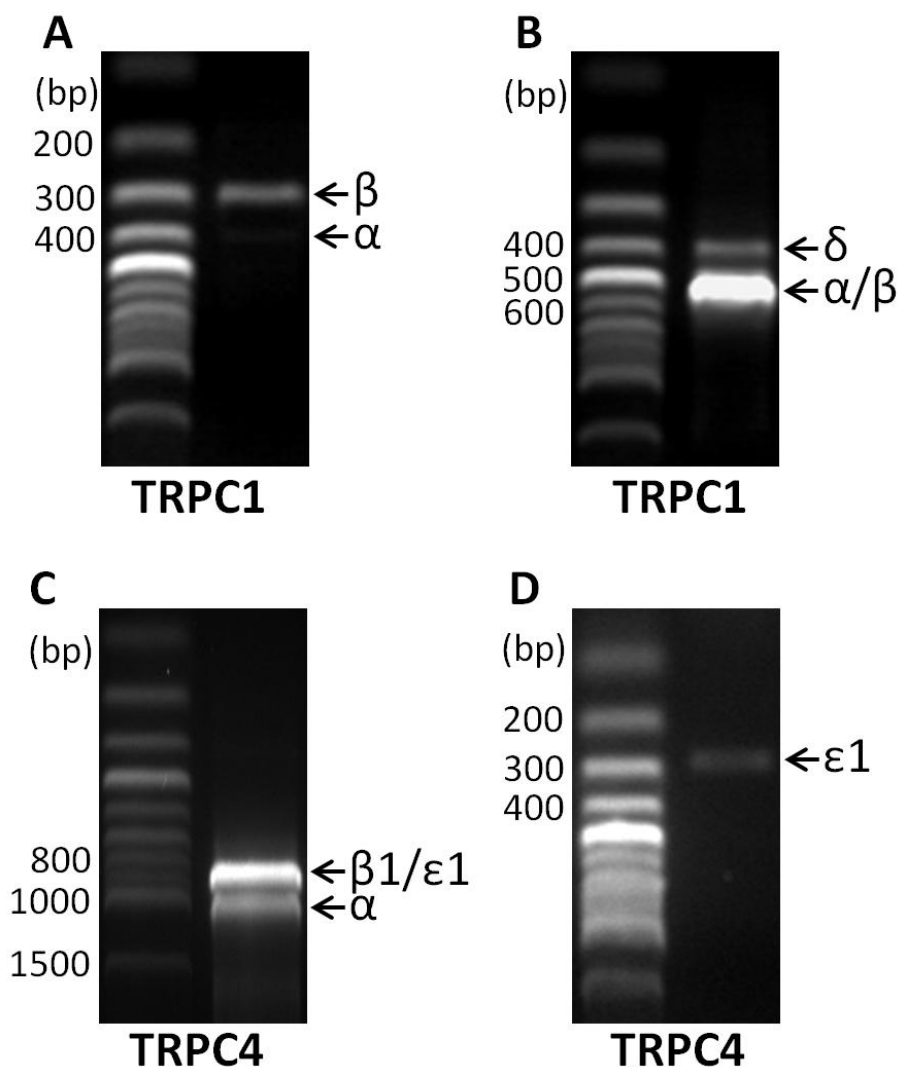
Fig. 3.1 Detection of TRPC1 and TRPC4 spliced variants in human aortic endothelial cells (HAECs). (A) PCR amplification with primers TRPC1S-F and TRPC1E4E5-R from cDNA of HAECs generated two bands, one is bright and the other is very faint, after electrophoresis in 1.5% agarose gel, which correspond to the β (301 bp) and α (403 bp) isoforms of TRPC1. (B) The amplification with primers TRPC1E8E11-F and TRPC1E8E11-R produced two bands with expected sizes of the α and β isoforms (549 bp) and a new δ isoform with Exon 9 deleted (405 bp). (C) Primers TRPC4E6E11-F and TRPC4E12-R amplified DNA fragments with the sizes of the α (1137 bp), β1 (882 bp) and ε1 (897 bp) isoforms of TRPC4. (D) A fragment of the ε1 isoform (283 bp) was amplified using the forward primer TRPC4E7E9-F and the ε-specific reverse primer TRPC4E-R.

A

```
TRPC1α    FLLACDKGDY YMVKKILEEN SSGDLNINCV DVLGRNAVTI TIENENLDIL  [100]
TRPC1β    FLLACDKGDY YMVKKILEEN SSGDLNINCV DVLGRNAVTI TIENENLDIL  [100]

TRPC1α    QLLLDYGCQ- ---------- ---------- ---------- ---KLMERIQ  [150]
TRPC1β    QLLLDYGCQS ADALLVAIDS EVVGAVDILL NHRPKRSSRP TIVKLMERIQ  [150]
                                   Exon 3
TRPC1α    NPEYSTTMDV APVILAAHRN NYEILTMLLK QDVSLPKPHA VGCECTLCSA  [200]
TRPC1β    NPEYSTTMDV APVILAAHRN NYEILTMLLK QDVSLPKPHA VGCECTLCSA  [200]


TRPC1α    IWSDIKRLWY EGLEDFLEES RNQLSFVMNS LYLATFALKV VAHNKFHDFA  [450]
TRPC1δ    IWSDIKRLWY EGLEDFLEES RNQLSFVMNS LYLATFALKV VAHNK-----  [450]

TRPC1α    DRKDWDAFHP TLVAEGLFAF ANVLSYLRLF FMYTTSSILG PLQISMGQML  [500]
TRPC1δ    ---------- ---------- ---------- ---------- ---ISMGQML  [500]
                                   Exon 9
TRPC1α    QDFGKFLGMF LLVLFSFTIG LTQLYDKGYT SKEQKDCVGI FCEQQSNDTF  [550]
TRPC1δ    QDFGKFLGMF LLVLFSFTIG LTQLYDKGYT SKEQKDCVGI FCEQQSNDTF  [550]
```

B

```
TRPC4α    GTLPTPFNVI PSPKSLWYLI KWIWTHLCKK KMRRKPESFG TIG-----RR  [700]
TRPC4β1   GTLPTPFNVI PSPKSLWYLI KWIWTHLCKK KMRRKPESFG TIG-----RR  [700]
TRPC4ε1   GTLPTPFNVI PSPKSLWYLI KWIWTHLCKK KMRRKPESFG TIGVRTQHRR  [700]
                                   Exon 8
TRPC4α    AADNLRRHHQ YQEVMRNLVK RYVAAMIRDA KTEEGLTEEN FKELKQDISS  [750]
TRPC4β1   AADNLRRHHQ YQEVMRNLVK RYVAAMIRDA KTEEGLTEEN FKELKQDISS  [750]
TRPC4ε1   AADNLRRHHQ YQEVMRNLVK RYVAAMIRDA KTEEGLTEEN FKELKQDISS  [750]

TRPC4α    FRFEVLGLLR GSKLSTIQSA NASKESSNSA DSDEKSDSEG NSKDKKKNFS  [800]
TRPC4β1   FRFEVLGLLR GSKLSTIQSA NASKESSNSA DSDEKSDSE- ----------  [800]
TRPC4ε1   FRFEVLGLLR GSKLSTIQSA NASKESSNSA DSDEKSDSE- ----------  [800]
                                   Exon 11
TRPC4α    LFDLTTLIHP RSAAIASERH NISNGSALVV QEPPREKQRK VNFVTDIKNF  [850]
TRPC4β1   ---------- ---------- ---------- ---------- ----------  [850]
TRPC4ε1   ---------- ---------- ---------- ---------- ----------  [850]

TRPC4α    GLFHRRSKQN AAEQNANQIF SVSEEVARQQ AAGPLERNIQ LESRGLASRG  [900]
TRPC4β1   ---------- ---------- ----EVARQQ AAGPLERNIQ LESRGLASRG  [900]
TRPC4ε1   ---------- ---------- ----EVARQQ AAGPLERNIQ LESRGLASRG  [900]
                                       Exon 12
```

C

Fig. 3.2 Sequence alignment and schematic illustration of the spliced variants of TRPC1 and TRPC4. (A) The alignment of partial amino-acid sequences of TRPC1α, TRPC1β and TRPC1δ. Dashes indicate the deletion of amino acids. (B) The alignment of partial amino-acid sequences of TRPC4α, TRPC4β1 and TRPC4ε1. (C) Structures of the spliced variants of TRPC1 and TRPC4.

of the TRPC4ε isoform (NM_003306). The variations in these TRPC1 or TRPC4 isoforms do not cause any shifting in the open reading frames, suggesting these isoforms are able to encode functional ion channels in HAECs.

3.2.2. Localisation of STIM1, ORAI and TRPC proteins in HEK293 cells

3.2.2.1. STIM1, ORAI1, ORAI2 and ORAI3

The STIM1-EYFP fused proteins were predominantly localised at the intracellular compartments including perinuclear region and ER-like structures across the cytoplasm at resting state (Fig. 3.3A, left). Once the cells were treated with TG and the Ca^{2+} stores were depleted, some of the STIM1-EYFP proteins aggregated at the plasma membrane, forming bright puncta (Fig. 3.3A, right).

The mCherry-ORAI1 and mCherry-ORAI2 proteins were present at the plasma membrane and also in some intracellular vesicles (Fig. 3.3B, left and middle). The mCFP-ORAI3 proteins were mostly distributed at the plasma membrane, with small amount of aggregations in the cells (Fig. 3.3B, right).

In STIM1/ORAI-coexpressing cells, the localisation of STIM1-EYFP and mCherry/mCFP-ORAI proteins was similar to those proteins expressed alone in the cells at resting state (Fig. 3.3C, left). When the Ca^{2+} stores were depleted by TG, the STIM1 puncta were induced and colocalised with ORAI proteins at the plasma membrane. Among the three ORAI proteins, mCFP-ORAI3 showed most evident puncta with STIM1, whilst mCherry-ORAI1 retained a smooth distribution at the plasma membrane (Fig. 3.3C, right).

3.2.2.2. TRPC1, TRPC4, TRPC3 and TRPC6

The mCFP-TRPC1 and mCFP-TRPC1δ proteins showed an ER-like localisation in T-REx HEK293 cells and had almost no distribution at the plasma membrane (Fig. 3.4A). The EYFP-TRPC4α/β1/ε1 proteins were mostly evident at the plasma membrane, with very little distribution in the cells (Fig. 3.4B). The mCherry-TRPC3 proteins were localised at the plasma membrane and in some vesicular compartments in the cells (Fig. 3.4C, left). The mCFP-TRPC6 proteins were exclusively distributed at the plasma membrane (Fig. 3.4C, right).
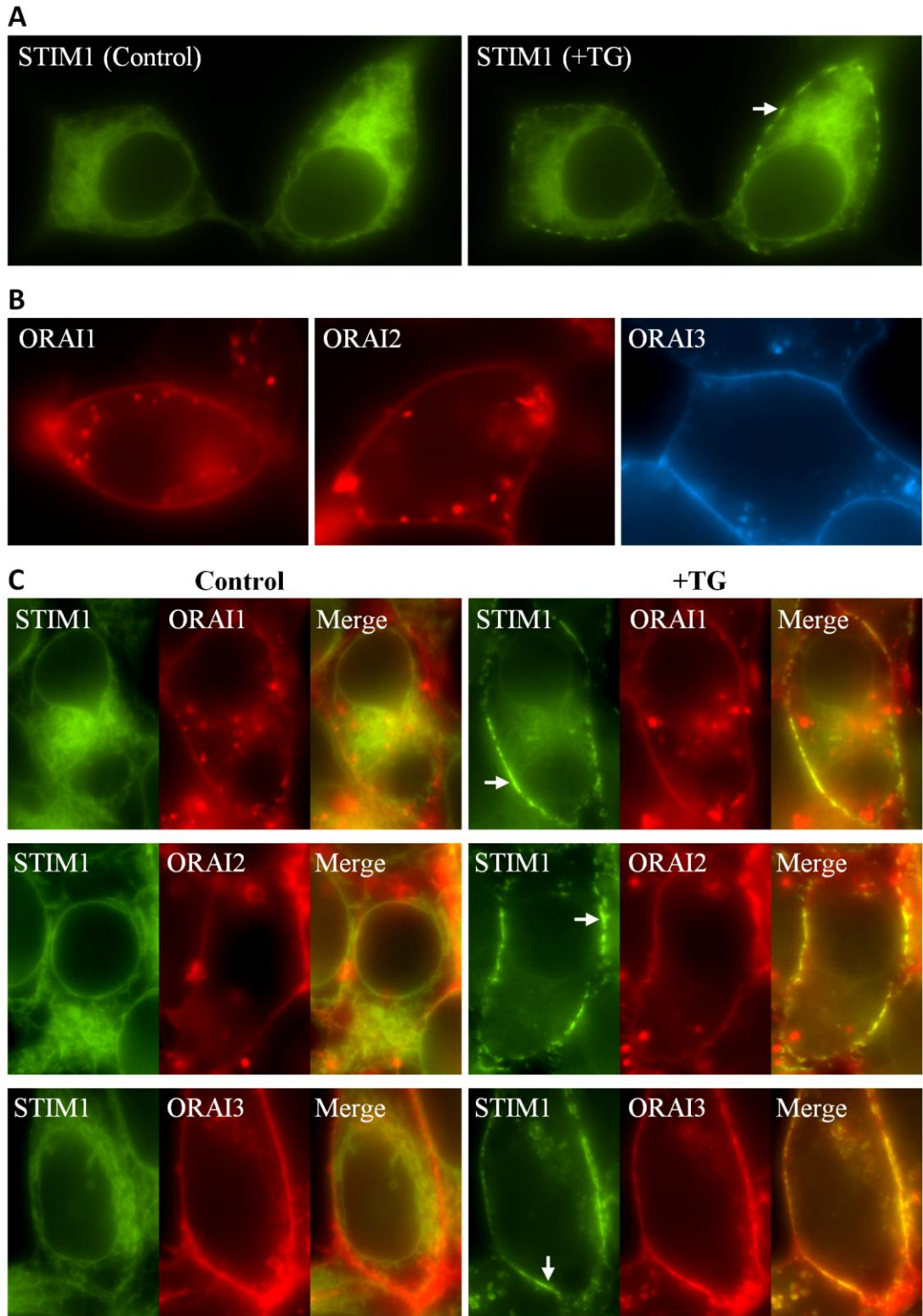
Fig. 3.3 Subcellular localisation of STIM1 and ORAI proteins in HEK293 cells.
(A) STIM1-EYFP before and after TG (1μM) treatment. (B) mCherry-ORAI1,
mCherry-ORAI2 and mCFP-ORAI3 at resting state. (C) STIM1-EYFP coexpressed
with mCherry-ORAI1, mCherry-ORAI2 or mCFP-ORAI3 before and after TG
(1μM) treatment. The mCFP fluorescence is converted into red pseudocolour in the
pictures at the bottom. The STIM1 puncta at the plasma membrane are indicated by
arrows.
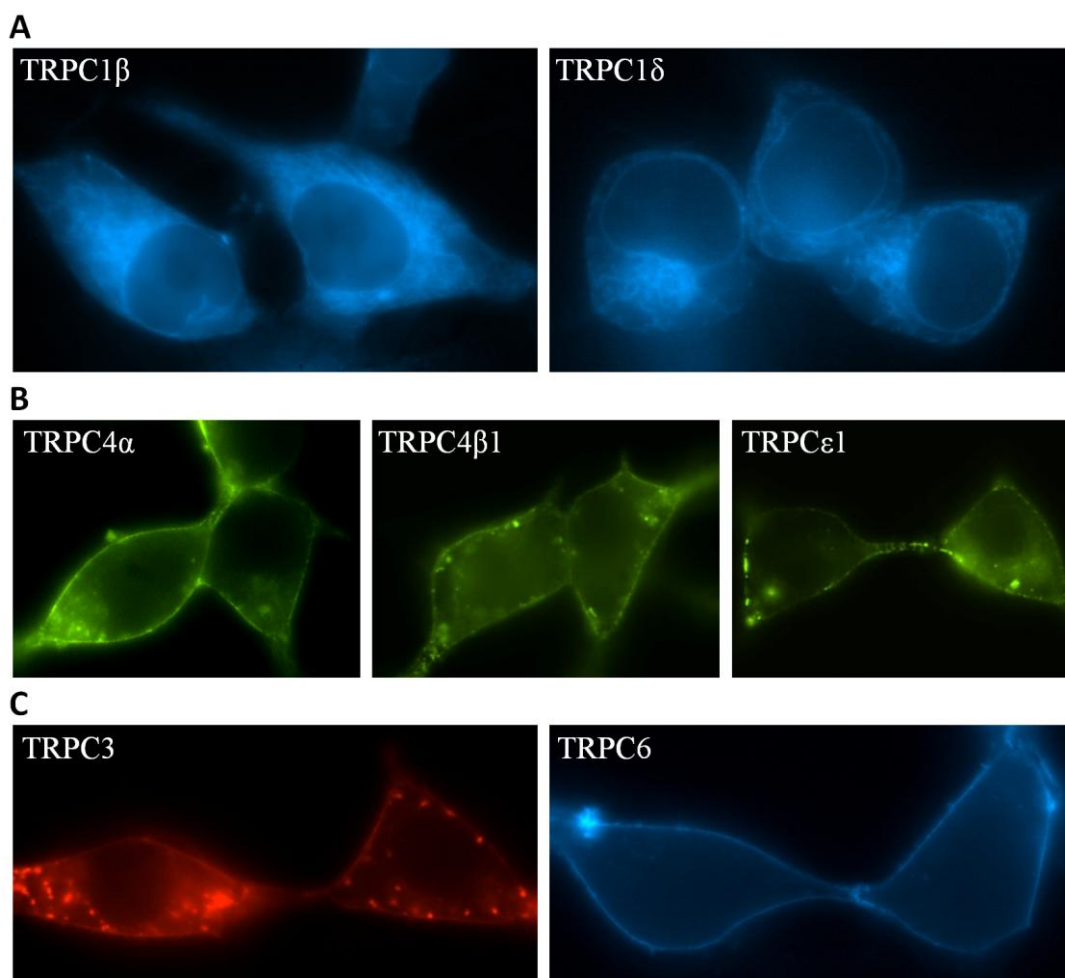
Fig. 3.4 Subcellular localisation of TRPC channels in HEK293 cells. (A) mCFP-TRPC1β and mCFP-TRPC1δ. (B) EYFP-TRPC4α, EYFP-TRPC4β1 and EYFP-TRPCε1. (C) mCherry-TRPC3 and mCFP-TRPC6.

3.2.2.3. STIM1/TRPC1, STIM1/TRPC4 and STIM1/TRPC6

STIM1-EYFP and mCFP-TRPC1 proteins exhibited colocalisation at the perinuclear region and ER-like structures when they were coexpressed in the cells (Fig. 3.5A, left). However, mCFP-TRPC1 did not move to the plasma membrane and form puncta with STIM1-EYFP after Ca^{2+} store depletion by TG (Fig. 3.5A, right). The same phenomenon was observed in STIM1-EYFP cells transiently transfected with mCFP-TRPC1δ (Fig. 3.5B). Coexpression of STIM1 with TRPC4 or TRPC6 did not change the localisation of these proteins (Fig. 3.5C-D, left). TRPC4 and TRPC6 did not affect TG-evoked translocation of STIM1, and the formation of STIM1 puncta at the plasma membrane did not induce clustering of TRPC4 or TRPC6 neither (Fig. 3.5C-D, right).
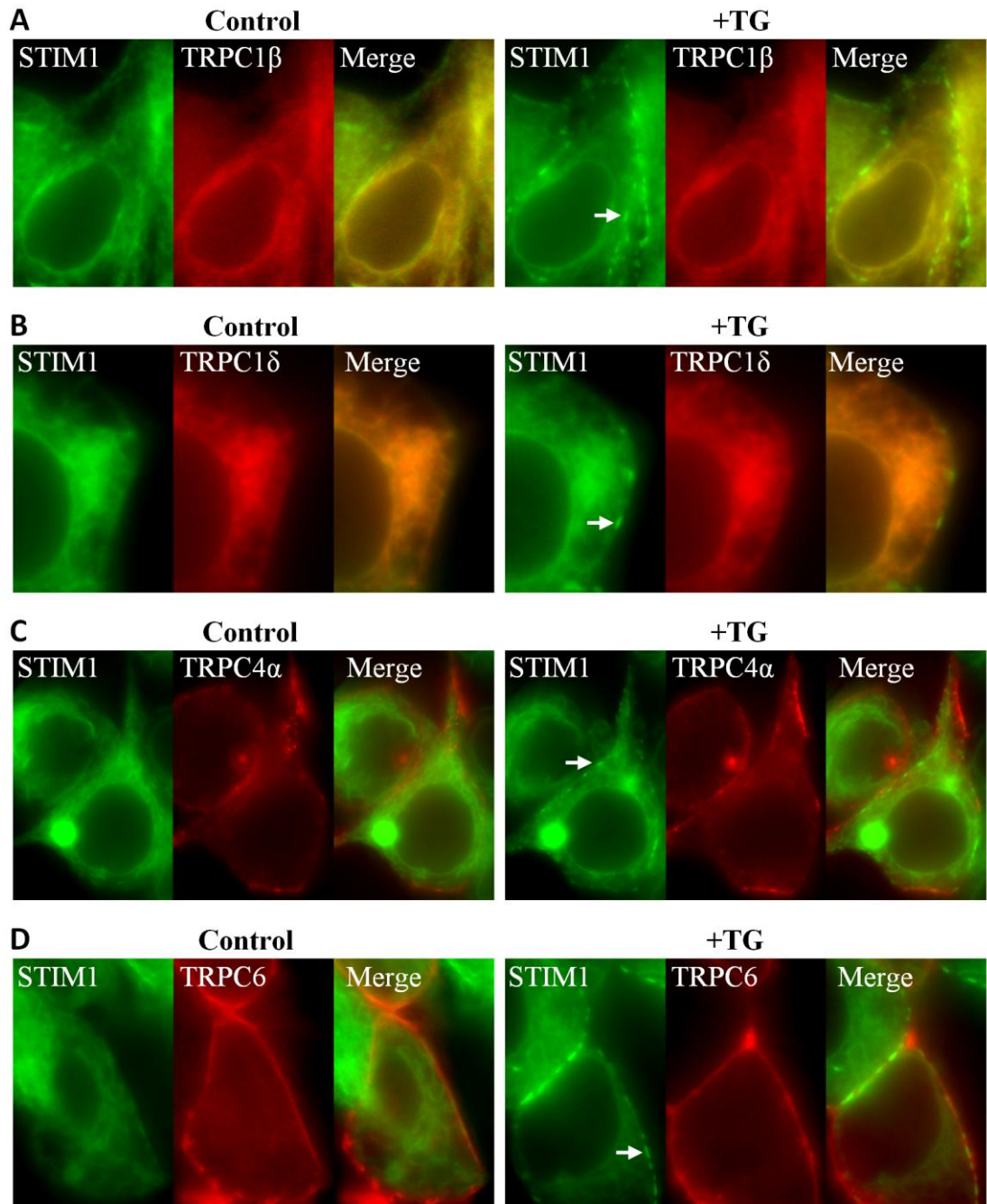
Fig. 3.5 Subcellular localisation of STIM1 and TRPC proteins coexpressed in HEK293 cells. (A) STIM1-EYFP and mCFP-TRPC1β before and after TG (1μM) treatment. (B) STIM1-EYFP and mCFP-TRPC1δ. (C) STIM1-EYFP and mCFP-TRPC4α. (D) STIM1-EYFP and mCFP-TRPC6. The mCFP fluorescence is converted into red pseudocolour in the pictures. The STIM1 puncta at the plasma membrane are indicated by arrows.

3.2.3. Electrophysiological properties of STIM1/ORAI and TRPC channels overexpressed in HEK293 cells

3.2.3.1. STIM1/ORAI1, STIM1/ORAI2, STIM1/ORAI3 and ORAI3

Inward-rectifying whole-cell currents were elicited by 1 μM TG in STIM1/ORAI1 and STIM1/ORAI2 cells (Fig. 3.6A-B). In the control cells without exogenous expression of STIM1 and ORAIs (non-induced), TG (1 μM) did not stimulate any inward or outward current (Fig. 3.6C). 2-APB at 100 μM potently activated ORAI3 current, showing an inward current similar to those of ORAI1 and ORAI2, and a much larger outward current (Fig. 3.6D). In cells overexpressing ORAI3 alone a current with same properties was observed after 2-APB perfusion (Fig. 3.6E). In the non-induced ORAI3 cells, application of 100 μM 2-APB only suppressed the endogenous current (Fig. 3.6F).

3.2.3.2. TRPC4α, TRPC4β1, TRPC4ε1, TRPC3 and TRPC6

After perfusion with 100 μM Gd^{3+}, the whole-cell currents of TRPC4α and TRPC4β1 cells were rapidly increased, showing a typical "*N*"-shape *I-V* relationship (Fig. 3.7A-B). The whole-cell current of TRPC4ε1 cells was partially inhibited by 100 μM Gd^{3+} (Fig. 3.7C).The current in the non-induced TRPCα cells was rather small, and also inhibited by 100 μM Gd^{3+} (Fig. 3.7D).

In TRPC4α and TRPC4β1 cells, the whole-cell currents were significantly augmented by 0.5 μM trypsin (Fig. 3.8A-B). The activation process was fast and transient, with the currents decreased to a lower level within 2 min. The whole-cell current in TRPC4ε1 cells was also increased by 0.5 μM trypsin but the amplitude was very small (0.47±0.09 nA, -0.15±0.03 nA, *n*=4), compared to that of TRPC4α (5.10±0.65 nA, -3.04±0.35 nA, *n*=4) and TRPC4β1 (3.55±0.31 nA, -2.59±0.32 nA, *n*=4), and the *I-V* curve was almost linear (Fig. 3.8C). In the control cells without exogenous TRPC4 expression, trypsin (0.5 μM) gradually stimulated the whole-cell current and this current did not decay in 4 min (Fig. 3.8D). Similar as in TRPC4α and TRPC4β1 cells, trypsin (0.5 μM) showed stimulatory effect on the whole-cell currents of TRPC3 and TRPC6 cells, and the characteristic "*N*"-shape *I-V* curves were also observed (Fig. 3.8E-F).
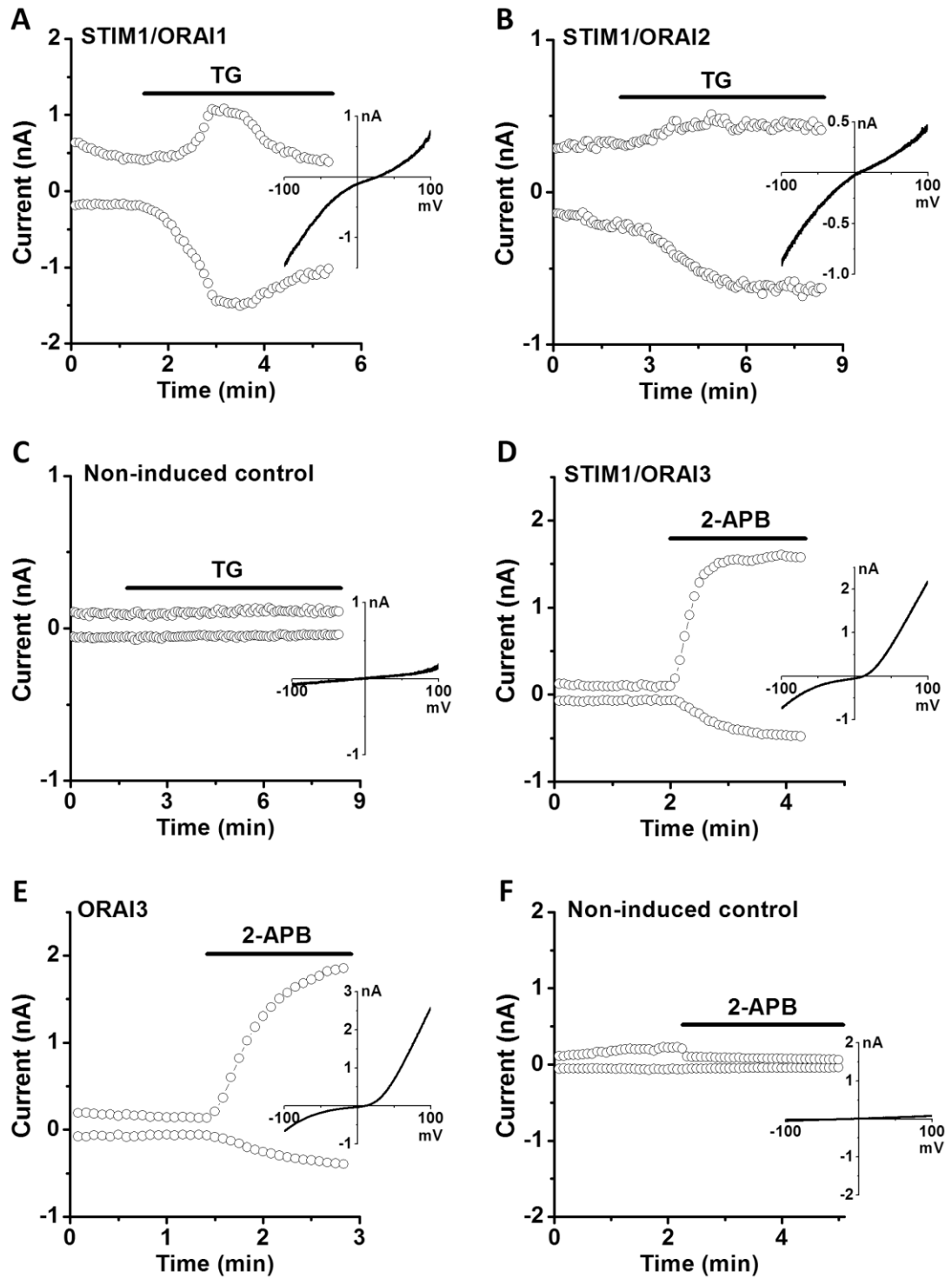
Fig. 3.6 Activation of ORAI channels by TG and 2-APB. (A-B) TG (1 μM) induced store-operated currents in STIM1/ORAI1 and STIM1/ORAI2-coexpressing HEK293 cells. (C) No TG (1 μM)-induced current in non-induced control cell. (D-E) Potentiation of ORAI3 currents by 100 μM 2-APB in STIM1/ORAI3 and ORAI3 cells. (F) 2-APB (100 μM) inhibited the endogenous current in non-induced control cell. The currents in the time-course plots were measured at +80 and -80 mV. The *I-V* curves of the currents at the end of each recording are inset.
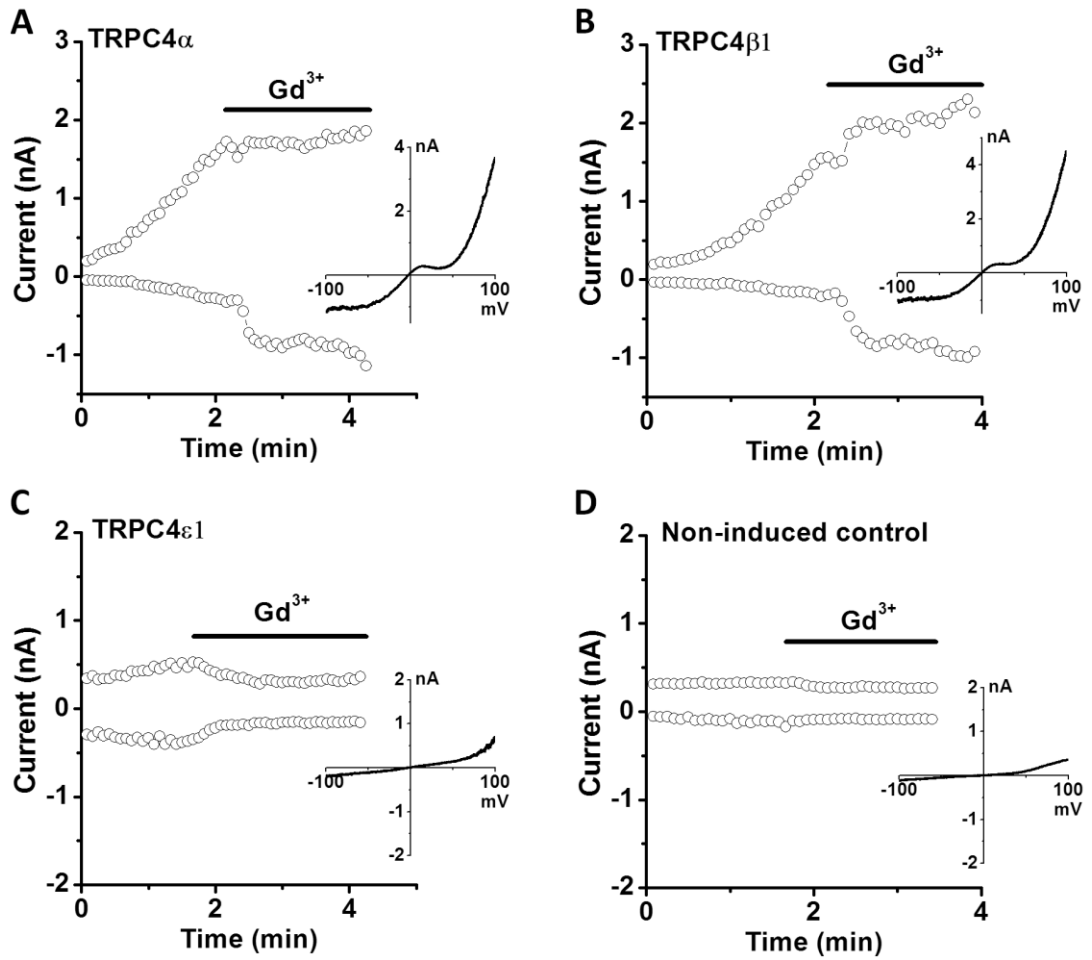
Fig. 3.7 The effects of Gd³⁺ on the whole-cell currents of TRPC4 variants. (A-B) Gd^{3+} (100 µM) activated typical "*N*"-shape TRPC currents in TRPC4α and TRPC4β1 cells. (C) The current of TRPC4ε1 cell was inhibited by 100 µM Gd^{3+}. (D) In non-induced control cell 100 µM Gd^{3+} showed no potentiating effect on the whole-cell current. The *I-V* curves of the currents at the end of each recordingare inset.
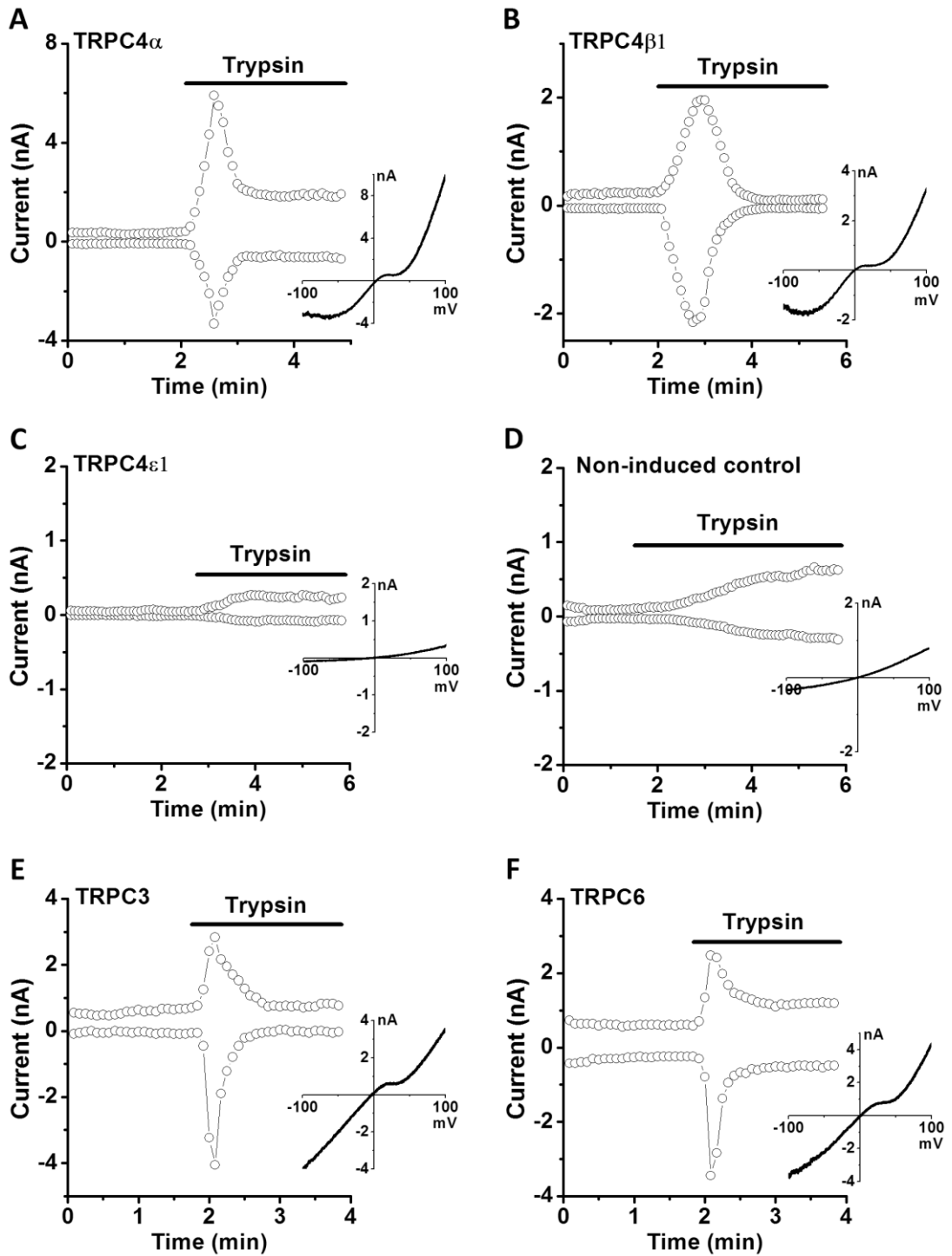
Fig. 3.8 The effects of trypsin on TRPC channels. (A-B) Trypsin (0.5 μM) transiently activated typical "*N*"-shape whole-cell currents in TRPC4α and TRPC4β1 cells. (C) Trypsin (0.5 μM) slightly increased the current in TRPC4ε1 cell. (D) Trypsin (0.5 μM) potentiated the current in non-induced control cell. (E-F) The effects of 0.5 μM trypsin on the whole-cell currents of TRPC3 and TRPC6 cells. The *I-V* curves of the peak currents (A, B, E and F) or currents at the end of recordings (C and D) are inset.

3.3. Discussion

3.3.1. Localisation and interaction of fluorescent protein-tagged STIM1, ORAI and TRPC proteins

In this study I generated HEK293 cell lines overexpressing store-operated channel proteins including STIM1, ORAI1/2/3 and TRPC1/3/4/6. The localisation of these proteins was revealed by the tagged fluorescent proteins mCFP, EYFP and mCherry. STIM1-EYFP and mCFP-TRPC1 are present at ER-like intracellular compartments, whilst mCherry-ORAI1, mCherry-ORAI2, mCFP-ORAI3, mCherry-TRPC3, EYFP-TRPC4 and mCFP-TRPC6 are mostly found at the plasma membrane. These results are as expected and suggest that the three fluorescent proteins are useful tools for protein localisation studies. However, it is noticeable that the proteins tagged with mCherry (ORAI1, ORAI2 and TRPC3) showed more intracellular aggregations compared with other proteins tagged with mCFP or EYFP (Fig. 3.3-3.4). These vesicle-like protein aggregations are most likely in lysosomes, which are responsible for intracellular protein degradation. The inclusion of mCherry-tagged proteins in lysosome-like organelles suggests that these proteins are probably misfolded and thus being degraded. The misfolding of these proteins may be caused by the conjugation with mCherry, because the cells overexpressing mCFP or EYFP-tagged proteins do not have so many intracellular vesicles with bright fluorescence. Accordingly, it is suggested that mCFP and EYFP are better than mCherry for protein localisation studies using fluorescent protein conjugation method.

The characteristic feature of STIM1 is its movement from intracellular compartments to the plasma membrane upon Ca^{2+} store depletion. This translocation process is confirmed in STIM1-EYFP cells, and also in cells coexpressing ORAI or TRPC channels with STIM1. Colocalisation of STIM1 puncta and ORAI channels at the plasma membrane was observed; however, there was no such phenomenon in STIM1/TRPC-coexpressing cells after Ca^{2+} store depletion. These results suggest that the affinity between STIM1 and TRPC proteins is much lower than that between STIM1 and ORAI proteins, if the direct interaction between STIM1 and TRPC proteins really exists. There is evidence that Ca^{2+} influx through ORAI1 is crucial for the activation of TRPC1 during SOCE (Cheng *et al.*, 2011), which may be a common mechanism for the STIM1/ORAI/TRPC complex. Future studies using

STIM1/ORAI/TRPC-coexpressing cells and gene knockout/down techniques will give more important evidences on this topic.

3.3.2. Electrophysiological properties of STIM1/ORAI channels

According to previous reports, overexpression of STIM1 and ORAI1 resulted in a large and characteristic I_{CRAC} (Peinelt *et al.*, 2006; Soboloff *et al.*, 2006; Mercer *et al.*, 2006). This is confirmed in present study, i.e. the whole-cell current elicited by TG in STIM1/ORAI1 cells showed an inward-rectifying property (Fig. 3.6A). However, the outward current observed in this study was larger than that described by other groups, which may result from the opening of other endogenous SOCs, probably TRPC channels. A similar phenomenon was observed in STIM1/ORAI2 cells (Fig. 3.6B). The lack of TG-induced current in non-induced control cells suggests that the inward-rectifying currents in STIM1/ORAI1 and STIM1/ORAI2 cells are due to the overexpression of STIM1, ORAI1 and ORAI2, and the activation of these exogenous channels enhances the activity of other endogenous SOCs.

2-APB is a direct activator of ORAI3 channel, so it was used to verify the functionality of STIM1/ORAI3 and ORAI3 cells. Chacraristic ORAI3 currents were evoked in these two types of cells after 2-APB application, which is distinct from the inhibition of current in non-induced control cells with the same treatment. The comparable currents in STIM1/ORAI3 and ORAI3 cells suggest that the overexpression of STIM1 does not affect the activation of ORAI3 by 2-APB, which is consistent with previous studies (DeHaven *et al.*, 2008; Peinelt *et al.*, 2008). Although the activation of ORAI3 channel by 2-APB has been well addressed in overexpression systems, there is no report stating this effect in native cells. This may be due to the low expression of ORAI3 channels in native cells, where the increased ORAI3 activity is masked by the inhibition of other channels when 2-APB is applied. Moreover, the assembly of ORAI1 and ORAI3 as heteromeric channel has been demonstrated (Mignen *et al.*, 2009; Schindl *et al.*, 2009), which may be another reason for the lack of 2-APB-evoked current in native ORAI3-expressing cells, because the activity of ORAI1/3 heteromeric channel is greatly reduced compared to homomeric ORAI3 channel in the presence of 2-APB (Schindl *et al.*, 2009).

3.3.3. Functions of novel TRPC1 and TRPC4 variants

TRPC1β and TRPC1δ are two TRPC1 isoforms detected in endothelial cells in this study. After transfection into HEK293 cells, they were found to be localised at intracellular compartments, most probably the ER. This is inconsistent with previous reports using fluorescent protein-tagged TRPC1 in HEK293 cells (Hofmann *et al.*, 2002; Alfonso *et al.*, 2008). It was found that TRPC1 could move to the plasma membrane when it was coexpressed with TRPC4 or TRPC5 channels; however, there are still considerable amount of TRPC1 proteins remaining in the cells (Hofmann *et al.*, 2002; Alfonso *et al.*, 2008). Apart from forming heteromeric channels with other TRPCs at the plasma membrane, TRPC1 can also operate as homomeric Ca^{2+}-leaking channels at the sarcopalsmic reticulum, as found in skeletal muscle cells (Berbey *et al.*, 2009). The ER-localised TRPC1 in HEK293 cells may have the same function, which needs to be confirmed by future studies using ER-specific Ca^{2+} indicators. The intracellular localisation of TRPC1 has hindered the electrophysiological studies on homomeric TRPC1 channels. So far there is no convincing report for the whole-cell current of TRPC1-overexpressing cells, probably because the current is very small and difficult to be distinguished from the endogenous currents. For the same reason, I have not compared the electrophysiological difference of the two TRPC1 isoforms in this study.

The eletrophysiological property of the new TRPC4 isoform TRPC4ε1 was found to be distinct from other two TRPC4 isoforms, TRPC4α and TRPC4β1. The TRPC4ε1 cells did not respond to the TRPC4/5 selective activator Gd^{3+}, and showed very little activation by the GPCR agonist trypsin. However, this trypsin-stimulated current (0.47±0.09 nA, -0.15±0.03 nA, *n*=4) was even smaller than that in the non-induced control cells (0.81±0.09 nA, -0.52±0.07 nA, *n*=4), suggesting that TRPC4ε1 may serve as a negative regulator of endogenous receptor-operated channels. The dominant negative modulation of TRP channels by their alternatively spliced variants have been reported, such as the inhibition of full-length TRPV1 and TRPM8 channels by their short variants (Wang *et al.*, 2004a; Bidaux *et al.*, 2012; Fernandez *et al.*, 2012). The exact role of TRPC4ε1 needs to be investigated by coexpression with other functional TRPC isoforms in the future.

3.3.4. Activation mechanisms of TRPC channels

Lanthanides are selective activators of TRPC4 and TRPC5 channels. The actions of La^{3+} and Gd^{3+} on TRPC5 are complex, including the increase of channel open probability, reduction of channel conductance, potentiation at low concentrations (10-100 μM) and inhibition at high concentrations (>100 μM) (Jung *et al.*, 2003). The molecular targets of La^{3+} and Gd^{3+} on TRPC5 are the negatively charged glutamic acid residues (E543, E595 and E598) situated in the extracellular pore region of the channel. Neutrolisation of these residues resulted in the inhibition of TRPC5 channels by La^{3+}. These residues are conserved in TRPC4 and TRPC5, but absent in other TRPC members. Therefore, La^{3+} and Gd^{3+} have only inhibitory effect on TRPC3/6/7 channels (Jung *et al.*, 2003). The TRPC4ε1 isoform identified in this study has the same pore region as TRPC4α and TRPC4β1, and possesses only five additional amino acids (VRTQH) in the cytoplasmic C-terminus. This amino acid stretch may work as a molecular lock that keeps the channel at closing conformation. The loss of Gd^{3+} potentiation on TRPC4ε1 may be related to this speculative mechanism.

Trypsin is a searine proteinase and the agonist of proteinase-activated receptor 2 (PAR2). Trypsin activates PAR2 by cleaving the N-terminus of the receptor, which leads to the activation of G proteins (Macfarlane *et al.*, 2001). It has been reported that TRPC4 and TRPC5 channels are directly activated by the specific G protein isoform $G\alpha_i$ (Jeon *et al.*, 2012), which is coupled to PAR2 (Ricks and Trejo, 2009). The G proteins then activate phospholipase C (PLC) in the subplasmalemmal area. PLC cleaves the plasma membrane component phosphatidylinositol 4,5-bisphosphate (PIP_2) into inositol 1,4,5-trisphosphate (IP_3) and diacylglycerol (DAG). DAG is a direct activator of TRPC3 and TRPC6 channels, and also activates protein kinase C (PKC) (Hofmann *et al.*, 1999). Because activated PKC blocks TRPC channel activity (Venkatachalam *et al.*, 2003), the effect of trypsin on TRPC currents will be activation at first and then inhibition, which is confirmed in current study (Fig. 3.8). The decay of TRPC currents should be taken into consideration when trypsin or other GPCR agonist is used as channel activators in the experiment to test TRPC blockers. PKC inhibitors, such as cheletythrine and GF109203X, may be used in future studies to prevent the rundown of TRPC currents stimulated by GPCR agonists.

3.4. Conclusions

In this chapter I identified three novel alternatively spliced isoforms of TRPC1 and TRPC4 (TRPC1δ, TRPC4β1 and TRPC4ε1) from HAECs. Expression vectors containing the complete coding sequences of STIM1, ORAI1/2/3 and TRPC1/4/3/6, including the three new isoforms, were constructed and transfected into HEK293 cells. Stable cell lines for STIM1, ORAI1/2/3 and TRPC1/4/3/6, and coexpression cell lines for STIM1-ORAI1/2/3 and STIM1-TRPC1/4/6 were generated and the functional properties of these cell lines were tested by fluorescence microscopy and patch-clamp recordings.

TRPC1β, TRPC1δ and STIM1 showed a similar ER-like localisation in HEK293 cells at resting state. TRPC4α/β1/ε1, TRPC3/6 and ORAI1/2/3 were mostly localised at the plasma membrane. Depletion of ER Ca^{2+} store induced STIM1 translocation to the plasma membrane, where it formed complex with ORAI1/2/3. TRPC1β and TRPC1δ did not move to the plasma membrane with STIM1 upon Ca^{2+} store depletion. TRPC4 and TRPC6 were not colocalised with STIM1 puncta at the plasma membrane.

Store-operated Ca^{2+} currents were observed in STIM1-ORAI1/2 coexpressing cells, and the ORAI3 current was substantially potentiated by its selective activator 2-APB in STIM1/ORAI3 and ORAI3 cells. The eletrophysiological property of TRPC4ε1 was distinct from TRPC4α and TRPC4β1, as it did not respond to the channel activators Gd^{3+} and trypsin. TRPC3 and TRPC6 channels were significantly activated by trypsin. All these results suggest that the STIM1, ORAI and TRPC proteins are functionally expressed in the stably transfected cell lines generated in this study, which can be used in further electrophysiological and pharmacological studies.

Chapter 4

Cytosolic Clustering of STIM1 as a Novel Mechanism for the Inhibition of Store-Operated Ca^{2+} Entry

4.1. Introduction

The activation of G protein-coupled receptors (GPCRs) and receptor tyrosine kinases (RTKs) induces a Ca^{2+} release from internal stores, which in turn triggers a sustained Ca^{2+} influx across the plasma membrane (PM) via store-operated Ca^{2+} channels (SOCs). This Ca^{2+} influx through SOCs, termed as store-operated Ca^{2+} entry (SOCE) or capacitative Ca^{2+} entry, mediates numerous physiological functions including cell growth, muscle contraction, exocytosis, gene transcription and apoptosis (Parekh and Putney, 2005). The molecular basis for SOCs has been linked to the two major ion channel families, i.e., ORAI channels and transient receptor potential (TRP) channels. ORAI channels mediate a highly Ca^{2+}-selective and inward rectifying Ca^{2+} release-activated Ca^{2+} current (I_{CRAC}) (Vig *et al.*, 2006a; Yeromin *et al.*, 2006), while TRPC channels mediate a non-selective Ca^{2+}-permeable cationic current with a current-voltage (*IV*) relationship of outward rectification, such as TRPC1, TRPC3, TRPC7 and the heteromeric TRPC1/TRPC5 channel (Xu *et al.*, 2012; Xu *et al.*, 2006b; Yuan *et al.*, 2007), or "N" shape *I-V* curve with inward and outward rectification (Xu *et al.*, 2008a). ORAI channels, as well as TRPCs, are interacted or triggered by the endoplasmic reticulum (ER) Ca^{2+} sensor STIM1 (stromal interaction molecule 1) that signals the Ca^{2+} depletion of ER to the SOCs (Hogan *et al.*, 2010; Liou *et al.*, 2005; Zhang *et al.*, 2005; Lee *et al.*, 2010; Pani *et al.*, 2009).

STIM1 was originally identified as a stromal cell molecule that is potentially relevant for interactions with precursor B cells. It is a type I membrane protein and mainly located in the ER, but also to a limited extent in the PM (Spassova *et al.*, 2006; Hogan *et al.*, 2010). STIM1 relocation has been suggested as the mechanism for coupling the ER Ca^{2+} store depletion to SOCs in the PM (Liou *et al.*, 2005; Zhang *et al.*, 2005). It has been demonstrated that the ER-luminal domain of STIM1 is responsible for Ca^{2+} sensing, and the dissociation of Ca^{2+} from STIM1 leads to oligomerization (clustering) and redistribution of STIM1 to the subplasmalemmal area (translocation) (Smyth *et al.*, 2008; Hogan *et al.*, 2010). STIM1 then triggers ORAI channels (ORAI1, 2 and 3) in the PM via the binding to the N-terminus of ORAI, which results in Ca^{2+} entry into the cell (Hogan *et al.*, 2010).

Dysfunction of SOCs causes some diseases, for example, the mutations of ORAI1 and STIM1 causing the deficiency of I_{CRAC} in T cells that has been regarded as the aetiology of severe combined immune deficiency syndrome (Feske *et al.*, 2010). ORAI1 deficiency in mice results in resistance to pathological thrombus formation, which is an important new clue for preventing ischemic cardiovascular and cerebrovascular events (Braun *et al.*, 2009b). In addition, the alteration of channel expression or channel activity is implicated in angiogenesis (Grigoriev *et al.*, 2008), smooth muscle cell proliferation and migration (Potier *et al.*, 2009) and cardiomyocyte hypertrophy (Ohba *et al.*, 2009), suggesting the signalling of STIM1-associated activation of SOCs could act as new therapeutic targets. However, the regulation of STIM1 movement is still unclear.

In order to examine the possibility of STIM1 movement as a new potential drug target, the pharmacological profile of STIM1 translocation and clustering was investigated in this study using a variety of modulators that potentially change the activity of SOCs or target to the signalling pathways associated with SOCE. HEK293 cells stably transfected with STIM1-EYFP fused gene were used. It is demonstrated that the localisation of STIM1 puncta has two different patterns in response to different regulators, i.e., cytosolic clusters and subplasmalemmal clusters. The ER Ca^{2+} store-independent mechanism for the cytosolic STIM1 movement is crucial for the pharmacological regulation of SOCE.

4.2. Results

4.2.1. STIM1 translocation induced by Ca^{2+} store depletion

Passive depletion of ER Ca^{2+} store by sarco/endoplasmic reticulum Ca^{2+}-ATPase (SERCA) inhibitor thapsigargin (TG, 1μM) induced STIM1-EYFP subplasmalemmal translocation and puncta formation (Fig. 4.1A), which is consistent with previous reports (Liou *et al.*, 2005; Zhang *et al.*, 2005; Walsh *et al.*, 2010). The STIM1 puncta at PM became evident after 4 min incubation with TG and achieved maximum after ~6 min (Fig. 1A). The TG-induced STIM1 clustering and translocation occurred in both Ca^{2+} free and Ca^{2+} containing bath solution, suggesting the extracellular Ca^{2+} is not the determinant for intracellular STIM1 movement.
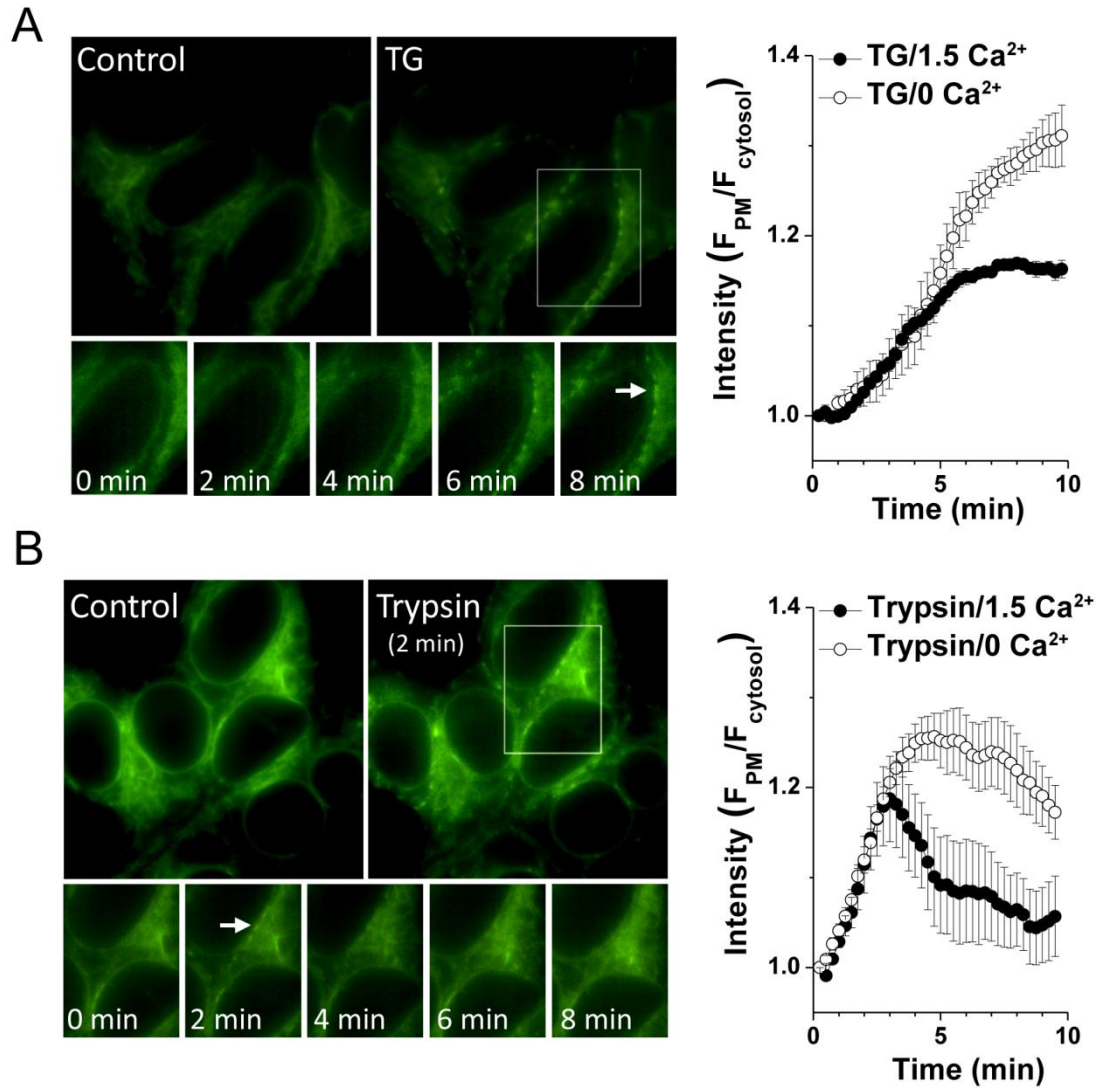
Fig. 4.1 STIM1 subplasmalemmal translocation and clustering in response to Ca²⁺-store depletion in the stably transfected STIM1-EYFP cells. (A) TG (1 μM) induced STIM1 puncta formation at the PM of cells in Ca²⁺ bath solution. The time course of STIM1 subplasmalemmal translocation and clustering in the boxed area is showed in the lower panels. The arrow indicates the subplasmalemmal STIM1 clusters (puncta). The ratio of fluorescent intensity in the PM (F_{PM}) and the cytosol ($F_{cytosol}$) of cells in response to TG (1 μM) in 1.5 mM Ca²⁺ or Ca²⁺-free bath solution ($n = 5$ cells in each group). The regions of interest (ROIs) of the PM and the nearby cytosol were manually selected. (B) Trypsin-induced STIM1 clustering and translocation in standard bath solution. The dynamic changes of ratio of fluorescent intensity ($F_{PM}/F_{cytosol}$) for the STIM1 translocation induced by trypsin (0.1 nM) are shown in the chart ($n = 5$ cells in each group).

The time course for the onset of the TG-induced STIM1 translocation was a slow process, which could be due to the slow Ca^{2+} leakage from the ER induced by passive Ca^{2+} store depletion.

The depletion of ER Ca^{2+} store via GPCR activation is another way to induce STIM1 translocation. Protease-activated receptor is a unique subclass of GPCR and can be activated by cleavage of the extracellular N-terminus with trypsin or thrombin (Hollenberg and Compton, 2002). Trysin at 0.1 nM significantly induced STIM1 clustering and translocation in standard bath solution or Ca^{2+} free bath solution (Fig. 4.1B). Unlike the SERCA blockers or Ca^{2+} chelators, the STIM1 translocation evoked by trypsin was much faster, but the subplasmalemmal clustering was transient and the puncta gradually disappeared after 4 min in standard bath solution containing 1.5 mM Ca^{2+} (Fig. 4.1B), however, the disassembly of STIM1 puncta was not observed in Ca^{2+} free solution, suggesting that this process is dependent on Ca^{2+} influx that leads to ER Ca^{2+} store refilling. The relocation of STIM1 from PM to cytosol seen in the active store-depletion suggests that the STIM1 clustering and translocation is a reversible process, which may act as a drug target.

4.2.2. Ryanodine-sensitive Ca^{2+} store and STIM1 movement

The entire ER/SR Ca^{2+} store could also be depleted by activation of ryanodine receptors (RyRs), which leads to SOCE (Fellner and Arendshorst, 2000). Therefore, STIM1 movement in response to the depletion of ryanodine-sensitive Ca^{2+} store was investigated. The expression of endogenous RyRs has been demonstrated in the HEK293 cells (Querfurth et al., 1998). Application of RyR direct activator 4-chloro-3-ethylphenol (4-CEP, 500 μM) led to STIM1 translocation toward the PM. Interestingly, unlike trypsin, the 4-CEP-induced STIM1 puncta at the PM disappeared after 3 min incubation with 4-CEP, and was followed by substantial STIM1 clusters retained in the cytosol (Fig. 4.2A). However, caffeine ranged from 10 to 50 mM that can increase the sensitivity of RyRs to Ca^{2+} did not cause cytosolic STIM1 puncta, instead the formation of subplasmalemmal STIM1 puncta (Fig. 4.2B). Both 4-CEP and caffeine induced intracellular Ca^{2+} release, however, Ca^{2+} release induced by 4-CEP was higher and lasted longer than that by caffeine. In addition, 4-CEP nearly abolished the Ca^{2+} influx when external 1.5 mM Ca^{2+} was added, but caffeine
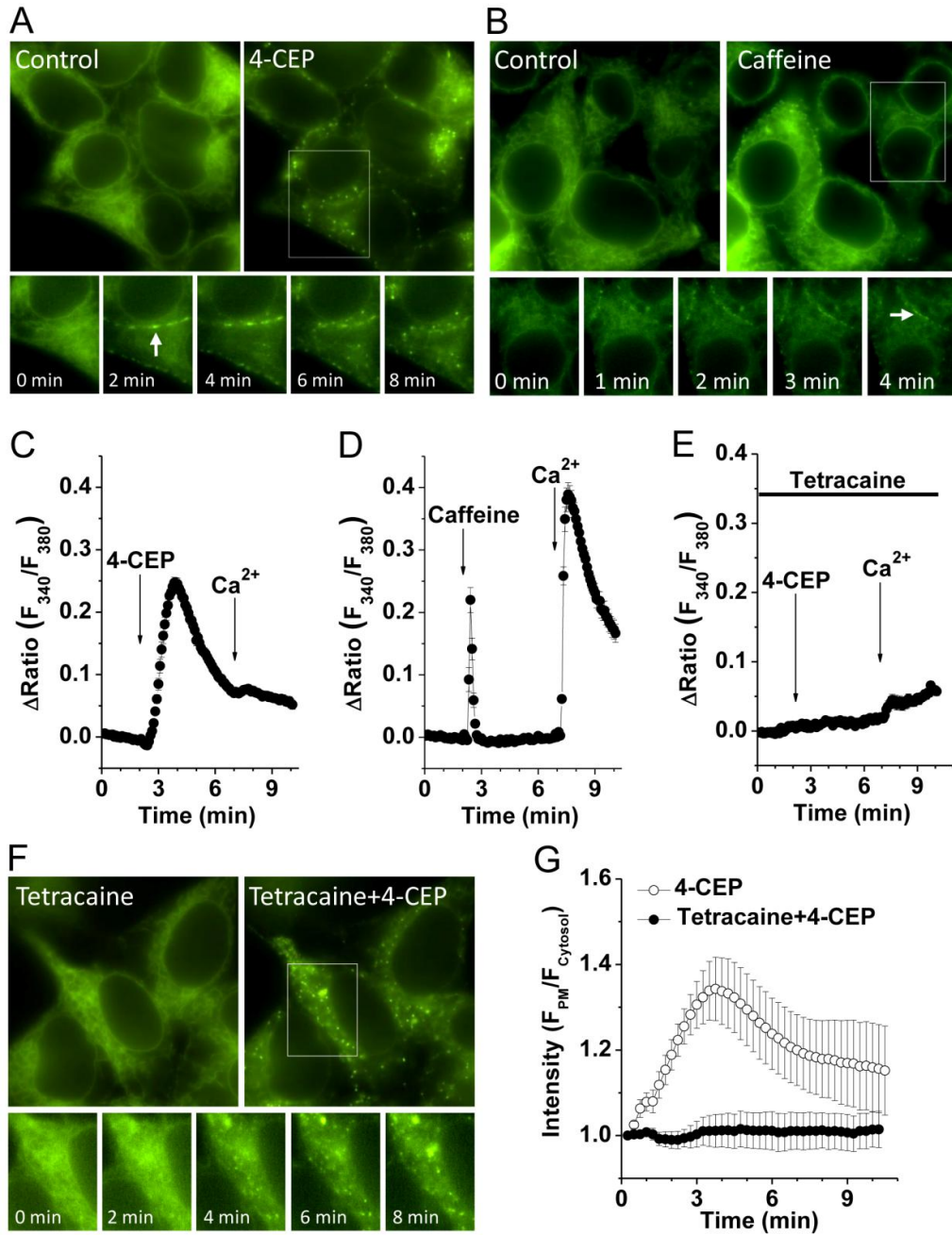
Fig. 4.2 STIM1 translocation induced by RyR agonists in the STIM1-EYFP cells. (A) 4-CEP (500 µM) induced transient STIM1 puncta formation at the PM and then cytosolic clustering in Ca^{2+} bath solution. The time course of STIM1 translocation in the boxed area is shown in the lower figures. The arrow indicates the subplasmalemmal STIM1 puncta. (B) Caffeine (10 mM) induced STIM1 puncta formation at the PM in Ca^{2+} bath solution. (C) 4-CEP (500 µM) induced Ca^{2+} release but abolished Ca^{2+} entry in STIM1-EYFP cells ($n = 23$). (D) Caffeine (10 mM) induced Ca^{2+} release and Ca^{2+} entry in the STIM1-EYFP cells ($n = 21$). (E) STIM1-EYFP cells perfused with tetracaine (500 µM) for 10 min and followed by 4-CEP and 1.5 mM Ca^{2+} ($n = 21$). (F) Tetracaine (500 µM) prevented the formation of subplasmalemmal STIM1 puncta, but not the cytosolic clusters, in Ca^{2+} bath solution. (G) The time course of fluorescent intensity changes ($F_{PM}/F_{cytosol}$) for the

STIM1 translocation induced by 4-CEP (500 μM) in the absence or presence of 500 μM tetracaine ($n = 10$ cells in each group).

had no such effect (Fig. 4.2C-D), suggesting the pharmacological difference between the two agonists in the regulation of STIM1 clustering and Ca^{2+} influx. In order to examine the relationship of cytosolic STIM1 clustering and Ca^{2+} release, the STIM1-EYFP cells were pretreated with RyR antagonist tetracaine (500 μM) for 10 min and then perfused with 4-CEP (500 μM). The 4-CEP-induced Ca^{2+} release signal and STIM1 subplasmalemmal translocation were completely blocked by tetracaine pretreatment, however, the cytosolic clustering of STIM1 was still present (Fig. 4.2E-F), suggesting that the cytosolic STIM1 clustering is independent of ER Ca^{2+} store release or store depletion.

4.2.3. Mitochondrial Ca^{2+} release is involved in cytosolic STIM1 clustering

Mitochondria are important Ca^{2+}-storing organelles closely associated with ER. Although it has been established that depletion of ER Ca^{2+} stores leads to STIM1 translocation to the PM, little is known about the effect of mitochondrial Ca^{2+} release on STIM1 movement. Flufenamic acid (FFA) is a non-steroidal anti-inflammatory drug with Ca^{2+} releasing effect from mitochondria whereas its analogue niflumic acid (NFA) has little effect on mitochondrial Ca^{2+} release (Tu *et al.*, 2009; Jiang *et al.*, 2012), which suggests that the two chemicals are ideal for investigating the effect of mitochondrial Ca^{2+} release on STIM1 movement. In the current study, FFA (100 μM) caused STIM1 clustering in the cytosol, and further addition of 1 μM TG failed to induce STIM1 puncta translocation toward the PM in the standard bath solution (Fig. 4.3A). However, NFA (100 μM) neither induced any cytosolic STIM1 clusters nor blocked the TG-induced STIM1 subplasmalemmal translocation to the PM, although much more sparse puncta were also observed in the cytosol after addition of TG (Fig. 4.3A-B). The differences of FFA and NFA on Ca^{2+} release and store-depleted Ca^{2+} entry in the STIM1-EYFP cells were also observed. The Ca^{2+} release induced by FFA was much higher than the group treated by NFA, but the inhibition on the store-depleted Ca^{2+} entry was similar (Fig. 4.3C-E).

The effect of mitochondrial metabolic inhibitors on STIM1 movement was examined. The uncoupling agent FCCP, which abolishes the obligatory linkage between the respiratory chain and the phosphorylation system, can also cause

mitochondrial Ca^{2+} release (Gurney *et al.*, 2000). Pretreatment with FCCP (5 µM) for 10 min did not prevent TG-induced STIM1 puncta formation near the plasma membrane, however, some STIM1 puncta were observed in the cytosol after FCCP treatment in both TG- or non-TG-treated cells (Fig. 4.3F), which could be due to its small transient Ca^{2+} release effect from mitochondria (Fig. 4.3G).
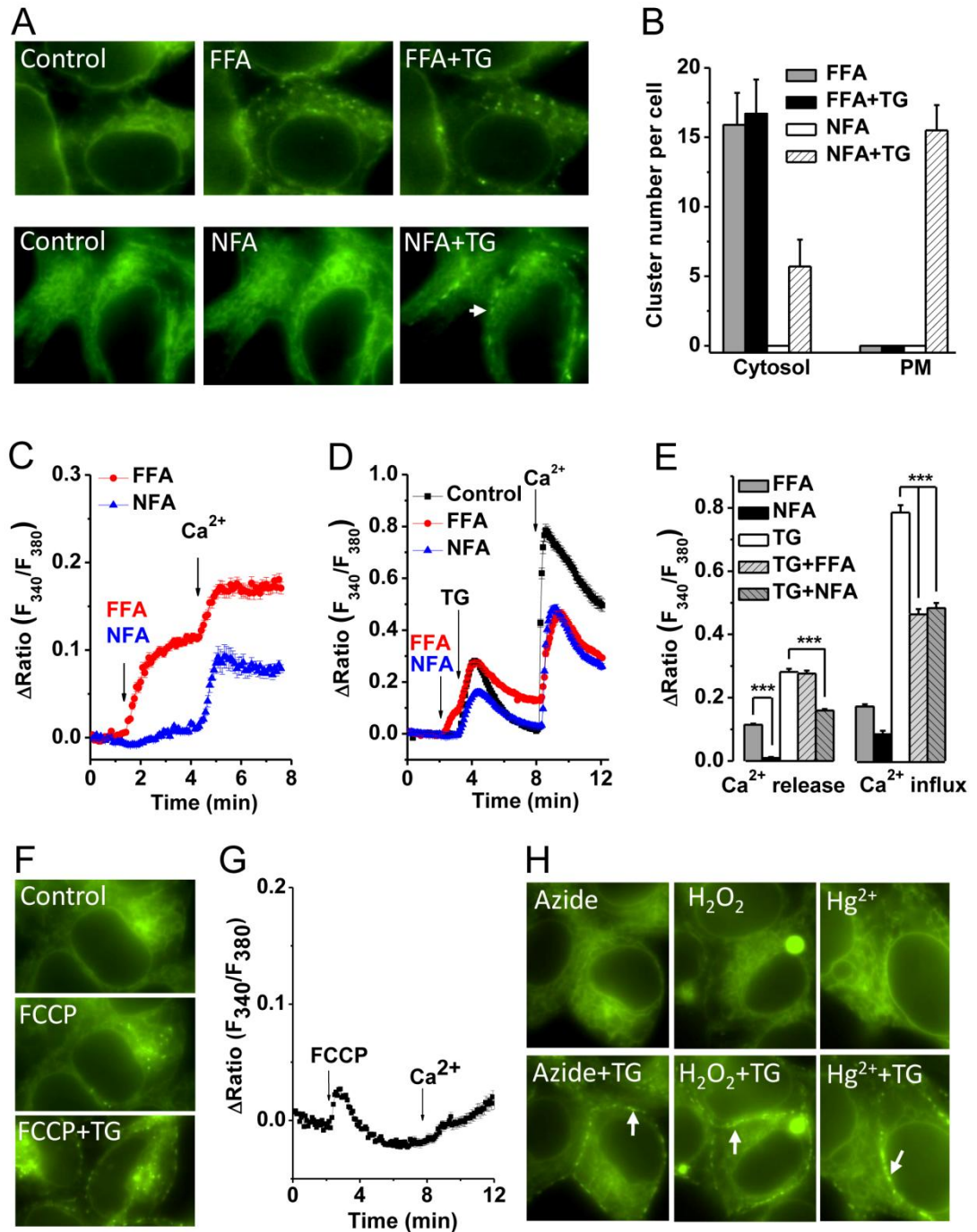
Fig. 4.3 Effects of flufenamic acid (FFA), niflumic acid (NFA) and mitochondrial metabolic inhibitors on STIM1 movement and store-operated Ca^{2+} entry in STIM1-EYFP cells. (A) FFA (100 µM) caused cytosolic STIM1 clustering and blocked TG-induced STIM1 subplasmalemmal translocation. NFA

(100 µM) did not change STIM1 localisation at resting state, but potentiated cytosolic STIM1 clustering after addition of TG (1 µM). (B) The number of STIM1 clusters induced by FFA or NFA before and after addition of 1 µM TG ($n = 10$ cells in each group). (C) FFA (100 µM) induced robust cytosolic Ca^{2+} increase in the absence of external Ca^{2+}, but NFA (100 µM) had no significant effect on Ca^{2+} release in the STIM1-EYFP cells. (D) Effect of FFA and NFA on TG-induced Ca^{2+} release and Ca^{2+} entry. The standard bath solution containing 1.5 mM Ca^{2+} was perfused after store depletion. (E) Comparison of Ca^{2+} release and Ca^{2+} influx induced by FFA (100 µM), NFA (100 µM) and TG (1 µM) ($n = 16\text{-}37$ cells in each group). (***$P<0.001$). (F) Example of FCCP (5 µM) induced cytosolic STIM1 clusters. (G) FCCP (5 µM) induced a small Ca^{2+} release ($n =26$). (H) Sodium azide (2.5 mM), H_2O_2 (500 µM) and Hg^{2+} (5 µM) did not alter TG (1 µM)-induced STIM1 puncta formation at the PM.
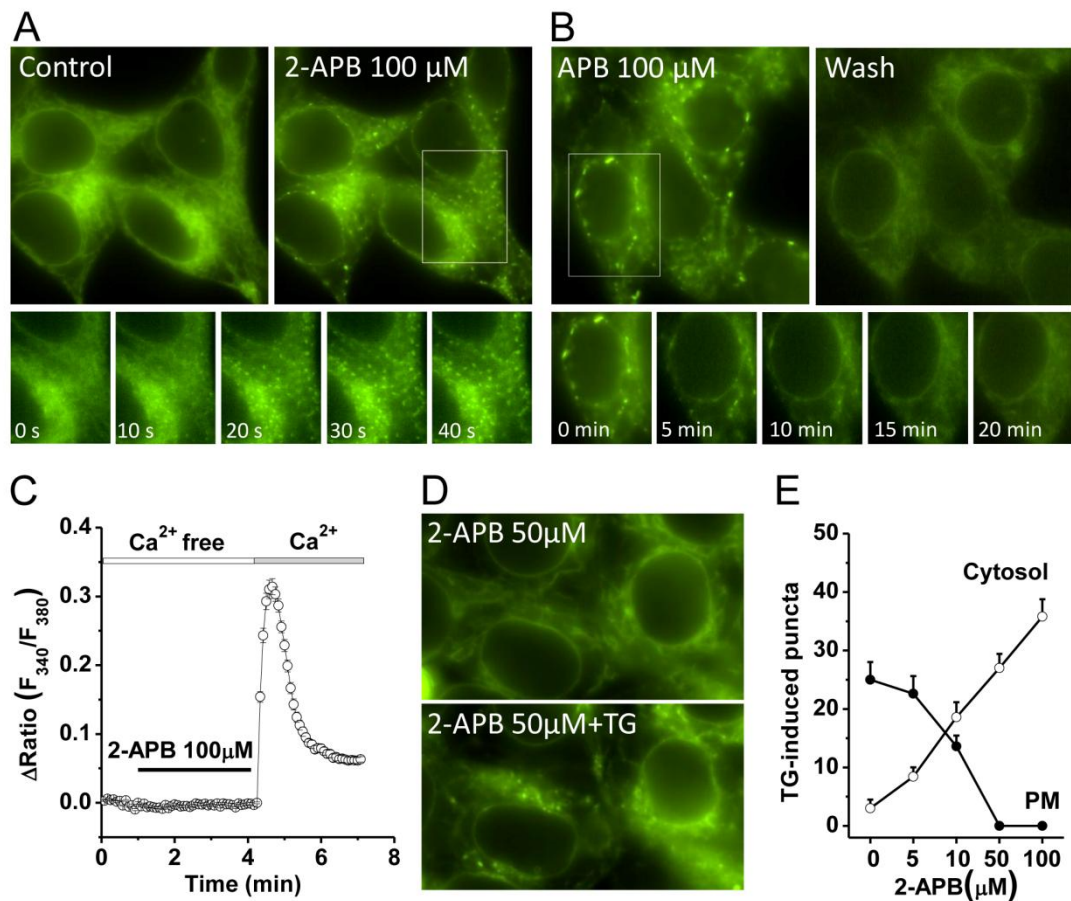
Fig. 4.4 2-APB induced STIM1 clustering in STIM1-EYFP cells. (A) Application of 100 µM 2-APB resulted in STIM1 clustering in the cytosol. Lower small figures show the time course of STIM1 clustering in the boxed area. (B) Cytosolic STIM1 clusters induced by 100 µM 2-APB were fully reversed after washing out for 20 min. (C) No effect of 2-APB (100 µM) on Ca^{2+} release in the STIM1-EYFP cells. (D) 2-APB (50 µM) blocked the STIM1 subplasmalemmal translocation after addition of 1 µM TG and caused cytosolic STIM1 clustering. (E) The mean ± SEM

data for the number of STIM1 at the PM or in the cytosol induced by TG (1 μM) in the absence or presence of 2-APB (5-100 μM) (n = 5 cells in each group).

Sodium azide is a potent inhibitor of mitochondrial respiration that blocks cytochrome c oxidase. Pretreament with sodium azide (2.5 mM) for 5 min did not change the TG-induced STIM1 subplasmalemmal translocation and clustering (Fig. 4.3H). Application of azide alone did not evoke STIM1 clustering and translocation. Moreover, the reagents affecting mitochondrial oxidative stress were examined. Incubating the cells with H_2O_2 (100-1000 μM) for 15 min did not evoke STIM1 clustering, and showed no effect on TG-induced STIM translocation (Fig. 4.3H). Mercury is a toxic heavy metal that causes severe mitochondrial oxidative damage leading to cell death, but STIM1 clustering and translocation showed no changes in the presence of Hg^{2+} (5 μM) for 10 min. Hg^{2+} also showed no effect on TG-induced STIM translocation and subplasmalemmal clustering (Fig. 4.3H). These data suggested the mitochondrial Ca^{2+} release is involved in the formation of cytosolic STIM1 clustering, as with FFA and FCCP, but the other inhibitors not affecting mitochondrial Ca^{2+} movement may have less or no direct effect on STIM1 movement.

4.2.4. Cytosolic STIM1 clustering induced by 2-APB in cells with replete ER Ca^{2+} store

2-APB is a non-specific blocker of SOCs with multiple effects on other cationic channels (Xu *et al.*, 2005a). 2-APB at 100 μM significantly induced STIM1 clustering in the cytosol in the absence of TG (Fig. 4.4A), and the clustering induced by 2-APB was reversible (Fig. 4.4B). In addition, 2-APB at 100 μM did not cause Ca^{2+} release (Fig. 4.4C), which suggests that the 2-APB-induced cytosolic STIM1 clustering is independent of Ca^{2+} store depletion. The inhibitory effect of 2-APB on TG-induced STIM1 translocation was also observed. 2-APB at low concentrations (5-50 μM) did not cause STIM1 clustering in the cells, but prevented the subplasmalemmal translocation and clustering evoked by 1 μM TG, and resulted in the retention of STIM1 puncta in the cytosol (Fig. 4.4D-E).

2-APB has been reported to inhibit ORAI1 and ORAI2, but activate ORAI3 channels (Peinelt *et al.*, 2008). To understand the difference, the effect of 2-APB on STIM1 movement was also investigated in STIM1/ORAI-coexpressing cells. 2-APB induced a small transient increase of ORAI1 and ORAI2 currents, which was followed by a sustained inhibition, but activated ORAI3 current (Fig. 4.5A).
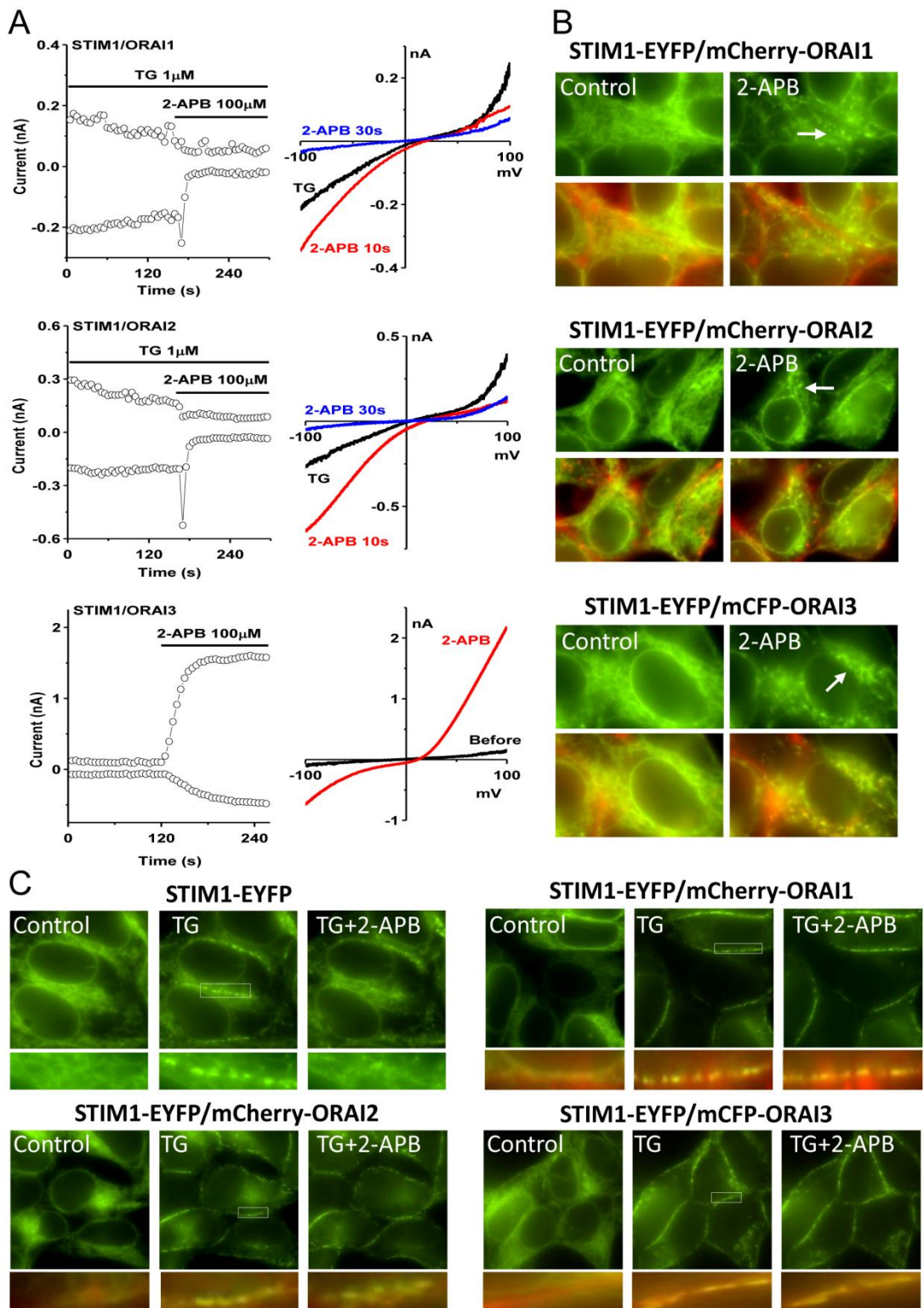
Fig. 4.5 Effects of 2-APB on STIM1/ORAI-coexpressing cells. (A) 2-APB (100 μM) transiently increased and then blocked the whole-cell currents of STIM1/ORAI1 and STIM1/ORAI2 cells. The current in STIM1/ORAI3 cells was substantially activated by 100 μM 2-APB. (B) 2-APB (100 μM) induced cytosolic STIM1 clustering in STIM1/ORAI1, STIM1/ORAI2 and STIM1/ORAI3 cells. The STIM1 only and STIM1/ORAI-merged images are shown. The mCFP fluorescence was converted into red pseudocolour in the merged images. (C) Application of 2-

APB (100 µM) disassembled the subplasmalemmal STIM1 clusters induced by TG (1 µM) in STIM1-EYFP cells, but no disassembling effect was observed in the STIM1-EYFP cells coexpressing mCherry-ORAI1, mCherry-ORAI2, or mCFP-ORAI3. The boxed area is amplified and shown under each corresponding picture with STIM1 clusters alone (green) or co-localised with ORAI channels (red) at the PM.

The *I-V* relationship of STIM1/ORAI1 and STIM1/ORAI2 induced by TG or STIM1/ORAI3 induced by 2-APB was similar to the report (Peinelt *et al.*, 2008). 2-APB-evoked cytosolic STIM1 clustering occurred in all the three cell lines coexpressing each ORAI isoform with STIM1 (Fig. 4.5B). However, the subplasmalemmal clusters induced by TG were disassembled by perfusion with 2-APB in the STIM1-EYFP cells, but 2-APB did not disassemble the subplasmalemmal clusters in the cells coexpressing STIM1 with ORAI channels (Fig. 4.5C).

4.2.5. Coexpression with TRPC1 does not affect cytosolic STIM1 clustering

The functional interaction of TRPC1 with STIM1 has been demonstrated (Pani *et al.*, 2009; Zeng *et al.*, 2008), implying the potential interference of STIM1 movement by TRPC1. The stable STIM1-EYFP cells were transfected with human TRPC1 tagged with mCFP. Like the localisation of STIM1-EYFP, the overexpressed mCFP-TRPC1 was mainly located in the cytosol, which is consistent with previous report (Gervasio *et al.*, 2008). The cytosolic STIM1 clusters induced by 2-APB were evident and the logarithmic fluorescence spectra showed many fluctuations by line-scan intensity analysis, but the TRPC1 did not show significant clusters after 2-APB treatment, although the distribution pattern of STIM1 and TRPC1 in the cells looked similar before the treatment of 2-APB (Fig. 4.6A). Moreover, the co-expression of TRPC1 did not change the TG-induced STIM1 subplasmalemmal translocation (Fig. 4.6B). These results suggest that the cytosolic TRPC1 does not form STIM1/TRPC1 complex in the cytosol or change the cytosolic STIM1 movement.
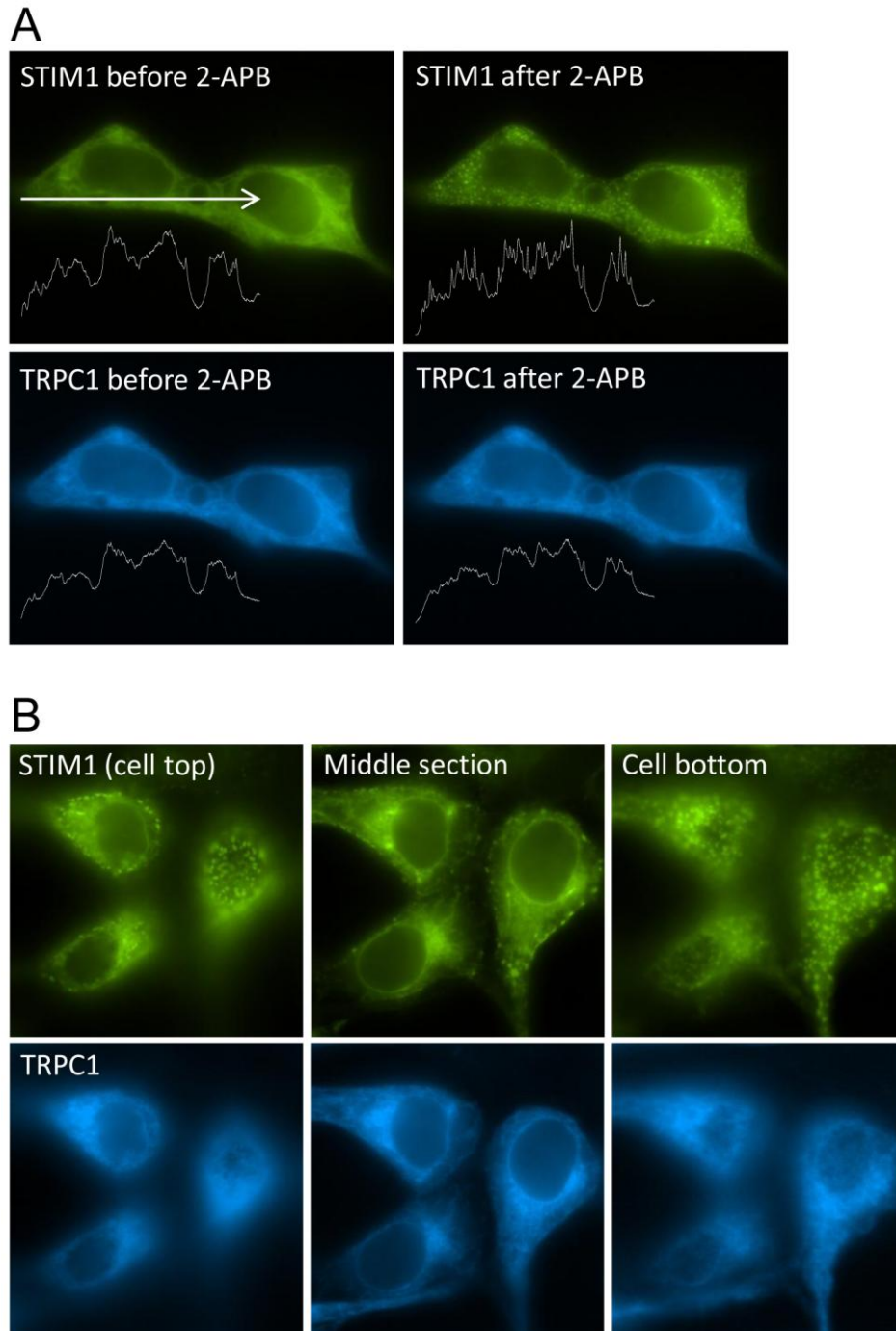
Fig. 4.6 Coexpression of TRPC1 does not affect 2-APB or TG-induced STIM1 clustering. (A) The localisation of STIM1-EYFP and mCFP-TRPC1 expressed in the same cells. The logarithmic fluorescence spectra show the florescence intensity of STIM1 (green) and TRPC1 (blue) of the arrow area using line-scan intensity software. Cytosolic STIM1 clusters induced by 2-APB (100 μM) and more small fluctuations were observed, but no more fluctuations for TRPC1. (B) TRPC1 did not translocate to and form puncta at the PM with STIM1 after TG (1 μM) treatment. The images focusing on the top, middle and bottom sections of the cells are shown.

4.2.6. Effects of other store-operated channel blockers on STIM1 movement

Since the formation of cytosolic STIM1 clusters is related to application of 2-APB, 4-CEP and FFA, and the three reagents are inhibitors of SOCs or cationic channels, I therefore examined other commonly used SOC blockers for pharmacological comparison. Both SKF-96365 and Gd^{3+} showed no effect on TG-induced STIM1 clustering and translocation (Fig. 4.7A-B). Pretreatment with diethylstilbestrol (DES, 10 μM), a potent inhibitor of I_{CRAC} and SOCE (Zakharov *et al.*, 2004), had no effect on STIM1 clustering and translocation (Fig. 4.7C). These results suggest that the blockade on SOCs or Ca^{2+} influx does not change the cytosolic STIM1 clustering, and also suggest the pharmacological difference on STIM1 movement among the modulators of SOCs.
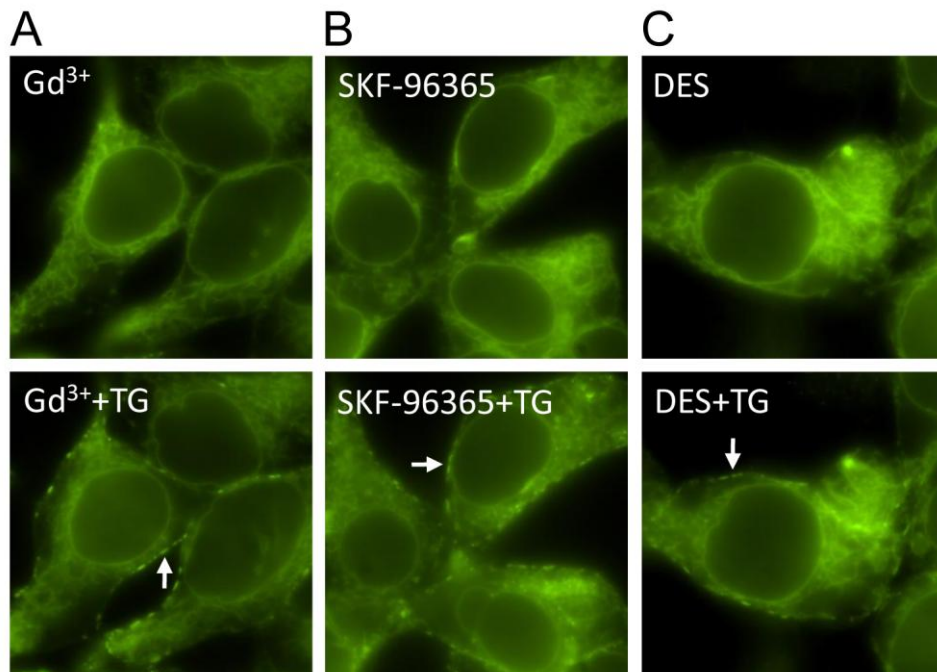
Fig. 4.7 Effect of store-operated Ca^{2+} channel blockers Gd^{3+}, SKF-96365 and diethylstilbestrol (DES) on STIM1 translocation. (A) Gd^{3+} (50 μM). (B) SKF-96365 (100 μM). (C) Diethylbestrol (DES) (10 μM). The STIM1 subplasmalemmal translocation (indicated by arrow) was induced by 1 μM TG.

4.2.7. Effects of signalling pathway modulators on STIM1 movement

STIM1 has been suggested as an important protein in regulating cell survival. It is unknown whether the pharmacological agents targeting to cell signalling pathways related to cell survival affect the STIM1 movement. Genistein at micromolar

concentrations has been regarded as a specific inhibitor for receptor tyrosine kinase (RTK) (Xu *et al.*, 2009b). Pretreatment with genistein (10 μM) for 5 min did not alter the STIM1 clustering and translocation toward PM evoked by store depletion (Fig. 4.8A). Incubation with phosphatidylinositol 3-kinase (PI$_3$K) inhibitor wortmannin (20 μM) for 30 min also showed no significant effect on TG-induced STIM1 translocation and clustering (Fig. 4.8B), suggesting the activity of RTK/PI$_3$K/Akt/mTOR pathway will not change the STIM1 movement.
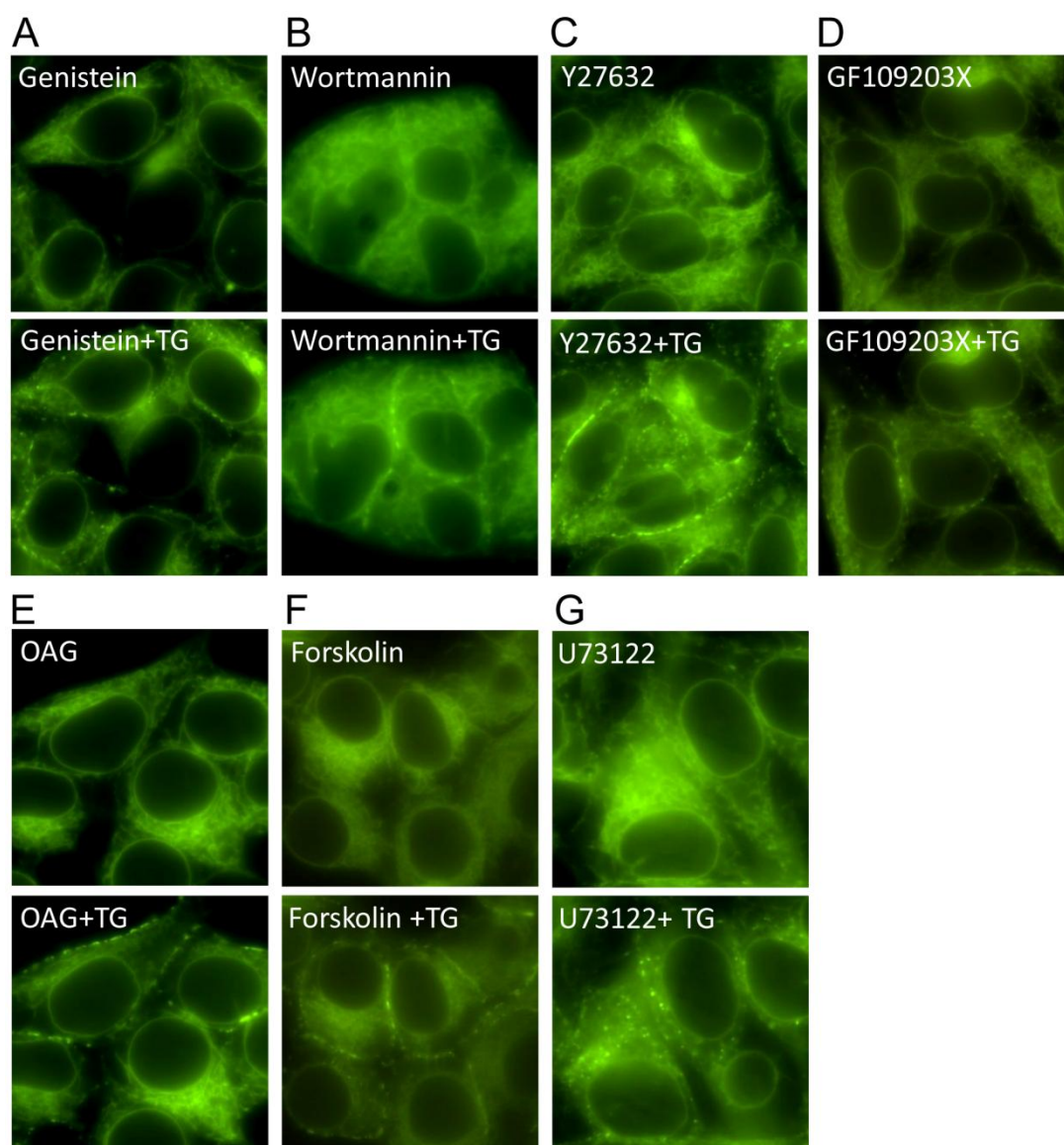
Fig. 4.8 Effect of signalling pathway regulators on TG-induced STIM1 translocation. (A) The protein tyrosine kinase (PTK) inhibitor genistein (10 μM). (B) Phosphatidylinositol 3-kinase (PI$_3$K) inhibitor wortmannin (20 μM). (C) Rho-associated protein kinase (ROCK) inhibitor Y-27632 (30 μM). (D) Protein kinase C (PKC) inhibitor GF109203X (30 μM). (E) PKC activator OAG (100 μM). (F) PKA activator forskolin (50 μM). (G) U73122 (10 μM) abolished TG-induced STIM1 translocation to the PM, and caused STIM1 clustering in the cytosol.

The RhoA/Rho kinase pathway has been implicated in various cellular functions including cytoskeleton reorganization, cell adhesion, motility and contraction and Y-27632 is a selective inhibitor of Rho-associated protein kinase (ROCK). Incubation with Y-27632 (30 µM) showed no effect on the TG-evoked STIM1 clustering and translocation (Fig. 4.8C).

The protein kinase C (PKC) inhibitor GF109203X (30 µM) and activator OAG (100 µM) were examined. Both of them did not change the TG-induced STIM1 movement (Fig. 4.8D-E). In addition, the protein kinase A (PKA) activator forskolin was also tested. Incubation with forskolin (50 µM) for 10 min did not cause cytosolic STIM1 clusters. Forskolin also had no effect on the TG-induced STIM1 translocation (Fig. 4.8F). Surprisingly, I found that the phospholipase C (PLC) inhibitor U73122 (10 µM) not only abolished TG-induced STIM1 translocation to the PM, but also caused STIM1 clustering in the cytosol (Fig. 4.8G). This unique effect of U73122 could be independent of the inhibition of PLC, because the TG-induced STIM1 translocation is unrelated to the PLC pathway.

4.2.8. Disruption of cytoskeleton does not prevent STIM1 translocation

Microtubules are filamentous polymers essential for cell viability and STIM1 has been shown to associate with the growth of microtubule ends (Grigoriev *et al.*, 2008), therefore, the involvement of cytoskeleton in STIM1 movement was examined. Incubation with CytD (10 µM) for 1 h, which inhibits actin polymerization (Patterson *et al.*, 1999), showed no effect on TG-induced STIM1 subplasmalemmal clustering and translocation (Fig. 4.9A), suggesting the actin is not directly involved in STIM1 movement. The effect of colchicine, a microtubule polymerization inhibitor, was also examined. Pretreatment of STIM1-EYFP cells with 100 µM colchicine for 30 min changed the cell morphology, but did not show any effects on TG-induced STIM1 subplasmalemmal clustering and translocation (Fig. 4.9A). The combined treatment with CytD and colchicine also showed no effect (Fig. 4.9A). However, the TG-induced SOCE was significantly reduced by the two agents (Fig. 4.9B-C). In addition, I found that the formation of cytosolic STIM1 clusters did not rely on cytoskeleton as well, because cells pretreated with CytD or colchicine showed the STIM1 clustering induced by 2-APB or 4-CEP similar to that in the untreated cells (Fig. 4.9D-E).
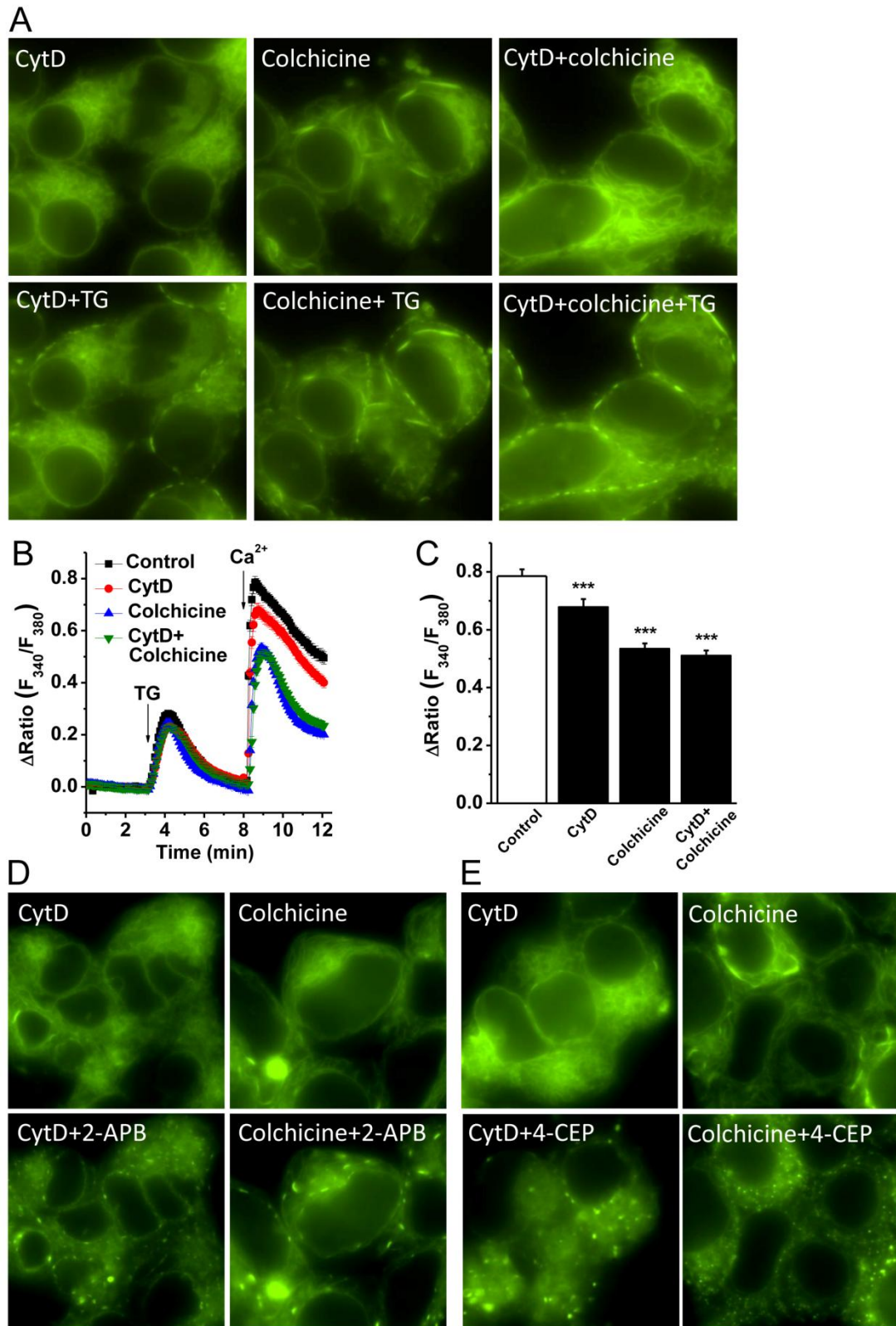
Fig. 4.9 Depolymerisation of cytoskeleton did not affect STIM1 clustering but reduced store-operated Ca²⁺ entry in STIM1-EYFP cells. (A) The cells were pretreated with 10 μM CytD for 1 h, or 100 μM colchicine for 30 min, or a combination of 10 μM CytD and 100 μM colchicine for 1 h. These procedures of cytoskeleton disruption did not prevent TG-induced STIM1 translocation. (B) The effects of CytD and colchicine on TG-induced Ca²⁺ release and Ca²⁺ entry ($n = 22$-

33 cells in each group). (C) CytD and colchicine significantly reduced TG-induced Ca^{2+} influx in STIM1-EYFP cells. (***P<0.001) (D) Pretreatment with CytD (10 μM, 1 h) or colchicine (100 μM, 30 min) did not affect cytosolic STIM1 clustering induced by 100 μM 2-APB in STIM1-EYFP cells. (E) Same as in (D), but 500 μM 4-CEP was used.

4.2.9. STIM1 subplasmalemmal translocation is inhibited by U73122 and calyculin A

It has been demonstrated that the cellular architecture of PM-ER junctions is the place for docking STIM1 clusters near PM and coupling to ORAI channels (Luik *et al.*, 2006). The PLC inhibitor U73122 at 1-10 μM has also been suggested to increase F-actin content (Kimata *et al.*, 2006; Scott *et al.*, 2005). Because the increase of F-actin is able to disrupt the PM-ER junctions and inhibit SOCE (Patterson *et al.*, 1999), I then examined this mechanism of U73122 on STIM1 movement. The STIM1-EYFP cells were cotransfected with Lifeact-mCFP cDNA, a marker to visualise F-actin (Riedl *et al.*, 2008). I found the fluorescence of Lifeact-mCFP at the PM was increased by U73122 (Fig. 4.10A), suggesting the accumulation of F-actin in the subplasmalemmal regions which spatially involve PM-ER junctions. The STIM1 subplasmalemmal translocation was blocked by the pretreatment of U73122, instead some STIM1 puncta in the cytosol (Fig. 4.10A). In cells pretreated with 10 μM CytD for 1 h to depolymerise F-actin filaments and then incubated with U73122 and TG, the TG-induced STIM1 subplasmalemmal translocation and puncta formation was restored (Fig. 4.10B-C), suggesting that the regulation of F-actin by U73122 is a novel mechanism for regulating SOC channels. In order to confirm the involvement of F-actin in the STIM1 translocation, calyculin A (CalyA), a serine/threonine phosphatase inhibitor that can disrupt the PM-ER junctions by increasing F-actin content, was also used (Lee *et al.*, 2005b; Patterson *et al.*, 1999). The STIM1-EYFP cells incubated with CalyA (10 nM) for 10 min showed no STIM1 subplasmalemmal translocation after TG treatment. Pretreatment with 10 μM CytD for 1 h abolished the effect of CalyA (Fig. 4.10B-C). Moreover, U73122 significantly reduced the SOCE, but had no effect on the amplitude of TG-induced Ca^{2+} release (Fig. 4.10D). Pretreatment with CytD partially reversed the inhibitory effect of U73122, but the Ca^{2+} entry was still much less than that in cells challenged with TG alone (Fig. 4.10F). CalyA treatment did not affect TG-induced Ca^{2+} release, and showed an effect on Ca^{2+} entry similar to that of U73122 (Fig. 4.10E-F).
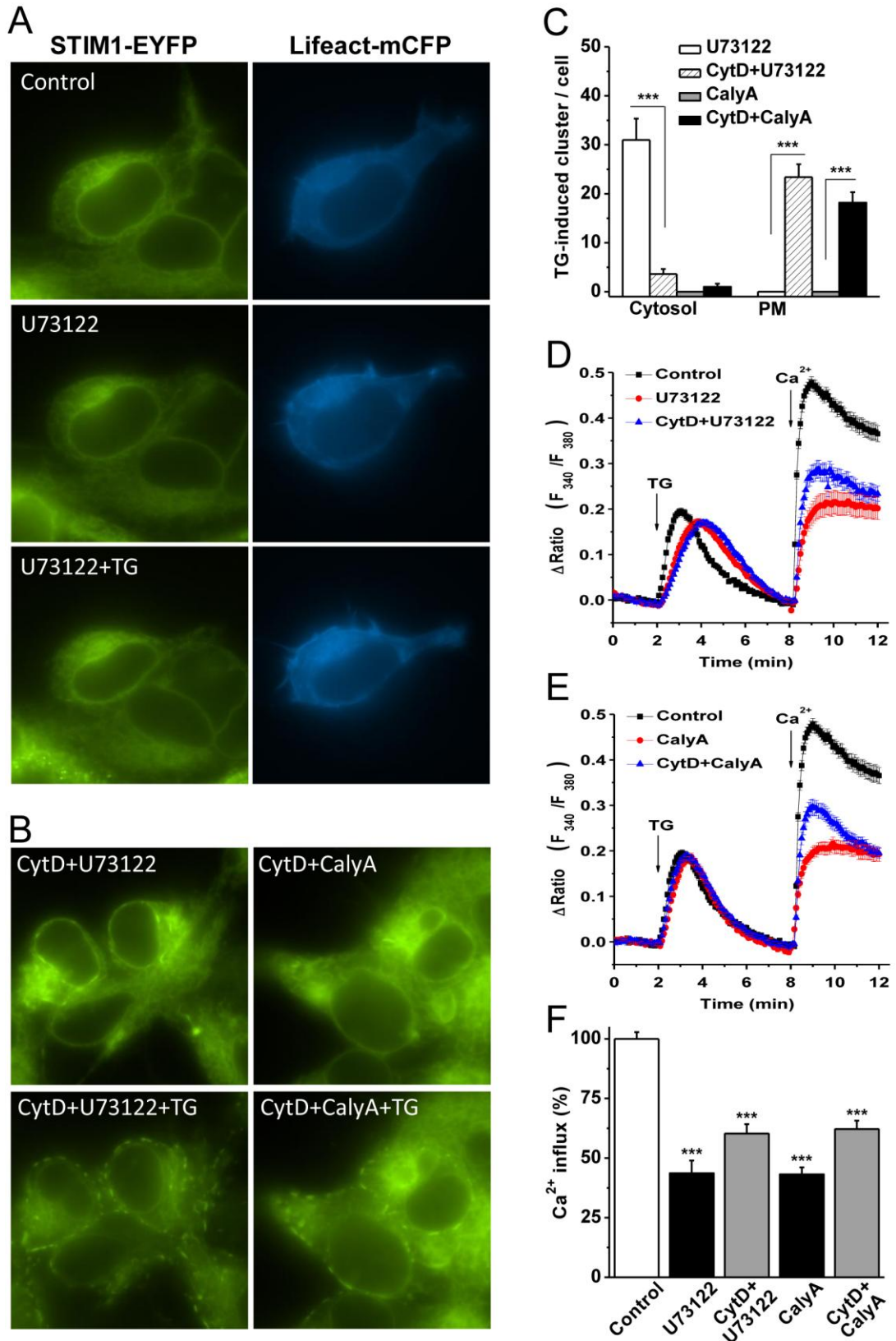
Fig. 4.10 Increase of F-actin content blocked TG-induced STIM1 translocation toward the PM and inhibited store-operated Ca²⁺ entry in STIM1-EYFP cells.
(A) U73122 (10 μM) increased the F-actin content marked as Lifeact-mCFP (blue) in the STIM1-EYFP cells cotransfected with Lifeact-mCFP. The TG-induced STIM1 clustering and subplasmalemmal translocation were prevented by U73122.

(B) Pretreatment with CytD abolished the effect of U73122 (10 μM) and CalyA (10 nM) on STIM1 movement. (C) The number of TG-induced STIM1 clusters in the cytosol and the PM in the presence of U73122 (10 μM) or CalyA (10 nM), with or without CytD (10 μM) pretreatment ($n = 10$ cells in each group). (D) U73122 (10 μM) inhibited TG-induced Ca^{2+} entry that was partially reversed by CytD pretreatment ($n = 19$-27 cells in each group). (E) CalyA (10 nM) inhibited TG-induced Ca^{2+} entry and partially reversed by CytD ($n = 21$-25 cells in each group). (F) Mean ± SEM data show the comparison of TG-induced Ca^{2+} influx among the groups treated with U73122, CalyA and CytD (***$P < 0.001$).

4.3. Discussion

4.3.1. ER Ca^{2+} store modulators and STIM1 translocation

Since the discovery of STIM1 as an essential component of SOCs, the coupling mechanisms of STIM1 to the pore-units of SOCs in the PM have been described and the ER Ca^{2+} store depletion is an essential step for STIM1 movement, such as by the application of SERCA blockers TG and cyclopiazonic acid (Zhang *et al.*, 2005; Liou *et al.*, 2005), or through IP_3R activation by many GPCR agonists including carbachol (Smyth *et al.*, 2008) and ATP/UTP (Chvanov *et al.*, 2008; Ross *et al.*, 2007). To further confirm the ER-dependent mechanism, I examined the ryanodine-sensitive Ca^{2+} store in this study. The Ca^{2+} release induced by RyR agonists also evoke STIM1 subplasmalemmal translocation, suggesting that STIM1 translocation can be regulated by the cooperation of the intracellular Ca^{2+} release channel IP_3Rs and RyRs. This finding could be an explanation of SOCs activated by RyR activators seen in some studies (Fellner and Arendshorst, 2000). In addition, I noticed the difference of the two RyR agonists, 4-CEP and caffeine, on cytosolic STIM1 clustering, Ca^{2+} release and Ca^{2+} influx. The concentration of 4-CEP used in this study is similar to the report on Ca^{2+} release (Islam *et al.*, 1998). 4-CEP at this concentration may cause membrane depolarization (Westerblad *et al.*, 1998), however, STIM1 movement is independent of extracellular Ca^{2+}, which suggests the contribution of membrane depolarization-induced Ca^{2+} influx, mainly through voltage-gated Ca^{2+} channels, should be very little. RyR antagonist tetracaine can prevent the Ca^{2+} release and STIM1 subplasmalemmal translocation induced by 4-CEP, but the cytosolic STIM1 clustering is still present, suggesting that the cytosolic STIM1 clustering is an ER Ca^{2+} store-independent mechanism.

4.3.2. Store-operated channel blockers and STIM1 movement

The existence of ER Ca^{2+} store-independent mechanism for cytosolic STIM1 clustering is also confirmed by the application of 2-APB. 2-APB at high concentrations inhibits IP_3Rs and blocks the IP_3-evoked ER Ca^{2+} release. Therefore the ER store should be regarded as non-depleted or filled. However, the STIM1 clustering can be quickly (~10 s) induced by 2-APB and the STIM1 puncta are retained in the cytosol without subplasmalemmal translocation. 2-APB at high concentrations has been shown to inhibit SERCA (Bilmen *et al.*, 2002), however I have not observed any Ca^{2+} release signal induced by 2-APB at 100 µM. In addition, the STIM1 translocation induced by SERCA blocker is a slow process with 1-2 min delay, however the cytosolic clusters induced by 2-APB induced is a fast process, which suggests that the effect of 2-APB on STIM1 clustering is unrelated to the SERCA inhibition. These findings further suggest that the 2-APB-induced STIM1 clustering is an ER store-independent process. I also observed that 2-APB at lower concentrations (10 and 50 µM) prevented the TG-induced STIM1 subplasmalemmal translocation, which is consistent with the recent report (He *et al.*, 2012). The detailed mechanism of cytosolic STIM1 clustering is still unclear, but it could be unrelated to the inhibition on Ca^{2+} influx, because other SOC blockers Gd^{3+}, SKF96365 and DES without ER Ca^{2+} store releasing effect do not induce cytosolic STIM1 clustering. It is also unrelated to the coexpression of TRPC1 and ORAI channels, because the two associated proteins do not change the pattern of cytosolic STIM1 clustering, although the ORAI channel coexpression can stabilize the subplasmalemmal clusters of STIM1/ORAI complexes.

4.3.3. Mitochondrial Ca^{2+} release and STIM1 clustering

FFA is a fenamate anti-inflammatory drug with a mitochondrial Ca^{2+} release effect, but has less effect on ER Ca^{2+} release (Tu *et al.*, 2009; Jiang *et al.*, 2012). In this study I found that FFA induced cytosolic STIM1 clustering, but its analogue NFA without affecting mitochondrial Ca^{2+} release did not cause cytosolic STIM1 clustering, further suggesting that the cytosolic STIM1 clustering is independent of ER store depletion, but the mitochondrial Ca^{2+} release could be related to cytosolic STIM1 clusters. To further confirm this, I tested the inhibitors of mitochondrial respiratory phosphorylation chain and metabolic pathways. FCCP, a mitochondrial uncoupler, causes STIM1 clustering in the cytosol, which could be due to the

mitochondrial Ca^{2+} release effect (Gurney *et al.*, 2000), however, FCCP does not block the TG-induced the STIM1 translocation. Similarly, the TG-induced STIM1 translocation cannot be prevented by oligomycin and antimycin A (Singaravelu *et al.*, 2011). Sodium azide, H_2O_2 and Hg^{2+} are mitochondrial metabolic inhibitors, however, acute application of these agents have no significant effect on STIM1 clustering and translocation, further suggesting that the agents only affecting mitochondrial Ca^{2+} release may change the intracellular STIM1 movement.

4.3.4. Signalling pathways and STIM1 translocation

The signalling pathway modulators of PTK and PI$_3$K, PKC and ROCK pathways have been examined in this study and no significant effects on TG-induced STIM1 movement are found, which is similar to the previous report (Smyth *et al.*, 2008). I have not tested those inhibitors on the STIM1 puncta induced by GPCR activation, because unlike TG-induced STIM1 clustering and subplasmalemmal translocation, the STIM1 puncta or movement induced by GPCR activation is transient and difficult to be quantified precisely.

4.3.5. Cytoskeleton and STIM1 movement

The importance of PM-ER junctions in the activation of SOCs has been described (Carrasco and Meyer, 2011). The increase of F-actin content in the PM-ER junctional regions resulted in the inhibition of SOCE (Lee *et al.*, 2005b; Patterson *et al.*, 1999). Both CalyA and U73122 are PM-ER disruptors by condensation of F-actin in the region. The inhibition of SOCE by U73122 and CalyA could be explained by the interruption of PM-ER junctions by the inhibition of STIM1 subplasmalemmal translocation, which leads to the uncoupling of STIM1 with the SOCs in the PM. However, other mechanisms for U73122 and CalyA may also exist, because the restoration of STIM1 translocation by CytD only partially recovered their inhibition on the SOCE. Moreover, I also examined the involvement of cytoskeleton in the STIM1 movement. CytD significantly inhibits SOCE in the STIM1-EYFP transfected cells, which is consistent to the observations in platelets (Harper and Sage, 2007), polymorphonuclear neutrophil (Itagaki *et al.*, 2004), hepocytes (Wang *et al.*, 2002), and vascular endothelial cells (Holda and Blatter, 1997), but no or increasing effects were reported in A7r5 cells, glioma C6 cells and transfected HEK293 cells (Sabala *et al.*, 2002; Galan *et al.*, 2011; Patterson *et al.*,

1999). I found that the TG-induced SOCE was inhibited by CytD in STIM1-EYFP cells; however, CytD had no effect on the TG-induced STIM1 movement. In this study, CytD at 10 μM was used, because a significant cell death occurred at the concentration of 100 μM, although this concentration was used in the A7r5 cells (Patterson *et al.*, 1999). The rearrangement of microtubules in the regulation of SOCE has also been demonstrated by the application of colchicine (Hajkova *et al.*, 2010; Galan *et al.*, 2011; Smyth *et al.*, 2007), however, colchicine has no effect on TG-induced STIM1 movement. In addition, disruption of lipid rafts in the PM does not change the STIM1 movement (DeHaven *et al.*, 2009).
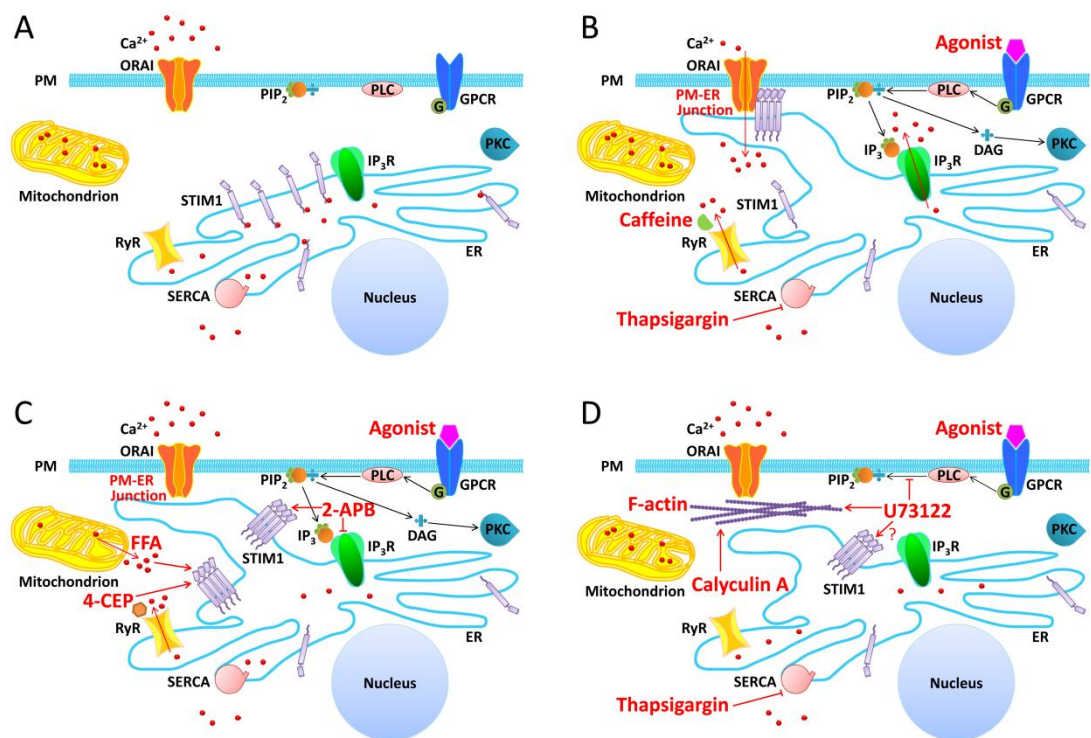
Fig. 4.11 Models for pharmacological regulation of STIM1 translocation and clustering. (A) STIM1 at resting state. (B) ER Ca^{2+} store-dependent STIM1 clustering and translocation to the newly formed PM-ER junction and Ca^{2+} influx through ORAI channel, which are induced by ER Ca^{2+} store depletion by GPCR agonist, thapsigargin or caffeine. (C) ER Ca^{2+} store-independent STIM1 clustering in the cytosol. 2-APB inhibits ER Ca^{2+} release through IP_3R and induces cytosolic STIM1 clustering. FFA and 4-CEP release Ca^{2+} from mitochondrion and ER respectively, and cause the formation of cytosolic STIM1 clusters. (D) U73122 blocks the activity of PLC, increases the cellular F-actin content and potentiates cytosolic STIM1 clustering in the presence of thapsigargin. Calyculin A also increases the F-actin content, prevents the formation of PM-ER junction and STIM1 translocation toward the PM.

4.4. Conclusions

In this study, it is confirmed that STIM1 translocation and clustering is regulated by ER Ca^{2+} store, and the extracellular Ca^{2+} level is not the determinant for this process. I found two patterns of STIM1 clustering in the cells that can be pharmacologically distinguished, i.e, subplasmalemmal clusters and cytosolic clusters. The subplasmalemmal clusters are mainly formed by STIM1 translocation after passive or active ER Ca^{2+} store depletion, whilst the cytosolic STIM1 clustering is specific for some drug effects, such as 2-APB, FFA, 4-CEP, U73122 and FCCP. The formation of cytosolic STIM1 clusters is independent of the ER Ca^{2+} store. In addition, increased content of F-actin in the PM-ER junctions by U73122 and CalyA blocks the STIM1 subplasmalemmal translocation. The proposed models for STIM1 movement are given in Fig. 4.11. The cytosolic STIM1 clustering independent of ER Ca^{2+} store discovered in this study is a new mechanism for the pharmacology of some channel blockers, which could be a useful target for future drug development.

Chapter 5

The Ryanodine Receptor Agonist 4-Chloro-3-Ethylphenol is a Non-Selective Blocker of ORAI and TRPC Channels

5.1. Introduction

Ca^{2+} is a second messenger that regulates a wide variety of physiological functions in human body. The cytosolic Ca^{2+} level is tightly controlled by Ca^{2+}-permeable channels residing in the plasma membrane and membranes of intracellular Ca^{2+} stores. Apart from IP_3 receptors (IP_3Rs), ryanodine receptors (RyRs) are another major class of ER/SR Ca^{2+} release channels. The RyR family consists of three members, RyR1-3, which are differentially expressed in many cell types including both electrically excitable and non-excitable cells (Lanner *et al.*, 2010). It has been demonstrated that activation of RyRs by ryanodine or repetitive depolarisation induced store-operated Ca^{2+} entry (SOCE) and Ca^{2+} release-activated current (I_{CRAC}) in smooth muscle and skeletal muscle cells, respectively (Fellner and Arendshorst, 2000; Yarotskyy and Dirksen, 2012), suggesting the functional coupling between RyRs and store-operated channels (SOCs) in excitable cells.

Chlorophenols and their derivatives are generally used as bactericides, fungicides or preservatives. Some of these compounds, including 4-chloro-3-ethylphenol (4-CEP) and 4-chloro-*m*-cresol (4-C*m*C) (Fig. 5.1), have been found to induce intracellular Ca^{2+} release by stimulating the RyRs (DiJulio *et al.*, 1997; Islam *et al.*, 1998; Westerblad *et al.*, 1998; Jacobson *et al.*, 2006), whlist their analogue 4-chlorophenol (4-ClP) (Fig. 5.1) is ineffective in triggering Ca^{2+} release through RyRs (Jacobson *et al.*, 2006). The activity of RyRs is considered particularly important in excitable cells such as cardiac and skeletal muscle cells. In these cells, Ca^{2+} entry through dihydropyridine receptor ($Ca_v1.1$, a voltage-gated L-type Ca^{2+} channel), which results in the depolarization of membrane potential, and subsequent Ca^{2+} release from the sarcoplasmic reticulum (SR), are believed to be the triggering mechanism of muscle contraction. This process, referred as excitation–contraction (EC) coupling, essentially relies on the activity of RyRs (Endo, 2009). RyR1 is the primary isoform expressed in skeletal muscles (Zorzato *et al.*, 1990; Lanner, 2012). The dysfunction of RyR1 has been associated with muscular or muscle-related diseases, such as central core disease (CCD) and malignant hyperthermia (MH). Patients affected by CCD or MH are mostly found to bear mutations in RyR1, which increase the sensitivity of the channel to anaesthetics and depolarizing muscle relaxants, such as halothane and succinylcholine (Robinson *et al.*, 2006). When the patients are exposed to such agents in general anaesthesia, drastic SR Ca^{2+} release and hypermetabolic responses including very high body temperature, tachycardia,

rigid muscles and rhabdamyolysis will be induced, which could be fatal if not treated quickly (Stowell, 2008). 4-CEP and 4-C*m*C have been used to test human and animal samples for malignant hyperthermia *in vitro* (Gerbershagen *et al.*, 2002; Gerbershagen *et al.*, 2005; Herrmann-Frank *et al.*, 1996; Baur *et al.*, 2000). 4-C*m*C was shown to trigger malignant hyperthermia in susceptible swine but not normal animals (Iaizzo *et al.*, 1999; Wappler *et al.*, 1999). These studies suggest that both 4-CEP and 4-C*m*C are useful tools in the diagnosis of malignant hyperthermia.

In Chapter 4, I found that the RyR sensitiser caffeine evoked Ca^{2+} release and SOCE in STIM1-overexpressing HEK293 cells. The RyR agonist 4-CEP also induced a robust Ca^{2+} release, but the following Ca^{2+} influx was completely abolished. This unexpected result implies that 4-CEP may be an inhibitor of SOCs, which is additive to its role as a RyR agonist. Indeed, as I have demonstrated in Chapter 4, 4-CEP triggers not only the formation of STIM1 puncta at the plasma membrane, but also cytosolic STIM1 clustering in the STIM1-overexpressing cells. In addition, it is also possible that 4-CEP may block Ca^{2+}-permeable channels in the plasma membrane directly. To address this question, I investigated the effects of 4-CEP on the activities of ORAI and TRPC channels, and compared the effects with the two analogues, 4-C*m*C and 4-ClP.
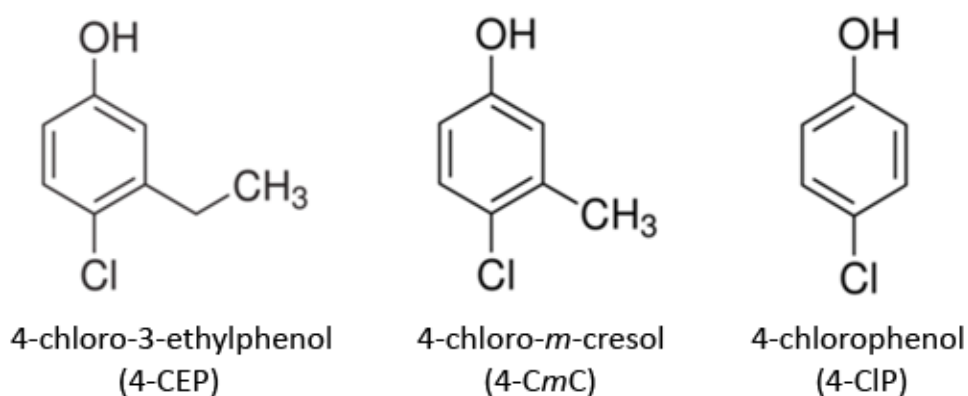
Fig. 5.1 Chemical structures of 4-chloro-3-ethylphenol (4-CEP), 4-chloro-*m*-cresol (4-C*m*C) and 4-chlorophenol (4-ClP).

5.2. Results

5.2.1. Effects of 4-CEP, 4-CmC and 4-ClP on Ca^{2+} release and SOCE in STIM1/ORAI1-coexpressing HEK293 cells

To characterise the functional contribution of RyRs in T-REx HEK293 cells overexpressing STIM1-EYFP and mCFP-ORAI1, 4-CEP (500 μM) was applied to the cells in Ca^{2+}-free solution. A robust Ca^{2+} release was observed immediately after the application of 4-CEP (Fig. 5.2A). In contrast, the cells exposed to 500 μM 4-CmC or 500 μM 4-ClP did not show any Ca^{2+} release signals (Fig. 5.2A). The differential responses to 4-CEP and 4-CmC suggest that the dominant isoform of RyRs expressed in these cells is most probably RyR3, because RyR3 is substantially activated by 4-CEP but almost insensitive to 4-CmC (Venkatachalam et $al.$, 2003; Hopkins, 2011). The effect on Ca^{2+} influx was also examined. As shown in Fig. 5.2A, Ca^{2+} influx in the 4-CEP-treated cells was nearly abolished after the addition of external Ca^{2+}, which is similar to the observation in the STIM1-overexpressing cells (Chapter 4, Fig. 4.2C). In 4-CmC-treated cells the Ca^{2+} influx was much higher than that in the 4-CEP group, but lower than that in the cells treated with 4-ClP (Fig. 5.2A and C). To further investigate the effect of 4-CEP, it was used together with thapsigargin (TG) to examine the Ca^{2+} release and SOCE in STIM1/ORAI1 cells. As expected, the application of 500 μM 4-CEP significantly increased the Ca^{2+} release signal, which was higher than the Ca^{2+} release evoked by 1 μM TG (Fig. 5.2B-C). However, the subsequent Ca^{2+} influx was completely inhibited in the 4-CEP/TG group (Fig. 5.2B-C). These results confirmed the role of 4-CEP as an inhibitor of SOCs. The inhibition of TG-induced SOCE by 4-CEP was found to be dose-dependent, with a 50% inhibitory concentration (IC$_{50}$) of 203.6 μM (Fig. 5.2D). In addition, 4-CmC and 4-ClP also showed dose-dependent inhibition on TG-induced SOCE with the IC$_{50}$ of 830.9 μM and 1437.1 μM, respectively (Fig. 5.4D).
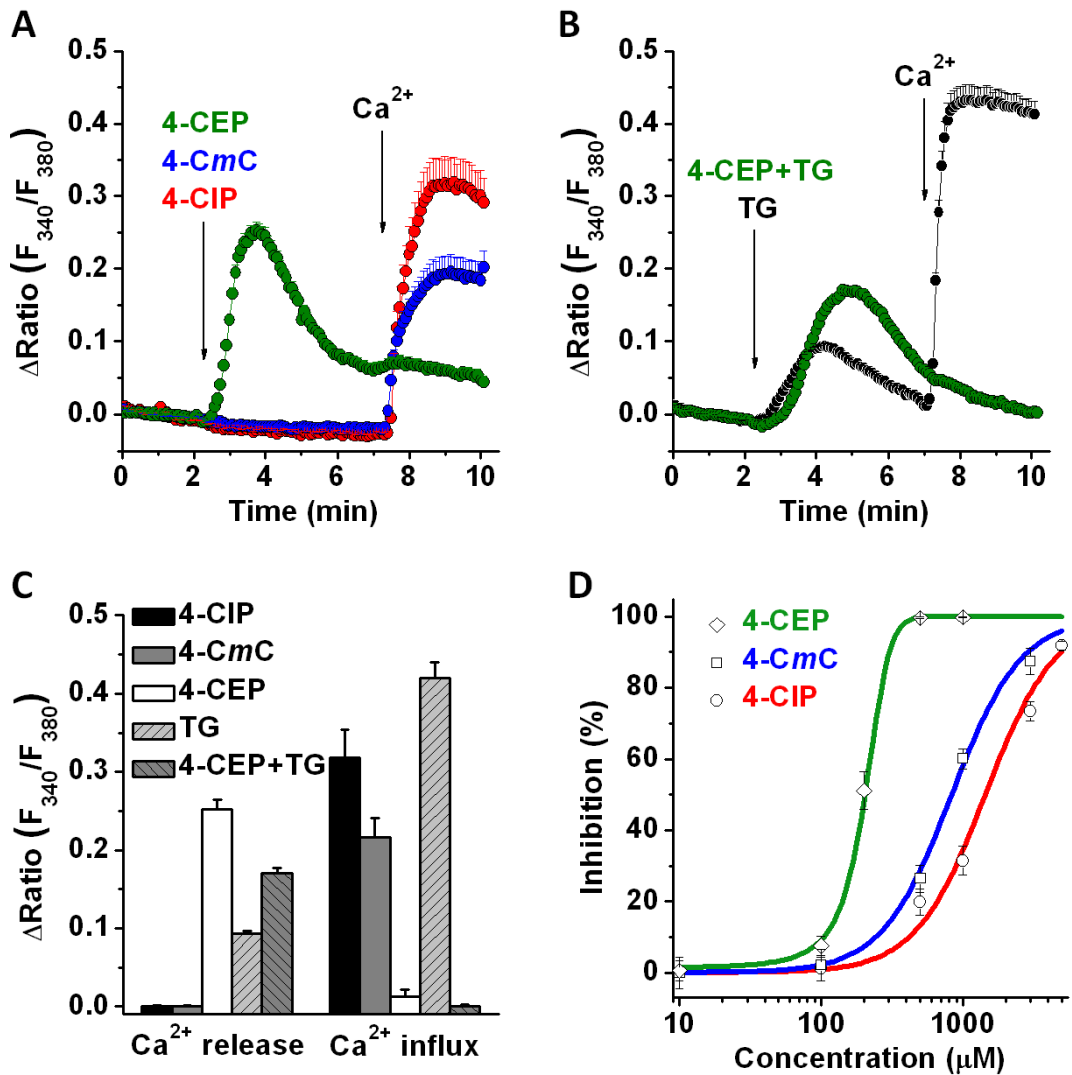
Fig. 5.2 The effects of 4-CEP, 4-C*m*C and 4-ClP on the Ca^{2+} release and store-operated Ca^{2+} entry in STIM1/ORAI1-coexpressing HEK293 cells. (A) The effects of 4-CEP, 4-C*m*C and 4-ClP (500 μM) on the cytosolic Ca^{2+} levels of STIM1/ORAI1 cells. The cells were maintained in Ca^{2+} free solution at first and then perfused with each drug in Ca^{2+} free and 1.5 mM Ca^{2+} solution as indicated by the arrows. (B) 4-CEP (500 μM) abolished TG (1 μM)-induced Ca^{2+} influx in STIM1/ORAI1 cells. (C) Comparison of the maximum amplitudes of Ca^{2+} release and influx induced by 4-ClP, 4-C*m*C, 4-CEP and TG in STIM1/ORAI1 cells (*n* = 18-26 cells in each group). (D) Dose-response curves of 4-CEP, 4-C*m*C and 4-ClP on the inhibition of store-operated Ca^{2+} entry in STIM1/ORAI1 cells (*n* = 17-29 cells for each point). The cells were pretreated with 1 μM TG for 30 min and then cytosolic Ca^{2+} were measured using the protocol in (A). The IC$_{50}$ of 4-CEP, 4-C*m*C and 4-ClP are 203.6, 830.9 and 1437.1 μM, respectively.
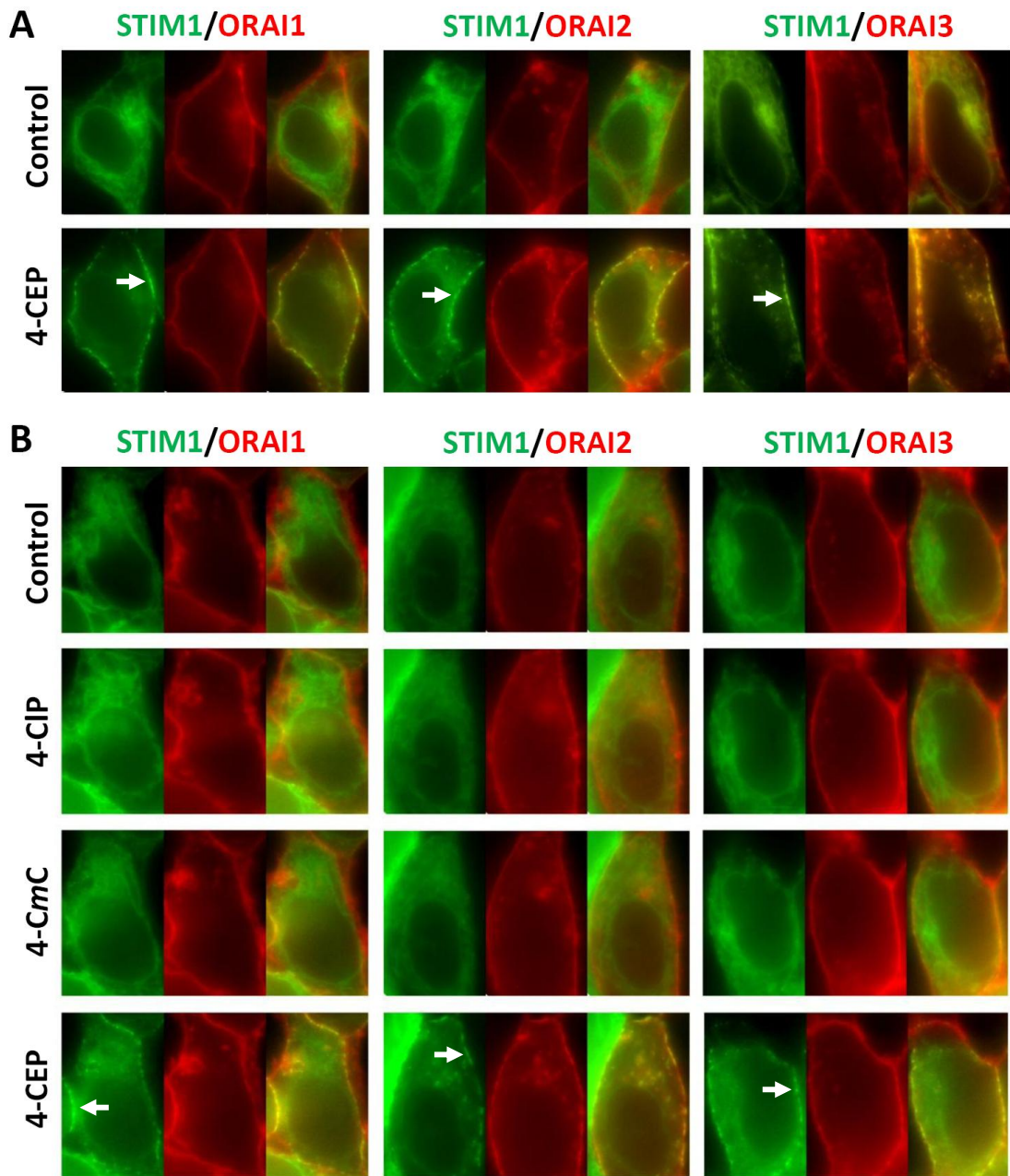
Fig. 5.3 4-CEP, but not 4-C*m*C and 4-ClP, induces STIM1 translocation in STIM1/ORAI1-3 cells. (A) Direct application of 500 µM 4-CEP induced persisted STIM1 puncta at the plasma membrane in STIM1-EYFP/mCFP-ORAI1-3 cells, whilst cytosolic clustering of STIM1 was not observed. The mCFP fluorescence was converted into red pseudocolour in the pictures. (B) The cells were successively challenged with 500 µM 4-ClP, 4-C*m*C and 4-CEP in 1.5 mM Ca^{2+} solution. Only 4-CEP induced STIM1 puncta at the plasma membrane. The STIM1 puncta are indicated by arrows.

5.2.2. 4-CEP, but not 4-C*m*C and 4-ClP, induces STIM1 translocation in STIM1/ORAI cells

In Chapter 4, I found 4-CEP induced STIM1 translocation to the plasma membrane at first, and then the formation of cytosolic STIM1 clusters in cells overexpressing

STIM1-EYFP alone. However, there was difference for such phenomenon in the STIM1/ORAI-coexpressing cells. The initial phase of STIM1 puncta formation at the plasma membrane was reproducible in the STIM1-EYFP/mCFP-ORAI1 cells after the exposure to 500 µM 4-CEP in Ca^{2+} solution. However, these puncta did not disappear, and there were almost no STIM1 clusters in the cytosol (Fig. 5.3A). A similar phenomenon was observed in STIM1-EYFP/mCFP-ORAI2 and STIM1-EYFP/mCFP-ORAI3 cells (Fig. 5.3A). These results suggest that the STIM1/ORAI complex is more stable than STIM1 oligomers, which is in consistent with the conclusion from the 2-APB experiments in Chapter 4. Furthermore, the persistence of STIM1/ORAI complexes implies that the STIM1 proteins may still be active to open ORAI channels, and the inhibition of SOCE by 4-CEP could be a direct action on ORAI channels. The effect of 4-C*m*C and 4-ClP was also tested in STIM1/ORAI1-3 cells. 4-ClP and 4-C*m*C at 500 µM failed to induce STIM1 translocation in all the three cell lines, whereas the subsequent perfusion of 500 µM 4-CEP clearly potentiated the formation of STIM1 puncta at the plasma membrane (Fig. 5.3B). These results are in accordance with the different abilities of these three drugs in triggering Ca^{2+} release from internal stores.

5.2.3. Inhibition of ORAI channels by 4-CEP, 4-C*m*C and 4-ClP

In STIM1/ORAI1-coexpressing cells, extracellular application of 1 µM TG elicited a store-operated current exhibiting distinct properties at different time points (Fig. 5.4A). A typical TRPC-like "*N*-shape" *I-V* curve was gradually developed after the addition of TG, and then both the inward and outward currents decreased to a medium level, showing a transitional type of *I-V* curve between the "*N*-shape" and the inward-rectifying shape. The currents kept decreasing and an I_{CRAC}-like inward-rectifying *I-V* curve was observed ~3 min after the occurrence of "*N*-shape" *I-V* curve. The dynamic changing of *I-V* curves was also observed in STIM1/ORAI1-3 cells with Ca^{2+} stores depleted by 1 µM TG in the internal solution, as shown by representative *I-V* curves with variable shapes in Fig. 5.4B-J. The store-operated currents induced in these cells were substantially inhibited by 500 µM 4-CEP in the bath solution without regard to the types of *I-V* curves (Fig. 5.4B-D). The currents were also inhibited by 500 µM 4-C*m*C and 4-ClP, and the residual currents could still be inhibited by 500 µM 4-CEP (Fig. 5.4E-J).
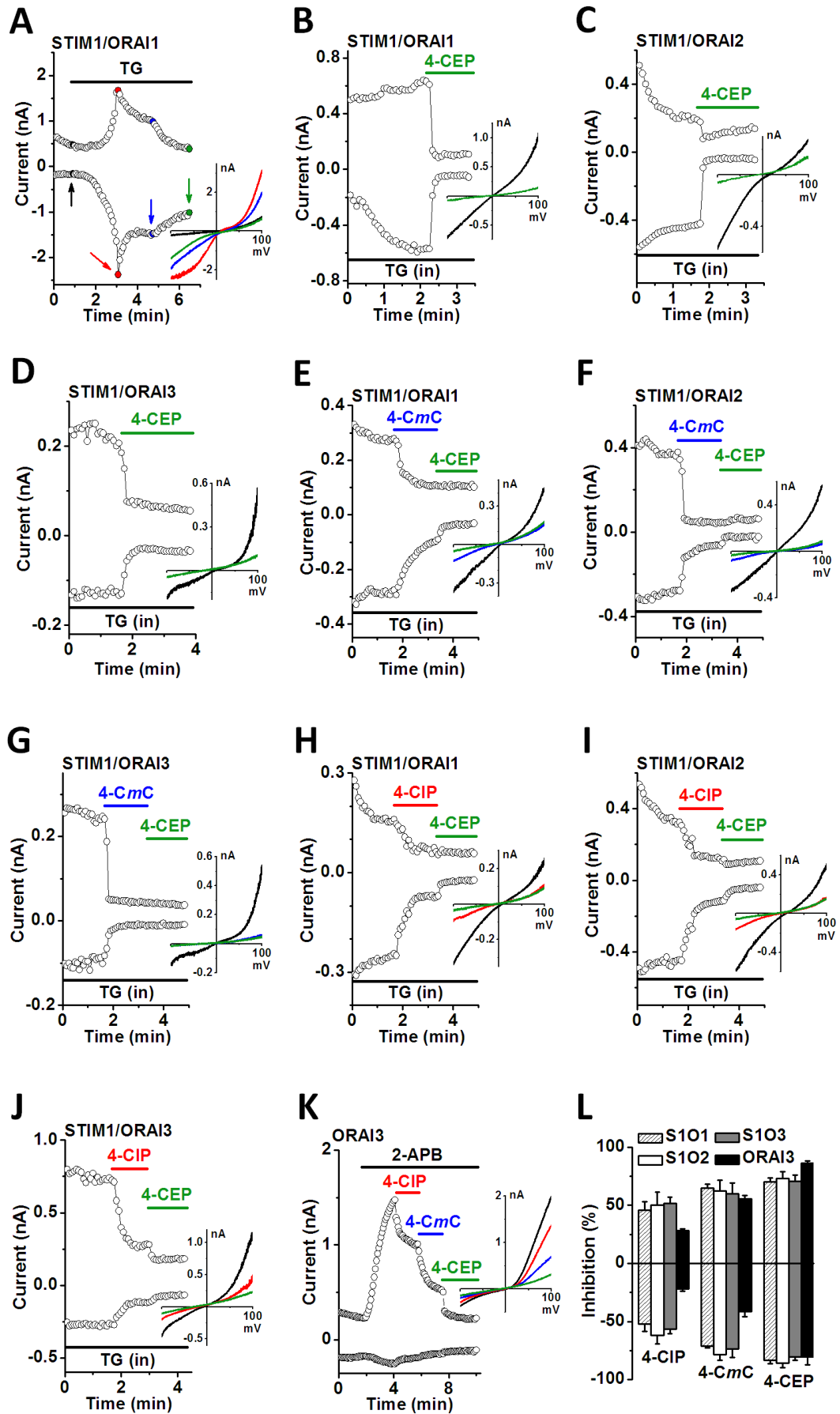
Fig. 5.4 4-CEP, 4-C*m*C and 4-ClP inhibited whole-cell currents evoked by TG or 2-APB in STIM1/ORAI1-3 cells. (A) The time course of TG (1 μM)-induced

currents measured at +80 and -80 mV in STIM1/ORAI1 cells. The *I-V* relationships at different time points are inset. (B-D) 4-CEP (500 µM) inhibited whole-cell currents evoked by TG (1 µM in pipette solution) in STIM1/ORAI1-3 cells. (E-J) 4-C*m*C and 4-ClP (500 µM) reduced TG-induced currents in STIM1/ORAI1-3 cells, which were further inhibited by 500 µM 4-CEP. (K) 4-ClP, 4-C*m*C and 4-CEP (500 µM) attenuated 2-APB (50 µM)-evoked currents in ORAI3 cells. (L) Percentages of inhibition on the whole-cell currents measured at +80 and -80 mV in STIM1/ORAI1-3 (with TG) and ORAI3 (with 2-APB) cells by 4-ClP, 4-C*m*C and 4-CEP (*n* = 5-10 in each group).

As TG failed to induce pure I_{CRAC} in STIM1/ORAI-coexpressing cells, I turned to use cells overexpressing ORAI3 alone to test whether the pure ORAI3 current could be inhibited by the three drugs. As shown in Fig. 5.4K, 2-APB (50 µM) potentiated a large outward current and a relatively small inward current in ORAI3 cells, which is independent of STIM1 and Ca^{2+} store depletion. The currents were then inhibited by 500 µM 4-ClP, 4-C*m*C and 4-CEP successively. These results suggested that both the TG-induced store-operated currents and 2-APB-activated ORAI3 currents were inhibited by the three drugs with potencies in the order of 4-CEP > 4-C*m*C > 4-ClP (Fig. 5.4L).

5.2.4. Inhibition of TRPC channels by 4-CEP, 4-C*m*C and 4-ClP

The effects of 4-CEP, 4-C*m*C and 4-ClP were further investigated in cells overexpressing TRPC4, TRPC5, TRPC3 or TRPC6 channels. Gd^{3+} (100 µM) was used to potentiate the whole-cell currents in TRPC4 and TRPC5 cells, which exhibited a typical "*N*-shape" *I-V* curve. The TRPC4 and TRPC5 currents were suppressed by 500 µM 4-ClP, 4-C*m*C and 4-CEP, among which 4-CEP was most effective and completely blocked the currents (Fig. 5.5A-B). The whole-cell currents in TRPC3 and TRPC6 cells were activated by trypsin (0.5 µM) via the G protein-coupled receptor PAR2 (proteinase-activated receptor 2) and phospholipase C pathway. The PKC inhibitor chelerythrine (10 µM) was added into the pipette solution to antagonise the PKC-induced decaying of TRPC3 and TRPC6 currents. Both the TRPC3 and TRPC6 currents were successively inhibited by 500 µM 4-ClP, 4-C*m*C and 4-CEP (Fig. 5.5C-D). These results suggest that these compounds are a new class of TRPC inhibitors with the potencies ranked as 4-CEP > 4-C*m*C > 4-ClP (Fig. 5.5E).
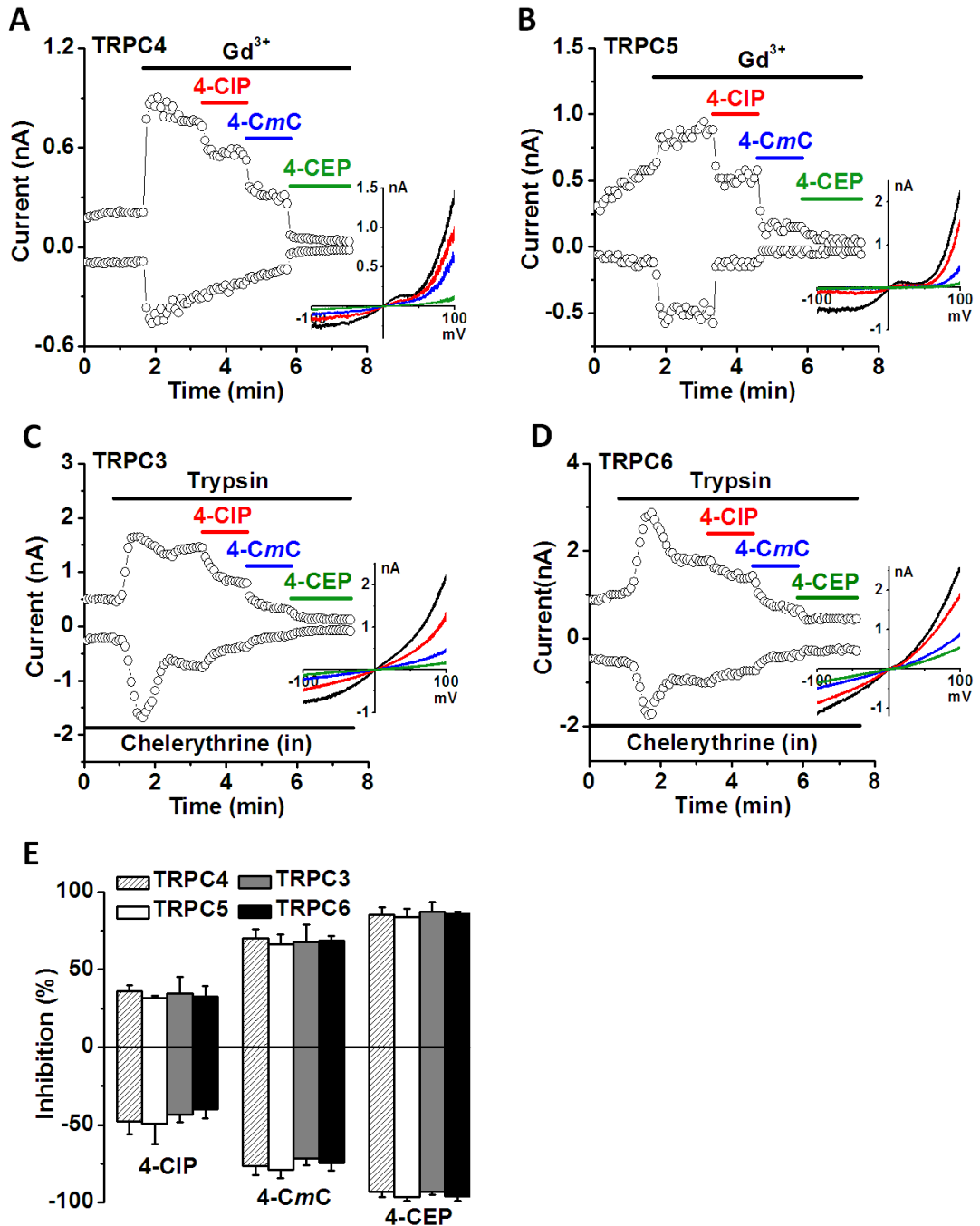
Fig. 5.5 4-ClP, 4-C*m*C and 4-CEP inhibited TRPC channels. (A-B) 4-ClP, 4-C*m*C and 4-CEP (500 µM) inhibited whole-cell currents potentiated by 100 µM Gd^{3+} in TRPC4 and TRPC5 cells. The time courses for currents measured at +80 and -80 mV are shown, and the *I-V* curves are inset. (C-D) 4-ClP, 4-C*m*C and 4-CEP (500 µM) inhibited whole-cell currents triggered by trypsin (0.5 µM) in TRPC3 and TRPC6 cells. The PKC inhibitor chelerythrine (10 µM) was added in the pipette solution to prevent the inhibition of TRPC3 and TRPC6 by PKC activation. (E) Percentages of inhibition on the whole-cell currents measured at +80 and -80 mV in TRPC4/5 (with Gd^{3+}) and TRPC3/6 (with trypsin) cells by 4-ClP, 4-C*m*C and 4-CEP (*n* = 5-7 in each group).
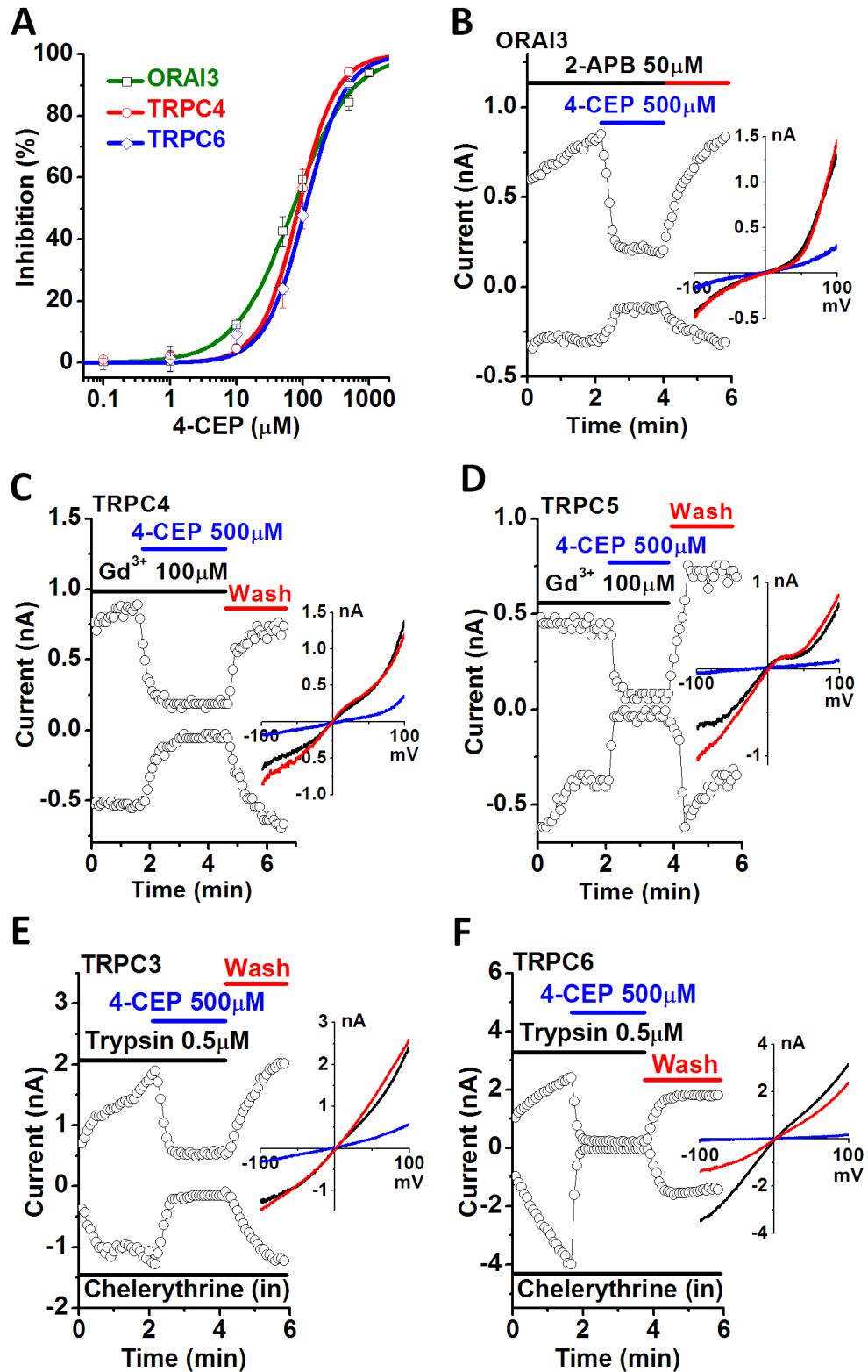
Fig. 5.6 Dose-dependent and reversible inhibition of ORAI3 and TRPC channels by 4-CEP. (A) Dose-response curves of 4-CEP on the inhibition of ORAI3, TRPC4 and TRPC6 channels ($n = 4\text{-}10$ for each point). The whole-cell currents measured at +80 mV were used for fitting with logistic model. The IC_{50} for ORAI3, TRPC4 and TRPC6 are 71.0, 85.6 and 108.4 μM, respectively. (B-F) The inhibitory effects of 500 μM 4-CEP on ORAI3 and TRPC4/5/3/6 channels were quickly reversed after 4-CEP was removed from the external solution.

5.2.5. Concentration-dependent and reversible inhibition of ORAI3 and TRPC channels by 4-CEP

4-CEP is the most potent blocker for ORAI and TRPC channels among the three compounds as shown above (Section 5.2.3 and 5.2.4) by comparing the effect at a single concentration (500 μM). To further determine the effect of 4-CEP, the dose-response experiments were conducted in ORAI3, TRPC4 and TRPC6 cells challenged by 50 μM 2-APB, 100 μM Gd^{3+} and 0.5 μM trypsin, respectively. Within the range of 0.1-1000 μM, the inhibition of these channels by 4-CEP is concentration-dependent, and the IC_{50} for ORAI3, TRPC4 and TRPC6 were found to be 71.0, 85.6 and 108.4 μM, respectively (Fig. 5.6A). The reversibility of 4-CEP inhibition was also examined. The inhibition of ORAI3 current in the presence of 50 μM 2-APB was gradually reversed after 4-CEP was removed (Fig. 5.6B). The TRPC4 and TRPC5 currents were fully restored after both the activator Gd^{3+} and inhibitor 4-CEP were washed away (Fig. 5.6C-D). Similarly, the whole-cell currents in TRPC3 and TRPC6 cells recovered quickly after the removal of trypsin and 4-CEP from the bath solution (Fig. 5.6E-F).

5.2.6. Extracellular effects of 4-CEP on ORAI3 and TRPC4 channels

The action side of 4-CEP on ORAI3 and TRPC4 channels was examined by two strategies. Firstly, the outside-out patch-clamp recordings was used and the characteristic ORAI3 and TRPC4 currents evoked by 50 μM 2-APB or 100 μM Gd^{3+} were inhibited by 500 μM 4-CEP in the external solution (Fig. 5.7A-B). Secondly, the intracellular application of 500 μM 4-CEP in the pipette solution failed to block the activation of ORAI3 by 50 μM 2-APB and TRPC4 currents by 100 μM Gd^{3+} in whole-cell configuration, whereas the subsequent addition of 500 μM 4-CEP into the extracellular solution rapidly abolished the currents (Fig. 5.7C-D). These results demonstrated that 4-CEP inhibited ORAI3 and TRPC4 activities from the extracellular side of the channels.
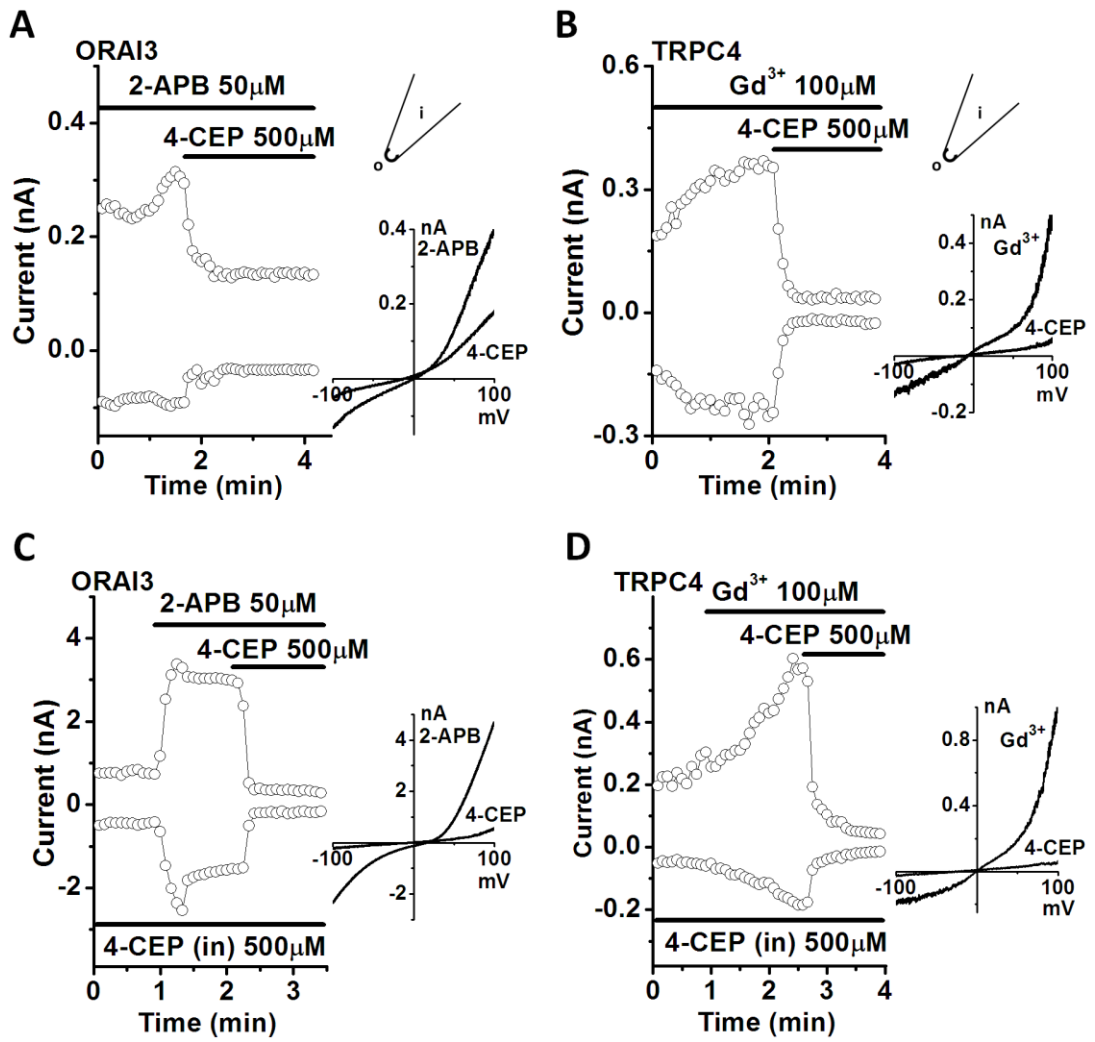
Fig. 5.7 4-CEP inhibits ORAI3 and TRPC4 channels from the cell surface. (A-B) 4-CEP (500 µM) inhibited ORAI3 and TRPC4 currents in outside-out patch configuration. The time courses for currents measured at +80 and -80 mV are shown, and the *I-V* curves are inset. (C-D) Intracellular application of 500 µM 4-CEP did not block the activation of ORAI3 and TRPC4 channels by 2-APB and Gd^{3+}, respectively.

5.3. Discussion

5.3.1. Structure determinants of 4-CEP analogues for the inhibition of ORAI and TRPC channels

In this chapter I found that the RyR agonist 4-CEP is a non-selective blocker of ORAI1/2/3 and TRPC3/4/5/6 channels. The inhibition of these channels, together with the cytoslic clustering of STIM1, lead to the abolishment of SOCE by this compound, despite the fact that it initially induces Ca^{2+} release from the ER store and STIM1 translocation toward the plasma membrane. The action of inhibition is independent of the Ca^{2+} release from RyRs because the other two analogues, 4-C*m*C and 4-ClP, also inhibit ORAI and TRPC channels, whilst they are unable to induce Ca^{2+} release in the HEK293 cells used in this study. The potency of the three compounds for channel inhibition is positively correlated with the length of the 3-alkyl group, i.e. 4-CEP (with an ethyl group) is the more effective than 4-C*m*C (with a methyl group) and 4-ClP (no side chain at 3' position). Nonetheless, the potency of 4-CEP (IC_{50} within 70-200 μM) is still much lower than that of other non-selective store-operated channel blockers, such as 2-APB (IC_{50} within 3-20 μM) (Xu *et al.*, 2005a; McGahon *et al.*, 2012) and SKF-96365 (IC_{50} within 1-3 μM) (Liu *et al.*, 2011; McGahon *et al.*, 2012). Elongation of the 3-alkyl chain of 4-CEP may produce analogues with higher potency, however this is not investigated in this study due to the availability of the compounds. The length of the alkyl side chain of chlorophenol derivatives is also associated with their potency on activating RyR1 (Beeler and Gable, 1993). Therefore, new compounds with longer alkyl chains may not only have increased potency on store-operated channel inhibition, but also strongly interfere with the ER/SR Ca^{2+} stores.

5.3.2. Action sites of 4-CEP on ORAI and TRPC channels

It has been widely acknowledged that 4-CEP and 4-C*m*C stimulate intracellular Ca^{2+} release by directly activating RyRs in intact cells. This suggests that these two compounds are highly membrane-permeable and thus may affect ion channels at the plasma membrane from the intracellular side. To test this hypothesis, I included 4-CEP in the pipette solution and performed whole-cell patch-clamp recordings on ORAI3 and TRPC4 channels. The results showed that intracellular application of 4-CEP do not inhibit the channels, suggesting that the action sites of 4-CEP should be located at the cell surface. Outside-out recordings confirmed the extracellular action

of 4-CEP on ORAI3 and TRPC4 channels. In another aspect, the 4-CEP-inhibited ORAI3 and TRPC currents were quickly restored when 4-CEP was removed from the bath solution, and the most reasonable explanation for this phenomenon is that the binding between 4-CEP and the channel proteins occurs at the cell surface and is easy to be disassociated. In addition to ORAI and TRPC channels, 4-CEP analogues also inhibit voltage-gated Na^+ channels (Haeseler $et\ al.$, 1999; Haeseler $et\ al.$, 2001). As these three types of ion channels have distinct structures and regulatory mechanisms, the action sites of 4-CEP on these channels are most likely located close to the outer pore-forming regions, where the channel activities can be directly modulated. Detailed work such as drug-amino acid binding assay and site-directed mutagenesis of ion channels will clarify the exact target positions of 4-CEP on these channels.

5.3.3. Implication for the use of 4-CEP and 4-CmC in diagnosis of malignant hyperthermia

SOCE has been shown to occur in skeletal muscle cells (Kurebayashi and Ogawa, 2001; Dirksen, 2009; Launikonis $et\ al.$, 2010) and proposed to contribute to the sustainment of hypermetabolic reactions in malignant hyperthermia (Duke $et\ al.$, 2010; Hopkins, 2011). SOCE is coupled to SR Ca^{2+} release in both normal and malignant hyperthermia-susceptible skeletal muscles (Launikonis $et\ al.$, 2003; Lyfenko and Dirksen, 2008; Duke $et\ al.$, 2010). High levels of STIM1 and ORAI1 have been detected in skeletal muscles and proved to be crucial for the SOCE after depletion of the SR Ca^{2+} store (Stiber $et\ al.$, 2008; Vig $et\ al.$, 2008; Stiber and Rosenberg, 2011). In addition, skeletal muscles also express multiple TRPC channels, including TRPC1/3/4/6 (Vandebrouck $et\ al.$, 2002; Brinkmeier, 2011; Gailly, 2012). The expression of these channels suggests that the regulation of myoplasmic Ca^{2+} may be more complicated than that in the classical model of muscle contraction. Although 4-CEP and 4-CmC have been found very useful in triggering Ca^{2+} release and promising for the diagnosis of malignant hyperthermia, it should be taken into consideration that these chemicals also affect the myoplasmic Ca^{2+} level by inhibiting SOCE, especially at concentrations over 100 μM. It has been shown that 4-CEP at 75 μM clearly distinguishes between the MH susceptible and nonsusceptible human skeletal muscle samples in the $in\ vitro$ muscle contracture tests, however 4-CEP at 100 and 200 μM were not diagnostically useful due to the overlapped results from two groups (Gerbershagen $et\ al.$, 2005). This can be

attributed to the maximum activation of both wildtype and mutant RyR1 channels in response to 4-CEP over 100 μM, and the inhibition of SOCE may further diminish the difference between two groups.

5.4. Conclusions

In this chapter I discovered that the RyR agonists 4-CEP and 4-C*m*C, as well as their analogue 4-ClP, are non-selective inhibitors of ORAI1/2/3 and TRPC3/4/5/6 channels. The potencies of inhibition are ranked as 4-CEP > 4-C*m*C > 4-ClP for all channels. These findings provided a new insight for the pharmacological mechanism of these compounds.

Chapter 6

Differential Effects of Divalent Copper on TRPC and TRPM2

Channels

6.1. Introduction

Metal ions are important factors or cofactors in cellular physiology (Mathie *et al.*, 2006). Among them, copper is a redox-active element and participates in many important cellular functions by binding to a variety of proteins such as ceruloplasmin, cytochrome *c* oxidase and superoxide dismutase (Jomova *et al.*, 2010). Both deficiency and elevated level of copper can induce oxidative stress that leads to cell or tissue damage (Uriu-Adams and Keen, 2005). Copper deficiency is seen in infants with Menkes' disease that is caused by genetic mutations in the copper transporter ATP7A (Chelly *et al.*, 1993) and in patients with gastrointestinal surgery, such as gastric bypass surgery (Shahidzadeh and Sridhar, 2008). In contrast, patients showing excessive copper accumulation in the body are due to exposure to excess copper in drinking water or other environmental sources (Brewer, 2009), or a genetic disorder with copper accumulation in the liver and the basal ganglia of the brain (Wilson's disease), which is caused by mutations in ATP7B, a transporter responsible for exporting copper out of the cells (Tanzi *et al.*, 1993). Moreover, the elevated copper level has also been reported in the plasma of diabetic patients (Walter *et al.*, 1991) and in the brain of patients with neurodegenerative disorders (Lovell *et al.*, 1998). It is unclear that the increased blood copper concentration is just a consequence of diabetes or the cause of dysfunction of insulin signaling and glucose homeostasis, however, treatment with a Cu^{2+} chelator to reverse diabetic copper overload seems effective in preventing diabetic organ damage (Cooper, 2011). With regard to neurological disorders, copper has been implicated in the pathogenesis of many neurodegenerative disorders including Alzheimer's disease, amyotrophic lateral sclerosis, Huntington's disease, Parkinson's disease, and prion disease (Desai and Kaler, 2008; Squitti, 2012). Excess copper can initiate or stimulate the progression of Alzheimer's disease by promoting the aggregation of amyloid-β peptides to form senile plaques in the brain (Meloni *et al.*, 2008; Tougu *et al.*, 2011) or by oxidative stress-driven cell death (Jomova *et al.*, 2010). Nevertheless, the effect of copper in Alzheimer's disease is still in much debate. The protective effect of copper against the formation of beta-sheet, the toxic secondary structure of amyloid-β, has also been demonstrated (Lin *et al.*, 2010; House *et al.*, 2009). These complex results could be due to the imbalance of copper in the affected region, rather than a bulk copper accumulation or deficiency (Faller, 2012; James *et al.*, 2012). The regulation of copper homeostasis and its

(patho)physiological consequences are not fully understood. In addition to its role in regulating oxidative stress, it is important to identify new functions of copper to further understand the pathogenesis of copper-related disorders.

Transient receptor potential (TRP) channels are a large family of cationic channels with a total of 27 members in mammalian genome. It has been found that the heat-sensitive channels TRPA1 and TRPV1, which belong to the ankyrin and vanilloid subfamily of TRP channels respectively, are activated by micromolar or millimolar Cu^{2+} (Gu and Lin, 2010; Riera *et al.*, 2007). To date there are no reports about the effect of Cu^{2+} on other TRP channels. The canonical subfamily of TRP channels are widely expressed Ca^{2+}-permeable channels consisting of seven members (TRPC1-7), among which TRPC2 is a pseudogene in human genome (Vannier *et al.*, 1999). TRPC channels can be activated by physiological stimulations such as G protein-coupled receptor (GPCR) signalling and depletion of intracellular Ca^{2+} stores, thus being involved in a variety of cellular and physiological functions. TRPC channels are also suggested to play important roles in copper-related diseases such as diabetes and neurological disorders. TRPC channels have been found to be associated with the development of diabetic complications including diabetic nephropathy, vasculopathy and neuropathy (Graham *et al.*, 2012). In neurodegenerative diseases, such as Parkinson's and Alzheimer's diseases, TRPC channels may contribute to the disturbance of cellular Ca^{2+} homeostasis in affected regions of the brain (Selvaraj *et al.*, 2010). As an important pathological factor in these diseases, oxidative stress has been shown to regulate the activity of TRPC channels. TRPC3, TRPC4 and TRPC6 are sensitive to reactive oxygen species (ROS) or H_2O_2 (Poteser *et al.*, 2006; Graham *et al.*, 2010; Cioffi, 2011). TRPC5 and TRPC1/5 heteromeric channels are activated by reduced thioredoxin, an endogenous redox protein (Xu *et al.*, 2008a). Considering the property of copper as a redox-active element in the body, it is likely that copper also participates in the regulation of TRPC channels in a direct or indirectly way.

TRPM2 is a member of the melastatin subfamily of TRP channels. It was previously known as TRPC7 or LTRPC2 with abundant expression in the brain (Nagamine *et al.*, 1998; Perraud *et al.*, 2001). Later studies showed that TRPM2 is a ubiquitously expressed channel found in many tissues including bone marrow, spleen, heart, liver, lung, pancreatic islets and immunocytes (Sumoza-Toledo and Penner, 2011). Several important physiological functions of TRPM2 channel have been

demonstrated using knockout animals or *in vitro* models including insulin release (Togashi *et al.*, 2006; Uchida *et al.*, 2011), cytokines and ROS production (Di *et al.*, 2011), cell motility and cell death (Hara *et al.*, 2002), and immune response (Knowles *et al.*, 2011). The genetic variants of TRPM2 have been linked to the pathogenesis of several neurological diseases like bipolar disorder (Xu *et al.*, 2009a), western pacific amyotrophic lateral sclerosis and parkinsonism-dementia (Hermosura *et al.*, 2008), and the regulation of amyloid beta-peptide (Aβ)-induced striatal cell death that involves in the Alzheimer's disease (Fonfria *et al.*, 2005). In addition, a number of endogenous modulators for TRPM2 channel have been identified, among which the most efficient direct channel activator is adenosine diphosphate ribose (ADPR). Free ADPR opens TRPM2 channels by binding to the Nudix-like motif in the C-terminus, and evokes a current with linear current-voltage (*I-V*) relationship (Perraud *et al.*, 2001; Sano *et al.*, 2001). The activation of TRPM2 channel by ADPR is dependent on the intracellular Ca^{2+} concentration (McHugh *et al.*, 2003) and negatively regulated by adenosine monophosphate (AMP) (Kolisek *et al.*, 2005) and acidic pH (Du *et al.*, 2009; Starkus *et al.*, 2010). H_2O_2 is another activator for TRPM2 channel, although the mechanism of H_2O_2-induced TRPM2 activation is still unclear (Sumoza-Toledo and Penner, 2011). Therefore, TRPM2 is a ROS-sensitive Ca^{2+}-permeable channel, which may play important roles in the oxidative stress-related diseases.

Given the evidences that TRPCs and TRPM2 are redox-sensitive channels and their association with neurodegenerative disorders and diabetes which are oxidative stress-related diseases, it is intriguing to suppose that the activity of TRPC and TRPM2 channels could be modulated by certain pathological factors related to these diseases, such as Cu^{2+} that plays an important role in regulating oxidative status in a cell. In this chapter, I investigated the effects of Cu^{2+} on TRPC3/4/5/6 and TRPM2 channels overexpressed in T-REx HEK293 cells by electrophysiological approaches.

6.2. Results

6.2.1. Cu^{2+} is a potent activator of TRPC channels

In TRPC4-overexpressing T-REx HEK293 cells, the whole-cell currents were inhibited immediately after the perfusion of 10 μM Cu^{2+} in bath solution, and then gradually potentiated to very large amplitude in 5 min, with the typical "*N*-shape" *I-V* curve (Fig. 6.1A). However, the whole-cell currents in the control cells, i.e. TRPC4 cells without tetracycline induction, were relatively small and the current amplitude was slightly increased after perfusion with 10 μM Cu^{2+} for 5 min (Fig. 6.1B). This suggests that the Cu^{2+}-evoked current is due to the activation of overexpressed TRPC4 channel, not the activity of endogenous ion channels. As in TRPC4-overexpressing cells, 10 μM Cu^{2+} also initially inhibited and then robustly stimulated both the inward and outward whole-cell currents of TRPC5, TRPC3 or TRPC6-overexpressing cells (Fig. 6.1C and Fig. 6.2). The *I-V* curves of these currents all exhibited a characteristic "*N*-shape", suggesting these exogenously expressed channels are responsible for the effect of Cu^{2+}.

6.2.2. Cu^{2+} activates TRPC4 channel in a dose-dependent manner

The effective range of Cu^{2+} on activation of TRPC4 channel was determined to be as low as to 1 μM (Fig. 6.3A). The potentiation of the whole-cell TRPC4 currents by 1 μM and 5 μM Cu^{2+} was very slow, whereas 10 μM and higher concentrations of Cu^{2+} showed a relatively fast effect (Fig. 6.3A-D). There are no significant differences among the amplitudes of currents measured at 2 min after application of Cu^{2+} at 10, 50, 100 and 500 μM. In contrast the currents evoked by 1 and 5 μM Cu^{2+} at the same time point were very small (Fig. 6.3E).
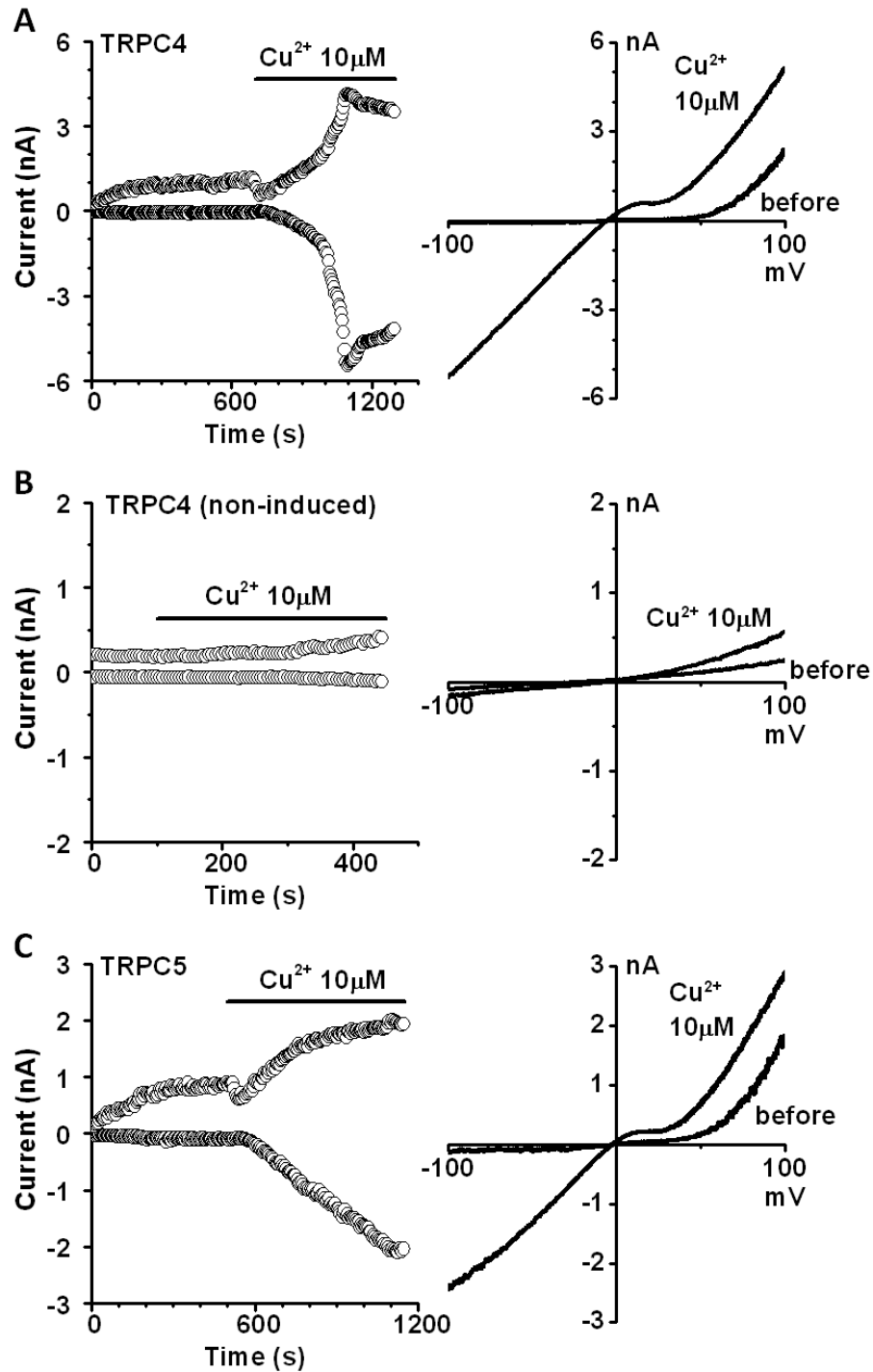
Fig. 6.1 Activation of TRPC4 and TRPC5 channels by Cu^{2+}. (A) The effect of extracellular Cu^{2+} (10 μM) on the whole-cell currents of T-REx HEK293 cells overexpressing EYFP-TRPC4. The currents measured at +80 and -80 mV were initially inhibited and then strongly potentiated by Cu^{2+}. The *I-V* curves before and after the application of Cu^{2+} are shown on the right. (B) Extracellular Cu^{2+} (10 μM) showed very little stimulation on the endogenous currents of control cells, where the expression of TRPC4 was not induced. The corresponding *I-V* curves are shown on the right. (C) In TRPC5-overexpressing T-REx HEK293 cells, extracellular Cu^{2+} (10 μM) had a similar effect on the whole-cell currents as in TRPC4 cells. The *I-V* curves before and after Cu^{2+} activation are shown on the right.
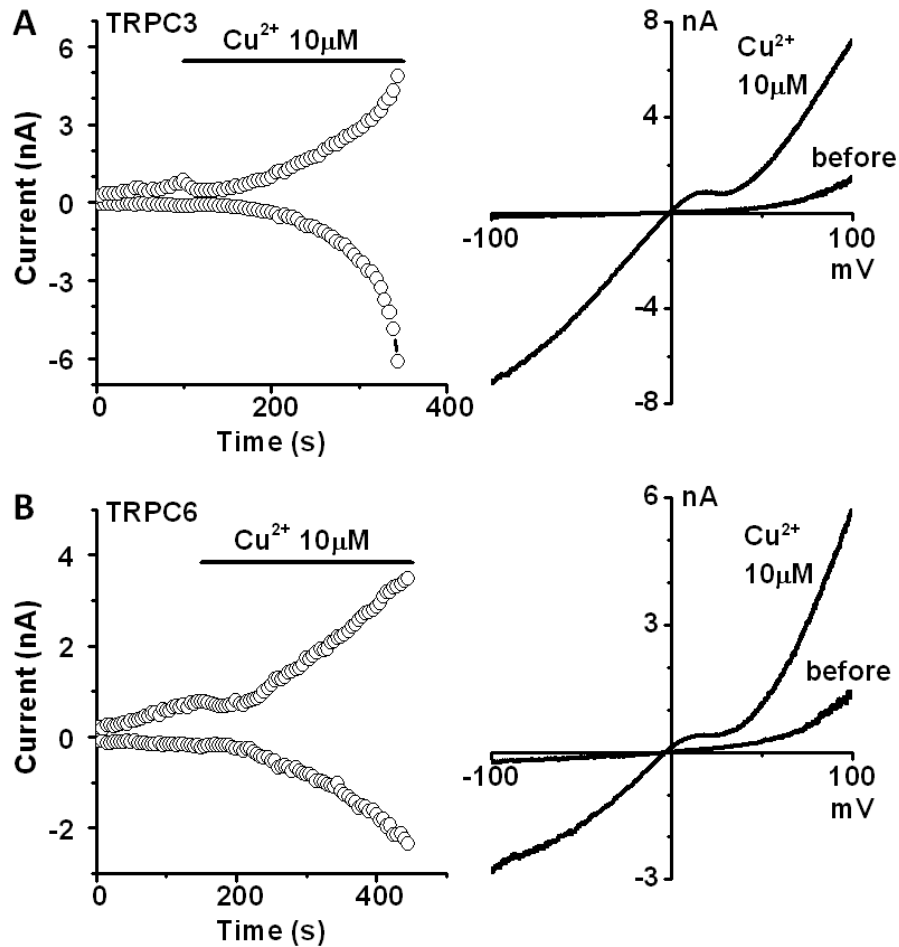
Fig. 6.2 Activation of TRPC3 and TRPC6 channels by Cu^{2+}. Extracellular Cu^{2+} (10 μM) initially inhibited and then strongly activated the whole-cell currents of T-REx HEK293 cells overexpressing mCherry-TRPC3 (A) or mCFP-TRPC6 (B). The time-courses of currents measured at +80 and -80 mV are shown on the left. The *I-V* curves before and after the application of Cu^{2+} are shown on the right.

6.2.3. Cu^{2+} activates TRPC4 channel from the cell surface

Due to the expression of Cu^{2+} transporters across the plasma membrane and intracellular membranes, and the variable Cu^{2+} concentrations in the extracellular cleft and cytoplasm (Mathie *et al.*, 2006), it is important to determine the action site of Cu^{2+} on TRPC channels. Outside-out patch recording was employed to examine which cellular side of TRPC4 is targeted by Cu^{2+}. Similar to the whole-cell currents, the membrane currents in outside-out configuration were suppressed by 10 μM Cu^{2+} in the external solution at first, and then gradually increased (Fig. 6.4A). This extracellular effect was then confirmed by whole-cell recordings with 20 μM Cu^{2+} in the internal solution. The intracellular application of Cu^{2+} did not significantly change the whole-cell currents, whereas subsequent perfusion of extracellular Cu^{2+} (10 μM) dramatically augmented the TRPC4 currents (Fig. 6.4B).
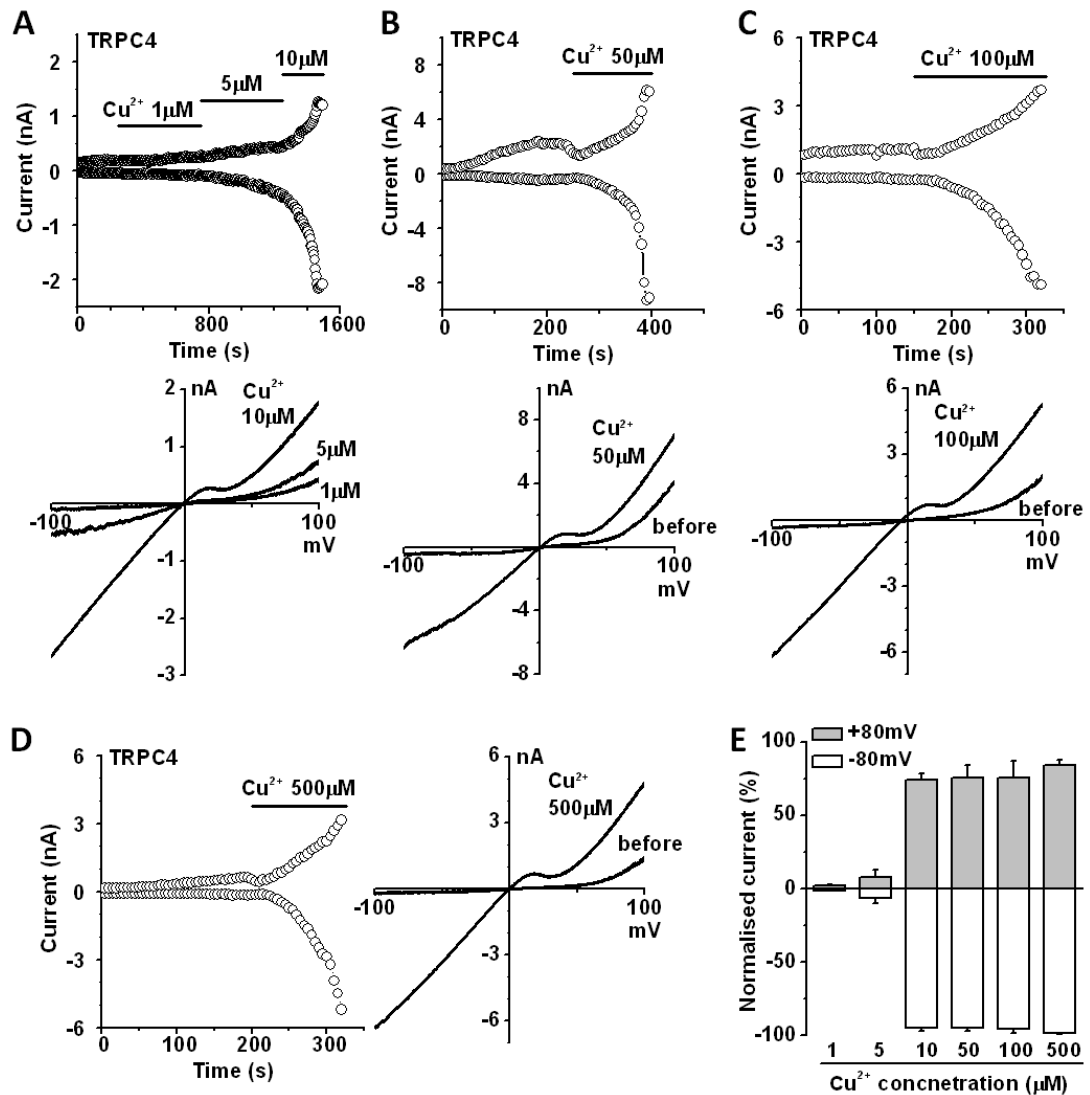
Fig. 6.3 Dose-dependent activation of TRPC4 channels by Cu²⁺. (A-D) The effects of extracellular Cu²⁺ (1-500 μM) on the whole-cell currents of T-REx HEK293 cells overexpressing EYFP-TRPC4. The corresponding *I-V* curves are shown below the time-course plots (A-C) or on the right (D). (E) Comparison of the amplitudes of TRPC4 currents after exposure to different concentrations of Cu²⁺ for 120 s (*n*=4-6 in each group). The currents were measured at +80 and -80 mV, and each of these currents was normalised to the maximum current recorded in the same cell.

6.2.4. Amino acid residues of TRPC4 related to Cu²⁺ activation

To determine the molecular targets of Cu²⁺ within TRPC4 channel, three TRPC4 mutants with altered amino acids in the pore-forming region between the fifth and sixth transmembrane segments were generated by PCR mutagenesis from the pcDNA4/TO-EYFP-TRPC4α vector. Three negatively charged glutamic acid
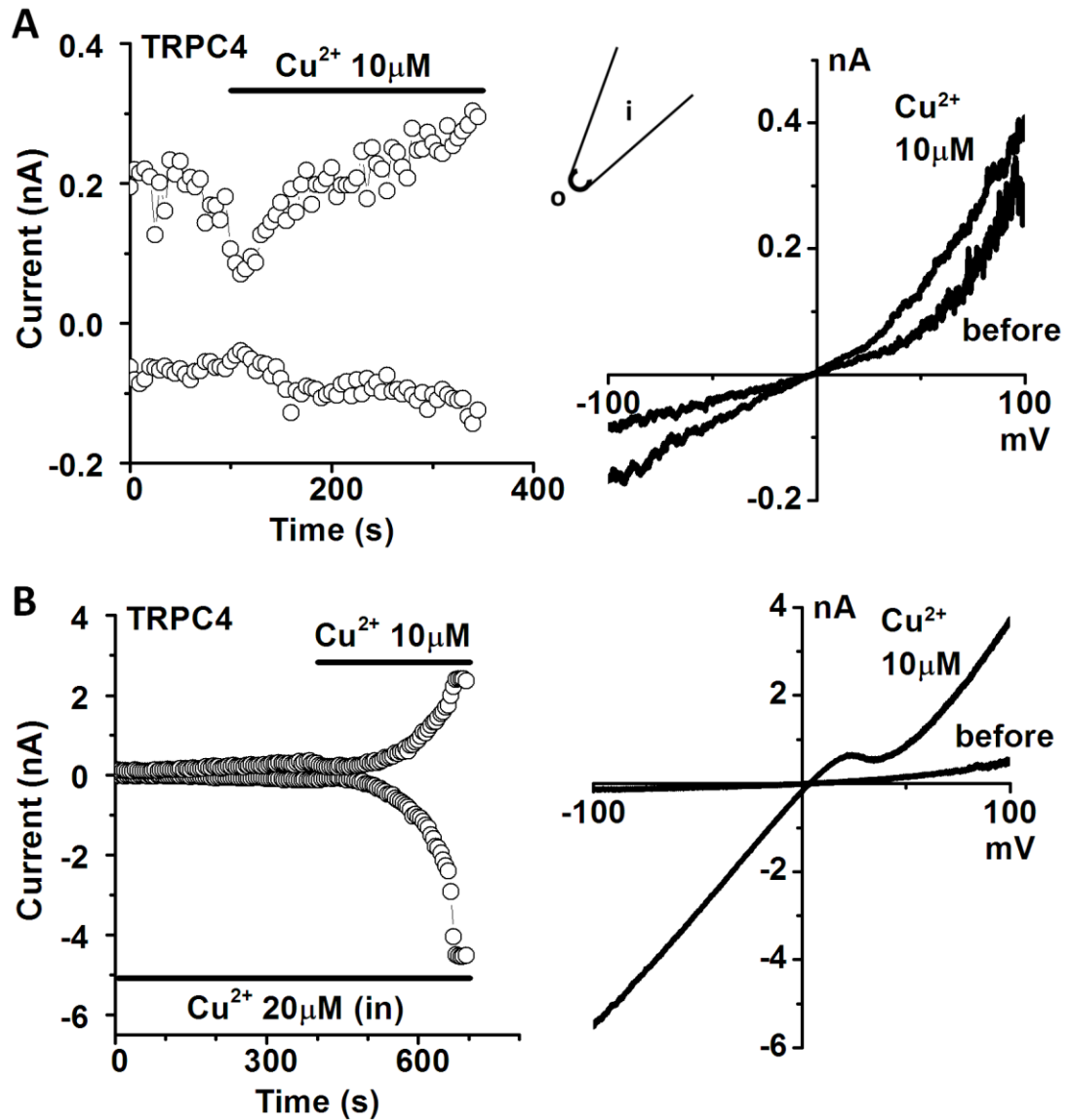
Fig. 6.4 Cu²⁺ activates TRPC4 channels from the extracellular side. (A) Cu^{2+} (10 µM) in external solution facilitated TRPC4 currents measured at +80 and -80 mV in outside-out configuration. The corresponding *I-V* curves are shown on the right. (B) Intracellular application of 20 µM Cu^{2+} did not potentiate the whole-cell currents in TRPC4 cells, whereas the later perfusion of 10 µM Cu^{2+} in the extracellular solution substantially augmented the currents. The *I-V* curves before and after the perfusion of external Cu^{2+} are shown on the right.

residues at the positions 542, 543 and 555 were changed into neutral glutamine residues to generate the mutants E542Q/E543Q and E555Q. The cysteine residue at position 554, which potentially forms a disulfide bridge with another cysteine residue at 549, was changed into neutral tryptophan residue to produce the mutant C554W. The E542Q/E543Q and E555Q mutants were mainly localised at the plasma membrane, which is similar to that of wildtype TRPC4 (Fig. 6.5A, E and G).

The C554W mutant showed many intracellular aggregations (Fig. 6.5C), suggesting the disruption of the disulfide bridge may cause misfolding of TRPC4 proteins, which are then transported into lysosomes and degraded. The electrophysiological properties also showed differences among the mutants. Cu^{2+} (10 μM) slightly increased the whole-cell current in the cells expressing E542Q/E543Q mutant by comparing with the maximum current evoked by 0.5 μM trypsin in the same cell (Fig. 6.5B). A similar phenomenon was observed for the C554W mutant (Fig. 6.5D). However, the Cu^{2+}-induced current was much bigger in cells expressing the E555Q mutant, and nearly achieved the maximum activation as trypsin (Fig. 6.5F and H). These results suggest that the glutamic acid residues at positions 542 and 543, and the cysteine residue at 554 are related to the TRPC4 channel activation by Cu^{2+}, whereas the receptor-operated channel opening is not affected by these mutations.

6.2.5. Cu^{2+} is a potent inhibitor of TRPM2 channel

TRP subfamilies may have different sensitivity to metal ions, such as lanthanides for TRPC5 and TRPM2 (Xu *et al.*, 2005a); therefore, I examined the effect of Cu^{2+} on TRPM2 channel. Unlike TRPC channels, direct application of Cu^{2+} failed to potentiate the whole-cell current in TRPM2 cells (data not shown). To test potential inhibitory effect of Cu^{2+} on TRPM2, the intracellular activator ADPR (500 μM) was included in the pipette solution. The whole-cell currents with a typical linear *I-V* curve were quickly evoked by ADPR in the tetracycline-induced TRPM2 cells (Tet+) and achieved maximum within 1 min after membrane breakthrough (Fig. 6.6A), which is consistent with previous reports (Perraud *et al.*, 2001; McHugh *et al.*, 2003; Xu *et al.*, 2008b). Perfusion with 10 μM Cu^{2+} abolished the TRPM2 current (Fig. 6.6A and C). The inhibitory effect of Cu^{2+} seemed to be irreversible on washout, which suggests that Cu^{2+} may form covalent bonds with the channel protein. In the control cells without tetracycline induction (Tet-), the whole-cell currents evoked by ADPR were very small, and also inhibited by 10 μM Cu^{2+} (Fig. 6.6B-C), suggesting that there is an endogenous current sensitive to Cu^{2+} in the native cells. The inhibition of Cu^{2+} on TRPM2 was concentration-dependent with an IC_{50} of 2.59 ± 0.66 μM and a slope factor of 1.50 ± 0.35 (Fig. 6.6D).
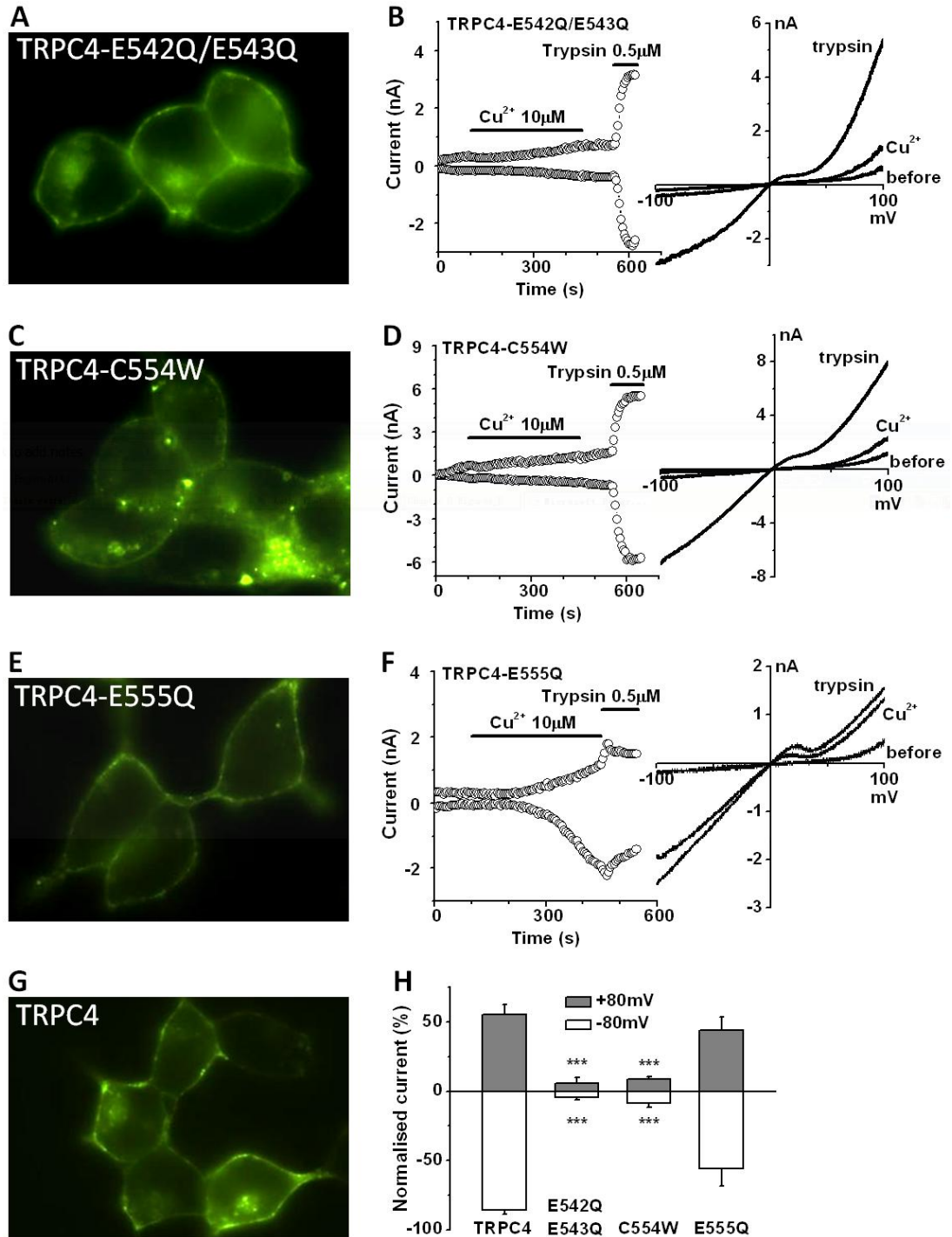
Fig. 6.5 Distinct properties of TRPC4 mutants in response to Cu²⁺. (A, C, E and G) Subcellular localisation of mutant and wildtype TRPC4 proteins tagged with EYFP in T-REx HEK293 cells. (B, D and F) The effects of extracellular Cu^{2+} (10 μM) and trypsin (0.5 μM) on the whole-cell currents of T-REx HEK293 cells overexpressing TRPC4 mutants. The corresponding *I-V* curves are shown on the right. (H) Comparison of the amplitudes of whole-cell currents evoked by 10 μM Cu^{2+} in cells overexpressing wildtype and mutant TRPC4 (*n*=4-6 in each group). The currents were measured at +80 and -80 mV, and each of these currents was normalised to the maximum current after trypsin stimulation in the same cell. (*** $P<0.001$)
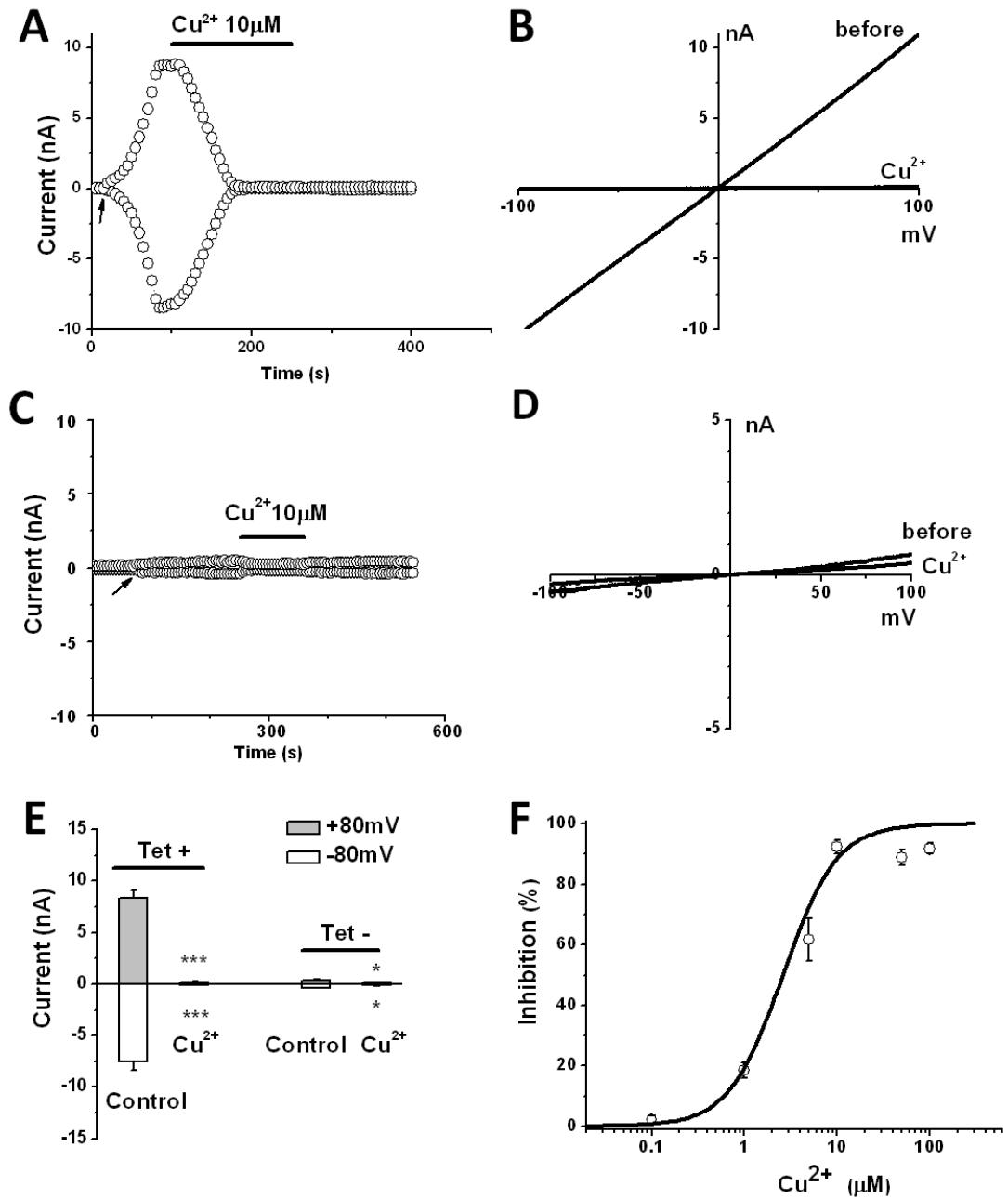
Fig. 6.6 Effects of Cu^{2+} on the whole-cell currents of TRPM2-overexpressing HEK293 cells. (A) The time course of the currents measured at +80 and -80 mV. Cu^{2+} (10 µM) inhibited the whole-cell TRPM2 currents evoked by 500 µM ADPR in the pipette solution. The arrow indicates the time point when the whole-cell configuration was formed. (B) Representative *I-V* curves before and after perfusion of Cu^{2+} in (A). (C) Cu^{2+} (10 µM) inhibited the endogenous currents in the cell without tetracycline induction. (D) Representative *I-V* curves before and after perfusion of Cu^{2+} in (C). (E) Mean ± SEM for the inhibition of Cu^{2+} on the currents of Tet-induced and non-induced cells. (*n*=4-10 in each group, **P<0.05, ***P<0.001*) (F) Dose-response curve for TRPM2 inhibition by Cu^{2+} (*n*=7-13 for each concentration).

6.2.6. Extracellular effect of Cu^{2+} on TRPM2 channel

To determine the action side of Cu^{2+} on TRPM2 channel, higher concentration (20 µM) of Cu^{2+} was added into the pipette solution to see whether the activation of TRPM2 current can be prevented. I found that intracellular application of Cu^{2+} failed to prevent the TRPM2 current induced by ADPR, but the subsequent perfusion of 10 µM Cu^{2+} in the bath solution abolished the current (Fig. 6.7A-B), suggesting that the action site of Cu^{2+} on TRPM2 is located at the external surface of the channel. To further confirm this extracellular effect, the outside-out patch was performed. Cu^{2+} (10 µM) significantly inhibited the TRPM2 current in the outside-out patches (Fig. 6.8A). The single channel activity of TRPM2 channel was also recorded (Fig. 6.8B-C). The slope conductance for TRPM2 channel stimulated by ADPR was 65.8 ±0.23 pS (n = 4), which is similar to 64 pS (Starkus et $al.$, 2010) and close to 60 pS recorded under the conditions of 100 nM Ca^{2+} and 100 µM ADP ribose (Perraud et $al.$, 2001). Bath perfusion with 10 µM Cu^{2+} abolished the single channel activity (Fig. 6.8C).
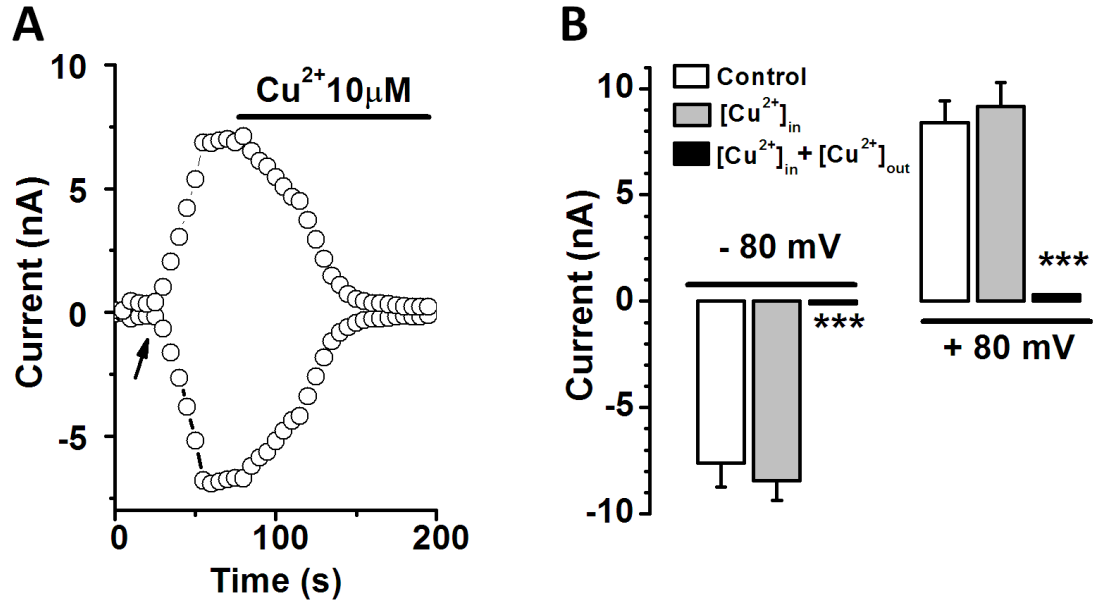
Fig. 6.7 Cu^{2+} inhibits TRPM2 channel from the cell surface. (A) Addition of Cu^{2+} (20 µM) into the internal solution did not prevent the channel activation by ADPR, whereas the perfusion of 10 µM Cu^{2+} in bath solution completely abolished the whole-cell currents. The arrow indicates the time point when the whole-cell configuration was achieved. (B) Comparison of the peak amplitudes of TRPM2 currents measured at +80 and -80 mV in the control group and in the presence of intracellular or extracellular Cu^{2+} (n = 3 in each group, ***$P<0.001$).
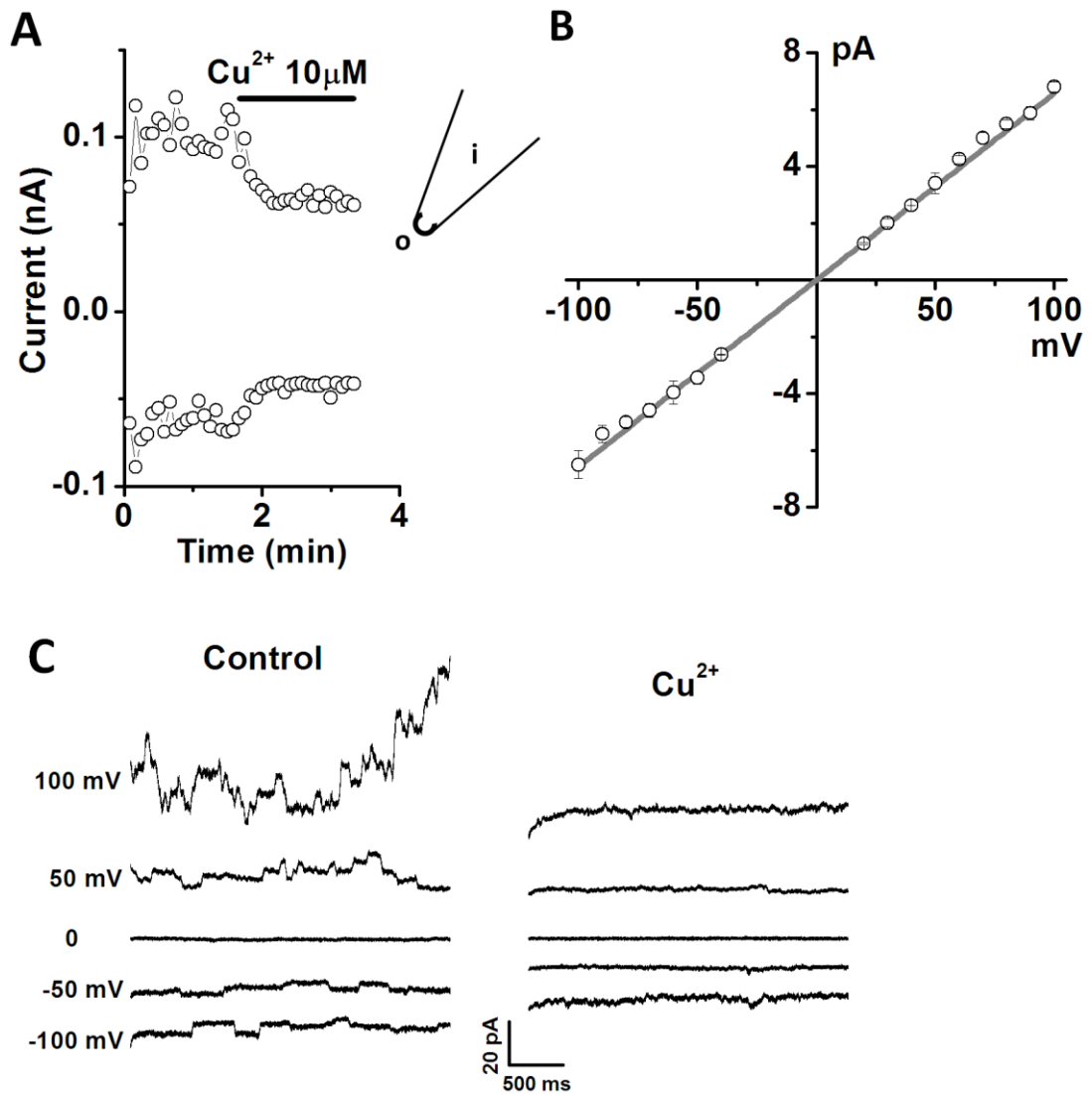
Fig. 6.8 Outside-out patch-clamp recordings showing the extracellular action of Cu^{2+} on TRPM2 channel. (A) Cu^{2+} (10 µM) in the external solution inhibited TRPM2 currents measured at +80 and -80 mV in outside-out patch configuration. (B) Mean unitary current sizes for ADPR-induced TRPM2 single channel events plotted against voltages. Straight line was fitted and the mean unitary slope conductance was 66 pS (0.5 mM ADPR). (C) Example of single channel activity of TRPM2 recorded by outside-out patches before and after perfusion with Cu^{2+}.

6.3. Discussion

6.3.1. Copper, oxidative stress, TRPC and TRPM2 channels in neurodegenerative diseases

Copper has been implicated in the pathogenesis of several neurodegenerative disorders including Alzheimer's disease, amyotrophic lateral sclerosis, Huntington's disease, Parkinson's disease, and prion disease (Desai and Kaler, 2008; Squitti, 2012). Excess of copper is associated with the production of ROS, which in turn triggers a series of events including oxidative stress-induced cell injury, intracellular protein deposits (neurofibrillary tangles), neuronal dysfunction and consequently cell death (Gaggelli $et\ al.$, 2006). On the other hand, ROS activate some Ca^{2+} channels, such as TRPM2, and cause the disruption of cellular Ca^{2+} homeostasis. The common change of Ca^{2+} homeostasis in Alzheimer's disease is an increased intracellular calcium level that could occur either indirectly through Aβ modulating an existing Ca^{2+} channel or directly through cation-selective channels formed by Aβ (Alarcon $et\ al.$, 2006). In this study, I found that extracellular Cu^{2+} significantly potentiated TRPC channels but inhibited TRPM2 channel, which provide new evidences for the relationship between ROS-sensitive TRP channels and Cu^{2+}. These channels are activated by ROS or H_2O_2, but have distinct responses to Cu^{2+}, which renders Cu^{2+} a complicated role in the regulation of cellular Ca^{2+} homeostasis. It has been suggested that TRPM2 mediates oxidative stress-driven neuronal cell death (Xie $et\ al.$, 2010; Naziroglu, 2011; Sumoza-Toledo and Penner, 2011). However, because of the extremely high copper levels in senile plaques (393±123 μM) (Lovell $et\ al.$, 1998), the activity of TRPM2 is likely to be completely inhibited by copper, instead of being enhanced by H_2O_2 and Aβ in the affected regions of the brain. The cell death induced by oxidative stress may be a result of hyperactivity of TRPC channels, which can be potentiated by ROS, H_2O_2 and Cu^{2+}. In another aspect, a recent study using TRPM2-deficient mice demonstrated that activation of TRPM2 inhibited ROS production in macrophages, which was mediated by the inhibition of NADPH oxidase activity through depolarization of the plasma membrane (Di $et\ al.$, 2011). This pathway may also exist in microglia, the resident phagocytes in the brain. TRPM2 expression has been detected in microglia, and the response to ADPR, H_2O_2 and endotoxin is similar to that in macrophages (Kraft $et\ al.$, 2004). Considering the abundance of microglia in senile plaques (Haga $et\ al.$, 1989), the inactivation of TRPM2 by copper would substantially promote the production of

ROS in these cells. Taken together, the oxidative stress in the brain could be severely augmented by excessive copper with regard to its oxidant property and effects on amyloid-β peptides and TRPM2 channels. The increased oxidative stress and excessive copper would lead to Ca^{2+} overload in the cells by activating TRPC channels, which eventually results in cell death. Thus, although TRPM2 and TRPC channels response to copper in distinct ways, they are both involved in the progression of neurodegenerative diseases.

6.3.2. Physiological and pathophysiological concentrations of copper in human body

Copper concentration in blood plasma is around 15 μM in normal population (Mathie *et al.*, 2006), however, copper accumulates in the brain and displays differential distribution patterns in the central nervous system. Much higher concentration has been estimated in the cerebrospinal fluid (~70 μM). The concentration in the synaptic cleft may reach 200-400 μM in some neuronal diseases, whereas the normal extracellular copper concentration in the brain is of the order of 0.2–1.7 μM (Mathie *et al.*, 2006). The elevated copper levels have also been reported in patients with type 1 or type 2 diabetes (Zargar *et al.*, 1998), which shares many pathogenetic mechanisms with Alzheimer's disease and vascular dementia. In addition, copper accumulation in the body is caused by genetic variants of copper transporter genes (ATP7A and ATP7B), i.e., Menkes syndrome and Wilson disease. These data suggest that the activation or inhibition of TRPC and TRPM2 channels by micromolar Cu^{2+} should exist in normal subjects and under some disease conditions.

6.3.3. Molecular targets of copper on TRPC4 and TRPM2 channels

Three amino acid residues are found to be potential Cu^{2+}-binding sites in TRPC4 channel in this study. The negatively charged E542 and E543 residues may bind Cu^{2+} by electrostatic interaction. Cysteine residue is an important ligand in copper-binding proteins and accounts for 35% of all copper ligands (Wu *et al.*, 2010b). The C554 residue in TRPC4 thus may form a complex with Cu^{2+} and then be oxidised. The oxidation of cysteine residues may catalyse the formation of disulphide bonds between physically adjacent cysteine residues, and thereby indirectly change protein structure and function (Song *et al.*, 2011). I have not examined the molecular targets of Cu^{2+} on TRPM channel in this study; however, Cu^{2+} may bind directly to amino

acids against most likely cysteine or the hydrophilic-charged amino acids (histidine, lysine, arginine, aspartate, and glutamate) to alter the channel activity. Indeed, the residue substitution in the outer vestibule of the pore including K952, H995 and D1002 significantly changed the sensitivity to Zn^{2+} (Yang *et al.*, 2011). Further investigation is needed to confirm these binding sites for Cu^{2+}. Moreover, a more indirect way that copper can modulate protein function is through the generation of free radicals, which can profoundly alter protein and cell function, particularly for the ROS-sensitive channels. Unlike the extracellular effect of Cu^{2+}, the action site for ROS or hydroxyl radical that generated by mixing with Fe^{2+} and H_2O_2 has been demonstrated as an intracellular effect, which is mainly related to the C-terminal Nudix-like domain (Ishii *et al.*, 2006; Sumoza-Toledo and Penner, 2011). Therefore, the channel appears to be opened by intracellular ROS, and closed by extracellular Cu^{2+}. On the other hand, higher concentrations of extracellular Cu^{2+} may enter cells via Cu^{2+} transporters that in turn regulate the ROS production. Recently, Zn^{2+} has been shown to inhibit TRPM2 channel, however, the potency of Zn^{2+} was much lower than that of Cu^{2+} (Yang *et al.*, 2011). The difference in potency for the two ions may have important physiological relevance because the plasma levels of copper and zinc are oppositely correlated in many diseased conditions such as diabetes and hypertension and the ratio of Zn^{2+}/Cu^{2+} have been evaluated in some diseases (Canatan *et al.*, 2004; Mathie *et al.*, 2006; Viktorinova *et al.*, 2009). Excessive copper and deficit of zinc would progressively disrupt the cellular Ca^{2+} homeostasis by tuning the activity of a number of TRP and other Ca^{2+} channels (Mathie *et al.*, 2006).

6.3.4. Other Ca^{2+} channels regulated by copper

Apart from the activation of TRPC and inhibition of TRPM2 channels, Cu^{2+} also inhibits the voltage-gated Ca^{2+} channels including T-, L-, N-, P-, and Q-type channels (Mathie *et al.*, 2006). The $Ca_v3.2$ channel is more sensitive to Cu^{2+} than other types of voltage-gated Ca^{2+} channels with an $IC_{50} = 0.9$ μM (Jeong *et al.*, 2003). In addition, high concentrations of Cu^{2+} stimulate TRPV1 and TRPA1 channels (Gu and Lin, 2010; Riera *et al.*, 2007), suggesting that the overall effect of Cu^{2+} on intracellular Ca^{2+} level may vary, which depends on the local concentration of Cu^{2+} and the expression of different Ca^{2+} channels.

6.4. Conclusions

In this study, I found that Cu^{2+} at micromolar concentrations potently activated TRPC4/5/3/6 channels but inhibited TRPM2 channel activated by ADP-Ribose. The action sites of Cu^{2+} on TRPC4 and TRPM2 are both extracellularly located. The E542, E543 and C554 residues of TRPC4 are related to the channel opening by Cu^{2+}. The inhibitory effect of Cu^{2+} on TRPM2 channel is irreversible. These findings provide novel insights into the functions of Cu^{2+} in human physiology. The dysfunction of TRP channels caused by excess copper may be one of the pathophysiological mechanisms that disrupt cellular Ca^{2+} homeostasis in diabetes and neurodegenerative diseases.

Chapter 7

TRPC Channels are Essential for Human Ovarian Cancer Cell Proliferation and Tumourigenesis

7.1. Introduction

Ca^{2+} signalling is believed to play a central role in the signalling cascades of tumorigenesis and neoplastic progression by controlling gene expression, progression through the cell cycle, and DNA synthesis. Inhibitors of Ca^{2+}-dependent signalling suppress the proliferation of cancer cells *in vitro* and in solid tumors *in vivo* (Holmuhamedov *et al.*, 2002). Store-operated Ca^{2+} influx is one of the Ca^{2+} entry pathways and closely related to cell proliferation and apoptosis. The importance of store-operated Ca^{2+} influx or capacitative Ca^{2+} influx in cancer development has been recognised for many years, however the role of TRP channels that act as the molecular constituents or subunits of SOCs or ROCs in cancer cell proliferation are still unclear (Prevarskaya *et al.*, 2007). It has been demonstrated that TRPC channel is involved in cell proliferation, and 2-aminoethyldiphenyl borate (2-APB) significantly inhibits the proliferation in HEK-293 cells (Xu *et al.*, 2005a). The mechanism is unrelated to its inhibitory action on inositol 1,4,5-trisphosphate receptors (IP$_3$R), since 2-APB also inhibits the proliferation of triple IP$_3$R knockout DT40 cells (Xu *et al.*, 2005a). This suggests the direct involvement of SOCs or TRPC channels in cell proliferation. Recently, several studies have demonstrated the expression of TRPC in different types of cancer cells or cancer tissues, such as TRPC1, 3, 6 in breast cancer MCF7 cells (Aydar *et al.*, 2009) and liver cancer HepG2 (El Boustany *et al.*, 2008), TRPC1, 3, 4 in prostate cancer LNCaP cells (Thebault *et al.*, 2006; Pigozzi *et al.*, 2006), TRPC1, 4, 6, 7 in renal cell carcinoma (Veliceasa *et al.*, 2007), TRPC1, 3, 5, 6 in human malignant gliomas (Bomben and Sontheimer, 2008), TRPC1, 3-7 in neuroblastoma IMR-32 cells (Nasman *et al.*, 2006), TRPC3 in human astrocytoma 1321N1 cells (Nakao *et al.*, 2008), TRPC6 in esophageal and gastric cancer (Cai *et al.*, 2009), TRPC3 in ovarian cancer (Yang *et al.*, 2009b), and TRPC1, 4 in basal cell carcinoma (Beck *et al.*, 2008). However, the detection of splicing activity of TRPCs and systematic examination of the role of each TRPC isoform in cancer growth has not been addressed.

In this chapter I aimed to identify the expression of TRPC genes and their splicing variants in human ovarian adenocarcinoma-derived cell line SKOV3, and determine the roles of TRPC isoforms in the regulation of cancer cell proliferation using TRPC siRNA interference and pharmacological tools including chemical modulators and

specific TRPC channel functional antibodies. I also examined the colony growth of ovarian cancer cells by overexpressing TRPC isoforms.

7.2. Results

7.2.1. Expression of TRPC spliced variants in SKOV3 Cells

The expression of TRPC genes and their spliced variants in SKOV3 cells were examined by RT-PCR using specific primer sets across introns (Table 2.2). The spliced variant of TRPC1 with exon 3 deletion (TRPC1β) was detected using the primer set across exon 3 (P1). The band density of TRPC1β is much stronger than the full-length isoform (TRPC1α) (Fig. 7.1A), suggesting that the β isoform is highly expressed in SKOV3 cells. Using the primer set across the exon 9 and 10 (P3), a novel spliced variant of TRPC1 with exon 9 deletion (TRPC1δ) was identified. The existence of TRPC1δ was also confirmed by using the TRPC1 primer set across exon 9 (P4). The band density of the TRPC1δ was less abundant than the non-spliced TRPC1 isoform in the region. The deletion of exon 9 did not cause open reading frame shift, suggesting this new spliced isoform may have a channel pore domain and C-terminus that seen in α or β isoforms. I also examined the possibility for other splicing regions using primer set P2 and P5, and the primer combination ranged from exon 1 to exon 13, but no other splicing site was identified.

Full-length human TRPC3 has 12 exons and a 58-base pair insert between exon 2 and exon 3. Using primer set across exon 2-5 (P1), or exon 3-5 (P2), exon 5-6 (P3) and exon 8-9 (P4), single PCR band with the expected size was detected (Fig. 7.1B). TRPC3 has an isoform with an extended N-terminus (TRPC3a) (Yildirim *et al.*, 2005). Using primer set across exon 1-5 (P0), this isoform was found to be expressed in SKOV3 cells. As shown in Fig. 7.1B, a band with an expected size of 1405 bp was detected, suggesting the existence of the TRPC3a isoform in SKOV3 cells. The regions across exon 5-9 and exon 8-12 were also amplified, but no other spliced isoforms were detected.

Eight spliced variants of human TRPC4 have been reported, including α, β, γ, δ, ε, ζ, η and an unnamed isoform truncated at exon 6. The α, β, γ, δ, ε and ζ isoforms have 100% identity for the region from exon 1 to exon 7 except that TRPC4ζ has exon 3
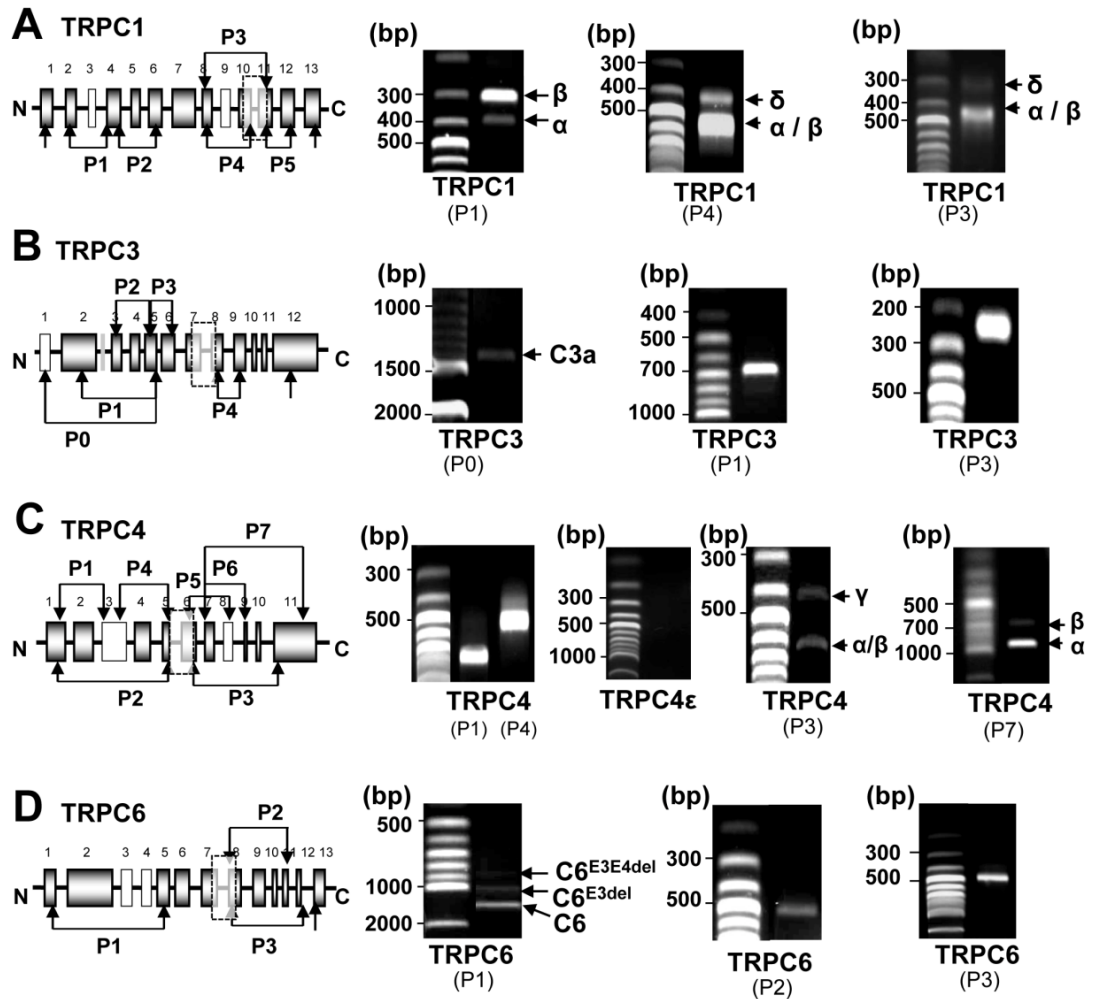
Fig. 7.1 Detection of TRPC spliced variants in human ovarian cancer SKOV-3 cells. (A) RT-PCR products of TRPC1 were amplified by specific primer set labelled as P1 to P5. Two products were amplified using primer set P1 with a size of 403 bp (TRPC1α) and 301 bp (TRPC1β). A small product with exon 9 deletion (TRPC1δ) was identified using primer set P4 (405 bp for TRPC1δ, and 549 bp for TRPC1α/β isoforms). The TRPC1δ was also detected using primer set P3 (423 bp for α/β isoforms; 279 bp for TRPC1δ). No other splicing region was detected using primer set P2 and P5. (B) The TRPC3 spliced variant with an extended N-terminus was detected using primer set P0 (1221 bp). Single PCR product was found using primer set P1, P3 and P4, or P2 and the primers amplifying exon 8 to exon 12. (C) TRPC4 isoforms were detected by primer set P1 and P4. The ε-isoform amplified by ε-specific primer was negative. The γ-isoform with exon 8 deletion was detected by primer set P3. Using primer set P7, both α-isoform (956 bp) and β-isoforms (704 bp) were detected. (D) Two TRPC6 spliced isoforms were detected using primer set P1. Single band of TRPC6 with expected size was detected by primer set P2 (551 bp) and P3 (476 bp).

deletion. The η-isoform has an early stop code due to open reading frame shift at the end of exon 3. Using primer set P1 and P4, TRPC4 fragments with the sizes of 740 bp and 519 bp were found (Fig. 7.1C). The ζ-isoform with exon 3 deletion was undetectable using the primer set across exon 1-5 (P2). The ε isoform of TRPC4 was also undetectable with the forward primer in exon 7 and the ε-specific reverse primer. However, two bands were detected with an expected size of 428 bp and 623 bp using the primer set (P3). The smaller band is specific for TRPC4γ with exon 8 deletion and the bigger band is the unspliced isoforms of TRPC4 (Fig. 7.1C). Similarly, two bands were detected if the primer set across the exon 8 alone (P6) was used, suggesting the TRPC4γ and other isoforms coexisted in the SKOV3 cells. To further distinguish the TRPC4 isoforms, the primer set (P7) amplifying exon 7 to exon 12 were used, the detected band with a predicted size of 956 bp is the α isoform, and the small band (704 bp) is the β isoform (Fig. 7.1C). Other possible splicing regions were also examined using the forward and reverse primer combinations ranged from exon 1 to exon 11, and no more alternative splicing was found. These data indicate that α, β and γ isoforms of TRPC4 coexist in the SKOV3 cells.

There are 13 exons for human TRPC6. Three bands were detected using primer set (P1) to amplify exon 1-5 (Fig. 7.1D). The size for the full-length TRPC6 is 1222 bp. The spliced isoform with exon 3 deletion is 1039 bp, and the shorter one with exon 3 and 4 deletion is 874 bp. No spliced region was found between exon 8 to exon 13 using primer sets P2 and P3 (Fig. 7.1D).

7.2.2. Ovarian cancer cell growth regulated by TRPC channel modulators

2-APB is a non-selective blocker of TRPC channels (Xu *et al.*, 2005a). The blockade of TRPC channels by 2-APB significantly inhibited the SKOV3 proliferation in a concentration-dependent manner with an EC_{50} of 5.9 μM (Fig. 7.2A). Since 2-APB has been shown to inhibit gap junctional channels, which might contribute to the anti-proliferative effect (Harks *et al.*, 2003; Vinken *et al.*, 2006), SKOV3 cells were pretreated with carbenoxolone, a gap junctional channel blocker, to pharmacologically dissect out the contribution of TRPC channels. Carbenoxolone at 200 μM and 400 μM significantly inhibited the cell proliferation (Fig. 7.2B), but
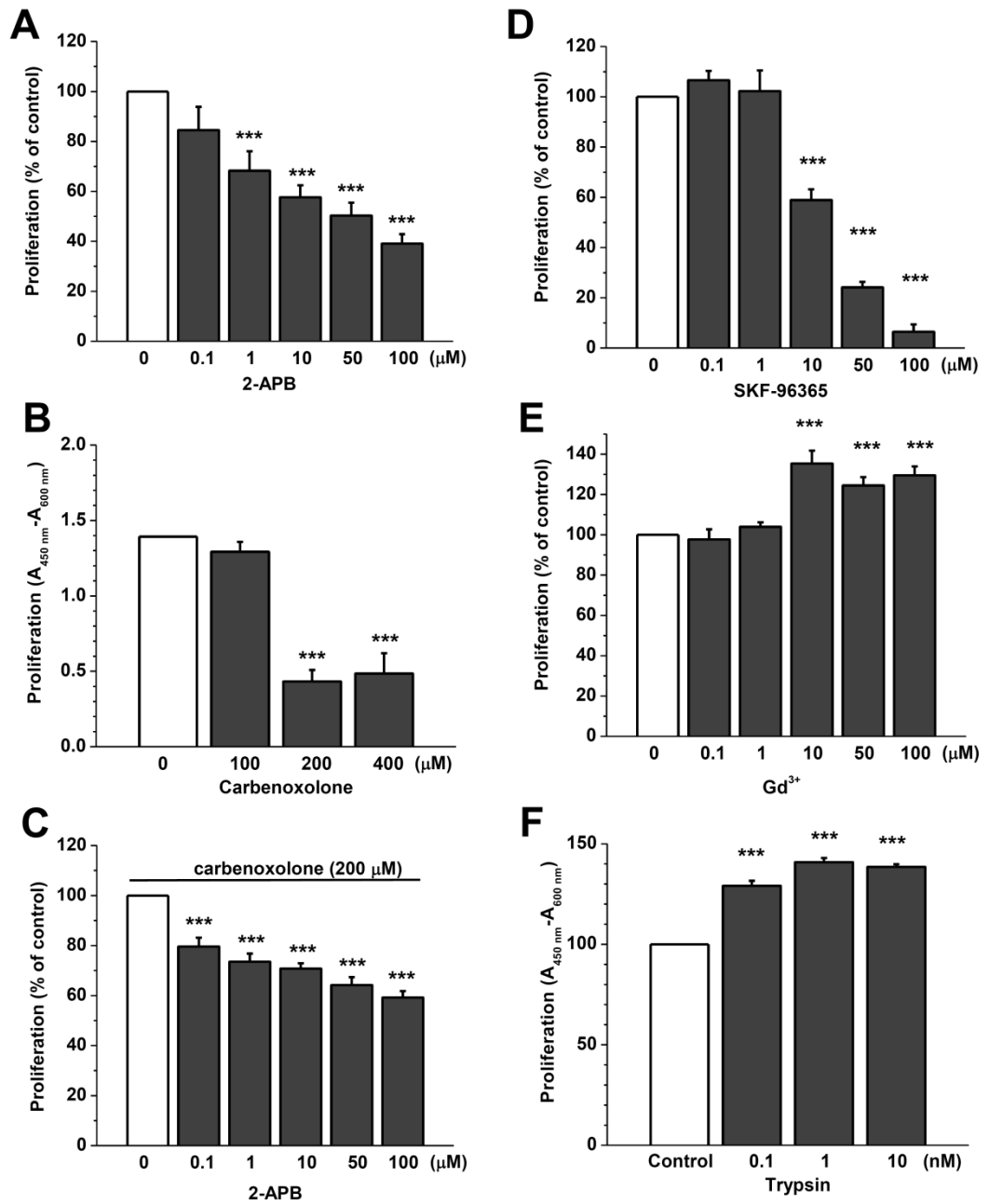
Fig. 7.2 Ovarian cancer cell proliferation was inhibited by store-operated channel blockers. (A) SKOV3 cells were incubated with different concentrations of 2-APB for 24 h. The cell proliferation was monitored by WST-1 assay and the absorbance was measured at a wavelength of 450 nm with a reference at 600 nm. (B) SKOV3 cells treated with carbenoxolone for 24 h. (C) SKOV3 cells incubated with carbenoxolone and 2-APB for 24 h. (D) Effect of SKF-96365 on SKOV3 cells with an IC_{50} of 14.5 μM after incubation for 24 h. (E) Effect of Gd^{3+} incubation for 24 h. (F) Incubation with trypsin for 24 h. Each experiment had 8 well repeats and the data were from ≥ two independent experiments. (*** $P<0.001$)

the anti-proliferative effect of 2-APB was still observed in the presence of carbenoxolone (Fig. 7.2C), suggesting that the anti-proliferative effect of 2-APB could be due to the inhibition of TRPC channels. The effect of SKF-96365, another non-specific TRPC channel blocker, was also tested. SKF-96365 significantly inhibited the proliferation of SKOV3 cells in a concentration-dependent manner with an EC_{50} of 14.5 μM (Fig. 7.2D). Gd^{3+} is an inhibitor of SOCs but selectively activates TRPC4 and TRPC5 channels. Gd^{3+} showed a stimulating effect on cell proliferation at the concentration of 10, 50 and 100 μM (Fig. 7.2E). In addition, the protease trypsin, which stimulates TRPC channels via protease-activated receptor activation, significantly promoted the cancer cell proliferation (Fig. 7.2F). These data suggest the importance of TRPC channel activity in regulating ovarian cancer cell growth, and the channel blockers have the potential for anti-cancer therapy.

7.2.3. Role of TRPC isoforms in ovarian cancer cell proliferation

To identify the role of individual TRPC isoforms on the cancer cell proliferation, SKOV3 cells were incubated with E3-targeting TRPC functional antibodies that can specifically inhibit Ca^{2+} influx via TRPC channels (Xu *et al.*, 2005b; Xu and Beech, 2001). The blockade of TRPC1, TRPC4 and TRPC6 channels by T1E3, T45E3 and T367E3 significantly decreased the cancer cell proliferation, but T5E3, which can block TRPC5 channel only, had no effect on cell proliferation (Fig. 7.3A), which confirmed the lack of TRPC5 expression in SKOV3 cells.

The isoform-specific TRPC siRNAs were used to further demonstrate the role of TRPCs in cancer cell proliferation. There was no difference among the groups transfected with scramble siRNA, pool siRNA and mock control transfection (no siRNA) on SKOV3 cell proliferation (Fig. 7.3B). However, the cell proliferation was significantly inhibited by the transfection with TRPC1, TRPC3, TRPC4 and TRPC6 siRNAs for 48 h (Fig. 7.3B). Bcl-2 siRNA, which targets the anti-apoptotic Bcl-2 gene, was used as a positive control, also significantly inhibited cell proliferation (Fig. 7.3B). These results were similar to the observations using specific anti-TRPC functional antibodies, suggesting that the silencing of TRPC channel expression is important for the inhibition of cancer cell proliferation.
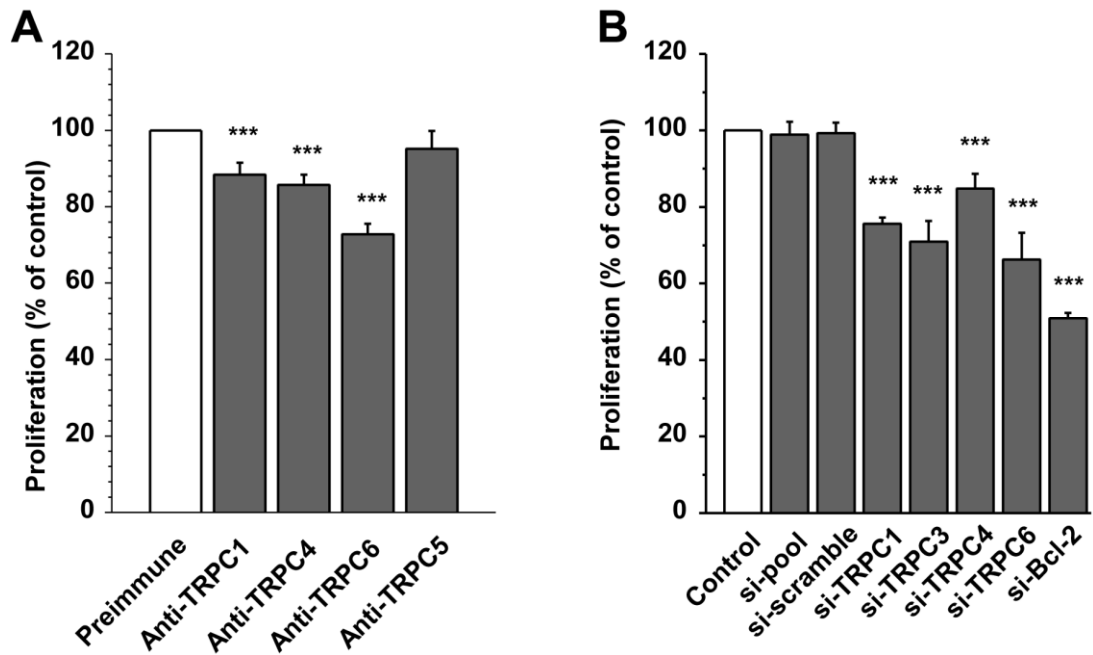
Fig. 7.3 Role of TRPC channels in the ovarian cancer cell growth. (A) SKOV3 cells were incubated with functional antibodies (1:500 dilution for anti-TRPC1 (T1E3); 1:250 dilution for anti-TRPC4 (T45E3), anti-TRPC5 (T5E3) and anti-TRPC6 (T367E3)) for 24 h and the cell proliferation was measured by WST-1 assay. $n =16$ for each group. (B) SKOV3 cells were transfected with TRPC siRNAs (100 nM siRNA for each group) using Lipofectamine 2000. Cell proliferation was measured by WST-1 assay 48 h after transfection. The sham transfection (control), pool siRNA and scramble siRNA were negative control. Bcl-2 siRNA was used as positive control. $n =16$ for each group. (*** $P<0.001$)

7.2.4. Overexpression of TRPC isoforms promoted colony growth of SKOV3 cells

There are no specific siRNAs or blocking antibody tools targeting to individual spliced variants of TRPCs, therefore I overexpressed different TRPC isoforms into SKOV3 cells to further confirm the role of TRPCs in ovarian cancer growth. SKOV3 cells were transfected with the plasmid encoding different TRPC isoforms and the cancer cell colony formation was observed. As shown in Figure 7.4A-B, the number of cell colonies larger than 2 mm^2 was greatly increased in the groups transfected with TRPC1β, TRPC1δ, TRPC3, TRPC4 and TRPC6 plasmids. I also examined the cancer colony growth using soft agar assay. The number of larger colonies with diameters >100 μm was much higher in the groups transfected with TRPC1β, TRPC1δ, TRPC3, TRPC4 and TRPC6 plasmids than that in the vector control group (Fig. 7.4C-D), which further suggested the involvement of TRPCs in the ovarian cancer development.
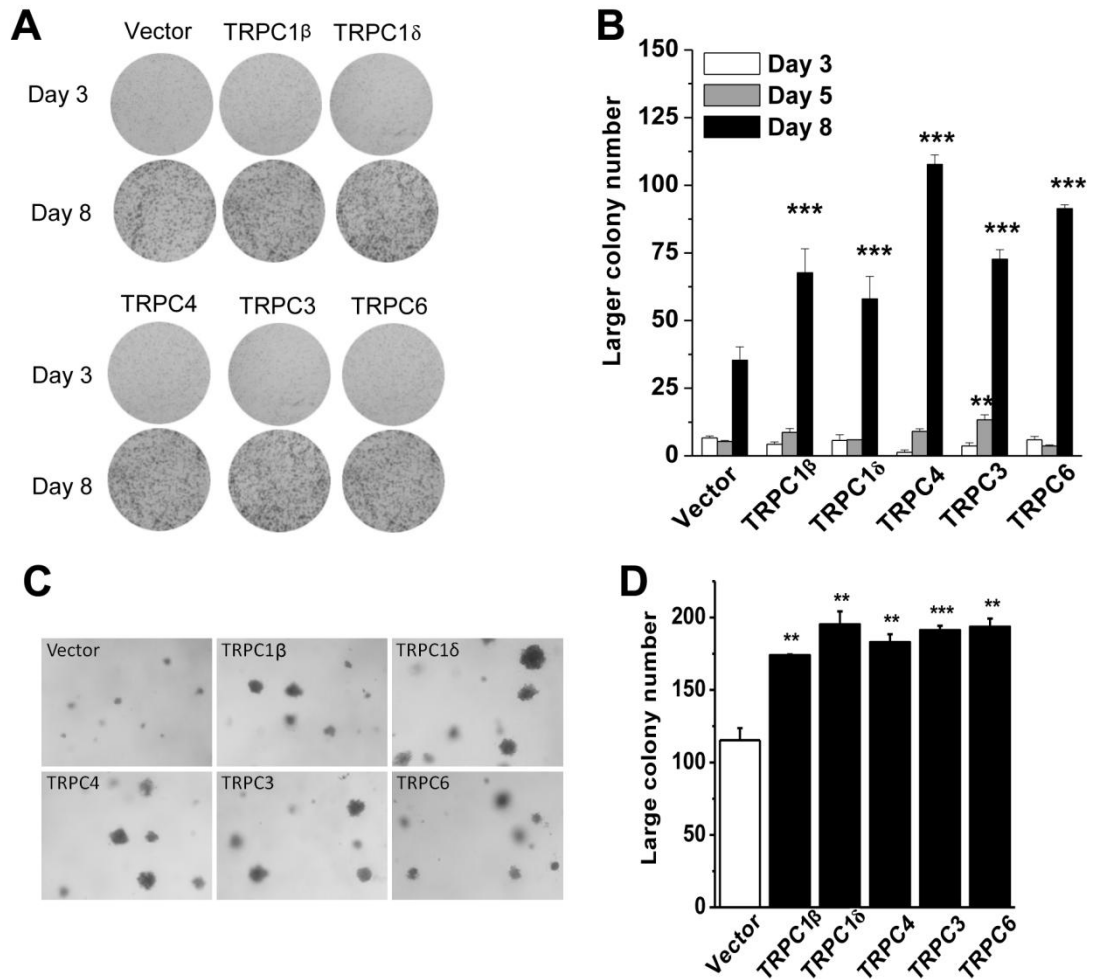
Fig. 7.4 Overexpression of TRPC channels promoted the colony growth of ovarian cancer cells. (A) SKOV3 cell colony formation assay on flat surface. The SKOV3 cells were transfected with TRPC cDNA plasmids or vector as indicated. The cell colonies were stained with crystal violet. (B) Mean ± SE data show the number of large colonies (>2 mm^2). Triplicate wells were used for each group. Results were reproduced in more than three independent experiments. (C) Examples of SKOV3 cell colonies grown in soft agar and stained with crystal violet. The cells were transfected with TRPC cDNA plasmids or vector as indicated. (D) Mean ± SE data show the number of large colonies with diameters >100 μm. Triplicate wells were used for each group. (** $P<0.01$, *** $P<0.001$)

7.2.5. TRPC channel blocker and gene silencing arrested SKOV3 cells at G$_2$/M phase

The cell cycle progression of SKOV3 cells was examined by fluorescence-activated cell sorting (FACS) using the propidium iodide staining procedure (Riccardi and Nicoletti, 2006). Incubation with the non-selective TRPC channel blocker SKF-96365 (10 μM) for 24 h substantially increased the population of SKOV3 cells at G$_2$/M phase and decreased the percentage of cells at G$_0$/G$_1$ phase (Fig. 7.5A), which

is in consistent with the previous report (Yang *et al.*, 2009b). SKF-96365 treatment also significantly increased the apoptosis of SKOV3 cells (Fig. 7.5A). To observe the effects of individual TRPC genes on cell cycle progress, SKOV3 cells were transfected with TRPC siRNAs. I found that more SKOV cells were arrested at G_2/M phase after transfection with siTRPC1, siTRPC4, siTRPC3, and siTRPC6 for
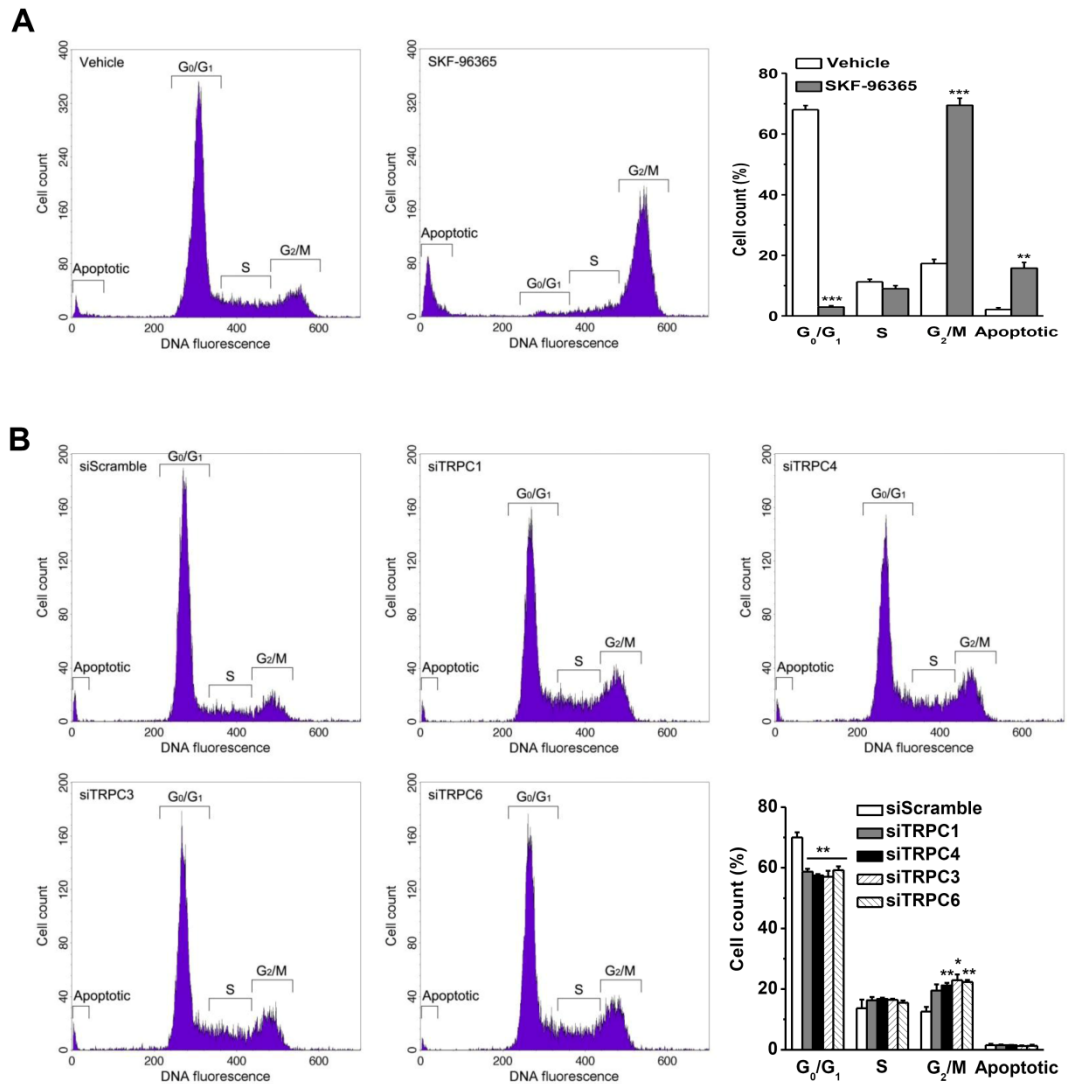
Fig. 7.5 Cell cycle arrested by TRPC channel blocker SKF-96365 and TRPC siRNAs in ovarian cancer cells. (A) The representative FACS histogram for SKOV3 cells treated with vehicle (DMSO) and SKF-96365 (10 µM) for 24 h. The mean ± SE data from three independent experiments are shown on the right. (B) Cell cycle analysis of SKOV3 cells transfected with scramble siRNA (siScramble) and TRPC siRNA (siTRPC1, siTRPC4, siTRPC3 and siTRPC6) for 72 hours. The percentages of propidium iodide-labelled cells at different phases of cell cycle were determined by FACS analysis. The mean ± SE data were from three independent experiments. * *P*<0.05, ** *P*<0.01, *** *P*<0.001 comparing with the vehicle group or the scramble siRNA-transfected group.

72 h comparing with the control group transfected with scramble siRNA (Fig. 7.5B), suggesting that the downregulation of TRPC gene expression can arrest the cell cycle progression through G_2/M to G_1. Unlike the channel blocker SKF-96365, the contribution of TRPC gene silencing on apoptosis was small. The down-regulation of TRPC expression did not significantly change the percentage of apoptotic ovarian cancer cells (Fig. 7.5B).

7.3. Discussion

7.3.1. Functional expression of TRPC isoforms in SKOV3 cells

TRPC channels have been identified in many cell types (Xu *et al.*, 2006b; Xu *et al.*, 2008a; Flemming *et al.*, 2003; Riccio *et al.*, 2002). These channels are differentially expressed at different stages of stem cell development, which may reflect their importance in cell differentiation (den Dekker *et al.*, 2001; Bodding, 2007). On the other hand, the thapsigargin-induced store-operated Ca^{2+} influx is higher in tumour cells than that in normal cells (Kovacs *et al.*, 2005), which further suggests the relevance of TRPC channels or store-operated channel molecules to cancer development. In this study, I have systematically detected the TRPC channels and their splice variants, and found that multiple TRPCs and their spliced isoforms existed in human ovarian cancer. TRPC1 has been suggested as a store-operated channel subunit and actively associates with other TRPC isoforms, such as TRPC1/4 or TRPC1/5 (Xu *et al.*, 2006b; Strubing *et al.*, 2001), or interacts with other channel proteins, such as Orai1 or STIM1 (Ong *et al.*, 2007), to constitute the heteromultimeric store-operated channels or channel complexes, which could be main molecular components in native cells. Interestingly, the existence of several spliced isoforms of TRPCs in a cell suggests the possibility of functional interaction or regulation on the channel activity. TRPC1γ1 and TRPC1γ2 have been reported in human myometrial cells (Yang *et al.*, 2002), but none of them have been detected in the ovarian cancer cells, and no inserts found between exon 8 to exon 10. Instead, I have identified a new TRPC1 isoform with exon 9 deletion, suggesting this TRPC1 spliced isoform lacks transmembrane segment 4 (S4). As shown in Chapter 2, TRPC1δ is mainly distributed in the cytosol with a similar subcellular distribution pattern to TRPC1β in HEK293 cells. However, other isoforms including TRPC3, TRPC4α, TRPC4β1, TRPC4ε1 and TRPC6 are located in the plasma membrane,

suggesting the potential functional difference between TRPC1 and other TRPC isoforms. Moreover, the spliced isoforms of TRPC1 with exon 2 and exon 3 deletion have been described in mice by Sakura & Ashcroft (Sakura and Ashcroft, 1997), but this splicing activity has not been found in human SKOV3 cells. TRPC3 and TRPC6 have a high similarity in sequence. Both of them have been demonstrated as receptor-operated channels that mediate the diacylglycerol-induced Ca^{2+} influx, although TRPC3 may also have store-operated channel properties (Estacion et al., 2004; Venkatachalam et al., 2002). In addition, co-existence of several TRPC4 isoforms in the SKOV cells could be important for protein interactions among the TRPC isoforms that may be required for precisely regulating the functionality of Ca^{2+} permeable channel complexes in cancer cells, and thus control cell growth. Indeed, some spliced TRPC isoforms have been demonstrated as an inhibitory subunit for TRPC homomultimeric channels in HEK-293 cells if co-overexpressed with the full-length isoforms (Schaefer et al., 2002; Satoh et al., 2002). Further investigation is needed to explore the functional difference among the alternative splicing of TRPCs in cancer development.

7.3.2. The role of TRPC channels in cancer cell proliferation and apoptosis

The anti-proliferative effect of 2-APB has been demonstrated in gastric cancer cell lines (Sakakura et al., 2003), colonic cancer cells (Kazerounian et al., 2005) and human hepatoma cells (Enfissi et al., 2004). Here I found that the effect of 2-APB was not altered by the gap junctional channel blocker, carbenoxolone, further suggesting that the anti-proliferative action of 2-APB is due to the inhibition on SOCs. 2-APB and SKF-96365 are broad-spectrum TRPC channel blockers and cannot distinguish the contribution of individual TRPC isoforms; therefore the isoform-specific functional antibodies were used in this study. The specificity of the antibodies has been confirmed by ELISA, western blotting, in vitro functional testing on Ca^{2+} influx and FACS-based assay in previous studies (Xu et al., 2005b; Xu et al., 2006b; Xu et al., 2008a). The block on TRPC1, TRPC4 and TRPC6 channels by E3-targeting functional antibodies caused a significant inhibition of cell proliferation, suggesting that TRPC1, TRPC4 and TRPC6 are important for cancer cell proliferation. This effect was further confirmed by the application of TRPC isoform-specific siRNAs. The inhibition of cancer cell proliferation by TRPC

knockdown is potentially due to the arrest of cells at G_2/M phase, as revealed by the cell cycle analysis in this study, which is similar to previous report using TRPC3 siRNA alone (Yang *et al.*, 2009b).

Cell apoptosis has been suggested to be related to SOCs (Skryma *et al.*, 2000). Thapsigargin can induce apoptosis of prostate cancer cells, but this effect cannot be prevented by an intracellular Ca^{2+} chelator, suggesting that the increase of cytosol Ca^{2+} is unnecessary for apoptosis (Skryma *et al.*, 2000). I found that the non-selective channel blocker SKF-96365 can evoke ovarian cancer cell apoptosis, but the specific TRPC siRNAs do not significantly change the apoptosis, suggesting that TRPC channels may be less important in the regulation of cancer cell apoptosis.

7.4. Conclusions

In this chapter I detected the expression of TRPC genes and their alternatively spliced variants in the human ovarian adenocarcinoma-derived cell line SKOV3. Blockade of TRPC channel activity by 2-APB, SKF-96365, TRPC isoform-specific functional antibodies or the transfection with TRPC siRNAs significantly inhibited the cancer cell proliferation. Overexpression of TRPC genes increased colony growth of ovarian cancer cells on flat surface and in soft agar. The TRPC channel blocker SKF-96365 and knockdown of TRPC expression by siRNAs arrested SKOV3 cells at G_2/M phase. These findings are novel and important for understanding the roles of TRPC channels in ovarian cancer development.

Chapter 8

General Discussion

8.1. Main results and significance of this study

8.1.1. Generation of HEK293 cells stably overexpressing STIM1, ORAI1/2/3 and TRPC1/3/4/6 channels

As the fundamental part of this study, stable overexpression HEK293 cell lines for STIM1, ORAI1/2/3 and TRPC1/3/4/6 were generated, which includes three new alternatively spliced isoforms (TRPC1δ, TRPC4β1 and TRPC4ε1) identified from human aortic endothelial cells. Each of these exogenously expressed proteins is tagged with a fluorescent protein (mCFP, EYFP or mCherry) to show its distribution in the cells. STIM1 and TRPC1 proteins are localised at ER-like intracellular compartments at resting state, whilst other ion channel-forming proteins (ORAI1/2/3 and TRPC3/4/6) are mostly found at the plasma membrane. Once the ER Ca^{2+} store is depleted, STIM1 proteins aggregate with ORAI1/2/3 channels at the plasma membrane. When STIM1 is coexpressed with TRPC proteins in the same cells, the translocation of STIM1 upon Ca^{2+} store depletion does affect the localisation of TRPC proteins, i.e. TRPC1 is retained in the ER, and TRPC4 and TRPC6 do not aggregate with STIM1 at the plasma membrane.

The electrophysioilogical properties of overexpressed ion channels are confirmed by patch-clamp recordings. Inward-rectifying currents are obtained from STIM1-ORAI1/2 coexpressing cells after Ca^{2+} store depletion with thapsigargin. ORAI3 channels expressed alone or coexpressed with STIM1 are substantially stimulated by 2-APB. TRPC4α and TRPC4β1 are potentiated by the selective activator Gd^{3+}, however TRPC4ε1 is not activated by this lanthanide. Activation of PAR2 receptor by trypsin leads to transient but dramatic opening of TRPC4α/β1 and TRPC3/6 channels, whereas TRPC4ε1 do not respond to this agonist.

These results suggest that the functions of STIM1, ORAI and TRPC proteins are well presented in the stably transfected cells. These cells are very useful tools for investigating the molecular mechanism, electrophysiology and pharmacology of store-operated Ca^{2+} channels. New findings on the subcellular localisation of STIM1 and TRPC channels, particularly the lack of direct association between STIM1 and TRPC1/4/6 after Ca^{2+} store depletion, raise an important question that which protein, STIM1 or ORAI1, determines the opening of TRPC channels during store-operated Ca^{2+} entry (SOCE). As TRPC channels are not consistently considered store-

operated Ca^{2+} channels, it is very important to understand the gating mechanism of TRPC channels when they are involed in the store-operated channel complex. Electrophysiological results on TRPC4ε1, a new TRPC4 variant found in endothelial cells, reveal that it is likely a dominant negative isoform of TRPC4 channels, which suppresses the activity of other TRPC4 subunits such as TRPC4α and TRPC4β1 in heterotetrameric channel configuration. The expression of this endogenous negative regulator may be associated with specific physiological or pathophysiological functions in endothelium, in which TRPC4 channels have been shown to play important roles, e.g. regulating endothelial permeability and vascular remodelling (Tiruppathi *et al.*, 2002; Fantozzi *et al.*, 2003).

8.1.2. Cytosolic STIM1 clustering as a new mechanism for the inhibition of store-operated Ca^{2+} entry

Cytosolic STIM1 clustering is a novel phenomenon observed in HEK293 cells overexpressing STIM1-EYFP fused proteins. Once cytosolic STIM1 clusters are formed, STIM1 proteins lose the ability to move to and aggregate at the subplasmalemmal region after Ca^{2+} store depletion, and the SOCE is also abolished. Cytosolic clustering of STIM1 proteins can be induced by pharmacological agents including 2-APB, flufenamic acid, 4-CEP, U73122 and FCCP. The triggering mechanism of cytosolic STIM1 clustering by 2-APB, 4-CEP and U73122 is unknown, whereas the action of flufenamic acid and FCCP is related to the Ca^{2+} release from mitochondria. The formation of cytosolic STIM1 clusters is independent of the ER Ca^{2+} store. The ER-localised TRPC1 proteins do not cluster with STIM1 when they are coexpressed in the same cells exposed to 2-APB.

The ER Ca^{2+} store-independent cytosolic clustering of STIM1 is a novel mechanism for the inhibition of SOCE. This mechanism is involved in the pharmacology of some channel blockers, and could be employed in the development of new drugs to selectively suppress SOCE. Since ORAI1 has been found to possess activity independent of the ER Ca^{2+} store and STIM proteins (Feng *et al.*, 2010), direct blockade of ORAI1 channel may result in unexpected pathophysiological consequence. Therefore, STIM1 could be a better target than ORAI1 for therapeutic store-operated channel blockers. Furthermore, gene silencing of STIM1 alone has been shown to sufficiently inhibit pathological cardiac hypertrophy *in vitro* and *in vivo* (Hulot *et al.*, 2011; Luo *et al.*, 2012), which is the first evidence for STIM1-

targeted gene therapy in animals. Due to the safety concerns on gene-delivery techniques, pharmacological inhibition of STIM1 function would be more feasible for clinical use than reducing gene expression by RNA interference. The cytosolic clustering of STIM1 has provided an unambiguous pharmacological target for drug development with this purpose.

8.1.3. The roles of cytoskeleton in STIM1 movement and store-operated Ca^{2+} entry

Neither depolymerisation of microtubule by colchicine nor disruption of microfilament by cytochalasin D showed any blocking effects on STIM1 translocation toward the plasma membrane upon Ca^{2+} store depletion. Complete disassembly of these two types of cytoskeleton by coapplication of colchicine and cytochalasin D also failed to inhibit the formation of subplasmalemmal STIM1 puncta. However, both colchicine and cytochalasin D significantly reduced SOCE in STIM1-overexpressing cells. The cytosolic clustering of STIM1 induced by 2-APB and 4-CEP was not affected by the disruption of microtubule and actin cytoskeleton.

The increase of F-actin content in subplasmalemmal region, which spatially involves the junctions between the plasma membrane and the ER, blocked the translocation of STIM1 toward the plasma membrane after Ca^{2+} store depletion. The two compounds U73122 and calyculin A are found to block thapsigargin-induced SOCE through this mechanism, which is independent of their roles as phospholipase C inhibitor or protein phosphatase inhibitor, respectively. Depolymerisation of F-actin by cytochalasin D recovered STIM1 translocation and partially restored SOCE in the presence of U73122 or calyculin A.

Both the results from this study and other reports (Smyth *et al.*, 2007; Galan *et al.*, 2011) suggest that the translocation of STIM1 proteins does not rely on cytoskeleton, instead they "slide" along the ER membrane. The reduction of SOCE in response to cytoskeleton depolymerisation is not unexpected because the store-operated channel subunits including STIM1, ORAI1 and TRPCs have been found to interact with several types of cytoskeleton (Grigoriev *et al.*, 2008; Odell *et al.*, 2008; Galan *et al.*, 2011; Stiber *et al.*, 2012). Loss of cytoskeleton support may change the architecture of store-operated channel complex and thus the SOCE is impaired. Another way to inhibit SOCE by manipulating cytoskeleton is increasing the subplasmalemmal F-

actin content, which disrupts the PM-ER junctions and blocks STIM1 translocation. This mechanism has been confirmed by a recent report using neuroendocrine-differentiated cells (Vanoverberghe *et al.*, 2012), suggesting that it is a common mechanism existing in different types of cells.

8.1.4. Inhibition of ORAI1/2/3 and TRPC3/4/5/6 channels by the ryanodine receptor agonoist 4-CEP

Apart from the roles in triggering Ca^{2+} release through ryanodine receptors and cytosolic STIM1 clustering, 4-CEP also inhibits SOCE by direct action on ORAI1/2/3 and TRPC3/4/5/6 channels. The chlorophenol analogues 4-C*m*C and 4-ClP have similar inhibitory effects on these channels as 4-CEP, and the potencies of these three compounds are ranked as 4-CEP > 4-C*m*C > 4-ClP. The inhibition of 4-CEP on ORAI3, TRPC4 and TRPC6 channels is concentrantion-dependent, with IC_{50} of 71.0, 85.6 and 108.4 µM, respectively. The activities of ORAI3 and TRPC3/4/5/6 channels are quickly recovered when 4-CEP is removed from the bath solution. The action sites of 4-CEP on ORAI3 and TRPC4 channels are located at the cell surface.

Ryanodine receptors are ER/SR Ca^{2+} release channels particularly important for the contraction of cardiac and skeletal muscle cells. RyR1 mutations which increase the channel sensitivity to general anaesthetic agents are the main cause for malignant hyperthermia, a skeletal muscle-related disease. Several RyR agonists are currently used in the diagnosis of malignant hyperthermia, among which 4-CEP and 4-C*m*C have been shown to sucessfully distinguish the malignant hyperthermia-susceptible skeletal muscles from normal samples. However, both drugs have not been included in the standard protocols for malignant hyperthermia diagnosis. The findings in this study have revealed a novel pharmacological aspect of these compounds, which could be useful for future drug development based on this class of molecules.

8.1.5. Cu^{2+} is a potent activator of TRPC3/4/5/6 channels and strong inhibitor of TRPM2 channel

Cu^{2+} at micromolar concentrations potently stimulates TRPC3/4/5/6 channels but inhibits TRPM2 channel activated by intracellular ADP-Ribose. Site-directed mutagenesis identified that the E542, E543 and C554 residues within the outer pore of TRPC4 are potential molecular targets of Cu^{2+}. The action site of Cu^{2+} on TRPM2 is also extracellularly located. The effects of Cu^{2+} on TRPC and TRPM2 channels

are concentration-dependent and cannot be reversed by removel of Cu^{2+} from the bath solution.

As copper has been considered an important pathophysiological factor of neurodegenerative diseases for long, understanding the modulation of TRP channels by Cu^{2+} will be helpful to demonstrate the exact roles of these channels in neurodegenerative diseases. Although TRPM2 channel has been suggested to mediate neuronal cell death induced by oxdative stress and Ca^{2+} overload, the findings in this study reveal that TRPC channels are much more likely to be responsible for this process, because the high concentrations of copper in the diseased regions of brain would completely abolish the activity of TRPM2 channel but substantially stimulate massive Ca^{2+} influx through TRPC channels. Therefore, blocking TRPC channels may be a novel and useful strategy in the treatment of neurodegenerative diseases.

8.1.6. TRPC channels promote the proliferation of human ovarian cancer cells and tumourigenesis

It is found that TRPC1/3/4/6 channels with multiple alternatively spliced variants are expressed in the human ovarian adenocarcinoma-derived SKOV3 cells. The proliferation of SKOV3 cells were significantly suppressed by TRPC channel blockers 2-APB and SKF-96365 and TRPC isoform-specific pore-blocking antibodies. Knockdown of TRPC gene expression by siRNAs also robustly inhibited the cancer cell proliferation. Colony growth of SKOV3 cells was promoted by overexpression of TRPC channels. Overall inhibition of TRPC channels by SKF-96365 arrested SKOV3 cells at G_2/M phase and significantly induced apoptosis, wheareas knockdown of individual TRPC gene expression by siRNA showed similar effect on cell cycle but did not increase the percentage of apoptotic cells.

TRP channels are increasingly recognised as very promising targets for anti-acncer therapy (Nilius *et al.*, 2007; Prevarskaya *et al.*, 2007; Fiorio Pla *et al.*, 2012). The abundant expression of TRPC channels in SKOV3 cells and their essential roles in cell proliferation and apoptosis discovered here have strongly evidenced the importance of Ca^{2+} homeostasis in ovarian cancer development. The inhibition of cell cycle progression by TRPC channel blockade and gene silencing provides a mechanistic view on the anti-proliferative effects of these treatments. As most TRPC channels are localised at the cell plasma membrane, they can be directly accessed by

pharmacological agents and antibodies delivered in blood stream, both of which have been used in this study and proved to be effective *in vitro*. These channel blockers are not only research tools for understanding the roles of TRPC channels in ovarian cancer development, but also potentially useful drugs for future anti-cancer therapy.

8.2. Study limitations and future directions

8.2.1. Localisation and functional interaction of store-operated channel components

In this study the localisation of STIM1, ORAI and TRPC proteins in HEK293cells is visualised by tagged fluorescent proteins, which is a generally used method for studying protein localisation in live cells. As this method requires transfection and overexpression of the genes, it cannot be used to show the localisation of endogenously expressed proteins. Immunostaining with specific primary antibody and fluorescent dye-conjugated secondary antibody is an important method to visualise the localisation of both endogenous and overexpressed proteins in fixed cells. The protein localisation shown by tagged fluorescent proteins in this study can be validated by immunofluorescence if reliable primary antibodies are provided. Similarly, the interaction between co-localised proteins can be further confirmed by co-immunoprecipitation and Western blotting.

8.2.2. Molecular mechanism of the cytosolic clustering of STIM1

Cytosolic clustering of STIM1 is found to be an unrecognised effect of some SOCE blockers, such as 2-APB, 4-CEP and flufenamic acid. Although STIM1 is known to oligomerise and form protein complex with ORAI channels at the plasma membrane, it is still unknown whether the formation of cytosolic STIM1 clusters requires any binding partners or scaffold proteins adjacent to the ER. As this phenomenon is described only in STIM1-overexpressing HEK293 cells, it needs to be confirmed in other types of cells. The response of endogenous STIM1 proteins in native cells to these drugs is also worthy to be investigated by immunofluorescence. Moreover, it is important to know whether STIM2 is able to form cytosolic clusters as its homologue STIM1, which may reveal more structural and functional aspects of these two proteins. Design and screening of novel compounds which selectively

regulate cytosolic STIM1 clustering would be a promising field in future drug development aiming to control SOCE.

8.2.3. Regulation of store-operated channel activity by cytoskeleton

The disruption of either microtubule or microfilament cytoskeleton leads to impaired SOCE, but does not affect the translocation of STIM1 toward the plasma membrane. A speculative mechanism for this is that loss of cytoskeleton changes the architecture and reduces the activity of the store-operated channel complex, which includes STIM1, ORAIs and possibly TRPCs. To investigate this mechanism, it needs to be demonstrated that which store-operated channel subunit interacts directly with tubulin, actin or other cytoskeletal proteins. In addition, cytoskeleton also supports the structure of caveolae (van Deurs *et al.*, 2003), which are a special type of lipid raft and important microdomains for Ca^{2+} signalling (Pani and Singh, 2009). Synchronous visualisation of lipid rafts and store-operated channels before and after cytoskeleton depolymerisation will further explain the regulatory mechanism of SOCE by cytoskeleton.

8.2.4. Interaction between chlorophenol derivatives and plasma membrane ion channels at molecular level

Three chlorophenol analogues, 4-CEP, 4-C*m*C and 4-ClP, are found to inhibit SOCE by blocking ORAI and TRPC channels. The action sites of 4-CEP on these channels are extracellularly located, but the exact target amino acids are not examined. Elongation of the 3-alkyl chain of these compounds is accompanied by increased potency on channel inhibition, which is an important clue for investigating the structural interaction between the drugs and channel proteins. Biophysical studies illustrating the crystal structures of the channel pore-forming regions will be helpful to understand the non-selective inhibitory mechanism of these compounds on ORAI and TRPC channels, and also voltage-gated Na^+ channels (Haeseler *et al.*, 1999; Haeseler *et al.*, 2001). Future electrophysiological studies on other ion channels are also required to give a comprehensive view on the pharmacology of chlorophenol derivatives.

8.2.5. Regulatory mechanisms of TRP channels by copper

The activation of TRPC channels by Cu^{2+} is a slow process compared to that by Gd^{3+} and trypsin. The mechanism for the initial inhibition and late potentiation is unclear. Although the amino acid residues E542, E543 and C554 of TRPC4 are found to be involved in the channel activation by Cu^{2+}, they seem not to be the exclusive determinants for the effect of Cu^{2+}, given the evidence that these three residues are not conserved in the corresponding regions of TRPC3 and TRPC6. Therefore, further mutagenesis work on TRPC3 and TRPC6 is required to demonstrate whether there is a universal mechanism responsible for the activation of all TRPC channels by Cu^{2+}.

The mechanism underlying the inhibition of TRPM2 channel by Cu^{2+} is possibly similar to the action of Zn^{2+} (Yang *et al.*, 2011). As the two residues K952 and D1002 of TRPM2 have been demonstrated to be the key determinants for the channel inactivation by Zn^{2+}, it is worthy to test the effect of Cu^{2+} on TRPM2 mutants with these two residues altered, which will give a conclusive result for the inhibitory mechanism of Cu^{2+} on TRPM2 channel.

8.2.6. TRPC channels as therapeutic targets for cancer and other diseases

Higher activity of TRPC channels is found to promote the proliferation and colony growth of human ovarian cancer cells. These findings from *in vitro* experiments are very important for ovarian cancer research if they can be confirmed in animal models and human patients. Genetically modified ovarian cancer cells with significantly upregulated or reduced TRPC expression can be injected into mice or rats to study the tumour growth *in vivo*, which will provide solid evidence for the role of TRPC channels in tumourigenesis. The expression levels of TRPC channels in human ovarian tumours and normal ovarian tissues can be compared by real-time quantitative PCR and Western blotting analyses, which may reveal a correlation between TRPC expression levels and the differentiation states of ovarian cancer. Development of clinically safe TRPC blockers will be an important field in pharmacological and pharmaceutical research, which would be useful in the treatment of cancer, pathological cardiac hypertrophy and many other diseases.

References

Abdullaev, I.F., Bisaillon, J.M., Potier, M., Gonzalez, J.C., Motiani, R.K. & Trebak, M. (2008) Stim1 and Orai1 mediate CRAC currents and store-operated calcium entry important for endothelial cell proliferation. *Circ Res.* 103 (11), pp. 1289-1299.

Abramowitz, J. & Birnbaumer, L. (2009) Physiology and pathophysiology of canonical transient receptor potential channels. *FASEB J.* 23 (2), pp. 297-328.

Alarcon, J.M., Brito, J.A., Hermosilla, T., Atwater, I., Mears, D. & Rojas, E. (2006) Ion channel formation by Alzheimer's disease amyloid beta-peptide (Abeta40) in unilamellar liposomes is determined by anionic phospholipids. *Peptides.* 27 (1), pp. 95-104.

Alfonso, S., Benito, O., Alicia, S., Angelica, Z., Patricia, G., Diana, K. & Luis, V. (2008) Regulation of the cellular localization and function of human transient receptor potential channel 1 by other members of the TRPC family. *Cell Calcium.* 43 (4), pp. 375-387.

Aydar, E., Yeo, S., Djamgoz, M. & Palmer, C. (2009) Abnormal expression, localization and interaction of canonical transient receptor potential ion channels in human breast cancer cell lines and tissues: a potential target for breast cancer diagnosis and therapy. *Cancer Cell Int.* 9 pp. 23.

Baba, Y., Nishida, K., Fujii, Y., Hirano, T., Hikida, M. & Kurosaki, T. (2008) Essential function for the calcium sensor STIM1 in mast cell activation and anaphylactic responses. *Nat Immunol.* 9 (1), pp. 81-88.

Bakowski, D., Burgoyne, R.D. & Parekh, A.B. (2003) Activation of the store-operated calcium current ICRAC can be dissociated from regulated exocytosis in rat basophilic leukaemia (RBL-1) cells. *J Physiol.* 553 (Pt 2), pp. 387-393.

Baur, C.P., Bellon, L., Felleiter, P., Fiege, M., Fricker, R., Glahn, K., Heffron, J.J., Herrmann-Frank, A., Jurkat-Rott, K., Klingler, W., Lehane, M., Ording, H., Tegazzin, V., Wappler, F., Georgieff, M. & Lehmann-Horn, F. (2000) A multicenter study of 4-chloro-m-cresol for diagnosing malignant hyperthermia susceptibility. *Anesth Analg.* 90 (1), pp. 200-205.

Beck, B., Lehen'kyi, V., Roudbaraki, M., Flourakis, M., Charveron, M., Bordat, P., Polakowska, R., Prevarskaya, N. & Skryma, R. (2008) TRPC channels determine human keratinocyte differentiation: new insight into basal cell carcinoma. *Cell Calcium.* 43 (5), pp. 492-505.

Beeler, T.J. & Gable, K.S. (1993) Activation of Ca2+ release from sarcoplasmic reticulum vesicles by 4-alkylphenols. *Archives of biochemistry and biophysics.* 301 (2), pp. 216-220.

Berbey, C., Weiss, N., Legrand, C. & Allard, B. (2009) Transient receptor potential canonical type 1 (TRPC1) operates as a sarcoplasmic reticulum calcium leak channel in skeletal muscle. *J Biol Chem.* 284 (52), pp. 36387-36394.

Bertram, R., Smolen, P., Sherman, A., Mears, D., Atwater, I., Martin, F. & Soria, B. (1995) A role for calcium release-activated current (CRAC) in cholinergic modulation of electrical activity in pancreatic beta-cells. *Biophys J.* 68 (6), pp. 2323-2332.

Bidaux, G., Beck, B., Zholos, A., Gordienko, D., Lemonnier, L., Flourakis, M., Roudbaraki, M., Borowiec, A.S., Fernandez, J., Delcourt, P., Lepage, G., Shuba, Y., Skryma, R. & Prevarskaya, N. (2012) Regulation of activity of transient receptor potential melastatin 8 (TRPM8) channel by its short isoforms. *J Biol Chem.* 287 (5), pp. 2948-2962.

Bilmen, J.G., Wootton, L.L., Godfrey, R.E., Smart, O.S. & Michelangeli, F. (2002) Inhibition of SERCA Ca^{2+} pumps by 2-aminoethoxydiphenyl borate (2-APB). 2-APB reduces both Ca^{2+} binding and phosphoryl transfer from ATP, by interfering with the pathway leading to the Ca^{2+}-binding sites. *Eur J Biochem.* 269 (15), pp. 3678-3687.

Bodding, M. (2007) TRP proteins and cancer. *Cell Signal.* 19 (3), pp. 617-624.

Bomben, V.C. & Sontheimer, H.W. (2008) Inhibition of transient receptor potential canonical channels impairs cytokinesis in human malignant gliomas. *Cell Prolif.* 41 (1), pp. 98-121.

Bordin, S., Boschero, A.C., Carneiro, E.M. & Atwater, I. (1995) Ionic mechanisms involved in the regulation of insulin secretion by muscarinic agonists. *J Membr Biol.* 148 (2), pp. 177-184.

Boulay, G., Zhu, X., Peyton, M., Jiang, M., Hurst, R., Stefani, E. & Birnbaumer, L. (1997) Cloning and expression of a novel mammalian homolog of Drosophila transient receptor potential (Trp) involved in calcium entry secondary to activation of receptors coupled by the Gq class of G protein. *J Biol Chem.* 272 (47), pp. 29672-29680.

Braun, A., Gessner, J.E., Varga-Szabo, D., Syed, S.N., Konrad, S., Stegner, D., Vogtle, T., Schmidt, R.E. & Nieswandt, B. (2009a) STIM1 is essential for Fcgamma receptor activation and autoimmune inflammation. *Blood.* 113 (5), pp. 1097-1104.

Braun, A., Varga-Szabo, D., Kleinschnitz, C., Pleines, I., Bender, M., Austinat, M., Bosl, M., Stoll, G. & Nieswandt, B. (2009b) Orai1 (CRACM1) is the platelet SOC channel and essential for pathological thrombus formation. *Blood.* 113 (9), pp. 2056-2063.

Brewer, G.J. (2009) The risks of copper toxicity contributing to cognitive decline in the aging population and to Alzheimer's disease. *J Am Coll Nutr.* 28 (3), pp. 238-242.

Brinkmeier, H. (2011) TRP channels in skeletal muscle: gene expression, function and implications for disease. *Adv Exp Med Biol.* 704 pp. 749-758.

Bush, E.W., Hood, D.B., Papst, P.J., Chapo, J.A., Minobe, W., Bristow, M.R., Olson, E.N. & McKinsey, T.A. (2006) Canonical transient receptor potential channels promote cardiomyocyte hypertrophy through activation of calcineurin signaling. *J Biol Chem.* 281 (44), pp. 33487-33496.

Bygrave, F.L. & Benedetti, A. (1996) What is the concentration of calcium ions in the endoplasmic reticulum? *Cell Calcium.* 19 (6), pp. 547-551.

Cai, R., Ding, X., Zhou, K., Shi, Y., Ge, R., Ren, G., Jin, Y. & Wang, Y. (2009) Blockade of TRPC6 channels induced G2/M phase arrest and suppressed growth in human gastric cancer cells. *Int J Cancer.* 125 (10), pp. 2281-2287.

Cai, X. (2007a) Molecular evolution and functional divergence of the Ca(2+) sensor protein in store-operated Ca(2+) entry: stromal interaction molecule. *PLoS One.* 2 (7), pp. e609.

Cai, X. (2007b) Molecular evolution and structural analysis of the Ca(2+) release-activated Ca(2+) channel subunit, Orai. *J Mol Biol.* 368 (5), pp. 1284-1291.

Calloway, N., Vig, M., Kinet, J.P., Holowka, D. & Baird, B. (2009) Molecular clustering of STIM1 with Orai1/CRACM1 at the plasma membrane depends dynamically on depletion of Ca^{2+} stores and on electrostatic interactions. *Mol Biol Cell.* 20 (1), pp. 389-399.

Canatan, H., Bakan, I., Akbulut, M., Halifeoglu, I., Cikim, G., Baydas, G. & Kilic, N. (2004) Relationship among levels of leptin and zinc, copper, and zinc/copper ratio in plasma of patients with essential hypertension and healthy normotensive subjects. *Biol Trace Elem Res.* 100 (2), pp. 117-123.

Carrasco, S. & Meyer, T. (2011) STIM proteins and the endoplasmic reticulum-plasma membrane junctions. *Annu Rev Biochem.* 80 pp. 973-1000.

Casteels, R. & Droogmans, G. (1981) Exchange characteristics of the noradrenaline-sensitive calcium store in vascular smooth muscle cells or rabbit ear artery. *J Physiol.* 317 pp. 263-279.

Chaudhuri, P., Colles, S.M., Bhat, M., Van Wagoner, D.R., Birnbaumer, L. & Graham, L.M. (2008) Elucidation of a TRPC6-TRPC5 channel cascade that restricts endothelial cell movement. *Mol Biol Cell.* 19 (8), pp. 3203-3211.

Chelly, J., Tumer, Z., Tonnesen, T., Petterson, A., Ishikawa-Brush, Y., Tommerup, N., Horn, N. & Monaco, A.P. (1993) Isolation of a candidate gene for Menkes disease that encodes a potential heavy metal binding protein. *Nat Genet.* 3 (1), pp. 14-19.

Chen, Y., Smith, M.L., Chiou, G.X., Ballaron, S., Sheets, M.P., Gubbins, E., Warrior, U., Wilkins, J., Surowy, C., Nakane, M., Carter, G.W., Trevillyan, J.M., Mollison, K. & Djuric, S.W. (2002) TH1 and TH2 cytokine inhibition by 3,5-bis(trifluoromethyl)pyrazoles, a novel class of immunomodulators. *Cell Immunol.* 220 (2), pp. 134-142.

Cheng, K.T., Liu, X., Ong, H.L. & Ambudkar, I.S. (2008) Functional requirement for Orai1 in store-operated TRPC1-STIM1 channels. *J Biol Chem.* 283 (19), pp. 12935-12940.

Cheng, K.T., Liu, X., Ong, H.L., Swaim, W. & Ambudkar, I.S. (2011) Local Ca(2)+ entry via Orai1 regulates plasma membrane recruitment of TRPC1 and controls cytosolic Ca(2)+ signals required for specific cell functions. *PLoS Biol.* 9 (3), pp. e1001025.

Chvanov, M., Walsh, C.M., Haynes, L.P., Voronina, S.G., Lur, G., Gerasimenko, O.V., Barraclough, R., Rudland, P.S., Petersen, O.H., Burgoyne, R.D. & Tepikin, A.V. (2008) ATP depletion induces translocation of STIM1 to puncta and formation of STIM1-ORAI1 clusters: translocation and re-translocation of STIM1 does not require ATP. *Pflugers Arch.* 457 (2), pp. 505-517.

Cioffi, D.L. (2011) Redox regulation of endothelial canonical transient receptor potential channels. *Antioxid Redox Signal.* 15 (6), pp. 1567-1582.

Clapham, D.E. (2003) TRP channels as cellular sensors. *Nature.* 426 (6966), pp. 517-524.

Cooper, G.J. (2011) Therapeutic potential of copper chelation with triethylenetetramine in managing diabetes mellitus and Alzheimer's disease. *Drugs.* 71 (10), pp. 1281-1320.

Dedkova, E.N. & Blatter, L.A. (2002) Nitric oxide inhibits capacitative Ca^{2+} entry and enhances endoplasmic reticulum Ca^{2+} uptake in bovine vascular endothelial cells. *J Physiol.* 539 (1), pp. 77-91.

Dedman, A.M., Majeed, Y., Tumova, S., Zeng, F., Kumar, B., Munsch, C., Bateson, A.N., Wittmann, J., Jack, H.M., Porter, K.E. & Beech, D.J. (2011) TRPC1 transcript variants, inefficient nonsense-mediated decay and low up-frameshift-1 in vascular smooth muscle cells. *BMC Mol Biol.* 12 pp. 30.

DeHaven, W.I., Jones, B.F., Petranka, J.G., Smyth, J.T., Tomita, T., Bird, G.S. & Putney, J.W., Jr. (2009) TRPC channels function independently of STIM1 and Orai1. *J Physiol.* 587 (Pt 10), pp. 2275-2298.

DeHaven, W.I., Smyth, J.T., Boyles, R.R., Bird, G.S. & Putney, J.W., Jr. (2008) Complex actions of 2-aminoethyldiphenyl borate on store-operated calcium entry. *J Biol Chem.* 283 (28), pp. 19265-19273.

den Dekker, E., Molin, D.G., Breikers, G., van Oerle, R., Akkerman, J.W., van Eys, G.J. & Heemskerk, J.W. (2001) Expression of transient receptor potential mRNA isoforms and Ca(2+) influx in differentiating human stem cells and platelets. *Biochim Biophys Acta.* 1539 (3), pp. 243-255.

Deng, X., Wang, Y., Zhou, Y., Soboloff, J. & Gill, D.L. (2009) STIM and Orai: dynamic intermembrane coupling to control cellular calcium signals. *J Biol Chem.* 284 (34), pp. 22501-22505.

Desai, V. & Kaler, S.G. (2008) Role of copper in human neurological disorders. *Am J Clin Nutr.* 88 (3), pp. 855S-858S.

Di, A., Gao, X.P., Qian, F., Kawamura, T., Han, J., Hecquet, C., Ye, R.D., Vogel, S.M. & Malik, A.B. (2011) The redox-sensitive cation channel TRPM2 modulates phagocyte ROS production and inflammation. *Nat Immunol.* 13 (1), pp. 29-34.

Dietrich, A., Kalwa, H., Storch, U., Mederos y Schnitzler, M., Salanova, B., Pinkenburg, O., Dubrovska, G., Essin, K., Gollasch, M., Birnbaumer, L. & Gudermann, T. (2007) Pressure-induced and store-operated cation influx in vascular smooth muscle cells is independent of TRPC1. *Pflugers Arch.* 455 (3), pp. 465-477.

Dietrich, A., Mederos, Y.S.M., Gollasch, M., Gross, V., Storch, U., Dubrovska, G., Obst, M., Yildirim, E., Salanova, B., Kalwa, H., Essin, K., Pinkenburg, O., Luft, F.C., Gudermann, T. & Birnbaumer, L. (2005) Increased vascular smooth muscle contractility in TRPC6-/- mice. *Mol Cell Biol.* 25 (16), pp. 6980-6989.

DiJulio, D.H., Watson, E.L., Pessah, I.N., Jacobson, K.L., Ott, S.M., Buck, E.D. & Singh, J.C. (1997) Ryanodine receptor type III (Ry3R) identification in mouse parotid acini. Properties and modulation of [3H]ryanodine-binding sites. *J Biol Chem.* 272 (25), pp. 15687-15696.

Dirksen, R.T. (2009) Checking your SOCCs and feet: the molecular mechanisms of Ca^{2+} entry in skeletal muscle. *J Physiol.* 587 (Pt 13), pp. 3139-3147.

Du, J., Xie, J. & Yue, L. (2009) Modulation of TRPM2 by acidic pH and the underlying mechanisms for pH sensitivity. *Journal of General Physiology.* 134 (6), pp. 471-488.

Duke, A.M., Hopkins, P.M., Calaghan, S.C., Halsall, J.P. & Steele, D.S. (2010) Store-operated Ca^{2+} entry in malignant hyperthermia-susceptible human skeletal muscle. *J Biol Chem.* 285 (33), pp. 25645-25653.

El Boustany, C., Bidaux, G., Enfissi, A., Delcourt, P., Prevarskaya, N. & Capiod, T. (2008) Capacitative calcium entry and transient receptor potential canonical 6 expression control human hepatoma cell proliferation. *Hepatology.* 47 (6), pp. 2068-2077.

Endo, M. (2009) Calcium-induced calcium release in skeletal muscle. *Physiol Rev.* 89 (4), pp. 1153-1176.

Enfissi, A., Prigent, S., Colosetti, P. & Capiod, T. (2004) The blocking of capacitative calcium entry by 2-aminoethyl diphenylborate (2-APB) and carboxyamidotriazole (CAI) inhibits proliferation in Hep G2 and Huh-7 human hepatoma cells. *Cell Calcium.* 36 (6), pp. 459-467.

Estacion, M., Li, S., Sinkins, W.G., Gosling, M., Bahra, P., Poll, C., Westwick, J. & Schilling, W.P. (2004) Activation of human TRPC6 channels by receptor stimulation. *J Biol Chem.* 279 (21), pp. 22047-22056.

Faller, P. (2012) Copper in Alzheimer disease: too much, too little, or misplaced? *Free Radical Biology and Medicine.* 52 (4), pp. 747-748.

Fantozzi, I., Zhang, S., Platoshyn, O., Remillard, C.V., Cowling, R.T. & Yuan, J.X. (2003) Hypoxia increases AP-1 binding activity by enhancing capacitative Ca^{2+} entry in human pulmonary artery endothelial cells. *Am J Physiol Lung Cell Mol Physiol.* 285 (6), pp. L1233-1245.

Fellner, S.K. & Arendshorst, W.J. (2000) Ryanodine receptor and capacitative Ca^{2+} entry in fresh preglomerular vascular smooth muscle cells. *Kidney Int.* 58 (4), pp. 1686-1694.

Feng, M., Grice, D.M., Faddy, H.M., Nguyen, N., Leitch, S., Wang, Y., Muend, S., Kenny, P.A., Sukumar, S., Roberts-Thomson, S.J., Monteith, G.R. & Rao, R. (2010) Store-independent activation of Orai1 by SPCA2 in mammary tumors. *Cell.* 143 (1), pp. 84-98.

Fernandez, J.A., Skryma, R., Bidaux, G., Magleby, K.L., Scholfield, C.N., McGeown, J.G., Prevarskaya, N. & Zholos, A.V. (2012) Short isoforms of the cold receptor TRPM8 inhibit channel gating by mimicking heat action rather than chemical inhibitors. *J Biol Chem.* 287 (5), pp. 2963-2970.

Feske, S. (2009) ORAI1 and STIM1 deficiency in human and mice: roles of store-operated Ca^{2+} entry in the immune system and beyond. *Immunol Rev.* 231 (1), pp. 189-209.

Feske, S., Gwack, Y., Prakriya, M., Srikanth, S., Puppel, S.H., Tanasa, B., Hogan, P.G., Lewis, R.S., Daly, M. & Rao, A. (2006) A mutation in Orai1 causes immune deficiency by abrogating CRAC channel function. *Nature.* 441 (7090), pp. 179-185.

Feske, S., Picard, C. & Fischer, A. (2010) Immunodeficiency due to mutations in ORAI1 and STIM1. *Clin Immunol.* 135 (2), pp. 169-182.

Fiorio Pla, A., Avanzato, D., Munaron, L. & Ambudkar, I.S. (2012) Ion channels and transporters in cancer. 6. Vascularizing the tumor: TRP channels as molecular targets. *Am J Physiol Cell Physiol.* 302 (1), pp. C9-15.

Flemming, R., Xu, S.Z. & Beech, D.J. (2003) Pharmacological profile of store-operated channels in cerebral arteriolar smooth muscle cells. *Br J Pharmacol.* 139 (5), pp. 955-965.

Fonfria, E., Marshall, I.C., Boyfield, I., Skaper, S.D., Hughes, J.P., Owen, D.E., Zhang, W., Miller, B.A., Benham, C.D. & McNulty, S. (2005) Amyloid beta-peptide(1-42) and hydrogen peroxide-induced toxicity are mediated by TRPM2 in rat primary striatal cultures. *J Neurochem.* 95 (3), pp. 715-723.

Freichel, M., Suh, S.H., Pfeifer, A., Schweig, U., Trost, C., Weissgerber, P., Biel, M., Philipp, S., Freise, D., Droogmans, G., Hofmann, F., Flockerzi, V. & Nilius, B. (2001) Lack of an endothelial store-operated Ca^{2+} current impairs agonist-dependent vasorelaxation in TRP4-/- mice. *Nat Cell Biol.* 3 (2), pp. 121-127.

Freichel, M., Vennekens, R., Olausson, J., Stolz, S., Philipp, S.E., Weissgerber, P. & Flockerzi, V. (2005) Functional role of TRPC proteins in native systems: implications from knockout and knock-down studies. *J Physiol.* 567 (1), pp. 59-66.

Gabashvili, I.S., Sokolowski, B.H., Morton, C.C. & Giersch, A.B. (2007) Ion channel gene expression in the inner ear. *J Assoc Res Otolaryngol.* 8 (3), pp. 305-328.

Gaggelli, E., Kozlowski, H., Valensin, D. & Valensin, G. (2006) Copper homeostasis and neurodegenerative disorders (Alzheimer's, prion, and Parkinson's diseases and amyotrophic lateral sclerosis). *Chem Rev.* 106 (6), pp. 1995-2044.

Gailly, P. (2012) TRP channels in normal and dystrophic skeletal muscle. *Curr Opin Pharmacol.* 12 (3), pp. 326-334.

Galan, C., Dionisio, N., Smani, T., Salido, G.M. & Rosado, J.A. (2011) The cytoskeleton plays a modulatory role in the association between STIM1 and the Ca(2+) channel subunits Orai1 and TRPC1. *Biochem Pharmacol.* 82 (4), pp. 400-410.

Gees, M., Colsoul, B. & Nilius, B. (2010) The Role of Transient Receptor Potential Cation Channels in Ca^{2+} Signaling. *Cold Spring Harb Perspect Biol.* 2 (10), pp. a003962.

Gemes, G., Bangaru, M.L., Wu, H.E., Tang, Q., Weihrauch, D., Koopmeiners, A.S., Cruikshank, J.M., Kwok, W.M. & Hogan, Q.H. (2011) Store-operated Ca^{2+} entry in sensory neurons: functional role and the effect of painful nerve injury. *J Neurosci.* 31 (10), pp. 3536-3549.

Gerbershagen, M.U., Fiege, M., Weisshorn, R., Kolodzie, K., Schulte am Esch, J. & Wappler, F. (2005) Cumulative and bolus in vitro contracture testing with 4-chloro-3-ethylphenol in malignant hyperthermia positive and negative human skeletal muscles. *Anesth Analg.* 101 (3), pp. 710-714.

Gerbershagen, M.U., Wappler, F., Fiege, M., Weilsshorn, R., Alberts, P.A., von Breunig, F. & Schulte am Esch, J. (2002) In vitro effects of 4-chloro-3-ethylphenol in skeletal muscle preparations from malignant hyperthermia susceptible and normal swine. *Eur J Anaesthesiol.* 19 (2), pp. 135-140.

Gervasio, O.L., Whitehead, N.P., Yeung, E.W., Phillips, W.D. & Allen, D.G. (2008) TRPC1 binds to caveolin-3 and is regulated by Src kinase - role in Duchenne muscular dystrophy. *J Cell Sci.* 121 (Pt 13), pp. 2246-2255.

Gracheva, E.O., Cordero-Morales, J.F., Gonzalez-Carcacia, J.A., Ingolia, N.T., Manno, C., Aranguren, C.I., Weissman, J.S. & Julius, D. (2011) Ganglion-specific splicing of TRPV1 underlies infrared sensation in vampire bats. *Nature.* 476 (7358), pp. 88-91.

Graham, S., Ding, M., Ding, Y., Sours-Brothers, S., Luchowski, R., Gryczynski, Z., Yorio, T., Ma, H. & Ma, R. (2010) Canonical transient receptor potential 6 (TRPC6), a redox-regulated cation channel. *J Biol Chem.* 285 (30), pp. 23466-23476.

Graham, S., Yuan, J.P. & Ma, R. (2012) Canonical transient receptor potential channels in diabetes. *Exp Biol Med (Maywood).* 237 (2), pp. 111-118.

Grigoriev, I., Gouveia, S.M., van der Vaart, B., Demmers, J., Smyth, J.T., Honnappa, S., Splinter, D., Steinmetz, M.O., Putney, J.W., Jr., Hoogenraad, C.C. & Akhmanova, A. (2008) STIM1 is a MT-plus-end-tracking protein involved in remodeling of the ER. *Curr Biol.* 18 (3), pp. 177-182.

Grosse, J., Braun, A., Varga-Szabo, D., Beyersdorf, N., Schneider, B., Zeitlmann, L., Hanke, P., Schropp, P., Muhlstedt, S., Zorn, C., Huber, M., Schmittwolf, C., Jagla, W., Yu, P., Kerkau, T., Schulze, H., Nehls, M. & Nieswandt, B. (2007) An EF hand mutation in Stim1 causes premature platelet activation and bleeding in mice. *J Clin Invest.* 117 (11), pp. 3540-3550.

Grynkiewicz, G., Poenie, M. & Tsien, R.Y. (1985) A new generation of Ca^{2+} indicators with greatly improved fluorescence properties. *J Biol Chem.* 260 (6), pp. 3440-3450.

Gu, Q. & Lin, R.L. (2010) Heavy metals zinc, cadmium, and copper stimulate pulmonary sensory neurons via direct activation of TRPA1. *J Appl Physiol.* 108 (4), pp. 891-897.

Gurney, A.M., Drummond, R.M. & Fay, F.S. (2000) Calcium signalling in sarcoplasmic reticulum, cytoplasm and mitochondria during activation of rabbit aorta myocytes. *Cell Calcium.* 27 (6), pp. 339-351.

Gwack, Y., Srikanth, S., Oh-Hora, M., Hogan, P.G., Lamperti, E.D., Yamashita, M., Gelinas, C., Neems, D.S., Sasaki, Y., Feske, S., Prakriya, M., Rajewsky, K. & Rao, A. (2008) Hair loss and defective T- and B-cell function in mice lacking ORAI1. *Mol Cell Biol.* 28 (17), pp. 5209-5222.

Haeseler, G., Leuwer, M., Kavan, J., Wurz, A., Dengler, R. & Piepenbrock, S. (1999) Voltage-dependent block of normal and mutant muscle sodium channels by 4-Chloro-m-Cresol. *Br J Pharmacol.* 128 (6), pp. 1259-1267.

Haeseler, G., Piepenbrink, A., Bufler, J., Dengler, R., Aronson, J.K., Piepenbrock, S. & Leuwer, M. (2001) Structural requirements for voltage-dependent block of muscle sodium channels by phenol derivatives. *Br J Pharmacol.* 132 (8), pp. 1916-1924.

Haga, S., Akai, K. & Ishii, T. (1989) Demonstration of microglial cells in and around senile (neuritic) plaques in the Alzheimer brain. An immunohistochemical study using a novel monoclonal antibody. *Acta Neuropathol.* 77 (6), pp. 569-575.

Hajkova, Z., Bugajev, V., Draberova, E., Vinopal, S., Draberova, L., Janacek, J. & Draber, P. (2010) STIM1-directed reorganization of microtubules in activated mast cells. *J Immunol.* 186 (2), pp. 913-923.

Hara, Y., Wakamori, M., Ishii, M., Maeno, E., Nishida, M., Yoshida, T., Yamada, H., Shimizu, S., Mori, E., Kudoh, J., Shimizu, N., Kurose, H., Okada, Y., Imoto, K. & Mori, Y. (2002) LTRPC2 Ca^{2+}-permeable channel activated by changes in redox status confers susceptibility to cell death. *Mol Cell.* 9 (1), pp. 163-173.

Harks, E.G., Camina, J.P., Peters, P.H., Ypey, D.L., Scheenen, W.J., van Zoelen, E.J. & Theuvenet, A.P. (2003) Besides affecting intracellular calcium signaling, 2-APB reversibly blocks gap junctional coupling in confluent monolayers, thereby allowing measurement of single-cell membrane currents in undissociated cells. *FASEB J.* 17 (8), pp. 941-943.

Harper, A.G. & Sage, S.O. (2007) A key role for reverse Na^+/Ca^{2+} exchange influenced by the actin cytoskeleton in store-operated Ca^{2+} entry in human platelets:

evidence against the de novo conformational coupling hypothesis. *Cell Calcium.* 42 (6), pp. 606-617.

Harper, J.L., Camerini-Otero, C.S., Li, A.H., Kim, S.A., Jacobson, K.A. & Daly, J.W. (2003) Dihydropyridines as inhibitors of capacitative calcium entry in leukemic HL-60 cells. *Biochem Pharmacol.* 65 (3), pp. 329-338.

Harteneck, C. & Gollasch, M. (2011) Pharmacological modulation of diacylglycerol-sensitive TRPC3/6/7 channels. *Curr Pharm Biotechnol.* 12 (1), pp. 35-41.

Hartmann, J., Dragicevic, E., Adelsberger, H., Henning, H.A., Sumser, M., Abramowitz, J., Blum, R., Dietrich, A., Freichel, M., Flockerzi, V., Birnbaumer, L. & Konnerth, A. (2008) TRPC3 channels are required for synaptic transmission and motor coordination. *Neuron.* 59 (3), pp. 392-398.

He, J., Yu, T., Pan, J. & Li, H. (2012) Visualisation and identification of the interaction between STIM1s in resting cells. *PLoS One.* 7 (3), pp. e33377.

He, L.P., Hewavitharana, T., Soboloff, J., Spassova, M.A. & Gill, D.L. (2005) A functional link between store-operated and TRPC channels revealed by the 3,5-bis(trifluoromethyl)pyrazole derivative, BTP2. *J Biol Chem.* 280 (12), pp. 10997-11006.

Henquin, J.C., Mourad, N.I. & Nenquin, M. (2012) Disruption and stabilization of beta-cell actin microfilaments differently influence insulin secretion triggered by intracellular Ca^{2+} mobilization or store-operated Ca^{2+} entry. *FEBS Lett.* 586 (1), pp. 89-95.

Hermosura, M.C., Cui, A.M., Go, R.C., Davenport, B., Shetler, C.M., Heizer, J.W., Schmitz, C., Mocz, G., Garruto, R.M. & Perraud, A.L. (2008) Altered functional properties of a TRPM2 variant in Guamanian ALS and PD. *Proc Natl Acad Sci U S A.* 105 (46), pp. 18029-18034.

Herrmann-Frank, A., Richter, M. & Lehmann-Horn, F. (1996) 4-Chloro-m-cresol: a specific tool to distinguish between malignant hyperthermia-susceptible and normal muscle. *Biochem Pharmacol.* 52 (1), pp. 149-155.

Hofmann, T., Obukhov, A.G., Schaefer, M., Harteneck, C., Gudermann, T. & Schultz, G. (1999) Direct activation of human TRPC6 and TRPC3 channels by diacylglycerol. *Nature.* 397 (6716), pp. 259-263.

Hofmann, T., Schaefer, M., Schultz, G. & Gudermann, T. (2002) Subunit composition of mammalian transient receptor potential channels in living cells. *Proc Natl Acad Sci U S A.* 99 (11), pp. 7461-7466.

Hogan, P.G., Lewis, R.S. & Rao, A. (2010) Molecular basis of calcium signaling in lymphocytes: STIM and ORAI. *Annu Rev Immunol.* 28 pp. 491-533.

Holda, J.R. & Blatter, L.A. (1997) Capacitative calcium entry is inhibited in vascular endothelial cells by disruption of cytoskeletal microfilaments. *FEBS Lett.* 403 (2), pp. 191-196.

Hollenberg, M.D. & Compton, S.J. (2002) International Union of Pharmacology. XXVIII. Proteinase-activated receptors. *Pharmacol Rev.* 54 (2), pp. 203-217.

Holmuhamedov, E., Lewis, L., Bienengraeber, M., Holmuhamedova, M., Jahangir, A. & Terzic, A. (2002) Suppression of human tumor cell proliferation through mitochondrial targeting. *FASEB J.* 16 (9), pp. 1010-1016.

Hopkins, P.M. (2011) Malignant hyperthermia: pharmacology of triggering. *Br J Anaesth.* 107 (1), pp. 48-56.

Hoth, M. (1995) Calcium and barium permeation through calcium release-activated calcium (CRAC) channels. *Pflugers Arch.* 430 (3), pp. 315-322.

Hoth, M. & Penner, R. (1992) Depletion of intracellular calcium stores activates a calcium current in mast cells. *Nature.* 355 (6358), pp. 353-356.

House, E., Mold, M., Collingwood, J., Baldwin, A., Goodwin, S. & Exley, C. (2009) Copper abolishes the beta-sheet secondary structure of preformed amyloid fibrils of amyloid-beta(42). *J Alzheimers Dis.* 18 (4), pp. 811-817.

Hsu, S., O'Connell, P.J., Klyachko, V.A., Badminton, M.N., Thomson, A.W., Jackson, M.B., Clapham, D.E. & Ahern, G.P. (2001) Fundamental Ca^{2+} signaling mechanisms in mouse dendritic cells: CRAC is the major Ca^{2+} entry pathway. *J Immunol.* 166 (10), pp. 6126-6133.

Hulot, J.S., Fauconnier, J., Ramanujam, D., Chaanine, A., Aubart, F., Sassi, Y., Merkle, S., Cazorla, O., Ouille, A., Dupuis, M., Hadri, L., Jeong, D., Muhlstedt, S., Schmitt, J., Braun, A., Benard, L., Saliba, Y., Laggerbauer, B., Nieswandt, B., Lacampagne, A., Hajjar, R.J., Lompre, A.M. & Engelhardt, S. (2011) Critical role for stromal interaction molecule 1 in cardiac hypertrophy. *Circulation.* 124 (7), pp. 796-805.

Iaizzo, P.A., Johnson, B.A., Nagao, K. & Gallagher, W.J. (1999) 4-chloro-m-cresol triggers malignant hyperthermia in susceptible swine at doses greatly exceeding those found in drug preparations. *Anesthesiology.* 90 (6), pp. 1723-1732.

Ishii, M., Shimizu, S., Hara, Y., Hagiwara, T., Miyazaki, A., Mori, Y. & Kiuchi, Y. (2006) Intracellular-produced hydroxyl radical mediates H_2O_2-induced Ca^{2+} influx and cell death in rat beta-cell line RIN-5F. *Cell Calcium.* 39 (6), pp. 487-494.

Ishikawa, J., Ohga, K., Yoshino, T., Takezawa, R., Ichikawa, A., Kubota, H. & Yamada, T. (2003) A pyrazole derivative, YM-58483, potently inhibits store-operated sustained Ca^{2+} influx and IL-2 production in T lymphocytes. *J Immunol.* 170 (9), pp. 4441-4449.

Islam, M.S., Leibiger, I., Leibiger, B., Rossi, D., Sorrentino, V., Ekstrom, T.J., Westerblad, H., Andrade, F.H. & Berggren, P.O. (1998) In situ activation of the type 2 ryanodine receptor in pancreatic beta cells requires cAMP-dependent phosphorylation. *Proc Natl Acad Sci U S A.* 95 (11), pp. 6145-6150.

Itagaki, K., Kannan, K.B., Singh, B.B. & Hauser, C.J. (2004) Cytoskeletal reorganization internalizes multiple transient receptor potential channels and blocks calcium entry into human neutrophils. *J Immunol.* 172 (1), pp. 601-607.

Jacobson, A.R., Moe, S.T., Allen, P.D. & Fessenden, J.D. (2006) Structural determinants of 4-chloro-m-cresol required for activation of ryanodine receptor type 1. *Mol Pharmacol.* 70 (1), pp. 259-266.

James, S.A., Volitakis, I., Adlard, P.A., Duce, J.A., Masters, C.L., Cherny, R.A. & Bush, A.I. (2012) Elevated labile Cu is associated with oxidative pathology in Alzheimer disease. *Free Radical Biology and Medicine.* 52 (2), pp. 298-302.

Jeon, J.P., Hong, C., Park, E.J., Jeon, J.H., Cho, N.H., Kim, I.G., Choe, H., Muallem, S., Kim, H.J. & So, I. (2012) Selective Galphai subunits as novel direct activators of transient receptor potential canonical (TRPC)4 and TRPC5 channels. *J Biol Chem.* 287 (21), pp. 17029-17039.

Jeong, S.W., Park, B.G., Park, J.Y., Lee, J.W. & Lee, J.H. (2003) Divalent metals differentially block cloned T-type calcium channels. *Neuroreport.* 14 (11), pp. 1537-1540.

Jiang, H., Zeng, B., Chen, G.L., Bot, D., Eastmond, S., Elsenussi, S.E., Atkin, S.L., Boa, A.N. & Xu, S.Z. (2012) Effect of non-steroidal anti-inflammatory drugs and new fenamate analogues on TRPC4 and TRPC5 channels. *Biochem Pharmacol.* 83 (7), pp. 923-931.

Jomova, K., Vondrakova, D., Lawson, M. & Valko, M. (2010) Metals, oxidative stress and neurodegenerative disorders. *Mol Cell Biochem.* 345 (1-2), pp. 91-104.

Jung, S., Muhle, A., Schaefer, M., Strotmann, R., Schultz, G. & Plant, T.D. (2003) Lanthanides potentiate TRPC5 currents by an action at extracellular sites close to the pore mouth. *J Biol Chem.* 278 (6), pp. 3562-3571.

Kazerounian, S., Pitari, G.M., Shah, F.J., Frick, G.S., Madesh, M., Ruiz-Stewart, I., Schulz, S., Hajnoczky, G. & Waldman, S.A. (2005) Proliferative signaling by store-

operated calcium channels opposes colon cancer cell cytostasis induced by bacterial enterotoxins. *J Pharmacol Exp Ther.* 314 (3), pp. 1013-1022.

Kimata, T., Nagaki, M., Ogiso, T., Naiki, T., Kato, T. & Moriwaki, H. (2006) Actin organization and hepatocyte differentiation are regulated by extracellular matrix via PI-4,5-bisphosphate in the rat. *Hepatology.* 44 (1), pp. 140-151.

Knowles, H., Heizer, J.W., Li, Y., Chapman, K., Ogden, C.A., Andreasen, K., Shapland, E., Kucera, G., Mogan, J., Humann, J., Lenz, L.L., Morrison, A.D. & Perraud, A.-L. (2011) Transient Receptor Potential Melastatin 2 (TRPM2) ion channel is required for innate immunity against Listeria monocytogenes. *Proc Natl Acad Sci U S A.* 108 (28), pp. 11578-11583.

Kolisek, M., Beck, A., Fleig, A. & Penner, R. (2005) Cyclic ADP-ribose and hydrogen peroxide synergize with ADP-ribose in the activation of TRPM2 channels. *Mol Cell.* 18 (1), pp. 61-69.

Korzeniowski, M.K., Manjarres, I.M., Varnai, P. & Balla, T. (2010) Activation of STIM1-Orai1 involves an intramolecular switching mechanism. *Sci Signal.* 3 (148), pp. ra82.

Kovacs, G.G., Zsembery, A., Anderson, S.J., Komlosi, P., Gillespie, G.Y., Bell, P.D., Benos, D.J. & Fuller, C.M. (2005) Changes in intracellular Ca^{2+} and pH in response to thapsigargin in human glioblastoma cells and normal astrocytes. *Am J Physiol Cell Physiol.* 289 (2), pp. C361-371.

Kozak, J.A., Kerschbaum, H.H. & Cahalan, M.D. (2002) Distinct properties of CRAC and MIC channels in RBL cells. *J Gen Physiol.* 120 (2), pp. 221-235.

Kraft, R., Grimm, C., Grosse, K., Hoffmann, A., Sauerbruch, S., Kettenmann, H., Schultz, G. & Harteneck, C. (2004) Hydrogen peroxide and ADP-ribose induce TRPM2-mediated calcium influx and cation currents in microglia. *Am J Physiol Cell Physiol.* 286 (1), pp. C129-137.

Kuang, C.Y., Yu, Y., Guo, R.W., Qian, D.H., Wang, K., Den, M.Y., Shi, Y.K. & Huang, L. (2010) Silencing stromal interaction molecule 1 by RNA interference inhibits the proliferation and migration of endothelial progenitor cells. *Biochem Biophys Res Commun.* 398 (2), pp. 315-320.

Kurebayashi, N. & Ogawa, Y. (2001) Depletion of Ca^{2+} in the sarcoplasmic reticulum stimulates Ca^{2+} entry into mouse skeletal muscle fibres. *J Physiol.* 533 (Pt 1), pp. 185-199.

Kwan, H.Y., Huang, Y. & Yao, X.Q. (2004) Regulation of canonical transient receptor potential isoform 3 (TRPC3) channel by protein kinase G. *Proc Natl Acad Sci U S A.* 101 (8), pp. 2625-2630.

Lanner, J.T. (2012) Ryanodine receptor physiology and its role in disease. *Adv Exp Med Biol.* 740 pp. 217-234.

Lanner, J.T., Georgiou, D.K., Joshi, A.D. & Hamilton, S.L. (2010) Ryanodine receptors: structure, expression, molecular details, and function in calcium release. *Cold Spring Harb Perspect Biol.* 2 (11), pp. a003996.

Larsson, L. & Ohman, S. (1978) Serum ionized calcium and corrected total calcium in borderline hyperparathyroidism. *Clin Chem.* 24 (11), pp. 1962-1965.

Launikonis, B.S., Barnes, M. & Stephenson, D.G. (2003) Identification of the coupling between skeletal muscle store-operated Ca^{2+} entry and the inositol trisphosphate receptor. *Proc Natl Acad Sci U S A.* 100 (5), pp. 2941-2944.

Launikonis, B.S., Murphy, R.M. & Edwards, J.N. (2010) Toward the roles of store-operated Ca^{2+} entry in skeletal muscle. *Pflugers Arch.* 460 (5), pp. 813-823.

Lee, C., Xu, D.Z., Feketeova, E., Kannan, K.B., Fekete, Z., Deitch, E.A., Livingston, D.H. & Hauser, C.J. (2005a) Store-operated calcium channel inhibition attenuates neutrophil function and postshock acute lung injury. *J Trauma.* 59 (1), pp. 56-63.

Lee, C.H., Kuo, K.H., Dai, J., Leo, J.M., Seow, C.Y. & Breemen, C. (2005b) Calyculin-A disrupts subplasmalemmal junction and recurring Ca^{2+} waves in vascular smooth muscle. *Cell Calcium.* 37 (1), pp. 9-16.

Lee, K.P., Yuan, J.P., So, I., Worley, P.F. & Muallem, S. (2010) STIM1-dependent and STIM1-independent Function of Transient Receptor Potential Canonical (TRPC) Channels Tunes Their Store-operated Mode. *J Biol Chem.* 285 (49), pp. 38666-38673.

Lewis, R.S. & Cahalan, M.D. (1989) Mitogen-induced oscillations of cytosolic Ca^{2+} and transmembrane Ca^{2+} current in human leukemic T cells. *Cell Regul.* 1 (1), pp. 99-112.

Liao, Y., Erxleben, C., Abramowitz, J., Flockerzi, V., Zhu, M.X., Armstrong, D.L. & Birnbaumer, L. (2008) Functional interactions among Orai1, TRPCs, and STIM1 suggest a STIM-regulated heteromeric Orai/TRPC model for SOCE/Icrac channels. *Proc Natl Acad Sci U S A.* 105 (8), pp. 2895-2900.

Lin, C.J., Huang, H.C. & Jiang, Z.F. (2010) Cu(II) interaction with amyloid-beta peptide: a review of neuroactive mechanisms in AD brains. *Brain Res Bull.* 82 (5-6), pp. 235-242.

Liou, J., Kim, M.L., Heo, W.D., Jones, J.T., Myers, J.W., Ferrell, J.E., Jr. & Meyer, T. (2005) STIM is a Ca^{2+} sensor essential for Ca^{2+}-store-depletion-triggered Ca^{2+} influx. *Curr Biol.* 15 (13), pp. 1235-1241.

Liu, D., Yang, D., He, H., Chen, X., Cao, T., Feng, X., Ma, L., Luo, Z., Wang, L., Yan, Z., Zhu, Z. & Tepel, M. (2009) Increased transient receptor potential canonical type 3 channels in vasculature from hypertensive rats. *Hypertension.* 53 (1), pp. 70-76.

Liu, H., Hughes, J.D., Rollins, S., Chen, B. & Perkins, E. (2011) Calcium entry via ORAI1 regulates glioblastoma cell proliferation and apoptosis. *Exp Mol Pathol.* 91 (3), pp. 753-760.

Liu, X., Cheng, K.T., Bandyopadhyay, B.C., Pani, B., Dietrich, A., Paria, B.C., Swaim, W.D., Beech, D., Yildrim, E., Singh, B.B., Birnbaumer, L. & Ambudkar, I.S. (2007) Attenuation of store-operated Ca^{2+} current impairs salivary gland fluid secretion in TRPC1(-/-) mice. *Proc Natl Acad Sci U S A.* 104 (44), pp. 17542-17547.

Liu, X., Wang, W., Singh, B.B., Lockwich, T., Jadlowiec, J., O'Connell, B., Wellner, R., Zhu, M.X. & Ambudkar, I.S. (2000) Trp1, a candidate protein for the store-operated Ca(2+) influx mechanism in salivary gland cells. *J Biol Chem.* 275 (5), pp. 3403-3411.

Liu, Y.J. & Gylfe, E. (1997) Store-operated Ca^{2+} entry in insulin-releasing pancreatic beta-cells. *Cell Calcium.* 22 (4), pp. 277-286.

Lovell, M.A., Robertson, J.D., Teesdale, W.J., Campbell, J.L. & Markesbery, W.R. (1998) Copper, iron and zinc in Alzheimer's disease senile plaques. *J Neurol Sci.* 158 (1), pp. 47-52.

Luik, R.M., Wu, M.M., Buchanan, J. & Lewis, R.S. (2006) The elementary unit of store-operated Ca^{2+} entry: local activation of CRAC channels by STIM1 at ER-plasma membrane junctions. *J Cell Biol.* 174 (6), pp. 815-825.

Luo, X., Hojayev, B., Jiang, N., Wang, Z.V., Tandan, S., Rakalin, A., Rothermel, B.A., Gillette, T.G. & Hill, J.A. (2012) STIM1-dependent store-operated Ca(2)(+) entry is required for pathological cardiac hypertrophy. *J Mol Cell Cardiol.* 52 (1), pp. 136-147.

Lyfenko, A.D. & Dirksen, R.T. (2008) Differential dependence of store-operated and excitation-coupled Ca^{2+} entry in skeletal muscle on STIM1 and Orai1. *J Physiol.* 586 (Pt 20), pp. 4815-4824.

Lytton, J., Westlin, M. & Hanley, M.R. (1991) Thapsigargin inhibits the sarcoplasmic or endoplasmic reticulum Ca-ATPase family of calcium pumps. *J Biol Chem.* 266 (26), pp. 17067-17071.

Macfarlane, S.R., Seatter, M.J., Kanke, T., Hunter, G.D. & Plevin, R. (2001) Proteinase-activated receptors. *Pharmacol Rev.* 53 (2), pp. 245-282.

Maroto, R., Raso, A., Wood, T.G., Kurosky, A., Martinac, B. & Hamill, O.P. (2005) TRPC1 forms the stretch-activated cation channel in vertebrate cells. *Nat Cell Biol.* 7 (2), pp. 179-185.

Maruyama, T., Kanaji, T., Nakade, S., Kanno, T. & Mikoshiba, K. (1997) 2APB, 2-aminoethoxydiphenyl borate, a membrane-penetrable modulator of Ins(1,4,5)P3-induced Ca^{2+} release. *J Biochem.* 122 (3), pp. 498-505.

Mathie, A., Sutton, G.L., Clarke, C.E. & Veale, E.L. (2006) Zinc and copper: pharmacological probes and endogenous modulators of neuronal excitability. *Pharmacol Therapeut.* 111 (3), pp. 567-583.

McGahon, M., McKee, J., Dash, D., Brown, E., Simpson, D., Curtis, T., McGeown, J. & Scholfield, C. (2012) Pharmacological profiling of store-operated Ca(2+) entry in retinal arteriolar smooth muscle. *Microcirculation.* pp.

McHugh, D., Flemming, R., Xu, S.Z., Perraud, A.L. & Beech, D.J. (2003) Critical intracellular Ca^{2+} dependence of transient receptor potential melastatin 2 (TRPM2) cation channel activation. *J Biol Chem.* 278 (13), pp. 11002-11006.

Meloni, G., Sonois, V., Delaine, T., Guilloreau, L., Gillet, A., Teissie, J., Faller, P. & Vasak, M. (2008) Metal swap between Zn7-metallothionein-3 and amyloid-beta-Cu protects against amyloid-beta toxicity. *Nat Chem Biol.* 4 (6), pp. 366-372.

Mercer, J.C., Dehaven, W.I., Smyth, J.T., Wedel, B., Boyles, R.R., Bird, G.S. & Putney, J.W., Jr. (2006) Large store-operated calcium selective currents due to co-expression of Orai1 or Orai2 with the intracellular calcium sensor, Stim1. *J Biol Chem.* 281 (34), pp. 24979-24990.

Merritt, J.E., Armstrong, W.P., Benham, C.D., Hallam, T.J., Jacob, R., Jaxa-Chamiec, A., Leigh, B.K., McCarthy, S.A., Moores, K.E. & Rink, T.J. (1990) SK&F 96365, a novel inhibitor of receptor-mediated calcium entry. *Biochem J.* 271 (2), pp. 515-522.

Mery, L., Magnino, F., Schmidt, K., Krause, K.H. & Dufour, J.F. (2001) Alternative splice variants of hTrp4 differentially interact with the C-terminal portion of the inositol 1,4,5-trisphosphate receptors. *FEBS Lett.* 487 (3), pp. 377-383.

Mignen, O., Thompson, J.L. & Shuttleworth, T.J. (2009) The molecular architecture of the arachidonate-regulated Ca2+-selective ARC channel is a pentameric assembly of Orai1 and Orai3 subunits. *J Physiol.* 587 (Pt 17), pp. 4181-4197.

Mori, Y., Wakamori, M., Miyakawa, T., Hermosura, M., Hara, Y., Nishida, M., Hirose, K., Mizushima, A., Kurosaki, M., Mori, E., Gotoh, K., Okada, T., Fleig, A., Penner, R., Iino, M. & Kurosaki, T. (2002) Transient receptor potential 1 regulates capacitative Ca(2+) entry and Ca(2+) release from endoplasmic reticulum in B lymphocytes. *J Exp Med.* 195 (6), pp. 673-681.

Motiani, R.K., Abdullaev, I.F. & Trebak, M. (2010) A novel native store-operated calcium channel encoded by Orai3: selective requirement of Orai3 versus Orai1 in estrogen receptor-positive versus estrogen receptor-negative breast cancer cells. *J Biol Chem.* 285 (25), pp. 19173-19183.

Muik, M., Frischauf, I., Derler, I., Fahrner, M., Bergsmann, J., Eder, P., Schindl, R., Hesch, C., Polzinger, B., Fritsch, R., Kahr, H., Madl, J., Gruber, H., Groschner, K. & Romanin, C. (2008) Dynamic coupling of the putative coiled-coil domain of ORAI1 with STIM1 mediates ORAI1 channel activation. *J Biol Chem.* 283 (12), pp. 8014-8022.

Nagamine, K., Kudoh, J., Minoshima, S., Kawasaki, K., Asakawa, S., Ito, F. & Shimizu, N. (1998) Molecular cloning of a novel putative Ca^{2+} channel protein (TRPC7) highly expressed in brain. *Genomics.* 54 (1), pp. 124-131.

Nakao, K., Shirakawa, H., Sugishita, A., Matsutani, I., Niidome, T., Nakagawa, T. & Kaneko, S. (2008) Ca^{2+} mobilization mediated by transient receptor potential canonical 3 is associated with thrombin-induced morphological changes in 1321N1 human astrocytoma cells. *J Neurosci Res.* 86 (12), pp. 2722-2732.

Nakayama, H., Wilkin, B.J., Bodi, I. & Molkentin, J.D. (2006) Calcineurin-dependent cardiomyopathy is activated by TRPC in the adult mouse heart. *FASEB J.* 20 (10), pp. 1660-1670.

Nasman, J., Bart, G., Larsson, K., Louhivuori, L., Peltonen, H. & Akerman, K.E. (2006) The orexin OX1 receptor regulates Ca^{2+} entry via diacylglycerol-activated channels in differentiated neuroblastoma cells. *J Neurosci.* 26 (42), pp. 10658-10666.

Naylor, J., Al-Shawaf, E., McKeown, L., Manna, P.T., Porter, K.E., O'Regan, D., Muraki, K. & Beech, D.J. (2011) TRPC5 channel sensitivities to antioxidants and hydroxylated stilbenes. *J Biol Chem.* 286 (7), pp. 5078-5086.

Naziroglu, M. (2011) TRPM2 cation channels, oxidative stress and neurological diseases: where are we now? *Neurochem Res.* 36 (3), pp. 355-366.

Ng, L.C., Wilson, S.M., McAllister, C.E. & Hume, J.R. (2007) Role of InsP3 and ryanodine receptors in the activation of capacitative Ca^{2+} entry by store depletion or hypoxia in canine pulmonary arterial smooth muscle cells. *Br J Pharmacol.* 152 (1), pp. 101-111.

Nilius, B., Owsianik, G., Voets, T. & Peters, J.A. (2007) Transient Receptor Potential Cation Channels in Disease. *Physiol Rev.* 87 (1), pp. 165-217.

Oberwinkler, J., Lis, A., Giehl, K.M., Flockerzi, V. & Philipp, S.E. (2005) Alternative splicing switches the divalent cation selectivity of TRPM3 channels. *J Biol Chem.* 280 (23), pp. 22540-22548.

Odell, A.F., Van Helden, D.F. & Scott, J.L. (2008) The spectrin cytoskeleton influences the surface expression and activation of human transient receptor potential channel 4 channels. *J Biol Chem.* 283 (7), pp. 4395-4407.

Oh-Hora, M., Yamashita, M., Hogan, P.G., Sharma, S., Lamperti, E., Chung, W., Prakriya, M., Feske, S. & Rao, A. (2008) Dual functions for the endoplasmic reticulum calcium sensors STIM1 and STIM2 in T cell activation and tolerance. *Nat Immunol.* 9 (4), pp. 432-443.

Ohana, L., Newell, E.W., Stanley, E.F. & Schlichter, L.C. (2009) The Ca^{2+} release-activated Ca^{2+} current (I(CRAC)) mediates store-operated Ca^{2+} entry in rat microglia. *Channels (Austin).* 3 (2), pp. 129-139.

Ohba, T., Watanabe, H., Murakami, M., Sato, T., Ono, K. & Ito, H. (2009) Essential role of STIM1 in the development of cardiomyocyte hypertrophy. *Biochem Biophys Res Commun.* 389 (1), pp. 172-176.

Oike, M., Gericke, M., Droogmans, G. & Nilius, B. (1994) Calcium entry activated by store depletion in human umbilical vein endothelial cells. *Cell Calcium.* 16 (5), pp. 367-376.

Okada, T., Inoue, R., Yamazaki, K., Maeda, A., Kurosaki, T., Yamakuni, T., Tanaka, I., Shimizu, S., Ikenaka, K., Imoto, K. & Mori, Y. (1999) Molecular and functional characterization of a novel mouse transient receptor potential protein homologue TRP7. Ca(2+)-permeable cation channel that is constitutively activated and enhanced by stimulation of G protein-coupled receptor. *J Biol Chem.* 274 (39), pp. 27359-27370.

Ong, H.L., Cheng, K.T., Liu, X., Bandyopadhyay, B.C., Paria, B.C., Soboloff, J., Pani, B., Gwack, Y., Srikanth, S., Singh, B.B., Gill, D.L. & Ambudkar, I.S. (2007) Dynamic assembly of TRPC1-STIM1-Orai1 ternary complex is involved in store-operated calcium influx. Evidence for similarities in store-operated and calcium release-activated calcium channel components. *J Biol Chem.* 282 (12), pp. 9105-9116.

Pani, B., Ong, H.L., Brazer, S.C., Liu, X., Rauser, K., Singh, B.B. & Ambudkar, I.S. (2009) Activation of TRPC1 by STIM1 in ER-PM microdomains involves release of the channel from its scaffold caveolin-1. *Proc Natl Acad Sci U S A.* 106 (47), pp. 20087-20092.

Pani, B. & Singh, B.B. (2009) Lipid rafts/caveolae as microdomains of calcium signaling. *Cell Calcium.* 45 (6), pp. 625-633.

Parekh, A.B. & Penner, R. (1997) Store depletion and calcium influx. *Physiol Rev.* 77 (4), pp. 901-930.

Parekh, A.B. & Putney, J.W., Jr. (2005) Store-operated calcium channels. *Physiol Rev.* 85 (2), pp. 757-810.

Park, C.Y., Hoover, P.J., Mullins, F.M., Bachhawat, P., Covington, E.D., Raunser, S., Walz, T., Garcia, K.C., Dolmetsch, R.E. & Lewis, R.S. (2009) STIM1 clusters and activates CRAC channels via direct binding of a cytosolic domain to Orai1. *Cell.* 136 (5), pp. 876-890.

Patterson, R.L., van Rossum, D.B. & Gill, D.L. (1999) Store-operated Ca^{2+} entry: evidence for a secretion-like coupling model. *Cell.* 98 (4), pp. 487-499.

Peinelt, C., Lis, A., Beck, A., Fleig, A. & Penner, R. (2008) 2-Aminoethoxydiphenyl borate directly facilitates and indirectly inhibits STIM1-dependent gating of CRAC channels. *J Physiol.* 586 (13), pp. 3061-3073.

Peinelt, C., Vig, M., Koomoa, D.L., Beck, A., Nadler, M.J., Koblan-Huberson, M., Lis, A., Fleig, A., Penner, R. & Kinet, J.P. (2006) Amplification of CRAC current by STIM1 and CRACM1 (Orai1). *Nat Cell Biol.* 8 (7), pp. 771-773.

Penner, R., Matthews, G. & Neher, E. (1988) Regulation of calcium influx by second messengers in rat mast cells. *Nature.* 334 (6182), pp. 499-504.

Perraud, A.L., Fleig, A., Dunn, C.A., Bagley, L.A., Launay, P., Schmitz, C., Stokes, A.J., Zhu, Q., Bessman, M.J., Penner, R., Kinet, J.P. & Scharenberg, A.M. (2001) ADP-ribose gating of the calcium-permeable LTRPC2 channel revealed by Nudix motif homology. *Nature.* 411 (6837), pp. 595-599.

Picard, C., McCarl, C.A., Papolos, A., Khalil, S., Luthy, K., Hivroz, C., LeDeist, F., Rieux-Laucat, F., Rechavi, G., Rao, A., Fischer, A. & Feske, S. (2009) STIM1 mutation associated with a syndrome of immunodeficiency and autoimmunity. *N Engl J Med.* 360 (19), pp. 1971-1980.

Pigozzi, D., Ducret, T., Tajeddine, N., Gala, J.L., Tombal, B. & Gailly, P. (2006) Calcium store contents control the expression of TRPC1, TRPC3 and TRPV6 proteins in LNCaP prostate cancer cell line. *Cell Calcium.* 39 (5), pp. 401-415.

Plant, T.D. & Schaefer, M. (2003) TRPC4 and TRPC5: receptor-operated Ca2+-permeable nonselective cation channels. *Cell Calcium.* 33 (5-6), pp. 441-450.

Poteser, M., Graziani, A., Rosker, C., Eder, P., Derler, I., Kahr, H., Zhu, M.X., Romanin, C. & Groschner, K. (2006) TRPC3 and TRPC4 associate to form a redox-sensitive cation channel. Evidence for expression of native TRPC3-TRPC4 heteromeric channels in endothelial cells. *J Biol Chem.* 281 (19), pp. 13588-13595.

Potier, M., Gonzalez, J.C., Motiani, R.K., Abdullaev, I.F., Bisaillon, J.M., Singer, H.A. & Trebak, M. (2009) Evidence for STIM1- and Orai1-dependent store-operated calcium influx through ICRAC in vascular smooth muscle cells: role in proliferation and migration. *FASEB J.* 23 (8), pp. 2425-2437.

Prakriya, M., Feske, S., Gwack, Y., Srikanth, S., Rao, A. & Hogan, P.G. (2006) Orai1 is an essential pore subunit of the CRAC channel. *Nature.* 443 (7108), pp. 230-233.

Prevarskaya, N., Zhang, L. & Barritt, G. (2007) TRP channels in cancer. *Biochim Biophys Acta.* 1772 (8), pp. 937-946.

Putney, J.W. (2009) Capacitative calcium entry: from concept to molecules. *Immunol Rev.* 231 (1), pp. 10-22.

Putney, J.W. (2010) Pharmacology of store-operated calcium channels. *Mol Interv.* 10 (4), pp. 209-218.

Putney, J.W., Jr. (1976a) Biphasic modulation of potassium release in rat parotid gland by carbachol and phenylephrine. *J Pharmacol Exp Ther.* 198 (2), pp. 375-384.

Putney, J.W., Jr. (1986) A model for receptor-regulated calcium entry. *Cell Calcium.* 7 (1), pp. 1-12.

Putney, J.W., Jr. (1977) Muscarinic, alpha-adrenergic and peptide receptors regulate the same calcium influx sites in the parotid gland. *J Physiol.* 268 (1), pp. 139-149.

Putney, J.W., Jr. (1976b) Stimulation of 45Ca influx in rat parotid gland by carbachol. *J Pharmacol Exp Ther.* 199 (3), pp. 526-537.

Querfurth, H.W., Haughey, N.J., Greenway, S.C., Yacono, P.W., Golan, D.E. & Geiger, J.D. (1998) Expression of ryanodine receptors in human embryonic kidney (HEK293) cells. *Biochem J.* 334 (Pt 1) pp. 79-86.

Rao, J.N., Platoshyn, O., Golovina, V.A., Liu, L., Zou, T., Marasa, B.S., Turner, D.J., Yuan, J.X. & Wang, J.Y. (2006) TRPC1 functions as a store-operated Ca^{2+} channel in intestinal epithelial cells and regulates early mucosal restitution after wounding. *Am J Physiol Gastrointest Liver Physiol.* 290 (4), pp. G782-792.

Riccardi, C. & Nicoletti, I. (2006) Analysis of apoptosis by propidium iodide staining and flow cytometry. *Nat Protoc.* 1 (3), pp. 1458-1461.

Riccio, A., Li, Y., Moon, J., Kim, K.S., Smith, K.S., Rudolph, U., Gapon, S., Yao, G.L., Tsvetkov, E., Rodig, S.J., Van't Veer, A., Meloni, E.G., Carlezon, W.A., Jr., Bolshakov, V.Y. & Clapham, D.E. (2009) Essential role for TRPC5 in amygdala function and fear-related behavior. *Cell.* 137 (4), pp. 761-772.

Riccio, A., Medhurst, A.D., Mattei, C., Kelsell, R.E., Calver, A.R., Randall, A.D., Benham, C.D. & Pangalos, M.N. (2002) mRNA distribution analysis of human TRPC family in CNS and peripheral tissues. *Brain Res Mol Brain Res.* 109 (1-2), pp. 95-104.

Ricks, T.K. & Trejo, J. (2009) Phosphorylation of protease-activated receptor-2 differentially regulates desensitization and internalization. *J Biol Chem.* 284 (49), pp. 34444-34457.

Riedl, J., Crevenna, A.H., Kessenbrock, K., Yu, J.H., Neukirchen, D., Bista, M., Bradke, F., Jenne, D., Holak, T.A., Werb, Z., Sixt, M. & Wedlich-Soldner, R. (2008) Lifeact: a versatile marker to visualize F-actin. *Nat Methods.* 5 (7), pp. 605-607.

Riera, C.E., Vogel, H., Simon, S.A. & le Coutre, J. (2007) Artificial sweeteners and salts producing a metallic taste sensation activate TRPV1 receptors. *Am J Physiol Regul Integr Comp Physiol.* 293 (2), pp. R626-634.

Rinne, A., Banach, K. & Blatter, L.A. (2009) Regulation of nuclear factor of activated T cells (NFAT) in vascular endothelial cells. *J Mol Cell Cardiol.* 47 (3), pp. 400-410.

Robinson, R., Carpenter, D., Shaw, M.A., Halsall, J. & Hopkins, P. (2006) Mutations in RYR1 in malignant hyperthermia and central core disease. *Hum Mutat.* 27 (10), pp. 977-989.

Rohini, A., Agrawal, N., Koyani, C.N. & Singh, R. (2010) Molecular targets and regulators of cardiac hypertrophy. *Pharmacol Res.* 61 (4), pp. 269-280.

Roos, J., DiGregorio, P.J., Yeromin, A.V., Ohlsen, K., Lioudyno, M., Zhang, S., Safrina, O., Kozak, J.A., Wagner, S.L., Cahalan, M.D., Velicelebi, G. & Stauderman, K.A. (2005) STIM1, an essential and conserved component of store-operated Ca^{2+} channel function. *J Cell Biol.* 169 (3), pp. 435-445.

Ross, K., Whitaker, M. & Reynolds, N.J. (2007) Agonist-induced calcium entry correlates with STIM1 translocation. *J Cell Physiol.* 211 (3), pp. 569-576.

Sabala, P., Targos, B., Caravelli, A., Czajkowski, R., Lim, D., Gragnaniello, G., Santella, L. & Baranska, J. (2002) Role of the actin cytoskeleton in store-mediated calcium entry in glioma C6 cells. *Biochem Biophys Res Commun.* 296 (2), pp. 484-491.

Sakakura, C., Miyagawa, K., Fukuda, K., Shimomura, K., Takemura, M., Takagi, T., Kin, S., Nakase, Y., Fujiyama, J., Mikoshiba, K., Okazaki, Y., Hayashizaki, Y., Hagiwara, A. & Yamagishi, H. (2003) [Possible involvement of inositol 1, 4, 5-trisphosphate receptor type 3 (IP3R3) in the peritoneal dissemination of gastric cancers]. *Gan To Kagaku Ryoho.* 30 (11), pp. 1784-1787.

Sakura, H. & Ashcroft, F.M. (1997) Identification of four trp1 gene variants murine pancreatic beta-cells. *Diabetologia.* 40 (5), pp. 528-532.

Saleh, S.N., Albert, A.P., Peppiatt-Wildman, C.M. & Large, W.A. (2008) Diverse properties of store-operated TRPC channels activated by protein kinase C in vascular myocytes. *J Physiol.* 586 (10), pp. 2463-2476.

Salido, G.M., Sage, S.O. & Rosado, J.A. (2009) TRPC channels and store-operated Ca(2+) entry. *Biochim Biophys Acta.* 1793 (2), pp. 223-230.

Sano, Y., Inamura, K., Miyake, A., Mochizuki, S., Yokoi, H., Matsushime, H. & Furuichi, K. (2001) Immunocyte Ca^{2+} influx system mediated by LTRPC2. *Science.* 293 (5533), pp. 1327-1330.

Satoh, E., Ono, K., Xu, F. & Iijima, T. (2002) Cloning and functional expression of a novel splice variant of rat TRPC4. *Circ J.* 66 (10), pp. 954-958.

Satoh, S., Tanaka, H., Ueda, Y., Oyama, J., Sugano, M., Sumimoto, H., Mori, Y. & Makino, N. (2007) Transient receptor potential (TRP) protein 7 acts as a G protein-activated Ca^{2+} channel mediating angiotensin II-induced myocardial apoptosis. *Mol Cell Biochem.* 294 (1-2), pp. 205-215.

Schaefer, M., Plant, T.D., Stresow, N., Albrecht, N. & Schultz, G. (2002) Functional differences between TRPC4 splice variants. *J Biol Chem.* 277 (5), pp. 3752-3759.

Schindl, R., Frischauf, I., Bergsmann, J., Muik, M., Derler, I., Lackner, B., Groschner, K. & Romanin, C. (2009) Plasticity in Ca2+ selectivity of Orai1/Orai3 heteromeric channel. *Proc Natl Acad Sci U S A.* 106 (46), pp. 19623-19628.

Schmidt, K., Dubrovska, G., Nielsen, G., Fesus, G., Uhrenholt, T.R., Hansen, P.B., Gudermann, T., Dietrich, A., Gollasch, M., De Wit, C. & Kohler, R. (2010) Amplification of EDHF-type vasodilatations in TRPC1-deficient mice. *Br J Pharmacol.* 161 (8), pp. 1722-1733.

Scott, C.C., Dobson, W., Botelho, R.J., Coady-Osberg, N., Chavrier, P., Knecht, D.A., Heath, C., Stahl, P. & Grinstein, S. (2005) Phosphatidylinositol-4,5-bisphosphate hydrolysis directs actin remodeling during phagocytosis. *J Cell Biol.* 169 (1), pp. 139-149.

Selinummi, J., Seppala, J., Yli-Harja, O. & Puhakka, J.A. (2005) Software for quantification of labeled bacteria from digital microscope images by automated image analysis. *BioTechniques.* 39 (6), pp. 859-863.

Selvaraj, S., Sun, Y. & Singh, B.B. (2010) TRPC channels and their implication in neurological diseases. *CNS Neurol Disord Drug Targets.* 9 (1), pp. 94-104.

Seth, M., Zhang, Z.-S., Mao, L., Graham, V., Burch, J., Stiber, J., Tsiokas, L., Winn, M., Abramowitz, J., Rockman, H.A., Birnbaumer, L. & Rosenberg, P. (2009). TRPC1 Channels Are Critical for Hypertrophic Signaling in the Heart Vol. 105, pp 1023-1030.

Shahidzadeh, R. & Sridhar, S. (2008) Profound copper deficiency in a patient with gastric bypass. *Am J Gastroenterol.* 103 (10), pp. 2660-2662.

Singaravelu, K., Nelson, C., Bakowski, D., de Brito, O.M., Ng, S.W., Di Capite, J., Powell, T., Scorrano, L. & Parekh, A.B. (2011) Mitofusin 2 regulates STIM1 migration from the Ca^{2+} store to the plasma membrane in cells with depolarized mitochondria. *J Biol Chem.* 286 (14), pp. 12189-12201.

Skryma, R., Mariot, P., Bourhis, X.L., Coppenolle, F.V., Shuba, Y., Vanden Abeele, F., Legrand, G., Humez, S., Boilly, B. & Prevarskaya, N. (2000) Store depletion and store-operated Ca^{2+} current in human prostate cancer LNCaP cells: involvement in apoptosis. *J Physiol.* 527 Pt 1 pp. 71-83.

Smyth, J.T., Dehaven, W.I., Bird, G.S. & Putney, J.W., Jr. (2008) Ca^{2+}-store-dependent and -independent reversal of Stim1 localization and function. *J Cell Sci.* 121 (Pt 6), pp. 762-772.

Smyth, J.T., DeHaven, W.I., Bird, G.S. & Putney, J.W., Jr. (2007) Role of the microtubule cytoskeleton in the function of the store-operated Ca^{2+} channel activator STIM1. *J Cell Sci.* 120 (Pt 21), pp. 3762-3771.

Smyth, J.T., Hwang, S.Y., Tomita, T., DeHaven, W.I., Mercer, J.C. & Putney, J.W. (2010) Activation and regulation of store-operated calcium entry. *J Cell Mol Med.* 14 (10), pp. 2337-2349.

Soboloff, J., Spassova, M.A., Tang, X.D., Hewavitharana, T., Xu, W. & Gill, D.L. (2006) Orai1 and STIM reconstitute store-operated calcium channel function. *J Biol Chem.* 281 (30), pp. 20661-20665.

Song, M.Y., Makino, A. & Yuan, J.X. (2011) Role of reactive oxygen species and redox in regulating the function of transient receptor potential channels. *Antioxid Redox Signal.* 15 (6), pp. 1549-1565.

Spassova, M.A., Soboloff, J., He, L.P., Xu, W., Dziadek, M.A. & Gill, D.L. (2006) STIM1 has a plasma membrane role in the activation of store-operated Ca(2+) channels. *Proc Natl Acad Sci U S A.* 103 (11), pp. 4040-4045.

Squitti, R. (2012) Copper dysfunction in Alzheimer's disease: From meta-analysis of biochemical studies to new insight into genetics. *J Trace Elem Med Biol.* pp. in press.

Starkus, J.G., Fleig, A. & Penner, R. (2010) The calcium-permeable non-selective cation channel TRPM2 is modulated by cellular acidification. *J Physiol.* 588 (8), pp. 1227-1240.

Stathopulos, P.B., Zheng, L., Li, G.Y., Plevin, M.J. & Ikura, M. (2008) Structural and mechanistic insights into STIM1-mediated initiation of store-operated calcium entry. *Cell.* 135 (1), pp. 110-122.

Stiber, J., Hawkins, A., Zhang, Z.S., Wang, S., Burch, J., Graham, V., Ward, C.C., Seth, M., Finch, E., Malouf, N., Williams, R.S., Eu, J.P. & Rosenberg, P. (2008) STIM1 signalling controls store-operated calcium entry required for development and contractile function in skeletal muscle. *Nat Cell Biol.* 10 (6), pp. 688-697.

Stiber, J.A. & Rosenberg, P.B. (2011) The role of store-operated calcium influx in skeletal muscle signaling. *Cell Calcium.* 49 (5), pp. 341-349.

Stiber, J.A., Tang, Y., Li, T. & Rosenberg, P.B. (2012) Cytoskeletal Regulation of TRPC Channels in the Cardiorenal System. *Current hypertension reports.* 14 (6), pp. 492-497.

Stowell, K.M. (2008) Malignant hyperthermia: a pharmacogenetic disorder. *Pharmacogenomics.* 9 (11), pp. 1657-1672.

Strubing, C., Krapivinsky, G., Krapivinsky, L. & Clapham, D.E. (2001) TRPC1 and TRPC5 form a novel cation channel in mammalian brain. *Neuron.* 29 (3), pp. 645-655.

Sumoza-Toledo, A. & Penner, R. (2011) TRPM2: a multifunctional ion channel for calcium signalling. *J Physiol.* 589 (Pt 7), pp. 1515-1525.

Sundivakkam, P.C., Freichel, M., Singh, V., Yuan, J.P., Vogel, S.M., Flockerzi, V., Malik, A.B. & Tiruppathi, C. (2012) The Ca(2+) sensor stromal interaction molecule 1 (STIM1) is necessary and sufficient for the store-operated Ca(2+) entry function of transient receptor potential canonical (TRPC) 1 and 4 channels in endothelial cells. *Mol Pharmacol.* 81 (4), pp. 510-526.

Szikra, T., Cusato, K., Thoreson, W.B., Barabas, P., Bartoletti, T.M. & Krizaj, D. (2008) Depletion of calcium stores regulates calcium influx and signal transmission in rod photoreceptors. *J Physiol.* 586 (Pt 20), pp. 4859-4875.

Takemura, H., Hughes, A.R., Thastrup, O. & Putney, J.W., Jr. (1989) Activation of calcium entry by the tumor promoter thapsigargin in parotid acinar cells. Evidence that an intracellular calcium pool and not an inositol phosphate regulates calcium fluxes at the plasma membrane. *J Biol Chem.* 264 (21), pp. 12266-12271.

Takemura, H. & Putney, J.W., Jr. (1989) Capacitative calcium entry in parotid acinar cells. *Biochem J.* 258 (2), pp. 409-412.

Tamarina, N.A., Kuznetsov, A. & Philipson, L.H. (2008) Reversible translocation of EYFP-tagged STIM1 is coupled to calcium influx in insulin secreting beta-cells. *Cell Calcium.* 44 (6), pp. 533-544.

Tamura, K., Dudley, J., Nei, M. & Kumar, S. (2007) MEGA4: Molecular Evolutionary Genetics Analysis (MEGA) software version 4.0. *Mol Biol Evol.* 24 (8), pp. 1596-1599.

Tanzi, R.E., Petrukhin, K., Chernov, I., Pellequer, J.L., Wasco, W., Ross, B., Romano, D.M., Parano, E., Pavone, L., Brzustowicz, L.M. & et al. (1993) The Wilson disease gene is a copper transporting ATPase with homology to the Menkes disease gene. *Nat Genet.* 5 (4), pp. 344-350.

Taylor, C.W. & Tovey, S.C. (2010) IP(3) receptors: toward understanding their activation. *Cold Spring Harb Perspect Biol.* 2 (12), pp. a004010.

Thastrup, O., Cullen, P.J., Drobak, B.K., Hanley, M.R. & Dawson, A.P. (1990) Thapsigargin, a tumor promoter, discharges intracellular Ca^{2+} stores by specific inhibition of the endoplasmic reticulum Ca^{2+}-ATPase. *Proc Natl Acad Sci U S A.* 87 (7), pp. 2466-2470.

Thastrup, O., Dawson, A.P., Scharff, O., Foder, B., Cullen, P.J., Drobak, B.K., Bjerrum, P.J., Christensen, S.B. & Hanley, M.R. (1989) Thapsigargin, a novel molecular probe for studying intracellular calcium release and storage. *Agents Actions.* 27 (1-2), pp. 17-23.

Thebault, S., Flourakis, M., Vanoverberghe, K., Vandermoere, F., Roudbaraki, M., Lehen'kyi, V., Slomianny, C., Beck, B., Mariot, P., Bonnal, J.L., Mauroy, B., Shuba, Y., Capiod, T., Skryma, R. & Prevarskaya, N. (2006) Differential role of transient receptor potential channels in Ca^{2+} entry and proliferation of prostate cancer epithelial cells. *Cancer Res.* 66 (4), pp. 2038-2047.

Thilo, F., Loddenkemper, C., Berg, E., Zidek, W. & Tepel, M. (2009) Increased TRPC3 expression in vascular endothelium of patients with malignant hypertension. *Mod Pathol.* 22 (3), pp. 426-430.

Tian, D.Q., Jacobo, S.M.P., Billing, D., Rozkalne, A., Gage, S.D., Anagnostou, T., Pavenstaedt, H., Hsu, H.H., Schlondorff, J., Ramos, A. & Greka, A. (2010) Antagonistic Regulation of Actin Dynamics and Cell Motility by TRPC5 and TRPC6 Channels. *Sci Signal.* 3 (145), pp. ra77.

Tiruppathi, C., Freichel, M., Vogel, S.M., Paria, B.C., Mehta, D., Flockerzi, V. & Malik, A.B. (2002) Impairment of store-operated Ca^{2+} entry in TRPC4(-/-) mice interferes with increase in lung microvascular permeability. *Circ Res.* 91 (1), pp. 70-76.

Togashi, K., Hara, Y., Tominaga, T., Higashi, T., Konishi, Y., Mori, Y. & Tominaga, M. (2006) TRPM2 activation by cyclic ADP-ribose at body temperature is involved in insulin secretion. *EMBO J.* 25 (9), pp. 1804-1815.

Tougu, V., Tiiman, A. & Palumaa, P. (2011) Interactions of Zn(II) and Cu(II) ions with Alzheimer's amyloid-beta peptide. Metal ion binding, contribution to fibrillization and toxicity. *Metallomics.* 3 (3), pp. 250-261.

Tran, Q.K., Watanabe, H., Le, H.Y., Pan, L., Seto, M., Takeuchi, K. & Ohashi, K. (2001) Myosin light chain kinase regulates capacitative ca(2+) entry in human monocytes/macrophages. *Arterioscler Thromb Vasc Biol.* 21 (4), pp. 509-515.

Trevillyan, J.M., Chiou, X.G., Chen, Y.W., Ballaron, S.J., Sheets, M.P., Smith, M.L., Wiedeman, P.E., Warrior, U., Wilkins, J., Gubbins, E.J., Gagne, G.D., Fagerland, J., Carter, G.W., Luly, J.R., Mollison, K.W. & Djuric, S.W. (2001) Potent inhibition of NFAT activation and T cell cytokine production by novel low molecular weight pyrazole compounds. *J Biol Chem.* 276 (51), pp. 48118-48126.

Tsvilovskyy, V.V., Zholos, A.V., Aberle, T., Philipp, S.E., Dietrich, A., Zhu, M.X., Birnbaumer, L., Freichel, M. & Flockerzi, V. (2009) Deletion of TRPC4 and TRPC6 in mice impairs smooth muscle contraction and intestinal motility in vivo. *Gastroenterology.* 137 (4), pp. 1415-1424.

Tu, P., Brandolin, G. & Bouron, A. (2009) The anti-inflammatory agent flufenamic acid depresses store-operated channels by altering mitochondrial calcium homeostasis. *Neuropharmacology.* 56 (6-7), pp. 1010-1016.

Uchida, K., Dezaki, K., Damdindorj, B., Inada, H., Shiuchi, T., Mori, Y., Yada, T., Minokoshi, Y. & Tominaga, M. (2011) Lack of TRPM2 impaired insulin secretion and glucose metabolisms in mice. *Diabetes.* 60 (1), pp. 119-126.

Uriu-Adams, J.Y. & Keen, C.L. (2005) Copper, oxidative stress, and human health. *Mol Aspects Med.* 26 (4-5), pp. 268-298.

Vaca, L. (2010) SOCIC: the store-operated calcium influx complex. *Cell Calcium.* 47 (3), pp. 199-209.

van Deurs, B., Roepstorff, K., Hommelgaard, A.M. & Sandvig, K. (2003) Caveolae: anchored, multifunctional platforms in the lipid ocean. *Trends in cell biology.* 13 (2), pp. 92-100.

van Kruchten, R., Braun, A., Feijge, M.A., Kuijpers, M.J., Rivera-Galdos, R., Kraft, P., Stoll, G., Kleinschnitz, C., Bevers, E.M., Nieswandt, B. & Heemskerk, J.W. (2012) Antithrombotic potential of blockers of store-operated calcium channels in platelets. *Arterioscler Thromb Vasc Biol.* 32 (7), pp. 1717-1723.

Vandebrouck, C., Martin, D., Colson-Van Schoor, M., Debaix, H. & Gailly, P. (2002) Involvement of TRPC in the abnormal calcium influx observed in dystrophic (mdx) mouse skeletal muscle fibers. *J Cell Biol.* 158 (6), pp. 1089-1096.

Vannier, B., Peyton, M., Boulay, G., Brown, D., Qin, N., Jiang, M., Zhu, X. & Birnbaumer, L. (1999) Mouse trp2, the homologue of the human trpc2 pseudogene, encodes mTrp2, a store depletion-activated capacitative Ca^{2+} entry channel. *Proc Natl Acad Sci U S A.* 96 (5), pp. 2060-2064.

Vanoverberghe, K., Lehen'kyi, V., Thebault, S., Raphael, M., Vanden Abeele, F., Slomianny, C., Mariot, P. & Prevarskaya, N. (2012) Cytoskeleton reorganization as an alternative mechanism of store-operated calcium entry control in neuroendocrine-differentiated cells. *PLoS One.* 7 (9), pp. e45615.

Varga-Szabo, D., Authi, K.S., Braun, A., Bender, M., Ambily, A., Hassock, S.R., Gudermann, T., Dietrich, A. & Nieswandt, B. (2008a) Store-operated Ca(2+) entry in platelets occurs independently of transient receptor potential (TRP) C1. *Pflugers Arch.* 457 (2), pp. 377-387.

Varga-Szabo, D., Braun, A., Kleinschnitz, C., Bender, M., Pleines, I., Pham, M., Renne, T., Stoll, G. & Nieswandt, B. (2008b) The calcium sensor STIM1 is an essential mediator of arterial thrombosis and ischemic brain infarction. *J Exp Med.* 205 (7), pp. 1583-1591.

Vazquez, G., Lievremont, J.P., St, J.B.G. & Putney, J.W., Jr. (2001) Human Trp3 forms both inositol trisphosphate receptor-dependent and receptor-independent store-operated cation channels in DT40 avian B lymphocytes. *Proc Natl Acad Sci U S A.* 98 (20), pp. 11777-11782.

Veliceasa, D., Ivanovic, M., Hoepfner, F.T., Thumbikat, P., Volpert, O.V. & Smith, N.D. (2007) Transient potential receptor channel 4 controls thrombospondin-1 secretion and angiogenesis in renal cell carcinoma. *FEBS J.* 274 (24), pp. 6365-6377.

Venkatachalam, K., van Rossum, D.B., Patterson, R.L., Ma, H.T. & Gill, D.L. (2002) The cellular and molecular basis of store-operated calcium entry. *Nat Cell Biol.* 4 (11), pp. E263-272.

Venkatachalam, K., Zheng, F. & Gill, D.L. (2003) Regulation of canonical transient receptor potential (TRPC) channel function by diacylglycerol and protein kinase C. *J Biol Chem.* 278 (31), pp. 29031-29040.

Vig, M., Beck, A., Billingsley, J.M., Lis, A., Parvez, S., Peinelt, C., Koomoa, D.L., Soboloff, J., Gill, D.L., Fleig, A., Kinet, J.P. & Penner, R. (2006a) CRACM1 multimers form the ion-selective pore of the CRAC channel. *Curr Biol.* 16 (20), pp. 2073-2079.

Vig, M., DeHaven, W.I., Bird, G.S., Billingsley, J.M., Wang, H., Rao, P.E., Hutchings, A.B., Jouvin, M.H., Putney, J.W. & Kinet, J.P. (2008) Defective mast cell effector functions in mice lacking the CRACM1 pore subunit of store-operated calcium release-activated calcium channels. *Nat Immunol.* 9 (1), pp. 89-96.

Vig, M., Peinelt, C., Beck, A., Koomoa, D.L., Rabah, D., Koblan-Huberson, M., Kraft, S., Turner, H., Fleig, A., Penner, R. & Kinet, J.P. (2006b) CRACM1 is a plasma membrane protein essential for store-operated Ca^{2+} entry. *Science.* 312 (5777), pp. 1220-1223.

Viktorinova, A., Toserova, E., Krizko, M. & Durackova, Z. (2009) Altered metabolism of copper, zinc, and magnesium is associated with increased levels of glycated hemoglobin in patients with diabetes mellitus. *Metabolism.* 58 (10), pp. 1477-1482.

Vinken, M., Vanhaecke, T., Papeleu, P., Snykers, S., Henkens, T. & Rogiers, V. (2006) Connexins and their channels in cell growth and cell death. *Cell Signal.* 18 (5), pp. 592-600.

Walsh, C.M., Chvanov, M., Haynes, L.P., Petersen, O.H., Tepikin, A.V. & Burgoyne, R.D. (2010) Role of phosphoinositides in STIM1 dynamics and store-operated calcium entry. *Biochem J.* 425 (1), pp. 159-168.

Walter, R.M., Jr., Uriu-Hare, J.Y., Olin, K.L., Oster, M.H., Anawalt, B.D., Critchfield, J.W. & Keen, C.L. (1991) Copper, zinc, manganese, and magnesium status and complications of diabetes mellitus. *Diabetes Care.* 14 (11), pp. 1050-1056.

Wang, C., Hu, H.Z., Colton, C.K., Wood, J.D. & Zhu, M.X. (2004a) An alternative splicing product of the murine trpv1 gene dominant negatively modulates the activity of TRPV1 channels. *J Biol Chem.* 279 (36), pp. 37423-37430.

Wang, X., Pluznick, J.L., Wei, P., Padanilam, B.J. & Sansom, S.C. (2004b) TRPC4 forms store-operated Ca^{2+} channels in mouse mesangial cells. *Am J Physiol Cell Physiol.* 287 (2), pp. C357-364.

Wang, Y.J., Gregory, R.B. & Barritt, G.J. (2002) Maintenance of the filamentous actin cytoskeleton is necessary for the activation of store-operated Ca^{2+} channels, but not other types of plasma-membrane Ca^{2+} channels, in rat hepatocytes. *Biochem J.* 363 (Pt 1), pp. 117-126.

Wappler, F., Scholz, J., Fiege, M., Kolodzie, K., Kudlik, C., Weisshorn, R. & Schulte am Esch, J. (1999) 4-chloro-m-cresol is a trigger of malignant hyperthermia in susceptible swine. *Anesthesiology.* 90 (6), pp. 1733-1740.

Watanabe, H., Takahashi, R., Zhang, X.X., Kakizawa, H., Hayashi, H. & Ohno, R. (1996) Inhibition of agonist-induced Ca^{2+} entry in endothelial cells by myosin light-chain kinase inhibitor. *Biochem Biophys Res Commun.* 225 (3), pp. 777-784.

Westerblad, H., Andrade, F.H. & Islam, M.S. (1998) Effects of ryanodine receptor agonist 4-chloro-*m*-cresol on myoplasmic free Ca^{2+} concentration and force of contraction in mouse skeletal muscle. *Cell Calcium.* 24 (2), pp. 105-115.

Wu, M.M., Buchanan, J., Luik, R.M. & Lewis, R.S. (2006) Ca^{2+} store depletion causes STIM1 to accumulate in ER regions closely associated with the plasma membrane. *J Cell Biol.* 174 (6), pp. 803-813.

Wu, X., Eder, P., Chang, B. & Molkentin, J.D. (2010a) TRPC channels are necessary mediators of pathologic cardiac hypertrophy. *Proc Natl Acad Sci U S A.* 107 (15), pp. 7000-7005.

Wu, Z., Fernandez-Lima, F.A. & Russell, D.H. (2010b) Amino acid influence on copper binding to peptides: cysteine versus arginine. *J Am Soc Mass Spectrom.* 21 (4), pp. 522-533.

Xie, Y.F., Macdonald, J.F. & Jackson, M.F. (2010) TRPM2, calcium and neurodegenerative diseases. *Int J Physiol Pathophysiol Pharmacol.* 2 (2), pp. 95-103.

Xu, C., Li, P.P., Cooke, R.G., Parikh, S.V., Wang, K., Kennedy, J.L. & Warsh, J.J. (2009a) TRPM2 variants and bipolar disorder risk: confirmation in a family-based association study. *Bipolar Disord.* 11 (1), pp. 1-10.

Xu, P., Lu, J., Li, Z., Yu, X., Chen, L. & Xu, T. (2006a) Aggregation of STIM1 underneath the plasma membrane induces clustering of Orai1. *Biochem Biophys Res Commun.* 350 (4), pp. 969-976.

Xu, S.Z. & Beech, D.J. (2001) TrpC1 is a membrane-spanning subunit of store-operated Ca(2+) channels in native vascular smooth muscle cells. *Circ Res.* 88 (1), pp. 84-87.

Xu, S.Z., Muraki, K., Zeng, F., Li, J., Sukumar, P., Shah, S., Dedman, A.M., Flemming, P.K., McHugh, D., Naylor, J., Cheong, A., Bateson, A.N., Munsch, C.M., Porter, K.E. & Beech, D.J. (2006b) A sphingosine-1-phosphate-activated calcium channel controlling vascular smooth muscle cell motility. *Circ Res.* 98 (11), pp. 1381-1389.

Xu, S.Z., Sukumar, P., Zeng, F., Li, J., Jairaman, A., English, A., Naylor, J., Ciurtin, C., Majeed, Y., Milligan, C.J., Bahnasi, Y.M., Al-Shawaf, E., Porter, K.E., Jiang, L.H., Emery, P., Sivaprasadarao, A. & Beech, D.J. (2008a) TRPC channel activation by extracellular thioredoxin. *Nature.* 451 (7174), pp. 69-72.

Xu, S.Z., Zeng, B., Daskoulidou, N., Chen, G.L., Atkin, S.L. & Lukhele, B. (2012) Activation of TRPC cationic channels by mercurial compounds confers the cytotoxicity of mercury exposure. *Toxicol Sci.* 125 (1), pp. 56-68.

Xu, S.Z., Zeng, F., Boulay, G., Grimm, C., Harteneck, C. & Beech, D.J. (2005a) Block of TRPC5 channels by 2-aminoethoxydiphenyl borate: a differential, extracellular and voltage-dependent effect. *Br J Pharmacol.* 145 (4), pp. 405-414.

Xu, S.Z., Zeng, F., Lei, M., Li, J., Gao, B., Xiong, C., Sivaprasadarao, A. & Beech, D.J. (2005b) Generation of functional ion-channel tools by E3 targeting. *Nat Biotechnol.* 23 (10), pp. 1289-1293.

Xu, S.Z., Zhong, W., Ghavideldarestani, M., Saurabh, R., Lindow, S.W. & Atkin, S.L. (2009b) Multiple mechanisms of soy isoflavones against oxidative stress-induced endothelium injury. *Free Radic Biol Med.* 47 (2), pp. 167-175.

Xu, S.Z., Zhong, W., Watson, N.M., Dickerson, E., Wake, J.D., Lindow, S.W., Newton, C.J. & Atkin, S.L. (2008b) Fluvastatin reduces oxidative damage in human vascular endothelial cells by upregulating Bcl-2. *J Thromb Haemost.* 6 (4), pp. 692-700.

Xue, T., Do, M.T., Riccio, A., Jiang, Z., Hsieh, J., Wang, H.C., Merbs, S.L., Welsbie, D.S., Yoshioka, T., Weissgerber, P., Stolz, S., Flockerzi, V., Freichel, M., Simon, M.I., Clapham, D.E. & Yau, K.W. (2011) Melanopsin signalling in mammalian iris and retina. *Nature.* 479 (7371), pp. 67-73.

Yamashita, M., Oki, Y., Iino, K., Hayashi, C., Yogo, K., Matsushita, F., Sasaki, S. & Nakamura, H. (2009) The role of store-operated Ca^{2+} channels in adrenocorticotropin release by rat pituitary cells. *Regul Pept.* 156 (1-3), pp. 57-64.

Yamashita, M., Somasundaram, A. & Prakriya, M. (2011) Competitive modulation of Ca^{2+} release-activated Ca^{2+} channel gating by STIM1 and 2-aminoethyldiphenyl borate. *J Biol Chem.* 286 (11), pp. 9429-9442.

Yang, M., Gupta, A., Shlykov, S.G., Corrigan, R., Tsujimoto, S. & Sanborn, B.M. (2002) Multiple Trp isoforms implicated in capacitative calcium entry are expressed

in human pregnant myometrium and myometrial cells. *Biol Reprod.* 67 (3), pp. 988-994.

Yang, S., Zhang, J.J. & Huang, X.Y. (2009a) Orai1 and STIM1 are critical for breast tumor cell migration and metastasis. *Cancer Cell.* 15 (2), pp. 124-134.

Yang, S.L., Cao, Q., Zhou, K.C., Feng, Y.J. & Wang, Y.Z. (2009b) Transient receptor potential channel C3 contributes to the progression of human ovarian cancer. *Oncogene.* 28 (10), pp. 1320-1328.

Yang, W., Manna, P.T., Zou, J., Luo, J., Beech, D.J., Sivaprasadarao, A. & Jiang, L.H. (2011) Zinc inactivates melastatin transient receptor potential 2 channels via the outer pore. *J Biol Chem.* 286 (27), pp. 23789-23798.

Yarotskyy, V. & Dirksen, R.T. (2012) Temperature and RyR1 Regulate the Activation Rate of Store-Operated Ca(2+) Entry Current in Myotubes. *Biophys J.* 103 (2), pp. 202-211.

Yeromin, A.V., Zhang, S.L., Jiang, W., Yu, Y., Safrina, O. & Cahalan, M.D. (2006) Molecular identification of the CRAC channel by altered ion selectivity in a mutant of Orai. *Nature.* 443 (7108), pp. 226-229.

Yetik-Anacak, G. & Catravas, J.D. (2006) Nitric oxide and the endothelium: History and impact on cardiovascular disease. *Vasc Pharmacol.* 45 (5), pp. 268-276.

Yildirim, E., Kawasaki, B.T. & Birnbaumer, L. (2005) Molecular cloning of TRPC3a, an N-terminally extended, store-operated variant of the human C3 transient receptor potential channel. *Proc Natl Acad Sci U S A.* 102 (9), pp. 3307-3311.

Yoshida, T., Inoue, R., Morii, T., Takahashi, N., Yamamoto, S., Hara, Y., Tominaga, M., Shimizu, S., Sato, Y. & Mori, Y. (2006) Nitric oxide activates TRP channels by cysteine S-nitrosylation. *Nat Chem Biol.* 2 (11), pp. 596-607.

Yuan, J.P., Kim, M.S., Zeng, W., Shin, D.M., Huang, G., Worley, P.F. & Muallem, S. (2009a) TRPC channels as STIM1-regulated SOCs. *Channels (Austin).* 3 (4), pp. 221-225.

Yuan, J.P., Kiselyov, K., Shin, D.M., Chen, J., Shcheynikov, N., Kang, S.H., Dehoff, M.H., Schwarz, M.K., Seeburg, P.H., Muallem, S. & Worley, P.F. (2003) Homer binds TRPC family channels and is required for gating of TRPC1 by IP3 receptors. *Cell.* 114 (6), pp. 777-789.

Yuan, J.P., Zeng, W., Dorwart, M.R., Choi, Y.J., Worley, P.F. & Muallem, S. (2009b) SOAR and the polybasic STIM1 domains gate and regulate Orai channels. *Nat Cell Biol.* 11 (3), pp. 337-343.

Yuan, J.P., Zeng, W., Huang, G.N., Worley, P.F. & Muallem, S. (2007) STIM1 heteromultimerizes TRPC channels to determine their function as store-operated channels. *Nat Cell Biol.* 9 (6), pp. 636-645.

Zagranichnaya, T.K., Wu, X. & Villereal, M.L. (2005) Endogenous TRPC1, TRPC3, and TRPC7 proteins combine to form native store-operated channels in HEK-293 cells. *J Biol Chem.* 280 (33), pp. 29559-29569.

Zakharov, S.I., Smani, T., Dobrydneva, Y., Monje, F., Fichandler, C., Blackmore, P.F. & Bolotina, V.M. (2004) Diethylstilbestrol is a potent inhibitor of store-operated channels and capacitative Ca(2+) influx. *Mol Pharmacol.* 66 (3), pp. 702-707.

Zanou, N., Shapovalov, G., Louis, M., Tajeddine, N., Gallo, C., Van Schoor, M., Anguish, I., Cao, M.L., Schakman, O., Dietrich, A., Lebacq, J., Ruegg, U., Roulet, E., Birnbaumer, L. & Gailly, P. (2010) Role of TRPC1 channel in skeletal muscle function. *Am J Physiol Cell Physiol.* 298 (1), pp. C149-162.

Zargar, A.H., Shah, N.A., Masoodi, S.R., Laway, B.A., Dar, F.A., Khan, A.R., Sofi, F.A. & Wani, A.I. (1998) Copper, zinc, and magnesium levels in non-insulin dependent diabetes mellitus. *Postgrad Med J.* 74 (877), pp. 665-668.

Zeng, W., Yuan, J.P., Kim, M.S., Choi, Y.J., Huang, G.N., Worley, P.F. & Muallem, S. (2008) STIM1 gates TRPC channels, but not Orai1, by electrostatic interaction. *Mol Cell.* 32 (3), pp. 439-448.

Zhang, S.L., Kozak, J.A., Jiang, W., Yeromin, A.V., Chen, J., Yu, Y., Penna, A., Shen, W., Chi, V. & Cahalan, M.D. (2008) Store-dependent and -independent modes regulating Ca^{2+} release-activated Ca^{2+} channel activity of human Orai1 and Orai3. *J Biol Chem.* 283 (25), pp. 17662-17671.

Zhang, S.L., Yeromin, A.V., Zhang, X.H., Yu, Y., Safrina, O., Penna, A., Roos, J., Stauderman, K.A. & Cahalan, M.D. (2006) Genome-wide RNAi screen of Ca(2+) influx identifies genes that regulate Ca(2+) release-activated Ca(2+) channel activity. *Proc Natl Acad Sci U S A.* 103 (24), pp. 9357-9362.

Zhang, S.L., Yu, Y., Roos, J., Kozak, J.A., Deerinck, T.J., Ellisman, M.H., Stauderman, K.A. & Cahalan, M.D. (2005) STIM1 is a Ca^{2+} sensor that activates CRAC channels and migrates from the Ca^{2+} store to the plasma membrane. *Nature.* 437 (7060), pp. 902-905.

Zhang, Z.Y., Pan, L.J. & Zhang, Z.M. (2010) Functional interactions among STIM1, Orai1 and TRPC1 on the activation of SOCs in HL-7702 cells. *Amino Acids.* 39 (1), pp. 195-204.

Zheng, L., Stathopulos, P.B., Li, G.Y. & Ikura, M. (2008) Biophysical characterization of the EF-hand and SAM domain containing Ca^{2+} sensory region of STIM1 and STIM2. *Biochem Biophys Res Commun.* 369 (1), pp. 240-246.

Zitt, C., Strauss, B., Schwarz, E.C., Spaeth, N., Rast, G., Hatzelmann, A. & Hoth, M. (2004) Potent inhibition of Ca^{2+} release-activated Ca^{2+} channels and T-lymphocyte activation by the pyrazole derivative BTP2. *J Biol Chem.* 279 (13), pp. 12427-12437.

Zorzato, F., Fujii, J., Otsu, K., Phillips, M., Green, N.M., Lai, F.A., Meissner, G. & MacLennan, D.H. (1990) Molecular cloning of cDNA encoding human and rabbit forms of the Ca^{2+} release channel (ryanodine receptor) of skeletal muscle sarcoplasmic reticulum. *J Biol Chem.* 265 (4), pp. 2244-2256.

Zweifach, A. & Lewis, R.S. (1996) Calcium-dependent potentiation of store-operated calcium channels in T lymphocytes. *J Gen Physiol.* 107 (5), pp. 597-610.

Appendix I: Pharmacological agents used in this study

Drug	Effect
EGTA	Ca^{2+} chelator (low affinity)
BAPTA	Ca^{2+} chelator (high affinity)
Thapsigargin	SERCA blocker, depleting ER/SR Ca^{2+} stores
2-APB	SOCE blocker; IP_3R inhibitor; ORAI3 activator
SKF-96365	Store-operated channel blocker
Diethylstilbestrol	Store-operated channel blocker
Colchicine	Microtubule polymerisation inhibitor
Cytochalasin D	Actin polymerisation inhibitor
Caffeine	RyR agonist
4-Chloro-3-ethylphenol	RyR agonist; store-operated channel blocker
4-Chloro-*m*-cresol	RyR agonist; store-operated channel blocker
4-Chlorophenol	Store-operated channel blocker
Genistein	Tyrosine kinase inhibitor
Wortmannin	Phosphatidylinositol 3-kinase (PI_3K) inhibitor
Y-27632	Rho-associated protein kinase (ROCK) inhibitor
Forskolin	Protein kinase A (PKA) activator
GF109203X	Protein kinase C (PKC) inhibitor
Chelerythrine	PKC inhibitor
OAG	TRPC3/6/7 activator; PKC activator
U73122	Phospholipase C inhibitor; increasing F-actin content
Calyculin A	Protein phosphatase inhibitor; increasing F-actin content
Flufenamic acid	SOCE inhibitor; releasing mitochondrial Ca^{2+}
Niflumic acid	SOCE inhibitor
FCCP	Mitochondrial oxidative phosphorylation inhibitor
Hg^{2+}	Mitochondrial oxidative phosphorylation inhibitor
Sodium azide	Mitochondrial cytochrome oxidase inhibitor
H_2O_2	Cellular oxidant, increasing oxidative stress
ADP-Ribose	TRPM2 channel activator
Cu^{2+}	TRPC3/4/5/6 activator; TRPM2 blocker
Gd^{3+}	TRPC4/5 activator; SOCE blocker
Trypsin	Protease-activated receptor 2 agonist

Appendix II: Publications during the PhD study

Zeng, B., Yuan, C., Yang, X., Atkin, S.L. and Xu, S.Z. (2013) TRPC channels and their splice variants are essential for promoting human ovarian cancer cell proliferation and tumorigenesis. *Current Cancer Drug Targets*. 13 (1), pp. 103-116.

Zeng, B., Chen, G.L. and Xu, S.Z. (2012) Store-independent pathways for cytosolic STIM1 clustering in the regulation of store-operated Ca^{2+} influx. *Biochemical Pharmacology*. 84 (8), pp. 1024-1035.

Zeng, B., Chen, G.L. and Xu, S.Z. (2012) Divalent copper is a potent extracellular blocker for TRPM2 channel. *Biochemical and Biophysical Research Communications*. 424 (2), pp. 279-284.

Chen, G.L., **Zeng, B.**, Eastmond, S., Elsenussi, S.E., Boa, A.N. and Xu, S.Z. (2012) Pharmacological comparison of novel synthetic fenamate analogues with econazole and 2-APB on the inhibition of TRPM2 channels. *British Journal of Pharmacology*. 167 (6), pp. 1232-1243.

Jiang, H., **Zeng, B.**, Chen, G.L., Bot, D., Eastmond, S., Elsenussi, S.E., Atkin, S.L., Boa, A.N. and Xu, S.Z. (2012) Effect of non-steroidal anti-inflammatory drugs and new fenamate analogues on TRPC4 and TRPC5 channels. *Biochemical Pharmacology*. 83 (7), pp. 923-931.

Xu, S.Z., **Zeng, B.**, Daskoulidou, N., Chen, G.L., Atkin, S.L. and Lukhele, B. (2012) Activation of TRPC cationic channels by mercurial compounds confers the cytotoxicity of mercury exposure. *Toxicological Sciences*. 125 (1), pp. 56-68.

TRPC Channels and Their Splice Variants are Essential for Promoting Human Ovarian Cancer Cell Proliferation and Tumorigenesis

Bo Zeng[1], Cunzhong Yuan[2], Xingsheng Yang[2], Stephen L. Atkin[1] and Shang-Zhong Xu[1,*]

[1]*Department of Diabetes, Endocrinology and Metabolism, Hull York Medical School, University of Hull, Hull, UK;*
[2]*Department of Obstetrics and Gynaecology, Qilu Hospital of Shandong University, Jinan 250012, China*

Abstract: TRPC channels are Ca^{2+}-permeable cationic channels controlling Ca^{2+} influx response to the activation of G protein-coupled receptors and protein tyrosine kinase pathways or the depletion of Ca^{2+} stores. Here we aimed to investigate whether TRPC can act as the potential therapeutic targets for ovarian cancer. The mRNAs of TRPC1, TRPC3, TRPC4 and TRPC6 were detected in human ovarian adenocarcinoma. The spliced variants of TRPC1β, TRPC3a, TRPC4β, TRPC4γ, and TRPC6 with exon 3 and 4 deletion were highly expressed in the ovarian cancer cells, and a novel spliced isoform of TRPC1 with exon 9 deletion (TRPC1^{E9del}) was identified. TRPC proteins were also detected by Western blotting and immunostaining. The expression of TRPC1, TRPC3, TRPC4 and TRPC6 was significantly lower in the undifferentiated ovarian cancer cells, but all-*trans* retinoic acid up-regulated the gene expression of TRPCs. The expression level was correlated to the cancer differentiation grade. The non-selective TRPC channel blockers, 2-APB and SKF-96365, significantly inhibited the cell proliferation, whilst the increase of TRPC channel activity by trypsin promoted the cell proliferation. Transfection with siRNA targeting TRPC1, TRPC3, TRPC4 and TRPC6 or application of specific blocking antibodies targeting to TRPC channels inhibited the cell proliferation. On the contrary, overexpression of TRPC1, TRPC1^{E9del}, TRPC3, TRPC4, and TRPC6 increased the cancer cell colony growth. These results suggest that TRPCs and their spliced variants are important for human ovarian cancer development and alteration of the expression or activity of these channels could be a new strategy for anticancer therapy.

Keywords: Calcium channels, ovarian cancer, proliferation, SKOV3 cells, TRPC.

INTRODUCTION

Ca^{2+} is a second messenger which plays a major role in the regulation of cellular functions, such as contraction, secretion, cell growth and death. The concentration of cytosolic Ca^{2+} ($[Ca^{2+}]_i$) is tightly controlled by Ca^{2+} transporters in the plasma membrane and intracellular Ca^{2+} stores. The transient receptor potential (TRP) proteins are novel class of Ca^{2+}-permeable cationic channels including six subfamilies, i.e., TRPC, TRPM, TRPV, TRPP, TRPML and TRPA. The canonical TRP (TRPC) is one of the subfamilies, which has been proposed as protein tyrosine kinase or G protein-coupled receptor-operated Ca^{2+} channels (ROCs) or internal Ca^{2+} store-operated channels (SOCs), which mediate the Ca^{2+} signalling pathway activated by many hormones and growth factors. TRPCs are ubiquitously distributed in the body and play essential roles in human physiology and pathophysiology [1, 2].

Ca^{2+} signalling is believed to play a central role in the signalling cascades of tumorigenesis and neoplastic progression by controlling gene expression, progression through the cell cycle, and DNA synthesis. The inhibitors of Ca^{2+}-dependent signalling suppress the proliferation of cancer cells *in vitro* and in solid tumors *in vivo* [3]. Store-operated Ca^{2+} influx is one of the Ca^{2+} entry pathways and closely related to cell proliferation and apoptosis. The importance of store-operated Ca^{2+} influx or capacitative Ca^{2+} influx in cancer development has been recognised for many years, however the role of TRP channels that act as the molecular constituents or subunits of SOCs or ROCs in cancer cell proliferation are still unclear [4]. In 2005, we demonstrated that TRPC channel is involved in cell proliferation, and 2-aminoethoxydiphenyl borate (2-APB) significantly inhibits the proliferation in HEK-293 cells. The mechanism is unrelated to its inhibitory action on inositol 1,4,5-trisphosphate receptors (IP$_3$R), since 2-APB also inhibits the proliferation of triple IP$_3$R knockout DT40 cells [5]. This suggests the direct involvement of SOCs or TRPC channels in cell proliferation. Recently, several studies have demonstrated the expression of TRPC in different types of cancer cells or cancer tissues, such as TRPC1, 3, 6 in breast cancer MCF7 cells [6] and liver cancer HepG2 [7], TRPC1, 3, 4 in prostate cancer LNCaP cells [8, 9], TRPC1, 4, 6, 7 in renal cell carcinoma [10], TRPC1, 3, 5, 6 in human malignant gliomas [11], TRPC1, 3-7 in neuroblastoma IMR-32 cells [12], TRPC3 in human astrocytoma 1321N1 cells [13], TRPC6 in esophageal and gastric cancer [14], TRPC3 in ovarian cancer [15], and TRPC1, 4 in basal cell carcinoma [16]. However, the detection of splicing activity of TRPCs and systematic examination of the role of each TRPC isoform in cancer growth has not been addressed.

Here we aimed to identify the expression of TRPCs and their splicing variants in human ovarian adenocarcinoma and the cancer-derived cell SKOV3, and determine the roles of TRPC isoforms in the regulation of cancer cell proliferation

*Address correspondence to this author at the Department of Diabetes, Endocrinology and Metabolism, Hull York Medical School, University of Hull, Cottingham Road, Hull, HU6 7RX, United Kingdom; Tel: +44 1482 465372; Fax: +44 1482 465390; E-mail: sam.xu@hyms.ac.uk

using TRPC siRNA interference and the pharmacological tools, such as the specific TRPC channel functional antibodies [5]. We also examined the colony growth of ovarian cancer cells by over-expressing TRPC isoforms. In addition, we compared the expression of TRPC genes in the human ovarian cancer tissues from patients with the normal ovarian tissues, and their involvement in ovarian cancer cell differentiation.

MATERIALS AND METHODS

Human Ovarian Cancer Tissues

Paraffin blocks of human ovarian adenocarcinoma tissue were obtained from patients undergoing ovariectomy at Hull and East Yorkshire NHS Trust (Hull, UK) with approval of the local ethics committee. The fresh ovarian cancer tissues were obtained from Qi Lu Hospital of Shandong University (Jinan, China) with ethical approval.

Cell Culture

Human ovarian adenocarcinoma cells (SKOV3, ATCC HTB-77) were purchased from LGC Promochem (Middlesex, UK). The SKOV3 cells were cultured in a flask with DMEM-F12 medium (Invitrogen, UK) supplemented with 10% fetal calf serum, 100 units/ml penicillin and 100 μg/ml streptomycin, and maintained at 37°C under 95% air and 5% CO_2.

RT-PCR and Real-time PCR

Total RNA was extracted from human ovarian tissues or cultured cells using Trizol reagent (Invitrogen, UK). The mRNA was reverse-transcribed to cDNA using M-MLV reserve transcriptase (RT) and random primers (Promega, UK). The primer set was designed across intron and the sequences were given in the Supplementary Table **1**. Non-template or non-RT was set as negative control, and the TRPC plasmid cDNAs or mouse brain cDNA were used as positive control. PCR products were detected on a 2 % agarose gel and confirmed by direct sequencing. Quantitative RT-PCR was performed using StepOne™ Real-Time PCR System (Applied Biosystems, UK). Each reaction volume was 10 μl, which contained 1 × Universal Master Mix (Applied Biosystems), 5 μl cDNA, 0.75 μl 300 nM forward primer, 0.75 μl 300 nM reverse primer. The human housekeeping gene GAPDH was used as an internal standard. Water was used as a non-template control. Non-reverse transcribed samples were run in parallel to confirm that positive results were not due to amplification of genomic DNA. The PCR cycle consisted of an initial cycle of 50 °C for 2 min followed by 95 °C for 10 minutes, then 50 repeated cycles of 95 °C for 15 s denaturation and 54 °C annealing temperature for 30 s, and primer extension at 72 °C for 30 s.

Antibodies and Western Blotting

Rabbit polyclonal anti-TRPC antibodies were generated against the extracellular third loop (E3) region near the channel pore [17] or targeting to C-terminus [18]. The specificity of E3-targeting antibodies (anti-TRPC1 (T1E3), anti-TRPC4 (T45E3), anti-TRPC5 (T5E3) and anti-TRPC6 (T367E3)) was tested by ELISA, Western blotting and functional assays [17]. The specific binding of E3-targeting antibodies was also confirmed by fluorescence activated cell sorting (FACS) (Fig. **S1**). The Western blotting procedure has been previously described [17].

Immunostaining

Cells were fixed with 4% paraformaldehyde and permeabilised by incubation in -20°C methanol for 1 minute and 0.1% Triton X-100 in phosphate buffered saline (PBS) for 1 hour at room temperature. For unpermeabilised staining, the steps for methanol and Triton X-100 were omitted. Cells were incubated in the appropriate TRPC primary antibodies (T1E3 at 1:500 dilution, T45E3, T367E3, anti-TRPC3 at 1:250 dilution) in PBS with 1% BSA at 4°C overnight. The anti-TRPC3 targeting C-terminus and the anti-TRPC6 targeting to N-terminus were purchased from Alomone Labs (Jerusalem, Israel) and used for comparison. The procedures for fluorescent staining and paraffin section staining using VECTASTAIN ABC kit (Vector laboratories) were similar to the previous reports [19]. Immunostaining was quantified by imaging software (Image-Pro Plus, Media Cybernetics, USA).

SiRNA Transfection

The TRPC siRNAs were purchased from Sigma-Aldrich (UK) (Supplementary Table **2**). TRPC siRNAs were transfected into SKOV3 cells using Lipofectamine 2000 (Invitrogen, UK) [2]. The wells or dishes without siRNA (no siRNA) or with scramble siRNA (Sigma-Aldrich, UK) or non-specific pool siRNA were set as negative control in parallel. The Bcl-2 siRNA was used as positive control. For cell cycle experiment, SKOV3 cells were transfected with TRPC siRNAs using the Neon electroporation system (Invitrogen, UK). The cells were resuspended to a density of 5×10^6/ml and mixed with 200 nM siRNA, and then pulsed twice at 1,170 V for 30 ms in a 100 μl tip. After electroporation the cells were maintained in antibiotic-free medium for 72 h and harvested for flow cytometry assay.

TRPC Cloning, Plasmid Construction and Expression

TRPC1, TRPC1^{E9del} and TRPC6 tagged with monomeric cyan fluorescent protein (CFP) were subcloned into pcDNA4/TO vector (Invitrogen, UK). TRPC3 tagged with monomeric red fluorescent protein (mCherry) and TRPC4 (α, β, and ε isoforms) tagged with enhanced yellow fluorescent protein (EYFP) were also subcloned into pcDNA4/TO vector. The plasmid cDNA of each TRPC isoform was transfected into HEK293 T-REx cells (Invitrogen, UK) using Lipofectamine 2000 and the expression was induced by tetracycline (1 μg/ml) and confirmed by fluorescent microscope examination. The channel activity was recorded by whole-cell patch clamp.

Cell Proliferation Assay and Colony Growth

Cell proliferation was determined using WST-1 assay (Roche, UK). This assay reflects the metabolic activity of the cultured cells. The overall cellular metabolic activity measured by optical absorption correlates well with the viable cell number in the culture dish/well. For colony growth, SKOV3 cells transfected with TRPC plasmid cDNAs using Lipofectamine 2000, and the cells were plated

in 6-cm culture dishes at a density of 500 cells per dish to allow to form colonies after 3-8 days culture. The colonies were fixed with 25% methanol, stained with 0.5% crystal violet dye in PBS, and automatically counted by CellC software (Version 1.2, Tampere University of Technology, Finland). For soft agar colony assay, the bottom layer of agar (0.7 %) was prepared in a 35-mm culture dish with 1.5 ml of DMEM-F12 medium containing agar, 10% FBS, 50 μg/ml penicillin and 50 μg/ml streptomycin. After solidification of the bottom layer, SKOV3 cells were suspended in 1 ml medium containing 0.35% agar at a density of 5000 cells/ml and poured into the dish to form a second layer. The dish was kept at 4 °C for 5 min and then the solidified second layer was covered with 1 ml medium to prevent the agar layer from drying out. The cells were incubated at 37°C in a humidified incubator and the top layer of medium was gently changed every 3 days. After 21 days of culture, the cells were stained with 0.005% crystal violet and the cell colonies with diameters >100 μm were counted under microscope with 4× objective.

Cell Cycle and Apoptosis Analyses

Simultaneous measurement of cell cycle and apoptosis was conducted using flow cytometric assay with propidium iodide staining as described by Riccardi and Nicoletti [20]. Briefly, SKOV3 cells at 70-80% confluency in a 100-mm culture dish were trypsinized, washed with PBS, fixed with 70% cold ethanol, incubated with DNA extraction buffer (0.2 M Na_2HPO_4, 0.004% Triton X-100, pH 7.8), treated with RNase (200 μg/ml), and stained with propidium iodide (20 μg/ml). The cells were then analysed with BD FACSCalibur Flow Cytometry System (Becton Dickinson, UK) with the CellQuest software. Events were counted at the limit of 20,000 or 10,000 for the drug-treated or siRNA-transfected groups. Cell debris was gated out according to the scatter plot and the percentages of cells at different phases of cell cycle were calculated based on the histogram plot of fluorescent intensities.

Reagents and Chemicals

2-Aminoethoxydiphenyl borate (2-APB), SKF-96365, carbenoxolone, trypsin, all-*trans* retinoic acid, PCR primers, TRPC1, 4, 6 siRNAs and scramble siRNA were purchased from Sigma-Aldrich. TRPC3 siRNA was purchased from Santa Cruz Biotechnology (USA). Bcl-2 siRNA and pool siRNA were from Upstate Biotech (USA).

Statistical Analysis

Data are expressed as mean ± S.E.M. The statistical significance was analysed using ANOVA and the difference among the groups was assessed with Dunnett's *t*-test in the SPSS software. The triplicate wells (or 8 wells/column) were set for cell proliferation assay.

RESULTS

Expression of TRPCs in Human Ovarian Cancer SKOV3 Cells

The mRNA of TRPCs in ovarian cancer cells was detected by RT-PCR (Fig. **1A**). TRPC1, TRPC3, TRPC4 and

TRPC6 were positive in human ovarian adenocarcinoma SKOV3 cells, while TRPC5 and TRPC7 were undetectable in the cells although the primer sets used for TRPC5 and TRPC7 was able to amplify the plasmid cDNAs (Fig. **1B**) or the total RNA extracted from mouse brain (Fig. **S2**). Two bands for TRPC1 were detected, suggesting splicing isoforms may exist in the cells.

The protein expression of TRPC channels was probed by western blotting (Fig. **1C**). The protein bands for TRPC1, TRPC3, TRPC4 and TRPC6 were detected using anti-TRPC1 (T1E3), anti-TRPC3, anti-TRPC4 (T45E3) and anti-TRPC6 (T367E3) antibodies, respectively, while no specific band was detected using preimmune serum or antibody pre-absorbed with antigenic peptide. Same size of TRPC6 protein band was detected by anti-TRPC6 antibody targeting the N-terminus (Fig. **1C**).

Identification of TRPC Spliced Variants

The expression of TRPC spliced variants in SKOV3 cells were examined by RT-PCR using specific primer sets across introns. The spliced variant of TRPC1 with exon 3 deletion (TRPC1β) was detected using the primer set across exon 3 (P1). The band density of TRPC1β is much stronger than the full-length isoform (TRPC1α) (Fig. **2A**), suggesting that the β-isoform is highly expressed in the cancer cells. Using the primer set across the exon 9 and 10 (P3), a novel spliced variant of TRPC1 with exon 9 deletion (TRPC1^{E9del}) was identified (GenBank accession No. GQ293239). The existence of TRPC1^{E9del} was also confirmed by using the TRPC1 primer set across exon 9 (P4). The band density of the TRPC1^{E9del} was less abundant than the non-spliced TRPC1 isoform in the region. The deletion of exon 9 did not cause open reading frame shift, suggesting this new spliced isoform may have a channel pore domain and C-terminus that seen in α or β isoforms. Interestingly, the TRPC1^{E9del} isoform was absent in normal mouse brain tissue (Fig. **S2**) and vascular smooth muscle cells or arteries detected by same primer set (P4) [21]. These data suggested that TRPC1 is actively spliced in cancer cells. In addition, we also examined the possibility for other splicing regions using primer set P2 and P5, and the primer combination ranged from exon 1 to exon 13, but no other splicing site was identified.

Full-length human TRPC3 has 12 exons and a 58-base pair insert between exon 2 and exon 3. Using primer set across exon 2-5 (P1), or exon 3-5 (P2), exon 5-6 (P3) and exon 8-9 (P4), single PCR band with the expected size was detected. TRPC3 has an isoform with an extended N-terminus (TRPC3a) [22], so we detected this isoform using primer set across exon 1-5 (P0). As shown in Fig. (**2B**), a band with an expected size of 1405 bp was detected, suggesting the TRPC3a isoform existed in the SKOV3 cells. We also amplified the regions of exon 5-9 and exon 8-12, but no other spliced isoforms were found in SKOV3 cells.

Eight spliced variants of human TRPC4 have been reported including α, β, γ, δ, ε, ζ, η and an unnamed isoform truncated at exon 6. Based on the sequence alignment (Fig. **S3**), the α, β, γ, δ, ε and ζ isoforms of TRPC4 have 100 % identity for the region from exon 1 to exon 7 except TRPC4ζ
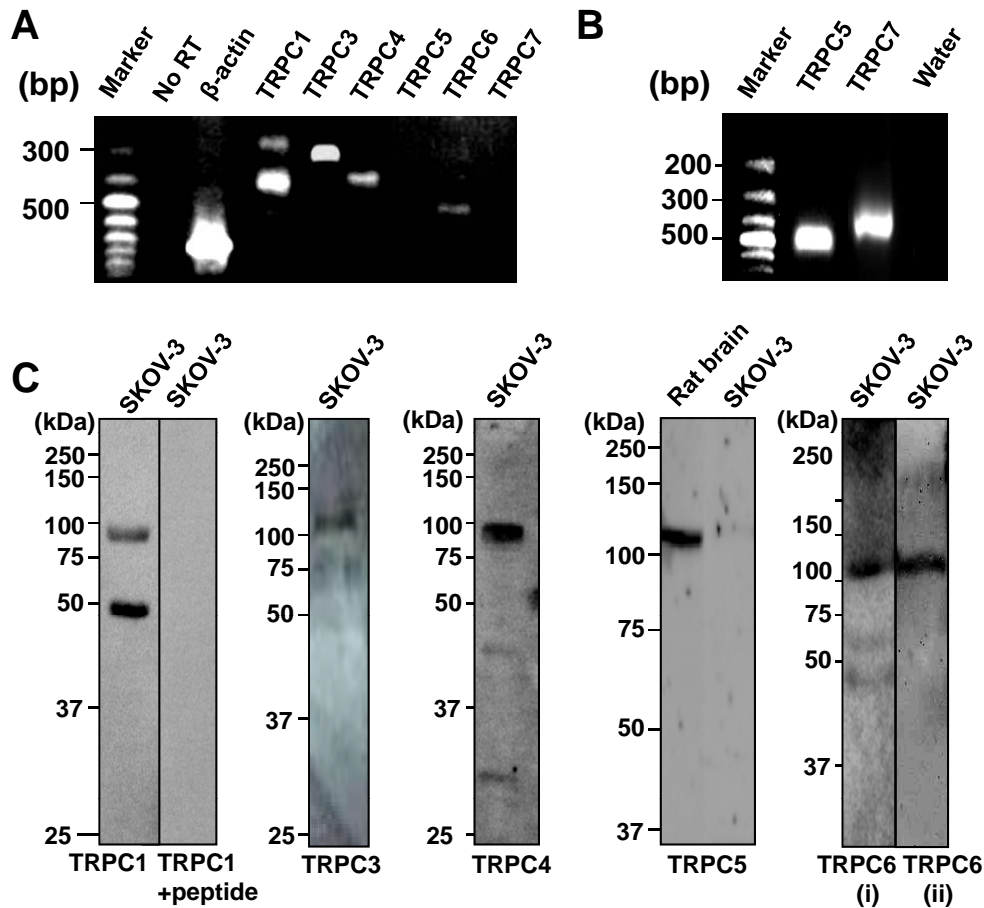
Fig. (1). Expression of TRPC channels in human ovarian cancer cells. A. Detection of TRPC mRNAs by RT-PCR using the primer set for TRPC1 (P3), TRPC3 (P4), TRPC4 (P5), TRPC5, TRPC6 (P3) and TRPC7 (see supplementary Table **1**). The β-actin was used as positive control, and the reverse transcript step omitting the reverse transcriptase (no RT) was set as negative control. **B**. TRPC5 and TRPC7 were undetectable in (**A**), but positive if the plasmid TRPC5 and TRPC7 cDNAs were used as positive control. **C**. Western blotting detection of TRPC proteins using anti-TRPC1 (T1E3), anti-TRPC3, anti-TRPC4 (T45E3) and anti-TRPC6 (T367E3 (i) and anti-TRPC6 targeting to N-terminal (ii)) antibodies. No band was detected by anti-TRPC5 antibody (T5E3) in SKOV3, but positive for the rat brain lysate. Two bands were detected by anti-TRPC1 (T1E3) and competed by antigenic peptide.

that has exon 3 deletion. The η-isoform has an early stop code due to open reading frame shift at the end of exon 3. Using primer set P1 and P4, TRPC4 was positive in SKOV3 cells with the size of 740 bp and 519 bp, respectively. However, the ζ-isoform with exon 3 deletion was undetectable using the primer set across exon 1-5 (P2) (data not shown). The ε-isoform of TRPC4 was also undetectable with the forward primer in exon 7 and the ε-isoform specific reverse primer. However, two bands were detected with an expected size of 428 bp and 623 bp using the primer set (P3). The smaller band is specific for TRPC4γ and the bigger band is the unspliced isoforms of TRPC4 without exon 8 deletion. Similarly, two bands were detected if the primer set across the exon 8 alone (P6) (data not shown) was used, suggesting the TRPC4γ and other isoforms co-existed in the SKOV3 cells. To further distinguish the TRPC4 isoforms, the primer set (P7) amplifying exon 7 to exon 12 were used, the detected band with a predicted size of 956 bp is α-isoform, and the small band (704 bp) for the β-isoform (Fig. **2C**). In addition, we also examined the possibility for other splicing regions using the forward and reverse primer combinations

ranged from exon 1 to exon 11, and no other splicing region was found. These data indicated that α-, β- and γ-isoforms of TRPC4 coexist in the SKOV3 cells.

There are 13 exons for human TRPC6. Three bands were detected using primer set (P1) to amplify exon 1-5. The size for the full-length TRPC6 is 1222 bp. The two spliced isoforms with exon 3 deletion is 1039 bp and with exon 3 and 4 deletion is 874 bp, respectively. No spliced region was found between exon 8 to exon 13 (Fig. **2D**).

Functional Properties of TRPC Isoforms

We examined the functional properties of TRPC isoforms using whole-cell patch recording. TRPC1, TRPC1[E9del], TRPC3, TRPC4α, TRPC4β, TRPC4ε and TRPC6 were inducibly expressed in HEK293 T-REx cells using pcDNA4/TO expression system. TRPC1 and TRPC1[E9del] were mainly located intracellularly (See Fig. **6C**) and the whole-cell current was small (data not shown), however the currents for TRPC3, TRPC4α and TRPC6 were robust and significantly evoked by trypsin *via* G protein-coupled
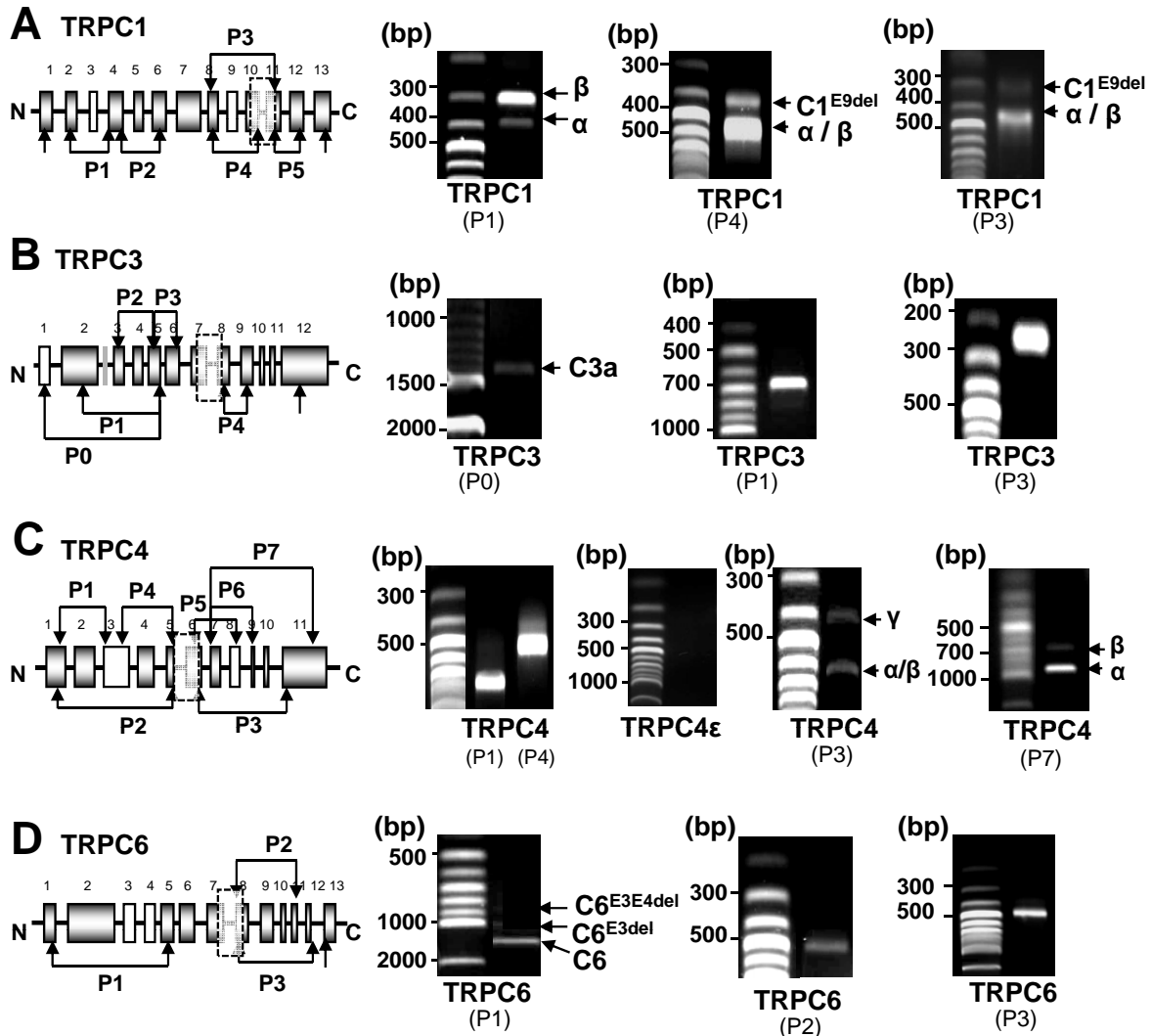
Fig. (2). Detection of TRPC spliced variants in human ovarian cancer SKOV-3 cells. A. RT-PCR products of TRPC1 were amplified by specific primer set labelled as P1 to P5. Two products were amplified using primer set P1 with a size of 403 bp (TRPC1α) and 301 bp (TRPC1β). A small product with exon 9 deletion (C1^{E9del}) was identified using primer set P4 (405 bp for C1^{E9del}, and 549 bp for TRPC1α/β isoforms). The C1^{E9del} was also detected using primer set P3 (423 bp for α/β isoforms; 279 bp for C1^{E9del}). No other splicing region was detected using primer set P2, P5 and the primer combinations amplifying exon 1-6 and exon 11-13. **B**. The TRPC3 spliced variant with an extended N-terminus was detected using primer set P0 (1221 bp). Single PCR product was found using primer set P1, P3 and P4, or P2 and the primers amplifying exon 8 to exon 12 (not shown). **C**. TRPC4 isoforms were detected by primer set P1 and P4. The ζ-isoform with exon 3 deletion (C4^{E3del}) amplified by set P2 (not shown) and ε-isoform amplified by isoform-specific primer were negative The γ-isoform with exon 8 deletion (C4^{E8del}) was detected by primer set P3, and P6 (not shown). Using primer set P7, both α-isoform (956 bp) and β-isoforms (704 bp) were detected. **D**. Two TRPC6 spliced isoforms were detected using primer set P1. Single band of TRPC6 with an expected size was detected by primer set P2 (551 bp) and P3 (476 bp). PCR products were confirmed by direct sequencing.

receptor activation and blocked by 2-APB (Fig. **S4**). We compared the functionality of TRPC4α, TRPC4β and TRPC4ε isoforms. TRPC4α and TRPC4β showed a similar current-voltage (*IV*) relationship and both of them were activated by Gd^{3+} and blocked by 2-APB, however the current for TRPC4ε was much smaller and the *IV* curve was linear, which is different from the *IV* curves for TRPC4α and TRPC4β with double rectifications (Fig. **S5**). These results suggest the potential functional differences among the TRPC isoforms due to the different subcellular distribution and channel properties.

Ovarian Cancer Cell Growth Regulated by TRPC Channel Modulators

2-APB is a non-selective blocker of TRPC channels [5]. The blockade of TRPC channels by 2-APB significantly inhibited the SKOV3 proliferation in a concentration-dependent manner with an EC$_{50}$ of 5.9 μM (Fig. **3A**). Since 2-APB has been shown to inhibit gap junctional channels, which might contribute to the anti-proliferative effect [23, 24], we pretreated the SKOV3 cells with carbenoxolone, a gap junctional blocker, to pharmacologically dissect out the

contribution of TRPC channels. Carbenoxolone at 200 μM and 400 μM significantly inhibited the cell proliferation (Fig. **3B**), but the anti-proliferative effect of 2-APB was still reserved in the presence of carbenoxolone (Fig. **3C**), suggesting that the anti-proliferative effect of 2-APB could be due to the inhibition on TRPC channels. We also observed the effect of SKF-96365, another non-specific TRPC channel blocker. SKF-96365 significantly inhibited the cell proliferation of SKOV3 in a concentration-dependent manner with an EC_{50} of 14.5 μM (Fig. **3D**), however Gd^{3+} which can differentially activate TRPC4 and TRPC5 channels showed a stimulating effect on cell proliferation (Fig. **3E**). In addition, we tested the channel activator trypsin

on cell proliferation. Trypsin significantly stimulated TRPC3, 4 and 6 channels as shown in Fig. (**S4**), which can be explained by the mechanism of protease-activated receptor activation. Incubation with trypsin promoted the cancer cell proliferation (Fig. **3F**). These data suggest the importance of TRPC channel activity in regulating ovarian cancer cell growth, and the channel blockers could have the potential for anti-cancer therapy.

Role of TRPC Isoforms in Ovarian Cancer Cell Proliferation

To identify the role of individual TRPC isoforms on the cancer cell proliferation, SKOV3 cells were incubated
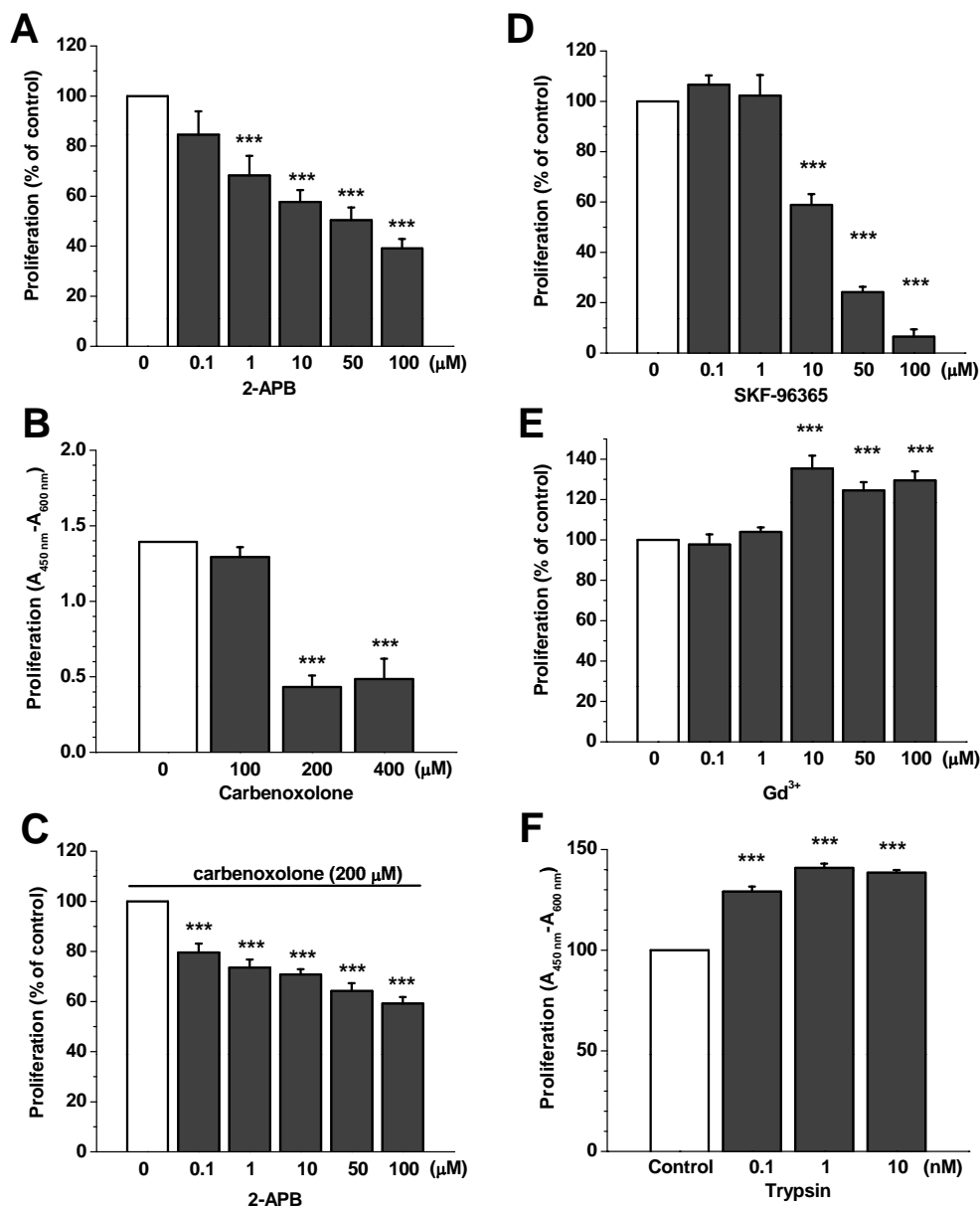
Fig. (3). Ovarian cancer cell proliferation was inhibited by store-operated channel blockers. A. SKOV3 were incubated with different concentrations of 2-APB for 24 h. The cell proliferation was monitored by WST-1 assay and the absorbance was measured at a wavelength of 450 nm with a reference at 600 nm. **B**. SKOV3 treated with carbenoxolone for 24 h. **C**. SKOV3 cells were incubated with carbenoxolone and 2-APB for 24 h. **D**. Effect of SKF-96365 on SKOV with a IC_{50} of 14.5 μM after 24 hour incubation. **E**. Effect of Gd^{3+}. **F**. Incubation with trypsin (0.1-10 nM). Each experiment had 8 well repeats and the data were from ≥ two independent experiments. *** $P<0.001$.
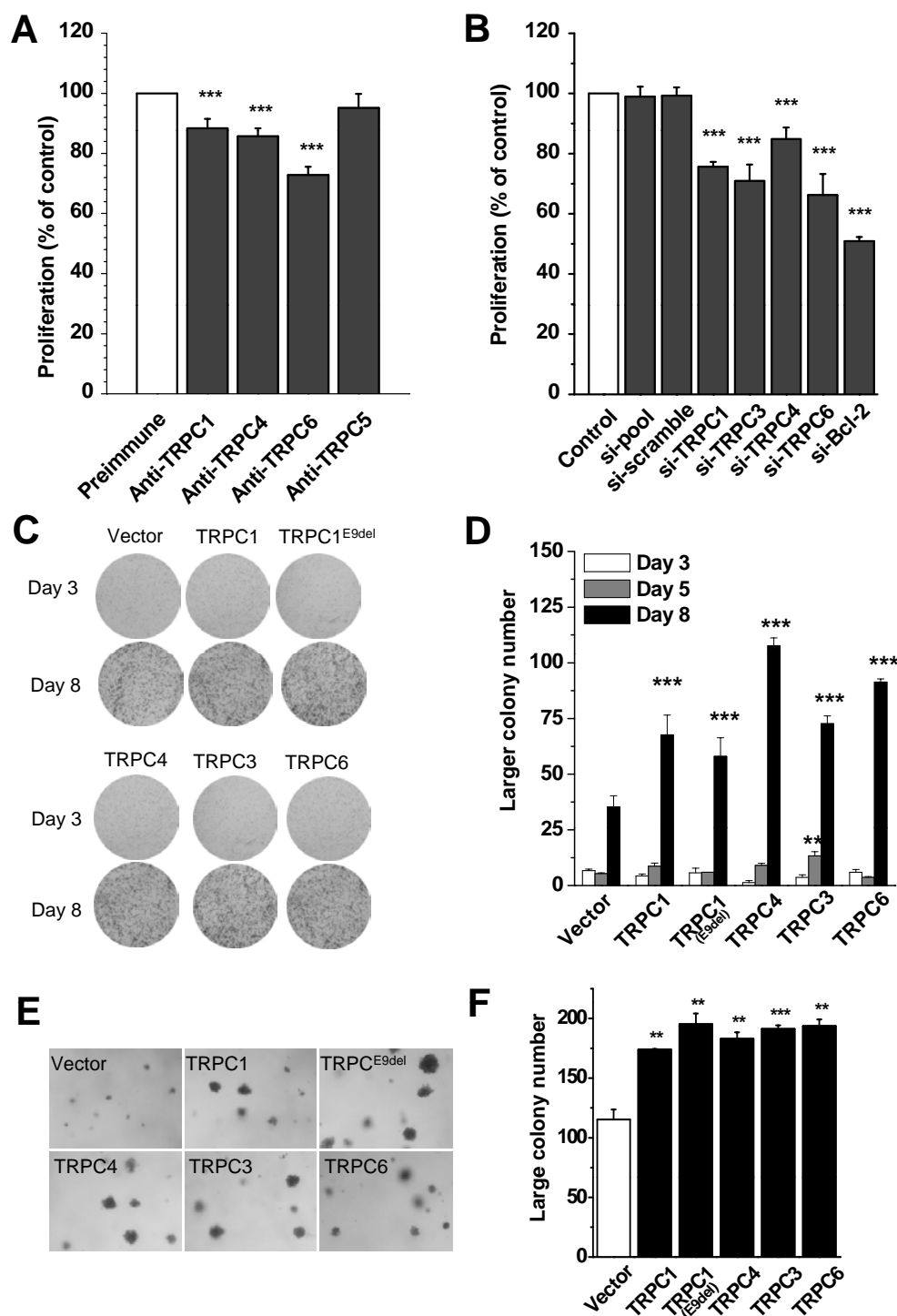
Fig. (4). Role of TRPC channels in the ovarian cancer growth. A. SKOV3 cells were incubated with functional antibodies (1:500 dilution for anti-TRPC1 (T1E3); 1:250 dilutions for anti-TRPC4 (T45E3), anti-TRPC5 (T5E3) and anti-TRPC6 (T367E3) for 24 hours and the cell proliferation was measured by WST-1 assay. n =16 for each group. **B.** SKOV3 cells were transfected with TRPC siRNAs (100 nM siRNA for each group) using Lipofectamine 2000. Cell proliferation was measured with WST-1 assay after 48 h transfection. The sham transfection (control), pool siRNA and scramble siRNA were negative control. Bcl-2 siRNA was used as positive control. n =16 for each group. **C.** Ovarian cancer colony formation assay. The SKOV3 cells over-expressing with plasmid TRPC cDNAs (indicated) or vector and the cancer colonies were stained with crystal violet. **D**. Mean ± SE data showed the large (>2 mm^2) colony number. Triplicate wells were used for each group. Results were reproducible in more than three independent experiments. **E.** Examples of ovarian cancer colonies grown in soft agar and stained with crystal violet. The SKOV3 cells over-expressing with plasmid TRPC cDNAs (indicated) or vector. **F**. Mean ± SE data showed the number of large colony with a diameter >100 μm. Triplicate wells were used for each group. ** $P<0.01$, *** $P<0.001$.

with E3-targeting TRPC functional antibodies that can specifically inhibit Ca^{2+} influx *via* TRPC channels [17, 21]. The specificity of antibody binding was confirmed by ELISA and FACS as shown in Fig. (**S1**). The blockade of TRPC1, TRPC4 and TRPC6 channels by T1E3, T45E3 and T367E3 significantly decreased the cancer cell proliferation (Fig. **4A**), but T5E3, which can block TRPC5 channel only,

had no effect on cell proliferation, further suggesting the lack of TRPC5 expression in SKOV3 cells.

The isoform-specific TRPC siRNAs were used to further demonstrate the role of TRPCs in cancer cell proliferation. The downregulation of TRPCs by siRNAs was confirmed by real-time PCR (data not shown). There was no difference
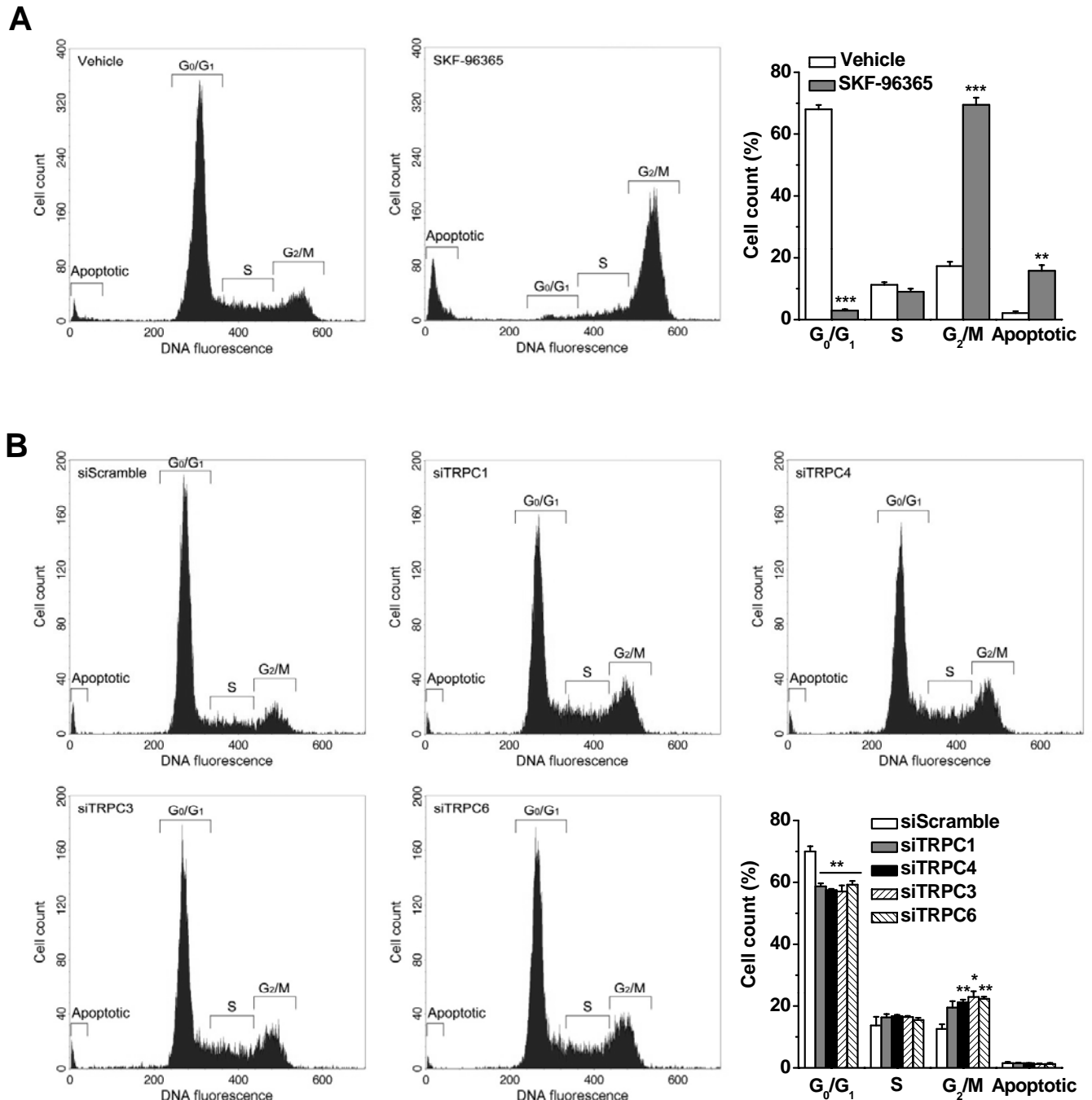
Fig. (5). Cell cycle arrested by TRPC channel blocker SKF-96365 and TRPC siRNAs in ovarian cancer cells. A. The representative FACS histogram for vehicle (DMSO) and SKF-96365 (10 μM), and the mean ± SE data from three independent experiments. B. SKOV3 cells transfected with scramble siRNA (siScramble) and TRPC siRNA (siTRPC1, siTRPC4, siTRPC3, and siTRPC6) for 72 hours. The percentage of propidium iodide -labelled cells at different cell cycle stage was determined by FACS analysis. The mean ± SE data were from three independent experiments. * $P<0.05$, ** $P<0.01$, *** $P<0.001$ comparing with the vehicle group or the scramble siRNA transfected group.

among the groups transfected with scramble siRNA, pool siRNA and mock control transfection (no siRNA) on SKOV3 cell proliferation. However, the cell proliferation was significantly inhibited by the transfection with TRPC1, TRPC3, TRPC4 and TRPC6 siRNAs for 48 hours. Bcl-2 siRNA, which targets the anti-apoptotic Bcl-2 gene, was used as a positive control, also significantly inhibited cell proliferation (Fig. **4B**). These results were similar to the observations using specific anti-TRPC functional antibodies, suggesting that the silencing of TRPC channel expression is important for the inhibition of cancer cell proliferation.

Overexpression of TRPC Isoforms Promotes Cancer Colony Growth

There are no specific siRNAs or blocking antibody tools targeting to individual spliced variants of TRPCs, therefore we overexpressed the TRPC isoforms to further confirm the role of TRPC in ovarian cancer growth. SKOV3 cells were transfected with the plasmid TRPC and TRPC1^{E9del} cDNAs and the cancer cell colony formation was observed. As shown in Fig. (**4C**-**D**), the large colony number (>2 mm^2) was greatly increased in the groups transfected with TRPC1, TRPC1^{E9del}, TRPC3, TRPC4 and TRPC6. We also examined
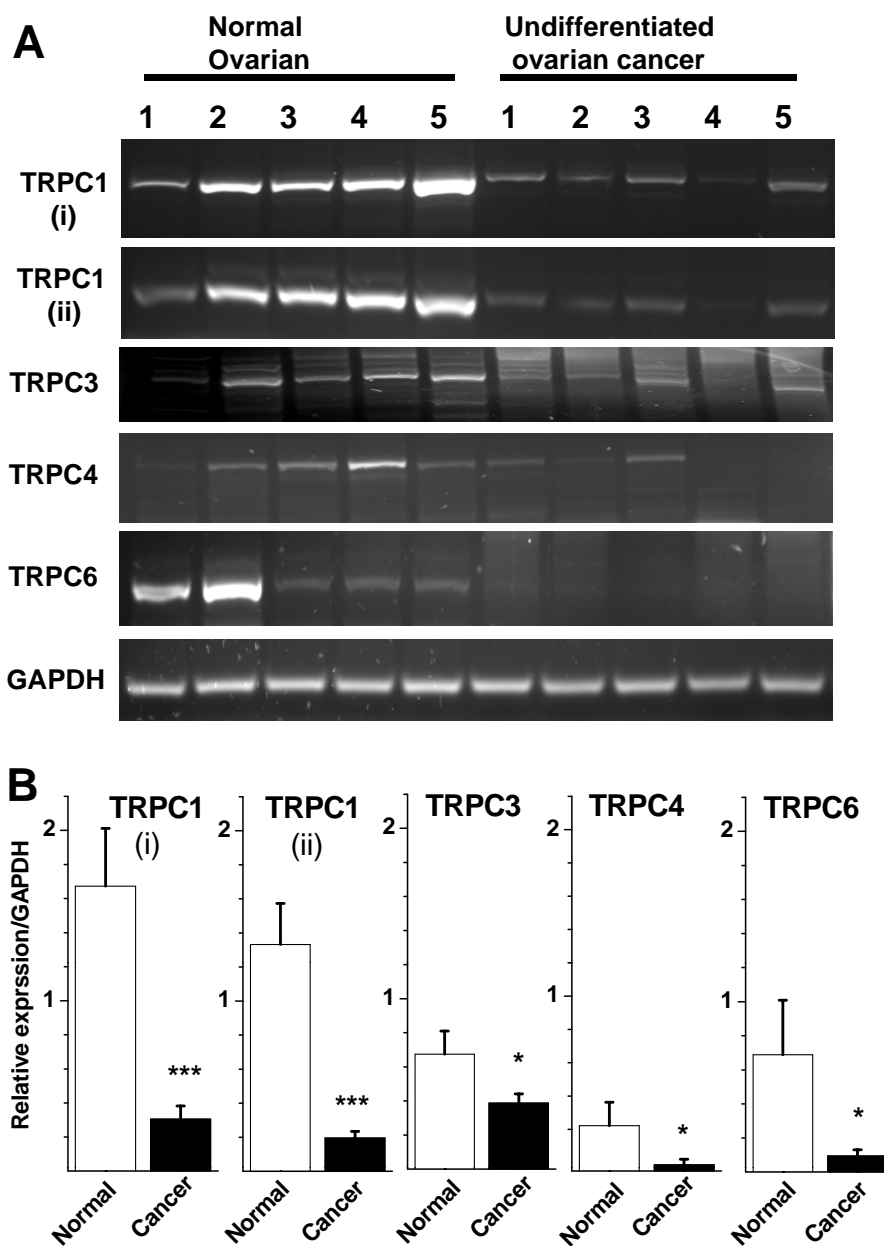
Fig. (6). TRPC expression detected in human ovarian adenocarcinoma. The mRNA was detected by RT-PCR. The PCR amplicons for TRPC1 (i: primer P1; ii: primer P3), TRPC3, TRPC4 and TRPC6 were shown in (**A**). Five cancer samples from patients with undifferentiated ovarian serous papillary adenocarcinoma, and five normal samples were run in parallel. The GAPDH was used as control. **B**. The band density was quantified by a gel documentation software (VisionWorks LS6.3). The relative expression of TRPC/GAPDH was given. * $P<0.05$, *** $P<0.001$.
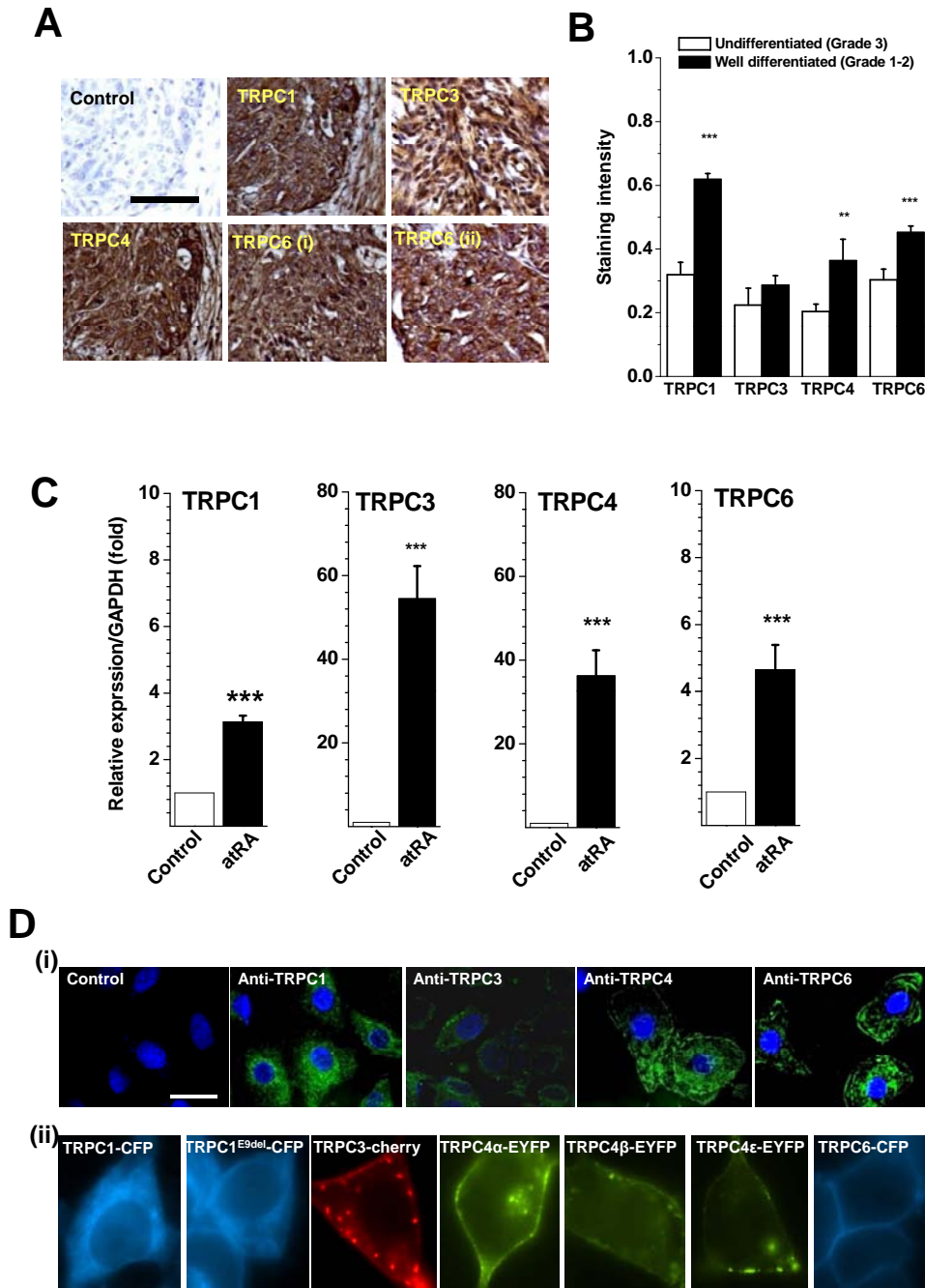
Fig. (7). Distribution of TRPC isoforms in human ovarian adenocarcinoma tissues and cells and the dependence of cell differentiation. A. Human ovarian adenocarcinoma tissue sections were stained with anti-TRPC1 (T1E3), anti-TRPC4 (T45E3), anti-TRPC3 (Alomone lab) and anti-TRPC6 (i:T367E3; ii:TRPC6 antibody from Alomone lab) using VECTASTAIN ABC Systems. The positive staining was shown as brown colour, and the nuclei were counter-stained by hematoxylin. The preimmue serum was used as control. Scale bar is 100 μm. **B**. Mean data for the staining intensity of the ovarian cancer. The *n* number is 15 microscopy fields for the quantification of the undifferentiated ovarian cancer from three patients, and *n* = 12 for the well differentiated ovarian tumour group from three patients. **C**. TRPC expression enhanced by all-*trans* retinoic acid (atRA). The mRNA was detected by real-time PCR. The GAPDH was used as a housekeeping gene for relative quantification. The $2^{(-\Delta\Delta Ct)}$ method was used for calculation. SKOV3 cells were treated with or without 1 μM atRA for 5 days. The culture media were refreshed every 24 hours. **D**. (i): SKOV3 cells stained with anti-TRPC1 (T1E3), anti-TRPC3, anti-TRPC4 (T45E3) and anti-TRPC6 antibodies at a dilution of 1:500 and the secondary anti-rabbit antibody conjugated with FITC (green). Same dilution of preimmune serum or no primary antibody was used as control. The nuclei were stained by 4',6-diamidino-2-phenylindole (DAPI, blue). Scale bar is 25 μm. (ii): Distribution of TRPC isoforms in the transfected HEK-293 T-REx cells. The TRPC1, TRPC1^{E9del} and TRPC6 cDNAs were tagged with CFP (blue), TRPC3 tagged with mCherry (Red), and TRPC4 (α, β and ε isoforms) tagged with EYFP. ** *P*<0.01, *** *P*<0.001.

the cancer colony growth using soft agar assay. The number of larger colony with a diameter >100 µm was much higher in the groups transfected with TRPC1, TRPC1^{E9del}, TRPC3, TRPC4 and TRPC6 than that in the vector control group, which further suggested the involvement of TRPCs in the ovarian cancer development.

Effects of TRPC Channel Blocker and Gene Silencing on Cell Cycle

The ovarian cancer cell cycle was determined by FACS using propidium iodide staining procedure [20]. Incubation with the non-selective TRPC channel blocker SKF-96365 (10 µM) substantially increased the G_2/M phase and decreased the G_0/G_1 phase in the SKOV3 cells (Fig. **5A**), which was accorded to the previous report [15]. To further observed the effects of individual TRPC genes on cell cycle progress, the SKOV3 cells were transfected with TRPC siRNAs. We found that more SKOV cells were arrested at G_2/M phase after transfection with siTRPC1, siTRPC4, siTRPC3, and siTRPC6 for 72 hours comparing with the control group transfected with scramble siRNA (Fig. **5B**), suggesting that the downregulation of TRPC gene expression can arrest the cell cycle progression through G_2/M to G_1. Unlike the channel blocker SKF-96365, the contribution of TRPC gene silencing on apoptosis was small (Fig. **5**). The down-regulation of TRPC expression did not significantly change the apoptosis in ovarian cancer.

Differentiation-associated TRPC Expression

The expression of TRPC was examined by RT-PCR using ovarian cancer tissues from five patients with undifferentiated ovarian serous papillary adenocarcinoma. The five normal ovarian tissues obtained from patients at a similar age but without ovarian cancer were used as control. The mRNAs for TRPC1, TRPC3, TRPC4 and TRPC6 were positive in normal and ovarian cancer tissues. However, the mRNA level of TRPC1, TRPC3, TRPC4 and TRPC6 was significantly lower in the undifferentiated ovarian cancer than that in normal ovarian tissue (Fig. **6**), suggesting that the expression of TRPCs was down-regulated in the cell type of undifferentiated ovarian cancer.

We also examined the protein expression of TRPCs in human ovarian adenocarcinoma tissues by immunostaining. The paraffin-embedded ovarian cancer tissue sections were stained using Vectastain ABC systems. TRPC1, TRPC4 and TRPC6 were positively stained by T1E3, T45E3 and T367E3 antibodies, while the control staining with preimmune serum or without primary anti-TRPC antibodies was negative. The staining pattern for TRPC6 was similar to that by an anti-TRPC6 antibody targeting to the N-terminus (Fig. **7A**). We compared the immunostaining density between the undifferentiated or poorly differentiated (Grade 3) and well differentiated (Grade 1-2) ovarian tissue sections. The expression of TRPC1, TRPC4 and TRPC6 were significantly lower in the undifferentiated ovarian cancer tissues (Fig. **7B**).

TRPC Expression Enhanced by all-*trans* Retinoic Acid (atRA)

AtRA is a potent regulator for cell differentiation in a variety of cell types and plays an important role in anticancer therapy by affecting gene transcription [25, 26]. To further examine the association of TRPC in ovarian cancer cell differentiation, we tested the effect of atRA on TRPC expression. Using real-time RT-PCR, we found that the mRNA level for TRPC1, TRPC3, TRPC4, and TRPC6 was significantly increased in the SKOV3 cells treated with 1 µM atRA for 5 days (Fig. **7C**), suggesting that TRPC expression is associated with atRA-induced cell differentiation.

Subcellular Distribution of TRPC Isoforms

The subcellular distribution of TRPC channel proteins was investigated in the SKOV3 cells and the TRPC-transfected cells. SKOV3 cells were stained with anti-TRPC1 (T1E3), anti-TRPC3, anti-TRPC4 (T45E3) and anti-TRPC6 (T367E3) antibodies. TRPC1 was more evident in the cytosol, but TRPC3, TRPC4 and TRPC6 were apparent in the plasma membrane (Fig. **7D**(i)). The cultured SKOV3 had an irregular and very flat cell shape and tightly attached onto the coverslips, so it was hard to obtain a Z-section with a typical imaging for plasma membrane staining. Therefore, the unpermeabilized staining was also performed for TRPC1, TRPC4 and TRPC6 using extracellular binding antibodies, and the stainings were also positive (Fig. **S6**). Due to the lack of TRPC spliced variant-specific antibodies, it is impossible to see the subcellular localization of TRPC1^{E9del} and TRPC4 isoforms in the native ovarian cancer cells, therefore, we explored the subcellular localization in the HEK-293 T-REx cells by over-expressing the isoforms tagged with fluorescence proteins. TRPC1^{E9del} protein was mainly intracellularly located, which is similar to that of the full-length TRPC1. However, channel proteins for TRPC3, TRPC4α, TRPC4β, TRPC4ε and TRPC6 were evident in the plasma membrane (Fig. **7D**(ii)).

DISCUSSION

We have shown that TRPC1, TRPC3, TRPC4 and TRPC6 exist in the tissue section of human ovarian adenocarcinoma and the ovarian adenocarcinoma-derived cell line SKOV3. We have also shown that several spliced variants of TRPC1, TRPC3, TRPC4 and TRPC6 co-express in the ovarian cancer cells. In addition, a new TRPC1 spliced variant with exon 9 deletion has been identified in this study. Blockade of TRPC channel activity by 2-APB, SKF-96365, or by TRPC isoform-specific functional antibodies or by the transfection with TRPC siRNAs significantly inhibits the cancer cell proliferation, whilst the increase of TRPC channel activity by G protein-coupled receptor activation promotes the ovarian cancer cell growth. Overexpression of TRPC genes also increases ovarian cancer colony growth. Moreover, the expression in undifferentiated human ovarian cancer is significantly lower than in normal ovarian tissues. These findings are novel and important for understanding the roles of TRPC channels in ovarian cancer development.

TRPC channels have been identified in many cell types [2, 18, 27, 28]. These channels are differentially expressed at different stages of stem cell development, which may reflect their importance in cell differentiation [29, 30]. On the other hand, the thapsigargin-induced store-operated Ca^{2+} influx is higher in tumour cells than that in normal cells [31], which further suggests the relevance of TRPC channels or store-

operated channel molecules to cancer development. In this study, we have systematically detected the TRPC channels and their splice variants, and found that multiple TRPCs and their spliced isoforms exist in human ovarian cancer. TRPC1 has been suggested as a store-operated channel subunit and actively associates with other TRPC isoforms, such as TRPC1/4 or TRPC1/5 [18, 32], or interacts with other channel proteins, such as ORAI1 or STIM1 [33], to constitute the heteromultimeric store-operated channels or channel complexes, which could be main molecular components in native cells. Interestingly, the existence of several spliced isoforms of TRPCs in a cell suggests the possibility of functional interaction or regulation on the channel activity. TRPC1γ1 and TRPC1γ2 have been reported in human myometrial cells [34], but none of them have been detected in the ovarian cancer cells, and no inserts found between exon 8 to exon 10. Instead, we have identified a new TRPC1 isoform with exon 9 deletion, suggesting this TRPC1 spliced isoform lacks transmembrane segment 4 (S4). TRPC1^{E9del} is mainly distributed in the cytosol with a similar subcellular distribution pattern to the full length TRPC1. The nuclear membrane localisation for TRPC1 and TRPC^{E9del} is also evident. However, other isoforms including TRPC3, TRPC4α, TRPC4β, TRPC4ε and TRPC6 are located in the plasma membrane, suggesting the potential functional difference between TRPC1 and other TRPC isoforms. Since the current of over-expressed TRPC1 is small and difficult to be distinguished from the endogenous current, we have not compared the biophysical difference between TRPC1 and TRPC1^{E9del}. However, we believe that the TRPC1^{E9del} is a functional subunit, because the colony growth is significantly increased by the overexpression of TRPC1^{E9del}, although the underling mechanism is unclear and needed to be further investigated. Moreover, the spliced isoforms of TRPC1 with exon 2 and exon 3 deletion have been described in mice by Sakura & Ashcroft [35], but this splicing activity has not been found in human SKOV3 cells. TRPC3 and TRPC6 have a high similarity in sequence. Both of them have been demonstrated as receptor-operated channels that mediate the diacylglycerol-induced Ca^{2+} influx, although TRPC3 may also have store-operated channel properties [36, 37]. In addition, co-existence of several TRPC4 isoforms in the SKOV cells could be important for protein interactions among the TRPC isoforms that may be required for precisely regulating the functionality of Ca^{2+} permeable channel complexes in cancer cells, and thus control cell growth. Indeed, some spliced TRPC isoforms have been demonstrated as an inhibitory subunit for TRPC homomultimeric channels in HEK-293 cells if co-overexpressed with the full-length isoforms [38, 39]. We also found that the channel property of TRPC4ε is different from other TRPC4 isoforms. Further investigation is needed to explore the functional difference among the alternative splicing of TRPCs in cancer development.

The expression level of individual TRPCs in different type of cancer cells or cancer tissues are variable, suggesting the differential expression of TRPCs in cancer cells [4, 30]. We also found such differences in our study, such as TRPC4 expressed in SKOV3, but not in breast cancer MCF7 cells (data not shown). In addition, the expression level may depend on the differentiation status of the cancer cells,

because we found that the undifferentiated ovarian cancer has lower expression of TRPC1, TRPC4 and TRPC6, which is consistent to the observation of low level of TRPC4 and TRPC6 in immature stem cells [29]. This observation was further confirmed in the *in vitro* experiment using the cell differentiation regulator atRA. It has been reported that atRA at 1 μM inhibited SKOV3 cell proliferation and phenotype, although the ovarian cell line is less sensitive to atRA treatment [40, 41]. We were unable to compare the expression among the different ovarian cancer types and different grades of differentiation in this study due to the source of fresh ovarian sample, however, a large scale collaborative study is needed in the future.

The anti-proliferative effect of 2-APB has been demonstrated in gastric cancer cell lines [42], colon cancer cell [43] and human hepatoma cells [44]. Here we found that the effect of 2-APB was not altered by the gap junctional channel blocker, carbenoxolone, further suggesting that the anti-proliferative action of 2-APB is due to the inhibition on store-operated channels. 2-APB and SKF-96365 are broad-spectrum TRPC channel blockers and cannot distinguish the contribution of individual TRPC isoforms, therefore the isoform-specific functional antibody tools were used in this study. The specificity of the antibodies has been confirmed by ELISA, western blotting, *in vitro* functional testing on Ca^{2+} influx and FACS-based assay. The block on TRPC1, TRPC4 and TRPC6 channels by E3-targeting functional antibodies caused a significant inhibition of cell proliferation, suggesting that TRPC1, TRPC4 and TRPC6 are important for cancer cell proliferation. This effect was further confirmed by the application of TRPC isoform-specific siRNAs. The M phase was mainly arrested for the cell cycle progression, which is similar to the study using TRPC3 siRNA alone [15].

We have not examined other TRP subfamilies related to cancer, such as TRPM1 in melanoma [4], TRPM7 in human retinoblastoma cells [45] and human head and neck carcinoma cells [46], TRPM8 and TRPV6 in prostate cancer [30, 47]. The potential contribution of other molecules or subunits of store-operated channels, such as STIM and ORAI proteins and MS4A12 [48, 49], may also be important in the regulation of store-operated Ca^{2+} signalling in cancer.

Cell apoptosis has been suggested to be related to store operated channel [50]. Thapsigargin can induce apoptosis of prostate cancer cells, but this effect cannot be prevented by an intracellular Ca^{2+} chelator, suggesting that the increase of cytosol Ca^{2+} is unnecessary for apoptosis [50]. We found that the non-selective channel blocker 2-APB (data not shown) and SKF-96365 can evoke ovarian cancer cell apoptosis, but the specific TRPC siRNAs do not significantly change the apoptosis, suggesting the TRPC channels may be less important in the regulation of cancer cell apoptosis, therefore we have not explored the details of TRPCs in cancer cell apoptosis in this study.

Ca^{2+} is a key signal for cell growth or death. The specific activation of pathways and channels for precisely regulating Ca^{2+} influx is important for both normal and cancer cells. We found that TRPC1, TRPC3, TRPC4 and TRPC6 channels are expressed in ovary cancer, and the splicing variants of

TRPCs are highly expressed in the cancer cells, which is important for understanding the molecular pathways for Ca^{2+} entry. Inhibition of these channel activity or expression level leads to the anti-proliferative effect, so the TRPC channels should be considered as potential targets for cancer therapy. In addition, the lower expression of TRPC or its isoforms could be developed negative prognostic biomarkers for certain type of cancer, such as the undifferentiated type of ovarian cancer.

FOOTNOTES

GenBank accession number for TRPC1 spliced isoform: GQ293239.

CONFLICT OF INTEREST

The author(s) confirm that this article content has no conflict of interest.

ACKNOWLEDGEMENTS

SUPPLEMENTARY MATERIAL

Supplementary material is available on the publisher's web site along with the published article.

ABBREVIATIONS

2-APB	=	2-Aminoethoxydiphenyl borate
atRA	=	all-*trans* retinoic acid
CFP	=	cyan fluorescent protein
EYFP	=	enhanced yellow fluorescent protein
FACS	=	fluorescence activated cell sorting
GAPDH	=	glyceraldehyde 3-phosphate dehydrogenase
IP_3R	=	inositol 1,4,5-trisphosphate receptor
PBS	=	phosphate buffered saline
RT	=	reserve transcriptase
ROCs	=	receptor-operated Ca^{2+} channels
SOCs	=	store-operated Ca^{2+} channels
TRPC	=	transient receptor potential canonical

REFERENCES

[1] Clapham, D. E. TRP channels as cellular sensors. *Nature* **2003**, *426*, 517-524.

[2] Xu, S. Z.; Sukumar, P.; Zeng, F.; Li, J.; Jairaman, A.; English, A.; Naylor, J.; Ciurtin, C.; Majeed, Y.; Milligan, C. J.; Bahnasi, Y. M.; Al-Shawaf, E.; Porter, K. E.; Jiang, L. H.; Emery, P.; Sivaprasadarao, A.; Beech, D. J. TRPC channel activation by extracellular thioredoxin. *Nature* **2008**, *451*, 69-72.

[3] Holmuhamedov, E.; Lewis, L.; Bienengraeber, M.; Holmuhamedova, M.; Jahangir, A.; Terzic A. Suppression of human tumor cell proliferation through mitochondrial targeting. *Faseb. J.* **2002**, *16*, 1010-1016.

[4] Prevarskaya, N.; Zhang, L.; Barritt, G. TRP channels in cancer. *Biochim. Biophys. Acta* **2007**, *1772*, 937-946.

[5] Xu, S. Z.; Zeng, F.; Boulay, G.; Grimm, C.; Harteneck, C.; Beech, D. J. Block of TRPC5 channels by 2-aminoethoxydiphenyl borate: a differential, extracellular and voltage-dependent effect. *Br. J. Pharmacol.* **2005**, *145*, 405-414.

[6] Aydar, E.; Yeo, S.; Djamgoz, M.; Palmer, C. Abnormal expression, localization and interaction of canonical transient receptor potential ion channels in human breast cancer cell lines and tissues: a potential target for breast cancer diagnosis and therapy. *Cancer Cell Int.* **2009**, *9*, 23.

[7] El Boustany, C.; Bidaux, G.; Enfissi, A.; Delcourt, P.; Prevarskaya, N.; Capiod, T. Capacitative calcium entry and transient receptor potential canonical 6 expression control human hepatoma cell proliferation. *Hepatology* **2008**, *47*, 2068-2077.

[8] Thebault, S.; Flourakis, M.; Vanoverberghe, K.; Vandermoere, F.; Roudbaraki, M.; Lehen'kyi, V.; Slomianny, C.; Beck, B.; Mariot, P.; Bonnal, J.L.; Mauroy, B.; Shuba, Y.; Capiod, T.; Skryma, R.; Prevarskaya, N. Differential role of transient receptor potential channels in Ca2+ entry and proliferation of prostate cancer epithelial cells. *Cancer Res.* **2006**, *66*, 2038-2047.

[9] Pigozzi, D.; Ducret, T.; Tajeddine, N.; Gala, J. L.; Tombal, B.; Gailly, P. Calcium store contents control the expression of TRPC1, TRPC3 and TRPV6 proteins in LNCaP prostate cancer cell line. *Cell Calcium* **2006**, *39*, 401-415.

[10] Veliceasa, D.; Ivanovic, M.; Hoepfner, F. T.; Thumbikat, P.; Volpert, O. V. Smith, N. D. Transient potential receptor channel 4 controls thrombospondin-1 secretion and angiogenesis in renal cell carcinoma. *FEBS J.* **2007**, *274*, 6365-6377.

[11] Bomben, V. C.; Sontheimer, H. W. Inhibition of transient receptor potential canonical channels impairs cytokinesis in human malignant gliomas. *Cell Prolif.* **2008**, *41*, 98-121.

[12] Nasman, J.; Bart, G.; Larsson, K.; Louhivuori, L.; Peltonen, H.; Akerman, K. E. The orexin OX1 receptor regulates Ca2+ entry via diacylglycerol-activated channels in differentiated neuroblastoma cells. *J. Neurosci.* **2006**, *26*, 10658-10666.

[13] Nakao, K.; Shirakawa, H.; Sugishita, A.; Matsutani, I.; Niidome, T.; Nakagawa, T.; Kaneko, S. Ca2+ mobilization mediated by transient receptor potential canonical 3 is associated with thrombin-induced morphological changes in 1321N1 human astrocytoma cells. *J. Neurosci. Res.* **2008**, *86*, 2722-2732.

[14] Cai, R.; Ding, X.; Zhou, K.; Shi, Y.; Ge, R.; Ren, G.; Jin, Y.; Wang, Y. Blockade of TRPC6 channels induced G2/M phase arrest and suppressed growth in human gastric cancer cells. *Int. J. Cancer* **2009**, *125*, 2281-2287.

[15] Yang, S. L.; Cao, Q.; Zhou, K.C.; Feng, Y. J.; Wang, Y. Z. Transient receptor potential channel C3 contributes to the progression of human ovarian cancer. *Oncogene* **2009**, 28, 1320-1328.

[16] Beck, B.; Lehen'kyi, V.; Roudbaraki, M.; Flourakis, M.; Charveron, M.; Bordat, P.; Polakowska, R.; Prevarskaya, N.; Skryma, R. TRPC channels determine human keratinocyte differentiation: new insight into basal cell carcinoma. *Cell Calcium* **2008**, *43*, 492-505.

[17] Xu, S. Z.; Zeng, F.; Lei, M.; Li, J.; Gao, B.; Xiong, C.; Sivaprasadarao, A.; Beech, D. J. Generation of functional ion-channel tools by E3 targeting. *Nat. Biotechnol.* **2005**, *23*, 1289-1293.

[18] Xu, S. Z.; Muraki, K.; Zeng, F.; Li, J.; Sukumar, P.; Shah, S.; Dedman, A. M.; Flemming, P. K.; McHugh, D.; Naylor, J.; Cheong, A.; Bateson, A. N.; Munsch, C. M.; Porter, K. E.; Beech, D. J. A sphingosine-1-phosphate-activated calcium channel controlling vascular smooth muscle cell motility. *Circ. Res.* **2006**, *98*, 1381-1389.

[19] Kumar, B.; Dreja, K.; Shah, S. S.; Cheong, A.; Xu, S. Z.; Sukumar, P.; Naylor, J.; Forte, A.; Cipollaro, M.; McHugh, D.; Kingston, P. A.; Heagerty, A. M.; Munsch, C. M.; Bergdahl, A.; Hultgardh-Nilsson, A.; Gomez, M. F.; Porter, K. E.; Hellstrand, P.; Beech, D. J. Upregulated TRPC1 channel in vascular injury in vivo and its role in human neointimal hyperplasia. *Circ. Res.* **2006**, *98*, 557-563.

[20] Riccardi, C.; Nicoletti, I. Analysis of apoptosis by propidium iodide staining and flow cytometry. *Nat. Protoc.* **2006**, *1*, 1458-1461.

[21] Xu, S. Z.; Beech, D. J. TrpC1 is a membrane-spanning subunit of store-operated Ca(2+) channels in native vascular smooth muscle cells. *Circ. Res.* **2001**, *88*, 84-87.

[22] Yildirim, E.; Kawasaki, B. T.; Birnbaumer, L. Molecular cloning of TRPC3a, an N-terminally extended, store-operated variant of the

human C3 transient receptor potential channel. *Proc. Natl. Acad. Sci. U.S.A* **2005**, *102*, 3307-3311.

[23]   Harks, E. G.; Camina, J. P.; Peters, P. H.; Ypey, D. L.; Scheenen, W. J.; van Zoelen, E. J.; Theuvenet, A. P. Besides affecting intracellular calcium signaling, 2-APB reversibly blocks gap junctional coupling in confluent monolayers, thereby allowing measurement of single-cell membrane currents in undissociated cells. *FASEB J.* **2003**, *17*, 941-943.

[24]   Vinken, M.; Vanhaecke, T.; Papeleu, P.; Snykers, S.; Henkens, T.; Rogiers, V. Connexins and their channels in cell growth and cell death. *Cell Signal.* **2006**, *18*, 592-600.

[25]   Kaiser, P. C.; Korner, M.; Kappeler, A.; Aebi, S. Retinoid receptors in ovarian cancer: expression and prognosis. *Ann. Oncol.* **2005**, *16*, 1477-1487.

[26]   Um, S. J.; Lee, S. Y.; Kim, E. J.; Han, H. S.; Koh, Y. M.; Hong, K. J.; Sin, H. S.; Park, J. S. Antiproliferative mechanism of retinoid derivatives in ovarian cancer cells. *Cancer Lett.* **2001**, *174*, 127-134.

[27]   Flemming, R.; Xu, S. Z.; Beech, D. J. Pharmacological profile of store-operated channels in cerebral arteriolar smooth muscle cells. *Br. J. Pharmacol.* **2003**, *139*, 955-965.

[28]   Riccio, A.; Medhurst, A. D.; Mattei, C.; Kelsell, R. E.; Calver, A. R.; Randall, A. D.; Benham, C. D.; Pangalos, M. N. mRNA distribution analysis of human TRPC family in CNS and peripheral tissues. *Brain Res. Mol. Brain Res.* **2002**, *109*, 95-104.

[29]   den Dekker, E.; Molin, D. G.; Breikers, G.; van Oerle, R.; Akkerman, J. W.; van Eys, G. J.; Heemskerk, J. W. Expression of transient receptor potential mRNA isoforms and Ca(2+) influx in differentiating human stem cells and platelets. *Biochim. Biophys. Acta* **2001**, *1539*, 243-255.

[30]   Bodding, M. TRP proteins and cancer. *Cell Signal* **2007**, *19*, 617-624.

[31]   Kovacs, G. G.; Zsembery, A.; Anderson, S. J.; Komlosi, P.; Gillespie, G. Y.; Bell, P. D.; Benos, D. J.; Fuller, C. M. Changes in intracellular Ca2+ and pH in response to thapsigargin in human glioblastoma cells and normal astrocytes. *Am. J. Physiol. Cell Physiol.* **2005**, *289*, C361-371.

[32]   Strubing, C.; Krapivinsky, G.; Krapivinsky, L.; Clapham, D. E. TRPC1 and TRPC5 form a novel cation channel in mammalian brain. *Neuron.* **2001**, *29*, 645-655.

[33]   Ong, H. L.; Cheng, K. T.; Liu, X.; Bandyopadhyay, B. C.; Paria, B. C.; Soboloff, J.; Pani, B.; Gwack, Y.; Srikanth, S.; Singh, B. B.; Gill, D.; Ambudkar, I. S. Dynamic assembly of TRPC1-STIM1-Orai1 ternary complex is involved in store-operated calcium influx. Evidence for similarities in store-operated and calcium release-activated calcium channel components. *J. Biol. Chem.* **2007**, *282*, 9105-9116.

[34]   Yang, M.; Gupta, A.; Shlykov, S. G.; Corrigan, R.; Tsujimoto, S.; Sanborn, B. M. Multiple Trp isoforms implicated in capacitative calcium entry are expressed in human pregnant myometrium and myometrial cells. *Biol. Reprod.* **2002**, *67*, 988-994.

[35]   Sakura, H.; Ashcroft, F. M. Identification of four trp1 gene variants murine pancreatic beta-cells. *Diabetologia* **1997**, *40*, 528-532.

[36]   Estacion, M.; Li, S.; Sinkins, W. G.; Gosling, M.; Bahra, P.; Poll, C.; Westwick, J.; Schilling, W. P. Activation of human TRPC6 channels by receptor stimulation. *J. Biol. Chem.* **2004**, *279*, 22047-22056.

[37]   Venkatachalam, K.; van Rossum, D. B.; Patterson, R. L.; Ma, H. T.; Gill, D. L. The cellular and molecular basis of store-operated calcium entry. *Nat. Cell Biol.* **2002**, *4*, E263-272.

[38]   Schaefer, M.; Plant, T. D.; Stresow, N.; Albrecht, N.; Schultz, G. Functional differences between TRPC4 splice variants. *J. Biol. Chem.* **2002**, *277*, 3752-3759.

[39]   Satoh, E.; Ono, K.; Xu, F.; Iijima, T. Cloning and functional expression of a novel splice variant of rat TRPC4. *Circ. J.* **2002**, *66*, 954-958.

[40]   Hanna, E. A.; Umhauer, S.; Roshong, S. L.; Piechocki, M. P.; Fernstrom, M. J.; Fanning, J. D.; Ruch, R.J. Gap junctional intercellular communication and connexin43 expression in human ovarian surface epithelial cells and ovarian carcinomas in vivo and in vitro. *Carcinogenesis* **1999**, *20*, 1369-1373.

[41]   Guruswamy, S.; Lightfoot, S.; Gold, M. A.; Hassan, R.; Berlin, K. D.; Ivey, R. T.; Benbrook, D. M. Effects of retinoids on cancerous phenotype and apoptosis in organotypic cultures of ovarian carcinoma. *J. Natl. Cancer Inst.* **2001**, *93*, 516-525.

[42]   Sakakura, C.; Miyagawa, K.; Fukuda, K.; Shimomura, K.; Takemura, M.; Takagi, T.; Kin, S.; Nakase, Y.; Fujiyama, J.; Mikoshiba, K.; Okazaki, Y.; Hayashizaki, Y.; Hagiwara, A.; Yamagishi, H. [Possible involvement of inositol 1, 4, 5-trisphosphate receptor type 3 (IP3R3) in the peritoneal dissemination of gastric cancers]. *Gan To Kagaku Ryoho* **2003**, *30*, 1784-1787.

[43]   Kazerounian, S.; Pitari, G. M.; Shah, F. J.; Frick, G. S.; Madesh, M.; Ruiz-Stewart, I.; Schulz, S.; Hajnoczky, G.; Waldman, S. A. Proliferative signaling by store-operated calcium channels opposes colon cancer cell cytostasis induced by bacterial enterotoxins. *J. Pharmacol. Exp. Ther.* **2005**, *314*, 1013-1022.

[44]   Enfissi, A.; Prigent, S.; Colosetti, P.; Capiod, T. The blocking of capacitative calcium entry by 2-aminoethyl diphenylborate (2-APB) and carboxyamidotriazole (CAI) inhibits proliferation in Hep G2 and Huh-7 human hepatoma cells. *Cell Calcium* **2004**, *36*, 459-467.

[45]   Hanano, T.; Hara, Y.; Shi, J.; Morita, H.; Umebayashi, C.; Mori E.; Sumimoto, H.; Ito, Y.; Mori, Y.; Inoue, R. Involvement of TRPM7 in cell growth as a spontaneously activated Ca2+ entry pathway in human retinoblastoma cells. *J. Pharmacol. Sci.* **2004**, *95*, 403-419.

[46]   Jiang, J.; Li, M. H.; Inoue, K.; Chu, X. P.; Seeds, J.; Xiong, Z. G. Transient receptor potential melastatin 7 like current in human head and neck carcinoma cells: role in cell proliferation. *Cancer Res.* **2007**, *7*, 10929-10938.

[47]   Vanden Abeele, F.; Shuba, Y.; Roudbaraki, M.; Lemonnier, L.; Vanoverberghe, K.; Mariot, P.; Skryma, R.; Prevarskaya, N. Store-operated Ca2+ channels in prostate cancer epithelial cells: function, regulation, and role in carcinogenesis. *Cell Calcium* **2003**, *33*, 357-373.

[48]   Koslowski, M.; Sahin, U.; Dhaene, K.; Huber, C.; Tureci, O. MS4A12 is a colon-selective store-operated calcium channel promoting malignant cell processes. *Cancer Res.* **2008**, *68*, 3458-3466.

[49]   Prakriya, M.; Feske, S.; Gwack, Y.; Srikanth, S.; Rao, A.; Hogan, P. G. Orai1 is an essential pore subunit of the CRAC channel. *Nature* **2006**, *443*, 230-233.

[50]   Skryma, R.; Mariot, P.; Bourhis, X. L.; Coppenolle, F. V.; Shuba, Y.; Vanden Abeele, F.; Legrand, G.; Humez, S.; Boilly, B.; Prevarskaya, N. Store depletion and store-operated Ca2+ current in human prostate cancer LNCaP cells: involvement in apoptosis. *J. Physiol.* **2000**, *527*, 71-83.

22920441

Store-independent pathways for cytosolic STIM1 clustering in the regulation of store-operated Ca²⁺ influx

Bo Zeng, Gui-Lan Chen, Shang-Zhong Xu *

Centre for Cardiovascular and Metabolic Research, Hull York Medical School, University of Hull, Hull, HU6 7RX, United Kingdom

ARTICLE INFO

ABSTRACT

STIM1 is a Ca²⁺ sensing molecule. Once the Ca²⁺ stores are depleted, STIM1 moves towards the plasma membrane (PM) (translocation), forms puncta (clustering), and triggers store-operated Ca²⁺ entry (SOCE). Although this process has been regarded as a main mechanism for store-operated Ca²⁺ channel activation, the STIM1 clustering is still unclear. Here we discovered a new phenomenon of STIM1 clustering, which is not triggered by endoplasmic reticulum (ER) Ca²⁺ depletion.

STIM1 subplasmalemmal translocation and clustering can be induced by ER Ca²⁺ store depletion with thapsigargin (TG), G-protein-coupled receptor activator trypsin and ryanodine receptor (RyR) agonists caffeine and 4-chloro-3-ethylphenol (4-CEP) in the HEK293 cells stably transfected with STIM1–EYFP. The STIM1 clustering induced by TG was more sustained than that induced by trypsin and RyR agonists. Interestingly, 4-CEP-induced STIM1 clustering also happened in the cytosol without ER Ca²⁺ store depletion. Application of some pharmacological regulators including flufenamic acid, 2-APB, and carbonyl cyanide 4-(trifluoromethoxy)phenylhydrazone (FCCP) at concentrations without affecting ER Ca²⁺ store also evoked cytosolic STIM1 clustering. However, the direct store-operated ORAI channel blockers (SKF-96365, Gd³⁺ and diethylstilbestrol) or the signaling pathway inhibitors (genistein, wortmannin, Y-27632, forskolin and GF109203X) did not change the STIM1 movement. Disruption of cytoskeleton by colchicine and cytochalasin D also showed no effect on STIM1 movement.

We concluded that STIM1 clustering and translocation are two dynamic processes that can be pharmacologically dissociated. The ER Ca²⁺ store-independent mechanism for STIM1 clustering is a new alternative mechanism for regulating store-operated channel activity, which could act as a new pharmacological target.

© 2012 Elsevier Inc. All rights reserved.

1. Introduction

The activation of G-protein-coupled receptors (GPCRs) and receptor tyrosine kinases (RTKs) induces a Ca²⁺ release from internal stores, which in turn triggers a sustained Ca²⁺ influx across the plasma membrane (PM) via store-operated Ca²⁺ channels (SOCs). This Ca²⁺ influx through SOCs, also called store-operated Ca²⁺ entry or capacitative Ca²⁺ entry, mediates numerous physiological functions including cell growth, muscle contraction, exocytosis, gene transcription and apoptosis [1]. The molecular basis for SOCs has been linked to the two major ion channel families, i.e., ORAI channels and transient receptor potential (TRP) channels. ORAI channels mediate a highly Ca²⁺-selective and inward rectifying Ca²⁺ release-activated Ca²⁺ current (I_{CRAC}) [2,3], while TRPC channels mediate a non-selective Ca²⁺-permeable cationic current with a current–voltage (IV)

relationship of outward rectification, such as TRPC1, TRPC3, TRPC7 and the heteromeric TRPC1/TRPC5 channel [4–6], or "N" shape IV curve with inward and outward rectification [7]. ORAI channels, as well as TRPCs, are interacted or triggered by the endoplasmic reticulum (ER) Ca²⁺ sensor STIM1 (stromal interaction molecule 1) that signals the Ca²⁺ depletion of ER to the SOCs [8–12].

STIM1 was originally identified as a stromal cell molecule that is potentially relevant for interactions with pre-B cells. It is a type I membrane protein and mainly located in the ER, but also to a limited extent in the plasma membrane (PM) [8,13]. STIM1 relocation has been suggested as the mechanism for coupling the ER Ca²⁺ store depletion to the store-operated channels in the PM [9,10]. It has been demonstrated that the ER-luminal domain of STIM1 is responsible for Ca²⁺ sensing, and the dissociation of Ca²⁺ from STIM1 leads to oligomerization (clustering) and redistribution of STIM1 to the subplasmalemmal area (translocation) [8,14]. STIM1 then triggers ORAI channels (ORAI1, 2 and 3) in the PM via the binding to the N-terminus of ORAI, which results in Ca²⁺ entry into the cell [8].

Dysfunction of store-operated Ca^{2+} channels causes some diseases, for example, the mutations of ORAI1 and STIM1 causing the deficiency of I_{CRAC} in T cells that has been regarded as the aetiology of severe combined immune deficiency syndrome [15]. ORAI1 deficiency in mice results in resistance to pathological thrombus formation, which is an important new clue for preventing ischemic cardiovascular and cerebrovascular events [16]. In addition, the alteration of channel expression or channel activity is implicated in angiogenesis [17], smooth muscle cell proliferation and migration [18] and cardiomyocyte hypertrophy [19], suggesting the signaling of STIM1 associated store-operated Ca^{2+} channel activation could act as new therapeutic targets. However, the pharmacological regulation of STIM1 movement is still unclear.

In order to examine the possibility of STIM1 movement as a new potential drug target, we proposed this study to investigate the pharmacological profile of STIM1 translocation and clustering using store-operated Ca^{2+} channel modulators that potentially change the store-operated Ca^{2+} channel activity or target to the signaling pathways of store-operated channel activation. We demonstrated that the localization of STIM1 puncta shows two different patterns in response to different regulators, i.e., cytosolic clusters and subplasmalemmal clusters, and found the existence of an ER Ca^{2+} store-independent mechanism for the cytosolic STIM1 movement.

2. Materials and methods

2.1. Chemicals and reagents

Generally used salts and other chemicals including thapsigargin (TG), 2-aminoethoxydiphenyl borate (2-APB), $GdCl_3$, SKF-96365, diethylstilbestrol (DES), colchicine, cytochalasin D (CytD), caffeine, 4-chloro-3-ethylphenol (4-CEP), genistein, wortmannin, Y-27632, GF109203X, 1-oleoyl-2-acetyl-sn-glycerol (OAG), U73122, caly-culin A (CalyA), flufenamic acid (FFA), niflumic acid (NFA), carbonyl cyanide 4-(trifluoromethoxy)phenylhydrazone (FCCP), sodium azide, hydrogen peroxide (H_2O_2), $HgCl_2$, forskolin, and Fura-PE3/AM were purchased from Sigma–Aldrich (Poole, UK).

2.2. Gene cloning and plasmid construction

The coding sequences of monomeric red fluorescent protein (mCherry) and monomeric cyan fluorescent protein (mCFP) were subcloned into pcDNA4/TO vector (Invitrogen, Paisley, UK) using the primers HindIII-GFP-F and BamHI-GFP-R (Supplementary Table 1). Full-length ORAI1, ORAI2 and ORAI3 coding regions were amplified from the cDNA of human aortic endothelial cells with the primers in Supplementary Table 1. ORAI1 and ORAI2 were subcloned into the downstream of mCherry in pcDNA4/TO vector to make fused genes mCherry-ORAI1 and mCherry-ORAI2, and ORAI3 and TRPC1 were subcloned into pcDNA4/TO-mCFP vector in a same way to generate mCFP-ORAI3 and mCFP-TRPC1. The ORAI1, ORAI2, ORAI3 and TRPC1 sequences were identical to the GenBank reference sequences NM_032790, NM_032831, NM_152288 and NM_003304, respectively. The STIM1–EYFP plasmids were kindly provided by Prof AV Tepikin (University of Liverpool). The Lifeact sequence encoding a 17-amino-acid peptide that binds to filamentous actin (F-actin) in eukaryotic cells [20], was introduced into pcDNA4/TO-mCFP vector by PCR mutagenesis with three overlapped primers (Supplementary Table 1).

2.3. Cell culture and transfection

The plasmids encoding human STIM1 tagged with enhanced yellow fluorescent protein at the C-terminus (STIM1–EYFP) were transfected into T-REx HEK293 cells using Lipofectamine 2000 transfection reagent (Invitrogen, Paisley, UK). The cells were cultured in D-MEM/F-12 medium (Invitrogen, Paisley, UK) supplemented with 10% fetal calf serum, 100 units/ml penicillin and 100 mg/ml streptomycin, and maintained at 37 °C under 95% air and 5% CO_2. A cell line stably expressing STIM1–EYFP was manually selected from the transfected cells under a Nikon Eclipse Ti-E inverted fluorescence microscope and maintained in the cell culture medium containing G418 (200 μg/ml). Plasmids encoding mCherry-ORAI1, mCherry-ORAI2, mCFP-ORAI3, mCFP-TRPC1 and Lifeact-mCFP were transfected into STIM1–EYFP cells and the expression of these genes were induced with 1 μg/ml tetracycline in the culture medium. Stable cells coexpressing EYFP/mCherry or EYFP/mCFP tagged genes were manually selected under a fluorescent microscope and maintained for experiments.

2.4. Live cell imaging and Ca^{2+} measurement

The stably transfected cells were seeded on 13-mm glass coverslips and cultured for 24–48 h. Live cell images for EYFP/mCherry/mCFP fluorescence were captured using the microscope equipped with a Nikon Plan Fluor 100×/1.30 oil objective. The images were analyzed with the NIS-Elements software (Version 3.2, Nikon, Tokyo, Japan). The puncta around the PM with 1 μm thickness area (about one punctum) was counted as PM puncta, and other puncta were counted as cytosolic puncta. The fluorescence intensity of STIM1–EYFP was measured by NIS-Elements software and the regions of interest (ROIs) were drawn manually. For intracellular Ca^{2+} measurement, cells were loaded with 2 μM Fura-PE3/AM in standard bath solution for 30 min at 37 °C, followed by 5 min wash in standard bath solution at room temperature. Cells were excited alternately by 340 and 380 nm light and emission was collected via a 510-nm filter. Images were sampled every 5 s in pairs for the two excitation wavelengths by a CCD camera (ORCA-R2, Hamamatsu, Japan). The ratio of 340/380 nm fluorescence was used to represent the intracellular Ca^{2+} level. The standard bath solution contained (mM): NaCl 130, KCl 5, $MgCl_2$ 1.2, HEPES 10, glucose 8, and $CaCl_2$ 1.5 (pH 7.4). Ca^{2+}-free solution contained (mM): NaCl 130, KCl 5, $MgCl_2$ 1.2, HEPES 10, glucose 8, and EGTA 0.4 (pH 7.4). All experiments were performed at room temperature. The n values given are the numbers of cells from at least three independent Ca^{2+} imaging experiments.

2.5. Statistics

All values are expressed as mean ± SEM. The t test was used to assess the statistical difference and a P value less than 0.05 was considered as significant.

3. Results

3.1. STIM1 translocation induced by Ca^{2+} store depletion

Passive depletion of ER Ca^{2+} store by sarco/endoplasmic reticulum Ca^{2+}-ATPase (SERCA) inhibitor thapsigargin (TG, 1 μM) induced STIM1–EYFP subplasmalemmal translocation and puncta formation (Fig. 1A and Supplementary video 1), which is consistent with previous reports [9,10,21]. The STIM1 puncta at PM became evident after 4 min incubation with TG and achieved maximum after ~6 min (Fig. 1A). The TG-induced STIM1 clustering and translocation occurred in both Ca^{2+} free and Ca^{2+} containing bath solution, suggesting the extracellular Ca^{2+} is not the determinant for intracellular STIM1 movement. However, longer incubation (20 min) with the Ca^{2+} free bath solution containing 0.4 mM ethylene glycol-bis(2-aminoethylether)-N,N,N′,N′-tetraa-cetic acid (EGTA) also increased STIM1 translocation, which could
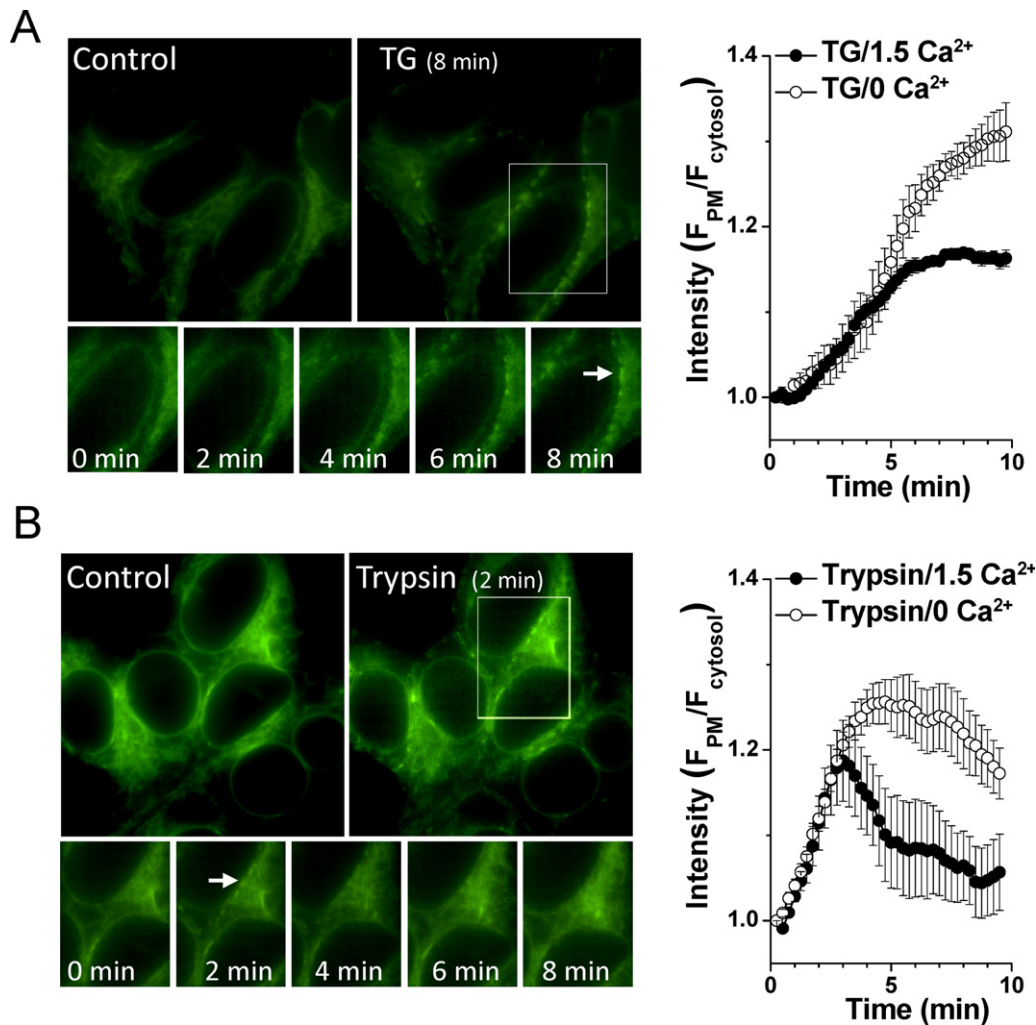
Fig. 1. STIM1 subplasmalemmal translocation and clustering in response to Ca^{2+}-store depletion in the stable transfected STIM1–EYFP cells. (A) TG (1 μM) induced STIM1 puncta formation at the PM of cells in Ca^{2+} bath solution. The time course of STIM1 subplasmalemmal translocation and clustering in the boxed area is showed in the lower panels. The arrow indicates the subplasmalemmal STIM1 clusters (puncta). The ratio of fluorescent intensity in the PM (F_{PM}) and the cytosol ($F_{cytosol}$) of cells in response to TG (1 μM) in 1.5 mM Ca^{2+} or Ca^{2+}-free bath solution ($n = 5$ cells in each group). The regions of interest (ROIs) of the PM and the nearby cytosol were manually selected. (B) Trypsin-induced STIM1 clustering and translocation in standard bath solution. The dynamic changes of ratio of fluorescent intensity ($F_{PM}/F_{cytosol}$) for the STIM1 translocation induced by trypsin (0.1 nM) are shown in the chart ($n = 5$ cells in each group).

be explained by ER Ca^{2+} leakage after longer incubation. This result is similar to the observation on STIM1 translocation with N,N,N′,N′-Tetrakis(2-pyridylmethyl)-ethylenediamine (TPEN), a membrane-permeable metal chelator that passively depletes ER Ca^{2+} store [22]. The time course for the onset of the TG-induced STIM1 translocation was a slow process, which could be due to the slow Ca^{2+} leakage from the ER induced by passive Ca^{2+} store depletion.

We also observed the STIM1 translocation induced by active ER Ca^{2+} store depletion via G-protein-coupled receptor (GPCR) activation. Protease-activated receptor is a unique subclass of GPCRs and can be activated by cleavage of the extracellular N-terminus with trypsin or thrombin [23]. We found trysin at 0.1 nM significantly induced STIM1 clustering and translocation in standard bath solution or Ca^{2+} free bath solution (Fig. 1B). Unlike the SERCA blockers or Ca^{2+} chelators, the STIM1 translocation evoked by trypsin was much faster, but the subplasmalemmal clustering was transient and the puncta gradually disappeared after 4 min in standard bath solution containing 1.5 mM Ca^{2+} (Fig. 1B and Supplementary video 2), however, the disassembly of STIM1 puncta was not observed in Ca^{2+} free solution, suggesting that this process is dependent on Ca^{2+} influx that leads to ER Ca^{2+} store refilling. The relocation of STIM1 from PM to cytosol seen in

the active store-depletion suggests that the STIM1 clustering and translocation is a reversible process, which may act as a drug target.

3.2. Ryanodine-sensitive Ca^{2+} store and STIM1 movement

The entire ER/SR Ca^{2+} store could also be depleted by activation of ryanodine receptors (RyRs), which leads to store-operated Ca^{2+} influx [24]. Therefore, we observed the effect of ryanodine-sensitive Ca^{2+} store depletion on STIM1 movement. The expression of endogenous RyRs has been demonstrated in the HEK293 cells [25]. Application of RyR1–3 direct activator 4-chloro-3-ethylphenol (4-CEP, 500 μM) led to STIM1 translocation toward PM. Interestingly, unlike trypsin, the 4-CEP-induced STIM1 puncta at the PM disappeared after 3 min incubation with 4-CEP, and followed by substantial STIM1 clusters retained in the cytosol (Fig. 2A and Supplementary video 3). However, caffeine ranged from 10 to 50 mM that can increase the sensitivity of RyRs to Ca^{2+} did not cause cytosolic STIM1 puncta, instead the formation of subplasmalemmal STIM1 puncta (Fig. 2B). Both 4-CEP and caffeine induced intracellular Ca^{2+} release, however, Ca^{2+} release induced by 4-CEP was higher and lasted longer than that by caffeine. In

addition, 4-CEP nearly abolished the Ca^{2+} influx when external 1.5 mM Ca^{2+} was added, but caffeine had no such effect (Fig. 2C and D), suggesting the pharmacological difference between the two agonists in the regulation of STIM1 clustering and Ca^{2+} influx.

In order to examine the relationship of cytosolic STIM1 clustering and Ca^{2+} release, the STIM1–EYFP cells were pretreated with RyR antagonist tetracaine (500 μM) for 10 min and then perfused with 4-CEP (500 μM). The 4-CEP-induced Ca^{2+} release signal and STIM1 subplasmalemmal translocation were completely blocked by tetracaine pretreatment, however, the cytosolic clustering of STIM1 was still present (Fig. 2E and F), suggesting that the cytosolic STIM1 clustering is independent of ER Ca^{2+} store release or store depletion.
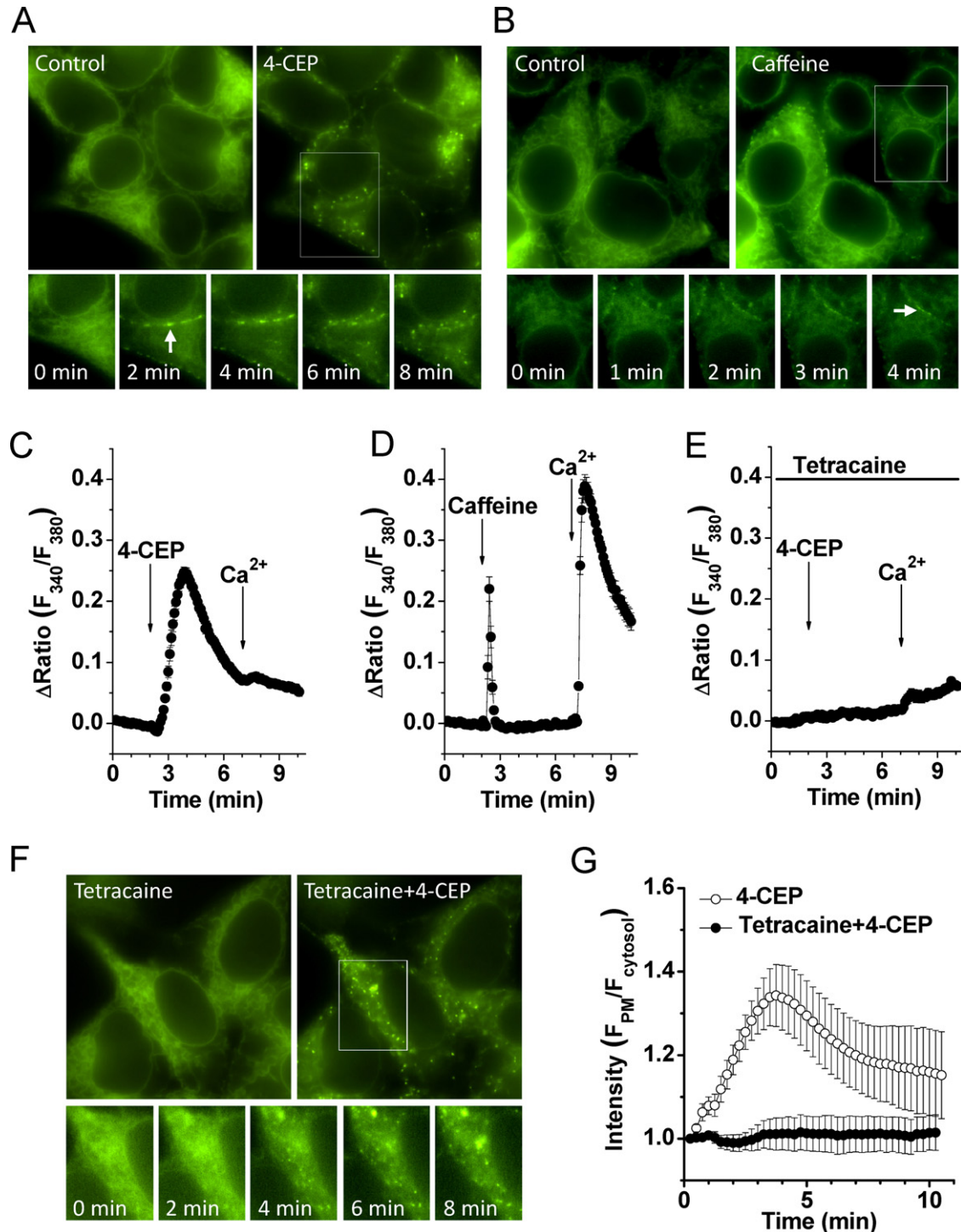
Fig. 2. STIM1 translocation induced by RyR agonists in the STIM1–EYFP cells. (A) 4-CEP (500 μM) induced transient STIM1 puncta formation at the PM and then cytosolic clustering. The time course of STIM1 translocation in the boxed area is shown in the lower figures. The arrow indicates the subplasmalemmal STIM1 puncta. (B) Caffeine (10 mM) induced STIM1 puncta formation at the PM. (C) 4-CEP (500 μM) induced Ca^{2+} release but abolished Ca^{2+} entry in STIM1–EYFP cells ($n = 23$). (D) Caffeine (10 mM) induced Ca^{2+} release and Ca^{2+} entry in the STIM1–EYFP cells ($n = 21$). (E) STIM1–EYFP cells perfused with tetracaine (500 μM) for 10 min and followed by 4-CEP and 1.5 mM Ca^{2+} ($n = 21$). (F) Tetracaine (500 μM) prevented the subplasmalemmal STIM1 puncta formation, but not the cytosolic clusters. (G) The time course of fluorescent intensity changes ($F_{PM}/F_{cytosol}$) for the STIM1 translocation induced by 4-CEP (500 μM) in the absence or presence of 500 μM tetracaine ($n = 10$ cells in each group).

3.3. Mitochondrial Ca²⁺ release is involved in cytosolic STIM1 clustering

Mitochondria are important Ca^{2+}-storing organelles closely associated with ER. Although it has been established that depletion of ER Ca^{2+} stores leads to STIM1 translocation to the PM, little is known about the effect of mitochondrial Ca^{2+} release on STIM1 movement. FFA is a non-steroidal anti-inflammatory drug with Ca^{2+} releasing effect from mitochondria whereas its analogue NFA

has little effect on mitochondrial Ca^{2+} release [26,27]. We therefore compared the two chemicals on STIM1 movement. FFA (100 μM) caused STIM1 clustering in the cytosol, and further addition of 1 μM TG failed to induce STIM1 puncta translocation toward the PM in the standard bath solution (Fig. 3A), however, NFA (100 μM) neither induced any cytosolic STIM1 clusters nor blocked the TG-induced STIM1 subplasmalemmal translocation to the PM, although much more sparse puncta were also observed in the cytosol after addition of TG (Fig. 3A and B). We also observed the
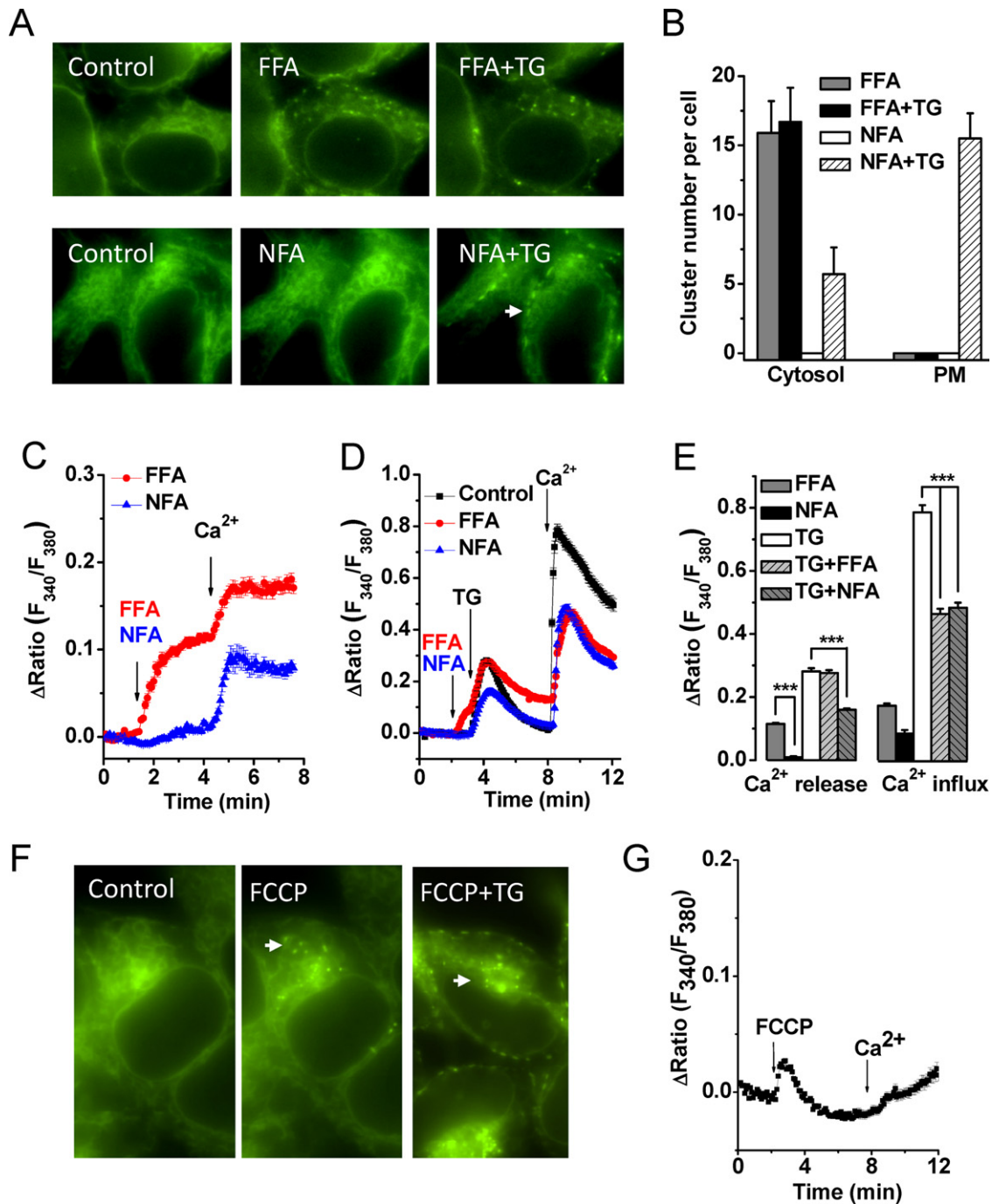
Fig. 3. Effects of flufenamic acid (FFA) and niflumic acid (NFA) on STIM1 movement and store-operated Ca^{2+} entry in STIM1–EYFP cells. (A) FFA (100 μM) caused cytosolic STIM1 clustering and blocked TG-induced STIM1 subplasmalemmal translocation. NFA (100 μM) did not change STIM1 localisation at resting state, but potentiated cytosolic STIM1 clustering after addition of TG (1 μM). (B) The number of STIM1 clusters induced by FFA or NFA before and after addition of 1 μM TG ($n = 10$ cells in each group). (C) FFA (100 μM) induced robust cytosolic Ca^{2+} increase in the absence of external Ca^{2+}, but NFA (100 μM) had no significant effect on Ca^{2+} release in the STIM1–EYFP cells. (D) Effect of FFA and NFA on TG-induced Ca^{2+} release and Ca^{2+} entry. The standard bath solution containing 1.5 mM Ca^{2+} was perfused after store depletion. (E) Comparison of Ca^{2+} release and Ca^{2+} influx induced by FFA (100 μM), NFA (100 μM) and TG (1 μM) ($n = 16–37$ cells in each group). ***$P < 0.001$. (F) Example of FCCP (5 μM) induced cytosolic STIM1 clusters. (G) FCCP (5 μM) induced a small Ca^{2+} release ($n = 26$).

effects of FFA and NFA on Ca^{2+} release and store-depleted Ca^{2+} entry in the STIM1–EYFP cells. The Ca^{2+} release induced by FFA was much higher than the group treated by NFA, but the inhibition on the store-depleted Ca^{2+} entry was similar (Fig. 3C–E).

We examined mitochondrial metabolic inhibitors on STIM1 movement. The uncoupling agent FCCP that can abolish the obligatory linkage between the respiratory chain and the phosphorylation system and cause mitochondrial Ca^{2+} release [28]. Pretreatment with FCCP (5 μM) for 10 min did not prevent TG-induced STIM1 puncta formation near the plasma membrane, however, some STIM1 puncta were observed in the cytosol after FCCP treatment in both TG- or non-TG-treated cells (Fig. 3F), which could be due to its small transient Ca^{2+} release effect from mitochondria (Fig. 3G). Sodium azide is a potent inhibitor of mitochondrial respiration that blocks cytochrome c oxidase. Pretreament with sodium azide (2.5 mM) for 5 min did not change the TG-induced STIM1 subplasmalemmal translocation and clustering (Fig. S1). Application of azide alone did not evoke STIM1 clustering and translocation (data not shown). Moreover, we examined the reagents affecting mitochondrial oxidative stress. Incubation with H_2O_2 (100–1000 μM) for 15 min did not evoke STIM1 clustering and showed no effect on TG-induced STIM translocation (Fig. S1). Mercury is a toxic heavy metal that causes severe mitochondrial oxidative damage leading to cell death, but STIM1 clustering and translocation showed no changes in the presence of Hg^{2+} (5 μM) for 10 min. Hg^{2+} also showed no effect on TG-induced STIM translocation and subplasmalemmal clustering (Fig. S1). These data suggested the mitochondrial Ca^{2+} release is involved in the formation of cytosolic STIM1 clustering, such as FFA and FCCP, but the other inhibitors without affecting mitochondrial Ca^{2+} movement may have less or no direct effect on STIM1 movement.

3.4. Cytosolic STIM1 clustering induced by 2-APB in cells with replete ER Ca^{2+} stores

2-APB is a non-specific store-operated channel blocker with multiple effects on other cationic channels [29]. 2-APB at 100 μM significantly induced STIM1 clustering in the cytosol in the absence of TG (Fig. 4A and Supplementary video 4), and the clustering induced by 2-APB was reversible (Fig. S2A). In addition, 2-APB at 100 μM did not cause Ca^{2+} release (Fig. 4B), which suggests that the 2-APB-induced cytosolic STIM1 clustering is independent of Ca^{2+} store depletion. We also observed the effect of 2-APB on TG-induced STIM1 translocation. 2-APB at low concentrations (5–50 μM) did not cause STIM1 clustering in the cells, but prevented the subplasmalemmal translocation and clustering evoked by 1 μM TG, and resulted in the retention of STIM1 puncta in the cytosol (Fig. 4C).

2-APB has been reported to inhibit ORAI1 and ORAI2, but activate ORAI3 channels [30]. To understand the difference, we observed the effect of 2-APB on STIM1 movement in the STIM1/ORAI cotransfected cells. 2-APB induced a small transient increase of ORAI1 and ORAI2 currents and followed by a sustained inhibition, but activated ORAI3 current (Fig. S2B). The *IV* relationship of STIM1/ORAI1 and STIM1/ORAI2 induced by TG or STIM1/ORAI3 induced by 2-APB was similar to the report [30]. 2-APB-evoked cytosolic STIM1 clustering occurred in all the three cell lines coexpressing each ORAI isoform with STIM1 (Fig. S2C), suggesting that the different sensitivity of ORAI isoforms to 2-APB is unrelated to cytosolic STIM1clustering. However, the subplasmalemmal clusters induced by TG were disassembled by perfusion with 2-APB in the STIM1–EYFP cells, but 2-APB did not disassemble the subplasmalemmal clusters in the cells coexpressing STIM1 with ORAI channels (Fig. 4D), suggesting that the clusters of STIM1/ORAI complexes formed by store-depletion at the PM become

more stable than the homomeric STIM1 clusters in the STIM1-EYFP cells.

3.5. Coexpression with TRPC1 does not affect the cytosolic STIM1 clustering

The functional interaction of TRPC1 with STIM1 has been demonstrated [12,31], therefore we tested the potential interference of STIM1 movement by TRPC1. The stable STIM1–EYFP cells were cotransfected with human TRPC1 tagged with mCFP. Like the STIM1, the overexpressed mCFP-TRPC1 was mainly located in the cytosol, which is accorded to the previous report [32]. The cytosolic STIM1 clusters induced by 2-APB were evident and the logarithmic fluorescence spectra showed many fluctuations by line-scan intensity analysis, but the TRPC1 did not show significant clusters after 2-APB treatment (Fig. 5), suggesting the two proteins are not physically associated in the cytosol during the STIM1 movement, although the distribution pattern of STIM1 and TRPC1 in the cells looks similar before the treatment of 2-APB. Moreover, the coexpression of TRPC1 did not change the TG-induced STIM1 subplasmalemmal translocation (data not shown). These results suggest that the cytosolic TRPC1 does not form STIM1/TRPC1 complexes in the cytosol or change the cytosolic STIM1 movement.

3.6. Effect of other store-operated channel blockers

Since the formation of cytosolic STIM1 clusters is related to application of 2-APB, 4-CEP and FFA, and the three reagents are cationic or store-operated channel inhibitors, we therefore examined other commonly used store-operated channel blockers for pharmacological comparison. Both SKF-96365 and Gd^{3+} showed no effect on TG-induced STIM1 clustering and translocation (Fig. S3). Pretreatment with diethylstilbestrol (DES, 10 μM), a potent store-operated channel inhibitor [33], had no effect on STIM1 clustering and translocation (Fig. S3). These results suggest that the blockade on store-operated channels or Ca^{2+} influx does not change the cytosolic STIM1 clustering, and also suggest the pharmacological difference on STIM1 movement among the store-operated channel modulators.

3.7. Effect of signaling pathway inhibitors on STIM1 movement

STIM1 has been suggested as an important protein in regulating cell survival, therefore we examined the potential mechanisms by the application of inhibitors targeting to cell signaling pathways regulating cell survival. Genistein at micromolar concentrations has been regarded as a specific inhibitor for receptor tyrosine kinase (RTK) [34]. Pretreatment with genistein (10 μM) for 5 min did not alter the STIM1 clustering and translocation toward PM evoked by store depletion (Fig. S4A). Incubation with phosphatidylinositol 3-kinase (PI_3K) inhibitor wortmannin (20 μM) for 30 min also showed no significant effect on TG-induced STIM1 translocation and clustering (Fig. S4B), suggesting the activity of RTK/PI_3K/Akt/mTOR pathway will not change the STIM1 movement.

The RhoA/Rho kinase pathway has been implicated in various cellular functions including cytoskeleton reorganization, cell adhesion, motility and contraction and Y-27632 is a selective inhibitor of Rho-associated protein kinase (ROCK). Incubation with Y-27632 (30 μM) showed no effect on the TG-evoked STIM1 clustering and translocation (Fig. S4C).

The protein kinase C (PKC) inhibitor GF109203X (30 μM) and activator OAG (100 μM) were examined. Both of them did not change the TG-induced STIM1 movement (Fig. S4D–E). However, we found that the phospholipase C (PLC) inhibitor U73122 (10 μM) not only abolished TG-induced STIM1 translocation to the PM, but
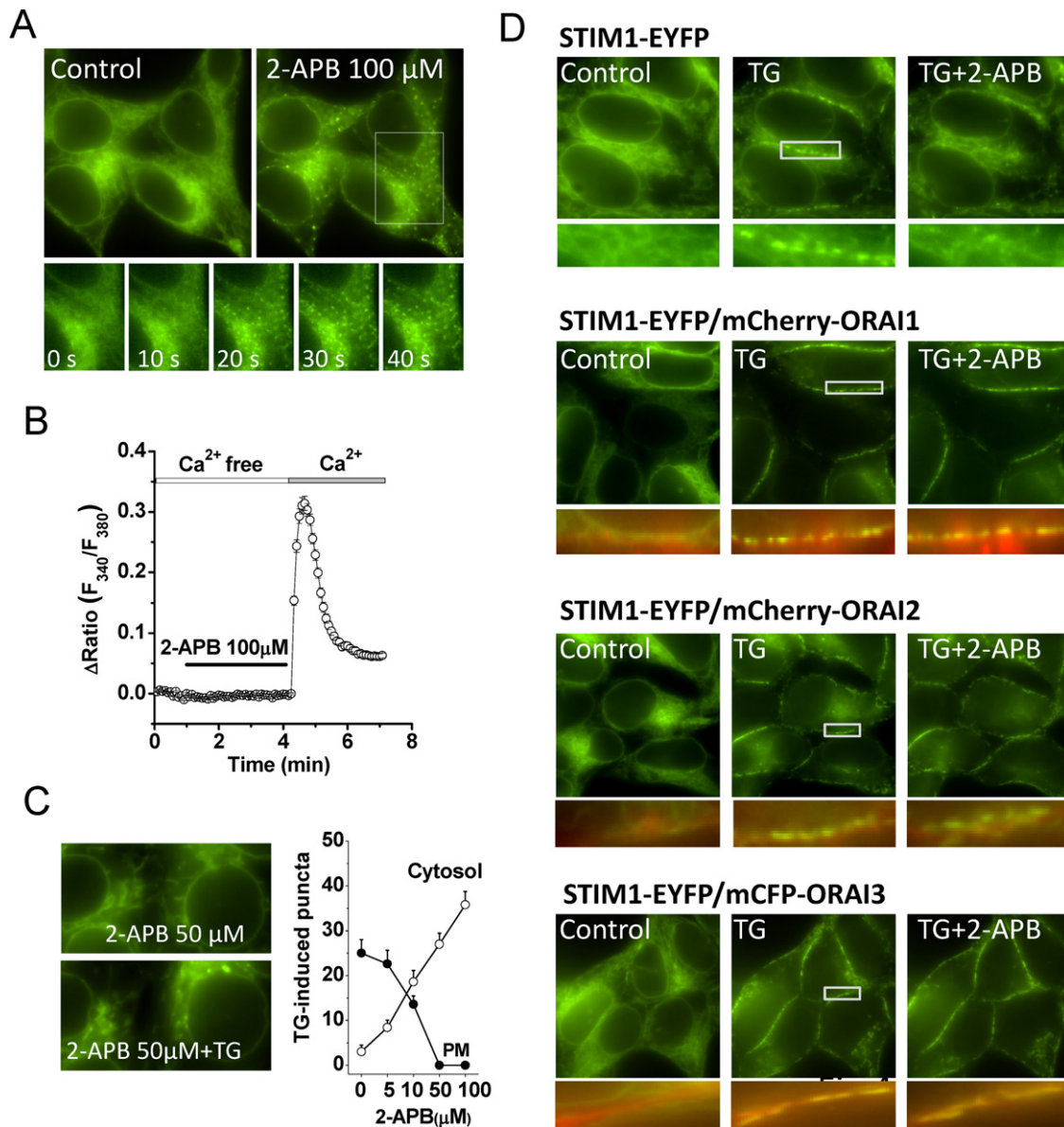
Fig. 4. 2-APB induced STIM1 clustering in STIM1–EYFP cells. (A) Application of 100 μM 2-APB resulted in STIM1 clustering in the cytosol. Lower small figures show the time course of STIM1 clustering in the boxed area. (B) No effect of 2-APB (100 μM) on Ca^{2+} release in the STIM1–EYFP cells. (C) 2-APB (50 μM) blocked the STIM1 subplasmalemmal translocation after addition of 1 μM TG and caused cytosolic STIM1 clustering. The mean ± SEM data for the number of STIM1 at the PM or in the cytosol induced by TG (1 μM) in the absence or presence of 2-APB (5–100 μM) are shown in the right chart (n = 5 cells in each group). (D) Application of 2-APB (100 μM) disassembled the subplasmalemmal STIM1 clusters induced by TG (1 μM) in the STIM1–EYFP cells, but no disassembling effect was observed in the STIM1–EYFP cells coexpressing with mCherry-ORAI1, mCherry-ORAI2, or mCFP-ORAI3. The boxed area is amplified and shown under each corresponding picture with STIM1 clusters alone (green) or co-localized with ORAI channels (red) in the PM. The mCFP fluorescence was converted into red pseudocolour in the images. (For interpretation of the references to colour in this figure legend, the reader is referred to the web version of this article.)

also caused STIM1 clustering in the cytosol (Fig. 7A and B). This unique effect of U73122 could be unrelated to the inhibition of PLC, because GPCR agonist or RTK inhibitor did not cause cytosolic STIM1 clustering. In addition, we tested the protein kinase A (PKA) activator forskolin. Incubation with forskolin (50 μM) for 10 min did not cause cytosolic STIM1 clusters. Forskolin also had no effect on the TG-induced STIM1 translocation (Fig. S4F).

3.8. Disruption of cytoskeleton did not prevent STIM1 subplasmalemmal translocation

Microtubules are filamentous polymers essential for cell viability and STIM1 has been shown to associate with the growth of microtubule ends [35], therefore, the involvement of cytoskeleton in

STIM1 movement was examined. Incubation with CytD (10 μM) for 1 h, which inhibits actin polymerization [36], showed no effect on TG-induced STIM1 subplasmalemmal clustering and translocation (Fig. 6A), suggesting the actin is not directly involved in STIM1 movement. We then examined the microtubule polymerization inhibitor, colchicine. Pretreatment of STIM1–EYFP cells with 100 μM colchicine for 30 min changed the cell morphology, but did not show any effects on TG-induced STIM1 subplasmalemmal clustering and translocation (Fig. 6A). The combined treatment with CytD and colchicine also showed no effect (Fig. 6A). However, the TG-induced SOCE was significantly reduced by the two agents (Fig. 6B and C). In addition, we found that the formation of cytosolic STIM1 clusters did not rely on cytoskeleton as well, because cells pretreated with CytD or colchicine showed the STIM1 clustering
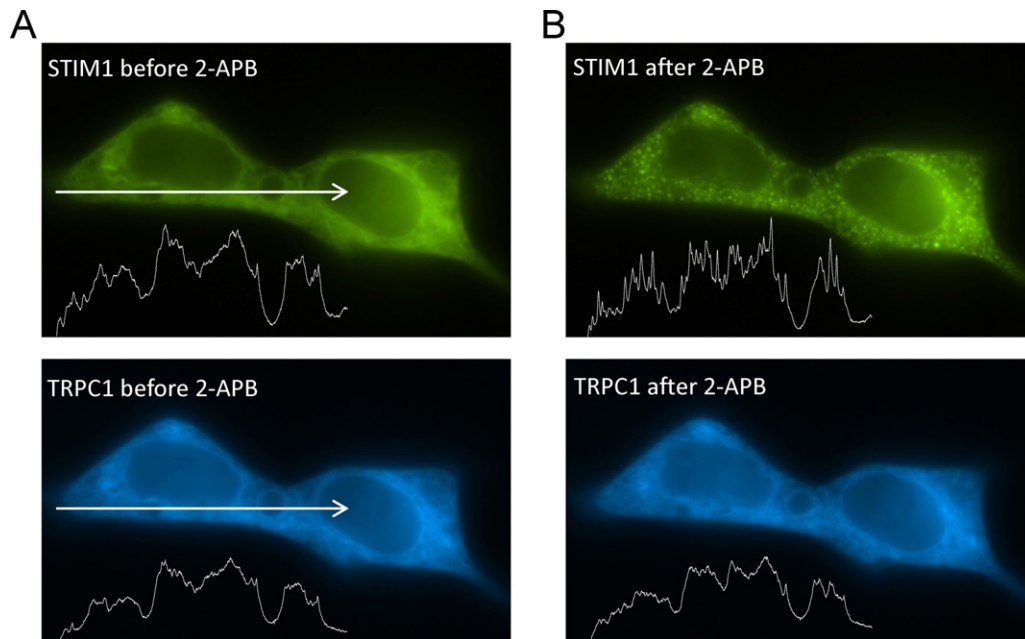
Fig. 5. Coexpression of TRPC1 on the 2-APB induced STIM1 clustering. (A) The STIM1–EYFP cells were cotransfected with mCFP-TRPC1. The logarithmic fluorescence spectra showed the florescence intensity of STIM1 (green) and TRPC1 (blue) of the arrow area using line-scan intensity software. (B) Cytosolic STIM1 clusters induced by 2-APB (100 μM) and more small fluctuations were observed, but no more fluctuations for TRPC1. (For interpretation of the references to colour in this figure legend, the reader is referred to the web version of this article.)

induced by 2-APB or 4-CEP similar to that in the untreated cells (Fig. S5).

3.9. STIM1 subplasmalemmal translocation inhibited by U73122 and calyculin A

It has been demonstrated that the cellular architecture of PM–ER junctions is the place for docking STIM1 clusters near PM and coupling to ORAI channels [37]. The PLC inhibitor U73122 at 1–10 μM has also been suggested to increase F-actin content [38,39], we then examined this mechanism of U73122 on STIM1 movement. The STIM1–EYFP cells were cotransfected with Lifeact-mCFP cDNA, a marker to visualize F-actin [20]. We found the fluorescence of Lifeact-mCFP at the PM was increased by U73122 (Fig. 7A), suggesting the accumulation of F-actin in the subplasmalemmal regions which spatially involve PM–ER junctions. The STIM1 subplasmalemmal translocation was blocked by the pretreatment of U73122, instead some STIM1 puncta in the cytosol (Fig. 7A). In cells pretreated with 10 μM CytD for 1 h to depolymerise F-actin filaments and then incubated with U73122 and TG, the TG-induced STIM1 subplasmalemmal translocation and puncta formation was restored (Fig. 7B and C), suggesting that the regulation of F-actin by U73122 is a novel mechanism for regulating SOC channels. In order to confirm the involvement of F-actin in the STIM1 translocation, calyculin A (CalyA), a serine/threonine phosphatase inhibitor that can disrupt the PM–ER junctions by increasing F-actin content, was also used [36,40]. The STIM1-EYFP cells incubated with CalyA (10 nM) for 10 min showed no STIM1 subplasmalemmal translocation after TG treatment. Pretreatment with 10 μM CytD for 1 h abolished the effect of CalyA (Fig. 7B and C). Moreover, U73122 significantly reduced the store-operated Ca^{2+} entry, but had no effect on the amplitude of TG-induced Ca^{2+} release signal (Fig. 7D). Pretreatment with CytD partially reversed the inhibitory effect of U73122, but the Ca^{2+} entry was still much less than that in cells challenged with TG alone (Fig. 7F). CalyA treatment did not affect TG-induced Ca^{2+}

release, and showed an effect on Ca^{2+} entry similar to that of U73122 (Fig. 7E and F).

4. Discussion

In this study, we confirm that STIM1 translocation and clustering is regulated by ER Ca^{2+} store, and the extracellular Ca^{2+} level is not the determinant for this process. We find two patterns of STIM1 clustering in the cells that can be pharmacologically distinguished, i.e., subplasmalemmal clusters and cytosolic clusters. The subplasmalemmal clusters are mainly formed by STIM1 translocation after passive or active ER Ca^{2+} store depletion, whilst the cytosolic STIM1 clustering is specific for some drug effects, such as 2-APB, FFA, 4-CEP, U73122 and FCCP. The formation of cytosolic STIM1 clusters is independent of ER Ca^{2+} store. In addition, increased content of F-actin in the PM–ER junctions by U73122 and CalyA blocks the STIM1 subplasmalemmal translocation. The proposed models for STIM1 movement are given in Fig. 8. The intracellular STIM1 clustering and translocation is a dynamic and reversible process, which could be a drug target for modulating store-operated channel activity.

Since the discovery of STIM1 as an essential component for store-operated Ca^{2+} channel function, the coupling mechanisms of STIM1 to the store-operated channels in the PM have been described and the ER Ca^{2+} store depletion is an essential step for STIM1 movement, such as by the application of SERCA blockers TG and cyclopiazonic acid [9,10], or through IP_3R activation by many GPCR agonists including carbachol [14] and ATP/UTP [22,41]. To further confirm the ER-dependent mechanism, we have examined the RyR sensitive ER Ca^{2+} store in this study. The Ca^{2+} release induced by RyR agonists also evoke STIM1 subplasmalemmal translocation, suggesting that STIM1 translocation can be regulated by the cooperation of the intracellular Ca^{2+} release channel IP_3Rs and RyRs. This finding could be an explanation of store-operated channel activated by RyR activators seen in some studies [42]. In addition, we noticed the difference of RyR agonists, 4-CEP
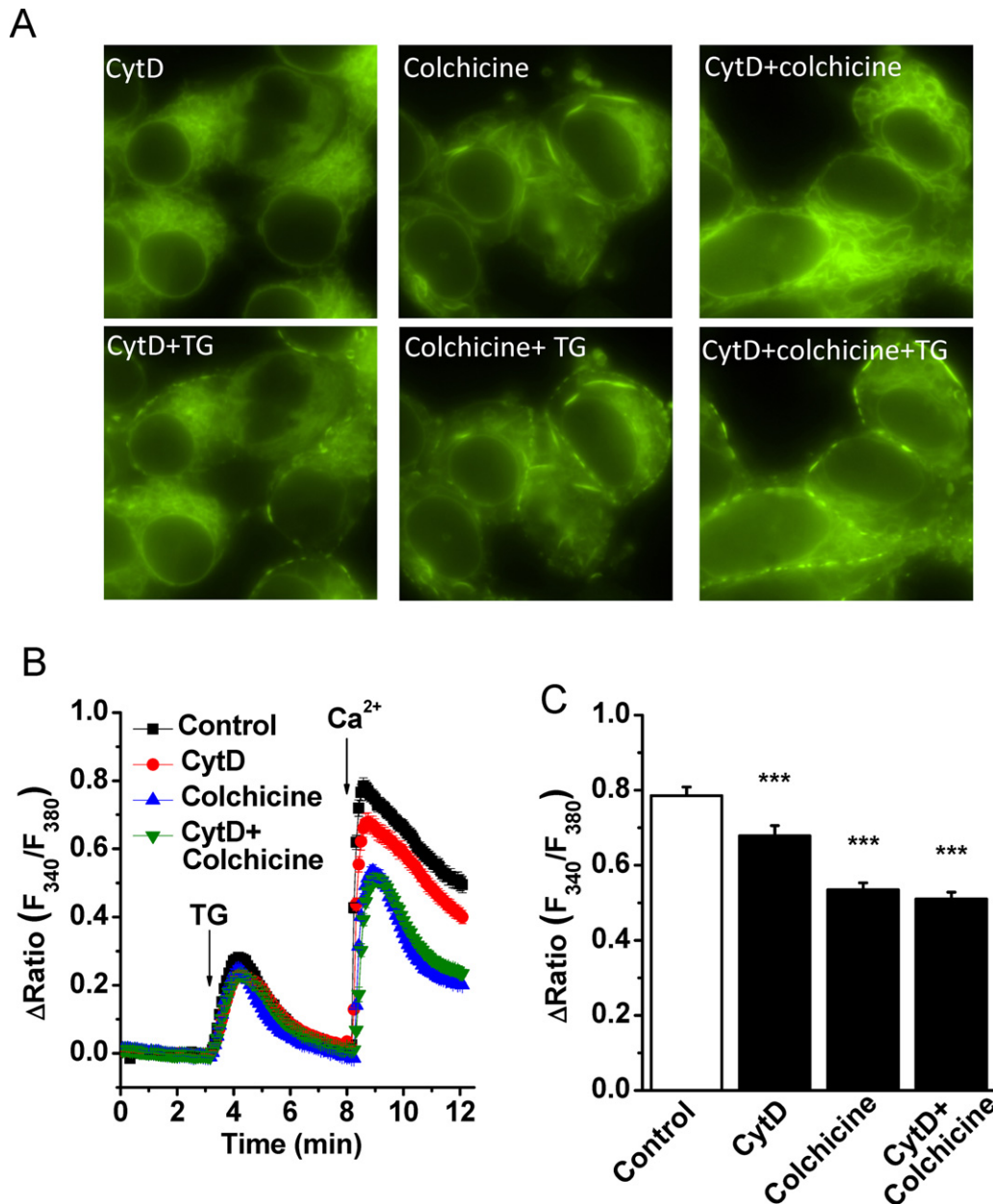
Fig. 6. Depolymerisation of cytoskeleton did not affect STIM1 translocation but reduced store-operated Ca^{2+} entry in STIM1–EYFP cells. (A) The cells were pretreated with 10 μM CytD for 1 h, or 100 μM colchicine for 30 min, or a combination of 10 μM CytD and 100 μM colchicine for 1 h. These procedures of cytoskeleton disruption did not prevent TG-induced STIM1 translocation. (B) The effects of CytD and colchicine on TG-induced Ca^{2+} release and Ca^{2+} entry (n = 22–33 cells in each group). (C) CytD and colchicine significantly reduced TG-induced Ca^{2+} influx in STIM1–EYFP cells. ***$P < 0.001$.

and caffeine, on cytosolic STIM1 clustering, Ca^{2+} release and Ca^{2+} influx. The concentration of 4-CEP used in this study is similar to the report on Ca^{2+} release [43]. 4-CEP at this concentration may cause membrane depolarization [44], however, STIM1 movement is independent of extracellular Ca^{2+}, which suggests the contribution of membrane depolarization-induced Ca^{2+} influx mainly through voltage-gated Ca^{2+} channels should be very little. RyR antagonist tetracaine can prevent the Ca^{2+} release and STIM1 subplasmalemmal translocation induced by 4-CEP, but the cytosolic STIM1 clustering is still present, suggesting that the cytosolic STIM1 clustering is an ER Ca^{2+} store-independent mechanism.

The existence of ER Ca^{2+} store-independent mechanism for cytosolic STIM1 clustering is also confirmed by the application of 2-APB. 2-APB at high concentrations inhibits IP$_3$R and blocks the

IP$_3$-evoked ER Ca^{2+} release, therefore the ER store should be regarded as non-depleted or filled. However, the STIM1 clustering can be quickly ($\sim$10 s) induced by 2-APB and the STIM1 puncta are retained in the cytosol without subplasmalemmal translocation. 2-APB at high concentrations has been shown to inhibit SERCA [45], however we have not observed any Ca^{2+} release signal induced by 2-APB at 100 μM. In addition, the STIM1 translocation induced by SERCA blocker is a slow process with 1–2 min delay, however the cytosolic clusters induced by 2-APB induced is a fast process, which suggests that the effect of 2-APB on STIM1 clustering is unrelated to the SERCA inhibition. These findings further suggest that the 2-APB-induced STIM1 clustering is an ER-store-independent process. 2-APB at lower concentrations (10 and 50 μM) prevented the TG-induced STIM1 subplasmalemmal translocation in our study, which is in agreement with the recent report [46]. The detail
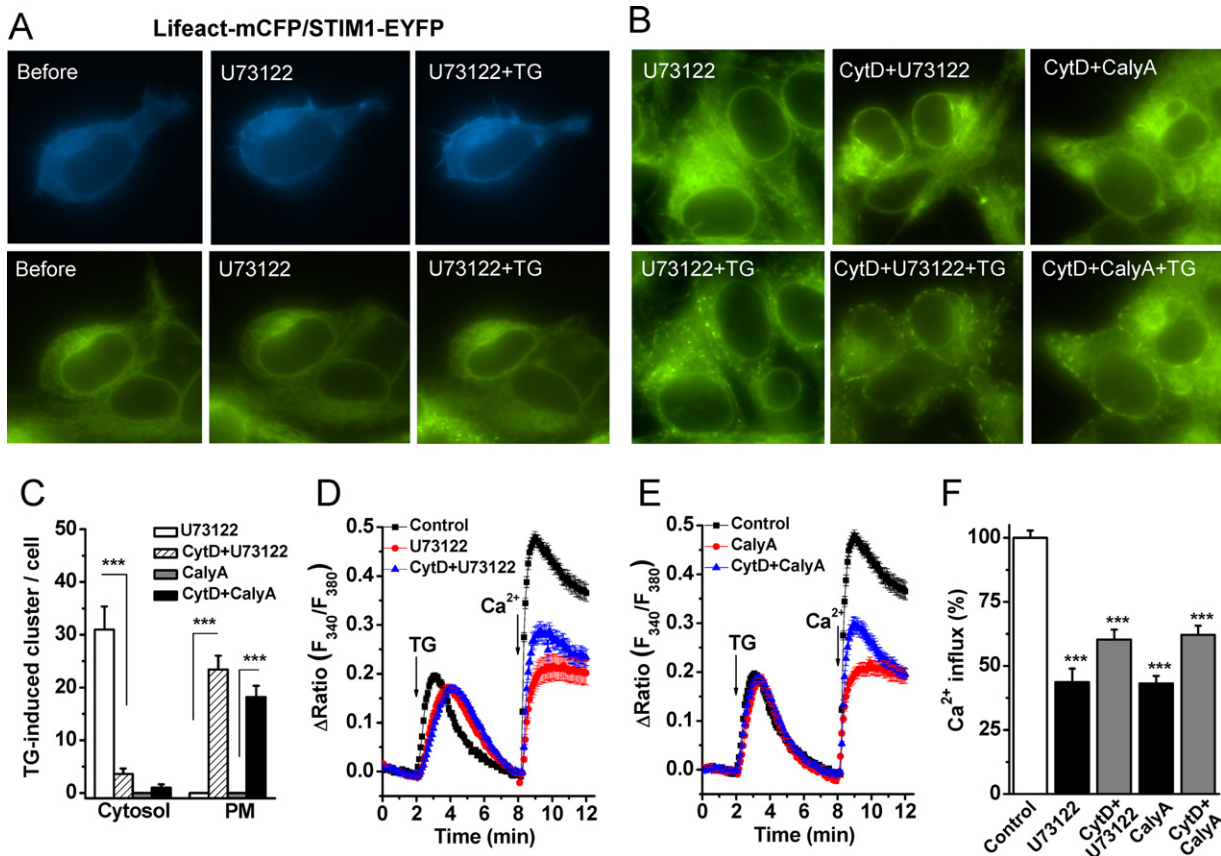
Fig. 7. Increase of F-actin content blocked TG-induced STIM1 translocation toward the PM and inhibited store-operated Ca^{2+} entry in STIM1–EYFP cells. (A) U73122 (10 μM) increased the F-actin content marked as Lifeact-mCFP (blue) in the STIM1–EYFP cells cotransfected with Lifeact-mCFP. The TG-induced STIM1 clustering and subplasmalemmal translocation were prevented by U73122 (A and B). Pretreatment with CytD abolished the effect of U73122 and CalyA (10 nM) on STIM1 movement (B). (C) The number of TG-induced STIM1 clusters in the cytosol and plasma membrane (PM) in the presence of U73122 (10 μM) or CalyA (10 nM), with or without CytD (10 μM) pretreatment ($n = 10$ cells in each group). (D) U73122 (10 μM) inhibited TG-induced Ca^{2+} entry that was partially reversed by CytD pretreatment ($n = 19$–27 cells in each group). (E) CalyA (10 nM) inhibited TG-induced Ca^{2+} entry and partially reversed by CytD ($n = 21$–25 cells in each group). (F) Mean ± SEM data show the comparison of TG-induced Ca^{2+} influx among the groups treated with U73122, CalyA and CytD (***$P < 0.001$). (For interpretation of the references to colour in this figure legend, the reader is referred to the web version of this article.)

mechanism of cytosolic STIM1 clustering is still unclear, but it could be unrelated to the inhibition on Ca^{2+} influx, because other store operated channel blockers Gd^{3+}, SKF96365 and DES without ER Ca^{2+} store releasing effect do not induce cytosolic STIM1 clustering. It is also unrelated to the coexpression of TRPC1 and ORAI channels, because the two associated proteins do not change the pattern of cytosolic STIM1 clustering, although the ORAI channel coexpression can stabilize the subplasmalemmal clusters of STIM1/ORAI complexes.

FFA is a fenamate anti-inflammatory drug with a mitochondrial Ca^{2+} release effect, but has less effect on ER Ca^{2+} release [26,27]. Our data show that FFA induces cytosolic STIM1 clustering, but its analogue NFA without affecting mitochondrial Ca^{2+} release does not cause cytosolic STIM1 clustering, further suggesting that the cytosolic STIM1 clustering is independent of ER store depletion, but the mitochondrial Ca^{2+} release could be related to cytosolic STIM1 clusters. To further confirm this, we tested the inhibitors of mitochondrial respiratory phosphorylation chain and metabolic pathways. FCCP, a mitochondrial uncoupler, causes STIM1 clustering in the cytosol, which could be due to the mitochondrial Ca^{2+} release effect [28], however, FCCP does not block the TG-induced the STIM1 translocation. Similarly, the TG-induced STIM1 translocation cannot be prevented by oligomycin and antimycin A [47]. Sodium azide, H$_2$O$_2$ and Hg^{2+} are mitochondrial metabolic inhibitors, however, acute application of these agents have no significant effect on STIM1 clustering and translocation, further

suggesting that the agents only affecting mitochondrial Ca^{2+} release may change the intracellular STIM1 movement.

The signaling pathway inhibitors of PTK and PI$_3$K, PKC and ROCK pathways have been examined in our study and no significant effects on TG-induced STIM1 movement are found, which is similar to the previous report [14]. We have not tested those inhibitors on the STIM1 puncta induced by GPCR activation, because unlike TG-induced STIM1 clustering and subplasmalemmal translocation, the STIM1 puncta or movement induced by GPCR activation is transient and difficult to be quantified precisely.

The importance of PM–ER junctions in the store-operated channel activation has been described [48]. The increase of F-actin content in the PM–ER junctional regions inhibits store-operated channel activity [36,40]. Both CalyA and U73122 are PM–ER disruptors by condensation of F-actin in the region. The inhibition of store-operated Ca^{2+} entry by U73122 and CalyA could be explained by the interruption of PM–ER junctions by the inhibition of STIM1 subplasmalemmal translocation, which leads to the uncoupling of STIM1 with the store-operated channels in the PM. However, other mechanisms for U73122 and CalyA may also exist, because the restore of STIM1 translocation by CytD only partially recovered their inhibition on the store-operated Ca^{2+} influx. Moreover, we also examined the involvement of cytoskeleton in the STIM1 movement. CytD significantly inhibits the store-operated Ca^{2+} entry in the STIM1–EYFP transfected cells, which is consistent to the observations in platelets [49], polymorphonuclear neutrophil

Fig. 8. Models for pharmacological regulation of STIM1 translocation and clustering. (A) STIM1 at resting state. (B) ER Ca^{2+} store-dependent STIM1 clustering and translocation to the newly formed PM–ER junction and Ca^{2+} influx through ORAI channel, which are induced by ER Ca^{2+} store depletion by GPCR agonist, thapsigargin or caffeine. (C) ER Ca^{2+} store-independent STIM1 clustering in the cytosol. 2-APB inhibits ER Ca^{2+} release through IP_3R and induces cytosolic STIM1 clustering. FFA and 4-CEP release Ca^{2+} from mitochondrion and ER respectively, and cause the formation of cytosolic STIM1 clusters. (D) U73122 blocks the activity of PLC, increases the cellular F-actin content and potentiates cytosolic STIM1 clustering in the presence of thapsigargin. Calyculin A also increases the F-actin content, prevents the formation of PM–ER junction and STIM1 translocation toward the PM.

(PMN) [50], hepocytes [51], and vascular endothelial cells [52], but no or increasing effects were reported in A7r5 cells, glioma C6 cells and transfected HEK293 cells [36,53,54]. We find that the TG-induced store-operated Ca^{2+} influx is inhibited by CytD in the STIM1–EYFP transfected cells, however, CytD has no effect on the TG-induced STIM1 movement. In our study, CytD at 10 μM was used, because we found a significant cell death occurred at the concentration of 100 μM, although this concentration has been used in the A7r5 cells [36]. The rearrangement of microtubules in the regulation of SOCE has also been demonstrated by the application of colchicine [54–56], however, colchicine has no effect on TG-induced STIM1 movement. In addition, disruption of lipid rafts in the PM does not change the STIM1 movement [57].

Store-operated Ca^{2+} entry coupled by STIM1 translocation has been demonstrated for ORAI and TRPC1 channels [10,58]. The activity of store-operated channels could be regulated by direct channel blockers or indirectly regulated by those agents affecting STIM1 clustering and subplasmalemmal translocation. The cytosolic STIM1 cluster formation independent of ER Ca^{2+} store discovered in this study is a new mechanism for the pharmacology of some channel blockers, which could be a useful target for future drug development.

Conflicts of interest

No potential conflicts of interest were disclosed.

Grant support

Appendix A. Supplementary data

Supplementary data associated with this article can be found, in the online version, at http://dx.doi.org/10.1016/j.bcp.2012.07.013.

References

[1] Parekh AB, Putney Jr JW. Store-operated calcium channels. Physiol Rev 2005;85:757–810.
[2] Vig M, Beck A, Billingsley JM, Lis A, Parvez S, Peinelt C, et al. CRACM1 multimers form the ion-selective pore of the CRAC channel. Curr Biol 2006;16:2073–9.
[3] Yeromin AV, Zhang SL, Jiang W, Yu Y, Safrina O, Cahalan MD. Molecular identification of the CRAC channel by altered ion selectivity in a mutant of Orai. Nature 2006;443:226–9.
[4] Xu SZ, Zeng B, Daskoulidou N, Chen GL, Atkin SL, Lukhele B. Activation of TRPC cationic channels by mercurial compounds confers the cytotoxicity of mercury exposure. Toxicol Sci 2012;125:56–68.
[5] Xu SZ, Muraki K, Zeng F, Li J, Sukumar P, Shah S, et al. A sphingosine-1-phosphate-activated calcium channel controlling vascular smooth muscle cell motility. Circ Res 2006;98:1381–9.
[6] Yuan JP, Zeng W, Huang GN, Worley PF, Muallem S. STIM1 heteromultimerizes TRPC channels to determine their function as store-operated channels. Nat Cell Biol 2007;9:636–45.

[7] Xu SZ, Sukumar P, Zeng F, Li J, Jairaman A, English A, et al. TRPC channel activation by extracellular thioredoxin. Nature 2008;451:69–72.

[8] Hogan PG, Lewis RS, Rao A. Molecular basis of calcium signaling in lymphocytes: STIM and ORAI. Annu Rev Immunol 2010;28:491–533.

[9] Liou J, Kim ML, Heo WD, Jones JT, Myers JW, Ferrell Jr JE, et al. STIM is a Ca^{2+} sensor essential for Ca^{2+}-store-depletion-triggered Ca^{2+} influx. Curr Biol 2005;15:1235–41.

[10] Zhang SL, Yu Y, Roos J, Kozak JA, Deerinck TJ, Ellisman MH, et al. STIM1 is a Ca^{2+} sensor that activates CRAC channels and migrates from the Ca^{2+} store to the plasma membrane. Nature 2005;437:902–5.

[11] Lee KP, Yuan JP, So I, Worley PF, Muallem S. STIM1-dependent and STIM1-independent function of transient receptor potential canonical (TRPC) channels tunes their store-operated mode. J Biol Chem 2010;285:38666–73.

[12] Pani B, Ong HL, Brazer SC, Liu X, Rauser K, Singh BB, et al. Activation of TRPC1 by STIM1 in ER-PM microdomains involves release of the channel from its scaffold caveolin-1. Proc Natl Acad Sci USA 2009;106:20087–92.

[13] Spassova MA, Soboloff J, He LP, Xu W, Dziadek MA, Gill DL. STIM1 has a plasma membrane role in the activation of store-operated Ca^{2+} channels. Proc Natl Acad Sci USA 2006;103:4040–5.

[14] Smyth JT, Dehaven WI, Bird GS, Putney Jr JW. Ca^{2+}-store-dependent and -independent reversal of Stim1 localization and function. J Cell Sci 2008;121:762–72.

[15] Feske S, Picard C, Fischer A. Immunodeficiency due to mutations in ORAI1 and STIM1. Clin Immunol 2010;135:169–82.

[16] Braun A, Varga-Szabo D, Kleinschnitz C, Pleines I, Bender M, Austinat M, et al. Orai1 (CRACM1) is the platelet SOC channel and essential for pathological thrombus formation. Blood 2009;113:2056–63.

[17] Li J, Sukumar P, Milligan CJ, Kumar B, Ma ZY, Munsch CM, et al. Interactions, functions, and independence of plasma membrane STIM1 and TRPC1 in vascular smooth muscle cells. Circ Res 2008;103:e97–104.

[18] Potier M, Gonzalez JC, Motiani RK, Abdullaev IF, Bisaillon JM, Singer HA, et al. Evidence for STIM1- and Orai1-dependent store-operated calcium influx through ICRAC in vascular smooth muscle cells: role in proliferation and migration. FASEB J 2009;23:2425–37.

[19] Ohba T, Watanabe H, Murakami M, Sato T, Ono K, Ito H. Essential role of STIM1 in the development of cardiomyocyte hypertrophy. Biochem Biophys Res Commun 2009;389:172–6.

[20] Riedl J, Crevenna AH, Kessenbrock K, Yu JH, Neukirchen D, Bista M, et al. Lifeact: a versatile marker to visualize F-actin. Nat Methods 2008;5:605–7.

[21] Walsh CM, Chvanov M, Haynes LP, Petersen OH, Tepikin AV, Burgoyne RD. Role of phosphoinositides in STIM1 dynamics and store-operated calcium entry. Biochem J 2010;425:159–68.

[22] Chvanov M, Walsh CM, Haynes LP, Voronina SG, Lur G, Gerasimenko OV, et al. ATP depletion induces translocation of STIM1 to puncta and formation of STIM1-ORAI1 clusters: translocation and re-translocation of STIM1 does not require ATP. Pflugers Arch 2008;457:505–17.

[23] Hollenberg MD, Compton SJ. International union of pharmacology. XXVIII. Proteinase-activated receptors. Pharmacol Rev 2002;54:203–17.

[24] Ng LC, Wilson SM, McAllister CE, Hume JR. Role of InsP3 and ryanodine receptors in the activation of capacitative Ca^{2+} entry by store depletion or hypoxia in canine pulmonary arterial smooth muscle cells. Br J Pharmacol 2007;152:101–11.

[25] Querfurth HW, Haughey NJ, Greenway SC, Yacono PW, Golan DE, Geiger JD. Expression of ryanodine receptors in human embryonic kidney (HEK293) cells. Biochem J 1998;334(Pt 1):79–86.

[26] Tu P, Brandolin G, Bouron A. The anti-inflammatory agent flufenamic acid depresses store-operated channels by altering mitochondrial calcium homeostasis. Neuropharmacology 2009;56:1010–6.

[27] Jiang H, Zeng B, Chen GL, Bot D, Eastmond S, Elsenussi SE, et al. Effect of non-steroidal anti-inflammatory drugs and new fenamate analogues on TRPC4 and TRPC5 channels. Biochem Pharmacol 2012;83:923–31.

[28] Gurney AM, Drummond RM, Fay FS. Calcium signalling in sarcoplasmic reticulum, cytoplasm and mitochondria during activation of rabbit aorta myocytes. Cell Calcium 2000;27:339–51.

[29] Xu SZ, Zeng F, Boulay G, Grimm C, Harteneck C, Beech DJ. Block of TRPC5 channels by 2-aminoethoxydiphenyl borate: a differential, extracellular and voltage-dependent effect. Br J Pharmacol 2005;145:405–14.

[30] Peinelt C, Lis A, Beck A, Fleig A, Penner R. 2-Aminoethoxydiphenyl borate directly facilitates and indirectly inhibits STIM1-dependent gating of CRAC channels. J Physiol 2008;586:3061–73.

[31] Zeng W, Yuan JP, Kim MS, Choi YJ, Huang GN, Worley PF, et al. STIM1 gates TRPC channels, but not Orai1, by electrostatic interaction. Mol Cell 2008;32:439–48.

[32] Gervasio OL, Whitehead NP, Yeung EW, Phillips WD, Allen DG. TRPC1 binds to caveolin-3 and is regulated by Src kinase – role in Duchenne muscular dystrophy. J Cell Sci 2008;121:2246–55.

[33] Zakharov SI, Smani T, Dobrydneva Y, Monje F, Fichandler C, Blackmore PF, et al. Diethylstilbestrol is a potent inhibitor of store-operated channels and capacitative Ca^{2+} influx. Mol Pharmacol 2004;66:702–7.

[34] Xu SZ, Zhong W, Ghavideldarestani M, Saurabh R, Lindow SW, Atkin SL. Multiple mechanisms of soy isoflavones against oxidative stress-induced endothelium injury. Free Radic Biol Med 2009;47:167–75.

[35] Grigoriev I, Gouveia SM, van der Vaart B, Demmers J, Smyth JT, Honnappa S, et al. STIM1 is a MT-plus-end-tracking protein involved in remodeling of the ER. Curr Biol 2008;18:177–82.

[36] Patterson RL, van Rossum DB, Gill DL. Store-operated Ca^{2+} entry: evidence for a secretion-like coupling model. Cell 1999;98:487–99.

[37] Luik RM, Wu MM, Buchanan J, Lewis RS. The elementary unit of store-operated Ca^{2+} entry: local activation of CRAC channels by STIM1 at ER-plasma membrane junctions. J Cell Biol 2006;174:815–25.

[38] Kimata T, Nagaki M, Ogiso T, Naiki T, Kato T, Moriwaki H. Actin organization and hepatocyte differentiation are regulated by extracellular matrix via PI-4,5-bisphosphate in the rat. Hepatology 2006;44:140–51.

[39] Scott CC, Dobson W, Botelho RJ, Coady-Osberg N, Chavrier P, Knecht DA, et al. Phosphatidylinositol-4,5-bisphosphate hydrolysis directs actin remodeling during phagocytosis. J Cell Biol 2005;169:139–49.

[40] Lee CH, Kuo KH, Dai J, Leo JM, Seow CY, Breemen C. Calyculin-A disrupts subplasmalemmal junction and recurring Ca^{2+} waves in vascular smooth muscle. Cell Calcium 2005;37:9–16.

[41] Ross K, Whitaker M, Reynolds NJ. Agonist-induced calcium entry correlates with STIM1 translocation. J Cell Physiol 2007;211:569–76.

[42] Fellner SK, Arendshorst WJ. Ryanodine receptor and capacitative Ca^{2+} entry in fresh preglomerular vascular smooth muscle cells. Kidney Int 2000;58:1686–94.

[43] Islam MS, Leibiger I, Leibiger B, Rossi D, Sorrentino V, Ekstrom TJ, et al. In situ activation of the type 2 ryanodine receptor in pancreatic beta cells requires cAMP-dependent phosphorylation. Proc Natl Acad Sci USA 1998;95:6145–50.

[44] Westerblad H, Andrade FH, Islam MS. Effects of ryanodine receptor agonist 4-chloro-m-cresol on myoplasmic free Ca^{2+} concentration and force of contraction in mouse skeletal muscle. Cell Calcium 1998;24:105–15.

[45] Bilmen JG, Wootton LL, Godfrey RE, Smart OS, Michelangeli F. Inhibition of SERCA Ca^{2+} pumps by 2-aminoethoxydiphenyl borate (2-APB), 2-APB reduces both Ca^{2+} binding and phosphoryl transfer from ATP, by interfering with the pathway leading to the Ca^{2+}-binding sites. Eur J Biochem 2002;269:3678–87.

[46] He J, Yu T, Pan J, Li H. Visualisation and identification of the interaction between STIM1s in resting cells. PLoS One 2012;7:e33377.

[47] Singaravelu K, Nelson C, Bakowski D, de Brito OM, Ng SW, Di Capite J, et al. Mitofusin 2 regulates STIM1 migration from the Ca^{2+} store to the plasma membrane in cells with depolarized mitochondria. J Biol Chem 2011;286:12189–201.

[48] Carrasco S, Meyer T. STIM proteins and the endoplasmic reticulum–plasma membrane junctions. Annu Rev Biochem 2011;80:973–1000.

[49] Harper AG, Sage SO. A key role for reverse Na$^+$/Ca^{2+} exchange influenced by the actin cytoskeleton in store-operated Ca^{2+} entry in human platelets: evidence against the de novo conformational coupling hypothesis. Cell Calcium 2007;42:606–17.

[50] Itagaki K, Kannan KB, Singh BB, Hauser CJ. Cytoskeletal reorganization internalizes multiple transient receptor potential channels and blocks calcium entry into human neutrophils. J Immunol 2004;172:601–7.

[51] Wang YJ, Gregory RB, Barritt GJ. Maintenance of the filamentous actin cytoskeleton is necessary for the activation of store-operated Ca^{2+} channels, but not other types of plasma-membrane Ca^{2+} channels, in rat hepatocytes. Biochem J 2002;363:117–26.

[52] Holda JR, Blatter LA. Capacitative calcium entry is inhibited in vascular endothelial cells by disruption of cytoskeletal microfilaments. FEBS Lett 1997;403:191–6.

[53] Sabala P, Targos B, Caravelli A, Czajkowski R, Lim D, Gragnaniello G, et al. Role of the actin cytoskeleton in store-mediated calcium entry in glioma C6 cells. Biochem Biophys Res Commun 2002;296:484–91.

[54] Galan C, Dionisio N, Smani T, Salido GM, Rosado JA. The cytoskeleton plays a modulatory role in the association between STIM1 and the Ca^{2+} channel subunits Orai1 and TRPC1. Biochem Pharmacol 2011.

[55] Hajkova Z, Bugajev V, Draberova E, Vinopal S, Draberova L, Janacek J, et al. STIM1-directed reorganization of microtubules in activated mast cells. J Immunol 2010;186:913–23.

[56] Smyth JT, DeHaven WI, Bird GS, Putney Jr JW. Role of the microtubule cytoskeleton in the function of the store-operated Ca^{2+} channel activator STIM1. J Cell Sci 2007;120:3762–71.

[57] DeHaven WI, Jones BF, Petranka JG, Smyth JT, Tomita T, Bird GS, et al. TRPC channels function independently of STIM1 and Orai1. J Physiol 2009;587:2275–98.

[58] Huang GN, Zeng W, Kim JY, Yuan JP, Han L, Muallem S, et al. STIM1 carboxyl-terminus activates native SOC, I(crac) and TRPC1 channels. Nat Cell Biol 2006;8:1003–10.

Divalent copper is a potent extracellular blocker for TRPM2 channel

Bo Zeng [a,1], Gui-Lan Chen [a,b,1], Shang-Zhong Xu [a,*]

[a] Centre for Cardiovascular and Metabolic Research, Hull York Medical School, University Hull, Hull, HU6 7RX, UK
[b] Key Laboratory of the Ministry of Education for Medical Electrophysiology, Luzhou Medical College, Luzhou, Sichuan 646000, China

ARTICLE INFO

ABSTRACT

Transient receptor potential melastatin 2 (TRPM2) is a Ca^{2+}-permeable cationic channel in the TRP channel family. The channel activity can be regulated by reactive oxygen species (ROS) and cellular acidification, which has been implicated to the pathogenesis of diabetes and some neuronal disorders. However, little is known about the effect of redox-active metal ions, such as copper, on TRPM2 channels. Here we investigated the effect of divalent copper on TRPM2.

TRPM2 channel was over-expressed in HEK-293 cells and the whole-cell current was recorded by patch clamp. We found the whole-cell current evoked by intracellular ADP-ribose was potently inhibited by Cu^{2+} with a half maximal inhibitory concentration (IC_{50}) of 2.59 μM. The inhibitory effect was irreversible. The single channel activity was abolished in the outside-out patches, and intracellular application of Cu^{2+} did not prevent the channel activation, suggesting that the action site of Cu^{2+} is located in the extracellular domains of the channel. TRPM2 current was also blocked by Hg^{2+}, Pb^{2+}, Fe^{2+} and Se^{2+}.

We concluded that Cu^{2+} is a potent TRPM2 channel blocker. The sensitivity of TRPM2 channel to heavy metal ions could be a new mechanism for the pathogenesis of some metal ion–related diseases.

© 2012 Elsevier Inc. All rights reserved.

1. Introduction

Transient receptor potential melastatin 2 (TRPM2) is a member of the melastatin subfamily of TRP channels which are permeable to cations such as Ca^{2+} and Na^+. TRPM2, previously known as TRPC7 or LTRPC2 [1,2], is abundantly expressed in the brain, and later studies show that TRPM2 is an ubiquitously expressed channel found in many tissues including bone marrow, spleen, heart, liver, lung, pancreatic islets and immunocytes [2,3]. Several important physiological functions of TRPM2 channel have been demonstrated using knockout animals or in vitro models including insulin release [3,4], cytokines and reactive oxygen species (ROS) production [5], cell motility and cell death [6], and immune response [7]. The genetic variants of TRPM2 have been linked to the pathogenesis of several neurological diseases like bipolar disorder [8], western pacific amyotrophic lateral sclerosis and parkinsonism-dementia [9], and the regulation of amyloid beta-peptide (Aβ)-induced striatal cell death that involves in the Alzheimer's disease [10]. In addition, a number of endogenous modulators for TRPM2 channel have been identified, among which the most efficient direct channel activator is adenosine diphosphate ribose (ADPR). Free ADPR opens TRPM2 channels by binding to the Nudix-like motif in the C-terminus, and evokes a current with linear current–voltage (IV) relationship

[1,11]. The activation of TRPM2 channel by ADPR is dependent on the intracellular Ca^{2+} concentration [12] and negatively regulated by adenosine monophosphate (AMP) [13] and acidic pH [14,15]. Hydrogen peroxide (H_2O_2) is another activator for TRPM2 channel, although the mechanism of H_2O_2-induced TRPM2 activation is still unclear [2]. Therefore, TRPM2 is a ROS-sensitive Ca^{2+}-permeable channel, which may play important roles in the oxidative stress-related diseases.

Metal ions are important factors or cofactors in cellular physiology [16]. Among them, copper is a redox-active element and participates in many important cellular functions by binding to a variety of proteins such as ceruloplasmin, cytochrome c oxidase and superoxide dismutase [17]. Both deficiency and elevated level of copper can induce oxidative stress that leads to cell or tissue damage [18]. Copper deficiency is seen in infants with Menkes' disease that is caused by genetic mutations in the copper transporter ATP7A [19] and in patients with gastrointestinal surgery, such as gastric bypass surgery [20]. In contrast, patients showing excessive copper accumulation in the body are due to exposure to excess copper in drinking water or other environmental sources [21], or the genetic disorder (Wilson's disease) with copper accumulation in the liver and the basal ganglia of the brain, which is caused by the mutations in ATP7B, a transporter responsible for exporting copper out of the cells [22]. Moreover, the elevated copper level has also been reported in the plasma of diabetic patients [23] and in the brain of patients with neurodegenerative disorders [24]. It is unclear that the increased blood copper concentration

is just a consequence of diabetes or the cause of dysfunction of insulin signaling and glucose homeostasis, however, the treatment with Cu^{2+} chelator to reverse diabetic copper overload seems effective in preventing diabetic organ damage [25]. With regard to neurological disorders, copper has been implicated in the pathogenesis of many neurodegenerative disorders including Alzheimer's disease, amyotrophic lateral sclerosis, Huntington's disease, Parkinson's disease, and prion disease [26,27]. Excess copper can initiate or stimulate the progression of Alzheimer's disease by promoting the aggregation of amyloid-beta peptides to form senile plaques in the brain [28,29] or by oxidative stress-driven cell death [17]. Nevertheless, the effect of copper in Alzheimer's disease is still in much debate. The protective effect against beta-sheet secondary structure formation by copper has also been demonstrated [30,31]. These mixed results could be due to the imbalance of Cu^{2+}

in the affected region, rather than a bulk Cu^{2+} accumulation or deficiency [32,33]. Therefore, the identification of potential new Cu^{2+} target is important for understanding the pathogenesis of Cu^{2+}-related disorders.

Given the evidences that TRPM2 is a redox-sensitive channel and mediates cell death, as well as its high expression in the brain and the association with neurodegenerative disorders and diabetes which are oxidative stress related diseases. It is intriguing to suppose that the activity of TRPM2 channels could be modulated by certain pathological factors related to these diseases, such as Cu^{2+} that plays an important role in regulating oxidative status in a cell. Therefore, we investigated the effect of Cu^{2+} on TRPM2 channels in the TRPM2 transfected HEK-293 cells by electrophysiological approach. Other heavy metal ions, such as Hg^{2+}, Pb^{2+}, Fe^{2+} and Gd^{3+}, and divalent selenium (Se^{2+}) were also studied for comparison.
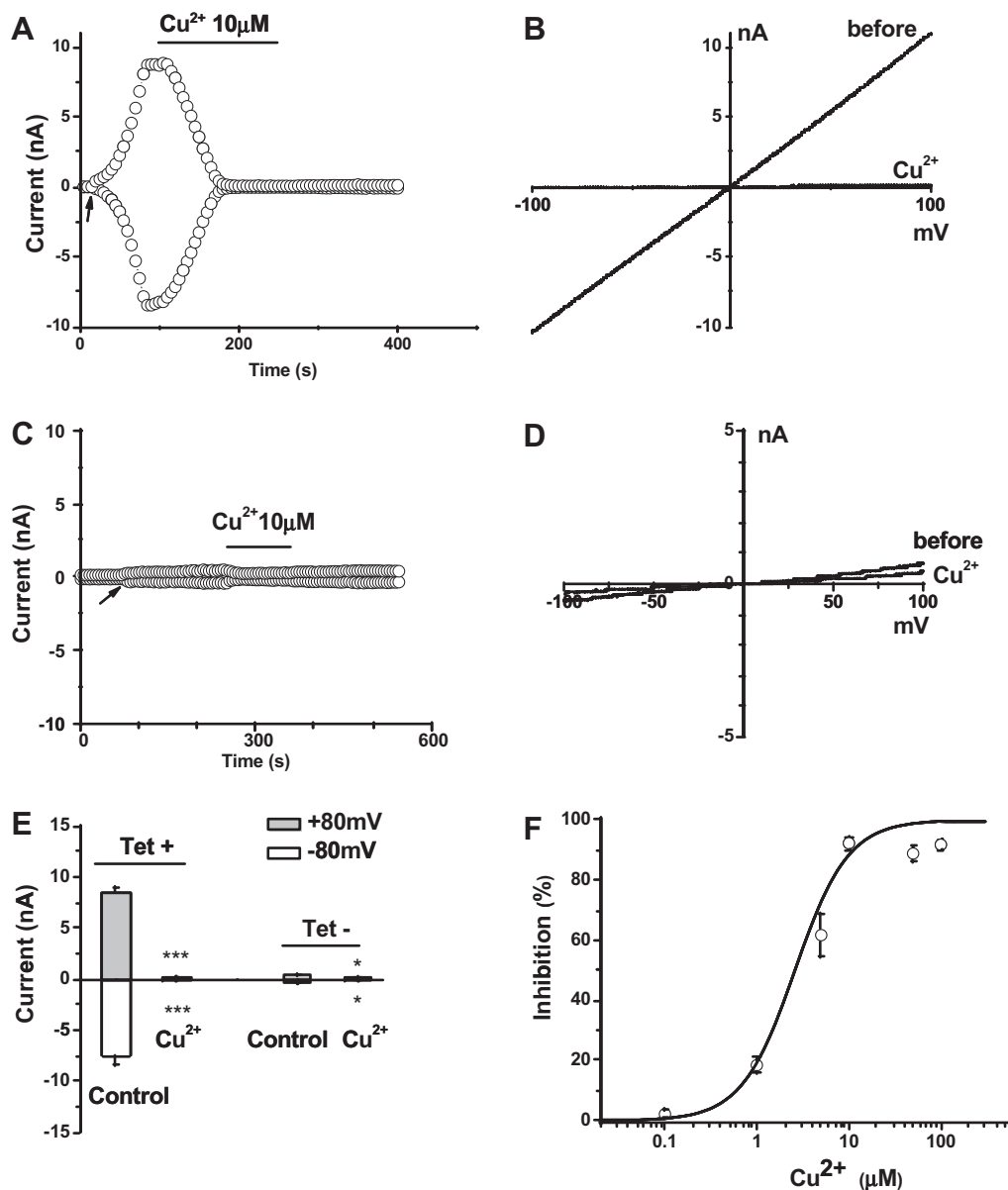
Fig. 1. Effects of Cu^{2+} on the currents of TRPM2-overexpressing HEK-293 cells. (A) The time course of the currents measured at +80 and −80 mV. Cu^{2+} (10 μM) inhibited the whole-cell TRPM2 currents evoked by 500 μM ADPR in the pipette solution. The arrow indicates the time point when the whole-cell configuration was formed. (B) Representative *IV* curves before and after perfusion of Cu^{2+} shown in (A). (C) Cu^{2+} (10 μM) inhibited the endogenous currents in the cell without tetracycline induction. (D) *IV* curves for (C). (E) Mean ± SEM for the inhibition of Cu^{2+} on the current of Tet-induced and non-induced cells. (F) Dose–response curve for TRPM2 inhibition by Cu^{2+} (*n* = 7–13 for each concentration).

2. Materials and methods

2.1. Cell culture and transfection

A tetracycline-controlled expression system for human TRPM2 channel was generated using pcDNA4/TO vector and stably transfected into the HEK-293 T-REx cells (Invitrogen, Paisley, UK) as previously described [34]. The cells were maintained in DMEM/F-12 medium supplemented with 50 units/ml penicillin, 50 μg/ml streptomycin (Gibco, Paisley, UK) and 10% fetal bovine serum (Sigma–Aldrich, Poole, UK). The expression of TRPM2 was induced by 1 μg/ml tetracycline in the cell culture medium for 24–72 h before patch-clamp recording. Cells without tetracycline induction were used as control.

2.2. Electrophysiology

Whole-cell patch-clamp recording was performed at room temperature (23–26 °C). Briefly, signal was amplified with an Axopatch 200B amplifier and controlled by the software pClamp 10. A 1-s ramp voltage protocol from −100 mV to +100 mV was applied at a frequency of 0.2 Hz from a holding potential of 0 mV. Signals were sampled at 10 kHz and filtered at 1 kHz. The glass microelectrodes with resistance of 3–5 MΩ were used. The 200 nM Ca^{2+} buffered pipette solution contained (in mM) 115 CsCl, 10 EGTA, 2 $MgCl_2$, 10 HEPES, and 5.7 $CaCl_2$ (pH 7.2 adjusted with CsOH, and osmolarity

~290 mOsm adjusted with mannitol). The calculated free Ca^{2+} is 200 nM. ADP-ribose (0.5 mM) was included in the pipette solution to activate TRPM2 channels in the whole-cell configuration. The standard bath solution contained (mM) 130 NaCl, 5 KCl, 8 D-glucose, 10 HEPES, 1.2 $MgCl_2$ and 1.5 $CaCl_2$. The pH was adjusted to 7.4 with NaOH.

2.3. Chemicals

General salts, ADP-ribose (ADPR), H_2O_2, copper sulphate ($CuSO_4$), gadolinium chloride ($GdCl_3$), lead nitrate ($Pb(NO_3)_2$), selenium dioxide, mercury chloride ($HgCl_2$) ferrous chloride tetrahydrate ($FeCl_2 \cdot 4H_2O$) and 2-aminoethoxydiphenyl borate (2-APB) were purchased from Sigma–Aldrich (Poole, UK).

2.4. Statistics

Data are expressed as mean ± SEM. Data sets were compared using paired t test for the results before and after treatment with significance indicated if $P < 0.05$.

3. Results

3.1. TRPM2 channel inhibited by Cu^{2+}

The effect of divalent Cu^{2+} on TRPM2 channel was investigated using whole-cell patch clamp recording in the HEK-293 cells overexpressed with human TRPM2 gene in a tetracycline-regulated expression system [34]. The activity of TRPM2 channel was induced by ADP-ribose (500 μM) in the pipette solution (Fig. 1A) or by bath application of H_2O_2 (500 μM) (data not shown). The current with a typical linear current–voltage (IV) relationship was quickly evoked by ADP-ribose in the tetracycline-induced TRPM2 cells (Tet+) and achieved maximum within 1 min after membrane
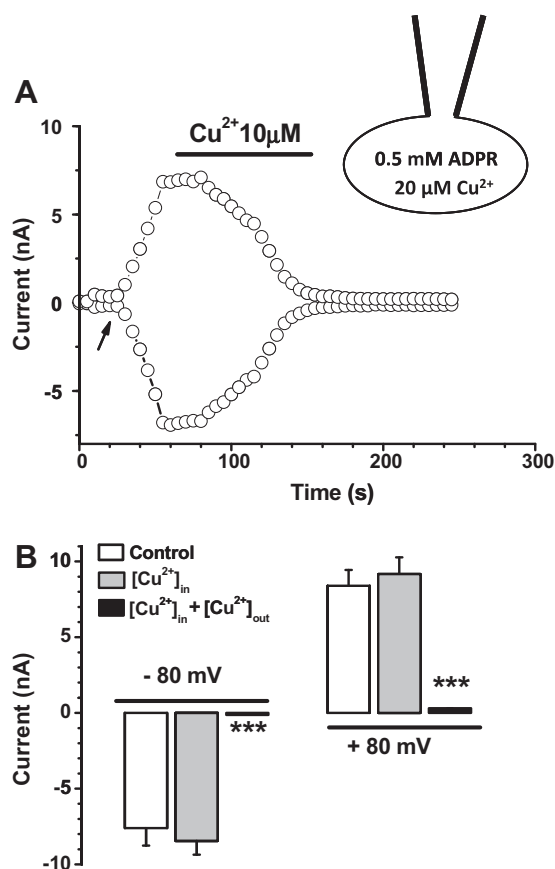
Fig. 2. Cu^{2+} inhibits TRPM2 channels from the cell surface. (A) Addition of Cu^{2+} (20 μM) into the pipette solution did not prevent the channel activation by ADPR, whereas the perfusion of Cu^{2+} in bath solution completely abolished the whole-cell currents. The arrow indicates the time point when the whole-cell configuration was achieved. (B) Comparison of the peak amplitudes of TRPM2 currents measured at +80 and −80 mV in the control group and in the presence of intracellular or extracellular Cu^{2+} ($n = 3$, ***$P < 0.001$).
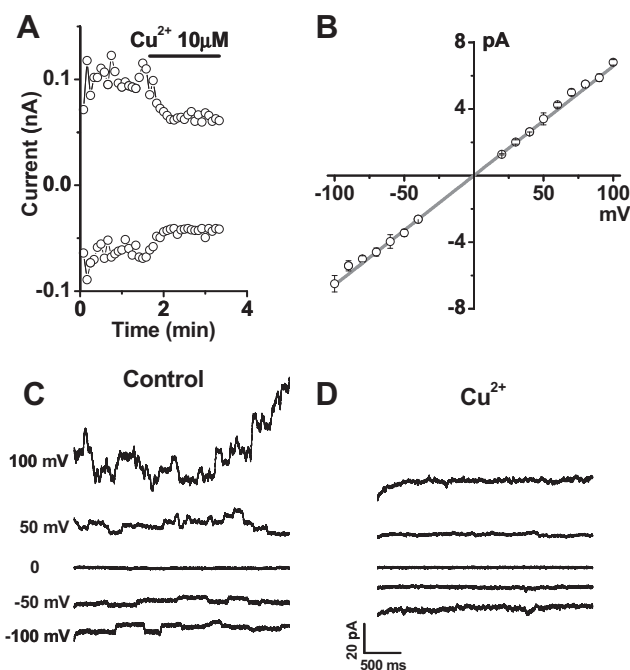
Fig. 3. Outside-out patches showing the effect of Cu^{2+}. (A) Example for the time course of the effect of Cu^{2+}. (B) Mean unitary current sizes for ADPR-induced TRPM2 single channel events plotted against voltages. Straight line was fitted and the mean unitary slope conductance was 66 pS (0.5 mM ADP-ribose). (C) Example of single channel activity of TRPM2 recorded by outside-out patches before perfusion with Cu^{2+}. (D) Cu^{2+} (10 μM).

breakthrough (Fig. 1A and B), which is consistent with our previous reports and others [1,12,35]. Perfusion with 10 μM divalent Cu^{2+} abolished the current of TRPM2. The inhibitory effect of Cu^{2+} seemed to be irreversible on washout, which suggests that Cu^{2+} may form covalent bonds with the channel protein. In the control cells without tetracycline induction (Tet-), the whole-cell current evoked by ADP-ribose was very small, and also inhibited by Cu^{2+} (10 μM), suggesting that there is an endogenous current sensitive to Cu^{2+} in the native cells (Fig. 1C and D). The inhibition of Cu^{2+} on TRPM2 was concentration-dependent with an IC_{50} of 2.59 ± 0.66 μM and a slope factor of 1.50 ± 0.35 (Fig. 1F).

3.2. Extracellular effect of Cu^{2+} on TRPM2

Due to the ubiquitous expression of Cu^{2+} transporters in the plasma membrane and intracellular membranes, and the different concentrations in the extracellular cleft and cytosol [16], we therefore determined the action site of Cu^{2+} on TRPM2 channel. We included higher concentration (20 μM) of Cu^{2+} into the pipette solution to see whether the activation of TRPM2 current can be prevented. We found that intracellular Cu^{2+} application failed to prevent the TRPM2 current induced by ADP-ribose, but the subsequent bath perfusion with 10 μM Cu^{2+} abolished the current (Fig. 2), suggesting that the
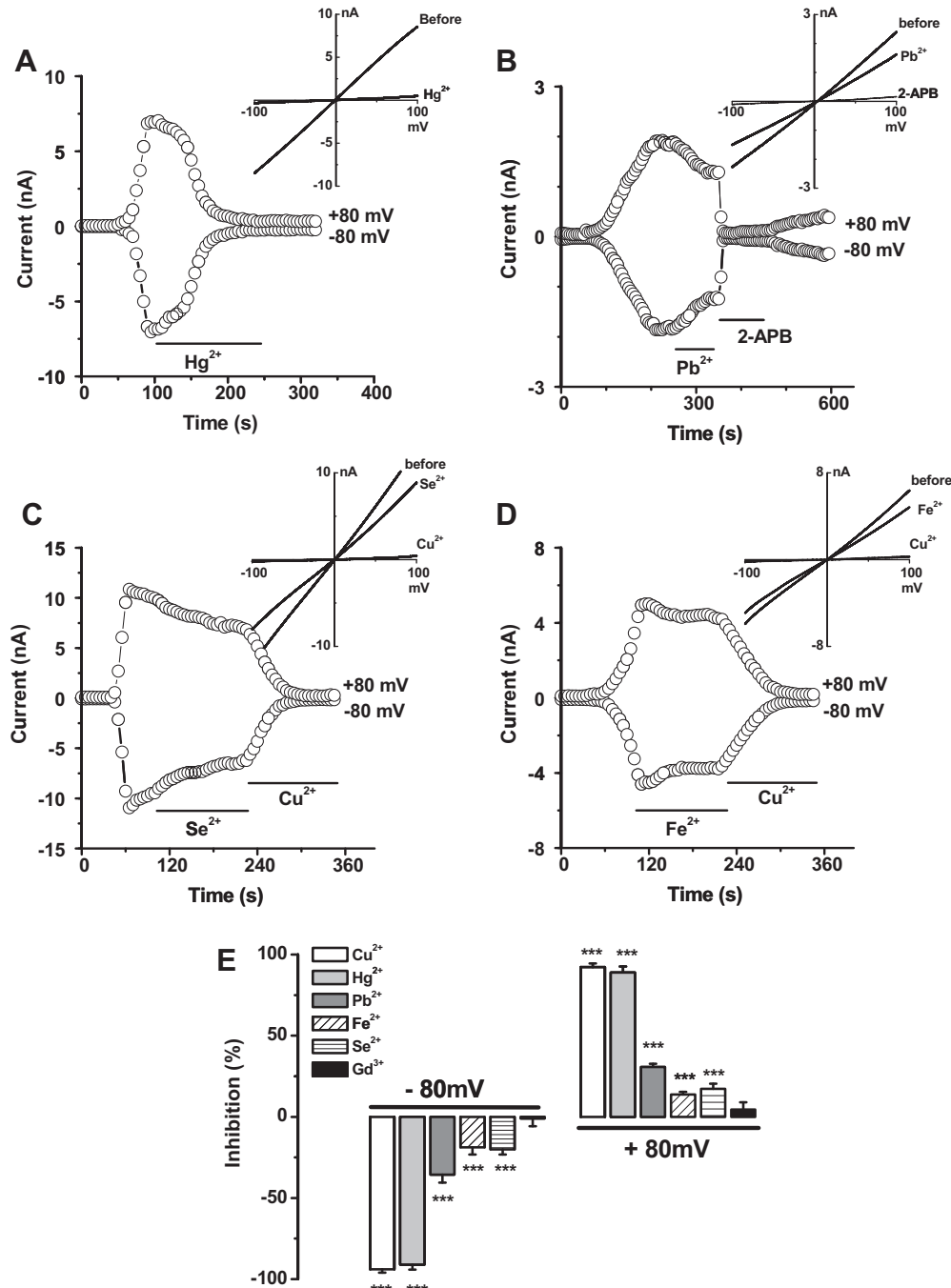
Fig. 4. Effect of Hg^{2+}, Pb^{2+}, Fe^{2+} and Se^{2+} on TRPM2 channels. (A) Hg^{2+} (10 μM) inhibited the whole-cell TRPM2 current activated by ADPR. (B) Pb^{2+} (10 μM) partially inhibited the TRPM2 current, and subsequent application of 2-APB (100 μM) dramatically reduced the currents. (C) Effect of Se^{2+} (10 μM). (D) Effect of Fe^{2+} (10 μM). (E) Comparison of the inhibitory effects of Hg^{2+}, Pb^{2+}, Fe^{2+}, Se^{2+}, Gd^{3+} at 10 μM on TRPM2 currents measured at +80 and −80 mV (n = 4–6 for each group).

action site of Cu^{2+} on TRPM2 channel could be located in the external surface of the transmembrane domains.

To further confirm the extracellular effect, the outside-out patch was performed. Cu^{2+} (10 μM) significantly inhibited the TRPM2 current in the outside-out patches (Fig. 3A). We also recorded the single channel activity of TRPM2. The slope conductance for the TRPM2 induced by ADP-ribose was 65.8 ± 0.23 pS (*n* = 4), which is similar to 64 pS [15] and close to 60 pS recorded under the conditions of 100 nM Ca^{2+} and 100 μM ADP-ribose [1]. Bath perfusion with 10 μM Cu^{2+} abolished the single channel activity (Fig. 3).

3.3. Comparison with other metal ions on TRPM2 channels

Mercury and lead are important metal ions related to neuronal development and dysfunction, therefore we investigated their effects on TRPM2 channel. Hg^{2+} at 10 μM completely inhibited the TRPM2 current, whilst Pb^{2+}, Fe^{2+}, and Se^{2+} at 10 μM showed a partial inhibition (Fig. 4A and D). The inhibitory effect of Hg^{2+} was difficult to be washed out. Fe^{2+} at 50 μM also showed inhibitory effect and the current was decreased by 25.3 ± 6.6% (*n* = 3), but higher concentrations of Fe^{2+} ($\geqslant$100 μM) caused a leak current due to cell damage. The percentage of inhibition was compared against the normalized effect (100%) of 2-APB at 100 μM on the same cell. The potency for Hg^{2+} and Cu^{2+} was similar, but stronger than that of Pb^{2+}, Fe^{2+} and Se^{2+} (Fig. 4F). No significant effect was observed for the trivalent cation Gd^{3+}, which is in agreement with our previous report [36].

4. Discussion

In this study, we demonstrate that Cu^{2+} at micromolar concentrations potently inhibits TRPM2 channel activity. The action site of Cu^{2+} is extracellularly located and the inhibitory effect of Cu^{2+} is irreversible. Hg^{2+}, Pb^{2+}, Fe^{2+} and Se^{2+} also show blocking effect on TRPM2 channel, but Pb^{2+}, Fe^{2+} and Se^{2+} are less potent than Cu^{2+} and Hg^{2+}. These findings provide a novel mechanism for the pathophysiology of Cu^{2+} in human diseases.

Copper has been implicated in the pathogenesis of several neurodegenerative disorders including Alzheimer's disease, amyotrophic lateral sclerosis, Huntington's disease, Parkinson's disease, and prion disease [26,27]. Excess of copper is associated with the production of ROS, which in turn triggers a series of events including oxidative stress-induced cell injury, intracellular protein deposits (neurofibrillary tangles), neuronal dysfunction and consequently cell death [37]. On the other hand, ROS activate some Ca^{2+} channels, such as TRPM2, and cause the disruption of cellular Ca^{2+} homeostasis. The common change of Ca^{2+} homeostasis in Alzheimer's disease is an increased intracellular calcium level that could occur either indirectly through Aβ modulating an existing Ca^{2+} channel or directly through cation-selective channels formed by Aβ [38]. In this study, we found that extracellular Cu^{2+} significantly inhibited the TRPM2 channels, which provide a new evidence for the relationship between ROS-sensitive Ca^{2+} channel TRPM2 and Cu^{2+}. The TRPM2 channel activity is activated by ROS or H_2O_2, but inhibited by Cu^{2+}, therefore Cu^{2+} seems to be protective in the Ca^{2+} homeostasis. Because of the extremely high copper levels in senile plaques (393 ± 123 μM) [24], we suppose that the activity of TRPM2 enhanced by H_2O_2 and Aβ in the affected regions of the brain is likely to be completely inhibited by Cu^{2+}. Nevertheless, the physiological significance of TRPM2 channel inhibited by Cu^{2+} still needs to be further investigated, because the inhibition by Cu^{2+} is an irreversible process, which may affect the normal function of TRPM2 in these cells. In primary cultures of rat striatum, the Aβ-induced Ca^{2+} increase and cell death can be prevented by a dominant negative isoform of TRPM2 (TRPM2-S), suggesting that lowering

activity of TRPM2 could be protective [10]. Moreover, the genetic variants of TRPM2 have been identified in several neurological diseases, but little is known about the channel functionality in the native cells related to these diseases [9].

Copper concentration in blood plasma is around 15 μM in normal population [16], however, copper accumulates in the brain and displays differential distribution patterns in the central nervous system. Much higher concentration has been estimated in the cerebrospinal fluid (~70 μM). The concentration in the synaptic cleft may reach 200–400 μM in some neuronal diseases, whereas the normal extracellular copper concentration in the brain is of the order of 0.2–1.7 μM [16]. The elevated copper levels have also been reported in patients with type 1 or type 2 diabetes [39], which shares many pathogenetic mechanisms with Alzheimer's disease and vascular dementia. In addition, copper accumulation in the body is caused by genetic variants of Cu^{2+} transporter genes (ATP7A and ATP7B), i.e., Menkes syndrome and Wilson disease. These suggest that the inhibitory mechanism by micromolar Cu^{2+} on TRPM2 channel should happen in normal subjects and under some disease conditions.

Apart from the inhibition on the oxidative stress-sensitive TRPM2 channels, Cu^{2+} also inhibits the voltage-gated Ca^{2+} channels including T-, L-, N-, P-, and Q-type currents [16]. The $Ca_v3.2$ channel is more sensitive to Cu^{2+} than other types of voltage-gated Ca^{2+} channels with an IC_{50} = 0.9 μM [40]. In addition, high concentrations of Cu^{2+} stimulate TRPV1 and TRPA1 channels [41,42], suggesting that the overall effect of Cu^{2+} on intracellular Ca^{2+} level may vary, which depends on the local concentration of Cu^{2+} and the expression of individual Ca^{2+} channels.

We have not examined the molecular targets of Cu^{2+} in this study, however, Cu^{2+} may bind directly to amino acids against most likely cysteine or the hydrophilic-charged amino acids (histidine, lysine, arginine, aspartate, and glutamate) to alter protein function. Indeed, the residue substitution in the outer vestibule of the pore including Lys952, His995 and Asp1002 significantly changed the sensitivity to Zn^{2+} [43]. Further investigation is needed to confirm these binding sites for Cu^{2+}. In addition, the binding to cysteine residues or oxidizing the residues may catalyse the formation of disulphide bonds between physically adjacent cysteine residues, and thereby indirectly change protein structure and function. Moreover, a third more indirect way that copper can modulate protein function is through the generation of free radicals, which can profoundly alter protein and cell function, particularly for the ROS-sensitive channels, such as TRPM2 channels in this study. Unlike the extracellular effect of Cu^{2+}, the action site for ROS or hydroxyl radical that generated by mixing with Fe^{2+} and H_2O_2 has been demonstrated as an intracellular effect, which is mainly related to the C-terminal Nudix-like domain [2,44]. Therefore, the channel appears to be opened by intracellular ROS, and closed by extracellular Cu^{2+}. On the other hand, higher concentrations of extracellular Cu^{2+} may enter cells via Cu^{2+} transporters that in turn regulate the ROS production. Recently, Zn^{2+} has been shown to inhibit TRPM2 channel, however, the potency of Zn^{2+} was much lower than that of Cu^{2+} [43]. The difference in potency for the two ions may have important physiological relevance because the plasma levels of copper and zinc are oppositely correlated in many diseased conditions such as diabetes and hypertension and the ratio of Zn^{2+}/Cu^{2+} have been evaluated in some diseases [16,45,46]. Excessive copper and deficit of zinc would progressively disrupt the cellular Ca^{2+} homeostasis by tuning the activity of a number of TRP and other Ca^{2+} channels [16]. The inhibition of TRPM2 channel by Pb^{2+}, Se^{2+} and Fe^{2+} was mild, suggesting these metal ions could be less important as direct channel regulators.

Besides the neurological disorders, TRPM2 channel is also important for insulin secretion in pancreatic β-cells [3,4]. Copper deficiency enhances the insulin secretion in isolated pancreatic

islets [47], suggesting that copper can regulate the insulin release, which could be related to TRPM2 channels. Taken together, the inhibition of TRPM2 by copper is an important mechanism for the normal physiological function in the body. The imbalance of TRPM2 channel activity caused by excess copper or ROS may be one of the pathophysiological mechanisms for disruption of Ca^{2+} homeostasis in diabetes and neurodegenerative disorders.

Acknowledgments

References

[1] A.L. Perraud, A. Fleig, C.A. Dunn, et al., ADP-ribose gating of the calcium-permeable LTRPC2 channel revealed by Nudix motif homology, Nature 411 (2001) 595–599.

[2] A. Sumoza-Toledo, R. Penner, TRPM2: a multifunctional ion channel for calcium signalling, J. Physiol. 589 (2011) 1515–1525.

[3] K. Uchida, K. Dezaki, B. Damdindorj, et al., Lack of TRPM2 impaired insulin secretion and glucose metabolisms in mice, Diabetes 60 (2011) 119–126.

[4] K. Togashi, Y. Hara, T. Tominaga, et al., TRPM2 activation by cyclic ADP-ribose at body temperature is involved in insulin secretion, EMBO J. 25 (2006) 1804–1815.

[5] A. Di, X.P. Gao, F. Qian, et al., The redox-sensitive cation channel TRPM2 modulates phagocyte ROS production and inflammation, Nat. Immunol. 13 (2011) 29–34.

[6] Y. Hara, M. Wakamori, M. Ishii, et al., LTRPC2 Ca^{2+}-permeable channel activated by changes in redox status confers susceptibility to cell death, Mol. Cell 9 (2002) 163–173.

[7] H. Knowles, J.W. Heizer, Y. Li, et al., Transient Receptor Potential Melastatin 2 (TRPM2) ion channel is required for innate immunity against Listeria monocytogenes, Proc. Natl. Acad. Sci. U.S.A. 108 (2011) 11578–11583.

[8] C. Xu, P.P. Li, R.G. Cooke, et al., TRPM2 variants and bipolar disorder risk: confirmation in a family-based association study, Bipolar Disord. 11 (2009) 1–10.

[9] M.C. Hermosura, A.M. Cui, R.C. Go, et al., Altered functional properties of a TRPM2 variant in Guamanian ALS and PD, Proc. Natl. Acad. Sci. U.S.A. 105 (2008) 18029–18034.

[10] E. Fonfria, I.C. Marshall, I. Boyfield, et al., Amyloid beta-peptide(1–42) and hydrogen peroxide-induced toxicity are mediated by TRPM2 in rat primary striatal cultures, J. Neurochem. 95 (2005) 715–723.

[11] Y. Sano, K. Inamura, A. Miyake, et al., Immunocyte Ca^{2+} influx system mediated by LTRPC2, Science 293 (2001) 1327–1330.

[12] D. McHugh, R. Flemming, S.Z. Xu, et al., Critical intracellular Ca^{2+} dependence of transient receptor potential melastatin 2 (TRPM2) cation channel activation, J. Biol. Chem. 278 (2003) 11002–11006.

[13] M. Kolisek, A. Beck, A. Fleig, et al., Cyclic ADP-ribose and hydrogen peroxide synergize with ADP-ribose in the activation of TRPM2 channels, Mol. Cell 18 (2005) 61–69.

[14] J. Du, J. Xie, L. Yue, Modulation of TRPM2 by acidic pH and the underlying mechanisms for pH sensitivity, J. Gen. Physiol. 134 (2009) 471–488.

[15] J.G. Starkus, A. Fleig, R. Penner, The calcium-permeable non-selective cation channel TRPM2 is modulated by cellular acidification, J. Physiol. 588 (2010) 1227–1240.

[16] A. Mathie, G.L. Sutton, C.E. Clarke, et al., Zinc and copper: pharmacological probes and endogenous modulators of neuronal excitability, Pharmacol. Ther. 111 (2006) 567–583.

[17] K. Jomova, D. Vondrakova, M. Lawson, et al., Metals, oxidative stress and neurodegenerative disorders, Mol. Cell. Biochem. 345 (2010) 91–104.

[18] J.Y. Uriu-Adams, C.L. Keen, Copper, oxidative stress, and human health, Mol. Aspects Med. 26 (2005) 268–298.

[19] J. Chelly, Z. Tumer, T. Tonnesen, et al., Isolation of a candidate gene for Menkes disease that encodes a potential heavy metal binding protein, Nat. Genet. 3 (1993) 14–19.

[20] R. Shahidzadeh, S. Sridhar, Profound copper deficiency in a patient with gastric bypass, Am. J. Gastroenterol. 103 (2008) 2660–2662.

[21] G.J. Brewer, The risks of copper toxicity contributing to cognitive decline in the aging population and to Alzheimer's disease, J. Am. Coll. Nutr. 28 (2009) 238–242.

[22] R.E. Tanzi, K. Petrukhin, I. Chernov, et al., The Wilson disease gene is a copper transporting ATPase with homology to the Menkes disease gene, Nat. Genet. 5 (1993) 344–350.

[23] R.M. Walter Jr., J.Y. Uriu-Hare, K.L. Olin, et al., Copper, zinc, manganese, and magnesium status and complications of diabetes mellitus, Diabetes Care 14 (1991) 1050–1056.

[24] M.A. Lovell, J.D. Robertson, W.J. Teesdale, et al., Copper, iron and zinc in Alzheimer's disease senile plaques, J. Neurol. Sci. 158 (1998) 47–52.

[25] G.J. Cooper, Therapeutic potential of copper chelation with triethylenetetramine in managing diabetes mellitus and Alzheimer's disease, Drugs 71 (2011) 1281–1320.

[26] V. Desai, S.G. Kaler, Role of copper in human neurological disorders, Am. J. Clin. Nutr. 88 (2008) 855S–858S.

[27] R. Squitti, Copper dysfunction in Alzheimer's disease: From meta-analysis of biochemical studies to new insight into genetics. J. Trace Elem. Med. Biol. (2012) in press.

[28] G. Meloni, V. Sonois, T. Delaine, et al., Metal swap between Zn7-metallothionein-3 and amyloid-beta-Cu protects against amyloid-beta toxicity, Nat. Chem. Biol. 4 (2008) 366–372.

[29] V. Tougu, A. Tiiman, P. Palumaa, et al., Interactions of Zn(II) and Cu(II) ions with Alzheimer's amyloid-beta peptide. Metal ion binding, contribution to fibrillization and toxicity, Metallomics 3 (2011) 250–261.

[30] C.J. Lin, H.C. Huang, Z.F. Jiang, Cu(II) interaction with amyloid-beta peptide: a review of neuroactive mechanisms in AD brains, Brain Res. Bull. 82 (2010) 235–242.

[31] E. House, M. Mold, J. Collingwood, et al., Copper abolishes the beta-sheet secondary structure of preformed amyloid fibrils of amyloid-beta(42), J. Alzheimers Dis. 18 (2009) 811–817.

[32] P. Faller, Copper in Alzheimer disease: too much, too little, or misplaced?, Free Radic Biol. Med. 52 (2012) 747–748.

[33] S.A. James, I. Volitakis, P.A. Adlard, et al., Elevated labile Cu is associated with oxidative pathology in Alzheimer disease, Free Radic. Biol. Med. 52 (2012) 298–302.

[34] S.-Z. Xu, B. Zeng, N. Daskoulidou, et al., Activation of TRPC Cationic Channels by Mercurial Compounds Confers the Cytotoxicity of Mercury Exposure, Toxicol. Sci. 125 (2012) 56–68.

[35] S.Z. Xu, W. Zhong, N.M. Watson, et al., Fluvastatin reduces oxidative damage in human vascular endothelial cells by upregulating Bcl-2, J. Thromb. Haemost. 6 (2008) 692–700.

[36] S.Z. Xu, F. Zeng, G. Boulay, et al., Block of TRPC5 channels by 2-aminoethoxydiphenyl borate: a differential, extracellular and voltage-dependent effect, Br. J. Pharmacol. 145 (2005) 405–414.

[37] E. Gaggelli, H. Kozlowski, D. Valensin, et al., Copper homeostasis and neurodegenerative disorders (Alzheimer's, prion, and Parkinson's diseases and amyotrophic lateral sclerosis), Chem. Rev. 106 (2006) 1995–2044.

[38] J.M. Alarcon, J.A. Brito, T. Hermosilla, et al., Ion channel formation by Alzheimer's disease amyloid beta-peptide (Abeta40) in unilamellar liposomes is determined by anionic phospholipids, Peptides 27 (2006) 95–104.

[39] A.H. Zargar, N.A. Shah, S.R. Masoodi, et al., Copper, zinc, and magnesium levels in non-insulin dependent diabetes mellitus, Post. Grad. Med. J 74 (1998) 665–668.

[40] S.W. Jeong, B.G. Park, J.Y. Park, et al., Divalent metals differentially block cloned T-type calcium channels, NeuroReport 14 (2003) 1537–1540.

[41] Q. Gu, R.L. Lin, Heavy metals zinc, cadmium, and copper stimulate pulmonary sensory neurons via direct activation of TRPA1, J. Appl. Physiol. 108 (2010) 891–897.

[42] C.E. Riera, H. Vogel, S.A. Simon, et al., Artificial sweeteners and salts producing a metallic taste sensation activate TRPV1 receptors, Am. J. Physiol. Regul. Integr. Comp. Physiol. 293 (2007) R626–634.

[43] W. Yang, P.T. Manna, J. Zou, et al., Zinc inactivates melastatin transient receptor potential 2 channels via the outer pore, J. Biol. Chem. 286 (2011) 23789–23798.

[44] M. Ishii, S. Shimizu, Y. Hara, et al., Intracellular-produced hydroxyl radical mediates H2O2-induced Ca^{2+} influx and cell death in rat beta-cell line RIN-5F, Cell Calcium 39 (2006) 487–494.

[45] A. Viktorinova, E. Toserova, M. Krizko, et al., Altered metabolism of copper, zinc, and magnesium is associated with increased levels of glycated hemoglobin in patients with diabetes mellitus, Metabolism 58 (2009) 1477–1482.

[46] H. Canatan, I. Bakan, M. Akbulut, et al., Relationship among levels of leptin and zinc, copper, and zinc/copper ratio in plasma of patients with essential hypertension and healthy normotensive subjects, Biol. Trace Elem. Res. 100 (2004) 117–123.

[47] G.D. Miller, C.L. Keen, J.S. Stern, et al., Copper deficiency and arachidonic acid enhance insulin secretion in isolated pancreatic islets from lean (FaFa) Zucker rats, Pancreas 17 (1998) 390–396.

RESEARCH PAPER

Pharmacological comparison of novel synthetic fenamate analogues with econazole and 2-APB on the inhibition of TRPM2 channels

Gui-Lan Chen[1]*, Bo Zeng[1]*, Sarah Eastmond[2], Sandra E Elsenussi[2], Andrew N Boa[2] and Shang-Zhong Xu[1]

[1]*Centre for Cardiovascular and Metabolic Research, Hull York Medical School, University of Hull, Hull, UK, and [2]Department of Chemistry, University of Hull, Hull, UK*

BACKGROUND AND PURPOSE

Fenamate analogues, econazole and 2-aminoethoxydiphenyl borate (2-APB) are inhibitors of transient receptor potential melastatin 2 (TRPM2) channels and are used as research tools. However, these compounds have different chemical structures and therapeutic applications. Here we have investigated the pharmacological profile of TRPM2 channels by application of newly synthesized fenamate analogues and the existing channel blockers.

EXPERIMENTAL APPROACH

Human TRPM2 channels in tetracycline-regulated pcDNA4/TO vectors were transfected into HEK293 T-REx cells and the expression was induced by tetracycline. Whole cell currents were recorded by patch-clamp techniques. Ca^{2+} influx or release was monitored by fluorometry.

KEY RESULTS

Flufenamic acid (FFA), mefenamic acid (MFA) and niflumic acid (NFA) concentration-dependently inhibited TRPM2 current with potency order FFA > MFA = NFA. Modification of the 2-phenylamino ring by substitution of the trifluoromethyl group in FFA with $-CH_3$, $-F$, $-CF_3$, $-OCH_3$, $-OCH_2CH_3$, $-COOH$, and $-NO_2$ at various positions, reduced channel blocking potency. The conservative substitution of 3-CF_3 in FFA by $-CH_3$ (3-MFA), however, gave the most potent fenamate analogue with an IC_{50} of 76 μM, comparable to that of FFA, but unlike FFA, had no effect on Ca^{2+} release. 3-MFA and FFA inhibited the channel intracellularly. Econazole and 2-APB showed non-selectivity by altering cytosolic Ca^{2+} movement. Econazole also evoked a non-selective current.

CONCLUSION AND IMPLICATIONS

The fenamate analogue 3-MFA was more selective than other TRPM2 channel blockers. FFA, 2-APB and econazole should be used with caution as TRPM2 channel blockers, as these compounds can interfere with intracellular Ca^{2+} movement.

Abbreviations

2-APB, 2-aminoethoxydiphenyl borate; 3-MFA, 2-(3-methylphenyl)aminobenzoic acid; ACA, *N*-(*p*-amylcinnamoyl)anthranilic acid; IP_3, inositol trisphosphate; *IV*, current–voltage; FFA, flufenamic acid; MFA, mefenamic acid; NFA, niflumic acid; NMDG, N-methyl-D-glucamine; NSAIDs, non-steroidal anti-inflammatory drugs; SERCA, sarco(endo)plasmic reticulum Ca^{2+}-ATPase; Tet, tetracycline; TRP, transient receptor potential; TRPC, transient receptor potential canonical; TRPM2, transient receptor potential melastatin 2

Introduction

Ca^{2+} ions are second messengers controlling many cell signalling processes. The transient receptor potential (TRP) channel family (channel and receptor nomenclature follows Alexander *et al.*, 2011) is a class of Ca^{2+}-permeable cationic channels that are important for maintaining intracellular Ca^{2+} level. The transient receptor potential melastatin 2 (TRPM2) channel is one member of the TRPM channel subfamily (Ramsey *et al.*, 2006), which was first cloned in 1998 (Nagamine *et al.*, 1998). TRPM2 channels are highly expressed in the brain and ubiquitously distributed in the body (Hecquet *et al.*, 2008; Wehrhahn *et al.*, 2010). The pathophysiological role of TRPM2 channels is still unclear, but they have been implicated in the free radical-induced cell death of hippocampal neurons (Olah *et al.*, 2009), striatal cells (Fonfria *et al.*, 2005) and other cell types (Zhang *et al.*, 2003; Yang *et al.*, 2006; Ishii *et al.*, 2007); the stress-related inflammatory processes (Yamamoto *et al.*, 2008; Wehrhahn *et al.*, 2010); insulin secretion (Uchida *et al.*, 2010); immune response (Sano *et al.*, 2001; Knowles *et al.*, 2011); and oxidant-induced endothelial injury (Hara *et al.*, 2002; Hecquet and Malik, 2009).

Heterologous expression of TRPM2 protein gives rise to a voltage-independent, Ca^{2+}-permeable, non-selective cationic channel with a linear current–voltage (*IV*) relationship (Perraud *et al.*, 2001; McHugh *et al.*, 2003) and a characteristic activation by intracellular ADP-ribose. Flufenamic acid (FFA), econazole, 2-aminoethoxydiphenyl borate (2-APB) and Zn^{2+} as all act as blockers of TRPM2 channels (Hill *et al.*, 2004a,b; Yang *et al.*, 2011). FFA is one of the fenamate non-steroidal anti-inflammatory drugs (NSAIDs), which affects a variety of channels, inducing inhibition of Cl^- channels, voltage-dependent Na^+ or Ca^{2+} channels, and TRPM2, TRPM4, TRPM5, TRPC3 and TRPC5 channels (Lee *et al.*, 2003; Kraft and Harteneck, 2005; Ullrich *et al.*, 2005). FFA also activates TRPC6 (Inoue *et al.*, 2001; Jung *et al.*, 2002; Foster *et al.*, 2009) and TRPA1 channels (Hu *et al.*, 2010). The action of FFA on ion channels is not mediated by cyclooxygenase (COX), because selective COX inhibitors were found to have no direct effect on TRP cationic channels (Jiang *et al.*, 2012), suggesting there is direct conformational interaction between FFA and the channel protein. The fenamate NSAIDs are anthranilic acid derivatives with structural similarity to the PLA2 inhibitor *N*-(*p*-amylcinnamoyl)anthranilic acid (ACA). However, although ACA inhibited TRPM2 channels (Kraft *et al.*, 2006), other PLA2 inhibitors without the skeleton of anthranilic acid had no effect on these channels, suggesting that the parent structure of anthranilic acid was essential for the channel blockade. Moreover, other fenamates with different substituents on the 2-phenylamino ring, such as FFA, mefenamic acid (MFA) and diclofenac, exert different effects on elevation of intracellular Ca^{2+} (Poronnik *et al.*, 1992). Recently, we found that the substituents on the 2-phenylamino ring of the fenamate skeleton were important for regulating TRPC4 and TRPC5 channel activity, especially the position of the methyl groups in MFA. The replacement of 2-methyl with a methoxy group gave an analogue showing activation, rather than inhibition on TRPC4 and TRPC5 channels (Jiang *et al.*, 2012). Therefore, we proposed that the modification of 2-phenylamino ring would be important for understanding the structure–activity relationship of

fenamate analogues on TRPM2 channels and might yield new leads for drug discovery.

In this study, we examined the effect of some new fenamate analogues on TRPM2 channels using inducible cells over-expressing TRPM2 protein. In order to understand the structure–activity relationship of the fenamates, we synthesized analogues with modifications of the 2-phenylamino ring and compared their potency on TRPM2 channels. To compare their pharmacological properties of the new compounds with those of known TRPM2 channel blockers, the effects of econazole and 2-APB were also investigated in our model system.

Methods

Cell culture and transfection

Human TRPM2 protein (GenBank accession number BC112342) in pcDNA4/TO tetracycline-regulatory vector was transfected into HEK-293 T-REx cells (Invitrogen, Paisley, UK). The expression was induced by 1 µg·mL^{-1} tetracycline for 24–72 h before recording. The non-induced cells without addition of tetracycline were used as control. Cells were grown in DMEM-F12 medium (Invitrogen) containing 10% fetal calf serum (FCS), 100 units·mL^{-1} penicillin and 100 µg·mL^{-1} streptomycin. Cells were maintained at 37°C under 95% air and 5% CO_2 and seeded on coverslips prior to experiments.

Electrophysiology

The procedure for whole-cell clamp is similar to that described earlier (Xu *et al.*, 2012). Experiments were performed at room temperature (25 °C). Briefly, electrical signal was amplified with an Axopatch 200B patch clamp amplifier and controlled with pClamp software 10. A 1 s ramp voltage protocol from –100 to +100 mV was applied at a frequency of 0.2 Hz from a holding potential of 0 mV. Signals were sampled at 3 kHz and filtered at 1 kHz. Glass microelectrodes with a resistance of 3–5 MΩ were used. The 200 nM Ca^{2+} buffered pipette solution (115 CsCl, 10 EGTA, 2 MgCl$_2$, 10 HEPES and 5.7 CaCl$_2$ in mM, pH was adjusted to 7.2 with CsOH and osmolarity was adjusted to ~290 mOsm with mannitol, and the calculated free Ca^{2+} was 200 nM) was used. ADP-ribose (0.5 mM) was added in the pipette solution. The same pipette solution was used for outside-out patches. The standard bath solution contained (mM) 130 NaCl, 5 KCl, 8 D-glucose, 10 HEPES, 1.2 MgCl$_2$ and 1.5 CaCl$_2$; pH was adjusted to 7.4 with NaOH.

Ca^{2+} measurement

Cells were pre-incubated with 2 µM fura-PE3 AM at 37°C for 30 min in Ca^{2+}-free bath solution, followed by a 20 min wash period in the standard bath solution at room temperature. Fura-PE3 fluorescence was monitored with an inverted epifluorescence microscope with a cooled Orca-R2 CCD camera (Hamamatsu, Hamamatsu City, Japan). The imaging system was controlled by software NIS-Elements 3.0 (Nikon, Tokyo, Japan). The ratio of Ca^{2+} dye fluorescence (F_{340}/F_{380}) was measured. For the experiment with single wavelength Ca^{2+} dye Fluo3-AM, the cuvette-based $[Ca^{2+}]_i$ assay system was used as described previously (Xu *et al.*, 2008). All experiments were performed at room temperature.

Materials

All general salts and reagents were from Sigma (Dorset, UK). FFA, MFA, niflumic acid (NFA), diclofenac , aspirin, indomethacin, 2-APB, tetracycline, ADP-ribose, econazole and N-methyl-D-glucamine (NMDG) were purchased from Sigma. Fura-PE3 AM was purchased from Invitrogen. Fura-PE3 AM (5 mM) and 2-APB (100 mM) were made up as stock solutions in 100% dimethyl sulphoxide (DMSO). Fenamate derivatives were synthesized in the Chemistry Department following the method reported by Mei *et al.* (2006) using the copper-catalysed coupling of either 2-chloro- or 2-bromobenzoic acid with the appropriate aniline derivative. For example, 2-chlorobenzoic acid (9.0 mmol), the appropriate aniline (9.5 mmol), K_2CO_3 (9.0 mmol), Cu (0.8 mmol), Cu_2O (0.4 mmol) and 5 mL of 2-ethoxyethanol were heated under a nitrogen atmosphere for 24 h. The cooled reaction mixture was poured into water; activated charcoal was added then the solution filtered. The crude product was precipitated upon acidification of the filtrate with 1 M HCl. The residue was purified by dissolution in 5% aqueous Na_2CO_3 solution, filtration and then re-precipitation by careful addition of 1 M HCl. In the case of compound 8 in Figure 3, 5[2-(4′-carboxyphenylamino)benzoic acid], the starting material was ethyl 4-aminobenzoate, but the ethyl ester group suffered *in situ* hydrolysis. All products gave satisfactory ^{1}H, ^{13}C-NMR and mass spectra; and their purity was estimated to be >95%.

Statistics

Data are expressed as mean ± SEM. where *n* is the cell number for electrophysiological recordings and Ca^{2+} imaging. Mean data were compared using paired *t*-test for the results before and after treatment, or ANOVA with Dunnett's *post hoc* test for comparing more than two groups, with significance indicated if $P < 0.05$.

Results

TRPM2 channels activated by ADP-ribose and H_2O_2

The expression of human TRPM2 protein in HEK-293 T-REx cells was induced by tetracycline and confirmed by Western blotting as we previously described (Xu *et al.*, 2008; 2012). The whole cell current was recorded by patch clamp after 24–48 h induction of gene expression, and the current carried by TRPM2 channels was activated by intracellular ADP-ribose with a linear *IV* curve (Figure 1A and B), in accordance with previous reports (Perraud *et al.*, 2001; Sano *et al.*, 2001; Hara *et al.*, 2002; Wehage *et al.*, 2002; McHugh *et al.*, 2003). The activation achieved its maximum within 30 s after the formation of whole-cell patch configuration and was fully blocked by 2-APB (100 µM). Substitution of Na^+ with equimolar concentrations of $NMDG^+$ rapidly abolished the inward current and the outward current gradually decreased (Figure 1C). In the non-induced cells, a small current (<1 nA) was activated by ADP-ribose, which could be due to endogenous channel activity. 2-APB fully inhibited the endogenous current (Figure 1D and E). We also examined the effect of H_2O_2 on the cells with inducible TRPM2 channels. Bath appli-

cation of H_2O_2 activated TRPM2 channels, but the current development was much slower and the maximum amplitude of the current was smaller than that after activation by ADP-ribose (Figure 1F). The *IV* curve induced by H_2O_2 showed an outward rectification and 2-APB at 100 µM did not fully block the current, suggesting that H_2O_2 may activate other 2-APB-insensitive channels. In addition, cytosolic Ca^{2+} concentrations were monitored using Ca^{2+}-sensitive dye. Influx of Ca^{2+} in cells with induced TRPM2 channels was robustly increased after perfusion with H_2O_2, but the non-induced cells showed a small increase (Figure 1G).

Comparison of the three experimental approaches indicated that whole-cell patch recording with intracellular ADP-ribose was the best methodology for examining TRPM2 channel pharmacology, as the large current (~10 nA) through TRPM2 channels evoked by ADP-ribose was clearly distinguished from the small endogenous current (0.64 ± 0.02 nA measured at –80 mV, $n = 12$) in the non-induced cells which also showed a linear *IV* relationship and 2-APB sensitivity. Therefore, the whole-cell patch was used in the subsequent experiments for pharmacological comparison.

Effect of NSAIDs on TRPM2 channels

We examined the effect of fenamates and non-fenamate NSAIDs on TRPM2 channels. FFA, NFA and MFA significantly inhibited the TRPM2 current; while diclofenac showed only a small inhibition. The IC_{50} values for FFA, MFA and NFA was 70 ± 2.5, 124 ± 11.9 and 149 ± 12.0 µM with a slope factor of 0.01776, 0.00872 and 0.00763 respectively. The non-fenamate NSAIDs, aspirin and indomethacin, had no significant effect (Figure 2). These data suggested that the blocking activity of fenamates could be a direct effect, rather than a class effect of NSAIDs on COX signalling pathways, as the non-fenamate COX inhibitors had no effect.

Fenamate analogues on TRPM2 channels

In order to explore the structure–activity relationship of varying the substituents on the 2-phenylamino ring of the fenamate skeleton, 10 analogues were synthesized replacing the 3-trifluoromethyl group of FFA with –F, –CH_3, –OCH_3, –OCH_2CH_3, –COOH and –NO_2 substituents at various positions in the 2-phenylamino ring (Figure 3). Potency on the TRPM2 current was compared with the known channel blockers 2-APB and FFA. Substitution with –3-CH_3 (**1**) (abbreviated as 3-MFA), 3-F (**2**), 3-CH_3O (**3**) and –3-NO_2 (**4**) showed a significant difference in the inhibition of TRPM2 channel. The methyl substituent in the *meta* position (3-MFA) was critical for channel blocking effect. A –CH_3 group in the *ortho* (**5**) or *para* (**6**) position reduced potency. Other substituents at the *meta* position (**2**, **3**, and **4**) also showed less potency. Substituents with –4-CH_3CH_2O (**7**) and –4-COOH (**8**) showed weak inhibition. MFA and the analogue (**9**) have two methyl substituents in the ring; however, they showed a significant difference in their inhibitory activity (see Figures 2C and 3), which further suggested the importance of the methyl substituent at the *meta* position. Substitution of the 2-methyl with a methoxy group (**10**) or introduction of two Cl^- substituents in the *ortho* positions (as in diclofenac) showed reduced inhibition (see Figures 2D and 3). Moreover, the replacement of the benzoic
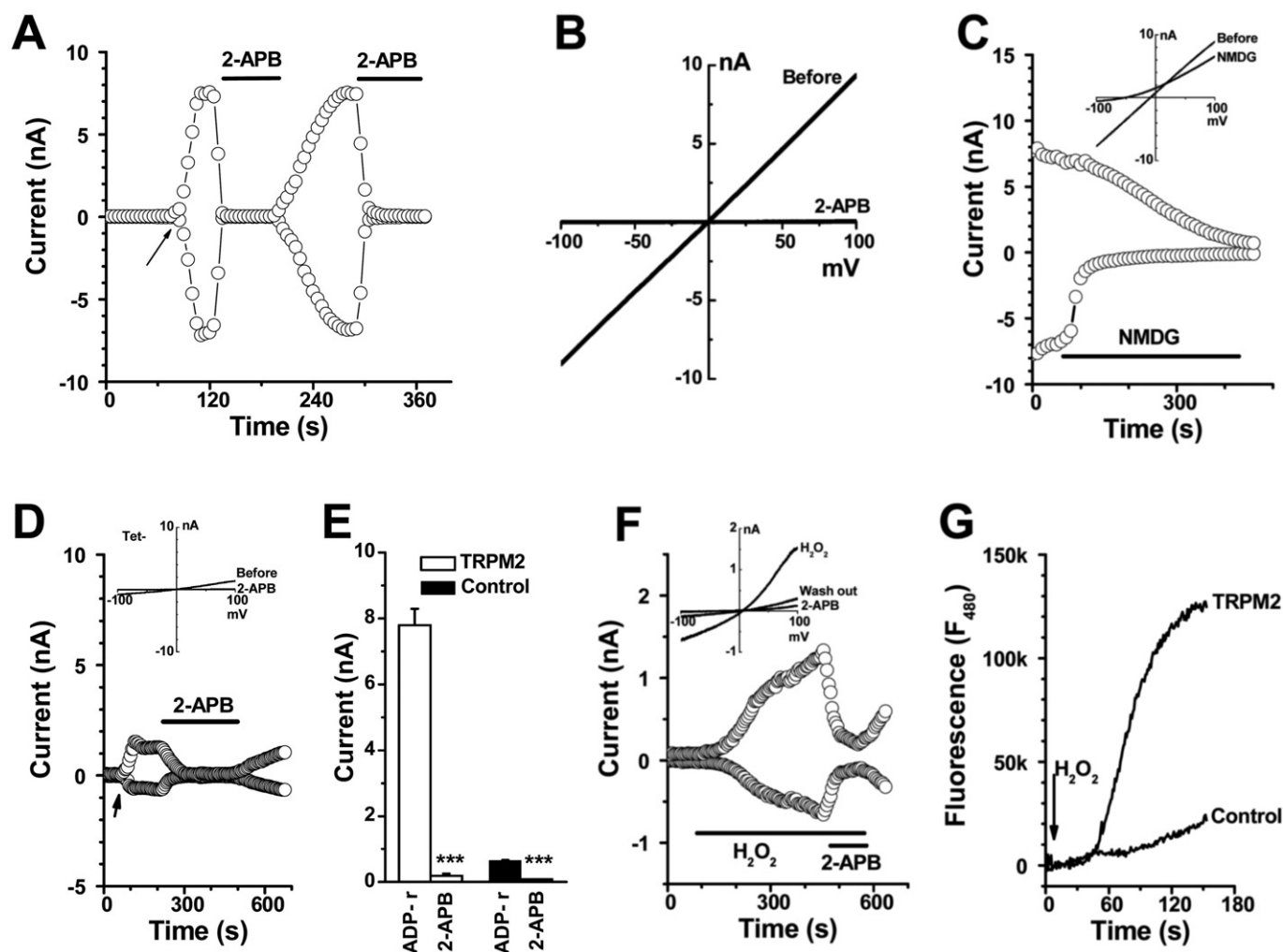
Figure 1

TRPM2 channels activated by ADP-ribose and H_2O_2. Whole-cell current in the HEK293 T-REx cells inducibly transfected with TRPM2 channels was recorded by patch clamp. (A) The time course for TRPM2 channel activation by 0.5 mM ADP-ribose (ADP-r) in pipette solution. The arrow shows the point of membrane breakthrough as whole-cell patch formation. 2-APB (100 μM) was used. (B) *IV* curve for (A). (C) Na^+ was substituted by equimolar concentrations of $NMDG^+$. The *IV* curves are shown in the inset. (D) Current recorded in the non-induced cells. (E) Summary data (means ± SEM) for the current at −80 mV in cells with induced TRPM2 channels (TRPM2) and non-induced cells (control) (*n* = 6). (F) TRPM2 channels activated by H_2O_2 (500 μM). (G) H_2O_2-evoked Ca^{2+} influx via TRPM2 channels. The cells without tetracycline induction (non-induced) were used as control.

acid ring in FFA with a nicotinic acid group (as in NFA) reduced potency, in comparison with FFA (Figure 2D). The dose–response curves of 3-MFA (**1**) and FFA were determined by single concentration application and fitted with the Boltzmann equation to yield IC_{50} values of 76 ± 2.8 and 70 ± 2.5 μM respectively. The inhibitory effect of 3-MFA on TRPM2 current was partially reversible but showed a voltage-independent block.

Intracellular effect of FFA and 3-MFA
The whole-cell patch recordings were performed using pipette solutions containing 200 μM FFA or 200 μM 3-MFA. The current induced by ADP-ribose was significantly prevented by the inclusion of FFA or 3-MFA in the pipette solution comparing with the control group with ADP-ribose only

in the pipette solution (Figure 4A). The outside-out excised membrane patches also showed no effect for FFA and 3-MFA but 2-APB significantly inhibited TRPM2 channel activity (Figure 4B and C). In addition, the single channel activity was recorded in the outside-out patches that formed immediately by standard procedures after the whole-cell TRPM2 current evoked by ADP-ribose. The mean slope conductance was 66 pS, which is similar to the channel conductance of TRPM2 channels (60–64 pS) recorded by others (Perraud *et al.*, 2001; Starkus *et al.*, 2010). Perfusion with FFA (100 μM) and 3-MFA (100 μM) did not change single channel conductance and the events of channel opening. However, 2-APB (100 μM) abolished the TRPM2 single channel events (Figure 4D). These data suggest that the site of action for FFA and 3-MFA was intracellularly located.
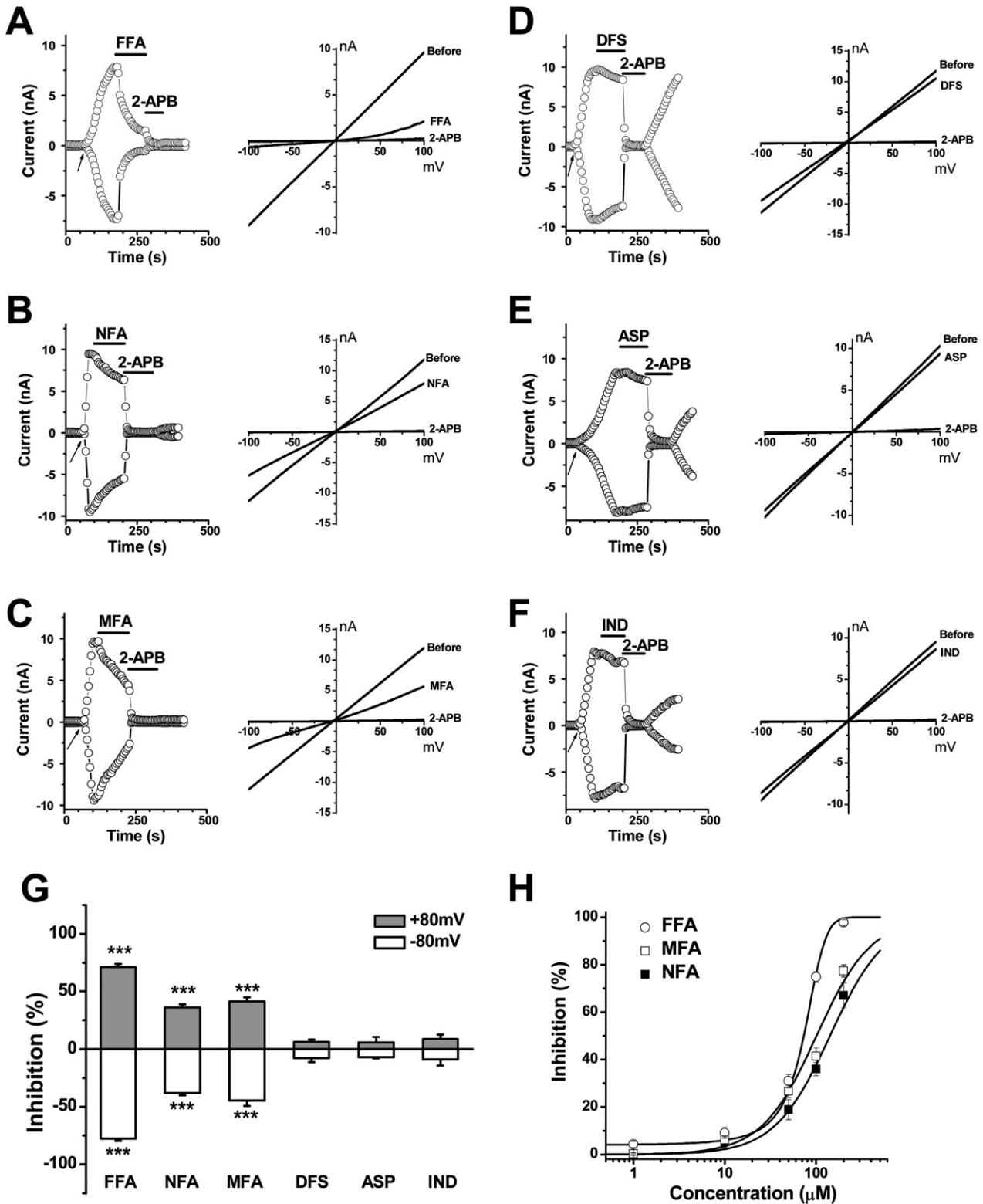
Figure 2

Effect of fenamates and non-fenamate NSAIDs on TRPM2 current. Representative time course and *IV* curves of TRPM2 channels were shown in (A–F). (A) FFA (100 µM). (B) NFA (100 µM). (C) MFA (100 µM). (D) diclofenac (DFS; 100 µM). (E) aspirin (ASP; 100 µM). (F) indomethacin (IND; 100 µM). (G) Summary data (means ± SEM) showing the percentage of inhibition of TRPM2 current. The amplitude was normalized to that blocked by 2-APB (100 µM) ($n = 3$–8). ***$P < 0.001$. (H) Concentration–response curves for FFA, MFA and NFA for the inhibition of TRPM2 current ($n = 5$–6 for each point).
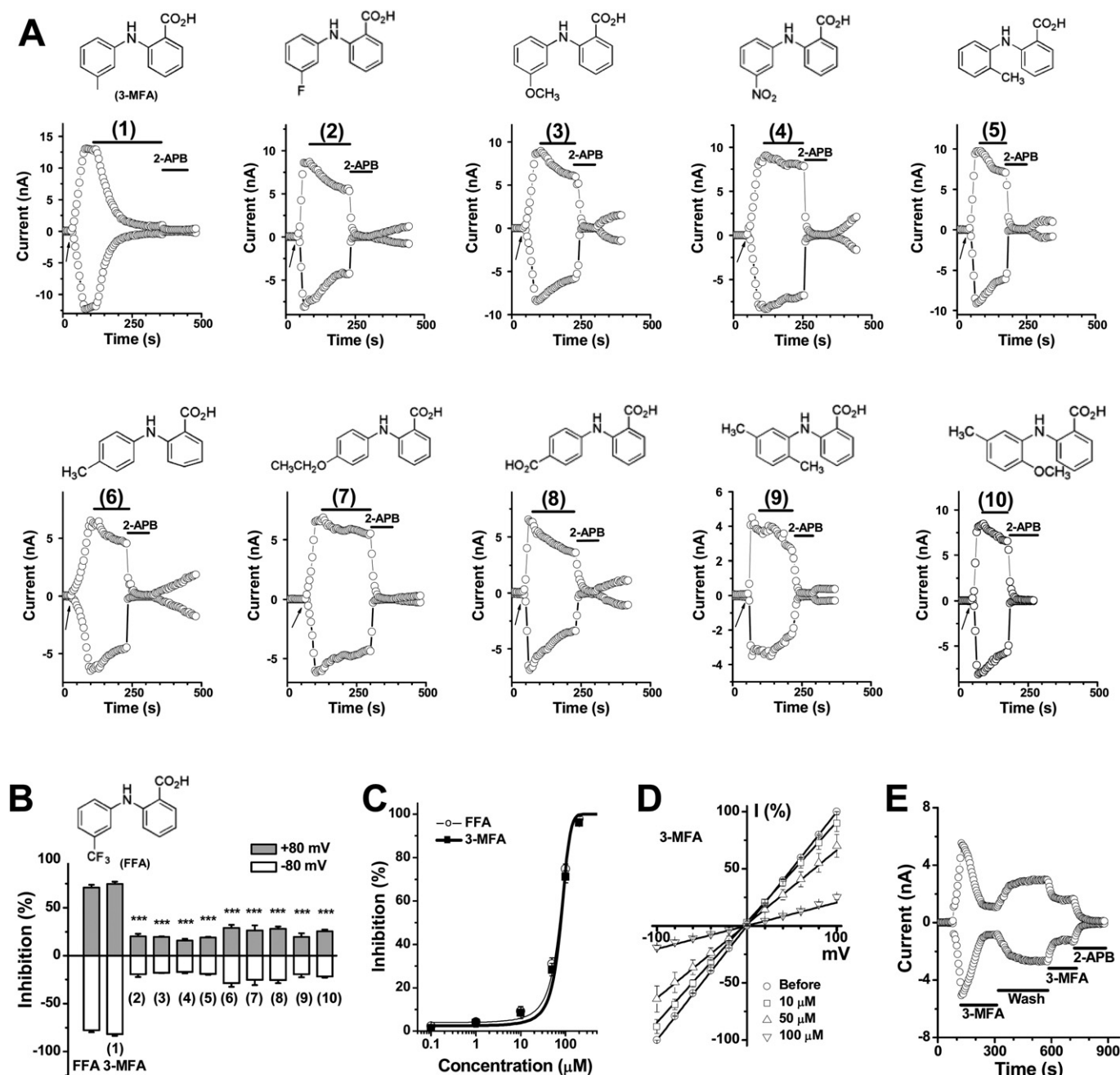
Figure 3

Synthetic fenamate analogues and the effect on TRPM2 current. (A) Time course showing the effect of fenamate analogues, compounds (**1**) to (**10**) at 100 μM. The structures are shown at the top of each panel. (B) Summary data (means ± SEM) for the effect on TRPM2 current. The current measured at ±80 mV was normalized to that blocked by 2-APB (100 μM). ***$P < 0.001$, significantly different from FFA group; ANOVA. $n = 3–6$ for each group. (C) Comparison of the concentration–response curves for 3-MFA (**1**) and FFA. (D) Current–voltage relationship and the inhibition of TRPM2 current by 3-MFA. (E) Inhibition of ADP-ribose-induced TRPM2 current by 3-MFA (100 μM) was partly reversed after wash-out and abolished by 2-APB (100 μM).

Comparison with fenamates, econazole and 2-APB

FFA, econazole and 2-APB are known to be TRPM2 channel blockers (Hill *et al.*, 2004a,b; Togashi *et al.*, 2008). Here we compared their pharmacological properties. FFA and 3-MFA

(**1**) showed a similar potency for blockade of TRPM2 channels (Figure 3C), but FFA also caused a significant Ca^{2+} release (Figure 5A). This effect was partly exerted on the endoplasmic reticulum (ER) Ca^{2+} store, because the sarco(endo)plasmic reticulum Ca^{2+}-ATPase (SERCA) blocker thapsigargin reduced by nearly half (46%), the effect of FFA-induced Ca^{2+} release
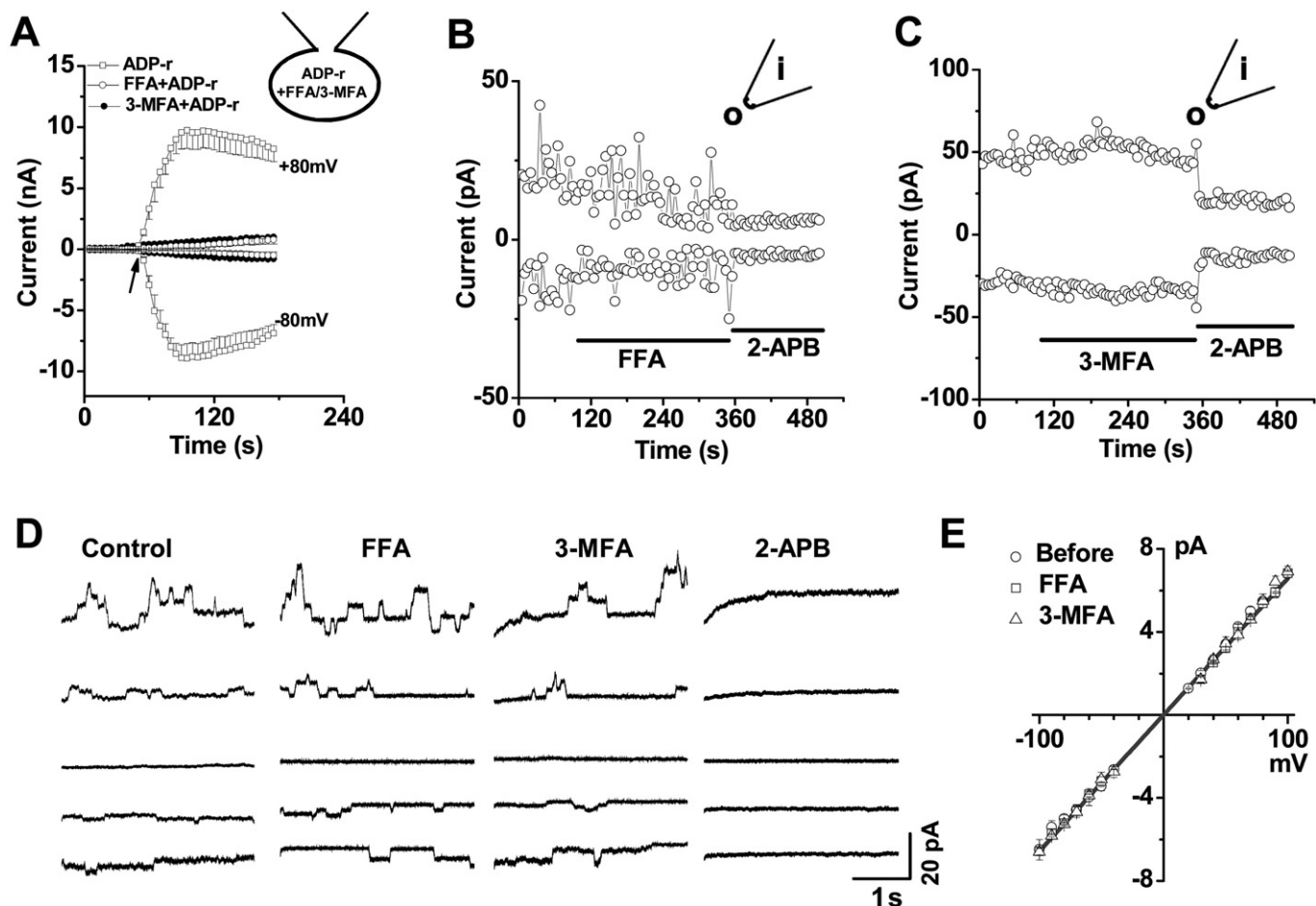
Figure 4

Effect of 3-MFA or FFA applied intracellularly. (A) Whole-cell patch was recorded in the TRPM2 cells using pipette solution containing 0.5 mM ADP-ribose (ADP-r) with or without FFA (200 μM) or 3-MFA (200 μM) ($n = 5$ for each group). (B) Example of outside-out patches showing the effect of FFA (100 μM) and 2-APB (100 μM). (C) Example of the effect of 3-MFA (100 μM) and 2-APB (100 μM). (D) Single channel activity of TRPM2 recorded by outside-out patches ($n = 4$). (E) Mean unitary current sizes for ADP-ribose-induced TRPM2 single channel events plotted against voltage. Straight lines were fitted, and the mean unitary slope conductance was 65.76 ± 0.23 pS (0.5 mM ADP-ribose). No effect of FFA (100 μM, 65.81 pS) and 3-MFA (100 μM, 65.61 pS) on the single channel conductance in the outside-out patches.

(Figure 5B). The other part of FFA-induced Ca^{2+} release could be due to mitochondrial Ca^{2+} release which has been described by us (Jiang *et al.*, 2012) and other groups (McDougall *et al.*, 1988; Poronnik *et al.*, 1992; Tu *et al.*, 2009). Although MFA had a small effect on Ca^{2+}-release, but its analogue 3-MFA (**1**) had no effect on this variable (Figure 5C and D). FFA-induced Ca^{2+} release was unrelated to the expression of TRPM2 channels, because the amplitude of the Ca^{2+} release signal in the induced cells (after tetracycline) was similar to that in the non-induced cells. These data suggested that 3-MFA was more selective than FFA and MFA as it did not affect Ca^{2+} release from intracellular stores.

Application of econazole (10 μM) inhibited TRPM2 current evoked by intracellular ADP-ribose. The onset of blockade was rapid and partly reversed by wash-out. However, econazole at 10–100 μM showed an inhibition at first and followed by a gradual increase of the whole cell current. 2-APB (100 μM) and FFA (100 μM) were unable to block the current evoked by econazole (Figure 6A–D, Supplementary Figure S1). Substitu-

tion of Na^+ with equimolar $NMDG^+$ showed a small reduction of the inward current through TRPM2 channels, but the inward current in the cells without econazole treatment was nearly abolished. In addition, the econazole-induced current was irreversible and resistant to the Cl^- channel blocker tamoxifen (10 μM) (Supplementary Figure S1C). The non-induced cells also showed the current induced by econazole (data not shown), suggesting that this econazole-induced current could be a non-selective current, which may result from the non-specific effects of antifungal drugs on membrane permeability. On the other hand, econazole (100 μM) induced significant Ca^{2+} oscillations in the T-REx cells. These oscillations were reversed on washing and inhibited by 100 μM 2-APB (Figure 6E and F). Pretreatment with the SERCA blocker thapsigargin (1 μM) prevented the Ca^{2+} oscillations (Figure 6G), suggesting that the econazole-induced Ca^{2+} oscillations were related to Ca^{2+} release from the ER.

2-APB at 100 μM nearly abolished the TRPM2 current, which was consistent with recent reports (Togashi *et al.*,
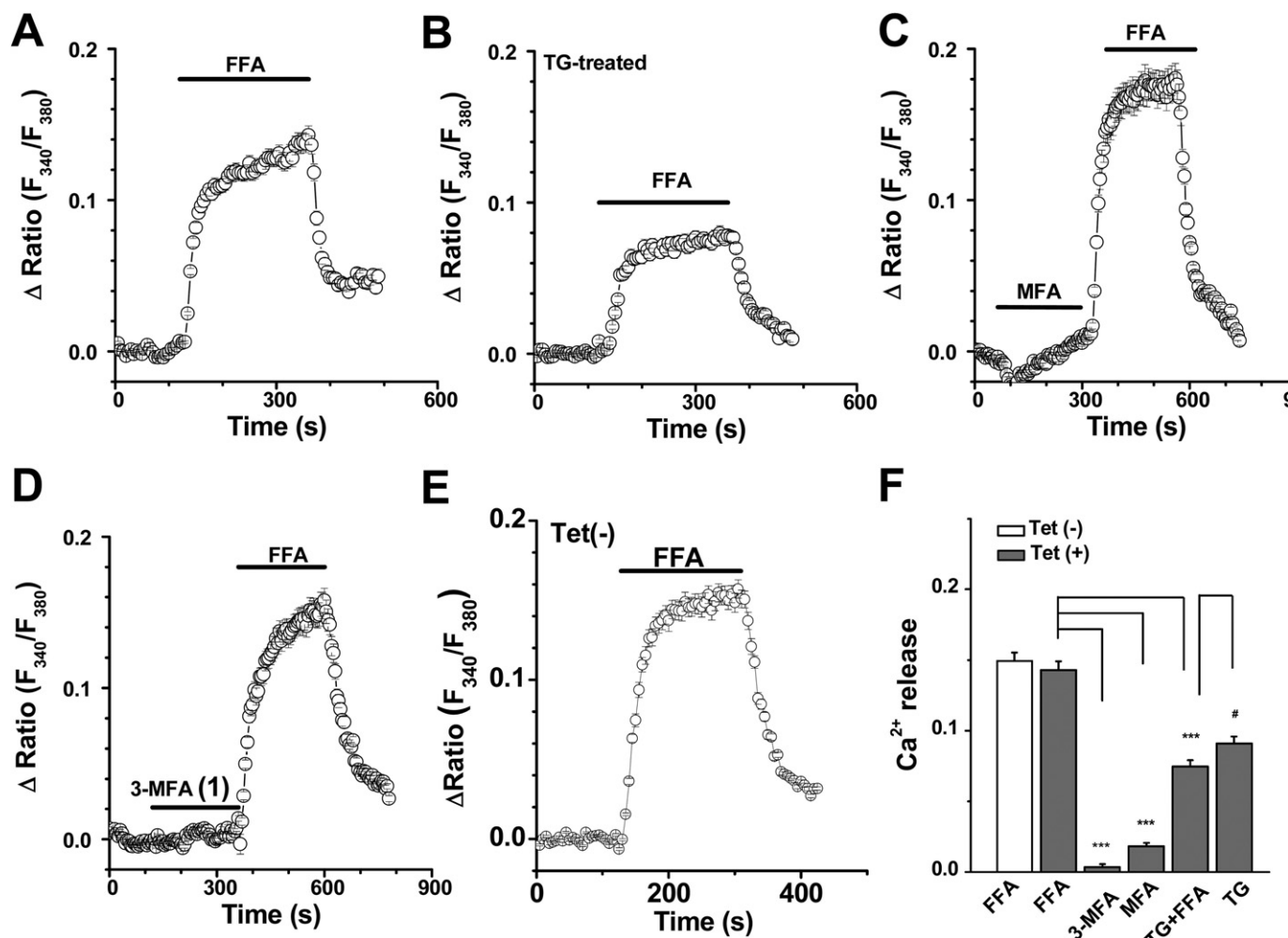
Figure 5

Ca^{2+} release induced by FFA. Cytosolic Ca^{2+} concentrations were monitored in the T-REx cells perfused with Ca^{2+}-free bath solution. (A) FFA (100 μM) induced Ca^{2+} release in the Ca^{2+}-free bath solution. (B) The FFA (100 μM) -induced Ca^{2+} release decreased in cells treated with 1 μM thapsigargin (TG). (C) Perfusion with MFA (100 μM) followed by FFA (100 μM). (D) No effect of 3-MFA (1) (100 μM) on Ca^{2+} release, but FFA (100 μM) evoked Ca^{2+} release. (E) FFA induced Ca^{2+} release in the non-induced cells [Tet(–)]. (F) Summary data (means ± SEM) for the amplitude of Ca^{2+} release signal. FFA, 3-MFA and MFA at 100 μM and TG at 1 μM were applied (n = 20–26 cells). ***$P < 0.001$, significantly different from FFA Tet(+) group. #$P < 0.05$ significantly different from TG+FFA group; ANOVA.

2008; Nazıroglu *et al.*, 2011). 2-APB not only blocked the TRPM2 current in the induced cells but also inhibited the current in the non-induced cells. The effect was rapid in onset and the current recovered fully after wash-out (see Figure 1). This result was contrary to our previous report (Xu *et al.*, 2005). After re-examining the effect of 2-APB, we believe the difference could be due to cell injury and membrane leak after long-lasting activation in our previous study. The massive Ca^{2+} influx through TRPM2 channels resulted in plasma membrane blebbing and cell shape change (Supplementary Figure S2). The non-induced TRPM2 cells had no such membrane blebbing phenomena after the membrane breakthrough with the patch pipette containing 0.5 mM ADP-ribose, suggesting that the plasma membrane blebbing was dependent on the activity of TRPM2 channels.

Discussion

In this study, we have compared the effect of some fenamate analogues, econazole and 2-APB on TRPM2 channels. Modification of the 2-phenylamino ring by substitution of the trifluoromethyl group in FFA with various substituents led to significant changes in channel blocking activity. The introduction of a *meta* –CH$_3$ group into the phenylamino ring (3-MFA, **1**) yielded a more selective inhibitor of TRPM2 channels that did not affect Ca^{2+} release from intracellular stores, but with a potency similar to FFA. This compound could therefore offer a new and useful tool for the selective study of this TRPM2 channel.

FFA and its analogues inhibit several types of ion channels. Early studies have shown that fenamates inhibited Ca^{2+}-activated Cl$^-$ channels (Korn *et al.*, 1991; Hogg *et al.*,
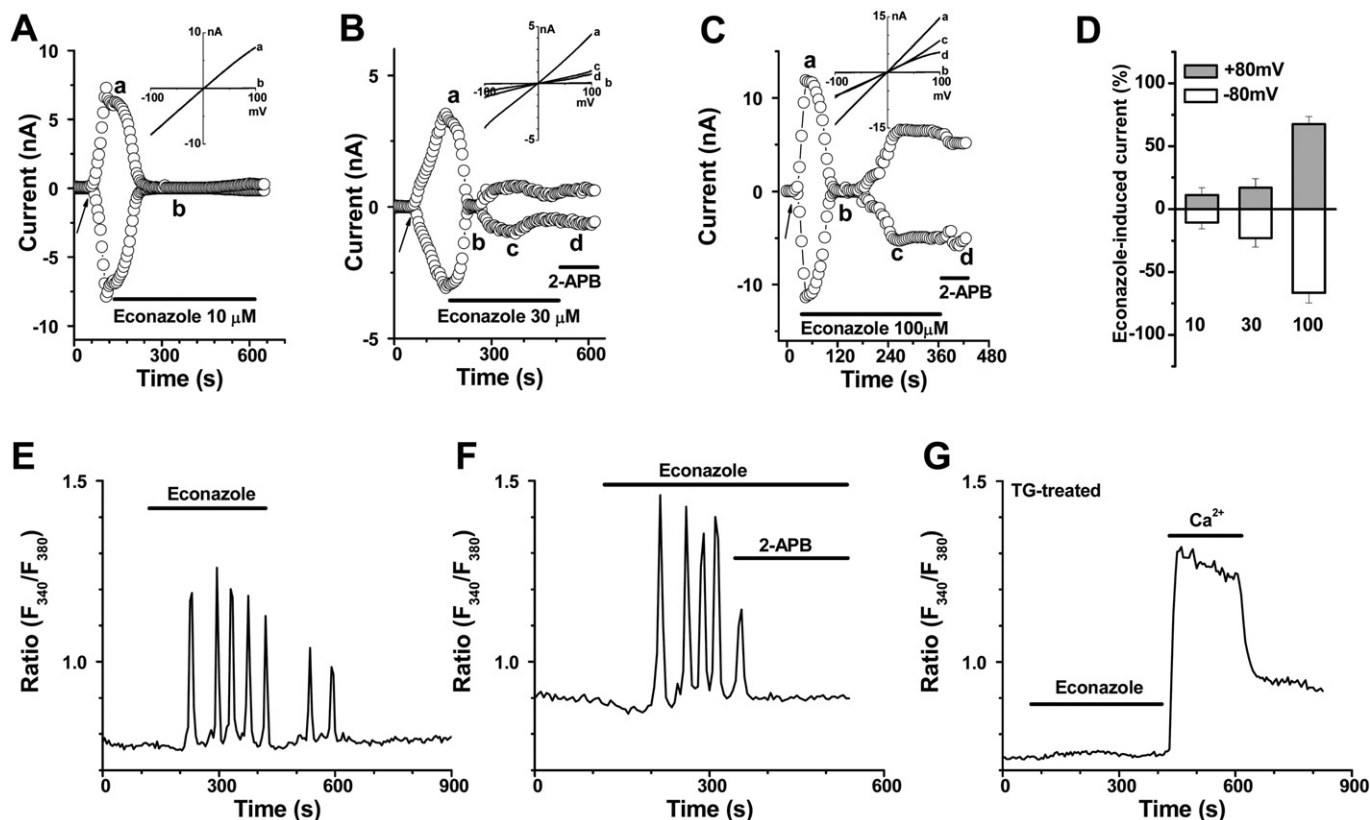
Figure 6

Effect of econazole on TRPM2 currents. (A–C) Examples of the time course for TRPM2 current inhibited by econazole (10, 30, 100 μM) and followed by an increase of the whole cell current. The *IV* curves are shown in the inset and the traces labelled as a, b, c, and d are indicated in the corresponding time course. (D) Summary data (means ± SEM) for current evoked by econazole. (E) Cytosolic Ca^{2+} oscillations induced by econazole (100 μM) in HEK-293 T-REx cells. (F) Ca^{2+} oscillations inhibited by 2-APB (100 μM) in the T-REx cells. (G) Ca^{2+} levels in cells pretreated with thapsigargin (TG; 1 μM) for 30 min and then perfused with econazole (100 μM) and then with a bath solution containing 1.5 mM Ca^{2+}.

1994; Shaw *et al*., 1995), Ca^{2+}-activated K^+ channels (Greenwood and Large, 1995), 1-oleoyl-2-acetyl-*sn*-glycerol (OAG)-sensitive cationic current (Jung *et al*., 2002), Ca^{2+}-activated non-selective cationic channel (Yamashita and Isa, 2003) and a cationic channel in cardiac myocytes (Macianskiene *et al*., 2010). For the TRP channel family, FFA activated TRPC6 (Inoue *et al*., 2001) and TRPA1 (Hu *et al*., 2010), but inhibited TRPM2, TRPM3, TRPM4 and TRPM5 channels (Hill *et al*., 2004a; Ullrich *et al*., 2005; Harteneck *et al*., 2007; Wilkinson *et al*., 2008; Klose *et al*., 2011; Naziroglu *et al*., 2011), suggesting that fenamate analogues are useful tools in the study of TRP cationic channels. However, there are several reports that FFA induced mitochondrial Ca^{2+} release (Poronnik *et al*., 1992; Hu *et al*., 2010), which could indirectly alter the activity of TRP channels, especially the Ca^{2+}-sensitive forms including TRPM2 (Tang *et al*., 2001; McHugh *et al*., 2003; Zeng *et al*., 2004). In order to find a relatively selective channel blocker, we modified the structure of FFA and found that 3-MFA (**1**) was the most promising compound among the analogues we synthesized. This compound had no effect on Ca^{2+} release and showed a slight inhibition of TRPC4 and TRPC5 channels (Jiang *et al*., 2012) but was potent as FFA in blocking TRPM2 channels, suggesting that 3-MFA (**1**) was a more selective compound for analysing TRPM2 channel func-

tion. However, further study is still required to characterize its specificity, because we have not tested the effect of 3-MFA on other TRPM channels or native cationic channels. The IC_{50} value for FFA was lower in this study than that measured by the FLIPR^{tetra} system (Klose *et al*., 2011), which could be due to different methodology and the channel activator used. We noticed that the TRPM2 current showed significant rundown after full current development, so we used a single concentration to determine the IC_{50}, rather than a series of cumulative concentrations. In addition, the percentage of inhibition was measured at 100 s after perfusion with each tested reagent and the current rundown was corrected by linear fitting.

Econazole is an antifungal imidazole and early reports showed that it inhibited I_{CRAC} channels (Franzius *et al*., 1994; Gamberucci *et al*., 1998). Inhibition of TRPM2 channels was reported by Hill *et al*. (2004b), and the binding site on TRPM2 channels was extracellularly located. Our data also showed potent inhibition of TRPM2 channels by econazole, with 10 μM producing nearly full block of TRPM2 current. However, longer perfusion with econazole evoked a non-specific current. The amplitude of the non-specific current induced by econazole was concentration-dependent and achieved nano-amp values for the whole cell current, when

high concentrations of econazole (100 μM) were applied. 2-APB and FFA did not inhibit the econazole-evoked current. Substitution of Na^+ with NMDG slightly reduced the inward current, and Cl^- channel blocker tamoxifen did not affect the current. These findings suggest that the econazole-induced current was not mediated by endogenous TRPC channels or gap junctional channels or a Cl^- channel, but was a non-specific current that could be due to the membrane hyperpermeability caused by antifungal drugs (Georgopapadakou et al., 1987; Matsui et al., 2008). In addition, we found econazole at 100 μM caused significant cytosolic Ca^{2+} oscillations. These oscillations were probably due to inositol trisphosphate-mediated Ca^{2+} release from ER Ca^{2+} stores (Hajnoczky and Thomas, 1997), because depletion of the ER Ca^{2+} stores by the SERCA blocker thapsigargin or the inhibition of inositol trisphosphate receptors by high concentration of 2-APB can abolished the activity. Such cytosolic Ca^{2+} increase was also reported by other groups with lower concentrations of econazole in human osteosarcoma cells (Chang et al., 2005), corneal epithelial cells (Chien et al., 2008) and lymphocytes (Mason et al., 1993), suggesting that econazole should be used with caution as a TRPM2 channel inhibitor.

The pH and temperature dependence of TRPM2 channels have been described (Hill et al., 2004a; Togashi et al., 2008; Yang et al., 2011). In our study, we did not measure blocking activities of 3-MFA or FFA at different pH or temperature. All the experiments were performed at room temperature (23–25°C) with normal bath and pipette solutions. Unlike 2-APB, which showed a rapid and reversible inhibition of TRPM2 channels, 3-MFA and FFA only showed a small recovery after wash-out, which was comparable to that after FFA (Hill et al., 2004a). The block of TRPM2 by 3-MFA was voltage-independent and its site of action was intracellularly located, in contrast to clotrimazole and 2-APB which are known to act on an extracellular site on the channel (Hill et al., 2004b). The TRPM2 channels are ubiquitously expressed Ca^{2+}-permeable channels. A relatively large TRPM2-like endogenous current has been reported in the rat insulinoma cell line CRI-G1, which was blocked by FFA (Hill et al., 2004a). We have not tested the effect of 3-MFA on such cells, but we have examined the effect of 3-MFA, FFA and 2-APB on the endogenous current in the non-induced HEK293 cells. 3-MFA only slightly changed the endogenous current, whereas both FFA and 2-APB showed clear inhibition and their inhibition was fully reversible after wash-out (data not shown), suggesting that the endogenous current may have different properties from the expressed TRPM2 channels or could be a non-specific current, sensitive to 2-APB and FFA, which needs to be further studied.

In conclusion, our results show that some fenamates, econazole and 2-APB are all useful blockers of TRPM2 channels. However, FFA, econazole and 2-APB have non-specific effects on intracellular Ca^{2+} movement and on other channels, so these unwanted effects should be considered when the blockers are used for pharmacological studies of TRPM2 channels. The fenamate analogue, 3-MFA (**1**), was as potent as FFA but had no effect on Ca^{2+} release from intracellular stores and may thus be used as a more selective TRPM2 channel blocker. However, we have not yet tested the effect of 3-MFA on other ion channels, which are targeted by FFA; therefore, the specificity and utility of 3-MFA as a TRPM2

blocker need to be further investigated. The information on structure-activity correlations would be useful for further improvement of the design of new fenamate-based channel blockers.

Acknowledgements

Conflicts of interest

None.

References

Alexander SP, Mathie A, Peters JA (2011). Guide to Receptors and Channels (GRAC), 5th edition. Br J Pharmacol 164 (Suppl. 1): S1–324.

Chang HT, Liu CS, Chou CT, Hsieh CH, Chang CH, Chen WC et al. (2005). Econazole induces increases in free intracellular Ca^{2+} concentrations in human osteosarcoma cells. Hum Exp Toxicol 24: 453–458.

Chien JM, Huang CC, Cheng HH, Lin KL, Chen WC, Tseng PL et al. (2008). Econazole-evoked $[Ca^{2+}]_i$ rise and non-Ca^{2+}-triggered cell death in rabbit corneal epithelial cells (SIRC). J Recept Signal Transduct Res 28: 567–579.

Fonfria E, Marshall IC, Boyfield I, Skaper SD, Hughes JP, Owen DE et al. (2005). Amyloid beta-peptide(1-42) and hydrogen peroxide-induced toxicity are mediated by TRPM2 in rat primary striatal cultures. J Neurochem 95: 715–723.

Foster RR, Zadeh MA, Welsh GI, Satchell SC, Ye Y, Mathieson PW et al. (2009). Flufenamic acid is a tool for investigating TRPC6-mediated calcium signalling in human conditionally immortalised podocytes and HEK293 cells. Cell Calcium 45: 384–390.

Franzius D, Hoth M, Penner R (1994). Non-specific effects of calcium entry antagonists in mast cells. Pflugers Arch 428: 433–438.

Gamberucci A, Fulceri R, Benedetti A, Bygrave FL (1998). On the mechanism of action of econazole, the capacitative calcium inflow blocker. Biochem Biophys Res Commun 248: 75–77.

Georgopapadakou NH, Dix BA, Smith SA, Freudenberger J, Funke PT (1987). Effect of antifungal agents on lipid biosynthesis and membrane integrity in Candida albicans. Antimicrob Agents Chemother 31: 46–51.

Greenwood IA, Large WA (1995). Comparison of the effects of fenamates on Ca-activated chloride and potassium currents in rabbit portal vein smooth muscle cells. Br J Pharmacol 116: 2939–2948.

Hajnoczky G, Thomas AP (1997). Minimal requirements for calcium oscillations driven by the IP3 receptor. EMBO J 16: 3533–3543.

Hara Y, Wakamori M, Ishii M, Maeno E, Nishida M, Yoshida T et al. (2002). LTRPC2 Ca^{2+}-permeable channel activated by changes in redox status confers susceptibility to cell death. Mol Cell 9: 163–173.

Harteneck C, Frenzel H, Kraft R (2007). N-(p-amylcinnamoyl)anthranilic acid (ACA): a phospholipase A(2) inhibitor and TRP channel blocker. Cardiovasc Drug Rev 25: 61–75.

Hecquet CM, Malik AB (2009). Role of H_2O_2-activated TRPM2 calcium channel in oxidant-induced endothelial injury. Thromb Haemost 101: 619–625.

Hecquet CM, Ahmmed GU, Vogel SM, Malik AB (2008). Role of TRPM2 channel in mediating H_2O_2-induced Ca^{2+} entry and endothelial hyperpermeability. Circ Res 102: 347–355.

Hill K, Benham CD, McNulty S, Randall AD (2004a). Flufenamic acid is a pH-dependent antagonist of TRPM2 channels. Neuropharmacology 47: 450–460.

Hill K, McNulty S, Randall AD (2004b). Inhibition of TRPM2 channels by the antifungal agents clotrimazole and econazole. Naunyn Schmiedebergs Arch Pharmacol 370: 227–237.

Hogg RC, Wang Q, Large WA (1994). Action of niflumic acid on evoked and spontaneous calcium-activated chloride and potassium currents in smooth muscle cells from rabbit portal vein. Br J Pharmacol 112: 977–984.

Hu H, Tian J, Zhu Y, Wang C, Xiao R, Herz JM et al. (2010). Activation of TRPA1 channels by fenamate nonsteroidal anti-inflammatory drugs. Pflugers Arch 459: 579–592.

Inoue R, Okada T, Onoue H, Hara Y, Shimizu S, Naitoh S et al. (2001). The transient receptor potential protein homologue TRP6 is the essential component of vascular alpha(1)-adrenoceptor-activated Ca^{2+}-permeable cation channel. Circ Res 88: 325–332.

Ishii M, Oyama A, Hagiwara T, Miyazaki A, Mori Y, Kiuchi Y et al. (2007). Facilitation of H_2O_2-induced A172 human glioblastoma cell death by insertion of oxidative stress-sensitive TRPM2 channels. Anticancer Res 27: 3987–3992.

Jiang H, Zeng B, Chen GL, Bot D, Eastmond S, Elsenussi SE et al. (2012). Effect of non-steroidal anti-inflammatory drugs and new fenamate analogues on TRPC4 and TRPC5 channels. Biochem Pharmacol 83: 923–931.

Jung S, Strotmann R, Schultz G, Plant TD (2002). TRPC6 is a candidate channel involved in receptor-stimulated cation currents in A7r5 smooth muscle cells. Am J Physiol Cell Physiol 282: C347–C359.

Klose C, Straub I, Riehle M, Ranta F, Krautwurst D, Ullrich S et al. (2011). Fenamates as TRP channel blockers: mefenamic acid selectively blocks TRPM3. Br J Pharmacol 162: 1757–1769.

Knowles H, Heizer JW, Li Y, Chapman K, Ogden CA, Andreasen K et al. (2011). Transient Receptor Potential Melastatin 2 (TRPM2) ion channel is required for innate immunity against Listeria monocytogenes. Proc Natl Acad Sci USA 108: 11578–11583.

Korn SJ, Bolden A, Horn R (1991). Control of action potentials and Ca^{2+} influx by the Ca^{2+}-dependent chloride current in mouse pituitary cells. J Physiol 439: 423–437.

Kraft R, Harteneck C (2005). The mammalian melastatin-related transient receptor potential cation channels: an overview. Pflugers Arch 451: 204–211.

Kraft R, Grimm C, Frenzel H, Harteneck C (2006). Inhibition of TRPM2 cation channels by N-(p-amylcinnamoyl)anthranilic acid. Br J Pharmacol 148: 264–273.

Lee YM, Kim BJ, Kim HJ, Yang DK, Zhu MH, Lee KP et al. (2003). TRPC5 as a candidate for the nonselective cation channel activated by muscarinic stimulation in murine stomach. Am J Physiol Gastrointest Liver Physiol 284: G604–G616.

McDougall P, Markham A, Cameron I, Sweetman AJ (1988). Action of the nonsteroidal anti-inflammatory agent, flufenamic acid, on calcium movements in isolated mitochondria. Biochem Pharmacol 37: 1327–1330.

McHugh D, Flemming R, Xu SZ, Perraud AL, Beech DJ (2003). Critical intracellular Ca^{2+} dependence of transient receptor potential melastatin 2 (TRPM2) cation channel activation. J Biol Chem 278: 11002–11006.

Macianskiene R, Gwanyanya A, Sipido KR, Vereecke J, Mubagwa K (2010). Induction of a novel cation current in cardiac ventricular myocytes by flufenamic acid and related drugs. Br J Pharmacol 161: 416–429.

Mason MJ, Mayer B, Hymel LJ (1993). Inhibition of Ca^{2+} transport pathways in thymic lymphocytes by econazole, miconazole, and SKF 96365. Am J Physiol 264: C654–C662.

Matsui H, Sakanashi Y, Oyama TM, Oyama Y, Yokota S, Ishida S et al. (2008). Imidazole antifungals, but not triazole antifungals, increase membrane Zn^{2+} permeability in rat thymocytes Possible contribution to their cytotoxicity. Toxicology 248: 142–150.

Mei XF, August AT, Wolf C (2006). Regioselective copper-catalyzed amination of chlorobenzoic acids: synthesis and solid-state structures of N-aryl anthranilic acid derivatives. J Org Chem 71: 142–149.

Nagamine K, Kudoh J, Minoshima S, Kawasaki K, Asakawa S, Ito F et al. (1998). Molecular cloning of a novel putative Ca^{2+} channel protein (TRPC7) highly expressed in brain. Genomics 54: 124–131.

Naziroglu M, Ozgul C, Celik O, Cig B, Sozbir E (2011). Aminoethoxydiphenyl borate and flufenamic acid inhibit Ca^{2+} influx through TRPM2 channels in rat dorsal root ganglion neurons activated by ADP-ribose and rotenone. J Membr Biol 241: 69–75.

Olah ME, Jackson MF, Li H, Perez Y, Sun HS, Kiyonaka S et al. (2009). Ca^{2+}-dependent induction of TRPM2 currents in hippocampal neurons. J Physiol 587: 965–979.

Perraud AL, Fleig A, Dunn CA, Bagley LA, Launay P, Schmitz C et al. (2001). ADP-ribose gating of the calcium-permeable LTRPC2 channel revealed by Nudix motif homology. Nature 411: 595–599.

Poronnik P, Ward MC, Cook DI (1992). Intracellular Ca^{2+} release by flufenamic acid and other blockers of the non-selective cation channel. FEBS Lett 296: 245–248.

Ramsey IS, Delling M, Clapham DE (2006). An introduction to TRP channels. Annu Rev Physiol 68: 619–647.

Sano Y, Inamura K, Miyake A, Mochizuki S, Yokoi H, Matsushime H et al. (2001). Immunocyte Ca^{2+} influx system mediated by LTRPC2. Science 293: 1327–1330.

Shaw T, Lee RJ, Partridge LD (1995). Action of diphenylamine carboxylate derivatives, a family of non-steroidal anti-inflammatory drugs, on $[Ca^{2+}]_i$ and Ca^{2+}-activated channels in neurons. Neurosci Lett 190: 121–124.

Starkus JG, Fleig A, Penner R (2010). The calcium-permeable non-selective cation channel TRPM2 is modulated by cellular acidification. J Physiol 588: 1227–1240.

Tang J, Lin Y, Zhang Z, Tikunova S, Birnbaumer L, Zhu MX (2001). Identification of common binding sites for calmodulin and inositol 1,4,5-trisphosphate receptors on the carboxyl termini of trp channels. J Biol Chem 276: 21303–21310.

Togashi K, Inada H, Tominaga M (2008). Inhibition of the transient receptor potential cation channel TRPM2 by 2-aminoethoxydiphenyl borate (2-APB). Br J Pharmacol 153: 1324–1330.

Tu P, Brandolin G, Bouron A (2009). The anti-inflammatory agent flufenamic acid depresses store-operated channels by altering mitochondrial calcium homeostasis. Neuropharmacology 56: 1010–1016.

Uchida K, Dezaki K, Damdindorj B, Inada H, Shiuchi T, Mori Y et al. (2010). Lack of TRPM2 impaired insulin secretion and glucose metabolisms in mice. Diabetes 60: 119–126.

Ullrich ND, Voets T, Prenen J, Vennekens R, Talavera K, Droogmans G et al. (2005). Comparison of functional properties of the Ca^{2+}-activated cation channels TRPM4 and TRPM5 from mice. Cell Calcium 37: 267–278.

Wehage E, Eisfeld J, Heiner I, Jungling E, Zitt C, Luckhoff A (2002). Activation of the cation channel long transient receptor potential channel 2 (LTRPC2) by hydrogen peroxide. A splice variant reveals a mode of activation independent of ADP-ribose. J Biol Chem 277: 23150–23156.

Wehrhahn J, Kraft R, Harteneck C, Hauschildt S (2010). Transient receptor potential melastatin 2 is required for lipopolysaccharide-induced cytokine production in human monocytes. J Immunol 184: 2386–2393.

Wilkinson JA, Scragg JL, Boyle JP, Nilius B, Peers C (2008). H$_2$O$_2$-stimulated Ca^{2+} influx via TRPM2 is not the sole determinant of subsequent cell death. Pflugers Arch 455: 1141–1151.

Xu SZ, Zeng F, Boulay G, Grimm C, Harteneck C, Beech DJ (2005). Block of TRPC5 channels by 2-aminoethoxydiphenyl borate: a differential, extracellular and voltage-dependent effect. Br J Pharmacol 145: 405–414.

Xu SZ, Zhong W, Watson NM, Dickerson E, Wake JD, Lindow SW et al. (2008). Fluvastatin reduces oxidative damage in human vascular endothelial cells by upregulating Bcl-2. J Thromb Haemost 6: 692–700.

Xu SZ, Zeng B, Daskoulidou N, Chen GL, Atkin SL, Lukhele B (2012). Activation of TRPC cationic channels by mercurial compounds confers the cytotoxicity of mercury exposure. Toxicol Sci 125: 56–68.

Yamamoto S, Shimizu S, Kiyonaka S, Takahashi N, Wajima T, Hara Y et al. (2008). TRPM2-mediated Ca^{2+} influx induces chemokine production in monocytes that aggravates inflammatory neutrophil infiltration. Nat Med 14: 738–747.

Yamashita T, Isa T (2003). Fulfenamic acid sensitive, Ca^{2+}-dependent inward current induced by nicotinic acetylcholine receptors in dopamine neurons. Neurosci Res 46: 463–473.

Yang KT, Chang WL, Yang PC, Chien CL, Lai MS, Su MJ et al. (2006). Activation of the transient receptor potential M2 channel and poly(ADP-ribose) polymerase is involved in oxidative stress-induced cardiomyocyte death. Cell Death Differ 13: 1815–1826.

Yang W, Manna PT, Zou J, Luo J, Beech DJ, Sivaprasadarao A et al. (2011). Zinc inactivates melastatin transient receptor potential 2 channels via the outer pore. J Biol Chem 286: 23789–23798.

Zeng F, Xu SZ, Jackson PK, McHugh D, Kumar B, Fountain SJ et al. (2004). Human TRPC5 channel activated by a multiplicity of signals in a single cell. J Physiol 559: 739–750.

Zhang W, Chu X, Tong Q, Cheung JY, Conrad K, Masker K et al. (2003). A novel TRPM2 isoform inhibits calcium influx and susceptibility to cell death. J Biol Chem 278: 16222–16229.

Supporting information

Additional Supporting Information may be found in the online version of this article:

Figure S1 Econazole-induced current and the effect of NMDG$^+$, tamoxifen and FFA. (A) TRPM2 current was induced by 0.5 mM ADP-ribose in the pipette solution. Perfusion with econazole (30 μM) inhibited the TRPM2 current and followed by the activation of another current. Perfusion with solutions containing NMDG$^+$ (140 mM), an equimolar substitute for Na$^+$, slightly reduced the inward current. (B) TRPM2 current inhibited by Na$^+$ substitution with NMDG$^+$ in the cells without econazole treatment. (C) Effect of FFA (100 μM) on econazole-induced current. (D) Effect of tamoxifen (10 μM).
Figure S2 Plasma membrane blebbing in cells with induced TRPM2 channels, during the patch recording. (A) Image showing the cells after the formation of whole-cell configuration for 3 min. (B) The same cells as in (A) photographed at 10 min after TRPM2 channels had been fully activated. Membrane blebbing is indicated by arrow.

Please note: Wiley-Blackwell are not responsible for the content or functionality of any supporting materials supplied by the authors. Any queries (other than missing material) should be directed to the corresponding author for the article.

Effect of non-steroidal anti-inflammatory drugs and new fenamate analogues on TRPC4 and TRPC5 channels

Hongni Jiang [a], Bo Zeng [a], Gui-Lan Chen [a], David Bot [a], Sarah Eastmond [b], Sandra E. Elsenussi [b], Stephen L. Atkin [a], Andrew N. Boa [b], Shang-Zhong Xu [a,*]

[a] Centre for Cardiovascular and Metabolic Research, Hull York Medical School, University of Hull, Hull HU6 7RX, UK
[b] Department of Chemistry, University of Hull, UK

ABSTRACT

Non-steroidal anti-inflammatory drugs (NSAIDs) are widely used anti-inflammatory therapeutic agents, among which the fenamate analogues play important roles in regulating intracellular Ca^{2+} transient and ion channels. However, the effect of NSAIDs on TRPC4 and TRPC5 is still unknown. To understand the structure–activity of fenamate analogues on TRPC channels, we have synthesized a series of fenamate analogues and investigated their effects on TRPC4 and TRPC5 channels.

Human TRPC4 and TRPC5 cDNAs in tetracycline-regulated vectors were transfected into HEK293 T-REx cells. The whole cell current and Ca^{2+} movement were recorded by patch clamp and calcium imaging, respectively.

Flufenamic acid (FFA), mefenamic acid (MFA), niflumic acid (NFA) and diclofenac sodium (DFS) showed inhibition on TRPC4 and TRPC5 channels in a concentration-dependent manner. The potency was FFA > MFA > NFA > DFS. Modification of 2-phenylamino ring by substitution of the trifluoromethyl group in FFA with –F, –CH₃, –OCH₃, –OCH₂CH₃, –COOH, and –NO₂ led to the changes in their channel blocking activity. However, 2-(2′-methoxy-5′-methylphenyl)aminobenzoic acid stimulated TRPC4 and TRPC5 channels. Selective COX1-3 inhibitors (aspirin, celecoxib, acetaminophen, and indomethacin) had no effect on the channels. Longer perfusion (>5 min) with FFA (100 μM) and MFA (100 μM) caused a potentiation of TRPC4 and TRPC5 currents after their initial blocking effects that appeared to be partially mediated by the mitochondrial Ca^{2+} release.

Our results suggest that fenamate analogues are direct modulators of TRPC4 and TRPC5 channels. The substitution pattern and conformation of the 2-phenylamino ring could alter their blocking activity, which is important for understanding fenamate pharmacology and new drug development targeting the TRPC channels.

© 2012 Elsevier Inc. All rights reserved.

1. Introduction

The transient receptor potential (TRP) channel family is a class of Ca^{2+}-permeable channels. To date, 28 mammalian TRP channels have been identified and divided into six subfamilies on the basis of amino acid sequence homology: TRPC ("canonical"), TRPM ("melastatin"), TRPV ("vanilloid"), TRPA ("ankyrin"), TRPML ("mucolipin"), and TRPP (or PKD) ("polycystin"). The canonical TRP subfamily (TRPC) has seven members that can be grouped into three subgroups: TRPC1/4/5, TRPC3/6/7, and TRPC2 (a pseudogene in human) [1]. Human TRPC channels seem to be ubiquitously distributed and mediate the Ca^{2+} influx evoked by G-protein coupled receptor activation or/and Ca^{2+} store depletion which are involved in many cellular functions, such as cell proliferation, apoptosis, secretion, smooth muscle contraction and migration [2–4]. TRPCs have been demonstrated as the potential therapeutic targets for neointimal growth, segmental glomerulosclerosis, overexposure to mercury, and rheumatoid arthritis [2–7]. Therefore, the identification of regulators of these channels is important for understanding their physiological properties in native cells that may lead to new therapeutic agents.

Non-steroidal anti-inflammatory drugs (NSAIDs) are widely used for the treatment of fever, pain and inflammation. Some like aspirin have the potential for the prevention of ischemic heart diseases, but some NSAIDs may increase the cardiovascular risk, such as the fenamate analogue diclofenac [8–11]. The cardiovascular risk associated with NSAIDs seems to be not determined by the selectivity of COX-2 [8]. In addition, the risk of some types of cancer was reduced by aspirin [12,13] and non-aspirin NSAIDs [14]. These observations suggest that mechanisms other than COX-2 inhibition may exist. Indeed, several possible mechanisms have been proposed for the action of NSAIDs including anti-proliferative

effects by regulating several target genes [12], stabilization of DNA mismatch repair [15], and regulation of cytosolic and mitochondrial Ca^{2+} homeostasis [12,16].

The relevance of NSAIDs to Ca^{2+} signalling has been recognized through the inhibition of production of prostaglandins and leukotrienes from arachidonic acid (AA) by cyclooxygenase (COX) inhibition, and AA and its metabolites themselves can influence Ca^{2+} influx through a number of Ca^{2+}-permeable channels [17–19]. In addition, AA release from membrane phospholipids by phospholipase A2 (PLA2) is also Ca^{2+}-related, since the group IVA PLA2 (also known as cytosol PLA2α) activation is Ca^{2+}-dependent [20]. These indirect effects on Ca^{2+} signal through COX inhibition could be a class effect of NSAIDs. On the other hand, the PLA2 inhibitor N-(p-amylcinnamoyl)anthranilic acid (ACA) inhibited TRPM2 channels, but PLA2 inhibitors without the skeleton of anthranilic acid had no effect on the channel [21], suggesting the parent structure of anthranilic acid is essential for the channel blocking effect. The fenamate NSAIDs are anthranilic acid derivatives with structural similarity to ACA [22], and their effects on a variety of channels have been demonstrated including the Ca^{2+}-activated Cl$^-$ channels, the voltage-dependent Na$^+$ or Ca^{2+} channels, and the TRP channels [23], for example, flufenamic acid (FFA) inhibited TRPM2, TRPM4, TRPM5, TRPC3, and TRPC5 [24,25], but activated TRPC6 [26–28] and TRPA1 [29]. These observations indicated that NSAIDs can influence intracellular Ca^{2+} level or Ca^{2+}-permeable channels in both direct and indirect ways, and the compounds with the skeleton of anthranilic acid are critical for the direct effect. Therefore, we hypothesized that non-fenamate NSAIDs may exert their effects mainly through PLA2/COX pathway or other mechanisms, while the fenamate NSAIDs could modulate Ca^{2+}-permeable channel activity directly. Structure modification on the fenamate skeleton could directly alter the potency of the channel blocking effect.

To test our hypothesis, we examined the effects of fenamate analogues, non-fenamate NSAIDs, and selective COX1-3 inhibitors on TRPC4 and TRPC5 channels. The subgroup of TRPC4/5 was used in this study, because the current for TRPC4 and TRPC5 is robust and stable after channel activation and therefore suitable for screening new drugs to address the unknown effect of NSAIDs on TRPC4/5 channels. To understand the structure–activity relationship of fenamates, we synthesized fenamate analogues by the 2-phenylamino ring modification and compared their effects on the TRPC channels. Moreover, as several reports have suggested that NSAIDs may interfere with mitochondria Ca^{2+} release [30,31], the involvement of intracellular Ca^{2+} homeostasis in the TRPC channel activity regulated by NSAIDs was also investigated.

2. Materials and methods

2.1. Cell culture and transfection

Human TRPC4α (GenBank accession number NM_016179) and TRPC5 (AF054568) in a tetracycline-regulatory vector were transfected into HEK-293 T-REx cells (Invitrogen, Paisley, UK). TRPC4 was tagged with enhanced yellow fluorescent protein (EYFP) at the N-terminus. The expression was induced by 1 μg ml^{-1} tetracycline for 48–72 h before recording. The non-induced cells without addition of tetracycline were used as control. Cells were grown in DMEM-F12 medium (Invitrogen, Paisley, UK) containing 10% foetal calf serum (FCS), 100 units ml^{-1} penicillin and 100 μg ml^{-1} streptomycin. Cells were maintained at 37 °C under 95% air and 5% CO$_2$ and seeded on coverslips prior to experiments.

2.2. Smooth muscle cell isolation and culture

Eight-week-old male rats were killed by inhalation of CO$_2$ in accordance with the Schedule 1 in the Code of Practice of UK Animals Scientific Procedures Act 1986. The thoracic aorta was dissected out and the adventitia was carefully removed. The endothelium was removed by gently rubbing the luminal surface with a curved forceps. The smooth muscle layer was cut into 0.5 mm^2 segments and cultured in DMEM-F12 including 10% FBS and antibiotics for cell expansion. The cultured smooth muscle cells at passage 4–5 were used for calcium imaging experiment.

2.3. Electrophysiological recordings

Whole-cell clamp was performed at room temperature (23–26 °C) [5]. Briefly, signal was amplified with an Axoclamp 2B or Axopatch B200 patch clamp amplifier and controlled with pClamp software 10. A 1-s ramp voltage protocol from −100 mV to +100 mV was applied at a frequency of 0.2 Hz from a holding potential of 0 mV. Signals were sampled at 10 kHz and filtered at 1 kHz. The glass microelectrode with a resistance of 3–5 MΩ was used. The 200 nM Ca^{2+} buffered pipette solution contained 115 CsCl, 10 EGTA, 2 MgCl$_2$, 10 HEPES, and 5.7 CaCl$_2$ in mM, pH was adjusted to 7.2 with CsOH and osmolarity was adjusted to ~290 mOsm with mannitol, and the calculated free Ca^{2+} was 200 nM using EQCAL (Biosoft, Cambridge, UK). The standard bath solution contained (mM): 130 NaCl, 5 KCl, 8 D-glucose, 10 HEPES, 1.2 MgCl$_2$ and 1.5 CaCl$_2$. The pH was adjusted to 7.4 with NaOH.

2.4. Ca^{2+} measurements

The rat aortic smooth muscle cells were preincubated with 2 μM fura-PE3 AM at 37 °C for 30 min in Ca^{2+}-free bath solution, followed by a 20-min wash period in the standard bath solution at room temperature. Fura-PE3 fluorescence was monitored with an inverted epifluorescence microscope (Nikon Ti-E, Japan). A xenon arc lamp provided excitation light, the wavelength of which was selected by a Nikon imaging system controlled by software Element 3.0. Emission was collected via 510 nm filter for fura-PE3 AM and a cooled Orca-R2 CCD camera (Hamamatsu, Japan). Images were analyzed using regions of interest (ROIs), which selected parts of the image frame corresponding to individual smooth muscle cells. The ratio of Ca^{2+} dye fluorescence (F_{340}/F_{380}) was measured by NIS-Element Ca^{2+} imaging software. Agents were applied to smooth muscle cells using a continuous bath perfusion system with a flow rate of 4 ml min^{-1}. All the experiments were performed at room temperature.

2.5. Reagents and drugs

All general salts and reagents were purchased from Sigma–Aldrich (Poole, UK). FFA, mefenamic acid (MFA), niflumic acid (NFA), diclofenac sodium (DFS), aspirin (ASP), acetaminophen (APAP), indomethacin (IND), gadolinium chloride (Gd^{3+}), 2-aminoethoxydiphenyl borate (2-APB), cyclosporine A, and foetal calf serum were purchased from Sigma–Aldrich. Celecoxib (CXB) was purchased from Cayman Chemical (Ann Arbor, MI, USA) and Fura-PE3 AM from Invitrogen (Paisley, UK). Fura-PE3 AM (5 mM) and 2-APB (100 mM) were made up as stock solutions in 100% dimethyl sulphoxide (DMSO). Ten fenamate derivatives (Fig. 2, table entries 1–10) were synthesized by the copper-catalysed coupling of either 2-chloro- or 2-bromobenzoic acid with the appropriate aniline derivative [32]. In the case of entry 5 [2-(4′-carboxyphenylamino)benzoic acid] ethyl 4-aminobenzoate was used but the ethyl ester group suffered in situ hydrolysis. Products gave satisfactory ^{1}H,^{13}C-NMR and mass spectra and their purity was estimated to be >95%.

2.6. Statistics

Data are expressed as mean ± S.E.M. where *n* is the cell number for electrophysiological recordings and Ca^{2+} imaging. Data sets were compared using paired *t*-test for the results before and after treatment, or the ANOVA Dunnett's post hoc analysis for comparing more than two groups with significance indicated if $P < 0.05$.

3. Results

3.1. Effect of fenamates on TRPC4 and TRPC5 channels

To examine the effect of fenamates on TRPC4 and TRPC5 channels, the whole-cell current was recorded in HEK-293 cells stably transfected with human TRPC4 or TRPC5. The expression
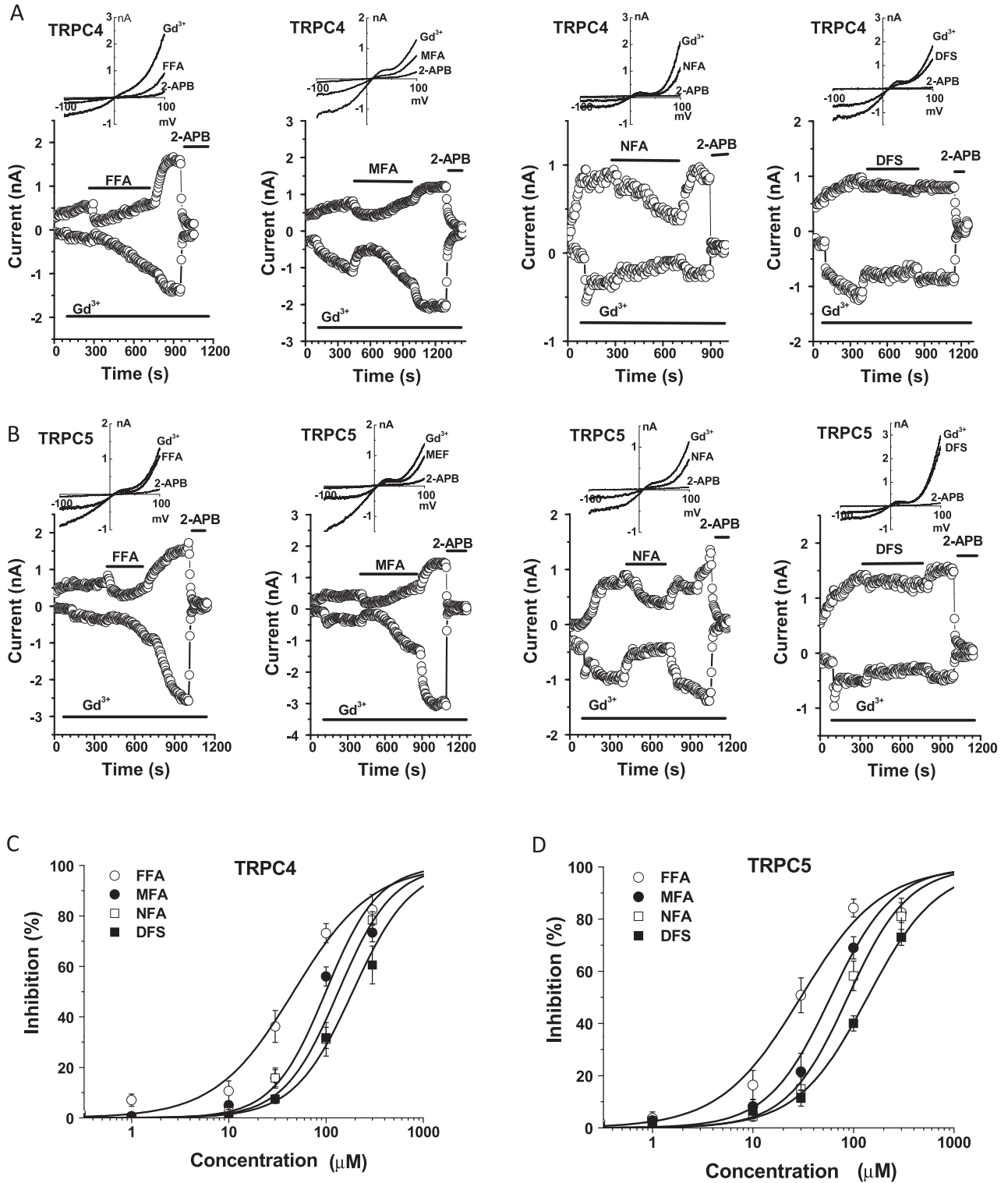
Fig. 1. Effect of fenamates on TRPC4 and TRPC5 channels. Whole cell currents in the HEK-293 T-REx cells transfected with TRPC4 and TRPC5 were recorded by whole-cell patch clamp. (A) The time course (lower) and IV curve (upper) for the effect of fenamates (FFA, MFA, NFA, and DFS) at 100 μM on TRPC4 channel. Gd^{3+} (100 μM) was used as a channel activator, and 2-APB (100 μM) was used at the end of fenamate perfusion. The current amplitude was measured at ±80 mV. (B) Similar to (A), but TRPC5 current was recorded. (C) Concentration–response curves for FFA, MFA, NFA, and DFS on TRPC4 channel (*n* = 6 for each group). (D) Concentration–response curves for TRPC5 (*n* = 6 for each group).

of TRPC4 and TRPC5 was induced by tetracycline and the current was characterized by the Gd^{3+} activation with a unique "N" shaped current–voltage (*IV*) relationship, and by fully blockade by 100 μM 2-APB (Fig. 1). FFA, MFA, NFA and DFS significantly inhibited the TRPC4 and TRPC5 currents in a concentration-dependent manner. The IC_{50} for FFA, MFA, NFA and DFS on TRPC4 was 55 $\pm$ 5 μM, 84 $\pm$ 8 μM, 102 $\pm$ 9 μM, and 138 $\pm$ 7 μM, respectively; and the IC_{50} for TRPC5 was 37 $\pm$ 5 μM, 80 $\pm$ 5 μM, 80 $\pm$ 9 μM, and 170 $\pm$ 9 μM, respectively. These data suggested that fenamates are inhibitors on TRPC4 and TRPC5 channels. The potency of inhibition was FFA > MFA > NFA > DFS.

3.2. Synthesis of fenamate analogues and the effect on TRPC4

Ten analogues were synthesized based on the 2-phenylamino-benzoic acid skeleton replacing the trifluoromethyl group of FFA with –F, –CH_3, –OCH_3, –OCH_2CH_3, –COOH, and –NO_2 substituents at various positions in the 2-phenylamino ring (Fig. 2A). The effect of these analogues at 100 μM on the TRPC4 current was compared with FFA by whole-cell patch recording. The substitution with –CH_3

(**1**), single –F atom (**2**), –OCH_3 (**3**) and –NO_2 (**4**) reduced the potency of inhibition on TRPC4 channel, and the percentage of inhibition was 67%, 40%, 32%, and 14% of the FFA inhibition (100%), respectively (Fig. 2B). The position of a single methyl substituent (analogue **1**, **5**, and **6**) also affected the potency (Fig. 2C). The substitution of –CH_3 at R^4 with –OCH_2CH_3 (**7**) increased the blocking activity with a similar potency on the inward current, however the introduction of –COOH (**8**) to the ring in the same position showed the loss of blocking effect (Fig. 2D), suggesting that the polarity of modifying group at R^4 could be important. In addition, we observed the effect of modifications with two substituents in the ring (Fig. 2E). MFA and analogue (**9**) showed a significant difference in their inhibitory activity. However replacement of the 2-methyl in (**9**) with a methoxy group (**10**) gave an analogue which potentiated the channel activity of TRPC4. The introduction of negative charges, such as –COOH (**8**) and Cl– (DFS), decreased the potency of blocking effect. Moreover, the modification on the benzoic acid by C to N substitution (i.e., NFA) showed a significant decrease in the blocking activity comparing to FFA (31 $\pm$ 7% vs. 73 $\pm$ 4% at the concentration of 100 μM) (see Fig. 1C).
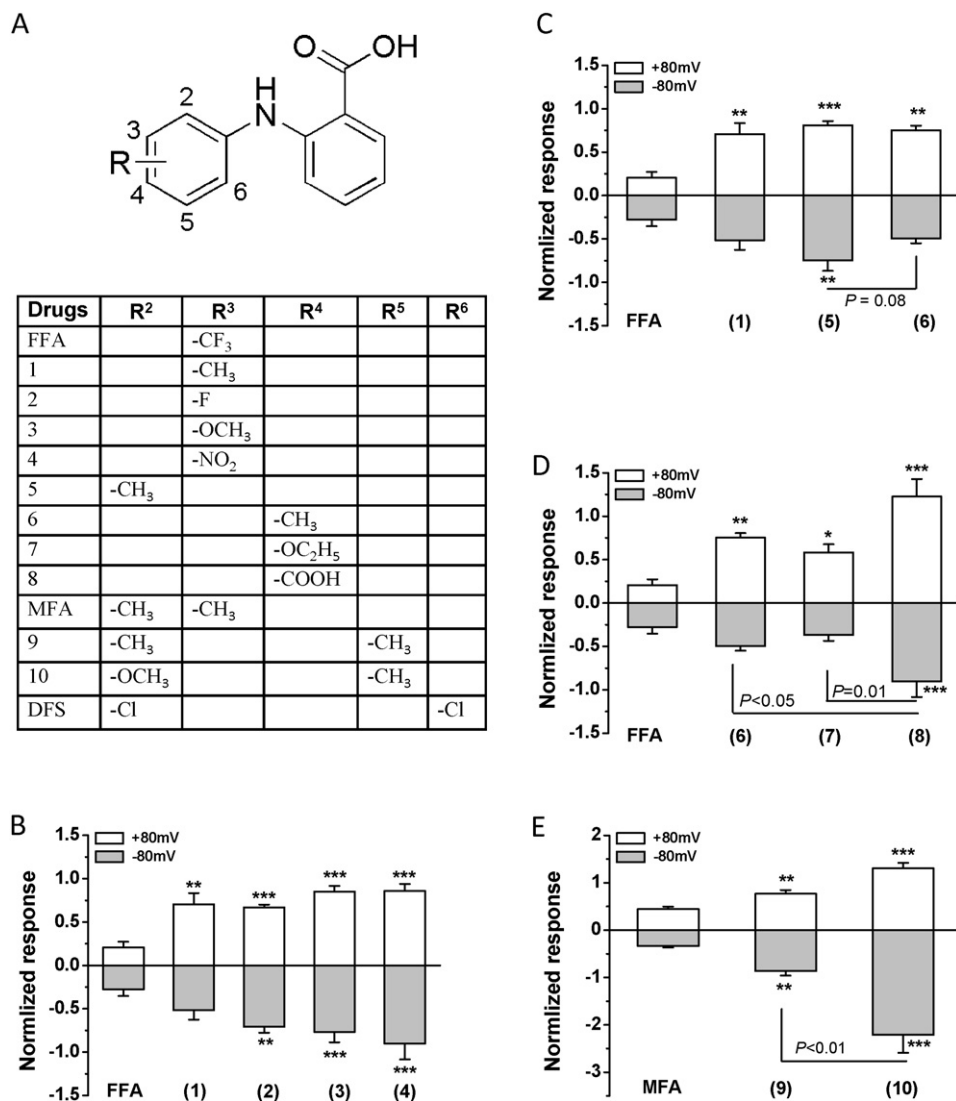
Fig. 2. Fenamate analogues and effect on TRPC4 channel. (A) The structures of fenamate analogues. (B) Mean $\pm$ S.E.M. data for the effect on TRPC4 current by the modification at R^3 position. FFA group (100 μM) was used as control for comparison between the groups. (C) Effect of the position of methyl substituent on the channel blocking activity. (D) Effect of the modification at R^4 position. (E) Location of two methyl substituents on the TRPC4 channel activity. MFA group (100 μM) was used as control for statistical comparison between the groups. The current measured at $\pm$80 mV after exposure to each compound for 5 min was normalized by the amplitude blocked by 2-APB (100 μM). ANOVA test was used and n = 6 for each group. *P < 0.05, **P < 0.01 and ***P < 0.001 for the comparisons with FFA group in (B, C, and D).
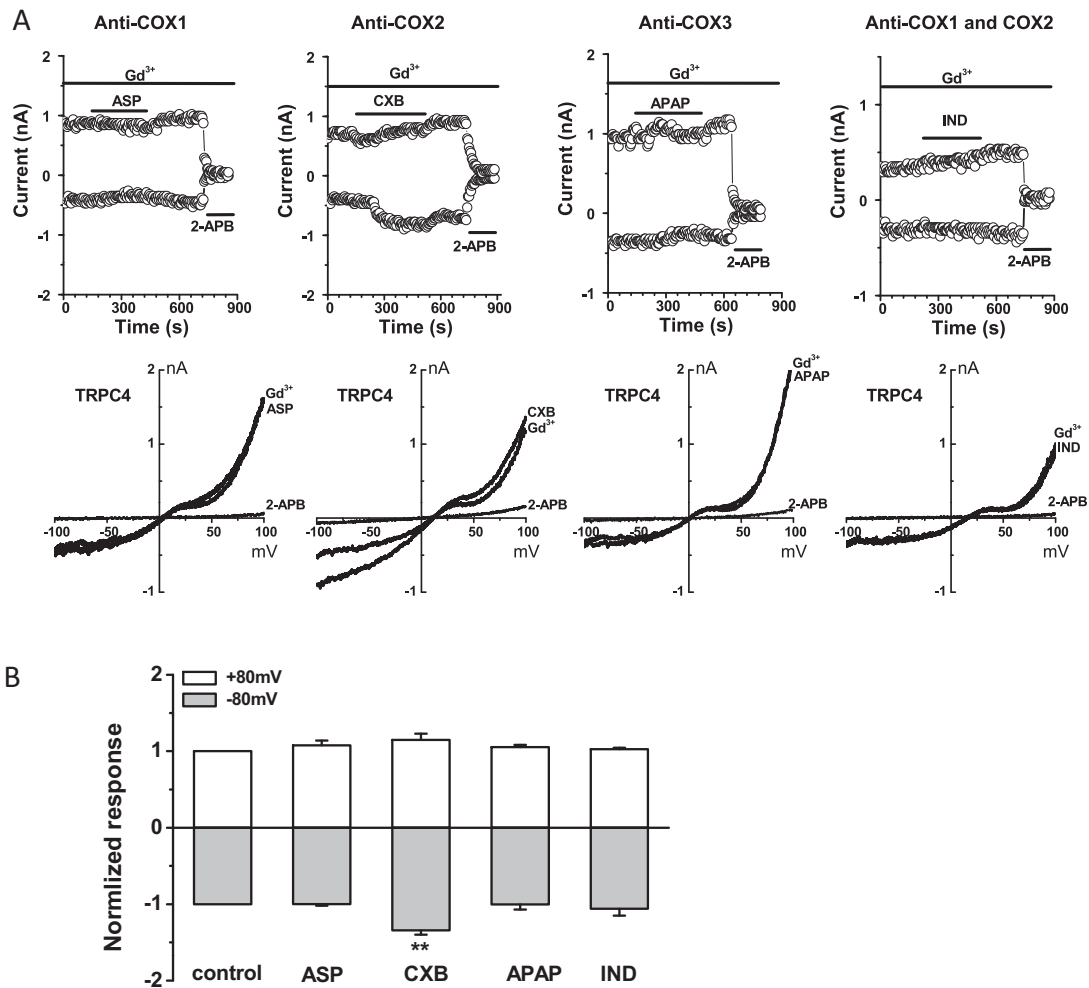
Fig. 3. Effect of non-fenamate COX inhibitors on TRPC4 channel. (A) Representative time course and IV curve for selective COX inhibitors on TRPC4 channels. Aspirin (ASP, 100 μM), celecoxib (CXB, 10 μM), acetaminophen (APAP, 100 μM), and indomethacin (IND, 10 μM) was used. (B) Mean ± S.E.M. data (n = 6–8, **P < 0.01).

3.3. Non-fenamate COX inhibitors on TRPC4 channels

The effect of selective COX inhibitors on TRPC channels is unknown, therefore we examined the direct effect of non-fenamate COX1-3 inhibitors on TRPC4 (Fig. 3). Aspirin, celecoxib and acetaminophen are selective inhibitors for COX1, COX2 and COX3, and indomethacin inhibits both COX1 and COX2 [8]. The COX1 and COX3 inhibitors had no effect on TRPC4, however, the COX2 inhibitor celecoxib showed a small stimulating effect on TRPC4. Similar stimulating effect of celecoxib was observed on TRPC5 current (Supplementary Fig. 1). Indomethacin showed no effect on TRPC4, suggesting that the inhibition of COX1 and COX2 are not involved in the channel activation. Aspirin, celecoxib, acetaminophen and indomethacin are structurally different from the fenamate analogues, therefore the blocking effect of fenamates is supposed to be a direct interaction between the chemical structures and the channel protein, rather than the COX pathways.

3.4. TRPC4 and TRPC5 channels potentiated by FFA but not by NFA

As shown in Fig. 4, FFA initially inhibited the TRPC4 and TRPC5, and then gradually increased the currents of TRPC4 and TRPC5. This delayed channel potentiation occurred after the exposure to FFA for 3 min and achieved the steady-state at 8–10 min. This channel potentiating effect was observed in the TRPC4 or TRPC5 transfected cells, but not the non-induced cells, after perfusion

with FFA and MFA at concentrations higher than 50 μM. However, NFA and DFS did not show potentiation on TRPC4 and TRPC5 channels. The FFA-induced IV curve showed a typical TRPC4 or TRPC5 current. These results suggested the delayed channel potentiation is due to the increased activity of TRPC4 or TRPC5 channels and specific for some structures of fenamate analogues.

3.5. Mitochondria Ca²⁺ release involved in the channel potentiation

In order to examine the underlying mechanism of the delayed channel potentiation on TRPC4 and TRPC5 channels, we compared the effects of FFA and NFA on mitochondrial Ca^{2+} release using primary cultured rat aortic smooth muscle cells (SMCs). The Ca^{2+} dye distribution in the mitochondria was evident after incubation with Fura-PE3 AM in Ca^{2+}-free solution for 30 min (Fig. 5). The pattern of mitochondrial Ca^{2+} dye loaded in the SMCs was similar to the previous report [33]. FFA robustly increased the intracellular Ca^{2+} concentration in both Ca^{2+}-free and 1.5 mM Ca^{2+} standard bath solutions, but MFA, NFA, DFS, ASP, and IND showed a small cytosolic Ca^{2+} increase compared to FFA, and CXB and APAP had no effect (Fig. 5C). The Ca^{2+} increase induced by FFA in the SMCs could be mainly contributed to by mitochondrial Ca^{2+} release, because pre-application of the sarco/endoplasmic reticulum Ca^{2+}-ATPase (SERCA) blocker thapsigargin (TG) did not inhibit the FFA-induced Ca^{2+} release (Fig. 5D).

Cytosolic Ca^{2+} increase evoked by FFA was also evident in the TRPC4 transfected HEK-293 cells even in the presence of TG, but
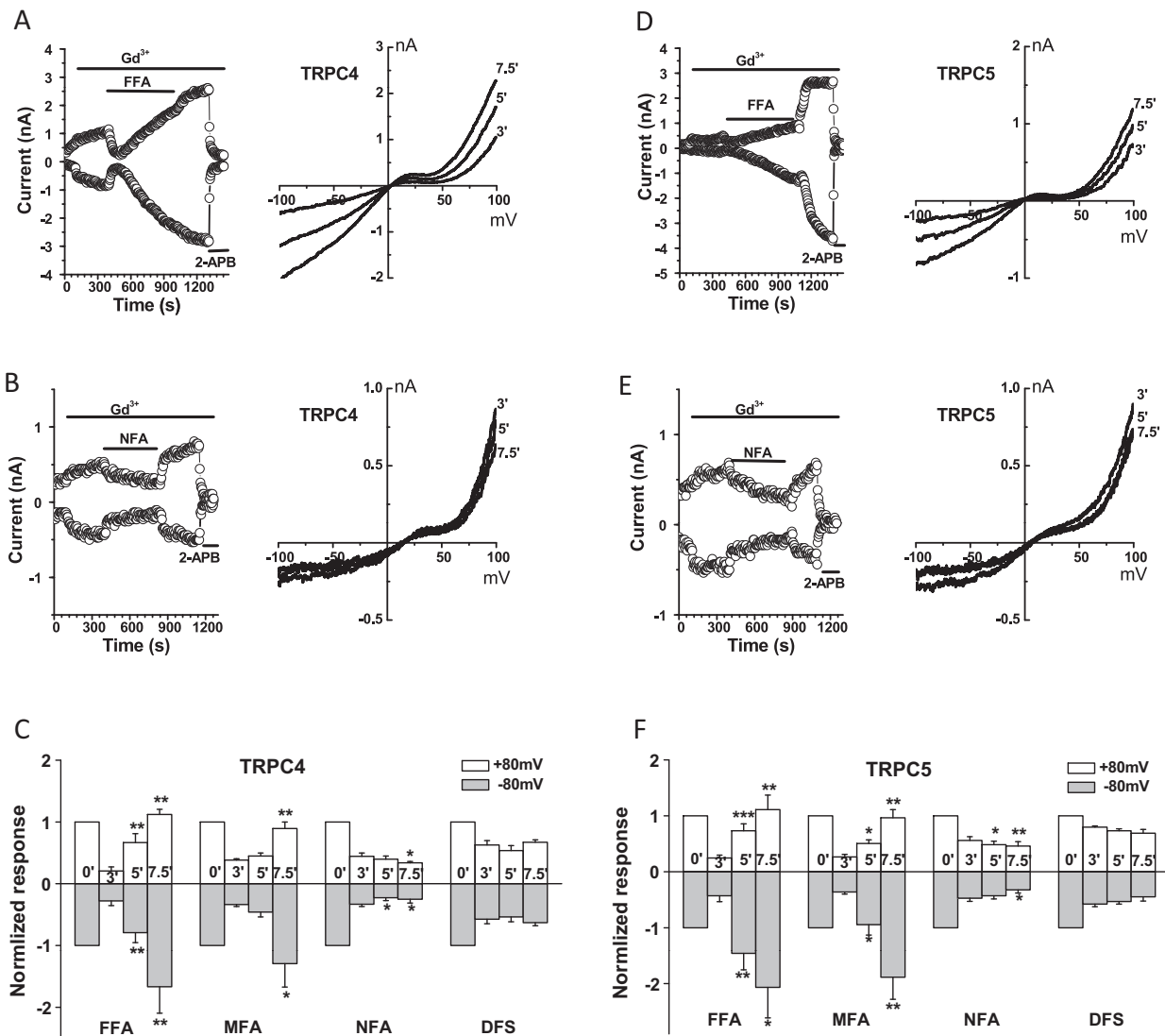
Fig. 4. Delayed potentiation on TRPC4 and TRPC5 currents by FFA. (A) FFA (100 μM) initially blocked the TRPC4 current and the gradually increased the amplitude of TRPC4 current in the presence of 100 μM Gd^{3+}. The *IV* curves were showed at 3, 5, and 7.5 min after initial blockade. (B) No potentiation by NFA (100 μM). The *IV* curves were shown in the right panel. (C) Mean ± S.E.M. data for the TRPC4 amplitude measured at ±80 mV after perfusion with FFA, MFA, NFA, and DFS for 3, 5 and 7.5 min. (D–F) As shown in A–C, but the cells expressing TRPC5 were used. $n = 6$–8 for each group, $^*P < 0.05$, $^{**}P < 0.01$, and $^{***}P < 0.001$.

the amplitude was reduced after the treatment with TG (Supplementary Fig. 2), suggesting that Ca^{2+} release from ER also contributes to the FFA-induced Ca^{2+} increase in this cell type. However, ER Ca^{2+} store depletion with TG was unable to abolish the channel potentiating effect of FFA (Fig. 5E and F), which further suggested the involvement of mitochondrial Ca^{2+} store in the mechanism.

To examine the role of mitochondrial Ca^{2+} release in the FFA-induced channel potentiation, we pre-treated the stable TRPC4 cells with cyclosporine A (CsA). CsA is an inhibitor of mitochondrial permeability transition pore, which also inhibits mitochondrial Ca^{2+} movement across the membrane [34,35]. Preincubation with CsA (10 μM) significantly decreased the FFA-induced TRPC4 channel potentiation (Fig. 5G), suggesting the involvement of mitochondrial Ca^{2+} release in the FFA-induced TRPC4 channel potentiation.

4. Discussion

In this study, we have found that the fenanates FFA, MFA, NFA and DFS showed inhibition on TRPC4 and TRPC5 channels with a

potency sequence of FFA > MFA > NFA > DFS. Replacement of the trifluoromethyl group in FFA with a range of substituents leads to a significant change in the channel blocking activity for those derivatives. Introduction of 2-methoxy-5-methyl substituents to the phenylamino ring (**10**) gave an analogue with a stimulating effect on the channels. COX-1 and COX-3 inhibitors did not show any direct effect on TRPC4 or TRPC5 channels, but the highly selective COX-2 inhibitor celecoxib slightly increased the activity of TRPC4 and TRPC5. Interestingly, there was differential effect of fenamate analogues on TRPC4 and TRPC5 channels, i.e., FFA and MFA showed a potentiating effect after initial inhibition, but NFA and DFS did not potentiate the channels. The TRPC4 and TRPC5 channel potentiation by FFA is likely explained by Ca^{2+} release from mitochondria, because the inhibition of mitochondrial permeability transition pore by CsA partially prevented the FFA-induced channel potentiation. In addition, NFA did not show any channel potentiation, which could be explained by its low potency in mitochondrial Ca^{2+} release compared with FFA [31].

Fenamates are effective anti-inflammatory agents through COX-1 and COX-2 inhibition, and also inhibit a variety of ion channel activities in many cell types. Early studies have shown that
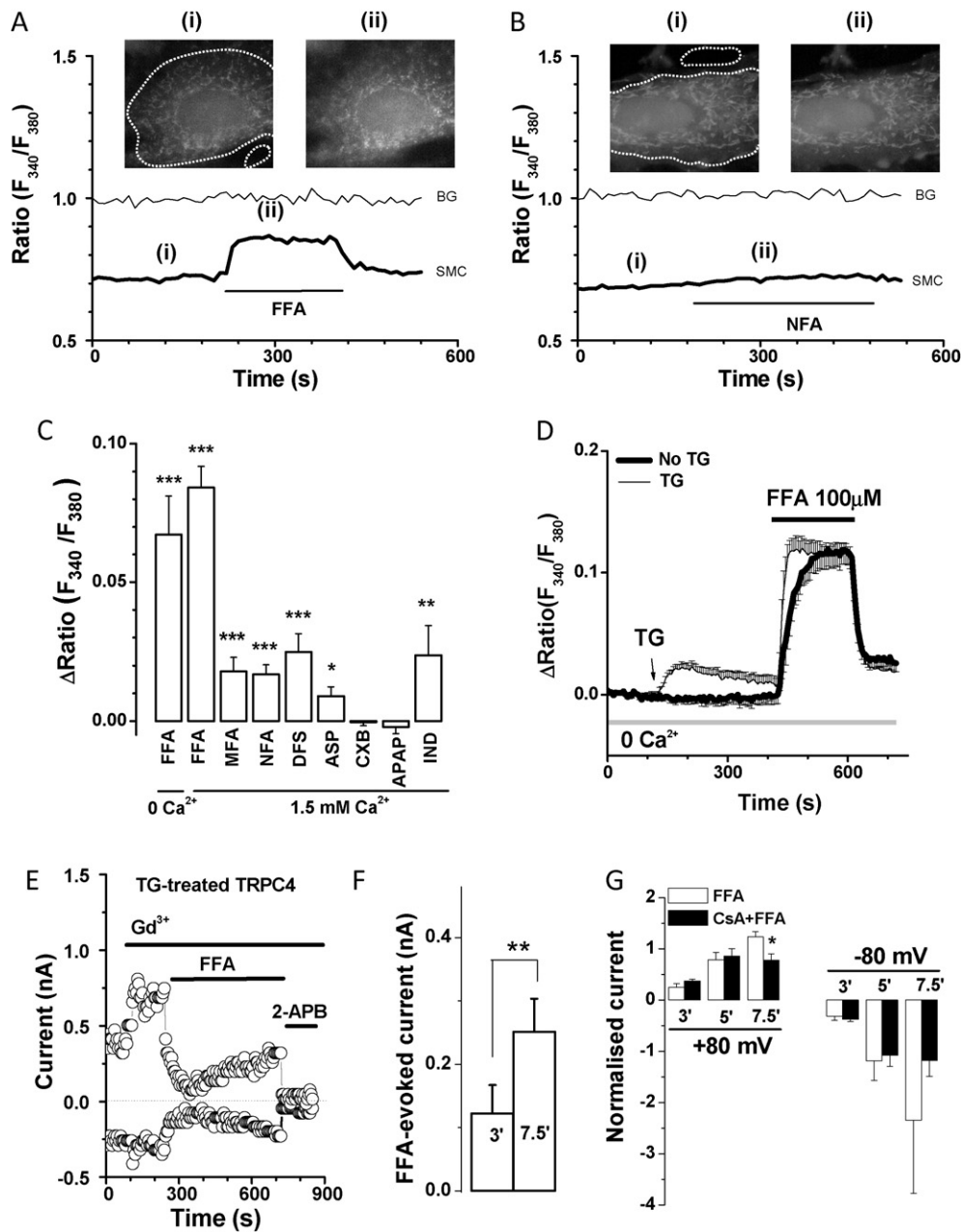
Fig. 5. Involvement of mitochondrial Ca^{2+} release on the TRPC4 channel potentiation. (A) Rat aortic smooth muscle cells were loaded with Fura-PE3 AM. The cytosolic Ca^{2+} increase induced by FFA at 100 μM. (i) and (ii) are the images before and after FFA treatment. The thin trace is the background (BG) signal and the thick line is smooth muscle cell (SMC). (B) Effect of NFA (100 μM). (C) Mean ± S.E.M. data for the intracellular Ca^{2+} increase in the SMCs induced by 100 μM of FFA, MFA, NFA, DFS, ASP, APAP, and IND and CXB (10 μM), $n = 17$–26 cells for each group. (D) SMCs were incubated with 1 μM TG ($n = 7$) or without TG ($n = 10$). (E) TRPC4 cells were pre-treated with TG (1 μM) for 10 min. The whole cell current was recorded in the presence of TG. FFA (100 μM), Gd^{3+} (100 μM) and 2-APB (100 μM) were used. (F) Mean data for FFA-induced current after perfusion with FFA for 3 and 7.5 min. The amplitude of TRPC4 current was measured at −80 mV ($n = 6$). (G) Pretreatment with CsA (10 μM) for 5 min, the amplitude of TRPC4 current was measured at ±80 mV after perfusion with FFA for 3, 5 and 7.5 min. $n = 6$–8 for each group, $^*P < 0.05$, $^{**}P < 0.01$, $^{***}P < 0.001$.

fenamates inhibited Ca^{2+}-activated chloride channels [36–38], Ca^{2+}-activated potassium channels [39], and the Ca^{2+}-activated non-selective cationic channel [40]. Recently, it has been demonstrated that FFA activated TRPC6 [28], TRPA1 [29], and an OAG-sensitive cationic current in A7r5 cells [26], but inhibited TRPM2, TRPM3, TRPM4 and TRPM5 channels [22,24,41–44]. Here we give the new evidence that fenamates also inhibit TRPC4 and TRPC5. The potency of inhibition depends on the modification on the skeleton of the 2-phenylaminobenzoate. Apart from the initial inhibition, there is a delayed channel potentiation evoked by some fenamate analogues, such as FFA and MFA. The delayed channel potentiation could be explained by the mitochondrial Ca^{2+} release

evoked by FFA, because both TRPC4 and TRPC5 channels have been demonstrated as Ca^{2+}-sensitive channels [45–48], and thus the increased cytosolic Ca^{2+} level caused by Ca^{2+} release from mitochondria in turn facilitates TRPC4/TRPC5 channel activity [45,47]. Our data showed that the FFA-induced Ca^{2+} increase in the cytosol was fast, robust and reversible in SMCs, while the effect for NFA was small. This difference has also been described in mouse submandibular salivary cells [31]. Our data suggested that the FFA-induced Ca^{2+} increase in the smooth muscle cells was mainly contributed by mitochondrial Ca^{2+} release, because the Ca^{2+} release signal was not influenced by the depletion of ER Ca^{2+} store. Tu and co-workers also showed that FFA-induced mitochondrial

Ca^{2+} release occurred in the presence of TG [30]. Therefore the TRPC4 and TRPC5 channel potentiation by FFA could be explained as the increased cytosolic Ca^{2+} due to mitochondrial Ca^{2+} release. In addition, the contribution of mitochondrial Ca^{2+} release to the channel potentiation was further demonstrated by the application of CsA that can partially prevent the mitochondrial Ca^{2+} movement in this study.

The delayed potentiation on TRPC4 and TRPC5 channel could be a mechanism for the pharmacology of fenamate NSAIDs, especially in situations with high dosage or long-term medication. The peak plasma concentration of FFA or MFA achieved 6-20 μg ml^{-1} (equal to 21–71 μM) in volunteers [49,50], suggesting that the effect on mitochondrial Ca^{2+} release and channel potentiation could happen in patients receiving fenamate drug treatment. The cardiovascular risks of some NSAIDs have been recognized and some NSAIDs have been withdrawn from the market by FDA due to the cardiovascular side effects [51]. The mechanisms for these side effects are unclear, but the interference with intracellular Ca^{2+} homeostasis or TRPC4/5 channel potentiation could be a new explanation for hypertension related to some fenamate analogues and celecoxib, which needs to be investigated further.

The effect of non-fenamate selective COX inhibitors was also examined in this study. COX-1 is involved in platelet aggregation, gastric mucosa protection and renal electrolyte homeostasis. Aspirin is a selective COX-1 inhibitor and irreversibly acetylates platelet COX-1 and inhibits the formation of the potent platelet agonist thromboxane A$_2$ (TXA$_2$) [52]. Perfusion with aspirin did not change the activity of TRPC4 and TRPC5 channels, suggesting that COX-1 is not directly involved in their modulation. In order to dissect COX-2 involvement, we tested the selective inhibitor celecoxib that significantly increased the channel activity of TRPC4 and TRPC5. The activation mechanism for celecoxib is unknown, but unlikely due to the COX2 inhibition, because other COX2 inhibitors have no direct effect.

Modification of the phenylamino ring in FFA is useful for finding the structure–activity relationship of those analogues. The substituents at R^3 position (analogues **1–4**) significantly changed the channel blocking potency, suggesting the importance of R^3 in the structural modification. The comparison between the methyl substituents at R^2, R^3 and R^4 (**5**, **1** and **6**) showed that the modification at *meta* and *para* positions could be more effective than the *ortho* position. Substituents at *para* position gave a compound (**7**) with similar potency to FFA, but the introduction of a polar substituent (**8**) could be ineffective. Our data also showed that the combination of groups at R^2 and R^5 could be a determinant as a channel opener or blocker, since the substituent –OCH$_3$ at R^2 (in **10**) yielded a channel stimulator, while the substituent –CH$_3$ at R^2 (in **9**) yielded a channel antagonist. We suggest that this could be due to the conformational changes in the diphenylamine core as the bulkier methoxy group is introduced into an *ortho* position. Introduction of a single –CH$_3$ or –OCH$_3$ group at R^3 (**1** or **5** respectively) however, without the second *meta* methyl residue, yielded channel inhibitors less effective than FFA.

In summary, our results show that fenamate analogues have differential effects on TRPC4 and TRPC5 channels with inhibition acutely and potentiation with long exposure. The analogues may have different properties for mitochondrial Ca^{2+} release and caution should be exercised in the explanation of drug class effect of these agents. The development of new fenamate analogues may have potential for identification of selective TRPC activators and inhibitors, which could yield new tools for investigating the roles of these channels in pathophysiological conditions.

Conflicts of interest

No potential conflicts of interest were disclosed.

Appendix A. Supplementary data

Supplementary data associated with this article can be found, in the online version, at doi:10.1016/j.bcp.2012.01.014.

References

[1] Wu LJ, Sweet TB, Clapham DE. International union of basic and clinical pharmacology. LXXVI. Current progress in the mammalian TRP ion channel family. Pharmacol Rev 2010;62:381–404.
[2] Bergdahl A, Gomez MF, Dreja K, Xu SZ, Adner M, Beech DJ, et al. Cholesterol depletion impairs vascular reactivity to endothelin-1 by reducing store-operated Ca2+ entry dependent on TRPC1. Circ Res 2003;93:839–47.
[3] Xu SZ, Muraki K, Zeng F, Li J, Sukumar P, Shah S, et al. A sphingosine-1-phosphate-activated calcium channel controlling vascular smooth muscle cell motility. Circ Res 2006;98:1381–9.
[4] Xu SZ, Sukumar P, Zeng F, Li J, Jairaman A, English A, et al. TRPC channel activation by extracellular thioredoxin. Nature 2008;451:69–72.
[5] Xu SZ, Zeng B, Daskoulidou N, Chen GL, Atkin SL, Lukhele B. Activation of TRPC cationic channels by mercurial compounds confers the cytotoxicity of mercury exposure. Toxicol Sci 2011;125:56–68.
[6] Winn MP, Conlon PJ, Lynn KL, Farrington MK, Creazzo T, Hawkins AF, et al. A mutation in the TRPC6 cation channel causes familial focal segmental glomerulosclerosis. Science 2005;308:1801–4.
[7] Li Y, Jia YC, Cui K, Li N, Zheng ZY, Wang YZ, et al. Essential role of TRPC channels in the guidance of nerve growth cones by brain-derived neurotrophic factor. Nature 2005;434:894–8.
[8] Warner TD, Mitchell JA. COX-2 selectivity alone does not define the cardiovascular risks associated with non-steroidal anti-inflammatory drugs. Lancet 2008;371:270–3.
[9] Friedewald VE, Bennett JS, Christo JP, Pool JL, Scheiman JM, Simon LS, et al. AJC Editor's consensus: selective and nonselective nonsteroidal anti-inflammatory drugs and cardiovascular risk. Am J Cardiol 2010;106:873–84.
[10] Trelle S, Reichenbach S, Wandel S, Hildebrand P, Tschannen B, Villiger PM, et al. Cardiovascular safety of non-steroidal anti-inflammatory drugs: network meta-analysis. BMJ 2011;342:c7086.
[11] McGettigan P, Henry D. Cardiovascular risk with non-steroidal anti-inflammatory drugs: systematic review of population-based controlled observational studies. PLoS Med 2011;8:e1001098.
[12] Elwood PC, Gallagher AM, Duthie GG, Mur LA, Morgan G. Aspirin, salicylates, and cancer. Lancet 2009;373:1301–9.
[13] Wang D, Dubois RN. The role of COX-2 in intestinal inflammation and colorectal cancer. Oncogene 2009;29:781–8.
[14] Daugherty SE, Pfeiffer RM, Sigurdson AJ, Hayes RB, Leitzmann M, Schatzkin A, et al. Nonsteroidal antiinflammatory drugs and bladder cancer: a pooled analysis. Am J Epidemiol 2011;173:721–30.
[15] McIlhatton MA, Tyler J, Burkholder S, Ruschoff J, Rigas B, Kopelovich L, et al. Nitric oxide-donating aspirin derivatives suppress microsatellite instability in mismatch repair-deficient and hereditary nonpolyposis colorectal cancer cells. Cancer Res 2007;67:10966–75.
[16] Nunez L, Valero RA, Senovilla L, Sanz-Blasco S, Garcia-Sancho J, Villalobos C. Cell proliferation depends on mitochondrial Ca2+ uptake: inhibition by salicylate. J Physiol 2006;571:57–73.
[17] Meves H. Arachidonic acid and ion channels: an update. Br J Pharmacol 2008;155:4–16.
[18] Toda N. Mechanism of action of carbocyclic thromboxane A2 and its interaction with prostaglandin I2 and verapamil in isolated arteries. Circ Res 1982;51:675–82.
[19] Di Capite J, Nelson C, Bates G, Parekh AB. Targeting Ca2+ release-activated Ca2+ channel channels and leukotriene receptors provides a novel combination strategy for treating nasal polyposis. J Allergy Clin Immunol 2009;124:1014–21. e1-3.
[20] Murakami M, Kudo I. Phospholipase A2. J Biochem 2002;131:285–92.
[21] Kraft R, Grimm C, Frenzel H, Harteneck C. Inhibition of TRPM2 cation channels by N-(p-amylcinnamoyl)anthranilic acid. Br J Pharmacol 2006;148:264–73.
[22] Harteneck C, Frenzel H, Kraft R. N-(p-amylcinnamoyl)anthranilic acid (ACA): a phospholipase A(2) inhibitor and TRP channel blocker. Cardiovasc Drug Rev 2007;25:61–75.
[23] Kraft R, Harteneck C. The mammalian melastatin-related transient receptor potential cation channels: an overview. Pflugers Arch 2005;451:204–11.
[24] Ullrich ND, Voets T, Prenen J, Vennekens R, Talavera K, Droogmans G, et al. Comparison of functional properties of the Ca2+-activated cation channels TRPM4 and TRPM5 from mice. Cell Calcium 2005;37:267–78.

[25] Lee YM, Kim BJ, Kim HJ, Yang DK, Zhu MH, Lee KP, et al. TRPC5 as a candidate for the nonselective cation channel activated by muscarinic stimulation in murine stomach. Am J Physiol Gastrointest Liver Physiol 2003;284:G604–16.

[26] Jung S, Strotmann R, Schultz G, Plant TD. TRPC6 is a candidate channel involved in receptor-stimulated cation currents in A7r5 smooth muscle cells. Am J Physiol Cell Physiol 2002;282:C347–59.

[27] Foster RR, Zadeh MA, Welsh GI, Satchell SC, Ye Y, Mathieson PW, et al. Flufenamic acid is a tool for investigating TRPC6-mediated calcium signalling in human conditionally immortalised podocytes and HEK293 cells. Cell Calcium 2009;45:384–90.

[28] Inoue R, Okada T, Onoue H, Hara Y, Shimizu S, Naitoh S, et al. The transient receptor potential protein homologue TRP6 is the essential component of vascular alpha(1)-adrenoceptor-activated Ca(2+)-permeable cation channel. Circ Res 2001;88:325–32.

[29] Hu H, Tian J, Zhu Y, Wang C, Xiao R, Herz JM, et al. Activation of TRPA1 channels by fenamate nonsteroidal anti-inflammatory drugs. Pflugers Arch 2010;459:579–92.

[30] Tu P, Brandolin G, Bouron A. The anti-inflammatory agent flufenamic acid depresses store-operated channels by altering mitochondrial calcium homeostasis. Neuropharmacology 2009;56:1010–6.

[31] Poronnik P, Ward MC, Cook DI. Intracellular Ca2+ release by flufenamic acid and other blockers of the non-selective cation channel. FEBS Lett 1992;296:245–8.

[32] Mei XF, August AT, Wolf C. Regioselective copper-catalyzed amination of chlorobenzoic acids: synthesis and solid-state structures of N-aryl anthranilic acid derivatives. J Org Chem 2006;71:142–9.

[33] Szado T, Kuo KH, Bernard-Helary K, Poburko D, Lee CH, Seow C, et al. Agonist-induced mitochondrial Ca2+ transients in smooth muscle. FASEB J 2003;17:28–37.

[34] Chalmers S, McCarron JG. The mitochondrial membrane potential and Ca2+ oscillations in smooth muscle. J Cell Sci 2008;121:75–85.

[35] Montero M, Lobaton CD, Gutierrez-Fernandez S, Moreno A, Alvarez J. Calcineurin-independent inhibition of mitochondrial Ca2+ uptake by cyclosporin A. Br J Pharmacol 2004;141:263–8.

[36] Hogg RC, Wang Q, Large WA. Action of niflumic acid on evoked and spontaneous calcium-activated chloride and potassium currents in smooth muscle cells from rabbit portal vein. Br J Pharmacol 1994;112:977–84.

[37] Korn SJ, Bolden A, Horn R. Control of action potentials and Ca2+ influx by the Ca(2+)-dependent chloride current in mouse pituitary cells. J Physiol 1991;439:423–37.

[38] Shaw T, Lee RJ, Partridge LD. Action of diphenylamine carboxylate derivatives, a family of non-steroidal anti-inflammatory drugs, on [Ca2+]i and Ca(2+)-activated channels in neurons. Neurosci Lett 1995;190:121–4.

[39] Greenwood IA, Large WA. Comparison of the effects of fenamates on Ca-activated chloride and potassium currents in rabbit portal vein smooth muscle cells. Br J Pharmacol 1995;116:2939–48.

[40] Yamashita T, Isa T. Fulfenamic acid sensitive, Ca(2+)-dependent inward current induced by nicotinic acetylcholine receptors in dopamine neurons. Neurosci Res 2003;46:463–73.

[41] Naziroglu M, Luckhoff A, Jungling E. Antagonist effect of flufenamic acid on TRPM2 cation channels activated by hydrogen peroxide. Cell Biochem Funct 2007;25:383–7.

[42] Wilkinson JA, Scragg JL, Boyle JP, Nilius B, Peers C. H2O 2-stimulated Ca2+ influx via TRPM2 is not the sole determinant of subsequent cell death. Pflugers Arch 2008;455:1141–51.

[43] Hill K, Benham CD, McNulty S, Randall AD. Flufenamic acid is a pH-dependent antagonist of TRPM2 channels. Neuropharmacology 2004;47:450–60.

[44] Klose C, Straub I, Riehle M, Ranta F, Krautwurst D, Ullrich S, et al. Fenamates as TRP channel blockers: mefenamic acid selectively blocks TRPM3. Br J Pharmacol 2011;162:1757–69.

[45] Blair NT, Kaczmarek JS, Clapham DE. Intracellular calcium strongly potentiates agonist-activated TRPC5 channels. J Gen Physiol 2009;133:525–46.

[46] Tang J, Lin Y, Zhang Z, Tikunova S, Birnbaumer L, Zhu MX. Identification of common binding sites for calmodulin and inositol 1,4,5-trisphosphate receptors on the carboxyl termini of trp channels. J Biol Chem 2001;276:21303–10.

[47] Zeng F, Xu SZ, Jackson PK, McHugh D, Kumar B, Fountain SJ, et al. Human TRPC5 channel activated by a multiplicity of signals in a single cell. J Physiol 2004;559:739–50.

[48] Obukhov AG, Nowycky MC. A cytosolic residue mediates Mg2+ block and regulates inward current amplitude of a transient receptor potential channel. J Neurosci 2005;25:1234–9.

[49] Lentjes EG, van Ginneken CA. Pharmacokinetics of flufenamic acid in man. Int J Clin Pharmacol Ther Toxicol 1987;25:185–7.

[50] Rescigno A, Marzo A, Thyroff-Friesinger U. Mefenamic acid bioequivalence assessment with a new statistical procedure. Pharmacol Res 1996;34:149–52.

[51] Antman EM, Bennett JS, Daugherty A, Furberg C, Roberts H, Taubert KA. Use of nonsteroidal antiinflammatory drugs: an update for clinicians: a scientific statement from the American Heart Association. Circulation 2007;115:1634–42.

[52] Perrone MG, Scilimati A, Simone L, Vitale P. Selective COX-1 inhibition: a therapeutic target to be reconsidered. Curr Med Chem 2010;17:3769–805.

Activation of TRPC Cationic Channels by Mercurial Compounds Confers the Cytotoxicity of Mercury Exposure

Shang-Zhong Xu,[1] Bo Zeng, Nikoleta Daskoulidou, Gui-Lan Chen, Stephen L. Atkin, and Bhekithemba Lukhele

Centre for Cardiovascular and Metabolic Research, Hull York Medical School, University of Hull, Hull, HU6 7RX, U.K.

[1]To whom correspondence should be addressed. Fax: +(44) 1482-465390. E-mail: sam.xu@hyms.ac.uk.

Mercury is an established worldwide environmental pollutant with well-known toxicity affecting neurodevelopment in humans, but the molecular basis of cytotoxicity and the detoxification procedure are still unclear. Here we examined the involvement of the canonical transient receptor potential (TRPC) channel in the mercury-induced cytotoxicity and the potential detoxification strategy. Whole-cell and excised patches, Ca^{2+} imaging, and site-directed mutagenesis were used to determine the mechanism of action of mercurial compounds on TRPC channels overexpressed in HEK293 cells, and cytotoxicity and preventive effect were investigated in cell culture models using small interfering RNA and pharmacological blockers. Mercury potently activates TRPC4 and TRPC5 channels. The extracellular cysteine residues (C^{553} and C^{558}) near the channel pore region of TRPC5 are the molecular targets for channel activation by mercury. The sensitivity of mercury to TRPC5 is presumed to be specific because other divalent heavy metal pollutants, such as Cd^{2+}, Ni^{2+}, and Zn^{2+}, had no stimulating effect, and TRPC3, TRPC6, TRPV1, and TRPM2 were resistant to mercurial compounds. The channel activity of TRPC5, as well as TRPC4, induced by mercury, was prevented by 2-aminoethoxydiphenyl borate and modified by a reducing environment. The inhibition of TRPC5 channels by specific TRPC5 pore-blocking antibody or by SKF-96365 alleviated the cytotoxicity, whereas the mercury chelator, meso-2,3-dimercaptosuccinic acid, showed nonselective prevention of cell survival. Silencing of the *TRPC5* gene reduced the mercury-induced neuronal damage. These results indicate that mercurial compounds are activators for TRPC5 and TRPC4 channels. Blockade of TRPC channels could be a novel strategy for preventing mercury-induced cytotoxicity and neurodevelopment impairment.

Key Words: cationic channel; calcium channel; TRPC; mercury; methylmercury; dimercaptosuccinic acid; SKF-96365; 2-aminoethoxydiphenyl borate.

Despite increasing attempts to control industrial pollution, mercury poisoning still occurs through methylmercury (MeHg) from fish, ethylmercury from vaccine products, metallic mercury from dental amalgam fillings, cinnabar from Chinese herbal balls, and other domestic mercury pollution (Counter and Buchanan, 2004). There are three primary forms of mercury in the environment, that is, metallic, inorganic, and organic mercury. They can convert from one form to another in the environment and in the human body. Three forms show different clinical toxicological features including major damage to the brain by organic mercury, the kidney by inorganic divalent mercury, and the lungs by inhalation of mercury vapor, although many organs are susceptible to mercury exposure (Clarkson *et al.*, 2003). Young children are vulnerable to mercury exposure, which may cause the impairment of brain development and mental retardation (Costa *et al.*, 2004; Trasande *et al.*, 2005). In the elderly, the elevated mercury level in the blood has been suggested as a potential risk factor for cardiovascular and neurodegenerative diseases (Guallar *et al.*, 2002; Landrigan *et al.*, 2005).

MeHg exposure is of particular concern because of its high accumulation in fish, complete absorption from gastrointestinal tract, easy transportation across the placenta and blood-brain barrier, and tissue accumulation. MeHg can affect brain development in children and result in a lower IQ; however, the correlation of MeHg exposure to children's learning and performance capacity is still disputed, as the recent epidemiological studies from the Faroe Island, the Seychelles, and New Zealand have produced contradictory results (Axelrad *et al.*, 2007; Cohen *et al.*, 2005; Davidson *et al.*, 2011; Spurgeon, 2006). The mechanisms of how MeHg causes brain damage may include abnormality of neuronal migration, neuronal apoptosis, retraction of growth cone formation and extensions, and the loss of interneuronal contacts (Costa *et al.*, 2004). The network connections between neurons are critical for short-term and long-term memories, which require a series of biophysical and biochemical processes (Dasari and Yuan, 2009). Ca^{2+} is a second messenger in the processes and plays an essential role in axonal transport, growth cone motility, and extension (Zheng, 2000). The disturbance of Ca^{2+} homeostasis has been linked to mercury toxicity; for example, MeHg blocks voltage-gated Ca^{2+} channels (VGCC) but increases intracellular $[Ca^{2+}]$ in isolated nerve terminals (Limke *et al.*, 2004); MeHg inhibits the action potential–evoked neurotransmitter release but increases the spontaneous transmitter release

(Denny and Atchison, 1996). These observations suggest that an unidentified Ca^{2+} influx pathway might exist.

Canonical transient receptor potential (TRPC) channels are Ca^{2+}-permeable cationic channels. Seven members (TRPC1–7) have been identified in the TRPC subfamily, and TRPC2 is a pseudogene in human (Clapham, 2003). TRPC1, TRPC3, and TRPC6 have been shown to mediate chemotropic-guided axonal turning (Li et al., 2005; Wang and Poo, 2005), and TRPC3 and TRPC6 are also involved in the survival of cerebellum granule neuron (Jia et al., 2007). TRPC5 channel is highly expressed in the brain, which is encoded by the TRPC5 gene located in a region of human X-chromosome associated with nonsyndromic mental retardation, and thus, there is a putative genetic link with neuronal development (Sossey-Alaoui et al., 1999). It has also been shown that TRPC5 is involved in retardation of neurite outgrowth (Greka et al., 2003; Hui et al., 2006) and in vivo neurofunction (Riccio et al., 2009). Because TRPC channels play important roles in neuronal function and are critical for regulating Ca^{2+} homeostasis in a cell, we then hypothesized that TRPC channels could be important for the mechanisms of mercury-induced cytotoxicity and neuronal impairment.

In this study, we have examined the effect and underlying mechanism of TRPC channels acting as the molecular targets of mercury-evoked cytotoxicity. We found that mercurial compounds potently activated TRPC5 as well as TRPC4 channels via binding to the two extracellular cysteine residues near the channel pore. Silence of TRPC5 gene with small interfering RNA (siRNA) or blockade of TRPC channel activity with pharmacological tools alleviated the mercury-related cytotoxicity.

MATERIALS AND METHODS

Cell culture, cloning, and transfection. HEK-293 cells were transfected with human TRPC5 (accession number AF054568), TRPC3 (accession number U47050), TRPC6 (accession number BC093660), mouse TRPC4 (accession number NM_016984), mouse TRPM2 (NM_138301), and human TRPV1 (accession number AY131289) plasmid complementary DNAs (cDNAs) in a pcDNA3 vector using Lipofectamine 2000 (Invitrogen, U.K.). The procedure was previously described (Xu et al., 2005b). The stable transfected cells for TRPC3, TRPC6, TRPV1, and TRPM2 were selected and maintained in the cell culture medium containing G418 (400 μg/ml). The human TRPC4α (NM_016179) tagged with enhanced yellow fluorescent protein in a tetracycline-regulatory vector was stably expressed in HEK-293 T-REx cells (Invitrogen). For some electrophysiological experiments, the tetracycline-inducible TRPC5 cells were used as we reported (Xu et al., 2005a, 2005b; Zeng et al., 2004), where the expression of TRPC5 was induced by 1 μg/ml tetracycline for 24–72 h before recording. There was no difference in the current-voltage (IV) curve and Ca^{2+} influx response to stimuli for the TRPC5 stable cells and the tetracycline-induced TRPC5 cells. The noninduced cells without addition of tetracycline or the nontransfected cells were used as control. Cells were grown in Dulbecco's Modified Eagle Medium (DMEM)-F12 (Gibco, U.K.) medium containing 10% fetal calf serum (FCS), 100 units/ml penicillin, and 100 μg/ml streptomycin. Cells were maintained at 37°C under 95% air and 5% CO_2 and seeded on coverslips prior to experiments.

PC12 cells were grown in F12 medium containing 15% FCS and 50 ng/ml of nerve growth factor (NGF; Invitrogen) using collagen type IV–coated cell culture dishes (Hui et al., 2006). The cell number and axonal growth were measured manually on photos taken by a digital microscope camera (Nikon, Japan). The TRPC5 siRNA was purchased from Sigma (U.K.) and the effectiveness was validated by real-time PCR as described in a previous publication (Xu et al., 2008a). The electroporation was used for PC12 cell transfection using BTX Electro Square Porator ECM 830 with three pulses (Genetronics, San Diego, CA) and the efficiency achieved ~85% at optimal conditions.

Primary cell cultures. The isolation and culture of human umbilical vein endothelial cells (HUVECs) were similar to that published previously (Xu et al., 2008b). Patients gave informed consent in accordance with the Declaration of Helsinki, and the project was approved by the local ethical committee. Briefly, the isolated cells were cultured in a T-75 flask with endothelial cell growth media (PromoCell, Germany) supplemented with 2% FCS, 5.0 ng/ml epidermal growth factor, 0.5 ng/ml vascular endothelial growth factor, 10 ng/ml basic fibroblast factor, 20 ng/ml insulin-like growth factor-1, and 22.5 ng/ml heparin. Cells were kept at 37°C in a CO_2 incubator with a humidified atmosphere of 5% CO_2 in air and used at passages 2–3. Cells were seeded into 96- or 48-well cell culture plates at a density of 3.0×10^4 cells/ml and cultured for 15 h to allow the cells to attach before further treatments.

Electrophysiology and fluorescence measurements. Voltage clamp was performed at room temperature (23–26°C) with the whole-cell, outside-out, or inside-out patch configuration (Xu et al., 2006). Briefly, signal was amplified with an Axopatch 200B patch clamp amplifier and controlled with pClamp software 10. A 1-s ramp voltage protocol from –100 to +100 mV was applied at a frequency of 0.1 Hz from a holding potential of –60 mV. Signals were sampled at 3 kHz and filtered at 1 kHz. The salt-agar bridge was used to connect the ground wire (Ag-AgCl) in the bath chamber. The 200nM Ca^{2+}-buffered pipette solution (115 CsCl, 10 ethylene glycol-bis(2-aminoethylether)-N,N,N′,N′-tetraacetic acid, 2 $MgCl_2$, 10 4-(2-hydroxyethyl)-1-piperazineethanesulfonic acid [HEPES], and 5.7 $CaCl_2$ in mM, pH was adjusted to 7.2 with CsOH and osmolarity was adjusted to ~290 mOsm with mannitol, and the calculated free Ca^{2+} was 200nM) was used. The standard bath solution contained (mM): 130 NaCl, 5 KCl, 8 D-glucose, 10 HEPES, 1.2 $MgCl_2$, and 1.5 $CaCl_2$. The pH was adjusted to 7.4 with NaOH. The recording chamber had a volume of 150 μl and was perfused at a rate of about 2 ml/min.

For fluorescence measurements, HEK-293 cells transfected with individual genes were incubated with Fluo3-AM (5μM) for 30 min at room temperature in Ca^{2+}-free standard bath solution. Intracellular Ca^{2+} experiments were performed using cuvette-based $[Ca^{2+}]_i$ assay. Briefly, the loaded cells were washed and resuspended in standard bath solution. Volumes of 2 ml were pipetted into a cuvette as required and equilibrated to 22°C (3 min) in the chamber of a Perkin Elmer LS50B fluorimeter. The ratio of Ca^{2+} dye fluorescence (Fura-PE3 AM, F_{340}/F_{380}) was measured by a Nikon Ti-E system with NIS-Element Ca^{2+} imaging software. All the experiments were performed at room temperature.

Western blotting. The protocol was similar to that described previously (Xu et al., 2008a). Cells were lysed in Laemmli buffer. Proteins were separated on 8% SDS-PAGE gels and transferred to nitrocellulose membrane (Millipore) and probed with custom-made rabbit anti-TRPC5 (T5C3, 1:250 dilution) antibody (Xu et al., 2005b). Secondary antibody was conjugated with horseradish peroxidase. Membranes were washed with PBS and labeling detected by ECLplus (Amersham).

RT-PCR. Total RNA was isolated from HUVECs using a standard TriReagent protocol and treated with DNase I (Ambion). The isolated RNA was used for cDNA synthesis with oligo-dT primer and AMV reverse transcriptase, and the reaction without reverse transcriptase (no-RT) was set in parallel as a negative control. PCR primer sequences for TRPC5 were CATGACTGGTGGAACC and GTGGGAGTTGGCTGTGAA. Thermal cycling was 40 cycles of 94°C (30 s), 56.6°C (1 min), and 72°C (1 min). PCR products were electrophoresed on 1.5% agarose gels containing ethidium bromide and confirmed by direct sequencing.

Assay for cell viability/proliferation. The cell viability was determined using WST-1 assay (Roche; Xu *et al*., 2008b). WST-1 is a tetrazolium salt and can be cleaved by cellular enzymes, and thus, the assay reflects the metabolic activity of the cells. The overall metabolic activity measured by optical absorption correlates well with the viable cell number as determined by cell counting. Cell proliferation was also observed by direct cell counting with ethidium bromide nucleus staining (Xu *et al*., 2008b).

Materials. All general salts and reagents were from Sigma (U.K.) or from British Drug House (Poole, U.K.). Methylmercury chloride (PESTANAL), $HgCl_2$, gadolinium chloride (Gd^{3+}), $Pb(NO_3)_2$, $NiCl_2$, $ZnCl_2$, hydrogen peroxide, *p*-chloromercuricbenzene sulfonate sodium salt (pCMBS), dithio-threitol (DTT), dimercaptosuccinic acid (DMSA), 2-aminoethoxydiphenyl borate (2-APB), and bovine serum albumin were purchased from Sigma. Fura-PE3 AM and Fluo-3 AM were from Molecular Probes. Fluo-3 AM or Fura-PE3 AM (5mM) and 2-APB (75mM) were made up as stock solutions in 100% dimethyl sulfoxide, and MeHg (10mM) was dissolved in water.

Statistics. Data are expressed as mean ± SEM, where *n* is the cell number for electrophysiological recordings. For Ca^{2+} assay and cell proliferation study, the number of experiments was given. Data sets were compared using unpaired Student's *t*-test and ANOVA Dunnett's *post hoc* analysis with significance indicated if $p < 0.05$.

RESULTS

Activation of TRPC5 Channels by Mercurial Compounds

To assess the effect of mercury compounds on TRPC channels, the Ca^{2+} influx and current were measured in HEK-293 cells stably transfected with TRPC5. The expression of human TRPC5 channel was characterized by the activation by lanthanides and the unique "N"-shaped IV relationship (Figs. 1A and 1B), which has been previously described (Xu *et al*., 2005a). MeHg and divalent mercury (Hg^{2+}) significantly increased the Ca^{2+} influx via TRPC5 in a concentration-dependent manner (Figs. 1C–F). For the acute experiments with accumulative application of mercurial compounds, the EC_{50} for MeHg was 2.03μM with a slope of 0.22, and the EC_{50} for $HgCl_2$ was 3.07μM with a slope factor of 0.40. We also observed the effect of a single concentration of MeHg with longer incubation time, and the cytosolic Ca^{2+} in the TRPC5-transfected cells was significantly elevated by MeHg at as low as 0.01μM after incubation for 20 min ($n = 5$, $p < 0.001$). These results suggested that MeHg is a potent activator of TRPC5.

Mercurial compounds with different ionic charge and/or lipophilicity may have differential effects (Hewett and Atchison, 1992); therefore, we compared the divalent mercury ($HgCl_2$), monovalent (MeHg), and organomercurial pCMBS. The pCMBS has been regarded as a cell-impermeable reagent due to its lowest lipophilicity. The current of TRPC5 was significantly activated by pCMBS as well as MeHg and Hg^{2+} (Fig. 2), suggesting that the activation of TRPC5 channel by mercurial compounds is independent of lipophilicity and ion charge. This also indicated that the binding site to mercurials could be extracellularly accessible.

In addition, we found that the stimulating effect of mercurial compounds on TRPC5 channel was additive to lanthanides.

The rectification property of TRPC5 shown in the IV curve was distorted after perfusion with Hg^{2+} (Supplementary fig. 1B), suggesting that mercurials may have a different extracellular binding site beyond the glutamic acid residues that have been identified as the extracellular binding sites for lanthanides (Jung *et al*., 2003). The binding site could be located within the electrical field near the channel pore region.

Extracellular Effect on TRPC Channel

We performed outside-out excised membrane patches and found that the extracellular perfusion with MeHg significantly increased the TRPC5 current (Figs. 3A and 3B), but no effect if the intracellular surface was exposed to MeHg using the inside-out patch configuration recordings (Fig. 3C). Similarly, Hg^{2+} also showed the external effect (Figs. 3D–F). The orientation of excised membrane was confirmed by perfusion with 2-APB or Gd^{3+}, both of which have been shown to have extracellular effects (Xu *et al*., 2005a). These data suggested that the target for mercurial compounds is extracellularly located.

Role of Extracellular Cysteine Residues in the E3 Loop

Sequence alignment and channel topology analysis showed that two cysteine residues (C^{553} and C^{558}) are predicted in the third extracellular loop (E3) near the channel pore (Fig. 4A). The two cysteine residues have the highest probability to form a disulfide bond predicted by the software (Cheng *et al*., 2006). The predicted structures with and without disulfide bond between S5 and S6 were shown in Figure 4B. We substituted the two cysteines with alanines (C^{553A} and C^{558A}) and found that the double-cysteine mutant TRPC5 channel (TRPC5$^{C553A/C558A}$) was in the open state with a high basal activity, which is consistent with our observation (Xu *et al*., 2008a). The TRPC5$^{C553A/C558A}$ mutant channel was resistant to mercury (Fig. 4C), suggesting that the two cysteine residues are essential for the action of mercurial compounds. In addition, TRPC5 associates with TRPC1 to form a heteromultimeric TRPC1/5 channel (Strubing *et al*., 2001; Xu *et al*., 2006); therefore, we tested the mutant TRPC1/5 heteromultimeric channel (TRPC5$^{C553A/C558A}$ + TRPC1^{C537A}), and no effect was observed (Fig. 4D). However, these cysteine mutant channels were still sensitive to TRPC5 channel blocker 2-APB.

Effect of Mercurial Compounds on Other TRP Channels

The sensitivity of TRPC to mercury is presumed to be isoform specific because the effect was absent if a TRPC member without cysteine residues was present in the region, for example, TRPC3 and TRPC6 (Figs. 4E and 4F). TRPV1 and TRPM2 have cysteine residues in the S5–S6 region (C^{621} and C^{635} for TRPV1, C^{994} and C^{1006} for TRPM2), but there was no direct channel activation by MeHg (Figs. 4G and 4H), which suggested that both cysteine position and channel conformation are important
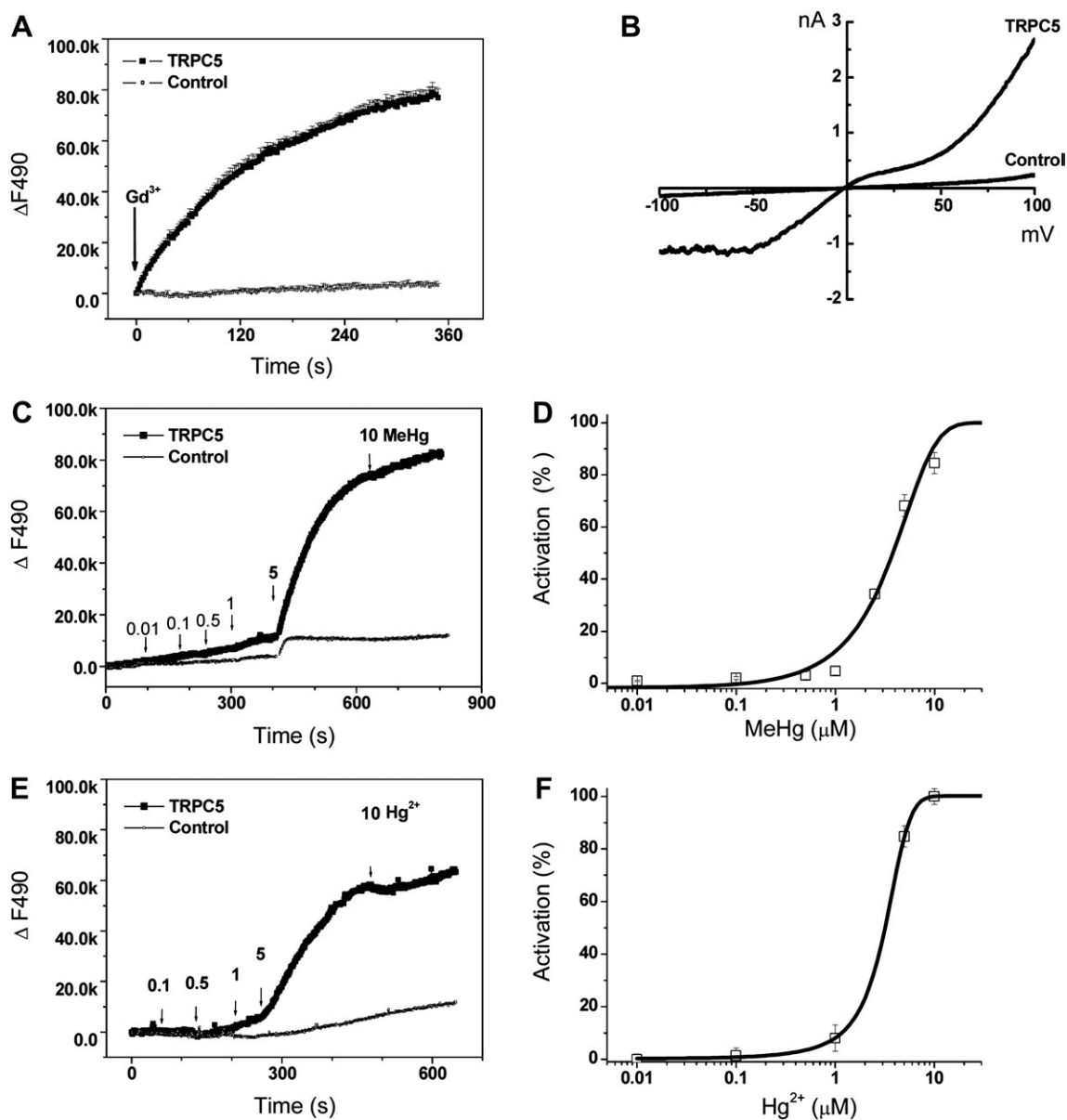
FIG. 1. Activation of TRPC5 channel by mercury compounds. (A) Ca^{2+} influx was activated by Gd^{3+} (100μM) in the TRPC5-transfected HEK-293 cells ($n = 30$ cells). The nontransfected HEK-293 cells (control) were set as control ($n = 28$ cells). (B) TRPC5 current with a typical ''N''-shaped IV curve was recorded with whole-cell patch in the presence of 100μM Gd^{3+}. The current in the nontransfected cells was small with a linear IV curve. (C) MeHg (0.01–10μM) activated the Ca^{2+} influx via TRPC5 channel, and the concentration-response curve is shown in (D) ($n = 6$). (E) Divalent Hg^{2+} (0.1–10μM) also significantly evoked the Ca^{2+} influx in the TRPC5 cells but only a very small effect in the nontransfected cells (control). The concentration-response curve for Hg^{2+} is shown in (F) ($n = 5$).

for mercury sensitivity. TRPC4 not only has a high identity to TRPC5 in amino acid sequence but also shows functional similarity, such as the sensitivity to lanthanides (Jung *et al.*, 2003). We found that human TRPC4α was also sensitive to Hg^{2+} and the channel activity was blocked by 2-APB (Supplementary fig. 2). However, we were unable to examine TRPC1 due to its relatively small Ca^{2+} signal in the transfected cells, which was difficult to distinguish from the endogenous channel signal.

Effect of Other Heavy Metals on TRPC5 Channel

The ion sensitivity of TRPC5 led us to examine other heavy metals. Pb^{2+} is another important pollutant in the environment and causes neurodevelopment disorders (Costa *et al.*, 2004). Pb^{2+} at low concentrations (0.01–5μM) had no effect but mildly increased Ca^{2+} influx at higher concentrations (Supplementary fig. 3A). In contrast, Pb^{2+} showed an inhibitory effect if the TRPC5 channel is at the opening state
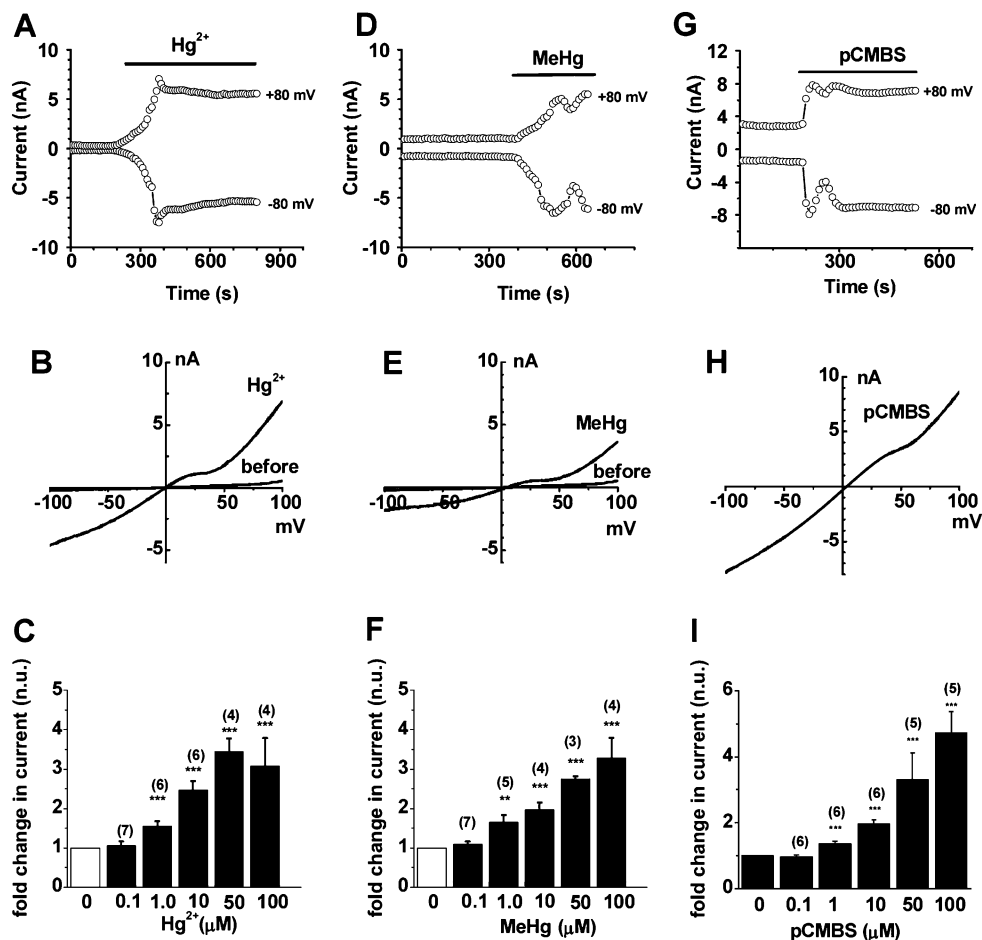
FIG. 2. TRPC5 current activated by mercury compounds. (A) The current was activated by Hg^{2+} (5μM) in the HEK-293 cells transfected with TRPC5. (B) IV relationship of Hg^{2+}-activated TRPC5 as shown in (A). (C) Mean ± SEM data for Hg^{2+} treatment. (D) Activation by MeHg (5μM) in the TRPC5-transfected cells. (E) IV curve for (D). (F) Mean ± SEM data for MeHg. (G) Effect of pCMBS (50μM) on TRPC5 channel. (H) The IV curve and the mean ± SEM data (I). The n numbers are given in the parentheses. Normalized unit (n.u.) is given as the ratio (after/before treatment) of the current at −60 mV. ANOVA test was used. **$p < 0.01$ and ***$p < 0.001$.

by pretreatment with 50μM Gd^{3+} (data not shown), suggesting a differential toxicological mechanism for Pb^{2+}. Ni^{2+} partially inhibited the Ca^{2+} influx, but Cd^{2+} and Zn^{2+} had no significant effect (Supplementary fig. 3B).

### TRPC Channel Regulators on Mercury Exposure

We tested the potential of TRP channel blockers for the treatment for mercury exposure. We found that 2-APB, a potent TRPC channel blocker, significantly inhibited the whole-cell current of TRPC5 activated by Hg^{2+} (Figs. 5A and 5B). This therapeutic effect was also demonstrated by outside-out excised membrane patch (see Figs. 3A and 3B). In addition, preincubation of 2-APB fully prevented the channel activation by Hg^{2+} (Fig. 5C).

Reducing agents with thiols or dithiols have been used for mercury detoxification (Rooney, 2007); therefore, we tested DTT and the therapeutic drug DMSA. Similar to our previous observation (Xu *et al.*, 2008a), DTT itself displayed channel

activation on TRPC5; however, the TRPC5-transfected cells pretreated with DTT resulted in the loss of stimulating action by Hg^{2+}, instead of a partial inhibition (Figs. 5D and 5E), suggesting that the reducing environment is important for modifying the action of mercury on TRPC channels. DMSA has been widely used in clinic as a thiol-reducing agent to chelate heavy metal ions. We found DMSA stimulated TRPC5 channels, and DMSA did not prevent the TRPC5 channel activation by Hg^{2+} (Supplementary fig. 4), suggesting that TRPC channel blocker could be developed as a potential therapeutic drug for mercury poisoning.

Involvement of TRPC in Mercury-Induced Cytotoxicity

We examined the involvement of TRPC5 channel in the cytotoxicity of mercury exposure. The expression of TRPC5 in HEK293 T-REx cells was induced by tetracycline using a tetracycline-regulatory gene expression system. The noninducible cells (without tetracycline) were used as control (Xu *et al.*, 2005a; Zeng *et al.*, 2004). We found that the overexpression of
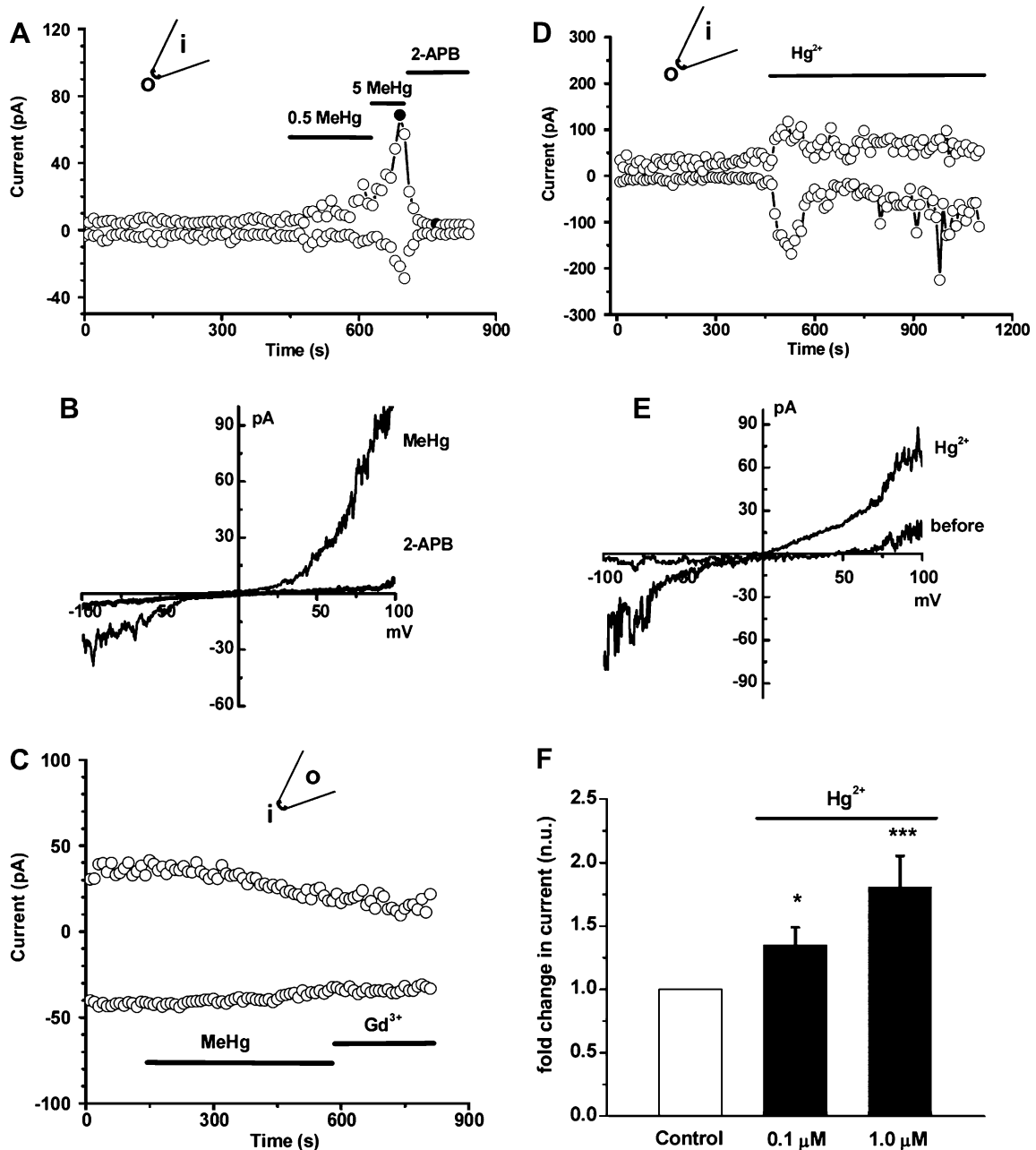
FIG. 3. Extracellular effect of mercury identified with excised membrane patches. (A) The current of TRPC5 channel was evoked by MeHg (0.5 and 5μM) in outside (o)-out patches and blocked by 2-APB (75μM). (B) Representative IV curve for TRPC5 as shown in (A) indicated as solid circle. (C) No effect was observed when MeHg (5μM) was applied in the intracellular surface via inside (i)-out patch recordings. Gd^{3+} (100μM) had no effect in inside-out membrane orientation because the binding site for Gd^{3+} was extracellularly located (Jung *et al.*, 2003; Xu *et al.*, 2005a). (D) Divalent Hg^{2+} (1μM) had a similar channel stimulating effect, and the representative IV curve is shown in (E). (F) Mean data for the outside-out patch experiments ($n = 6$, * $p < 0.05$ and *** $p < 0.001$). The currents in (A), (C), and (D) were given at the potential of ± 80 mV.

TRPC5 increased the proliferation of HEK-TRx cells by 27.6 ± 3.1% after 24 h cell culture determined by WST-1 assay. Incubation with Hg^{2+} at 1 and 5μM inhibited the cell proliferation in both TRPC5-transfected and nontransfected cells, but the inhibitory effect was more evident in the cells overexpressing TRPC5 (Fig. 6A), suggesting that the enhanced cytotoxicity could be due to the channel opening by Hg^{2+} and thus lead

to the intracellular toxicological processes through Hg^{2+} influx.

To explore the potential protection against mercury-induced cytotoxicity, the TRPC5-specific blocking antibody and the two nonselective TRPC channel blockers, 2-APB and SKF-96365, were tested (Xu *et al.*, 2005b). After incubation with Hg^{2+} for 24 h, the cell viability was significantly lower
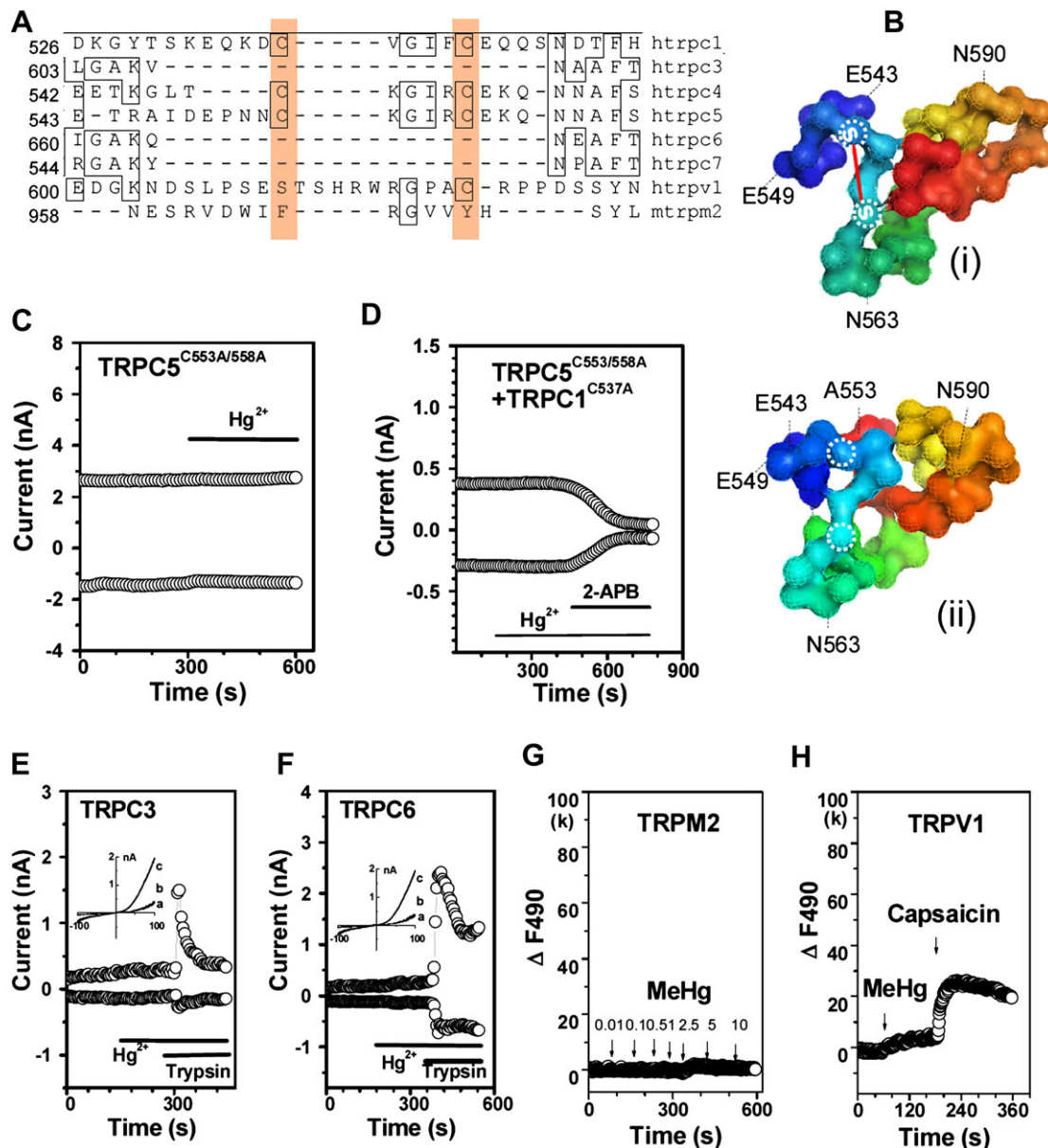
FIG. 4. Cysteine residues in the transmembrane domain (S5–S6) are essential for channel activation. (A) Sequence alignment of TRP channels near the putative channel pore region between S5 and S6 transmembrane. Two cysteine residues were highlighted. (B) Predicted topology of TRPC5 channel pore region (i) and mutant TRPC5 with double-cysteine substitution by alanine (TRPC5$^{C553A+C558A}$) (ii). Figures prepared by PYMOL (DeLano Scientific). The positions of C553 and C558 were indicated by dot circle, and disulfide bond was labeled as S–S. (C) TRPC5$^{C553A+C558A}$ mutant channel showed resistance to Hg^{2+} (5μM). (D) The heteromultimeric mutant channel (TRPC5$^{C553A+C558A}$ / TRPC1^{C537A}) was also resistant to Hg^{2+} (5μM) but sensitive to 2-APB (75μM). (E and F) No effect of Hg^{2+} (5μM) on TRPC3 and TRPC6 that has no cysteine residue in the region ($n = 5$ for each isoform) but sensitive to trypsin (0.1nM) or carbachol (100μM) (Xu *et al.*, 2005a). The IV curves of before (a) and after treatment with 5μM Hg^{2+} (b) and 0.1nM trypsin (c) are shown in the insets. (G and H) TRPM2 ($n = 4$) and TRPV1 ($n = 3$) did not display direct channel activation by MeHg (0.01–10μM); however, the expressed channels are sensitive to H$_2$O$_2$ (1mM; McHugh *et al.*, 2003) and capsaicin (1μM).

in the tetracycline-induced group (TRPC5) than that in the noninduced group (control). 2-APB (75μM) did not show any protective action on the Hg^{2+}-evoked cytotoxicity; instead, a deteriorating effect, which could be due to its inhibition on intracellular inositol trisphosphate (IP$_3$) receptors (Szatkowski *et al.*, 2010). However, SKF-96365 significantly prevented

the Hg^{2+}-evoked cytotoxicity in the TRPC5-transfected cells (Fig. 6A). The TRPC5-specific pore-blocking antibody also significantly showed protection against the mercury-induced cytotoxicity (Fig. 6B). In addition, we examined nonsulfhydryl and sulfhydryl-reducing agents. Tris (2-carboxyethyl) phosphine hydrochloride (TCEP), a membrane-impermeable nonsulfuric
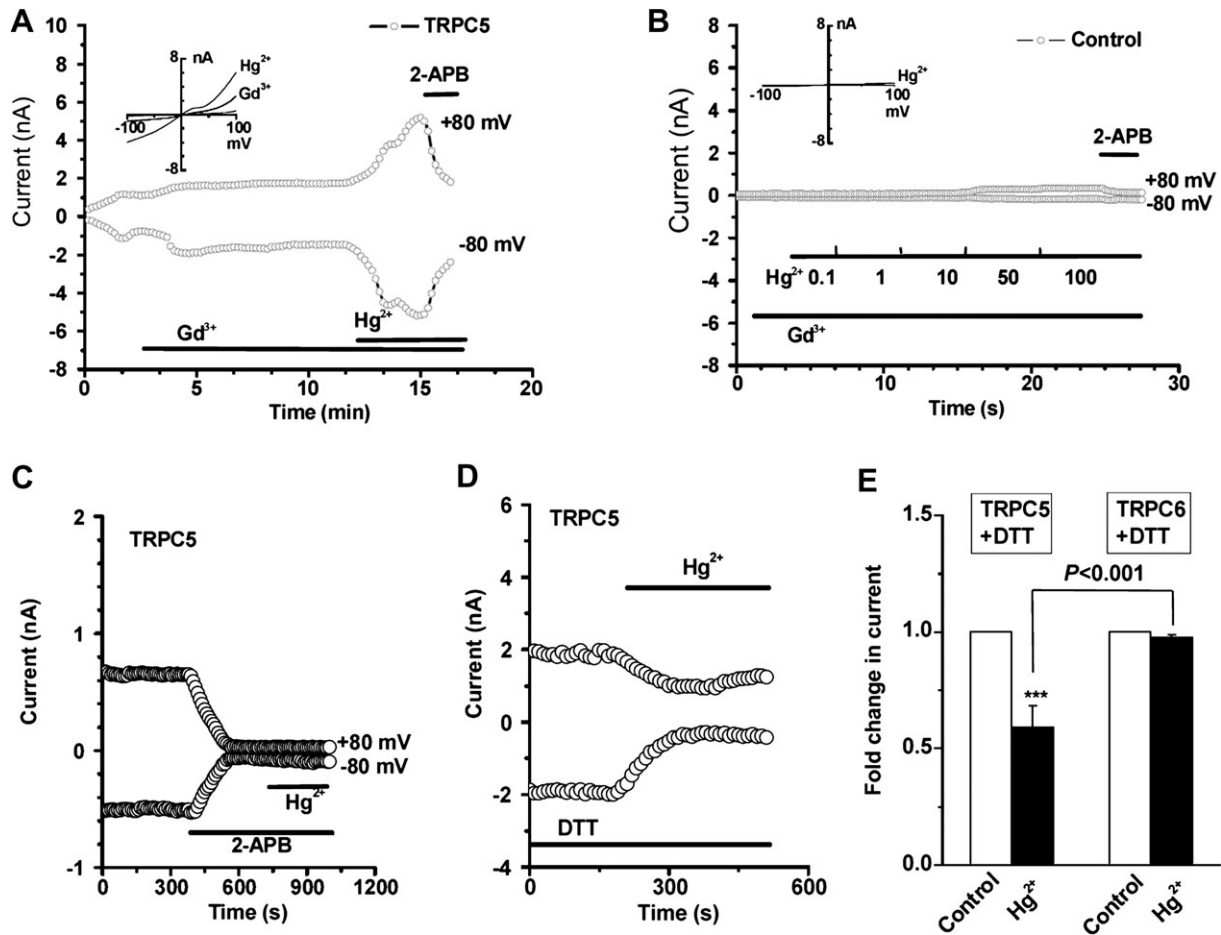
FIG. 5. Mercury-evoked current was blocked by 2-APB and modified by reducing agent DTT. TRPC5 channel activity was activated by Hg^{2+} (1μM) in TRPC5 cells in the presence of 10μM Gd^{3+} (A) but a small current in the nontransfected cells if high concentrations of Hg^{2+} (10–100μM) were applied (B). The IV curves are shown in the inset. (C) The activation by Hg^{2+} (1μM) was prevented by 2-APB (75μM). (D) Hg^{2+} (5μM) displayed as an inhibitory effect if the channel was activated by the reducing agent DTT (10 mM; Xu *et al.*, 2008a). (E) Mean ± SEM data showing mercury effect on TRPC5 ($n = 9$) and TRPC6 ($n = 6$) currents with DTT treatment.

reducing agent that can activate TRPC5 channels (Xu *et al.*, 2008a), had no protective effect, whereas the membrane-permeable sulfuric reducing agent DTT enhanced the cytotoxicity (Fig. 6C). DMSA with two thiol groups showed a significant protective effect on cell survival; however, the effect is more evident in the noninduced cells (Fig. 6D), suggesting that the protective mechanism for DMSA could be due to Hg^{2+} chelation, rather than the action on TRPC5 channels. The cell viability in the TRPC5-transfected group was decreased, which could be explained as the direct TRPC4 and TRPC5 channel activation by DMSA (Supplementary fig. 4) that may cause more Hg^{2+} influx and thus enhance the cytotoxicity via other mechanisms.

TRPC5 is widely expressed in central nervous system and involved in axonal growth (Greka *et al.*, 2003; Hui *et al.*, 2006). Therefore, we examined the TRPC5 channel in the neurotoxicity of mercury exposure. We found that the NGF-induced axonal growth was dramatically inhibited by mercurial compounds in a neuronal cell line (PC12), whereas Pb^{2+} at

1μM had no effect on axonal growth (Fig. 7A). The cell proliferation was also inhibited (Fig. 7B). Transfection with TRPC5 siRNA inhibited cell proliferation and axonal extension and partially alleviated Hg^{2+}-induced cytotoxicity (Figs. 7C and 7D).

Massive loss of cerebral cortex is another important pathological change in patients with mercury poisoning, and microvasculature formation is critical for maintaining the thickness of cerebral cortex (Eto and Takeuchi, 1978); we therefore tested the vascular hypothesis using endothelial cells derived from newborns. As shown in Figure S5A, TRPC5 was highly expressed in HUVECs. The cell growth of HUVECs was substantially inhibited by Hg^{2+} and MeHg, but not by Pb^{2+}. Inhibition of TRPC5 expression by TRPC5 siRNA also prevented the cell proliferation inhibition induced by 1μM Hg^{2+} (Supplementary fig. 5), suggesting that the Ca^{2+}-overloaded mechanism of mercury exposure via TRPC activation could be extended to vascular system.
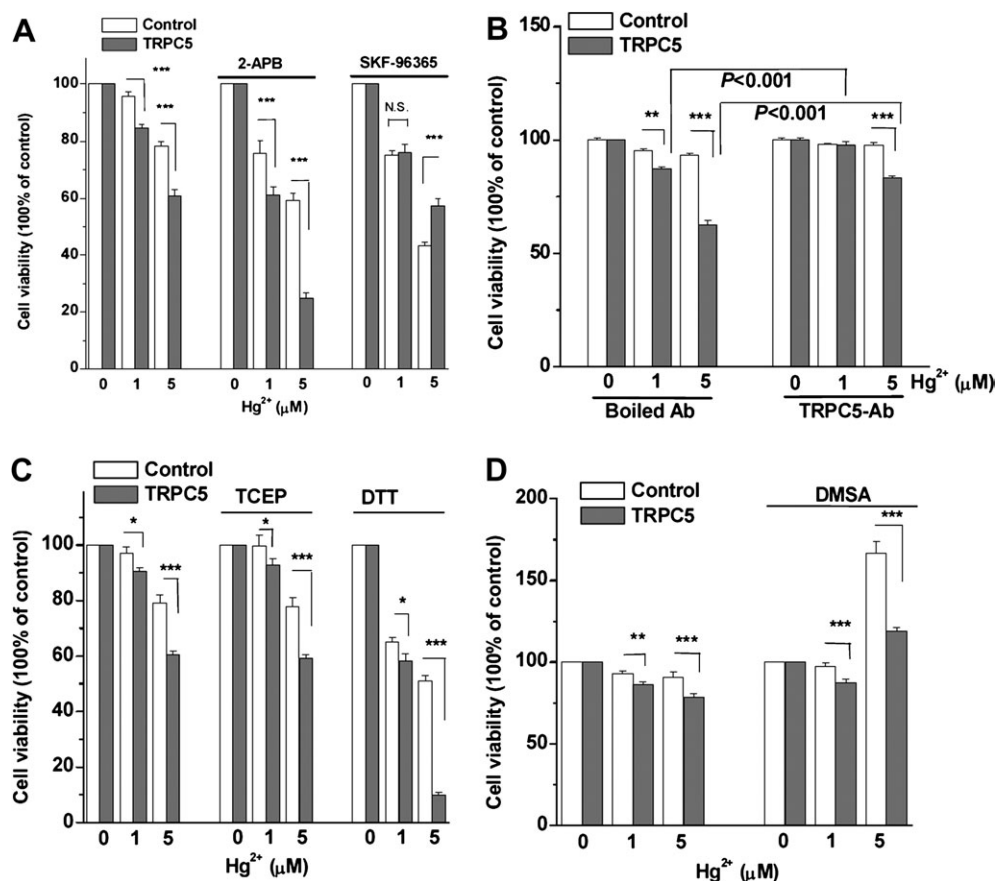
FIG. 6. Effect of pharmacological regulators on the mercury-induced inhibition of cell proliferation. The HEK-293 cells were inducibly expressed with TRPC5 with (TRPC5) and without tetracycline (control). The cell proliferation was detected by WST-1 assay. (A) Cells were incubated with Hg^{2+} in the DMEM-F12 medium containing 10% FCS for 24 h in the presence or absence of 2-APB (75μM) and SKF-96365 (25μM), $n = 8$ wells for each treated group. (B) TRPC5 E3-targeting pore-blocking antibody (TRPC5-Ab, 1:250) was used (Xu *et al.*, 2005b). Boiled TRPC5-Ab was used as control. (C) The reducing agents TCEP (100μM) and DTT (1mM) were used. The cells were incubated with Hg^{2+} for 24 h with and without reducing agents ($n = 16$ wells for each group). (D) Cells were incubated with and without chelating agent DMSA (100μM) for 24 h ($n = 16$ wells for each group). *$p < 0.05$; **$p < 0.01$; ***$p < 0.001$.

DISCUSSION

Our results provide first evidence that mercurial compounds can activate TRPC5 channels. The action site is related to the two extracellular cysteine residues (C^{553} and C^{558}) near the channel pore. The blockade of TRPC channel by 2-APB not only prevents the channel activation evoked by mercurial compounds but also shows therapeutic effect against the channel activation by mercury. TRPC channel blockers (SKF-96365 and TRPC5 pore-blocking antibody) modestly alleviate the cytotoxicity. These results give a new insight of TRPC4 and TRPC5 as the target proteins of mercury toxicity and a clue for the development of TRPC channel blockers as new therapeutic agents for mercury exposure.

The sensitivity of TRPC5 channels to trivalent lanthanides (La^{3+} or Gd^{3+}) has been described by Jung *et al.* (2003); however, the physiological or pathophysiological significance of the trivalent sensitivity of TRPC5 channel is unclear, especially lanthanides are very rare elements in the human body except their chelating complexes used as diagnostic and therapeutic agents (Bottrill *et al.*, 2006; Kostova, 2005). Therefore, we screened other heavy metal ions. Interestingly, we found that TRPC5 channel is sensitive to mercurial compounds. The channel can be activated by mercurials at micromolar concentrations, suggesting that TRPC5 channel is a novel target for mercury exposure. We examined the binding sites using excised membrane patch clamp and site mutagenesis and identified that two cysteine residues in the third extracellular loop of transmembrane region mediate the channel activation. This result suggested that there are at least two extracellular binding sites for heavy metal ions in TRPC5, that is, the two cysteine residues (C^{553} and C^{558}) bound to mercurial compounds and the glutamic acid residues (Glu^{543} and Glu^{595}/Glu^{598}) for lanthanides (Jung *et al.*, 2003).

Although nearly all ion channel proteins contain cysteine residues and the cytotoxicity of mercurials has been related to the formation of stable complexes with sulfhydryl-containing amino acids (Carvalho *et al.*, 2008; Rooney, 2007), the effect of mercurials is still specific for some ion channels; for
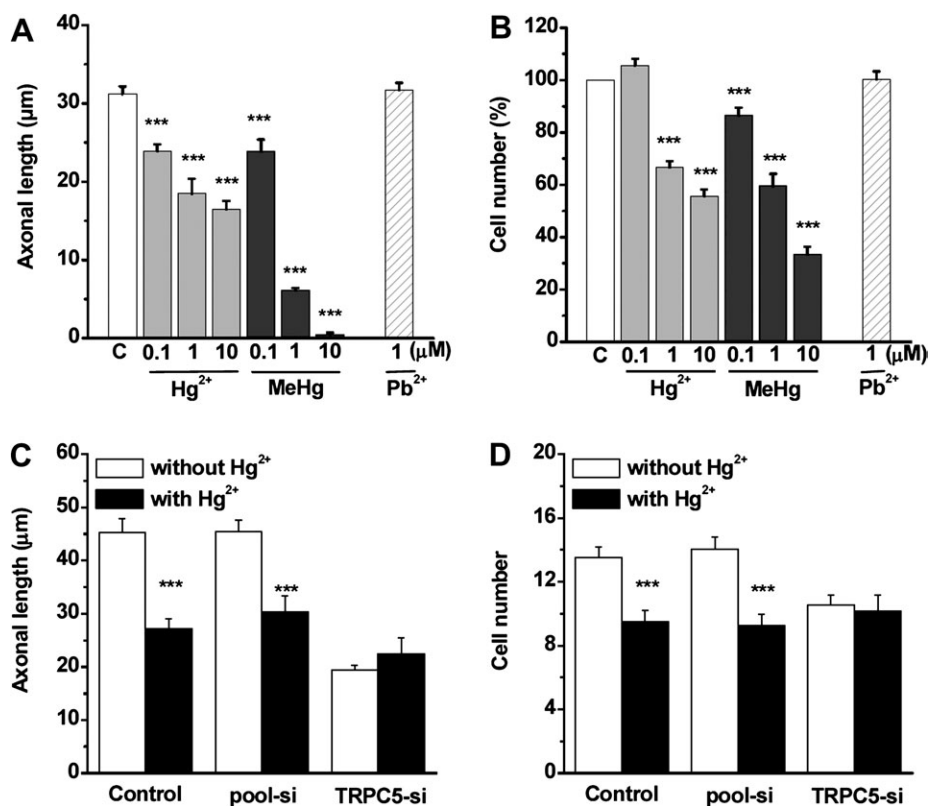
FIG. 7. Inhibition of axonal growth by mercury compounds in PC12 cells. PC12 cells were cultured in DMEM-F12 medium with 15% FCS and NGF (50 ng/ml) and treated with Hg^{2+}, MeHg, and Pb^{2+} for 4 days before taking photos. (A) Effect on axonal growth of PC12 cells (***$p < 0.001$, $n = 143–338$ neurite measurements for Hg^{2+}, and 68–201 measurements for MeHg, and 335 measurements for Pb^{2+}). (B) Effect on PC12 cell proliferation (***$p < 0.001$, $n = 40$ microscopic fields for each group). (C) The effect on axonal growth in PC12 cells after transfection with TRPC5 siRNA (TRPC5-si) and pool siRNA (pool-si) and mock transfection without siRNA (control) (***$p < 0.001$, $n = 112–253$ neurite measurements for each group). (D) Effect on PC12 cell proliferation after siRNA transfection (***$p < 0.001$, $n = 36$ microscopic fields for each group).

example, TRPC3 and TRPC6 without extracellular cysteine residues did not show any sensitivity to mercurial compounds; TRPM2 or TRPV1 with cysteine residues at different positions showed no direct activation, suggesting that the effect of mercurials on TRP channels is determined by the location and function of individual cysteine residue in a protein. This hypothesis needs to be further tested on other TRP channels in the future. In addition, we found that the action of mercury on TRPC5 channel could be modified by reducing agents. These findings suggested that both the cysteine residue position and channel conformation are important for mercury activation on TRP channels.

Several types of VGCC have been shown to be inhibited by mercurial compounds, such as L-type and T-type (Hajela *et al.*, 2003; Tarabova *et al.*, 2006); however, the cytosol $[Ca^{2+}]$ was increased in cells treated with mercury (Limke *et al.*, 2004). The activation of TRPC5 channel found in this study provides a good explanation for the increased $[Ca^{2+}]_i$ seen in mercury exposure. Although we tested TRPM2 in the TRPM subfamily and TRPV1 in the TRPV subfamily, we were unable to examine all the members in TRP superfamily; however, the sequence alignment of TRP superfamily shows no similar

location of cysteine residues in the S5–S6 regions (see Supplementary fig. 1C), suggesting that the TRPC5 or TRPC4 in TRPC subfamily is probably the only isoform for mercury activation.

The potential protective effect on the mercury cytotoxicity was examined in this study using *in vitro* cell models. The more evident inhibition on cell proliferation was seen in the TRPC5 overexpressing cells, which could be due to the channel activation and thus facilitates Hg^{2+} and Ca^{2+} influxes. The TRPC channel blocker 2-APB can potently protect against the channel-stimulating effect by mercurial compounds; however, there was no protective effect against cytotoxicity, which could be explained by the additional effects of 2-APB on cell survival, such as the inhibition on IP_3 receptor (Xu *et al.*, 2005a) or the blockage on gap junctional channel (Bai *et al.*, 2006). However, SKF-96365, another nonselective TRPC channel blocker, showed a significantly protective effect, suggesting that TRPC channel blocker may be useful for the treatment of mercury exposure. Importantly, we found that TRPC5-blocking antibody specifically prevented the cytotoxicity induced by mercury, which provided the direct evidence of TRPC5 acting as a therapeutic target for mercury

exposure. The protective effects are modest, which suggest that other toxicological mechanisms are also important, for example, the intracellular mechanisms (Calamita *et al.*, 2005; Castoldi *et al.*, 2000). On the other hand, thiol chemicals or thiol-containing proteins have been investigated for the treatment of mercury toxicity (Patrick, 2002). The reducing agents DTT and TCEP that can activate TRPC5 channel (Xu *et al.*, 2008a) did not show any protective effects, whereas DMSA, a chelating thiol agent with stimulating action on TRPC5 and TRPC4 channels, showed a nonselective protection. These results may give the explanations why mercury detoxification with reducing agents is not very effective.

Numerous studies have demonstrated that exposure to mercurial compounds causes neurodevelopmental disorders. Therefore, we examined the neuronal cell growth and the role of TRPC channels in mercury-induced neurotoxicity. We found that mercurial compounds significantly inhibited the PC 12 cell growth and axonal extension; this result is consistent with other reports (Leong *et al.*, 2001; Radio *et al.*, 2008). The inhibition on axonal extension and cell proliferation by Hg^{2+} was alleviated when the *TRPC5* gene was silenced by the specific TRPC5 siRNA (Xu *et al.*, 2008a), suggesting that the TRPC5 channel mediates the mercury neurotoxicity. On the other hand, the inhibition of VGCC has no direct relevance to the impairment of IQ or intelligence but rather to an improvement of memory or recognition (Veng *et al.*, 2003); therefore, we suppose that the IQ loss due to mercury exposure might be caused by the elevated $[Ca^{2+}]_i$ through TRPC5 activation and consequently affecting growth cone formation, axonal extension, and the connections between synapses. We also confirm the hypothesis that mercury cytotoxicity is mediated by TRPC5 channel in the vascular endothelial cells where the expression level of TRPC5 is high.

According to the U.S. Environment Protection Agency's reference dose, the level of mercury in blood less than 5.8 µg/l (equivalent to 0.029µM) has been considered "safe" without causing adverse health effects (Hightower *et al.*, 2006; Weil *et al.*, 2005), although it has been argued that the concentration should be lowered to 3.5 µg/l (Hightower *et al.*, 2006). In this study, we found that longer incubation with 10nM MeHg slightly increased Ca^{2+} influx and Hg^{2+} at 100nM significantly increased the outside-out patch current of TRPC5, which suggests that the effect of mercurial compounds on TRPC channel activity could happen in the population with elevated blood mercury level. In addition, the distribution and disposition of mercurial compounds in the body are tissue and organ specific; for example, the concentration of MeHg in brain is much higher than in plasma (50 times; Cernichiari *et al.*, 2007). Higher level (> 5.8 µg/l) of mercury has also been reported in the population living in polluted areas and frequent fish consumers (Trasande *et al.*, 2005). Therefore, the novel toxicological mechanism we reported here should be applicable for all cases of mercury overexposure. The removal of MeHg in the body is difficult, presumably due to its enterohepatic recirculation and poor reaction with chelating agents; therefore, the search for specific TRPC channel blockers may give rise to new therapeutics for mercury poisoning.

SUPPLEMENTARY MATERIAL

Supplementary data are available online at http://toxsci.oxfordjournals.org/.

REFERENCES

Axelrad, D. A., Bellinger, D. C., Ryan, L. M., and Woodruff, T. J. (2007). Dose-response relationship of prenatal mercury exposure and IQ: An integrative analysis of epidemiologic data. *Environ. Health Perspect.* **115**, 609–615.

Bai, D., del Corsso, C., Srinivas, M., and Spray, D. C. (2006). Block of specific gap junction channel subtypes by 2-aminoethoxydiphenyl borate (2-APB). *J. Pharmacol. Exp. Ther.* **319**, 1452–1458.

Bottrill, M., Kwok, L., and Long, N. J. (2006). Lanthanides in magnetic resonance imaging. *Chem. Soc. Rev.* **35**, 557–571.

Calamita, G., Ferri, D., Gena, P., Liquori, G. E., Cavalier, A., Thomas, D., and Svelto, M. (2005). The inner mitochondrial membrane has aquaporin-8 water channels and is highly permeable to water. *J. Biol. Chem.* **280**, 17149–17153.

Carvalho, C. M., Chew, E. H., Hashemy, S. I., Lu, J., and Holmgren, A. (2008). Inhibition of the human thioredoxin system. A molecular mechanism of mercury toxicity. *J. Biol. Chem.* **283**, 11913–11923.

Castoldi, A. F., Barni, S., Turin, I., Gandini, C., and Manzo, L. (2000). Early acute necrosis, delayed apoptosis and cytoskeletal breakdown in cultured cerebellar granule neurons exposed to methylmercury. *J. Neurosci. Res.* **59**, 775–787.

Cernichiari, E., Myers, G. J., Ballatori, N., Zareba, G., Vyas, J., and Clarkson, T. (2007). The biological monitoring of prenatal exposure to methylmercury. *Neurotoxicology* **28**, 1015–1022.

Cheng, J., Saigo, H., and Baldi, P. (2006). Large-scale prediction of disulphide bridges using kernel methods, two-dimensional recursive neural networks, and weighted graph matching. *Proteins* **62**, 617–629.

Clapham, D. E. (2003). TRP channels as cellular sensors. *Nature* **426**, 517–524.

Clarkson, T. W., Magos, L., and Myers, G. J. (2003). The toxicology of mercury–current exposures and clinical manifestations. *N. Engl. J. Med.* **349**, 1731–1737.

Cohen, J. T., Bellinger, D. C., and Shaywitz, B. A. (2005). A quantitative analysis of prenatal methyl mercury exposure and cognitive development. *Am. J. Prev. Med.* **29**, 353–365.

Costa, L. G., Aschner, M., Vitalone, A., Syversen, T., and Soldin, O. P. (2004). Developmental neuropathology of environmental agents. *Annu. Rev. Pharmacol. Toxicol.* **44**, 87–110.

Counter, S. A., and Buchanan, L. H. (2004). Mercury exposure in children: A review. *Toxicol. Appl. Pharmacol.* **198**, 209–230.

Dasari, S., and Yuan, Y. (2009). Low level postnatal methylmercury exposure in vivo alters developmental forms of short-term synaptic plasticity in the visual cortex of rat. *Toxicol. Appl. Pharmacol.* **240**, 412–422.

Davidson, P. W., Cory-Slechta, D. A., Thurston, S. W., Huang, L. S., Shamlaye, C. F., Gunzler, D., Watson, G., van Wijngaarden, E., Zareba, G., Klein, J. D., *et al.* (2011). Fish consumption and prenatal methylmercury exposure: Cognitive and behavioral outcomes in the main cohort at 17 years from the Seychelles child development study. *Neurotoxicology* **32**, 711–717.

Denny, M. F., and Atchison, W. D. (1996). Mercurial-induced alterations in neuronal divalent cation homeostasis. *Neurotoxicology* **17**, 47–61.

Eto, K., and Takeuchi, T. (1978). A pathological study of prolonged cases of Minamata disease. With particular reference to 83 autopsy cases. *Acta Pathol. Jpn.* **28**, 565–584.

Greka, A., Navarro, B., Oancea, E., Duggan, A., and Clapham, D. E. (2003). TRPC5 is a regulator of hippocampal neurite length and growth cone morphology. *Nat. Neurosci.* **6**, 837–845.

Guallar, E., Sanz-Gallardo, M. I., van't Veer, P., Bode, P., Aro, A., Gomez-Aracena, J., Kark, J. D., Riemersma, R. A., Martin-Moreno, J. M., and Kok, F. J. (2002). Mercury, fish oils, and the risk of myocardial infarction. *N. Engl. J. Med.* **347**, 1747–1754.

Hajela, R. K., Peng, S. Q., and Atchison, W. D. (2003). Comparative effects of methylmercury and Hg^{2+} on human neuronal N- and R-type high-voltage activated calcium channels transiently expressed in human embryonic kidney 293 cells. *J. Pharmacol. Exp. Ther.* **306**, 1129–1136.

Hewett, S. J., and Atchison, W. D. (1992). Effects of charge and lipophilicity on mercurial-induced reduction of $^{45}Ca^{2+}$ uptake in isolated nerve terminals of the rat. *Toxicol. Appl. Pharmacol.* **113**, 267–273.

Hightower, J. M., O'Hare, A., and Hernandez, G. T. (2006). Blood mercury reporting in NHANES: Identifying Asian, Pacific Islander, Native American, and multiracial groups. *Environ. Health Perspect.* **114**, 173–175.

Hui, H., McHugh, D., Hannan, M., Zeng, F., Xu, S. Z., Khan, S. U., Levenson, R., Beech, D. J., and Weiss, J. L. (2006). Calcium-sensing mechanism in TRPC5 channels contributing to retardation of neurite outgrowth. *J. Physiol.* **572**, 165–172.

Jia, Y., Zhou, J., Tai, Y., and Wang, Y. (2007). TRPC channels promote cerebellar granule neuron survival. *Nat. Neurosci.* **10**, 559–567.

Jung, S., Muhle, A., Schaefer, M., Strotmann, R., Schultz, G., and Plant, T. D. (2003). Lanthanides potentiate TRPC5 currents by an action at extracellular sites close to the pore mouth. *J. Biol. Chem.* **278**, 3562–3571.

Kostova, I. (2005). Lanthanides as anticancer agents. *Curr. Med. Chem. Anticancer Agents* **5**, 591–602.

Landrigan, P. J., Sonawane, B., Butler, R. N., Trasande, L., Callan, R., and Droller, D. (2005). Early environmental origins of neurodegenerative disease in later life. *Environ. Health Perspect.* **113**, 1230–1233.

Leong, C. C., Syed, N. I., and Lorscheider, F. L. (2001). Retrograde degeneration of neurite membrane structural integrity of nerve growth cones following in vitro exposure to mercury. *Neuroreport* **12**, 733–737.

Li, Y., Jia, Y. C., Cui, K., Li, N., Zheng, Z. Y., Wang, Y. Z., and Yuan, X. B. (2005). Essential role of TRPC channels in the guidance of nerve growth cones by brain-derived neurotrophic factor. *Nature* **434**, 894–898.

Limke, T. L., Heidemann, S. R., and Atchison, W. D. (2004). Disruption of intraneuronal divalent cation regulation by methylmercury: Are specific targets involved in altered neuronal development and cytotoxicity in methylmercury poisoning? *Neurotoxicology* **25**, 741–760.

McHugh, D., Flemming, R., Xu, S. Z., Perraud, A. L., and Beech, D. J. (2003). Critical intracellular Ca^{2+} dependence of transient receptor potential melastatin 2 (TRPM2) cation channel activation. *J. Biol. Chem.* **278**, 11002–11006.

Patrick, L. (2002). Mercury toxicity and antioxidants: Part 1: Role of glutathione and alpha-lipoic acid in the treatment of mercury toxicity. *Altern. Med. Rev.* **7**, 456–471.

Radio, N. M., Breier, J. M., Shafer, T. J., and Mundy, W. R. (2008). Assessment of chemical effects on neurite outgrowth in PC12 cells using high content screening. *Toxicol. Sci.* **105**, 106–118.

Riccio, A., Li, Y., Moon, J., Kim, K. S., Smith, K. S., Rudolph, U., Gapon, S., Yao, G. L., Tsvetkov, E., Rodig, S. J., *et al.* (2009). Essential role for TRPC5 in amygdala function and fear-related behavior. *Cell* **137**, 761–772.

Rooney, J. P. (2007). The role of thiols, dithiols, nutritional factors and interacting ligands in the toxicology of mercury. *Toxicology* **234**, 145–156.

Sossey-Alaoui, K., Lyon, J. A., Jones, L., Abidi, F. E., Hartung, A. J., Hane, B., Schwartz, C. E., Stevenson, R. E., and Srivastava, A. K. (1999). Molecular cloning and characterization of TRPC5 (HTRP5), the human homologue of a mouse brain receptor-activated capacitative Ca^{2+} entry channel. *Genomics* **60**, 330–340.

Spurgeon, A. (2006). Prenatal methylmercury exposure and developmental outcomes: Review of the evidence and discussion of future directions. *Environ. Health Perspect.* **114**, 307–312.

Strubing, C., Krapivinsky, G., Krapivinsky, L., and Clapham, D. E. (2001). TRPC1 and TRPC5 form a novel cation channel in mammalian brain. *Neuron* **29**, 645–655.

Szatkowski, C., Parys, J. B., Ouadid-Ahidouch, H., and Matifat, F. (2010). Inositol 1,4,5-trisphosphate-induced Ca^{2+} signalling is involved in estradiol-induced breast cancer epithelial cell growth. *Mol. Cancer* **9**, 156.

Tarabova, B., Kurejova, M., Sulova, Z., Drabova, M., and Lacinova, L. (2006). Inorganic mercury and methylmercury inhibit the cav3.1 channel expressed in human embryonic kidney 293 cells by different mechanisms. *J. Pharmacol. Exp. Ther.* **317**, 418–427.

Trasande, L., Landrigan, P. J., and Schechter, C. (2005). Public health and economic consequences of methyl mercury toxicity to the developing brain. *Environ. Health Perspect.* **113**, 590–596.

Veng, L. M., Mesches, M. H., and Browning, M. D. (2003). Age-related working memory impairment is correlated with increases in the L-type calcium channel protein alpha1D (Cav1.3) in area CA1 of the hippocampus and both are ameliorated by chronic nimodipine treatment. *Brain Res. Mol. Brain Res.* **110**, 193–202.

Wang, G. X., and Poo, M. M. (2005). Requirement of TRPC channels in netrin-1-induced chemotropic turning of nerve growth cones. *Nature* **434**, 898–904.

Weil, M., Bressler, J., Parsons, P., Bolla, K., Glass, T., and Schwartz, B. (2005). Blood mercury levels and neurobehavioral function. *JAMA* **293**, 1875–1882.

Xu, S. Z., Muraki, K., Zeng, F., Li, J., Sukumar, P., Shah, S., Dedman, A. M., Flemming, P. K., McHugh, D., Naylor, J., *et al.* (2006). A sphingosine-1-phosphate-activated calcium channel controlling vascular smooth muscle cell motility. *Circ. Res.* **98**, 1381–1389.

Xu, S. Z., Sukumar, P., Zeng, F., Li, J., Jairaman, A., English, A., Naylor, J., Ciurtin, C., Majeed, Y., Milligan, C. J., *et al.* (2008a). TRPC channel activation by extracellular thioredoxin. *Nature* **451**, 69–72.

Xu, S. Z., Zeng, F., Boulay, G., Grimm, C., Harteneck, C., and Beech, D. J. (2005a). Block of TRPC5 channels by 2-aminoethoxydiphenyl borate:

A differential, extracellular and voltage-dependent effect. *Br. J. Pharmacol.* **145,** 405–414.

Xu, S. Z., Zeng, F., Lei, M., Li, J., Gao, B., Xiong, C., Sivaprasadarao, A., and Beech, D. J. (2005b). Generation of functional ion-channel tools by E3 targeting. *Nat. Biotechnol.* **23,** 1289–1293.

Xu, S. Z., Zhong, W., Watson, N. M., Dickerson, E., Wake, J. D., Lindow, S. W., Newton, C. J., and Atkin, S. L. (2008b). Fluvastatin reduces oxidative damage in human vascular endothelial cells by upregulating Bcl-2. *J. Thromb. Haemost.* **6,** 692–700.

Zeng, F., Xu, S. Z., Jackson, P. K., McHugh, D., Kumar, B., Fountain, S. J., and Beech, D. J. (2004). Human TRPC5 channel activated by a multiplicity of signals in a single cell. *J. Physiol.* **559,** 739–750.

Zheng, J. Q. (2000). Turning of nerve growth cones induced by localized increases in intracellular calcium ions. *Nature* **403,** 89–93.